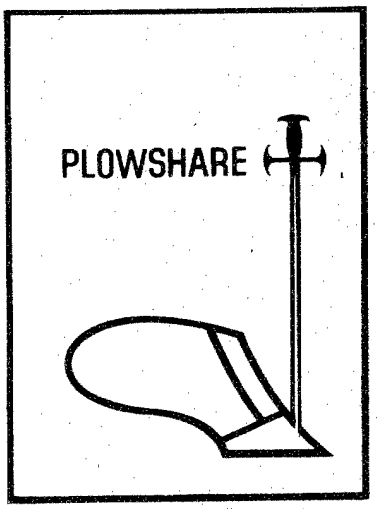

SC-RR-68-655
TID-4500 (52nd Ed.)
NUCLEAR EXPLOSIONS--
PEACEFUL APPLICATIONS

AIRBLAST AND CRATERS FROM ROWS OF TWO TO TWENTY-FIVE BURIED HE CHARGES

L. J. Vortman, 9111

January 1969

SANDIA LABORATORIES

OPERATED FOR THE U. S. ATOMIC ENERGY COMMISSION BY SANDIA CORPORATION | ALBUQUERQUE, NEW MEXICO; LIVERMORE, CALIFORNIA

Issued by Sandia Corporation
a prime contractor to the
United States Atomic Energy Commission

Printed in the United States of America
Available from
Clearinghouse for Federal Scientific and Technical Information
National Bureau of Standards, U. S. Department of Commerce
Springfield, Virginia 22151
Price: Printed Copy $3.00; Microfiche $0.65

TID-4500 (52nd Ed.)
NUCLEAR EXPLOSIONS--
PEACEFUL APPLICATIONS

SC-RR-68-655

AIRBLAST AND CRATERS FROM ROWS OF TWO TO TWENTY-FIVE BURIED HE CHARGES

L. J. Vortman, 9111
Sandia Laboratories, Albuquerque

January 1969

ABSTRACT

Airblast was measured perpendicular to and off the ends of row-charge explosions and compared with airblast from single charges. It was found that $p_{row} \approx n^{\beta} p_{single}$, where p is peak overpressure and n the number of charges. β was different for each blast parameter examined: ground-shock-induced peak overpressure, peak overpressure from venting gas, peak negative pressure, and positive and negative impulse. Values of β increased as spacing decreased. Airblast was always greater perpendicular to the row than off the end, by an amount which increased as the number of charges increased.

sbm

ACKNOWLEDGMENT

Field work for these experiments was accomplished by H. E. Gipson, R. E. Zumwalt, W. L. Gault, and C. D. Northam under direction of R. C. Holland, all of Sandia Corporation's Tonopah Test Range. Topographic mapping was done by American Aerial Surveys, Inc., of Covina, California. T. F. Laney guided data reduction, and G. E. Larsen, and J. M. Levesque assisted in data evaluation. The work was supported by the Atomic Energy Commission, Division of Peaceful Nuclear Explosives.

SUMMARY

Airblast measurements were made off the end of and perpendicular to rows of 2, 5, 11, and 25 charges and results were compared with the airblast from single charges at the same burial depth. Two series were used, each with a different combination of spacing and burial depth. In one case, the 64-pound charges were buried 6.9 feet deep and spaced 5.25 feet apart. In this series, no shot of 25 charges was detonated. The other series had 64-pound charges spaced 8 feet apart and buried 6 feet deep. On two 11-charge shots in this series, additional blast lines were located at 45 degrees off the end charges. The charges were detonated in playa at the Tonopah Test Range. Crater dimensions from row charges were obtained as a by-product of the experiments.

Wide system variations were encountered. Airblast from otherwise identical shots was not reproducible. Airblast attenuation rates were different from one shot to the next, and different parameters of the blast wave attenuated differently with distance, indicating that the blast wave was changing form. These, added to minor gage inaccuracies and small differences in meteorology, resulted in considerable data scatter.

Five parameters of airblast from row charges were examined and each was compared with the same parameter from single charges. Parameters were ground-shock-induced peak overpressure, peak overpressure from venting gas, peak negative pressure, positive phase impulse, and negative phase impulse. Two series of shots, each with different combinations of burial depth and spacing, were used. Burial depth was factored out by comparing each parameter for the row charges with the same parameter from a single charge at the same burial depth.

Each parameter of airblast was found to be approximately equal to n^{β} times that parameter for a single charge, where n is the number of charges. The power β was different for each parameter examined; it was a function of spacing and had a larger value for closer spacing.

Pressure and impulse were always greater perpendicular to the row than off the end of the row, and the difference increased with the number of charges. β was also greater perpendicular to the row.

Comparison of data from playa shots with limited data available from shots in other media shows that there is also a dependence on medium which the paucity of data precludes evaluating.

Effects from the type of explosive could not be separated from effects of medium because shots using other than TNT explosives also were detonated in different media.

Spacing between charges in a row will normally range from 1 to 1.3 times an optimum radius for single charges. A 64 lb, single charge optimum radius in playa is about 7.8 feet or 1.95 ft/lb$^{1/3}$. Because crater dimensions scale differently from cube root (probably between $W^{1/4}$ and $W^{1/3.4}$), the equivalent spacing for large yield nuclear shots is relatively smaller. The Sedan crater had between 610 and 795 feet. In Figure 19 this would correspond to 1.05 to 1.35 ft/lb$^{1/3}$.

Thus, in a practical application of the size of Sedan, the following would obtain:

1. Perpendicular to the row, β's for ground-shock-induced and gas-venting peaks are about equal and approximate 0.9.

2. Off the end of the row, β for the ground-shock-induced peaks is greater than that for the gas-venting peaks.

    a. Values of β for ground-shock-induced peaks would approximate 0.7.

    b. Values of β for gas-venting peaks would approximate 0.45.

Crater dimensions were generally greater for closer spacing in spite of a 15-percent greater depth of burial. Crater dimensions increased as the number of charges increased from 1 to 11, but became nearly constant for more than 11. An exception occurred in the case of average crater depth for the closer spacing, which at 11 charges, appeared to be still increasing at an appreciable rate.

CONTENTS

AIRBLAST AND CRATERS FROM ROWS OF TWO TO TWENTY-FIVE BURIED HE CHARGES

Introduction and Background

The use of nuclear explosives in large-scale excavations such as a sea-level interoceanic canal would involve rows containing two or more charges. Seismic disturbances and airblast are the two mechanical effects most likely to limit the use of such rows. Airblast is the principal subject of this investigation; crater dimension is a corollary subject.

Studies of airblast from buried single charges[1,2] have shown that the two principal constituents of the air pressure pulse from buried explosions are the ground-shock-induced (GSI) pulse and the pulse from venting gases. A Rayleigh-wave-induced pulse of low amplitude has been observed on certain high-explosive and nuclear-explosive events in rock, although no such pulse was observed on the explosions described herein.

The direct GSI pulse results from transmission of the ground shock across the interface into the air, as well as from propagation underground radially from the source. The air-transmitted GSI pulse travels upward and outward farther than the pressure pulse induced directly by ground shock.

As the explosion cavity grows, the mound over the cavity rises and the explosion gases vent at or near the crown of the mound, usually at many points.

For very shallow scaled burial depths, the direct and the air-transmitted GSI pulses are indistinguishable except very close to the epicenter. As burial depth is increased, time between the pulses increases. For shallow burial depths, the gas-venting pulse dominates, but is is suppressed more rapidly than the GSI pulse as the burial depth is increased, until at containment only the latter pulse remains.

At burial depths which maximize crater dimensions, nuclear shots in dry rock demonstrate a gas-venting pulse which is weak compared to the GSI pulse. The weakness is due in part to the small amount of explosion gas produced by a nuclear shot in this medium, and in part to the fact that the gas-venting pulse is superimposed on a negative phase which follows the GSI pulse.

For high-explosive shots in either rock or soil where gases produced are not medium-dependent, and for the Sedan nuclear shot[3] in alluvium where moisture content was about 10 percent, the amplitude of

the gas-venting pulse is greater than that of the GSI pulse. More experience is needed with nuclear shots of different yields in alluvium with varying moisture contents before the contributions of the three major constituents of the large amplitude observed on Sedan can be separated and evaluated. The constituents are these:

1. The Sedan cavity appears to have erupted relatively early, while the cavity was small and cavity pressure high.

2. The cavity gases were enhanced by vaporization of water in the soil; in effect a "steam-boosting" of the cavity.

3. There is some evidence of nonscalable aspects of the gas-venting pulse, in that escaping gas pressures increase with yield faster than the rate anticipated from cube root scaling. (This and the first point may be merely manifestations of the same mechanism.)

To the effects attributable to yield, medium, and burial depth effects, the use of row charges adds effects related to the number of charges, spacing between charges, and azimuth, as parameters influencing airblast.

Experiments predating the ones described here were conducted in a variety of media, frequently with different kinds of explosives, at various charge burial depths and spacings, and with different numbers of charges. Thus, it was important in this series to use the same explosive in the same medium, and to limit the parameters of burial depth and spacing to two combinations, so that the effect of the number of charges could be explored.

For a row charge, a peak overpressure not larger than

$$p_{row} = np_{single}$$

might be expected in the worst case (acoustic superposition of blast waves), where n is the number of charges in the row, and p is the peak overpressure. In the best case one might expect peak overpressure to be the same as for a single charge with a charge weight (or yield) equal to the sum of all charges in the row;* thus, for the acoustic case

$$p_{row} = n^{1/3} p_{single} \quad .$$

Since there are azimuthal variations, the above should represent limits perpendicular to a row of charges. Results from the Dugout HE row charge[4] in basalt, and results from an 11-charge row of 8-pound charges[5] in Albuquerque alluvium, were used to derive

$$\frac{p_{row}}{p_{single}} = n^{0.7}$$

*Assuming that very strong shocks are not being added.

The $n^{0.7}$ fell within the expected limits. However, the Dugout report gives reasons for being skeptical of the above equation:

> Peaks from the Dugout 5-charge explosion were those of the ground-shock-induced pulse while the peaks from the 11-charge shot may have come from venting gases. Thus, they may not be directly comparable, and the agreement which permitted the above relationships may be coincidence.

The inconsistency resulting from deducing a dependence on number of charges from such dissimilar wave forms made necessary a more controlled examination of the effects of number of charges.

Experiment Plan

Airblast measurements along five radii were available from two previous identical 11-charge rows (shots 211-10 and 211-13) of 64-pound charges, and from a 5-charge row (shot 211-16) with different burial depths and spacings between charges. Similar measurements were available along one radius from a single charge (211-4) at the same burial depth. The experiment was built around these and other completed shots as listed in Table I.

TABLE I

Shots with Airblast Measurements

Shot No.	Charge Size (lb)	DOB (ft)	Spacing (ft)	Charges/ Row	Date	Number of Blast Lines	Number of Gages each Station
211-42	64	6.9		1	10/25/66	2	2
211-46	64	6.9	5.25	2	3/27/67	2	2
211-16	64	6.9	5.25	5	5/27/65	2	1
211-45	64	6.9	5.25	11	2/24/67	2	2
211-4	64	6.0		1	5/22/64	1	5
211-41	64	6.0	8.00	2	10/5/66	2	2
211-44	64	6.0	8.00	5	11/22/66	2	2
211-10	64	6.0	8.00	11	8/20/64	5	1
211-13	64	6.0	8.00	11	3/3/65	5	1
211-43	64	6.0	8.00	25	11/18/66	2	2

Shot 211-4 had 5 gages, located at 50, 150, 500, and 1500 feet along the single blast line. Shots 211-10 and 211-13 had five blast lines--one perpendicular to the row opposite the midpoint of the row, one off each end, and one at 45 degrees from each end charge. Stations were at 50, 150, 500, and 1500 feet from the center charge for the perpendicular line and from the end charges for the other lines.

All other shots had two blast lines (one perpendicular and one off the end) with stations at the same distances, except in shot 211-16 where stations were located at 19.9, 40.9, 99.5, 269, and 567 feet. These locations were scaled from those of Project Dugout.

The pressure gages used throughout were Pace P-7 diaphragm type. An Ampex CP-100 magnetic tape recording system and Consolidated System D amplifiers with an 800-Hz response were used.

Crater dimensions were obtained from topographic maps prepared from "aerial" stereophotographs by American Aerial Survey, Inc., Covina, California. An unmodified aerial camera and its operator were suspended on a platform at heights of 40 to 60 feet by a crane boom. All other aspects of the photogrammetric mapping were conventional.

The site of the experiments was the southernmost dry lake bed of Cactus Flat basin at Tonopah Test Range, southeast of Tonopah, Nevada.

Airblast Results

It is doubtful if any attempt would have been made to measure airblast as a function of number of charges if it had been realized at the outset how difficult and complex a problem was involved. Many experimental variances which occurred singly or in combination were not anticipated, nor in all cases were the magnitudes of variances even suspected. The major variations were these:

1. Airblast from otherwise identical shots was not reproducible.
2. Airblast attenuated differently with distance from one shot to another.
3. Different constituents of the blast wave attenuated differently with distance; i.e., the blast wave changed form.
4. There were gage and gage-calibration inaccuracies.
5. Meteorology was not constant from one event to another (but this fact could explain only a small part of the difference noted in (2)).

With the exception of (4), these are system variations which cannot be reduced in a controllable manner. Hence, improvements can be achieved experimentally only by approaching the problem statistically--a time-consuming and costly approach.

In general, the airblast measurements were adequate. Ordinarily, there would be acoustical damping limitations on instrument response in blast measurements from charges as small as 64 pounds if the charges had been burst above ground. The peaks of the blast wave from buried explosions tend to be rounded, and the rise times increased, by charge burial. Any instrument acoustical damping would tend to reduce peaks of higher pressure more than it would those of weaker blast waves, and this may account for a few of the deviations observed in the following chapter.

Since the principal result (the effect of number of charges in a row) can be expressed by ratios of row-charge to single-charge values of each parameter, it is believed that acoustic damping of gages has not detracted from the value of conclusions reached.

The data have been analyzed by examining separately (a) the ground-shock-induced peak overpressure, (b) the peak overpressure from venting gas, (c) the peak negative pressure, (d) the positive-phase impulse, and (e) the negative-phase impulse. In determining attenuation rates, first-order least-square fits have been used because neither the quality nor quantity of the data justify the refinement of higher-order curve fitting. On some shots there was an indication that gas-venting peaks, measured by the closest gages, were lower than expected relative to those at more distant locations. This result tended to decrease attenuation rates if values from the closest gages were used. It is not clear whether the reduced values resulted from diffraction and shielding furnished at the closest locations by the mound of earth through which the gases vented, or whether they resulted from inadequate gage response to the higher pressure measured close-in.

Any lack of gage response caused by acoustic damping would be reflected in lower values for ground-shock-induced and gas-venting peak overpressure. The effect on positive and negative phase impulses or peak negative pressure should not be noticeable.

Rate of Attenuation of Overpressure with Distance

Spherical attenuation of shock overpressure with distance might be assumed to be nearly R^{-1} as the acoustic region is approached, but other theoretical treatments are inconsistent in this regard.

IBM Problem M[6] was not carried to the infinitesimal acoustic limit but in the region from 0.4 to 1 psi the peak overpressure followed an attenuation rate of about $R^{-1.2}$. Positive-phase impulse followed an attenuation rate of $R^{-0.9}$.

The Kirkwood-Brinkley free airburst curves for cast TNT[7] were carried only to about the 1-psi level. The region from 1 to 3 psi followed an attenuation rate of $R^{-1.35}$. The positive-phase impulse over the same region suggests an attenuation rate of R^{-1}. Thus, even in the spherical free air case, there are differences between attenuation rates of various models.

Experimental results from hemispherical HE tests[8] indicate that for the region from 0.01 to 0.1 psi the peak overpressure follows an attenuation rate of about $R^{-1.35}$. Positive-phase impulse follows $R^{-1.4}$ approximately.[9] When such variations are indicated by theoretical and

experimental results, differences in attenuation rates from the experiments described here should not be surprising. Examination of the attenuation rates of the five parameters described below will make it clear that a great deal of variation occurs and that there are only a few consistencies to be found.

Attenuation rates greater than R^{-1} can occur (a) if winds blow toward ground zero from the end of the blast line, and (b) if a temperature gradient exists, with warmer temperatures at ground level.

Attenuation rates would be less than R^{-1} if:

1. Winds were blowing toward the end of the blast line from ground zero
2. Temperature inversions exist, with the ground colder than the air above it
3. Close-in gages were shielded
4. Gages were not responding to peak overpressures
5. Waves starting with rounded peaks shock up with propagation over the distance range of the measurements.

Still another cause of a low rate of attenuation with distance is illustrated by 211-43, a 25 charge row. Perpendicular to the row the close gages see the shock front as coming from essentially a line source, with the more distant sources providing a later contribution. The more distant gages see the row more nearly as a point source because arrivals from individual charges are not separate in time by nearly as large an increment. Since arrivals are more nearly concurrent, peak pressures are greater and blast attenuation with distance is reduced.

No information was obtained on temperature gradients or inversions, so those effects cannot be evaluated. Shots were fired from 8:30 a.m. to 2:30 p.m., averaging about 11:30 a.m., so temperature differences would be expected.

Surface winds at the time of the shots ranged from calm to 4 miles per hour. No measurement was made of wind versus altitude. A 4-mph wind speed, uniform with altitude, could cause a change of less than 6 ft/sec in sonic velocity. Superposition of such a uniform flow field could change attenuation rates only by about ±0.005. Unfortunately, wind directions were not recorded because of the low velocity involved. The principal blast lines were 90 degrees apart, leaving a possibility that winds would affect one line more than the other.

Only for positive-phase impulse was the attenuation rate perpendicular to the row always higher than off the end of the row for all shots.

Tables IIa and IIb summarize the attenuation rates with distance for each blast parameter examined and for all shots fired. The table makes it clear that there is no consistent relationship or trend in the rate of attenuation with either the depth of burst and spacing combination or with the number of charges, and that attenuation is different for each parameter.

TABLE IIa

Summary of Attenuation in Rows

Shot No.	No. of Charges	Ground-Shock-Induced Peaks		Gas-Venting Peaks		Negative Peaks		Positive Impulse		Negative Impulse	
		a	b	a	b	a	b	a	b	a	b
211-42	1	1.038		0.983		1.001		0.989		0.982	
211-46	2	1.017	1.151	0.937	0.933	0.940	1.039	0.965	0.989	0.948	1.048
211-16	5	1.173	1.114	0.887	0.972	0.963	0.954	0.901	1.058	0.991	1.072
211-45	11	1.040	0.903	0.861	0.932	0.905	0.871	0.899	0.978	0.965	1.000
211-4	1	1.020		0.969		0.923		0.958		0.974	
211-41	2	1.042	1.073	0.934	1.006	0.939	1.017	0.907	1.026	1.079	1.052
211-44	5	0.990	1.051	0.892	1.004	0.954	0.953	0.924	0.998	0.965	1.011
211-10* 211-13	11	1.082	1.041	0.889	1.000	0.822	1.012	0.810	1.033	0.838	1.041
211-43	25	1.033	0.666	0.912	0.906	0.723	0.907	0.822	0.887	0.864	1.004

NOTES:
1. All values are negative.
2. Columns a: off end of row data.
3. Columns b: perpendicular to row data.

*Data from two separate shots were used to obtain values shown.

TABLE IIb

Standard Deviation of Attenuation in Rows

Shot No.	No. of Charges	Ground-Shock-Induced Peaks		Gas-Venting Peaks		Negative Peaks		Positive Impulse		Negative Impulse	
		a	b	a	b	a	b	a	b	a	b
211-42	1	0.019		0.047		0.015		0.015		0.016	
211-46	2	0.011	0.023	0.027	0.033	0.015	0.027	0.078	0.031	0.013	0.026
211-16	5	0.029	0.020	0.057	0.055	0.026	0.019	0.053	0.003	0.032	0.007
211-45	11	0.021	0.029	0.027	0.015	0.029	0.017	0.015	0.011	0.027	0.017
211-4	1	0.026		0.013		0.017		0.010		0.019	
211-41	2	0.008	0.018	0.016	0.018	0.029	0.019	0.015	0.020	0.010	0.015
211-44	5	0.033	0.027	0.034	0.018	0.018	0.020	0.024	0.015	0.026	0.021
211-10* 211-13	11	0.050	0.084	0.053	0.077	0.045	0.074	0.048	0.060	0.045	0.080
211-43	25	0.035	0.020	0.013	0.035	0.016	0.036	0.012	0.032	0.027	0.031

NOTES:
1. Columns a: off end of row data.
2. Columns b: perpendicular to row data.

*Data from two separate shots were used to obtain values shown.

In view of the variations in data discussed earlier, it is questionable whether the accuracy implied by Table IIa is warranted and whether a trend could be defined if it existed. Table IIb shows the standard deviation for each attenuation in Table IIa. The sigmas are highest for combined results of shots 211-10 and 211-13, and large deviations may be attributed to differences between otherwise identical shots. They are appreciably lower for most cases; less than 1 percent in some cases. The standard deviations are small relative to the variations in attenuation and a trend, if any, would not be obscured.

Analysis

The results for all shots are in Appendix A. For each shot, the pressure-time records are given, as well as tabulated values and results of least-square fits. First-order least-square fits were accomplished on two bases:

1. Where two gages were located at each station on a line, they were of different sensitivities to accommodate uncertainties in expected pressure. Values from the more sensitive gages were weighted twice as much as those from less sensitive gages. This was done separately for each blast line of each shot. If two gages were located at each station, only results of this weighting were used in analysis.

2. If gages with only one sensitivity were located at each station, these values were used in analysis. That is, on any one line and for any one parameter, data from all gages were weighted equally for that shot.

First-order log-log fits were determined for each parameter, although there is no a priori reason why blast-wave attenuation must follow a first-order approximation. A higher-order fit would better follow the data points, but data scatter seemed large enough that an estimation of attenuation to higher order did not appear warranted. On other shots there has been evidence of departure from log-log linear attenuation with distance, particularly for the gas-venting peak overpressure, in that the closest gages show lower values than would be predicted by a log-log approximation of data measured at other stations. This may be because the gas-venting pulse originated from the top of the mound through which the explosive erupts, and is subject both to diffraction down the mound and to travel over a longer distance than if it had originated at the preshot epicenter.

Using an expression* given by the data from each blast line on each shot (based on the criteria described above), the ratio of row-charge to single-charge airblast at distances of 50, 150, 500, and 1500 feet was obtained for each blast parameter. These ratios are plotted in Appendix B. In general, there is a power-law relationship between the number of charges and the ratio of row-charge to single-charge airblast. Again, the data scatter would not justify a fit of

*These expressions are noted on the pressure-distance plots in Appendix A.

higher than first order. If attenuation of the blast parameter with distance had been the same for the row charge as for the single charge, the ratios for the four distances would be coincident. Since attenuation rates are different, there is a spread in the ratios from 50 to 1500 feet.

This lack of uniformity in rate of attenuation, and the desire for a single number relating row-charge to single-charge data, led to another method of data evaluation. Average attenuation rates were obtained for the two single charges. Fits to row-charge data were made in which the rate of attenuation was forced to agree with attenuation rates from the single charges. Row charge/single charge ratios for each airblast parameter were obtained by using intercept values of the expressions obtained by forcing attenuations to be equal to single-charge averages. Table III summarizes interrupt values using attenuation rates thus obtained.

TABLE III

Intercept Values of Fits to Pressure/Distance Plots with Normalized Attenuation Rates

Shot No.	No. of Charges	Ground-Shock-Induced Peaks		Gas-Venting Peaks		Negative Peaks		Positive Impulse		Negative Impulse	
		a	b	a	b	a	b	a	b	a	b
c											
211-42	1	2.05		1.06		1.03		0.0469		0.0659	
211-46	2	3.00	4.06	1.82	1.87	2.28	2.54	0.0913	0.0930	0.1509	0.1579
211-16	5	4.06	8.93	3.78	4.38	3.01	3.56	0.1997	0.2171	0.2692	0.2904
211-45	11	4.92	20.2	4.72	8.56	4.15	5.79	0.3219	0.4281	0.4961	0.6399
d											
211-4	1	2.73		5.56		2.75		0.0945		0.1181	
211-41	2	3.14	5.06	3.73	5.39	2.75	2.60	0.1030	0.1142	0.1358	0.1493
211-44	5	2.78	13.9	5.41	9.52	4.31	4.81	0.2216	0.2723	0.2868	0.3463
211-10 211-13	11	3.13	18.7	7.88	19.9	5.13	7.91	0.3132	0.5135	0.4165	0.6117
211-43	25	3.14	29.6	6.84	19.8	4.59	13.70	0.3082	0.9159	0.5684	1.1480

NOTES:
1. Columns a: off the end of the row data.
2. Columns b: perpendicular to the row data.
3. Rows c: burial depth 6.9 feet; spacing 5.25 feet.
4. Rows d: burial depth 6 feet; spacing 8 feet.

Discussion of Airblast

Effect of Number of Charges in a Row

In Figures 1 through 10, the row-charge/single-charge ratios of the intercept values of each of the five blast parameters derived by the method last described are plotted against number of charges in the row. There were two series, each with a different spacing and burial-depth combination, and the data are separated accordingly. These ratios were obtained by a simple log-log fit,

$$\text{Ratio} = an^b .$$

There was an occasional suggestion, especially for negative peak pressures perpendicular to the row with an 8-foot spacing (see Figure 6), that the intercept given by a fit through the data might be less than 1. This could occur if the value used for the single charge (211-4) was too large relative to corresponding row charges. There was only one 64-pound single charge fired at a 6-foot DOB. However, a 700-pound charge had been detonated in the same medium at the same cube-root-scaled depth of burst. Pressure data from that event (211-7) was in excellent agreement with data from 211-4, suggesting that the shot used for nomalizing was not spurious.

A careful check of the data from each shot shows inconsistencies which could only be resolved by firing additional shots of the same type. For example, 211-41, a 2-charge shot, has a ground-shock-induced overpressure which is about in agreement with other shots in the series, both off the end of and perpendicular to the row. All other values resulting from this shot are quite low. In the case of 211-46, also a 2-charge row, the negative phase is quite large compared with other shots, although other values are in good agreement. Reference to the pressure/time records in Appendix A shows simply that this shot had an unusually large negative peak. Similar observations can be made in regard to 211-43, a 25-charge shot, where negative peaks, positive-impulse peaks, and gas-venting peaks appear low relative to the other shots. These peculiarities of certain shots add to data scatter and thus decrease the reliability of results. Unless repeat shots are fired, there is no way of distinguishing nonrepeatable variations from characteristic differences.

The exponents b are shown in Table IV. This table indicates that:

1. The increase in peak positive pressure or impulse with increase in the number of charges is always greater for the deeper row with the closer spacing. Such is not the case for peak negative pressure.

2. The rate of increase is always greater perpendicular to the row than off the end of the row. (This would be expected.)

3. The rate of increase is different for each parameter considered.

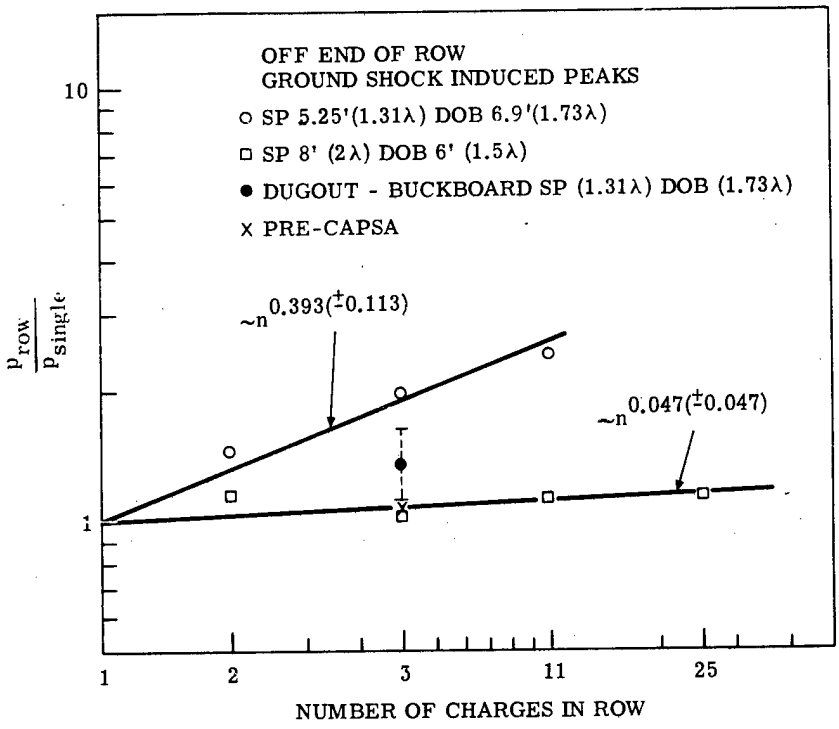

Figure 1.

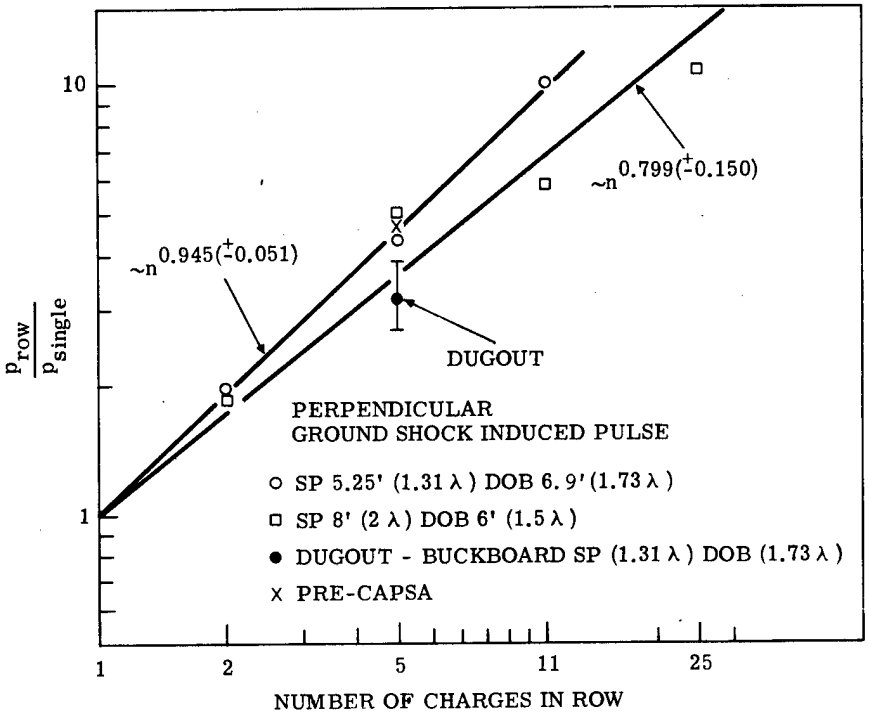

Figure 2.

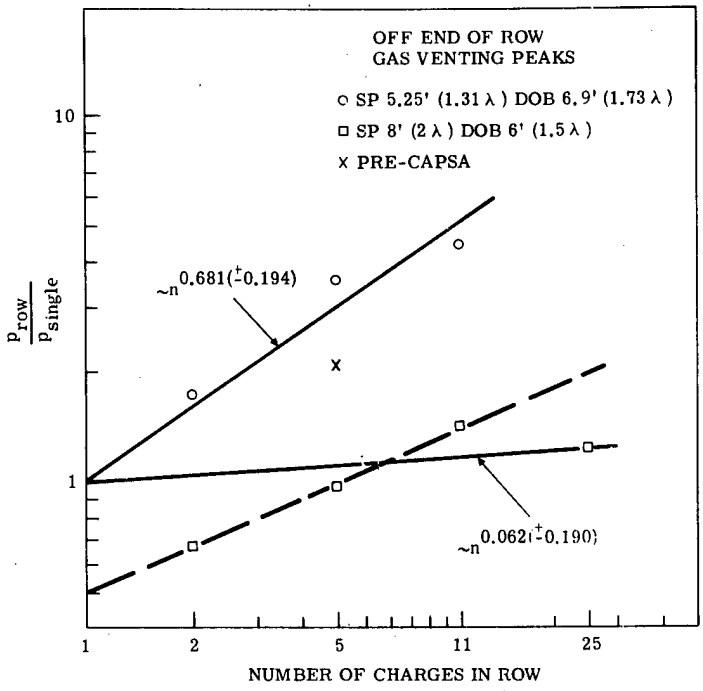

Figure 3.

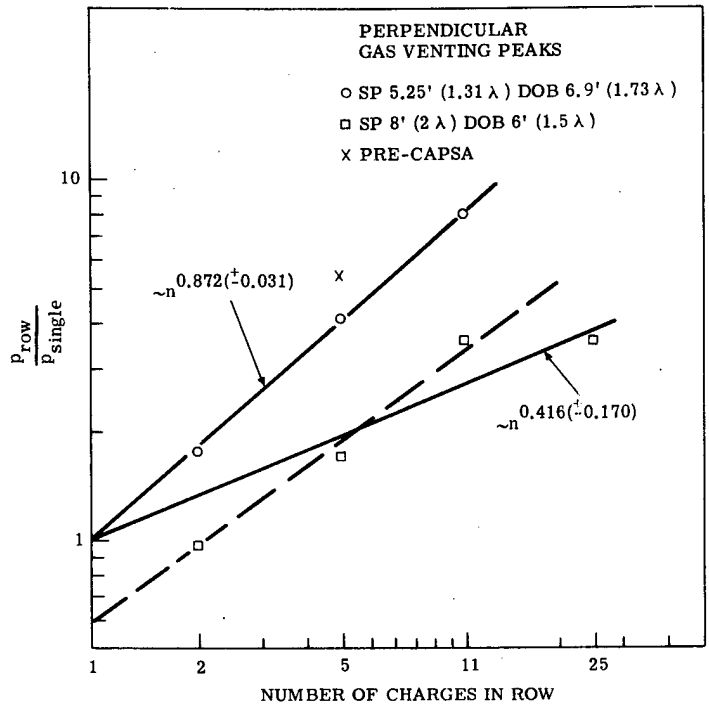

Figure 4.

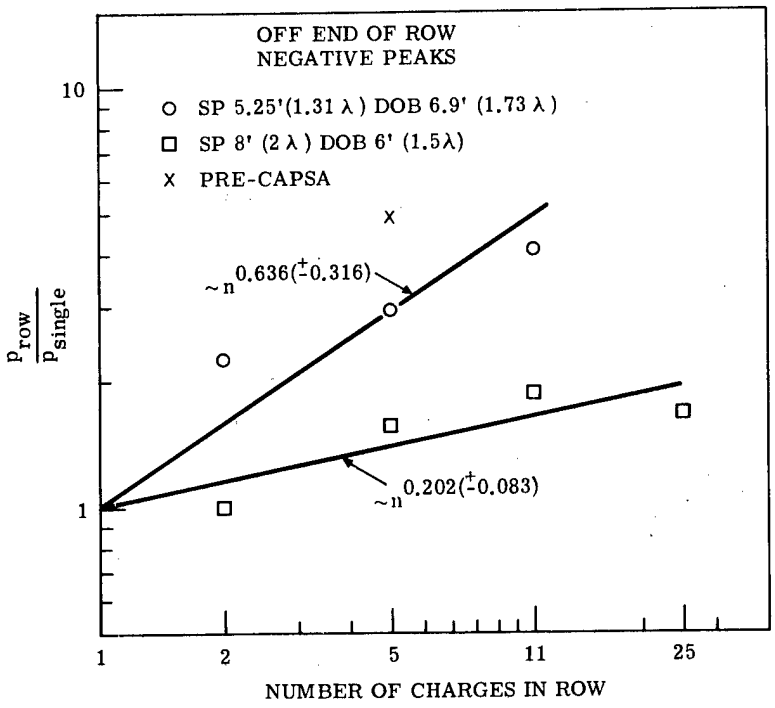

Figure 5.

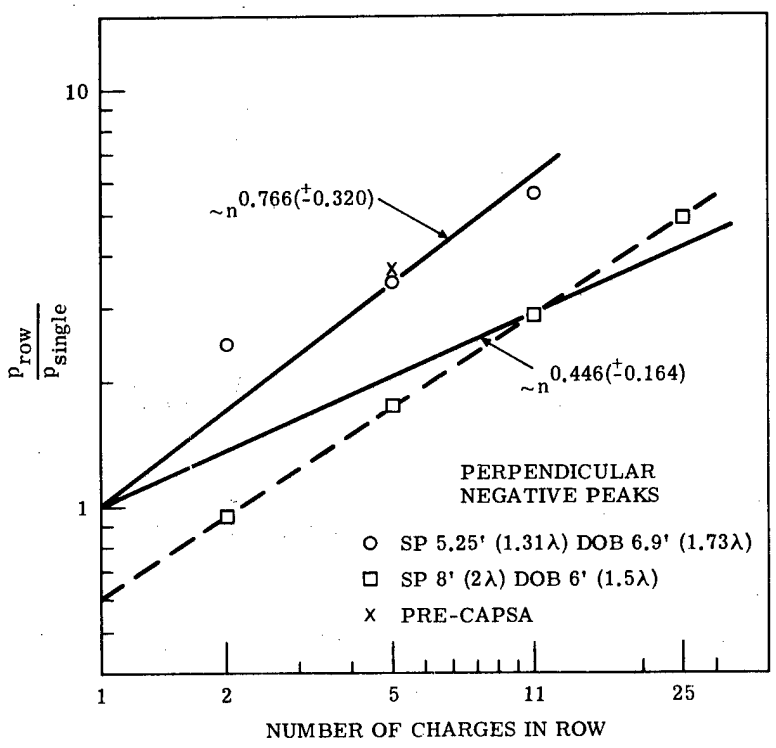

Figure 6.

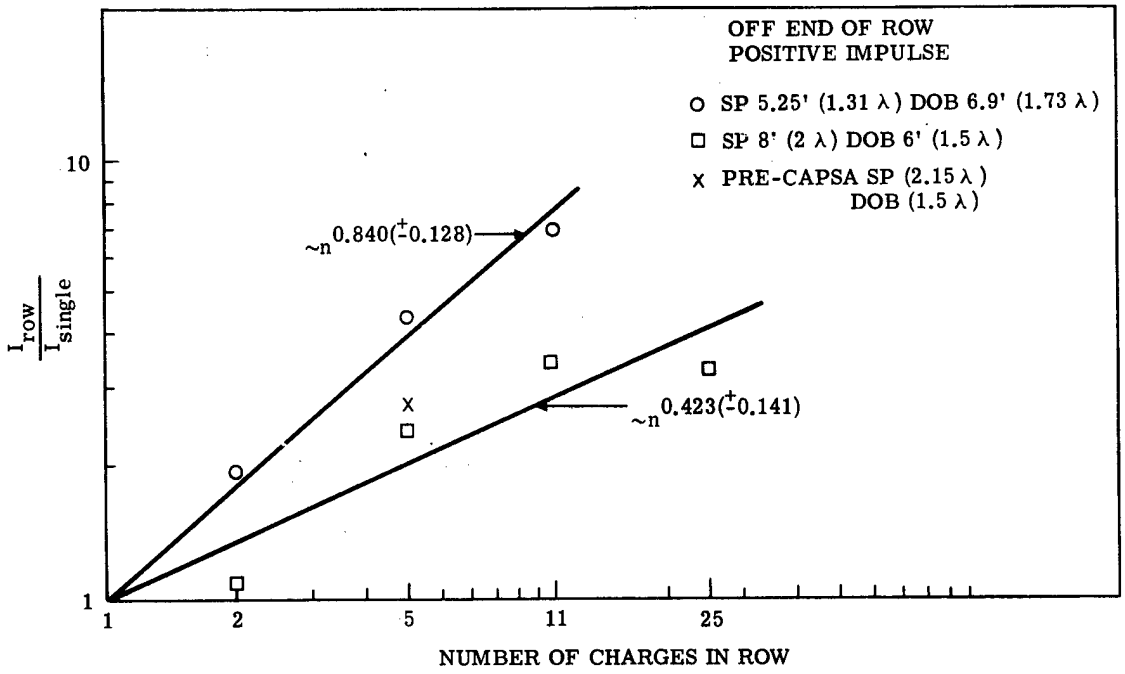

Figure 7.

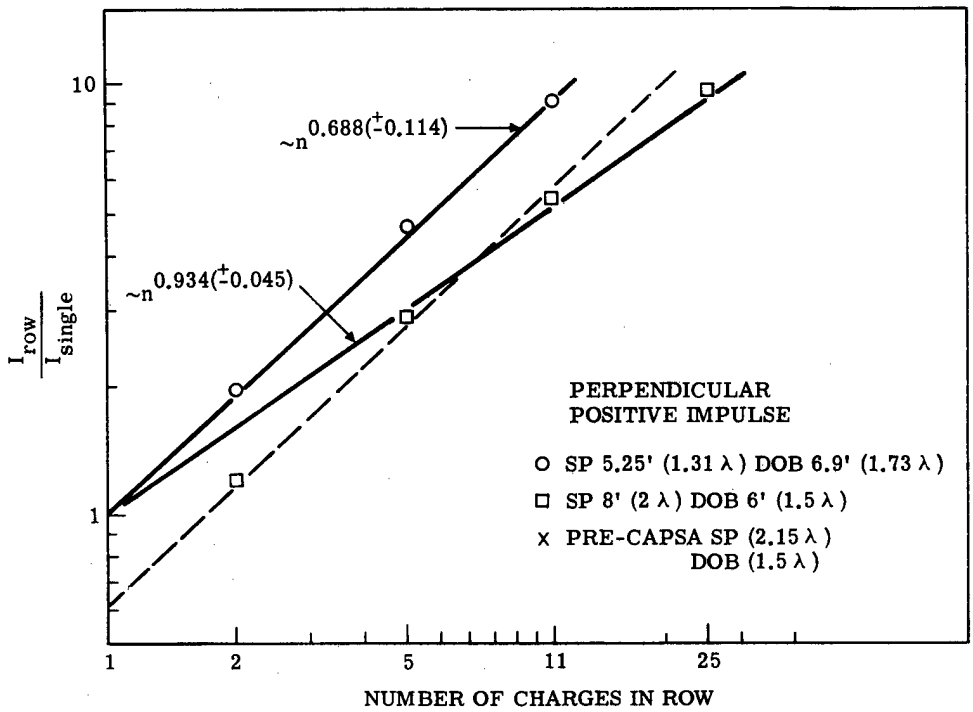

Figure 8.

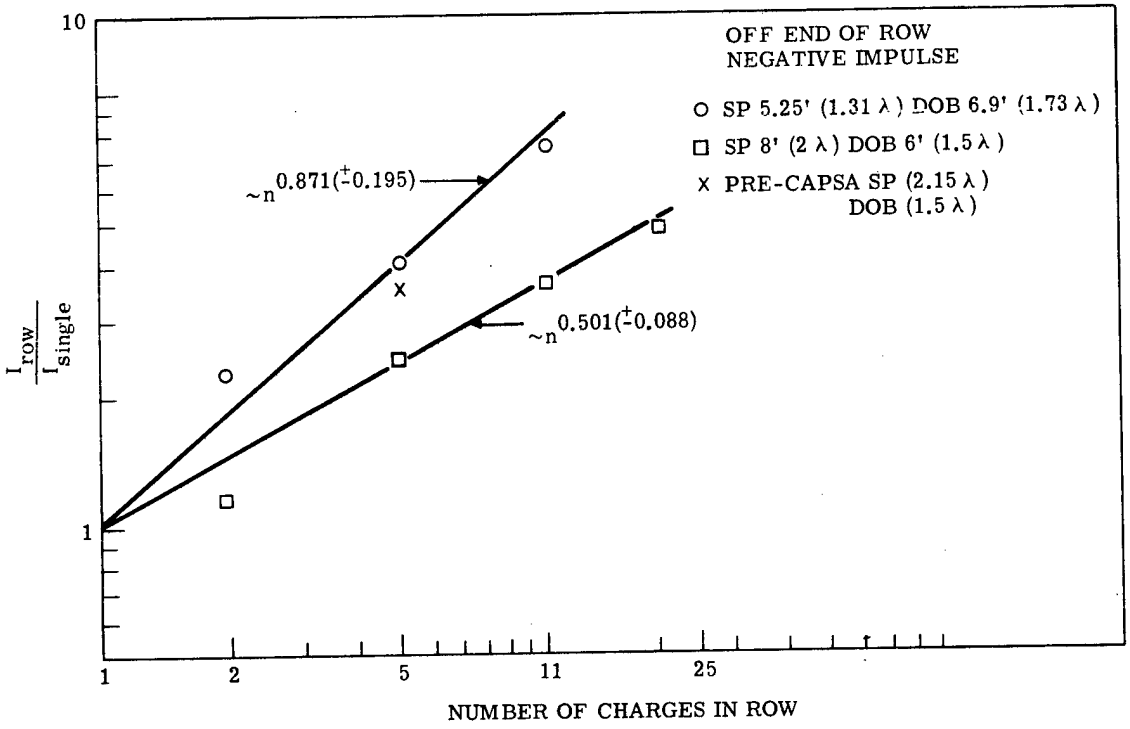

Figure 9.

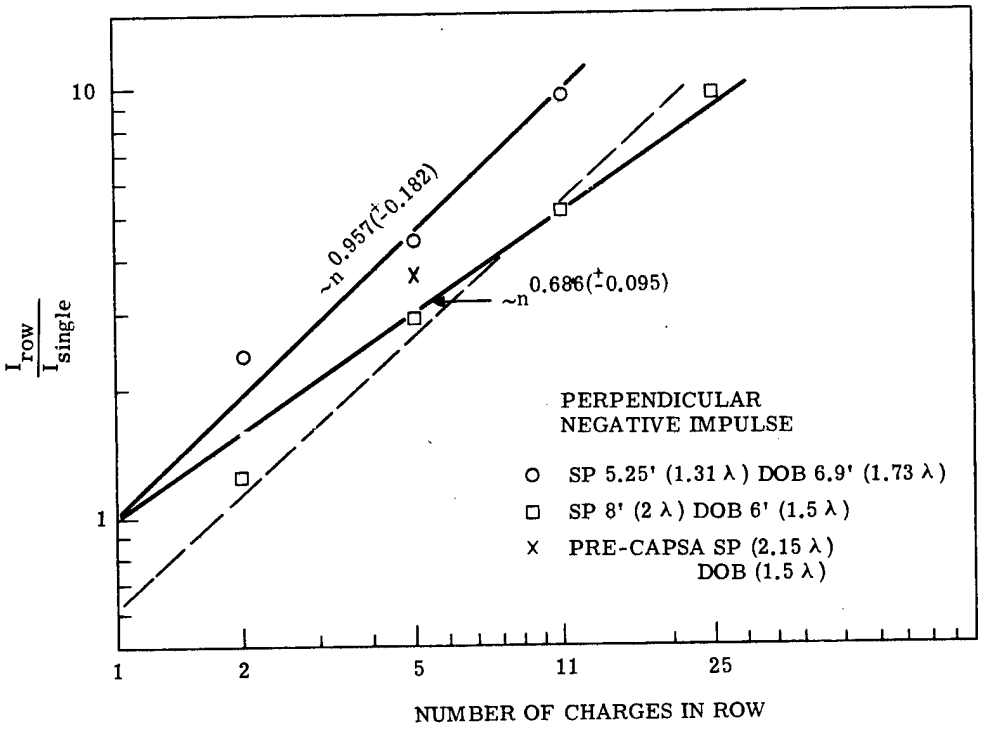

Figure 10.

TABLE IV

Exponents of Size-of-Row Dependence of Blast from Row Charges to Blast from Single Charges

Spacing and Depth of Burial	Ground-Shock-Induced Peaks		Gas-Venting Peaks		Negative Peaks		Positive Impulse		Negative Impulse	
	a	b	a	b	a	b	a	b	a	b
Sp = 5.25; DOB = 6.9	0.393	0.945	0.681	0.872	0.636	0.766	0.840	0.934	0.871	0.957
Sp = 8; DOB = 6.0	0.043	0.799	0.066	0.416	0.202	0.420	0.427	0.688	0.504	0.686

NOTE:
1. Columns a: off end of row data.
2. Columns b: perpendicular to row data.

Effect of Charge Burial Depth

Each of the two series of shots had a different combination of charge burial depth and spacing. It was assumed that to a first approximation it was possible to isolate the spacing effects by normalizing airblast from row charges to that from single charges. By using row-charge/single-charge ratios only from shots with a common burial depth, it was thought that effects of burial depth would be factored out. Once this was done, however, charge burial-depth effects could no longer be evaluated.

Effect of Azimuth

Some interesting observations can be made from Figures 11 and 12. As the number of charges is increased, the difference increases between airblast perpendicular to the row and airblast off the end; in fact, there is some suggestion that the rate of this increase may be increasing with added charges. For example, for two charges, the negative peaks and the positive and negative impulses perpendicular to and off the end of the row are about equal, and the ground-shock-induced and gas-venting peaks show only a slight difference; but by the time 25 charges are reached, the differences are quite large. As expected, the differences are less where the charge spacing is smaller. The limited data do not permit development of a generalized expression of azimuthal effects, though they do permit a demonstration of qualitative relationships for the two series examined.

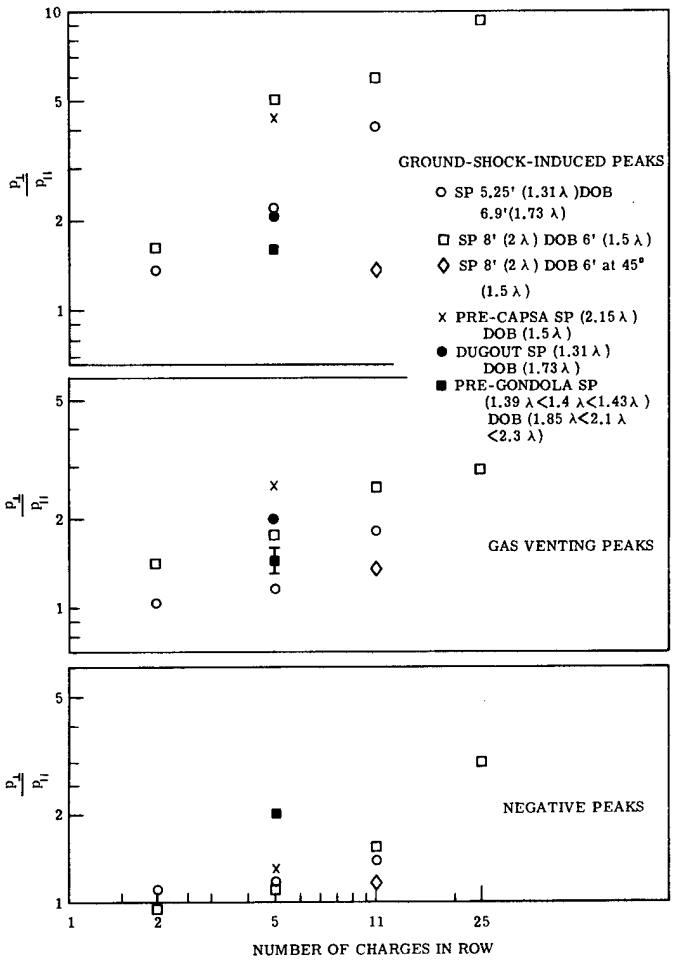

Figure 11.

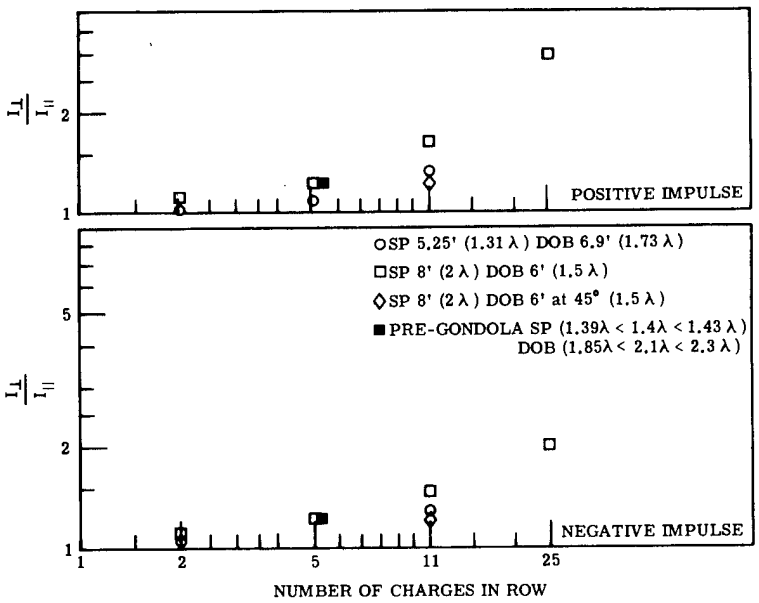

Figure 12.

On shots 211-10 and 211-13, measurements were made at 45 degrees. The increase in each blast parameter at 45 degrees over that off the end is less than half the increase perpendicular to the row.

Effect of Spacing

If the premise is accepted that burial depth effects can be factored out, it should then be possible to isolate effects of spacing.

In order to predict airblast from large-scale nuclear explosions, it is desirable to establish a relationship between airblast and charge spacing. Parameters of greatest safety concern are GSI and gas-venting peak pressures measured perpendicular to the row. Depending upon medium and burial depth, either of these two peaks may be the greater. The two charge spacings examined cover the range of spacings between that of a single-charge crater radius and that of about 0.6 times a single-charge radius. This includes the lower range of spacing which normally would be used for nuclear excavation. The increase in the row-charge/single-charge blast ratio (the slope of least-square fit to data of Figures 1-10) was summarized in Table IV. The increase with a larger number of charges is always smaller for the larger spacing; it is always larger perpendicular to the row than off the end of the row; and is different for each blast parameter, although ratios for positive and negative impulse are not very different.

The available information on the effect of charge spacing is illustrated in Figures 13-16. Blast-distance data were normalized to single-charge attenuations, and hence are more accurate over the range of the data (50 to 1500 feet) than at smaller or larger ranges. The figures show that the effect of spacing is different, depending on whether one is looking at GSI or gas-venting pulses, and whether one is looking at the pulses off the end of or perpendicular to the row. The limit case of zero spacing is a single charge whose weight is the sum of the weight of charges in the row. In these figures, the actual burial depth is held constant for each series. Thus, the limit case of zero spacing is at a relatively shallower scaled burial depth than for large spacings, and more blast gets out.

The limit case has been obtained from Figures 17 and 18 which show suppression of GSI and gas-venting peaks with charge burial depth, based on all available data from single charges. It can be observed from these figures that the GSI peaks for the charges in playa correspond more nearly to the peaks produced in basalt than to those produced in alluvium. The trends for the peaks from venting gases are not so obvious, some lying above and some below the basalt curves. The basalt relationship with depth of burst was used for playa in determining the ratios of row-charge pressures to single-charge pressures for the zero spacing limit. The ratios are essentially the same for the single-charge burial depth of both 6 and 6.9 feet.

GSI peak overpressures observed off the end of a row (Figure 13) decrease as spacing is increased, probably because of the greater distance the shock wave must travel from each additional charge in the row.

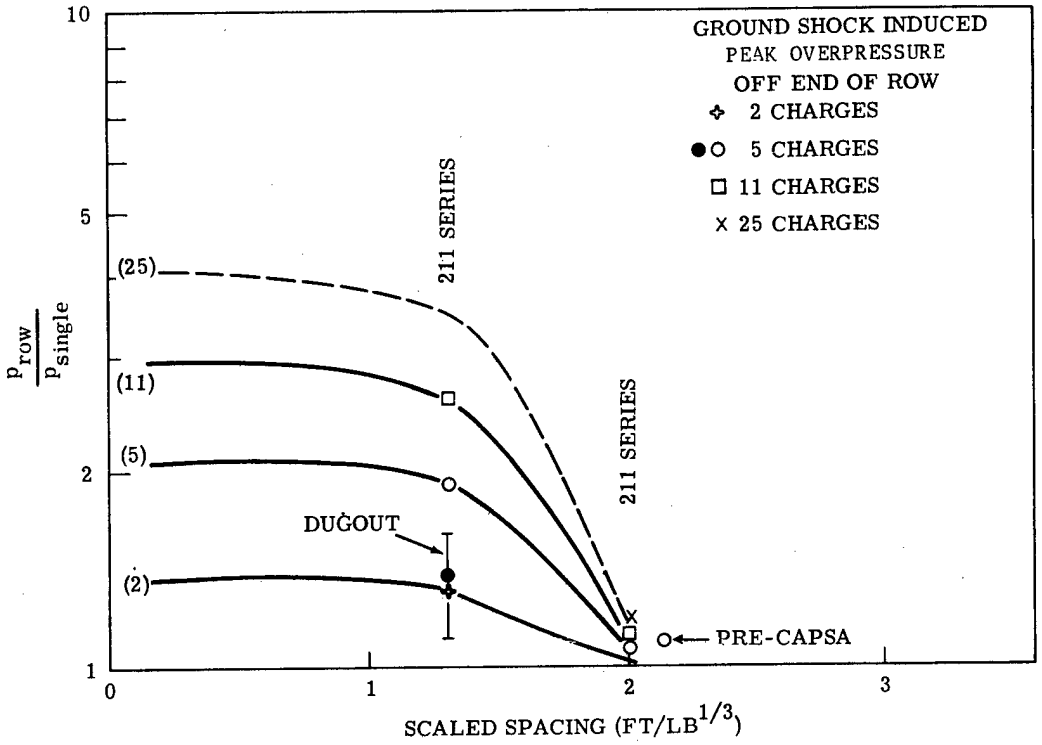

Figure 13.

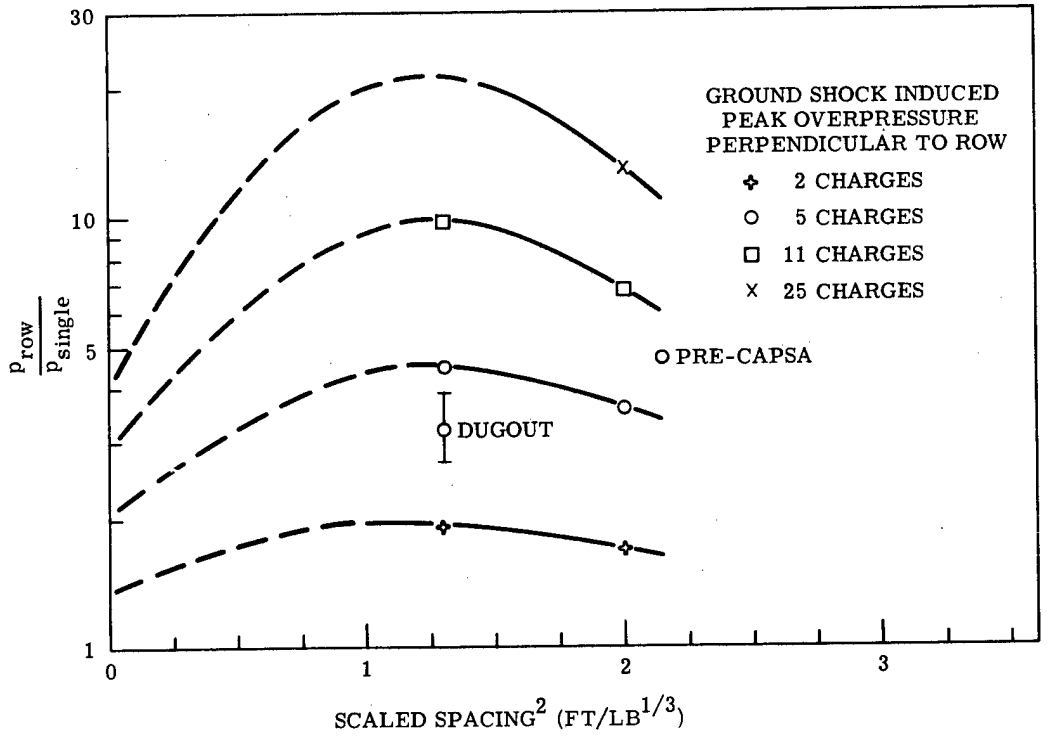

Figure 14.

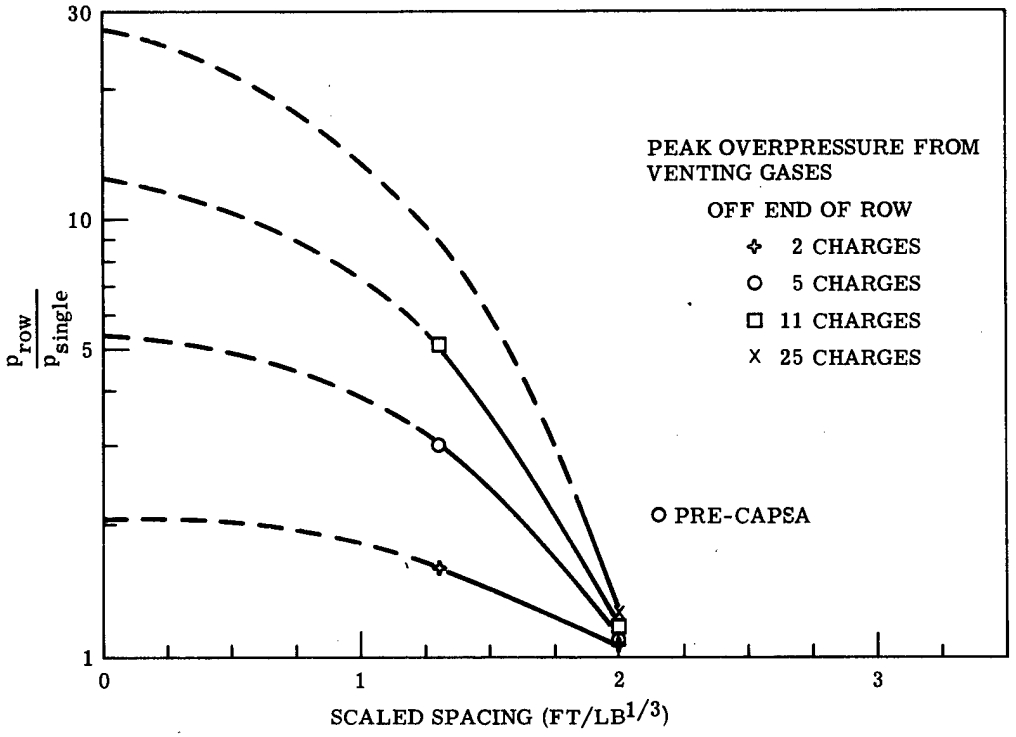

Figure 15.

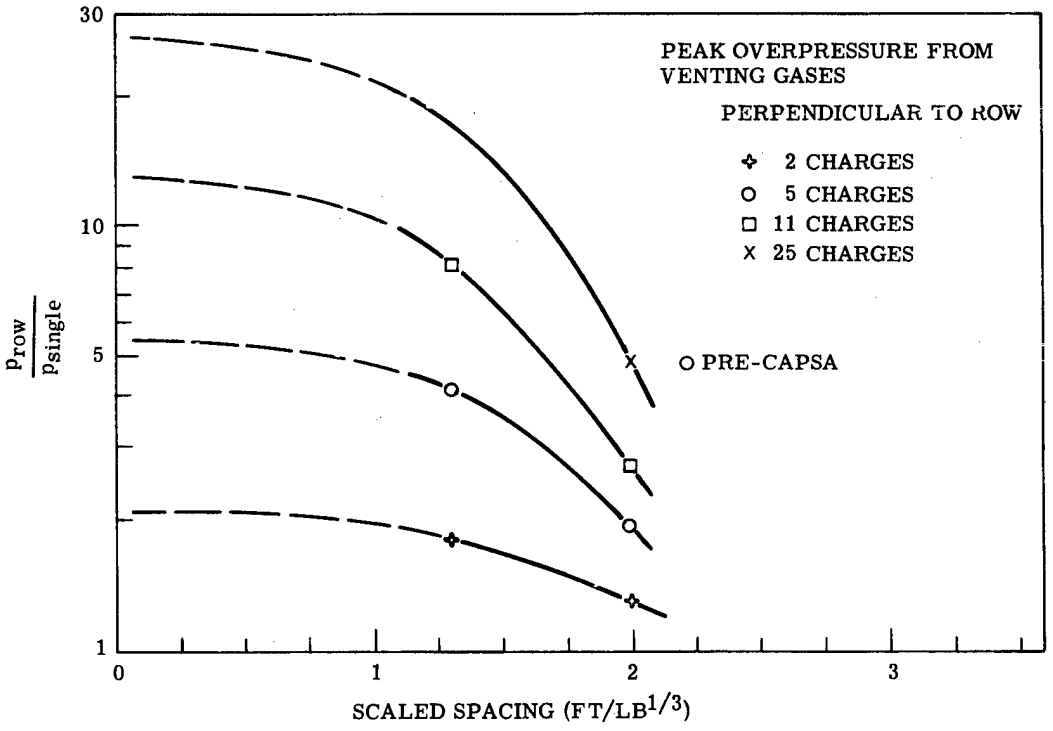

Figure 16.

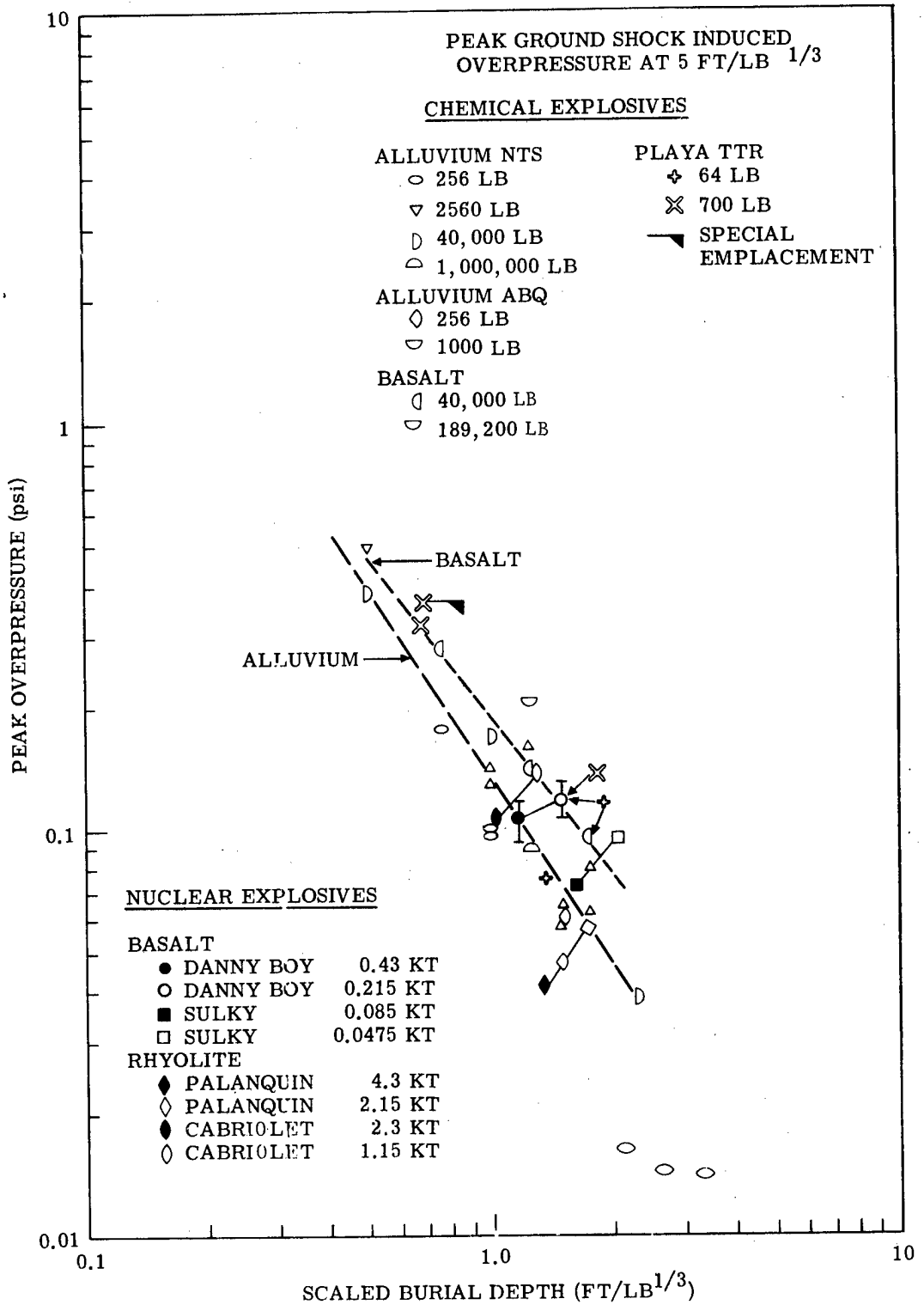
PEAK GROUND SHOCK INDUCED OVERPRESSURE AT 5 FT/LB 1/3
CHEMICAL EXPLOSIVES
ALLUVIUM NTS
256 LB
2560 LB
40,000 LB
1,000,000 LB
ALLUVIUM ABQ
256 LB
1000 LB
BASALT
40,000 LB
189,200 LB
PLAYA TTR
64 LB
700 LB
SPECIAL EMPLACEMENT
BASALT
ALLUVIUM
NUCLEAR EXPLOSIVES
BASALT
DANNY BOY 0.43 KT
DANNY BOY 0.215 KT
SULKY 0.085 KT
SULKY 0.0475 KT
RHYOLITE
PALANQUIN 4.3 KT
PALANQUIN 2.15 KT
CABRIOLET 2.3 KT
CABRIOLET 1.15 KT
PEAK OVERPRESSURE (psi)
10
1
0.1
0.01
0.1
1.0
10
SCALED BURIAL DEPTH (FT/LB1/3)

Figure 17.

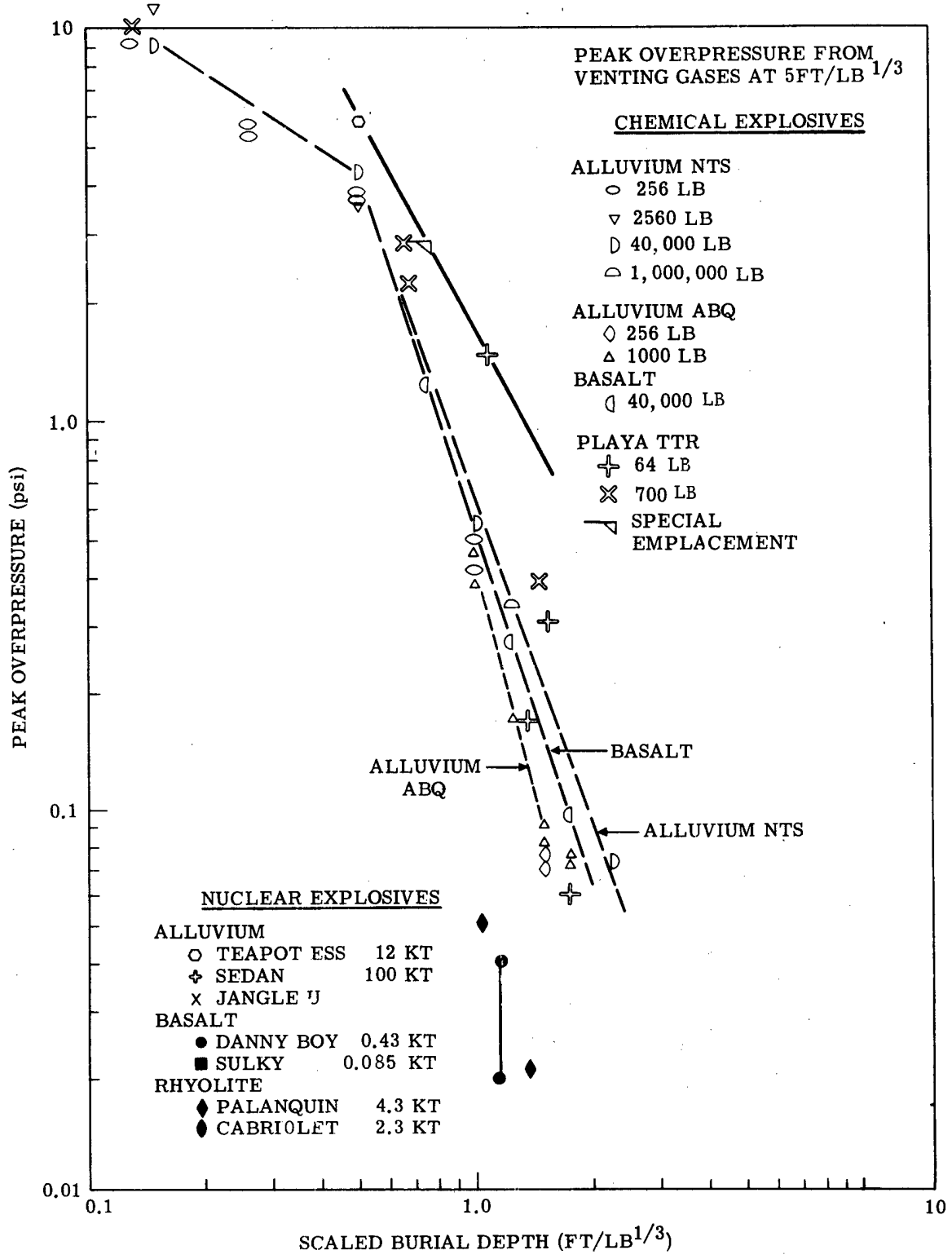
PEAK OVERPRESSURE FROM VENTING GASES AT 5FT/LB 1/3
CHEMICAL EXPLOSIVES
ALLUVIUM NTS
256 LB
2560 LB
40,000 LB
1,000,000 LB
ALLUVIUM ABQ
256 LB
1000 LB
BASALT
40,000 LB
PLAYA TTR
64 LB
700 LB
SPECIAL EMPLACEMENT
BASALT
ALLUVIUM ABQ
ALLUVIUM NTS
NUCLEAR EXPLOSIVES
ALLUVIUM
TEAPOT ESS 12 KT
SEDAN 100 KT
JANGLE U
BASALT
DANNY BOY 0.43 KT
SULKY 0.085 KT
RHYOLITE
PALANQUIN 4.3 KT
CABRIOLET 2.3 KT
PEAK OVERPRESSURE (psi)
10
1.0
0.1
0.01
0.1
1.0
10
SCALED BURIAL DEPTH (FT/LB1/3)

Figure 18.

GSI peaks measured perpendicular to the row (Figure 14) show an entirely different dependence on charge spacing. Because of acoustic addition, airblast from individual charges at the closer of the two spacings examined exceeds the zero spacing blast output, and the pressure ratio increases. At larger spacing, ratios again decrease.

Gas-venting peaks measured off the end of the row (Figure 15) and perpendicular to the row (Figure 16) show a continuous decrease as spacing between charges in the row is increased. This may be due in part to the increase in effective scaled burial depth as spacing is increased from zero. The decrease in pressure with increased spacing indicated by the two series examined here is quite rapid between scaled spacings of 1.3 and 2 ft/lb$^{1/3}$.

Theoretically the pressure ratio off the end should become asymptotic to 1 at a scaled spacing of approximately 36 ft/lb$^{1/3}$, where the positive and negative phases of blast from one charge pass, and pressure returns to ambient before the blast arrives from the next charge.

The spacing at which the ratio perpendicular to the row becomes asymptotic appears to be much greater than for blast measured off the end. It is a function both of the distance at which measurements are made and of the number of charges. The latter must be large enough so that an additional charge makes no contribution to peak overpressure. As the perpendicular distance increases, the number of charges at which the ratio becomes essentially constant must increase.

If the increase of a pressure parameter with number of charges is represented by

$$p \sim n^{\beta}$$

then β is also a function of spacing. The functional dependence is illustrated in Figure 19. The zero spacing intercept is defined as before. Again, the function β is different for each parameter, although β's for positive and negative impulses are similar and β's for positive and negative peak pressures from venting gases are also similar. Values of β for ground-shock-induced peak overpressures are unlike those for any other parameter.

It would be in order to examine spacings both larger and smaller than those investigated here (keeping burial depth constant), to better define the effect of spacing.

Spacing between charges in a row will normally range from 1 to 1.3 times an optimum radius for single charges. A 64 lb, single charge optimum radius in playa is about 7.8 feet or 1.95 ft/lb$^{1/3}$. Because crater dimensions scale differently from cube root (probably between $W^{1/4}$ and $W^{1/3.4}$), the equivalent spacing for large yield nuclear shots is relatively smaller. The Sedan crater had between 610 and 795 feet. In Figure 19 this would correspond to 1.05 to 1.35 ft/lb$^{1/3}$.

Thus, in a practical application of the size of Sedan, the following would obtain:

1. Perpendicular to the row, β's for ground-shock-induced and gas-venting peaks are about equal and approximate 0.9.

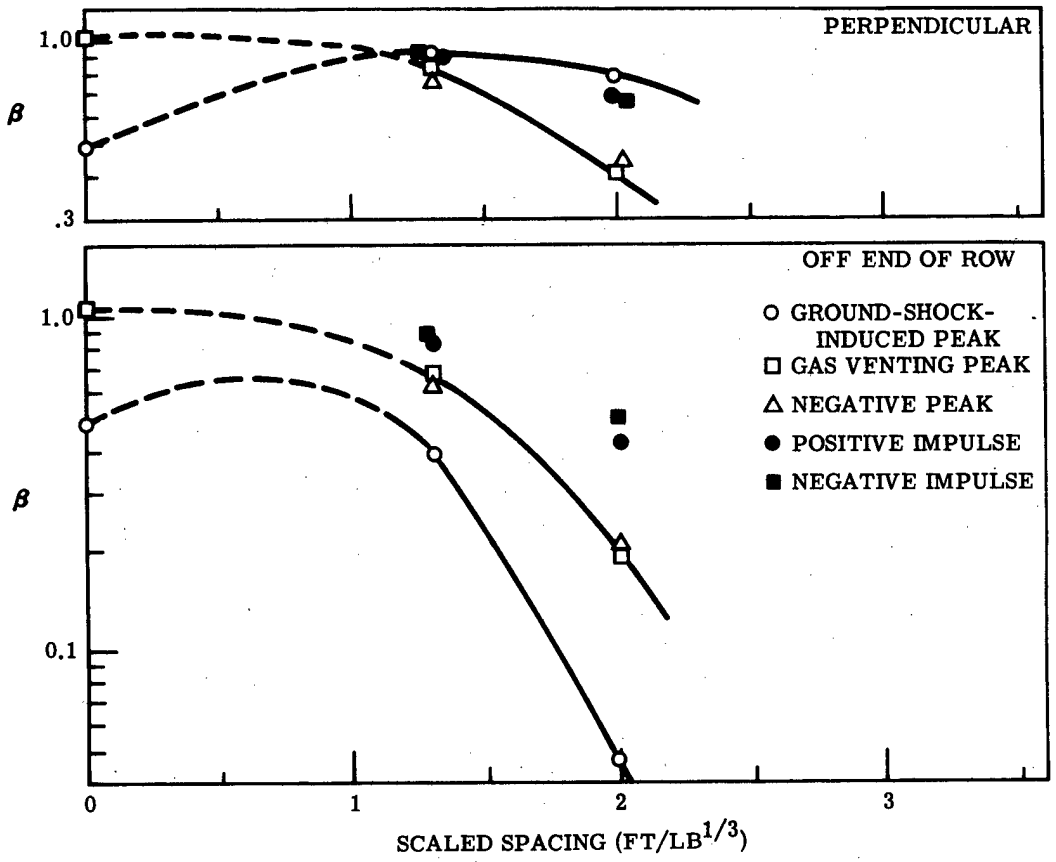
PERPENDICULAR
1.0
β
.3
OFF END OF ROW
GROUND-SHOCK-INDUCED PEAK
GAS VENTING PEAK
NEGATIVE PEAK
POSITIVE IMPULSE
NEGATIVE IMPULSE
1.0
β
0.1
0
1
2
3
SCALED SPACING (FT/LB$^{1/3}$)

Figure 19.

2. Off the end of the row, β for the ground-shock-induced peaks is greater than that for the gas-venting peaks.

   a. Values of β for ground-shock-induced peaks would approximate 0.7.

   b. Values of β for gas-venting peaks would approximate 0.45.

Effect of Medium

The effect of medium is not easily deduced because data which are directly applicable are lacking. Projects Buckboard and Dugout represent the only comparable single- and row-charge experience in basalt, and only the ground-shock-induced peaks can be compared for those two shots. Dugout versus Buckboard ratios have been added to Figures 1 and 2 to show that the ratio of row-charge to single-charge pressures is less than in the case of an identical combination of spacing and burial depth in playa. Similarly, the ratio is less in Figures 13 and 14 than for other shots. The Dugout-Buckboard ratio is somewhat tenuous because nitromethane explosive was used on Dugout, and TNT on Buckboard. Limited information from single charges[10,11] suggests larger pressures from nitromethane than from an equivalent weight of TNT. In view of this indication it is surprising that the Dugout-Buckboard ratios are lower than those based on uniform use of TNT. The comparison is carried to Figures 11 and 12, showing that the differences in pressure perpendicular to the row and off the end of the row are comparable to those of the similar shot in playa in the case of ground-shock-induced peaks, but are much higher in the case of peaks from venting gas.

One other comparison can be made using uniform explosives: the Pre-CAPSA series, which consisted of 256-pound charges buried 9.5 feet deep. One row of five charges was detonated with a spacing of 13.6 feet between charges. The experiment was run in Albuquerque alluvium. The Pre-CAPSA spacing is only slightly greater than for the larger of the two spacings in the playa series. For GSI peaks, the ratios of row-charge to single-charge pressures are not too different from those of playa (Figures 1 and 2). In the case of gas-venting and negative peaks the ratios are considerably larger for the Pre-CAPSA series (Figures 3-6). In the case of positive and negative impulses the values for alluvium are slightly above those for playa (Figures 7, 9, and 10). Similarly, the ratio of pressures perpendicular to the row to those off the end of the row is greater for the alluvium shots than for comparable shots in playa (Figure 11). The ratio for negative impulse is somewhat less (Figure 12). The fact that the ratios for peak overprssures are greater for the Pre-CAPSA series is also illustrated in Figures 13-16.

Airblast measurements also were made on Pre-Gondola II. In this experiment, there were three charges of 20 tons and two of 40 tons, all of nitromethane, with uniform spacing but irregular burial depths. No measurements were made on any of the comparable single-charge shots of Pre-Gondola, so it is not possible to derive ratios of row-charge to single-charge pressures for the Pre-Gondola series in saturated clay shale. The only information which this series contributes is illustrated in Figures 11 and 12, which show that ratios of blast perpendicular to the row to that off the end of the row are less than expected in the case of ground-shock-induced peaks, greater than expected in the case of negative peaks, and for impulses are about equal to comparable events in other media.

Effect of Type of Explosives

Information on the effects of different chemical explosives is limited to data from the Dugout shot and the Pre-Gondola series, both of which used nitromethane rather than TNT. In the case of Dugout, the ratio of row-charge to single-charge pressures is complicated by the fact that Buckboard, which constitutes the single-charge comparison, used TNT. This pair of shots also constitutes the only combination of single and row chemical explosive shots at a comparable depth in basalt. Observations about the ratio of pressures perpendicular to the row to those off the end of the row were made earlier in connection with medium effects, but inasmuch as a different explosive was used, any variances could as easily be the effect of a different explosive; or, more likely, a combination of the effects of different explosives and different media.

Pre-Gondola constitutes the other row charge in which an explosive other than TNT is used. Here there is no single-charge comparison, and no ratios of row-charge to single-charge blast can be derived. As in the case of Dugout, the difference in airblast perpendicular to the row to that off the end of the row could as well be attributed to explosive differences as to medium differences.

Craters

Results

Dimensions of craters from single and row charges are illustrated in Table V. No map was obtained for shot 211-4, and the crater from an identical shot of crater 211-49 has been substituted. Topographic maps and photos of the craters are reproduced in Appendix C.

Crater width has been defined as follows: let the area of the crater equal the area of a rectangle with semicircles at each end. The length of the rectangle is equal to the distance between the outermost charges. The diameter of the semicircles equals the width of the rectangle and is taken as the crater width.

Crater depths have been averaged over the distance between end charges and over the distance between the second charges from each end. Crater volumes were obtained separately over the same segments.

Discussion

Dimensions of craters from single and row charges have been plotted in Figures 20, 21, and 22. Allowing for the possibility that the single charge with a burial depth of 6.9 feet (shot 211-42) might be unusually small, the following trends can be noted:

1. Crater dimensions are larger for the closer spacing in spite of the 15 percent greater burial depth.

2. Crater dimensions generally increase as the number of charges in the row is increased, with evidence of little increase after 11 or 25 charges. The one exception is that average crater depth appears to be still increasing at an appreciable rate by the time the number of charges in the row has reached 11.

Conclusions

Five parameters of airblast from row charges were examined and compared with the same parameters from single charges. The parameters were ground-shock-induced peak overpressure, peak overpressure from venting gas, peak negative overpressure, positive phase impulse, and negative phase impulse. Two series of shots, each with different combinations of burial depth and spacing, were used. Burial depth was factored out by comparing each parameter for the row charges with the same parameter from a single charge at the same burial depth.

Each parameter of airblast was found to be approximately equal to n^{β} times that parameter for a single charge, where n is the number of charges. The power β is different for each parameter examined. It is a function of spacing and has a larger value for the closer spacing.

Pressure and impulse were always greater perpendicular to the row than off the end of the row, and the difference increased as the number of charges increased. The exponent β was also greater perpendicular to the row.

The limited data available imply that there is also a dependence upon medium which the paucity of data precludes evaluating.

Effects of the type of explosive cannot be separated from effects of medium because shots using other explosives also were detonated in different media.

Spacing between charges in a row will normally range from 1 to 1.3 times an optimum radius for single charges. A 64 lb, single charge optimum radius in playa is about 7.8 feet or 1.95 $ft/lb^{1/3}$. Because crater dimensions scale differently from cube root (probably between $W^{1/4}$ and $W^{1/3.4}$), the equivalent spacing for large yield nuclear shots is relatively smaller. The Sedan crater had between 610 and 795 feet. In Figure 19 this would correspond to 1.05 to 1.35 $ft/lb^{1/3}$.

Thus, in a practical application of the size of Sedan, the following would obtain:

1. Perpendicular to the row, β's for ground-shock-induced and gas-venting peaks are about equal and approximate 0.9.

2. Off the end of the row, β for the ground-shock-induced peaks is greater than that for the gas-venting peaks.

    a. Values of β for ground-shock-induced peaks would approximate 0.7.

    b. Values of β for gas-venting peaks would approximate 0.45.

Crater dimensions are generally greater for closer spacing in spite of the 15 percent greater depth of burial. Crater dimensions increase as the number of charges increases from 1 to 11, becoming nearly asymptotic for more than 11. An exception occurs in the case of average crater depth for the closer spacing, which appears to be still increasing at an appreciable rate in the case of 11 charges.

It is recommended that similar study be extended to charge spacings greater and less than those examined here.

TABLE V

Dimensions of Craters from Single and Row Charges

Shot No.	Charge Size (lb)	DOB (ft)	Spacing (ft)	Charges/ Row	Average Radius or Half Width (ft)	Depth			Volume				
						Maximum Depth (ft)	Average Depth Between End Charges (ft)	Average Depth Between Second Charge From Each End (ft)	End Area Volume (ft^3)	Volume Between End Charges (ft^3)	Volume Between Second Charge From Each End (ft^3)	Total Crater Volume (ft^3)	Crater Volume per Charge (ft^3)
211-48*	64	6.0	-	1	8.34	4.16	N/A	N/A	N/A	N/A	N/A	-	-
211-41	64	6.0	8.00	2	8.37	4.53	4.16	N/A	A 174.8 B 157.1	325.3	N/A	657.2	328.6
211-44	64	6.0	8.00	5	8.7	5.59	5.02	5.4	A 165.2 B 192.3	1595.5	849.9	1,953.0	390.6
211-10	64	6.0	8.00	11	9.03	6.03	4.85	4.94	A 207.4 B 212.0	4065.3	3301.8	4,484.7	407.7
211-13	64	6.0	8.00	11	8.47	4.74	3.94	4.17	A 129.9 B 162.6	3290.7	2787.9	3,583.2	3583.2
211-43	64	6.0	8.00	25	9.17	5.65	4.86	4.82	A 191.3 B 198.2	9726.3	8969.2	10,115.8	404.6
211-42	64	6.9	-	1	7.33	2.92	N/A	N/A	N/A	N/A	N/A	-	-
211-46	64	6.9	5.25	2	9.12	5.48	5.14	N/A	A 254.0 B 237.1	301.5	N/A	792.6	396.3
211-16	64	6.9	5.25	5	10.02	6.50	5.78	6.26	A 222.0 B 287.4	1502.3	832.9	2,011.7	402.3
211-45	64	6.9	5.25	11	10.43	7.34	6.55	6.86	A 263.7 B 332.7	4226.8	3497.5	4,823.2	438.5

*Substitute for 211-4

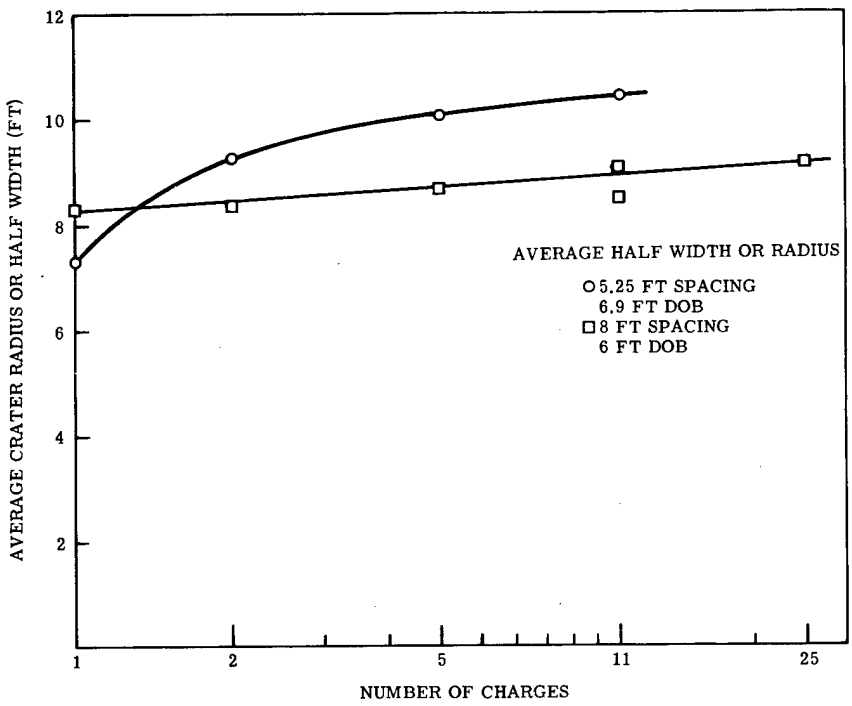

Figure 20.

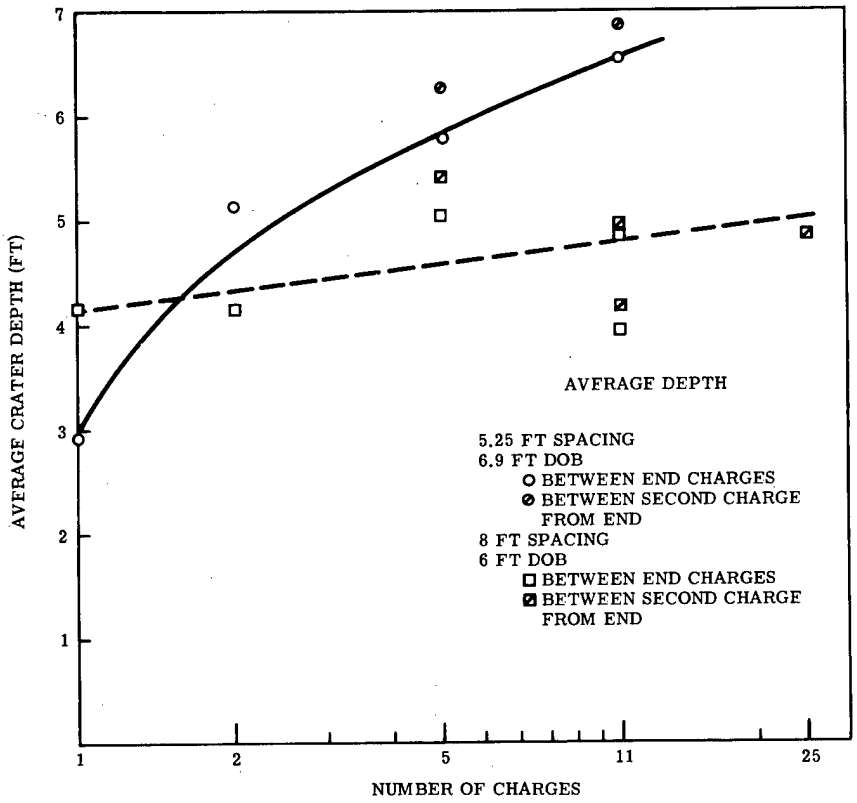

Figure 21.

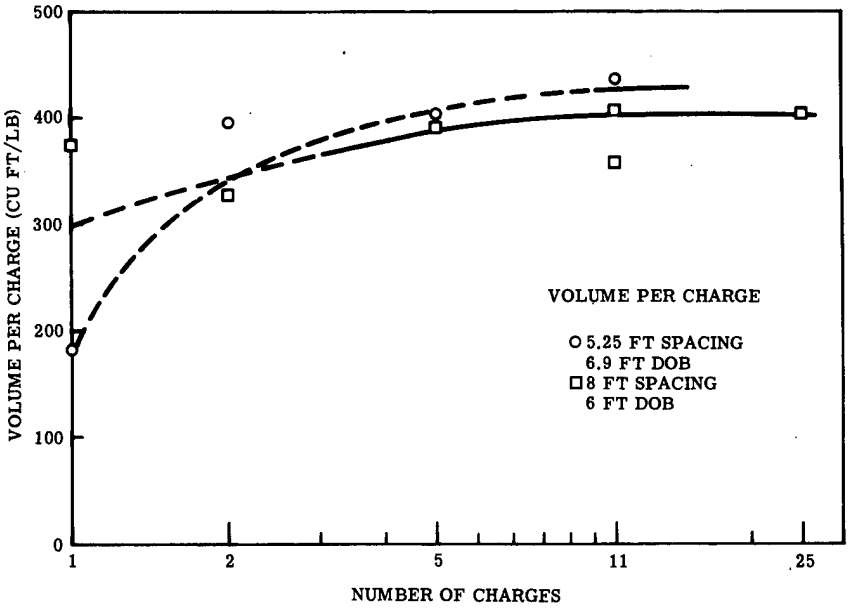

Figure 22.

References

1. Vortman, L. J., "Airblast Suppression as a Function of Explosive-Charge Burial Depth," Journal of the Acoustical Society of America, 40, pp. 229-230, July 1966.

2. Vortman, L. J., "Airblast from Underground Explosions as a Function of Charge Burial;" Proceedings of a Conference on Prevention of and Protection Against Accidental Explosion of Munitions, Fuels and Other Hazardous Mixtures, October 10-13, 1966, The New York Academy of Sciences, October 28, 1968.

3. Vortman, L. J., Close-in Airblast from a Nuclear Event in NTS Desert Alluvium, PNE-211F, Sandia Laboratory, Albuquerque, New Mexico, October 2, 1964.

4. Vortman, L. J., Close-in Airblast from a Row Charge in Basalt, PNE-608F, Sandia Laboratory, Albuquerque, New Mexico, August 4, 1965.

5. Unpublished data, Sandia Laboratory, Albuquerque, New Mexico.

6. Bethe, H., et al., Blast Wave, LA-2000, Los Alamos Scientific Laboratory, Los Alamos, New Mexico, March 27, 1958.

7. Kirkwood, J. G. and S. R. Brinkley, Jr., Theoretical Blast-Wave Curves for Cast TNT, OSRD 5481, NDRL A-341, Office of Scientific Research and Development, Washington 25, D. C., August 23, 1945.

8. Kingery, C. H. and B. F. Pannill, Peak Overpressure versus Scaled Distance for TNT Surface Bursts (Hemispherical Charges), BRL Memorandum Report No. 1518, Ballistic Research Laboratories, Aberdeen Proving Ground, Maryland, April 1964.

9. Kingery, C. H., Airblast Parameters versus Distance for Hemispherical TNT Surface Burst, BRL Report 1344, Ballistic Research Laboratories, Aberdeen Proving Ground, Maryland, September 1966.

10. Reed, J. W. and L. J. Vortman, Airblast Measurements - Pre-SCHOONER II, PNE-512, Sandia Laboratory, Albuquerque, New Mexico, to be published.

11. Unpublished data on Pre-CAPSA series, Sandia Laboratory, Albuquerque, New Mexico.

APPENDIX A

AIR BLAST DATA

Shot 211-4

A single 64-pound charge was buried 6 feet deep. There was one blast line with 5 gages (A1, A2, B3, C4, and C5) at each station.

Station and gage location	Arrival time (sec)	Ground shock induced peak (psi)	Time of peak (sec)	Peak from venting gas (psi)	Time of peak (sec)	Cross-over (sec)	Positive pulse duration (sec)	Positive phase impulse (psi-sec)	Negative peak (psi)	Time of peak (sec)	Cross-over (sec)	Negative pulse duration (sec)	Negative phase impulse (psi-sec)
50A-1	0.047	0.0459	0.052	0.1144	0.079	0.095	0.048	0.0021	-0.0606	0.117	0.185	0.090	-0.0005
50A-2	0.048	0.0462	0.053	0.1153	0.080	0.094	0.046	0.0020	-0.0637	0.121	0.196	0.102	-0.0007
50C-4	0.048	0.0568	0.051	0.1283	0.079	0.094	0.046	0.0022	-0.0636	0.120	0.195	0.101	-0.0005
50C-5	0.048	0.0593	0.051	0.1286	0.078	0.094	0.046	0.0022	-0.0615	0.118	0.186	0.092	-0.0004
150A-1	0.137	0.0152	0.141	0.0421	0.168	0.183	0.046	0.0008	-0.0237	0.210	0.262	0.079	-0.0001
150A-2	0.137	0.0131	0.142	0.0394	0.169	0.184	0.047	0.0008	-0.0217	0.211	0.264	0.080	-0.0001
150B-3	0.138	0.0139	0.142	0.0391	0.168	0.184	0.046	0.0007	-0.0194	0.210	0.270	0.086	-0.0001
150C-4	0.137	0.0146	0.140	0.0403	0.167	0.183	0.046	0.0008	-0.0191	0.210	0.261	0.078	+0.0001
150C-5	0.137	0.0155	0.140	0.0451	0.166	0.184	0.045	0.0007	-0.0234	0.207	0.276	0.094	-0.0003
500A-1	0.442	0.0046	0.445	0.0134	0.472	0.488	0.046	0.0002	-0.0070	0.513	0.572	0.084	-0.0001
500A-2	0.441	0.0048	0.445	0.0138	0.472	0.489	0.048	0.0003	-0.0069	0.509	0.567	0.078	-0.0000
500B-3	0.443	0.0045	0.446	0.0130	0.473	0.490	0.047	0.0002	-0.0073	0.513	0.571	0.081	-0.0001
500C-4	0.442	0.0046	0.445	0.0131	0.472	0.488	0.046	0.0002	-0.0073	0.512	0.571	0.083	-0.0001
500C-5	0.442	0.0046	0.446	0.0129	0.474	0.489	0.047	0.0002	-0.0070	0.517	0.568	0.079	-0.0001
1500A-2	1.320	0.0017	1.322	0.0043	1.348	1.364	0.044	0.0001*	-0.0029	1.393	1.448	0.084	-0.0000

*Dubious value due to accuracy of integration.

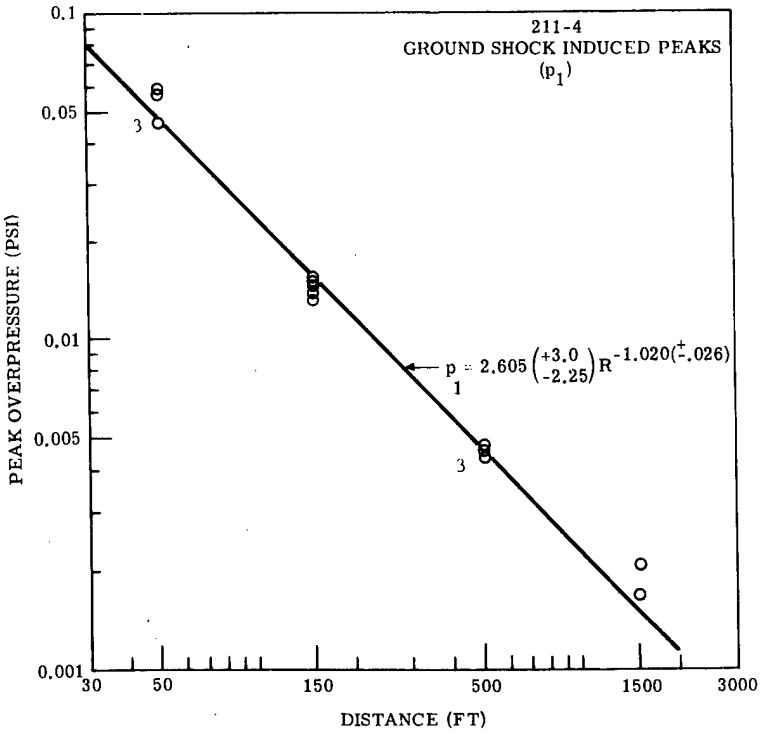

Figure A-1

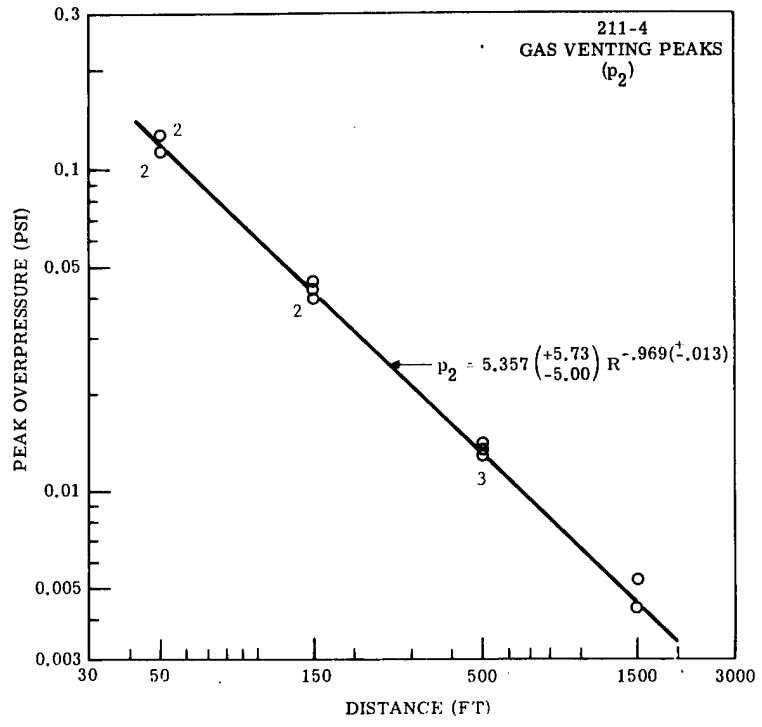

Figure A-2

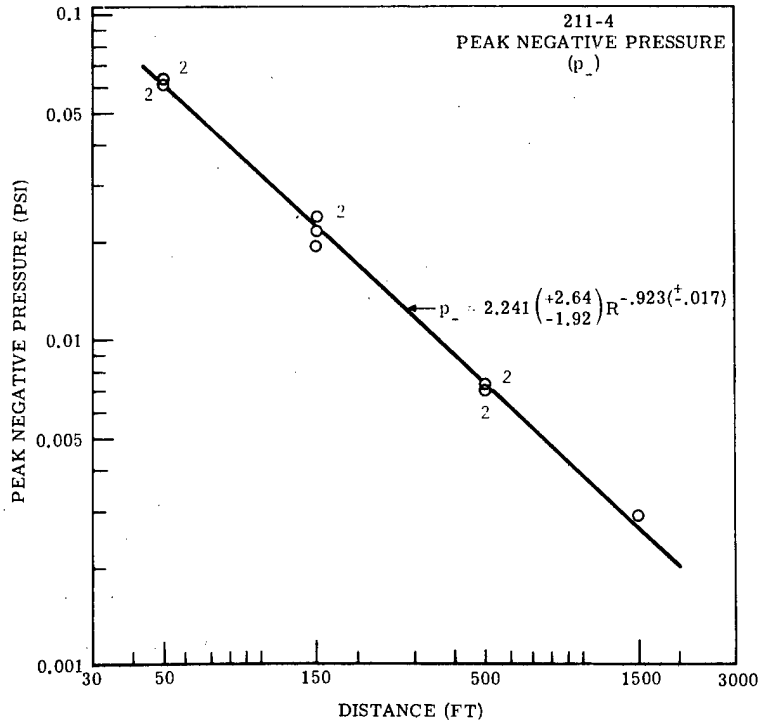

Figure A-3

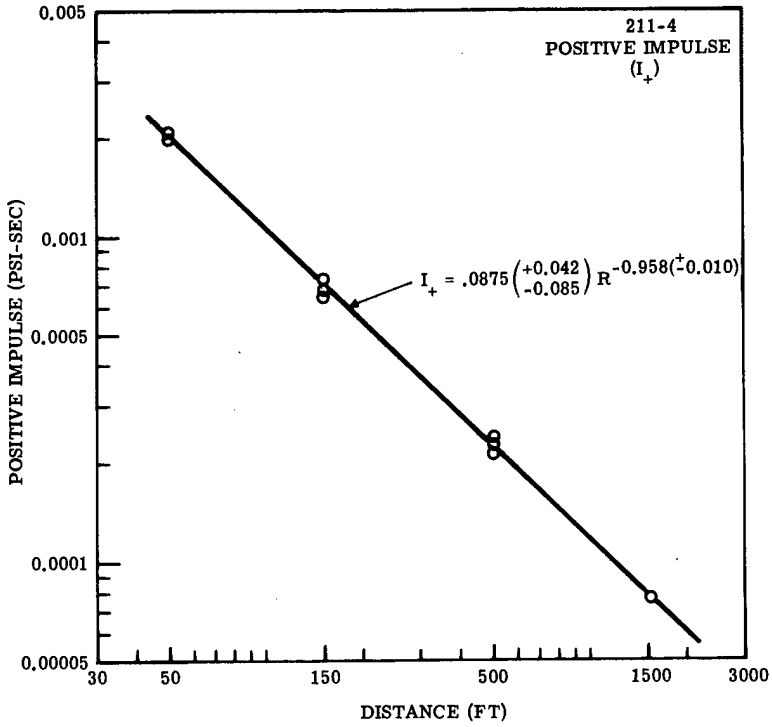

Figure A-4

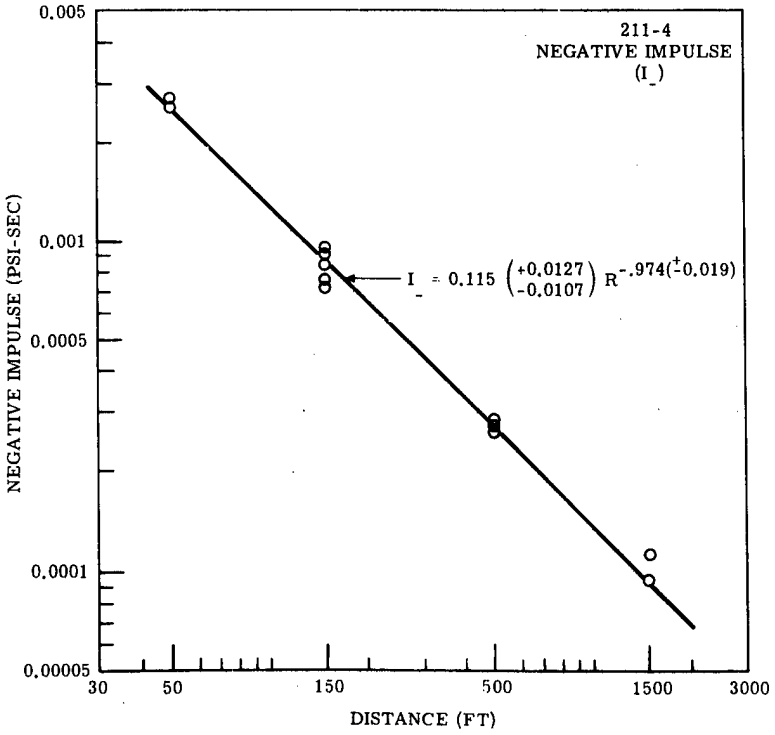
211-4
NEGATIVE IMPULSE
(I_-)
$I_- = 0.115 \left(^{+0.0127}_{-0.0107}\right) R^{-.974(\pm 0.019)}$
NEGATIVE IMPULSE (PSI-SEC)
0.005
0.001
0.0005
0.0001
0.00005
30
50
150
500
1500
3000
DISTANCE (FT)

Figure A-5

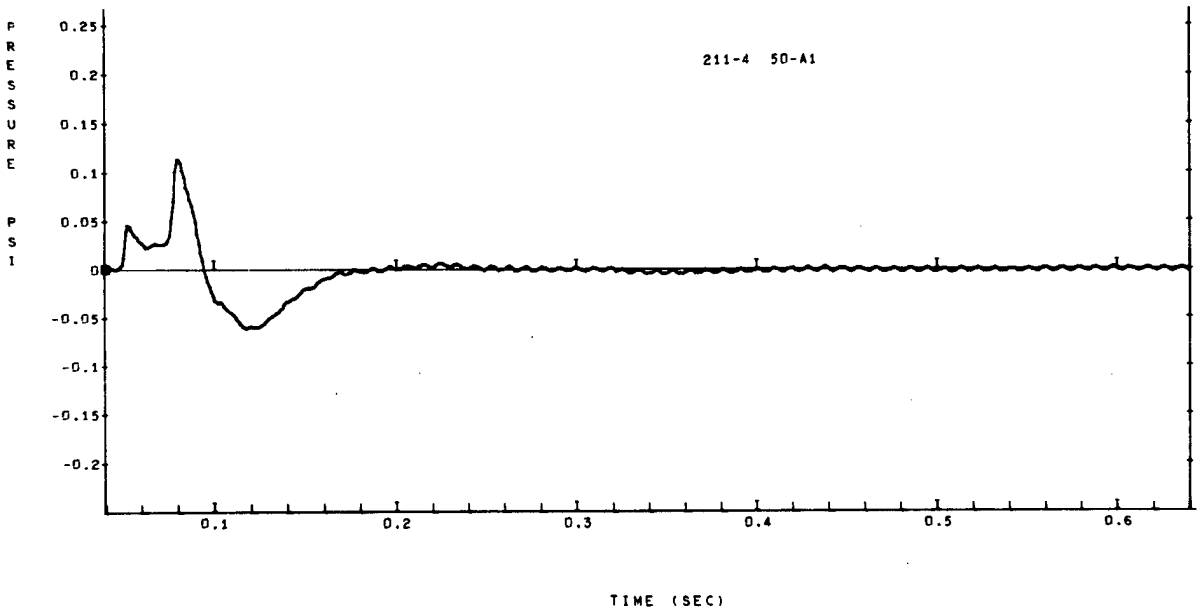

Figure A-6

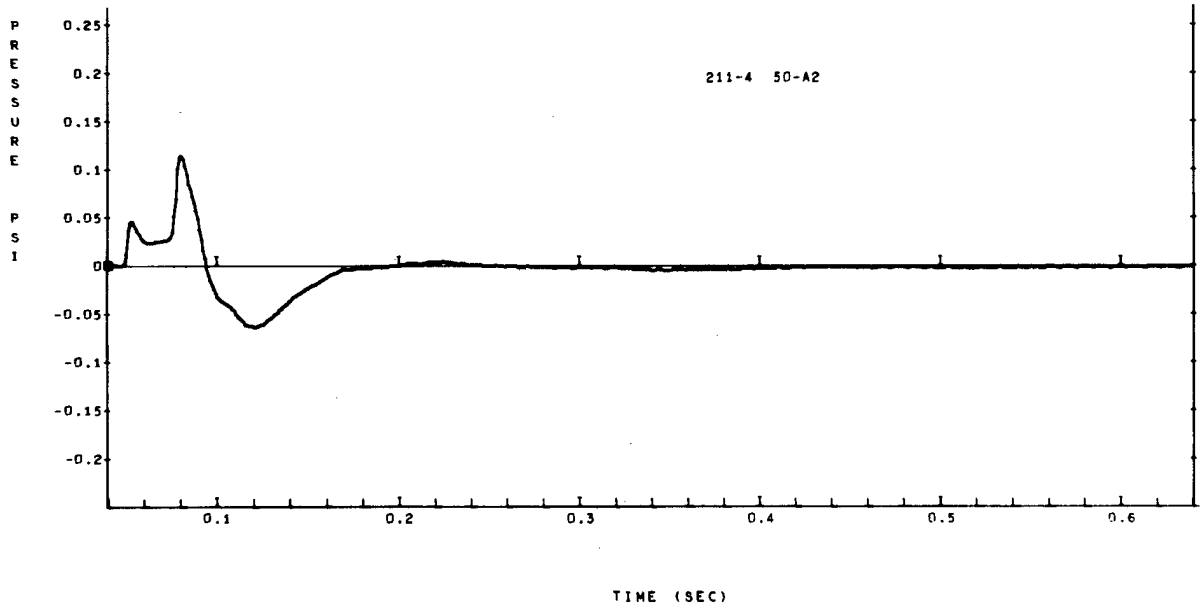

Figure A-7

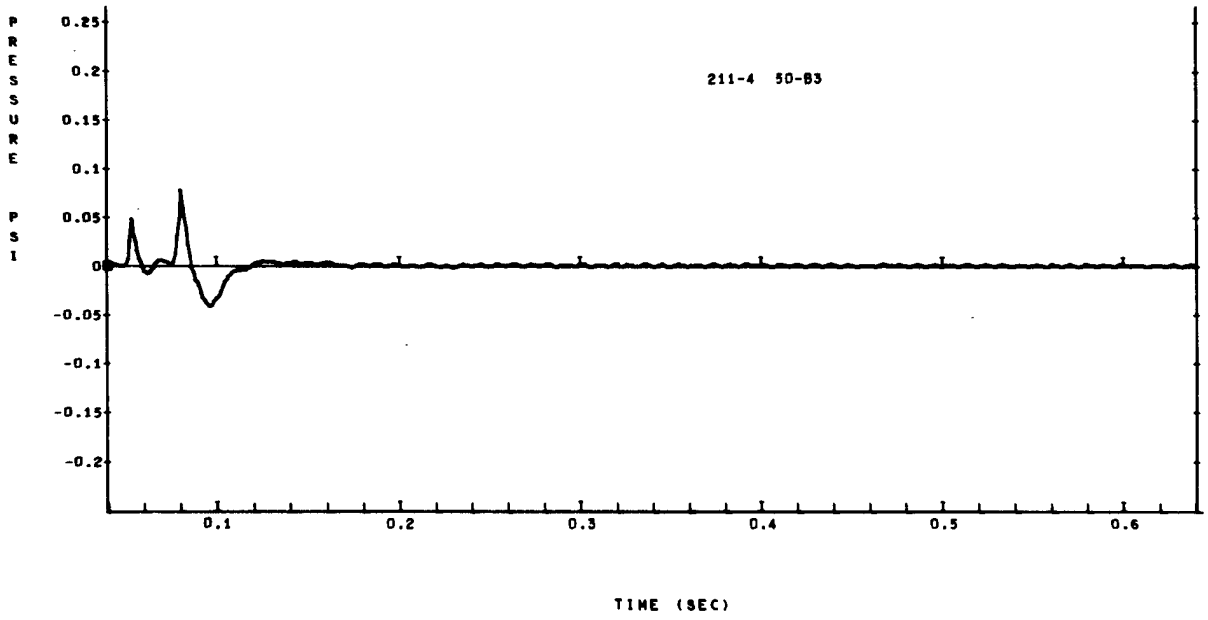

Figure A-8

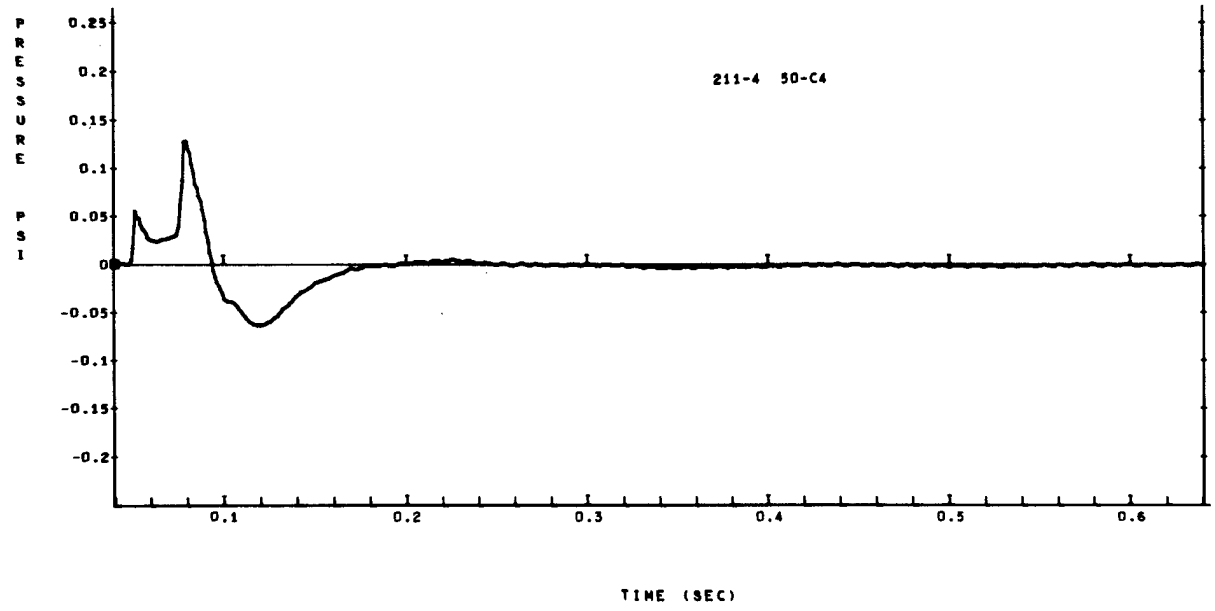

Figure A-9

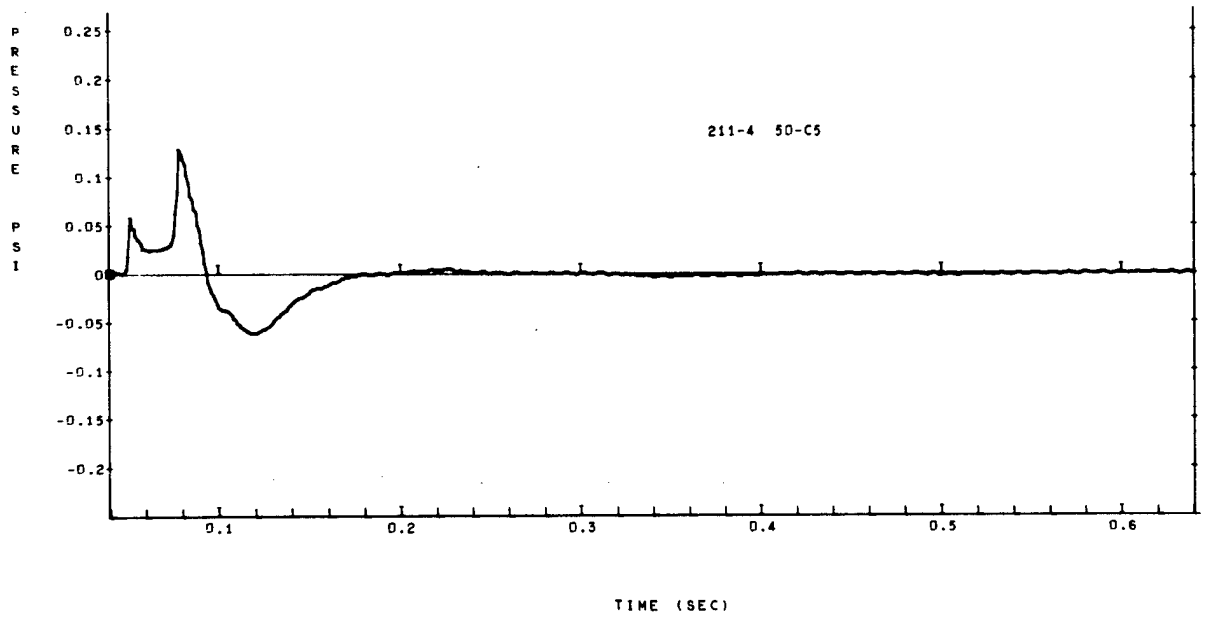

Figure A-10

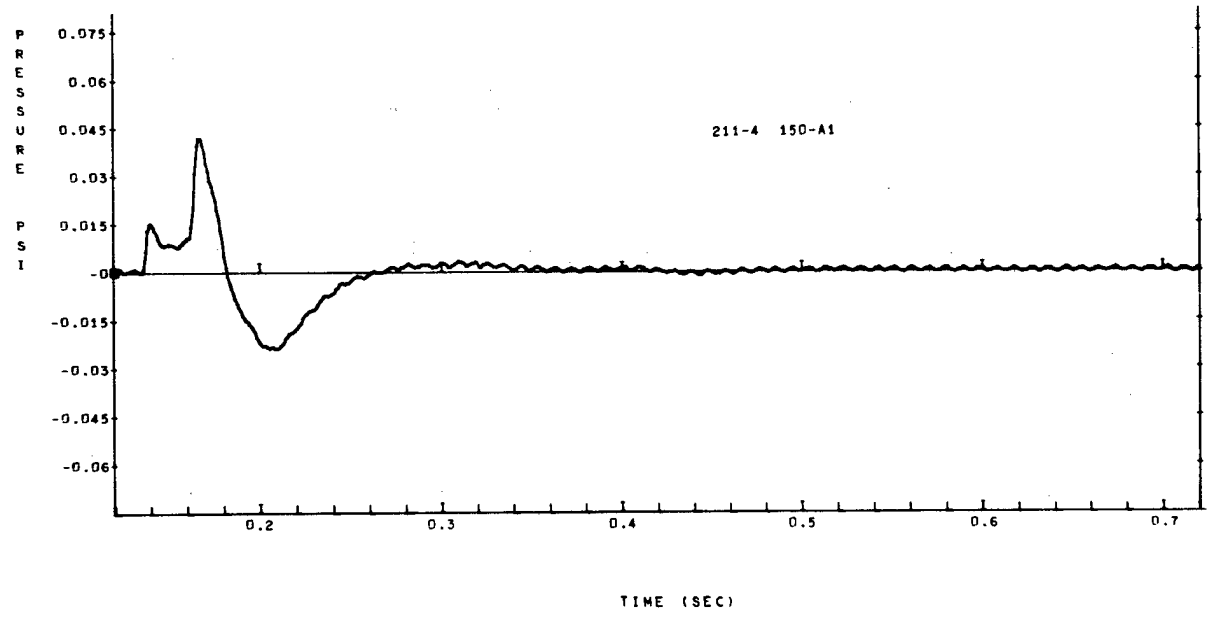

Figure A-11

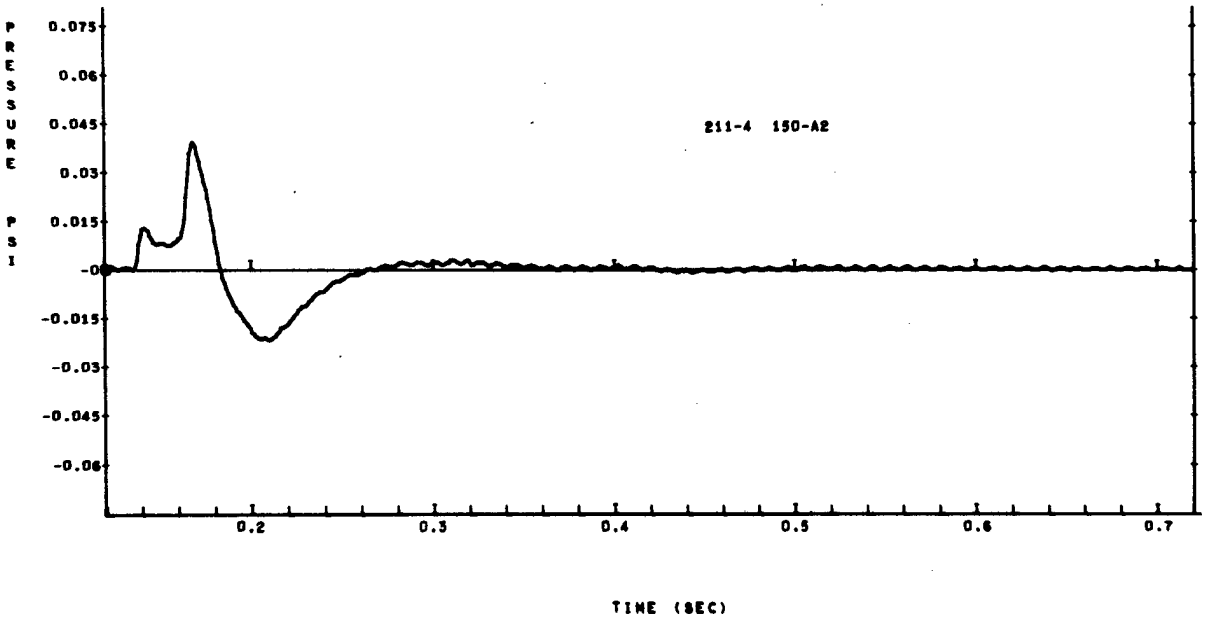

Figure A-12

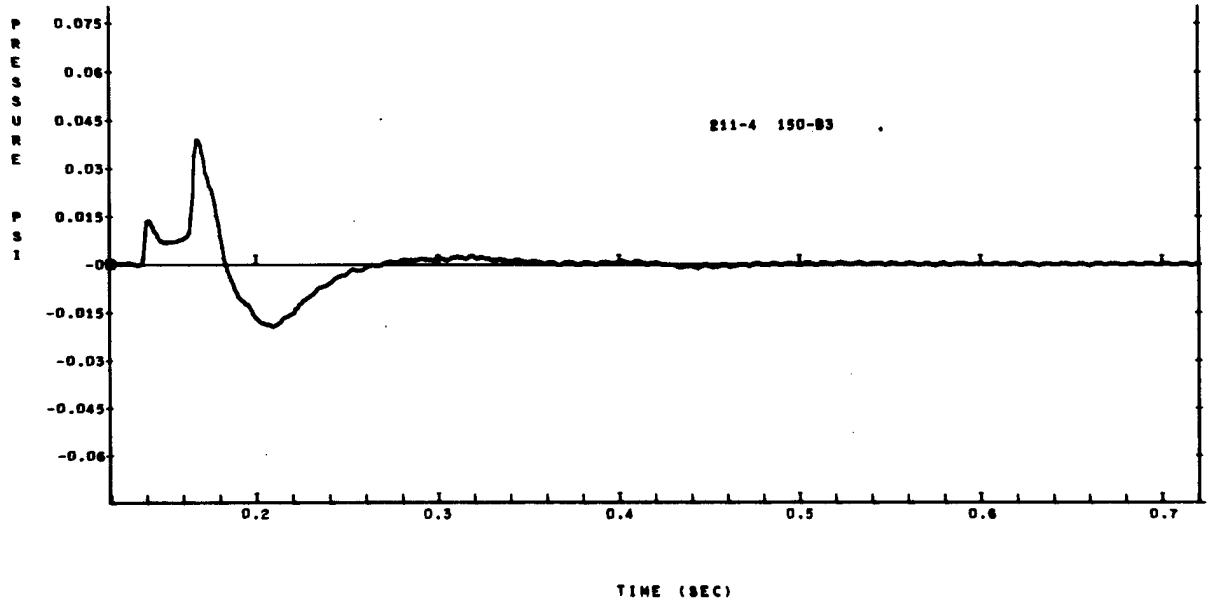

Figure A-13

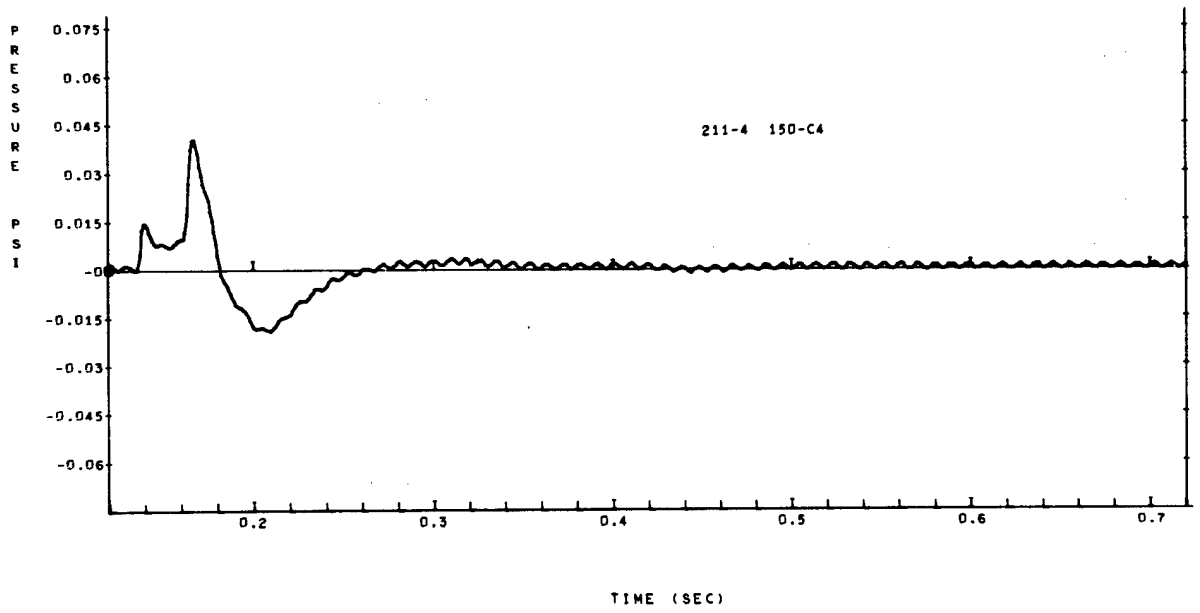

Figure A-14

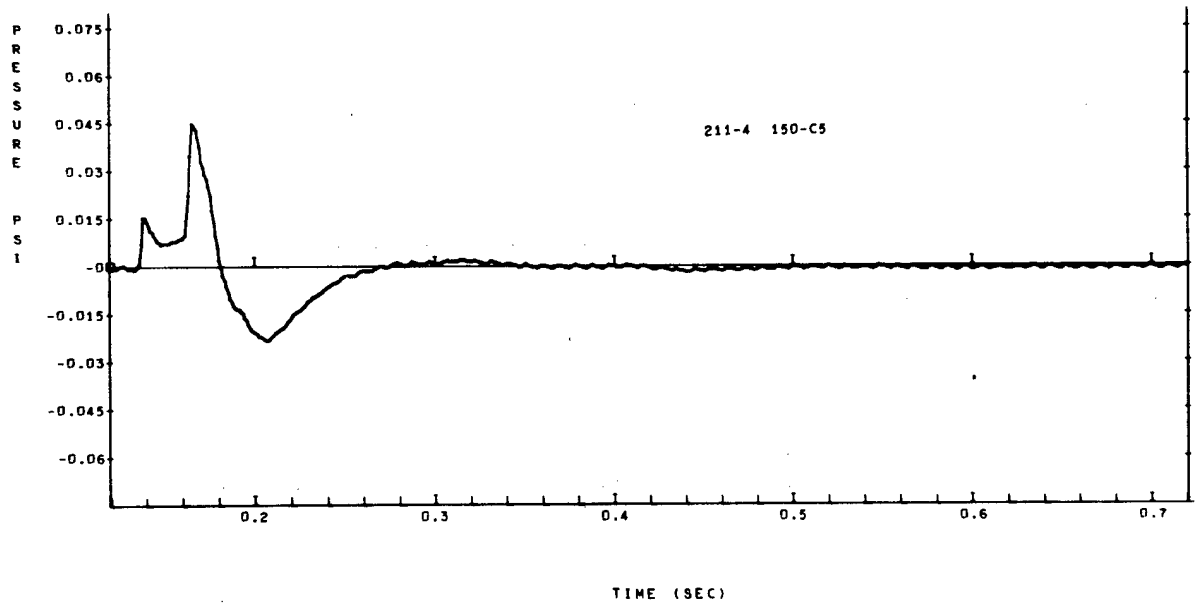

Figure A-15

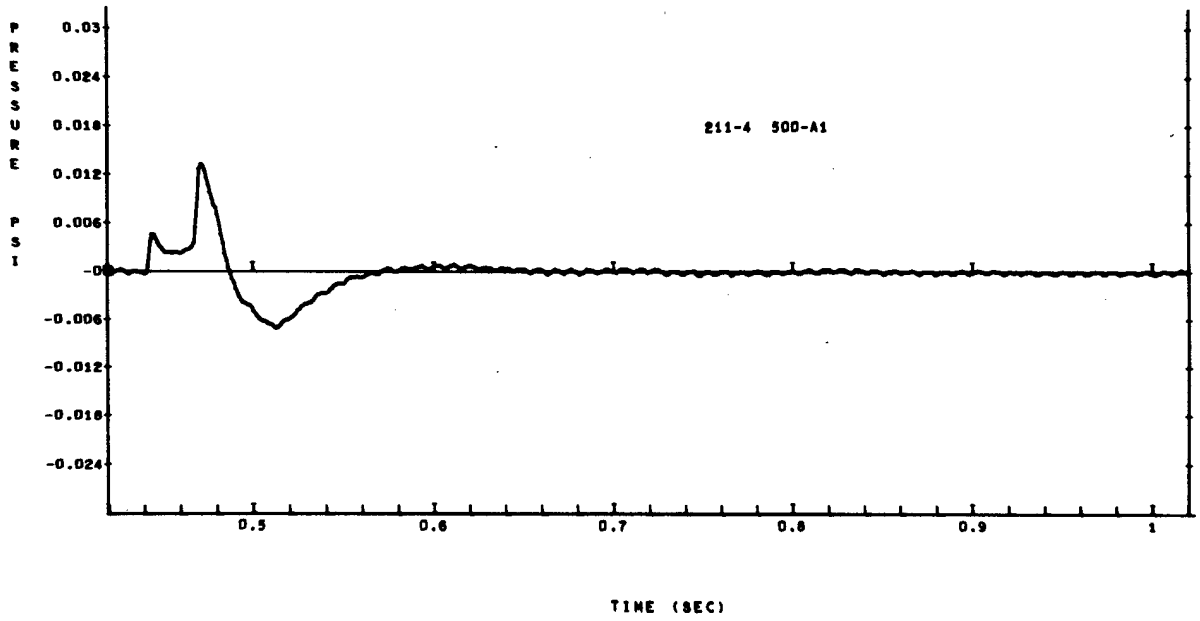

Figure A-16

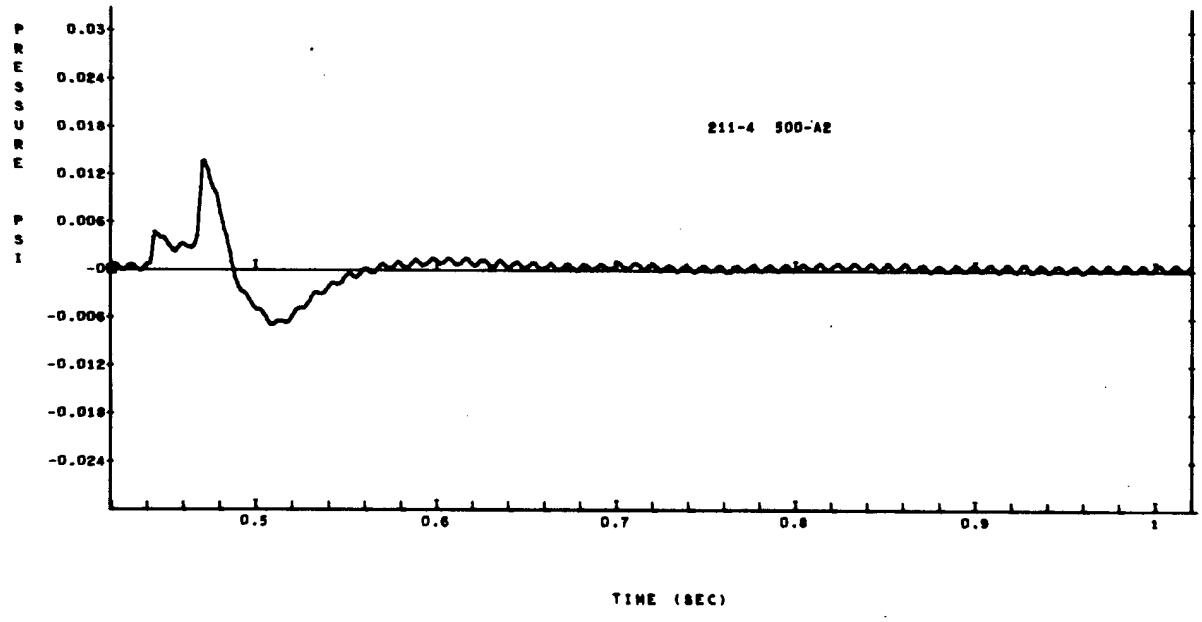

Figure A-17

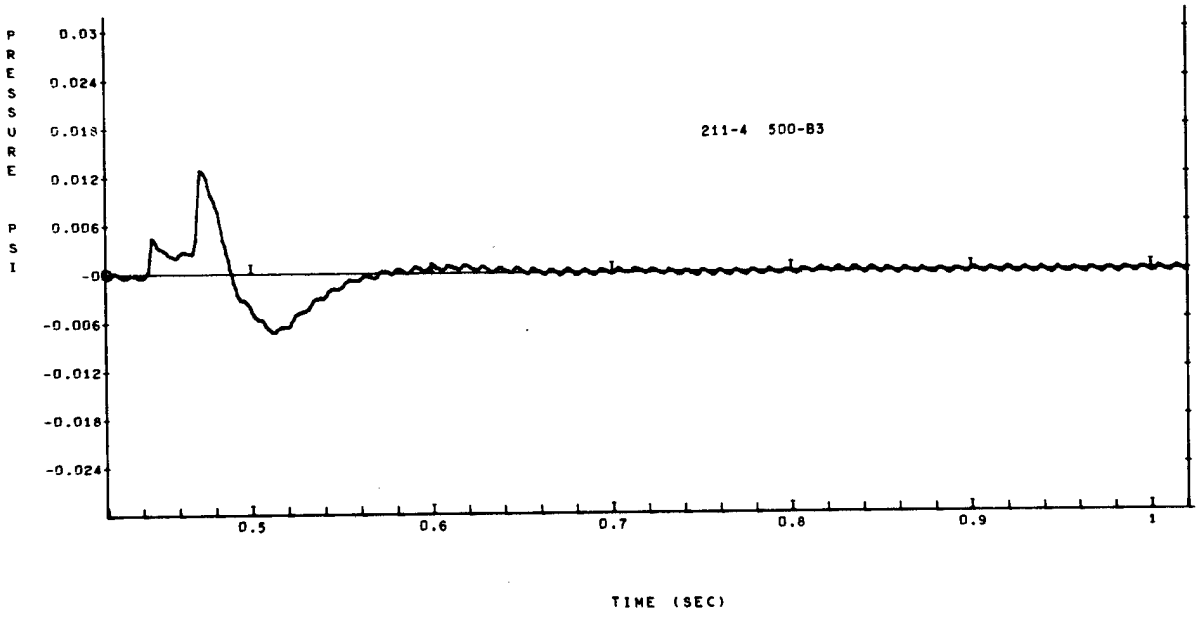

Figure A-18

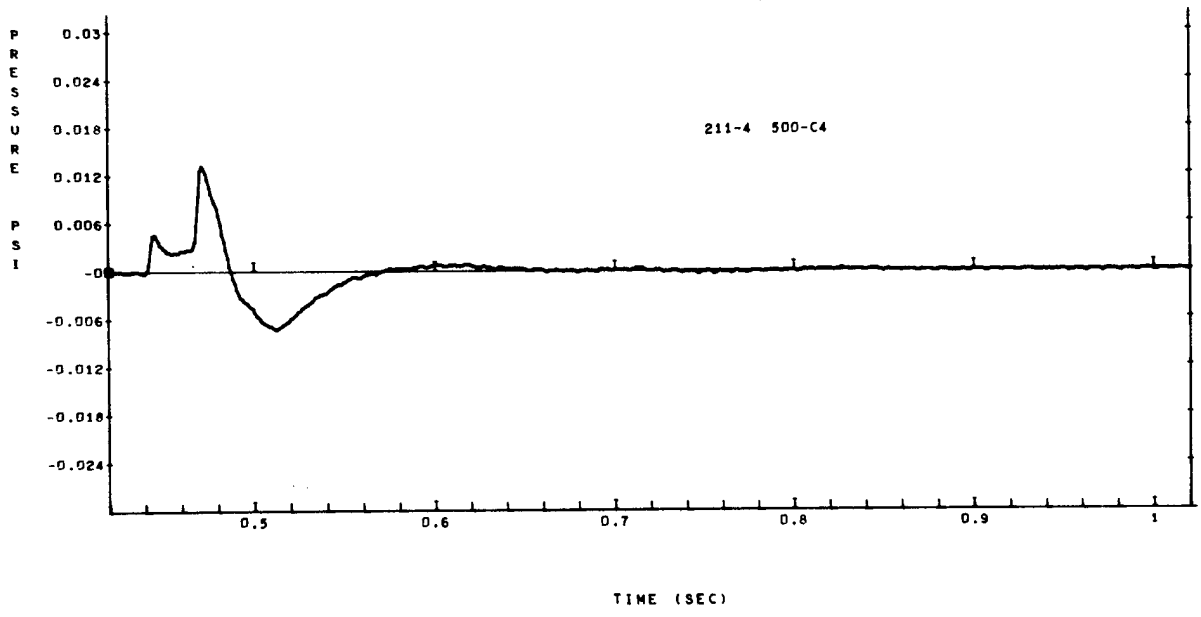

Figure A-19

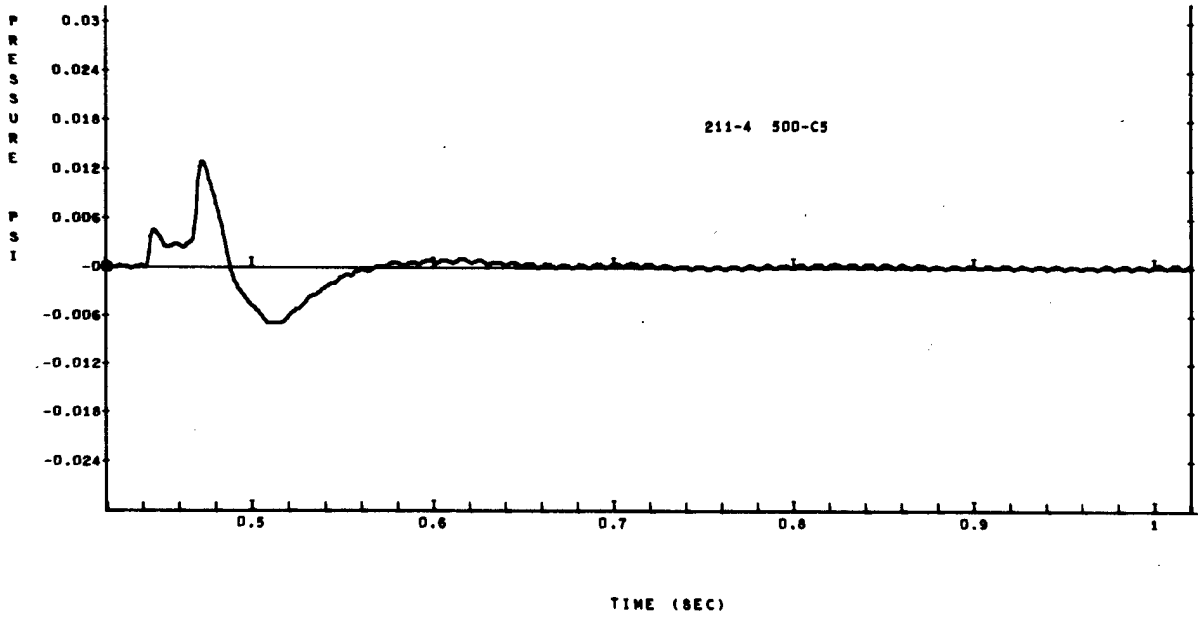

Figure A-20

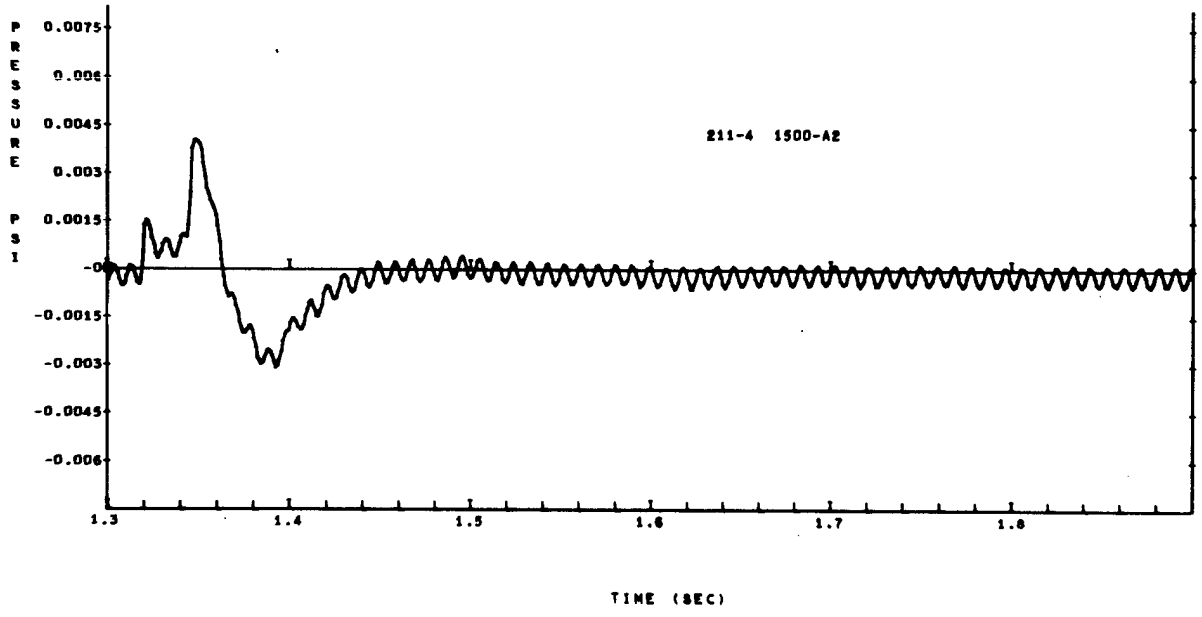

Figure A-21

Shot 211-41

Two 64-pound charges were buried 6 feet deep, spaced 8 feet apart. There were two blast lines: one off end of row (A), and one perpendicular to row (C). Two gages were places at each station; gage A is the less sensitive.

Gage	Arrival time (sec)	Ground shock induced peak (psi)	Time of peak (sec)	Peak from venting gas (psi)	Time of peak (sec)	Cross-over (sec)	Positive phase impulse (psi-sec)	Negative peak (psi)	Time of peak (sec)	Cross-over (sec)	Negative phase impulse (psi-sec)
A50A	0.047	0.0838	0.052	0.0184	0.079	0.094	0.00235	-0.0700	0.139	0.223	0.00381
A50B	0.047	0.0988	0.052	0.1235	0.079	0.096	0.00283	-0.0638	0.139	0.232	0.00369
A150A	0.137	0.0289	0.141	0.0443	0.170	0.184	0.000885	-0.0229	0.231	0.324	0.00116
A150B	0.137	0.0305	0.141	0.0432	0.169	0.191	0.000911	-0.0207	0.231	0.318	0.00104
A500A	0.452	0.0085	0.455	0.0125	0.483	0.5055	0.000268	-0.0056	0.546	0.626	0.000318
A500B	0.451	0.0083	0.455	0.0120	0.483	0.506	0.000265	-0.0061	0.546	0.640	0.000317
A1500A	1.357	0.00229	1.352	0.00379	1.381	1.402	0.000076	-0.00226	1.446	1.542	0.000107
B50A	0.046	0.0489	0.050	0.0791	0.076	0.097	0.00191	-0.0681	0.139	0.223	0.00376
B50B	0.046	0.0509	0.050	0.0774	0.076	0.096	0.00216	-0.0589	0.139	0.223	0.00331
B150B	0.136	0.0168	0.140	0.0264	0.179	0.1935	0.000754	-0.0223	0.232	0.316	0.00110
B500A	0.447		0.477	0.0088	0.491	0.5075	0.000243	-0.0061	0.548	0.624	0.000282
B1500A	1.338		1.347	0.0037	1.379	1.390	0.000086	-0.003206	1.428	1.5325	0.000089
B1500B	1.338	0.001457	1.347	0.003016	1.385	1.3975	0.000100	-0.002331	1.4275	1.5020	0.000089

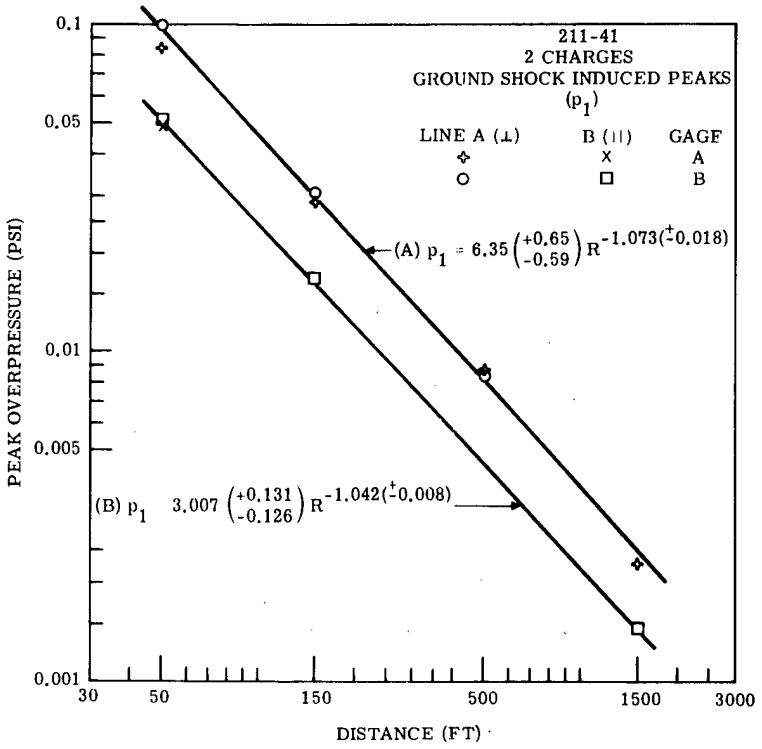

Figure A-22

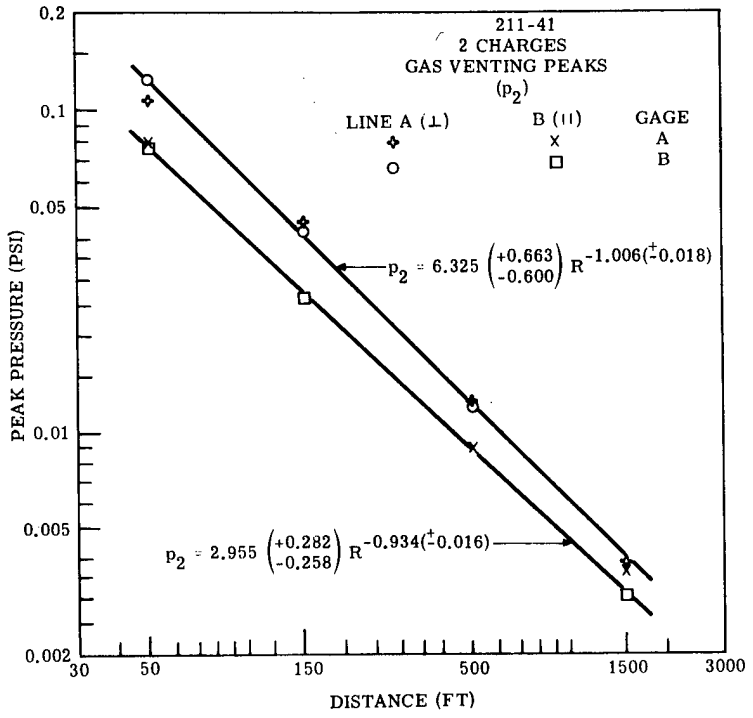

Figure A-23

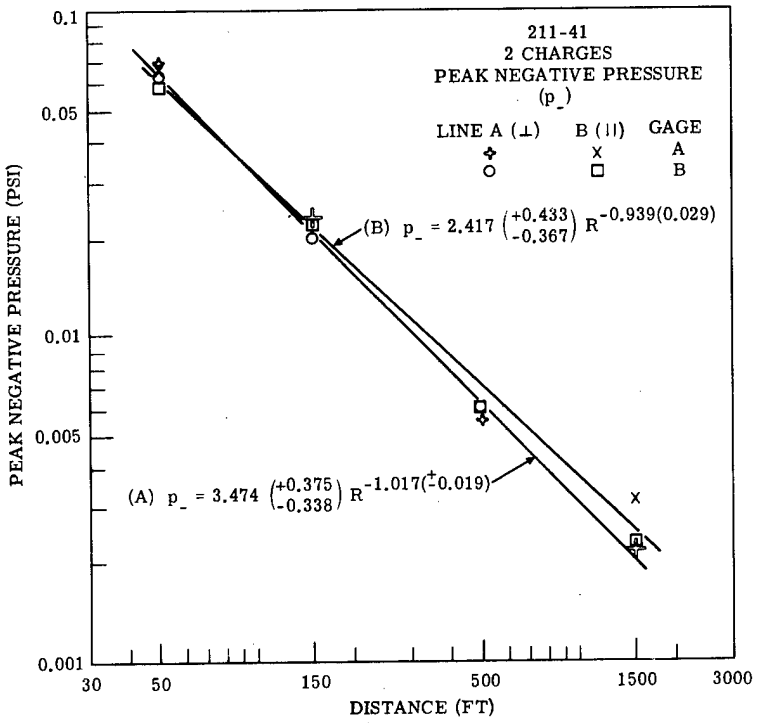

Figure A-24

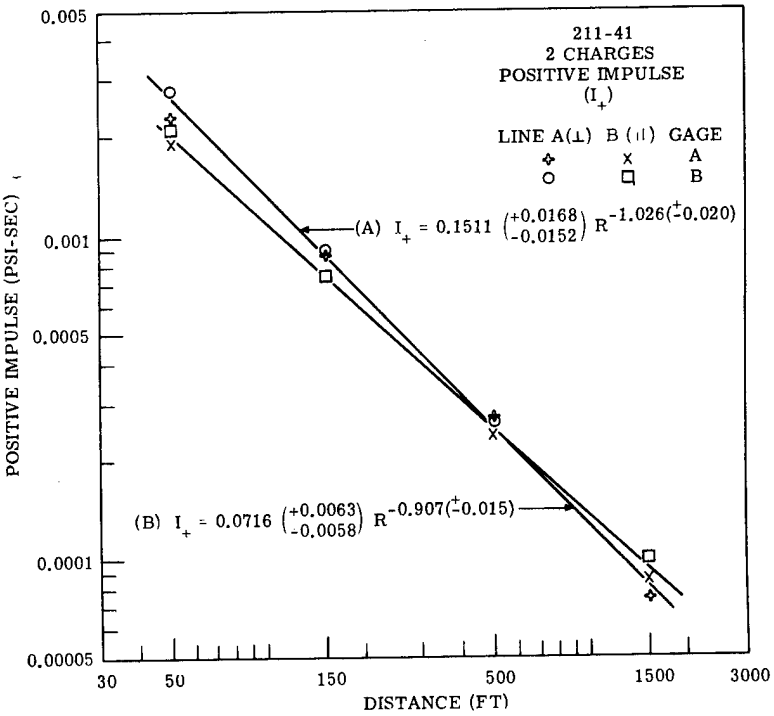

Figure A-25

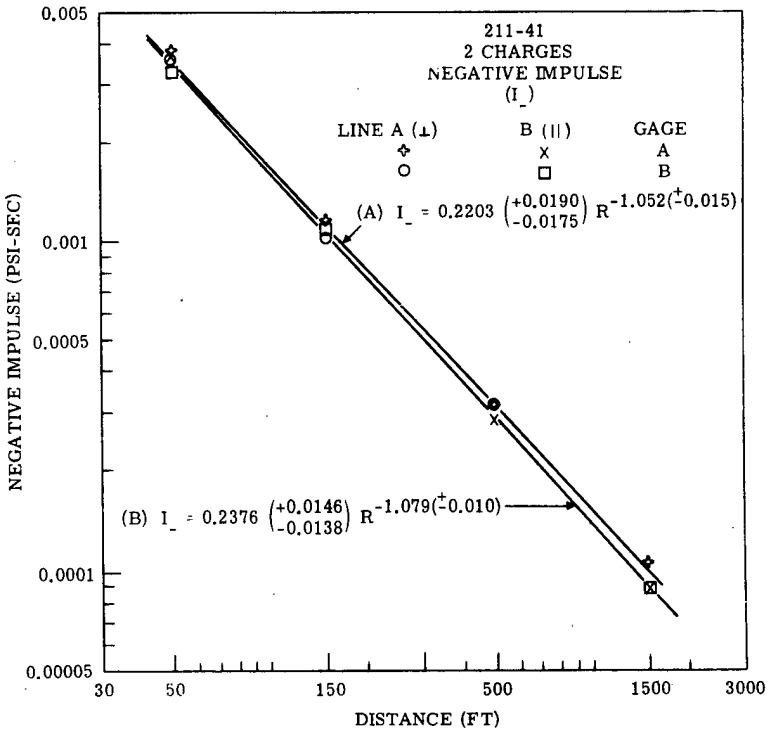
211-41
2 CHARGES
NEGATIVE IMPULSE
(I_)
LINE A (⊥)
B (||)
GAGE
A
B
(A) I_ = 0.2203 (+0.0190 / -0.0175) R^-1.052(±0.015)
(B) I_ = 0.2376 (+0.0146 / -0.0138) R^-1.079(±0.010)
NEGATIVE IMPULSE (PSI-SEC)
0.005
0.001
0.0005
0.0001
0.00005
30
50
150
500
1500
3000
DISTANCE (FT)

Figure A-26

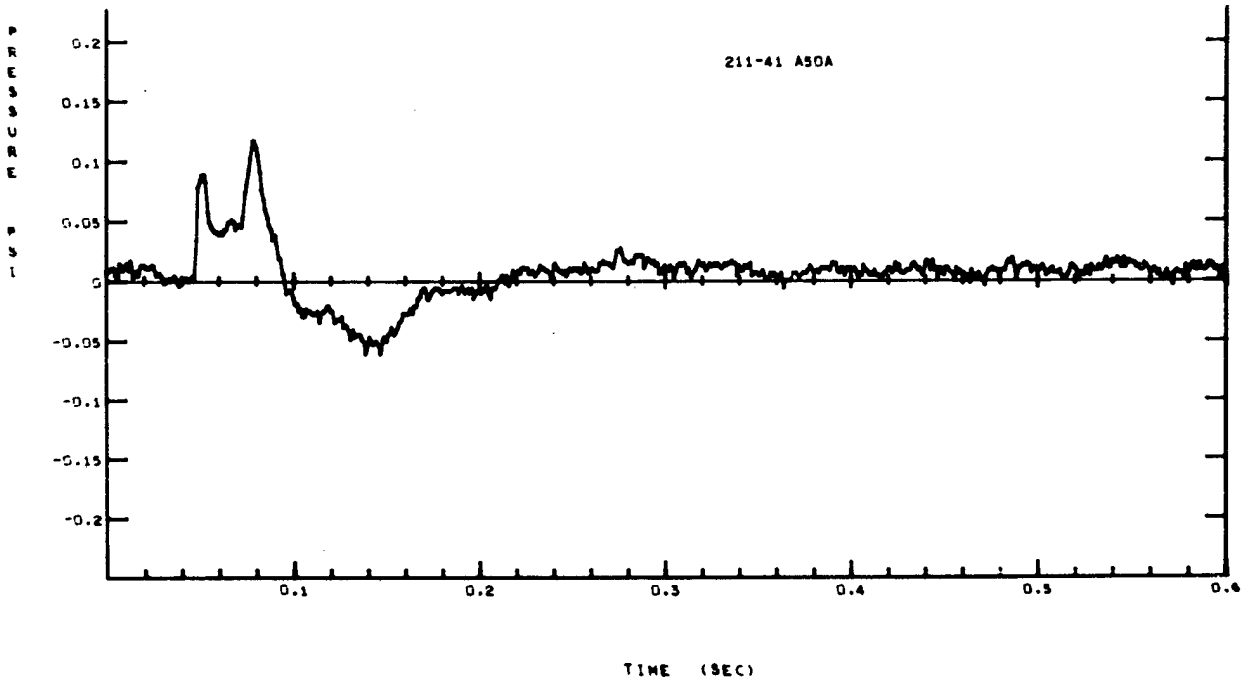

Figure A-27

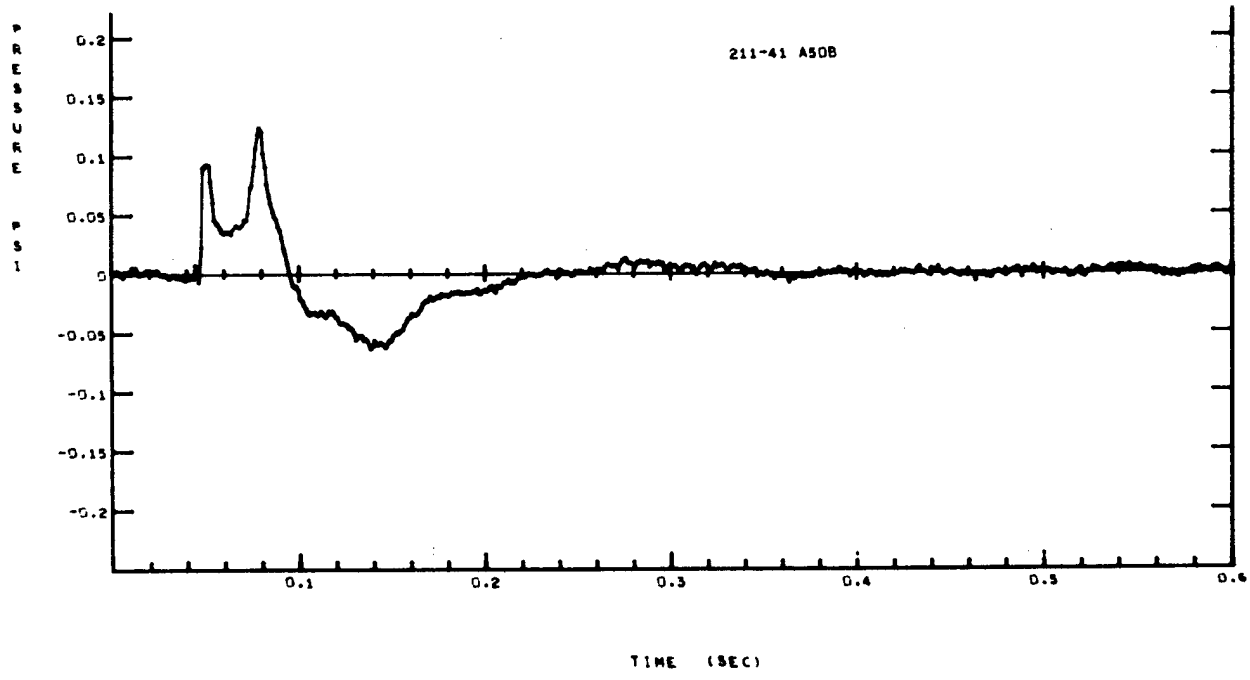

Figure A-28

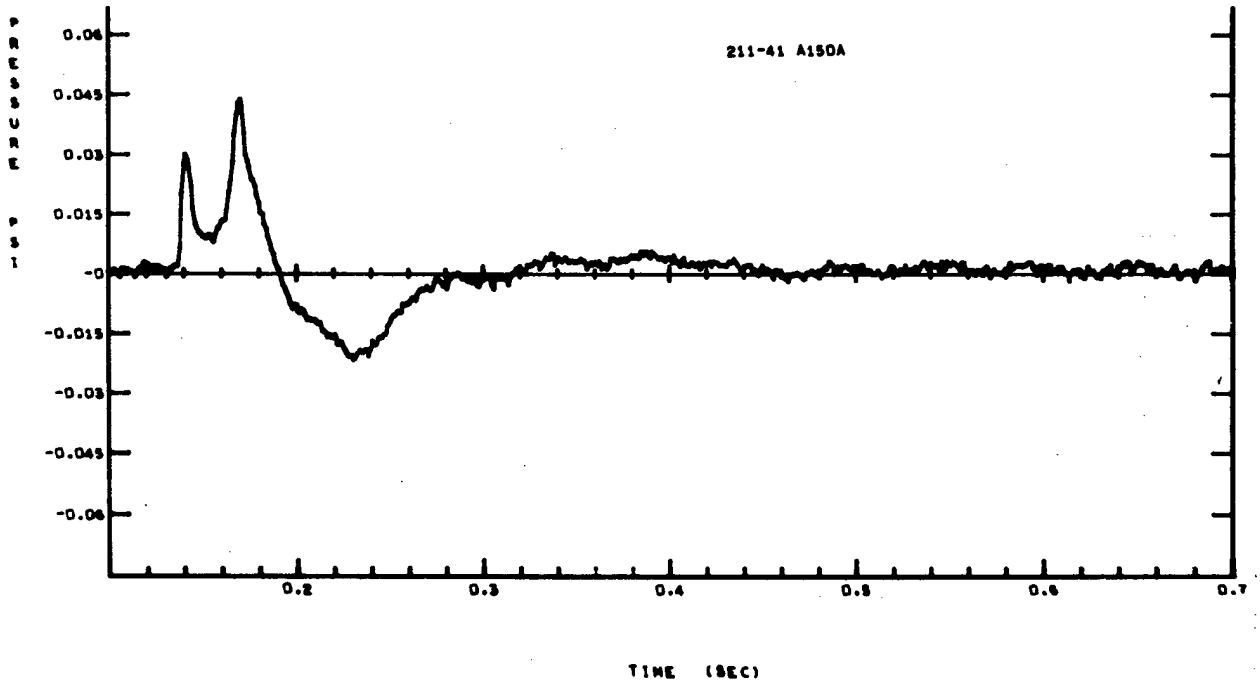

Figure A-29

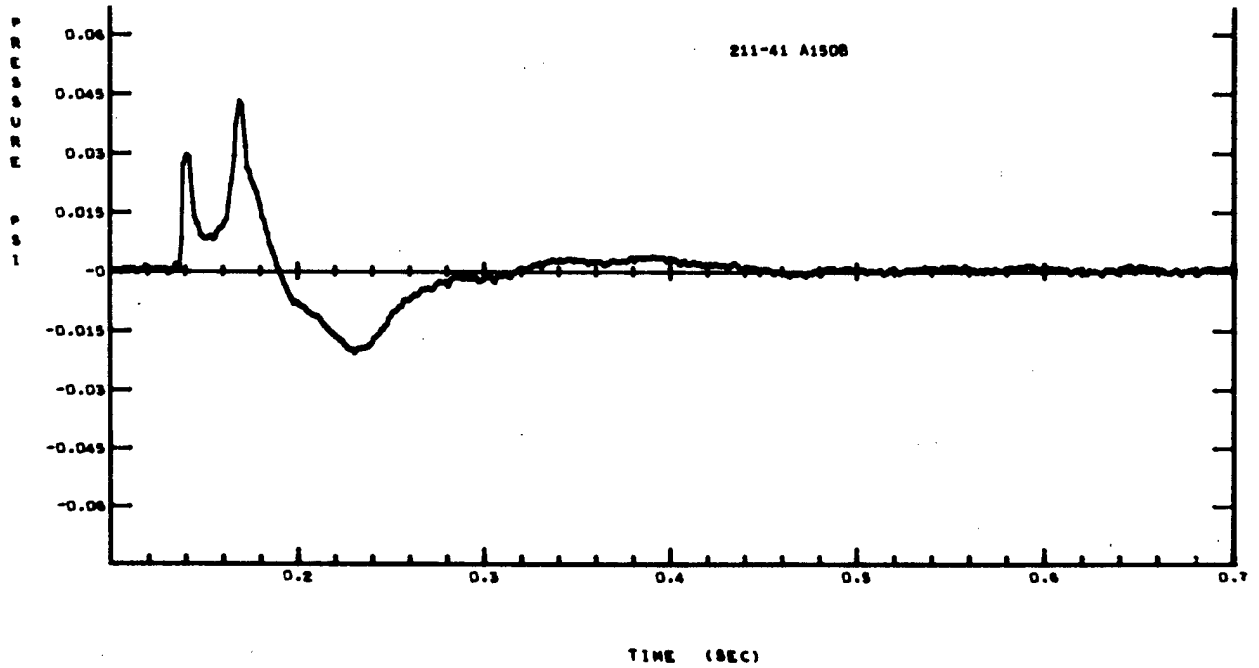

Figure A-30

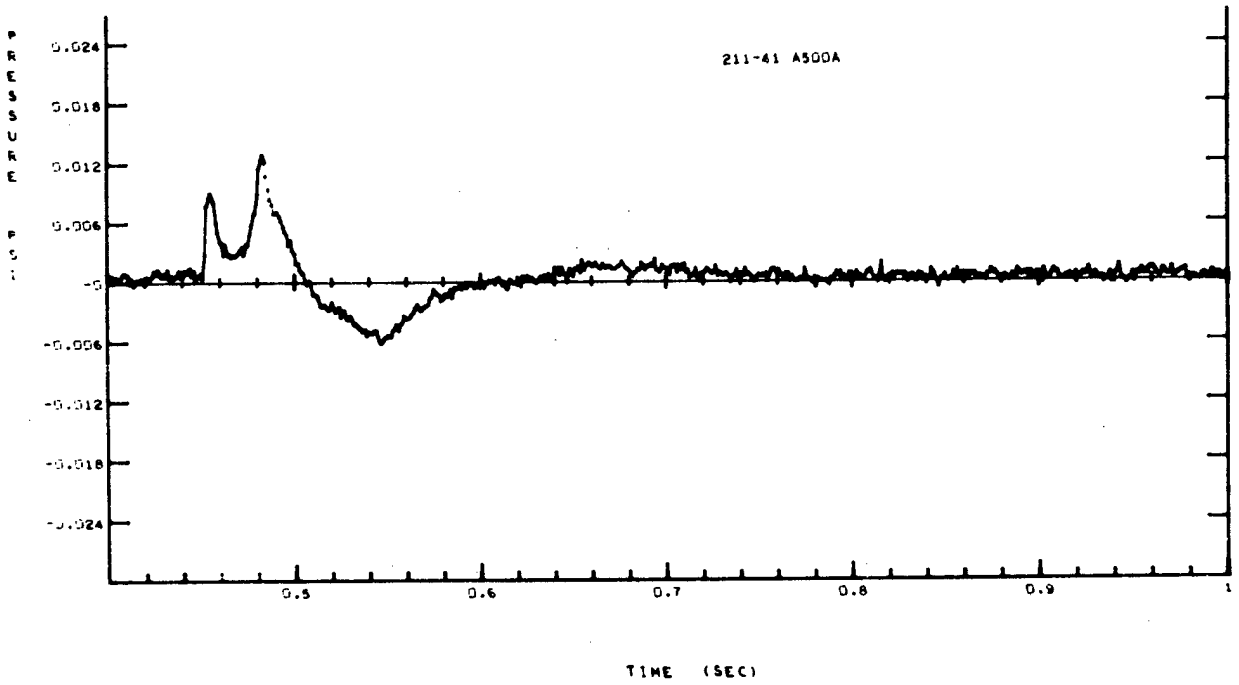

Figure A-31

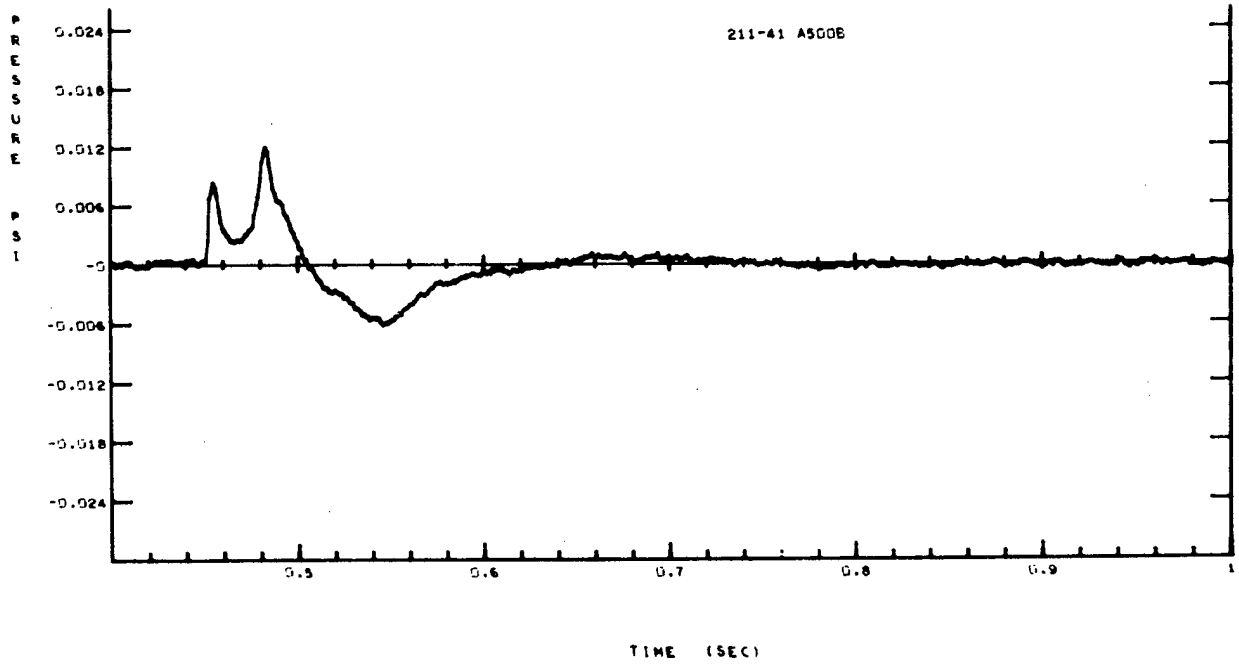

Figure A-32

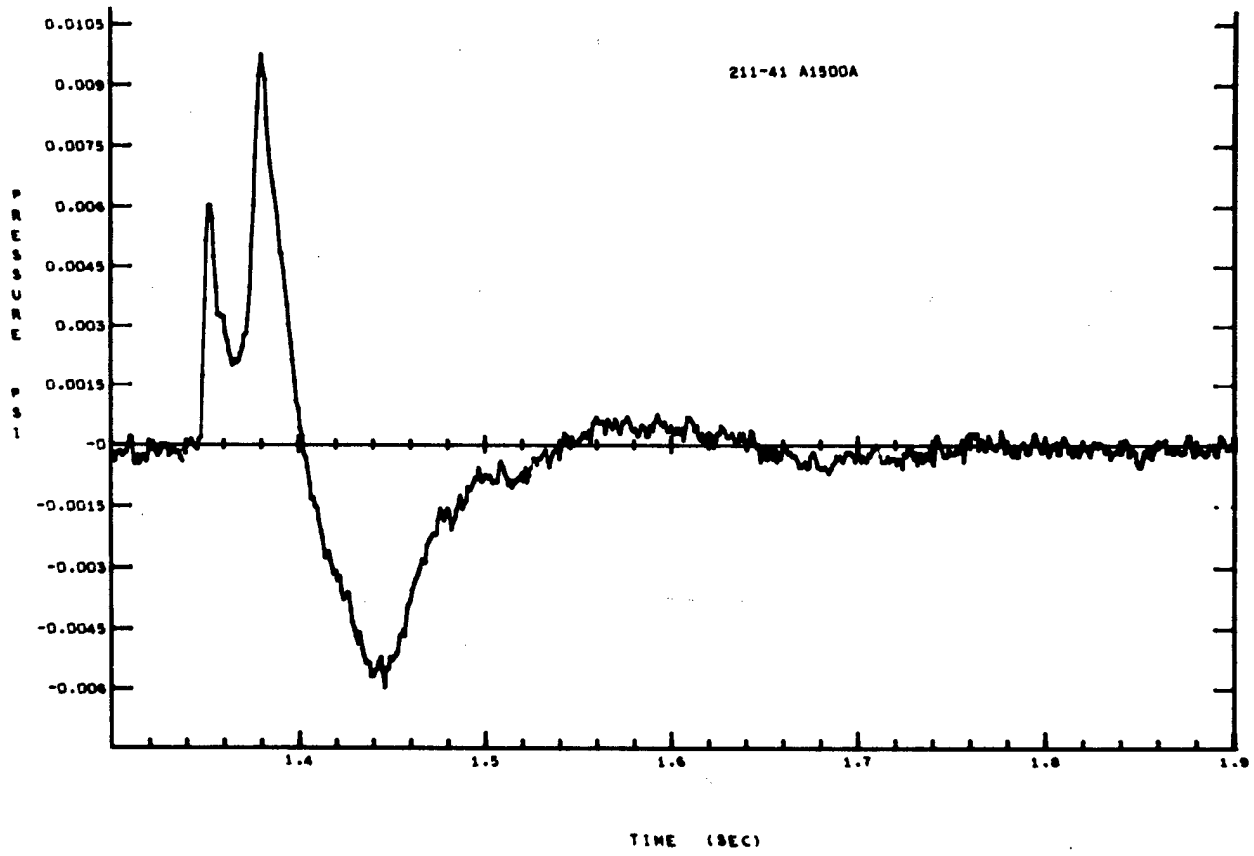

Figure A-33

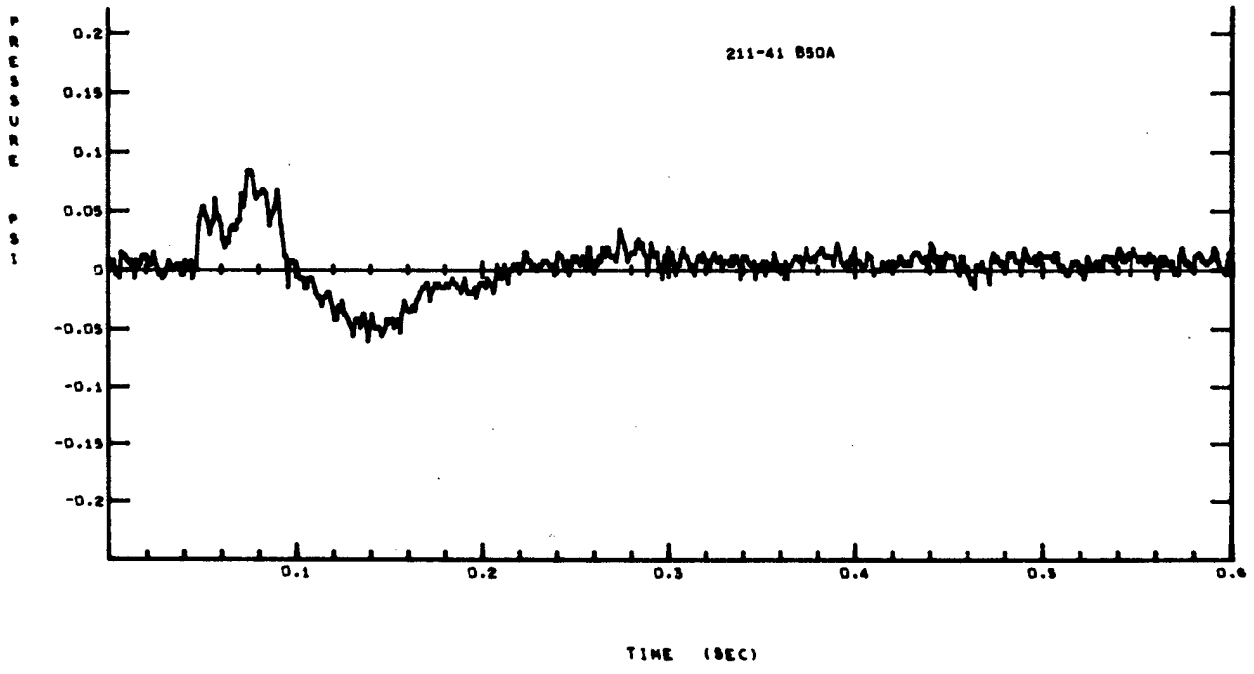

Figure A-34

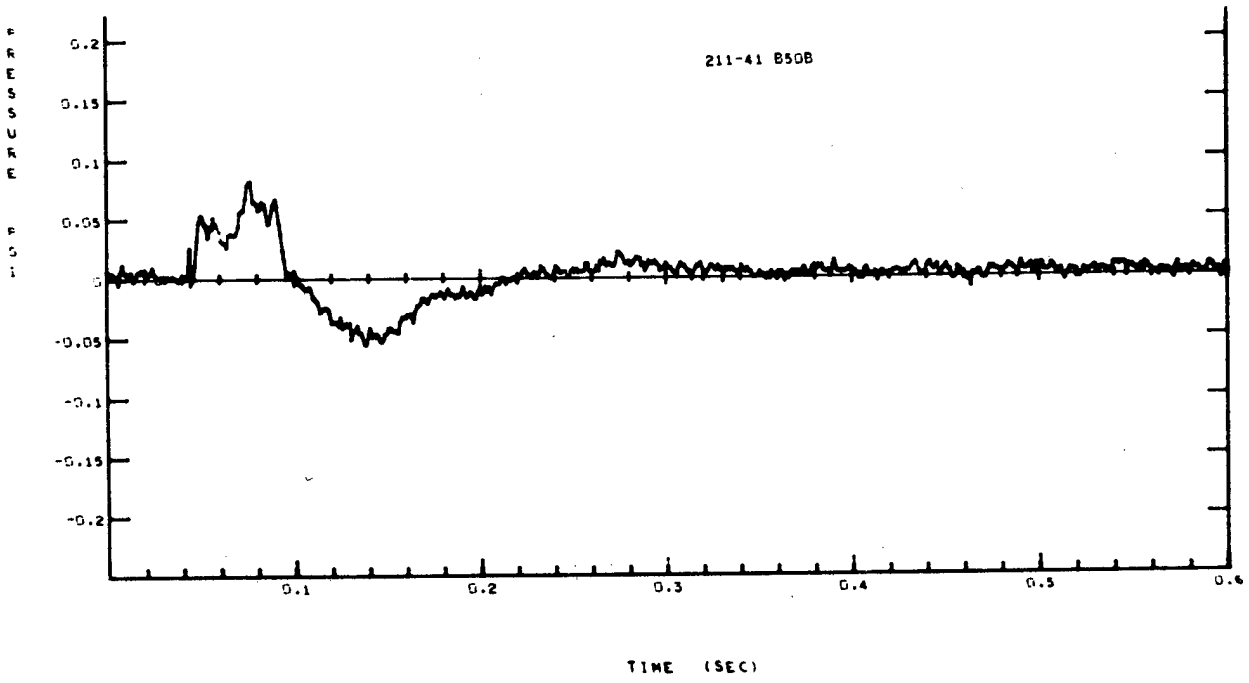

Figure A-35

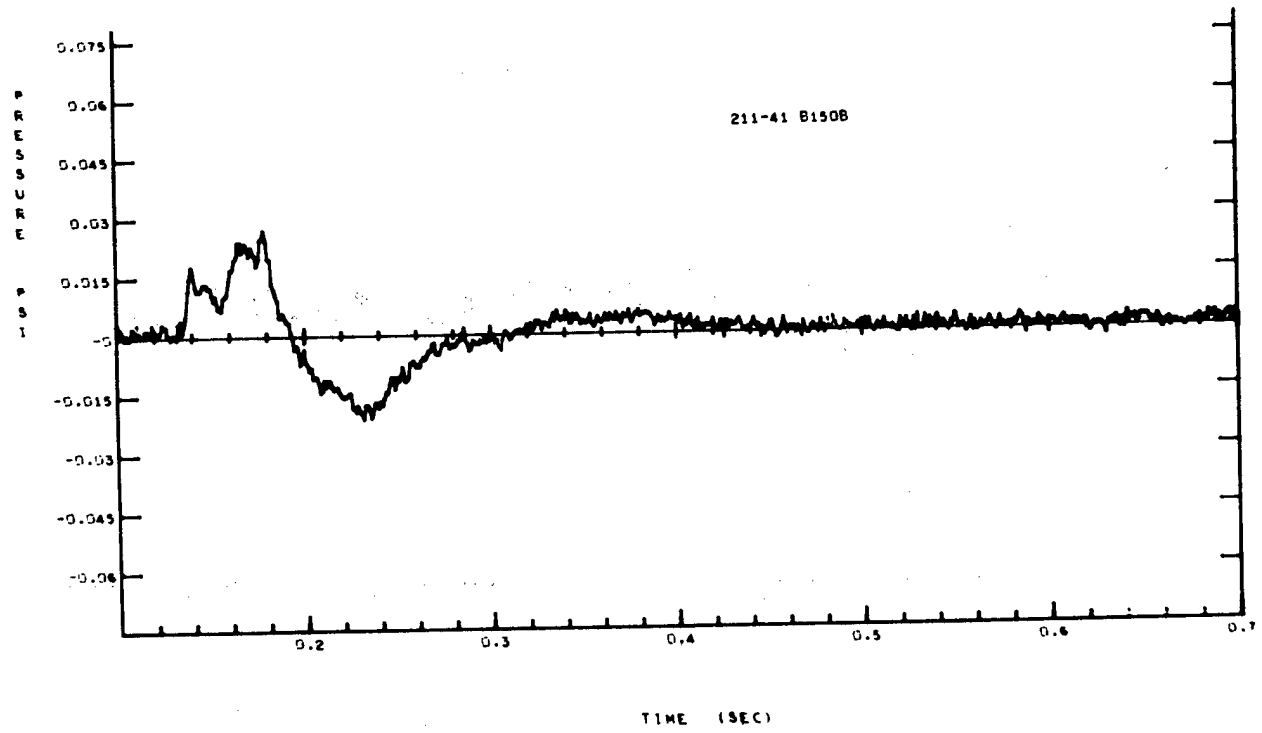

Figure A-36

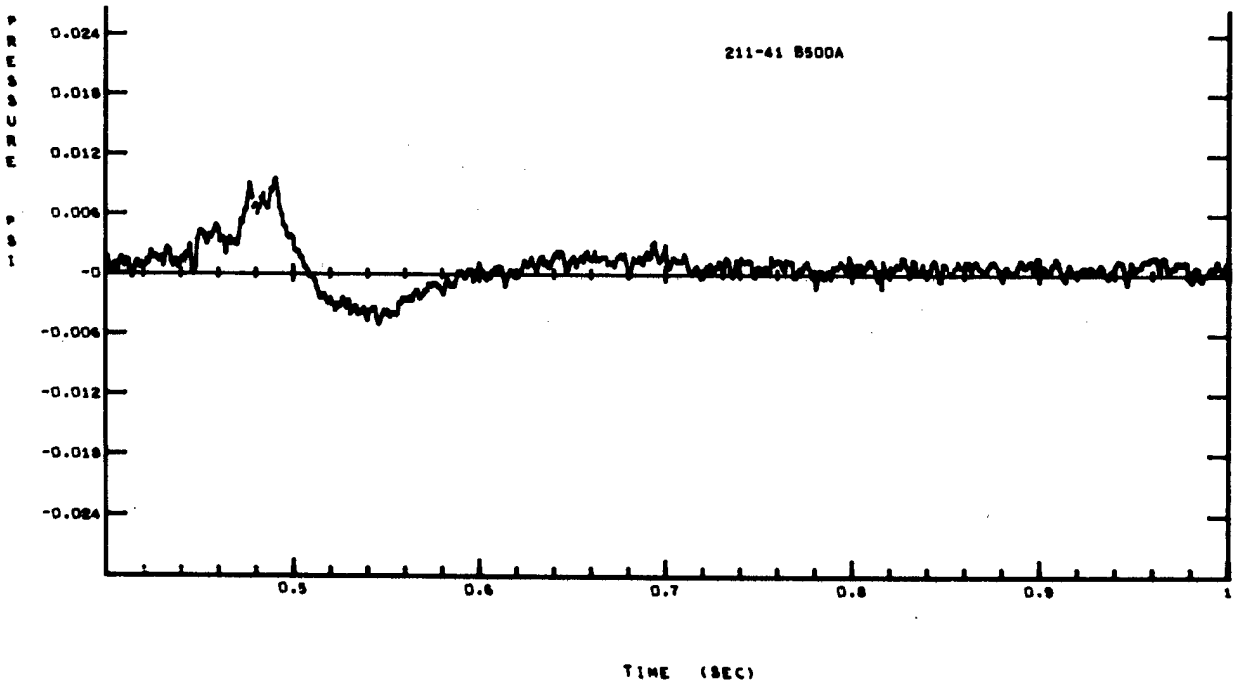

Figure A-37

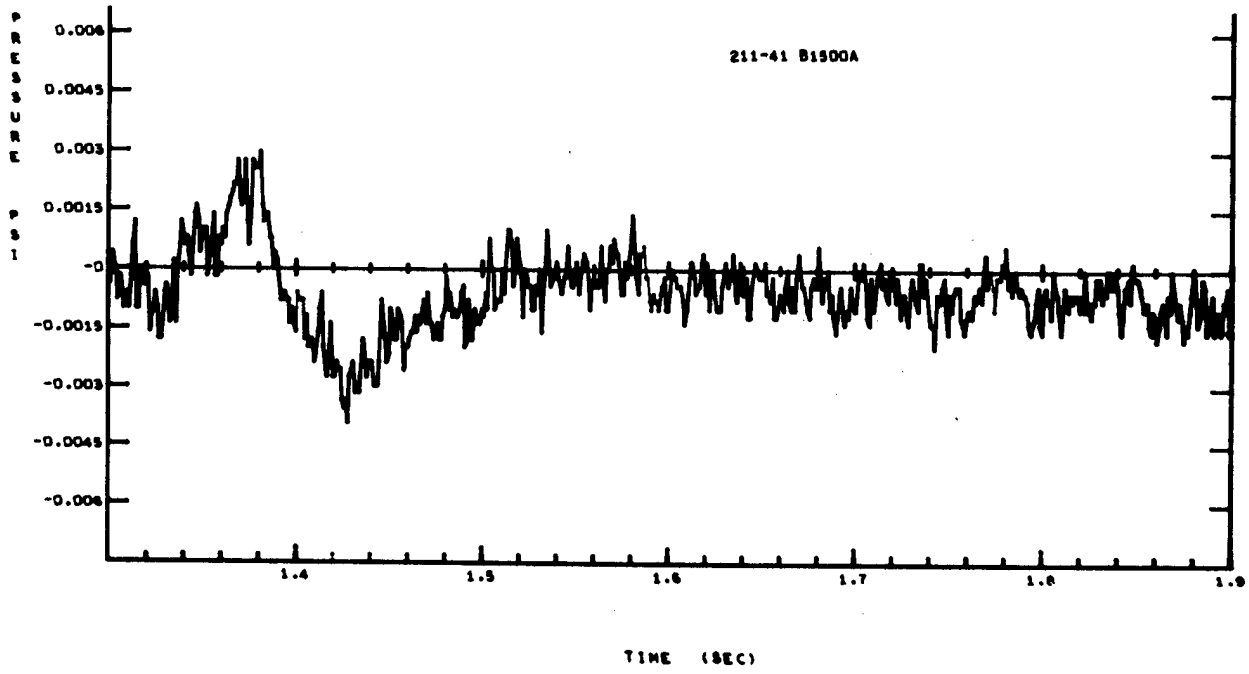

Figure A-38

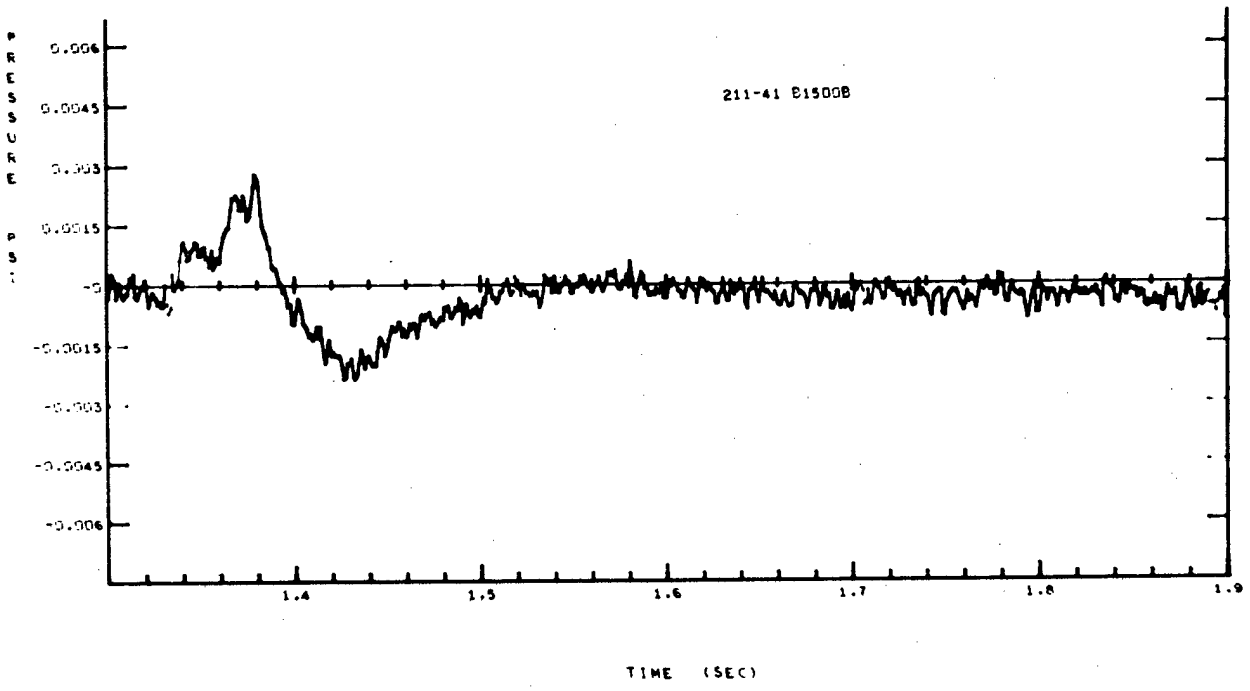
PRESSURE PSI
0.006
0.0045
0.003
0.0015
-0
-0.0015
-0.003
-0.0045
-0.006
211-41 B1500B
1.4
1.5
1.6
1.7
1.8
1.9
TIME (SEC)

Figure A-39

Shot 211-44

Five 64-pound charges were buried 6 feet deep, spaced 8 feet apart. One blast line off end of row (A), and one perpendicular to row (B). Two gages were placed at each station; gage A is the less sensitive.

Gage	Arrival time (sec)	Ground shock induced peak (psi)	Time of peak (sec)	Peak from venting gas (psi)	Time of peak (sec)	Cross-over (sec)	Positive phase impulse (psi-sec)	Negative peak (psi)	Time of peak (sec)	Cross-over (sec)	Negative phase impulse (psi-sec)
A50A	0.048	0.22641	0.054	0.188673	0.083	0.106	0.00576	-0.1154	0.147	0.267	0.00807
A50B	0.050	0.2367	0.054	0.2241	0.083	0.107	0.00640	-0.09947	0.143	0.297	0.00841
A150A	0.142	0.0964	0.144	0.077302	0.175	0.200	0.002278	-0.0458	0.242	0.364	0.002814
A150B	0.143	0.0884	0.145	0.075297	0.175	0.201	0.002138	-0.0416	0.243	0.366	0.002569
A500A	0.462	0.02377	0.464	0.02057	0.494	0.521	0.0005795	-0.011242	0.560	0.683	0.0006846
A500B	0.463	0.02543	0.464	0.02293	0.494	0.522	0.000659	-0.011568	0.557	0.680	0.0006805
A1500A	1.379	0.00584	1.382	0.00627	1.411	1.438	0.000189	-0.00420	1.477	1.601	0.000271
A1500B	1.378	0.00703	1.382	0.00745	1.411	1.439	0.000222	-0.00442	1.477	1.601	0.000284
B50A	0.046	0.0507	0.053	0.1038	0.083	0.123	0.00456	-0.08636	0.152	0.280	0.005424
B50B	0.047		0.071	0.09046	0.111	0.124	0.00432	-0.099507	0.147	0.265	0.00574
B150A	0.142	0.0175	0.145	0.05264	0.182	0.218	0.00209	-0.03976	0.246	0.363	0.00238
B150B	0.142	0.01344	0.146	0.04251	0.182	0.218	0.001614	-0.03546	0.239	0.378	0.00242
B1500A	1.376	0.001594	1.382	0.0050175	1.438	1.459	0.000209	-0.003572	1.483	1.595	0.000203
B1500B	1.379	0.00161	1.383	0.004698	1.438	1.459	0.0001864	-0.003892	1.484	1.596	0.0002306

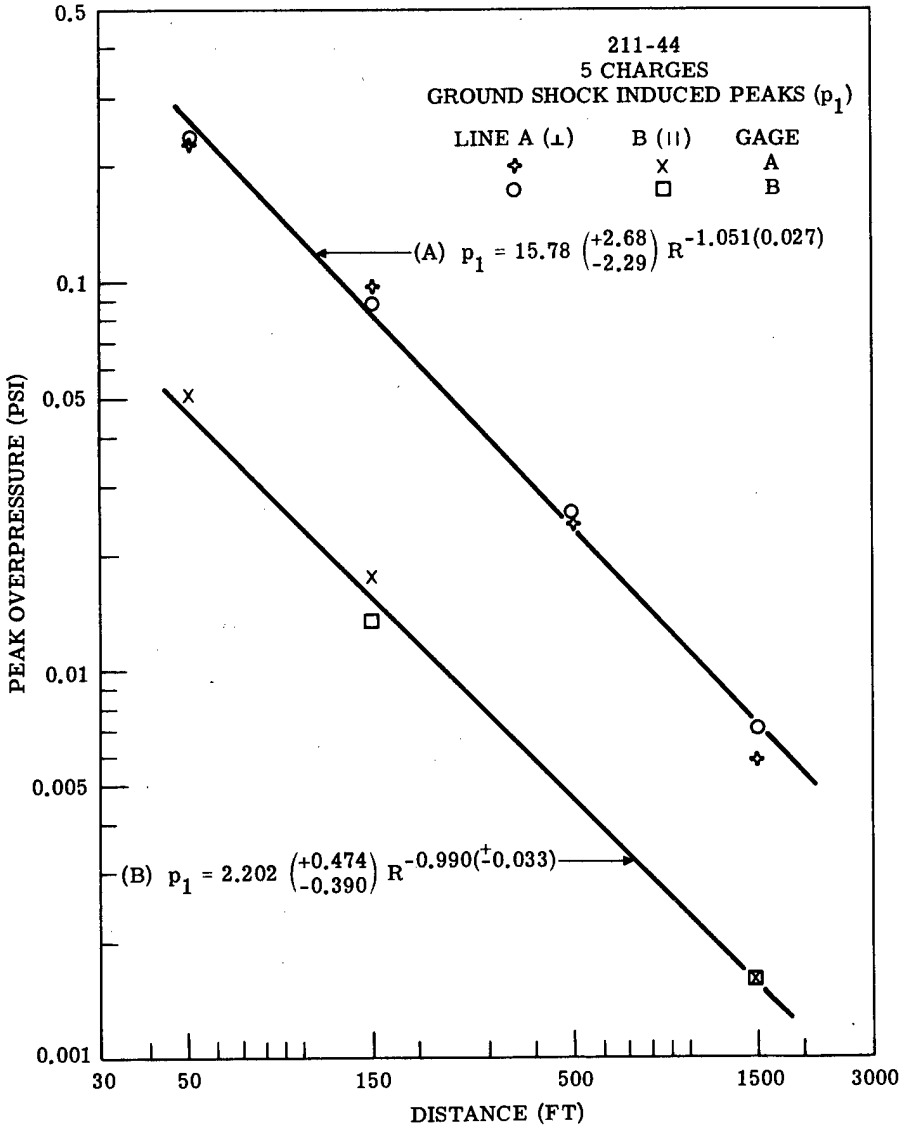
211-44
5 CHARGES
GROUND SHOCK INDUCED PEAKS (p_1)
LINE A (⊥) B (||) GAGE
A
B
(A) $p_1 = 15.78 \binom{+2.68}{-2.29} R^{-1.051(0.027)}$
(B) $p_1 = 2.202 \binom{+0.474}{-0.390} R^{-0.990(\pm 0.033)}$
PEAK OVERPRESSURE (PSI)
0.5
0.1
0.05
0.01
0.005
0.001
30
50
150
500
1500
3000
DISTANCE (FT)

Figure A-40

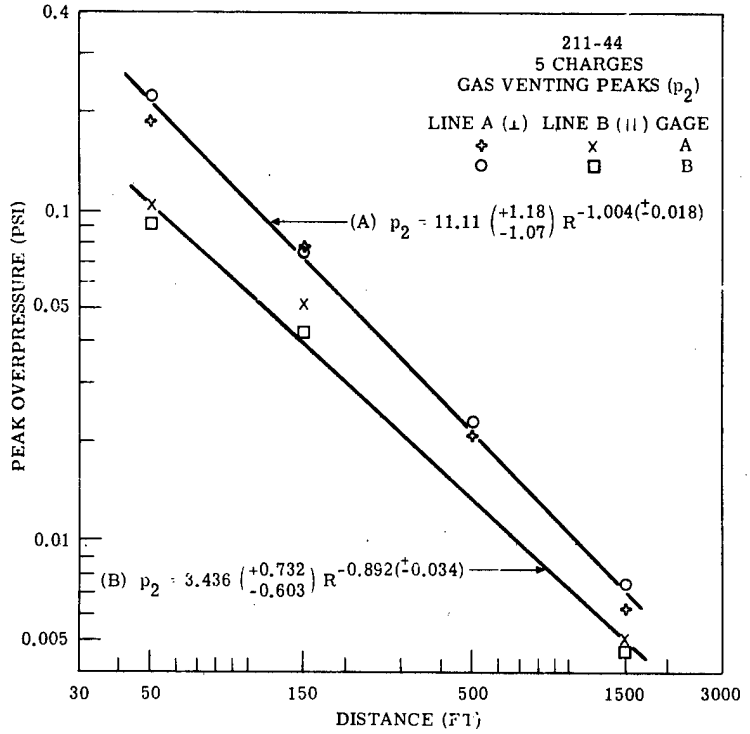

Figure A-41

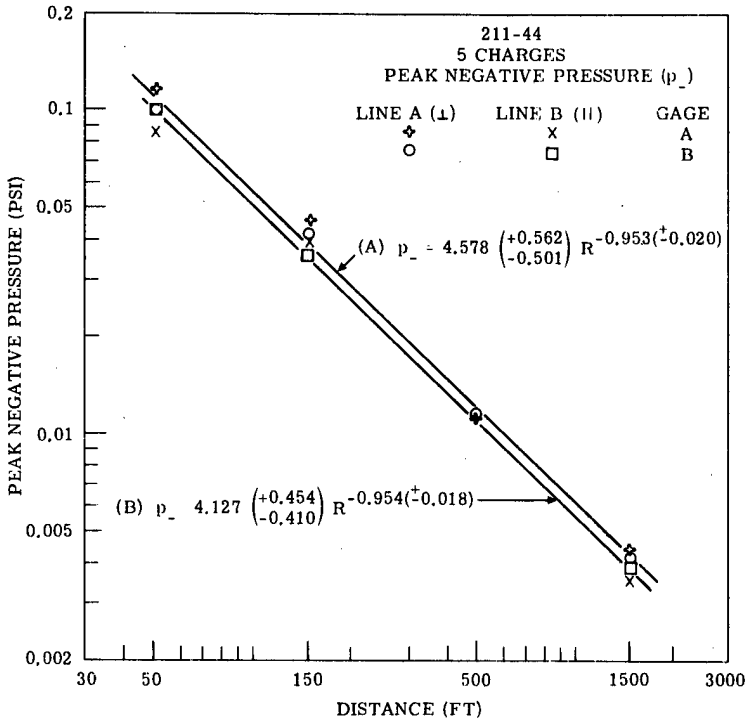

Figure A-42

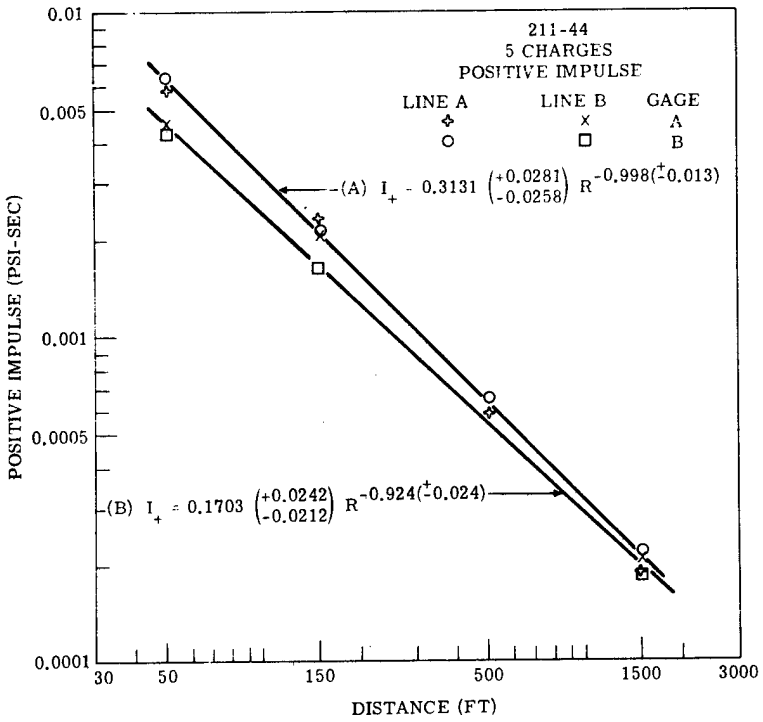

Figure A-43

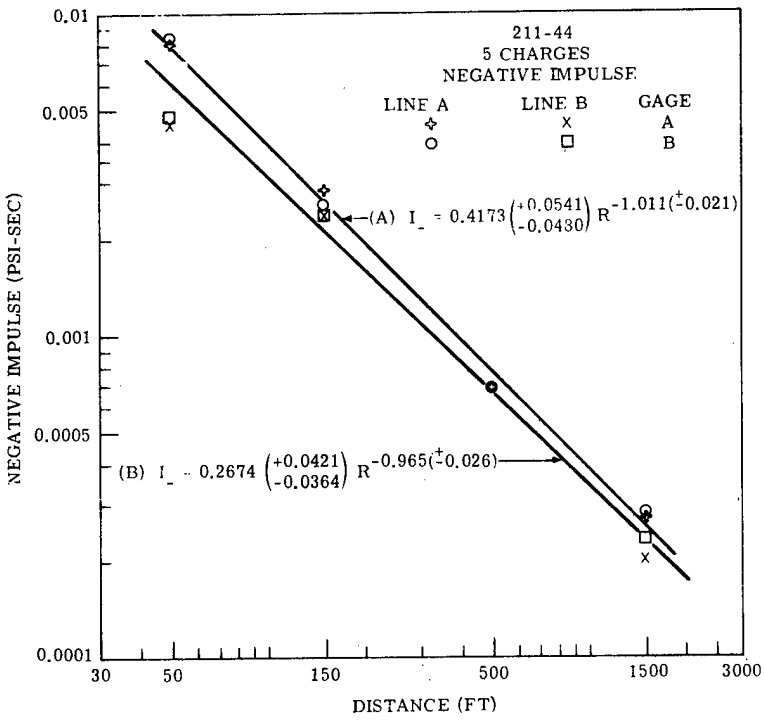

Figure A-44

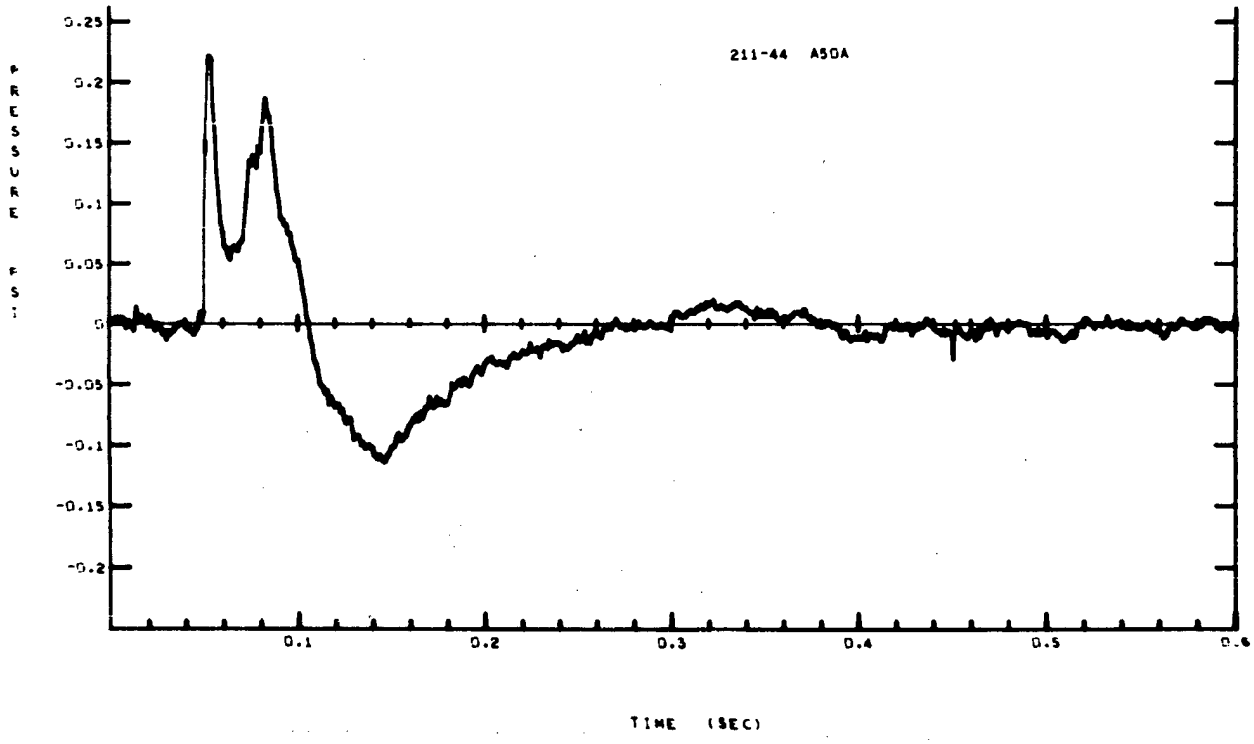

Figure A-45

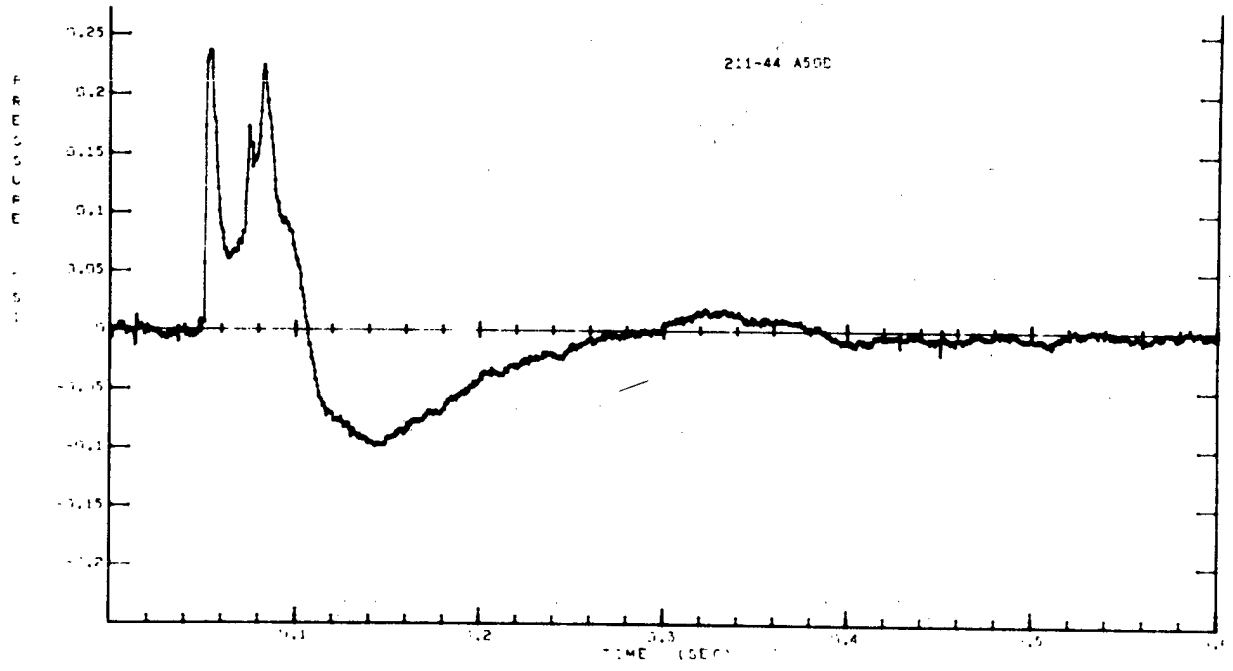

Figure A-46

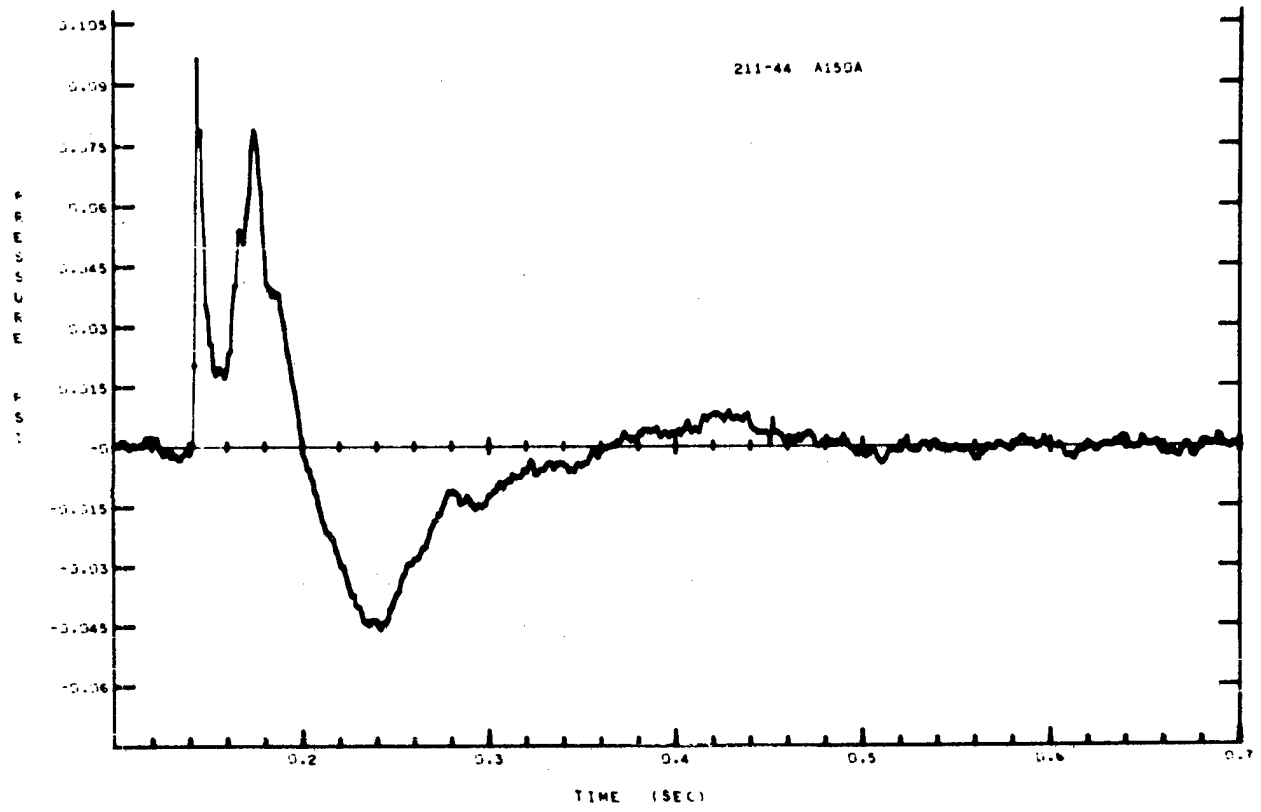

Figure A-47

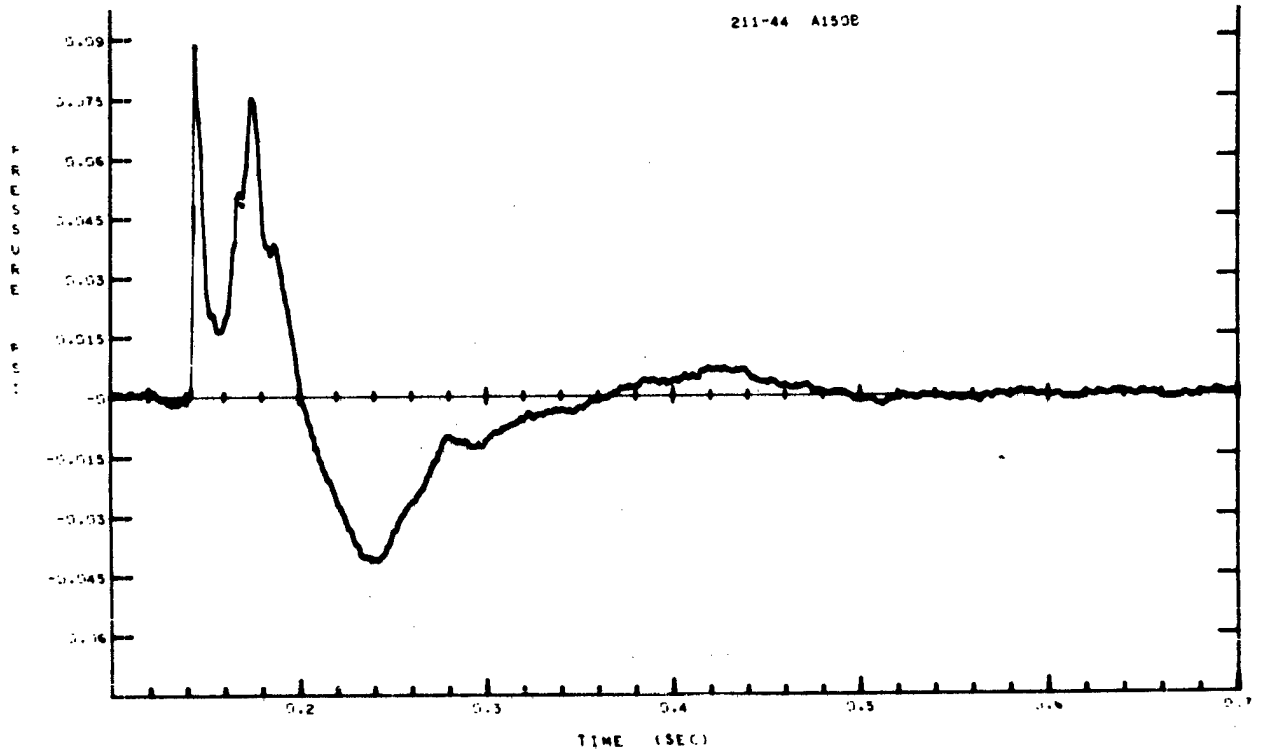

Figure A-48

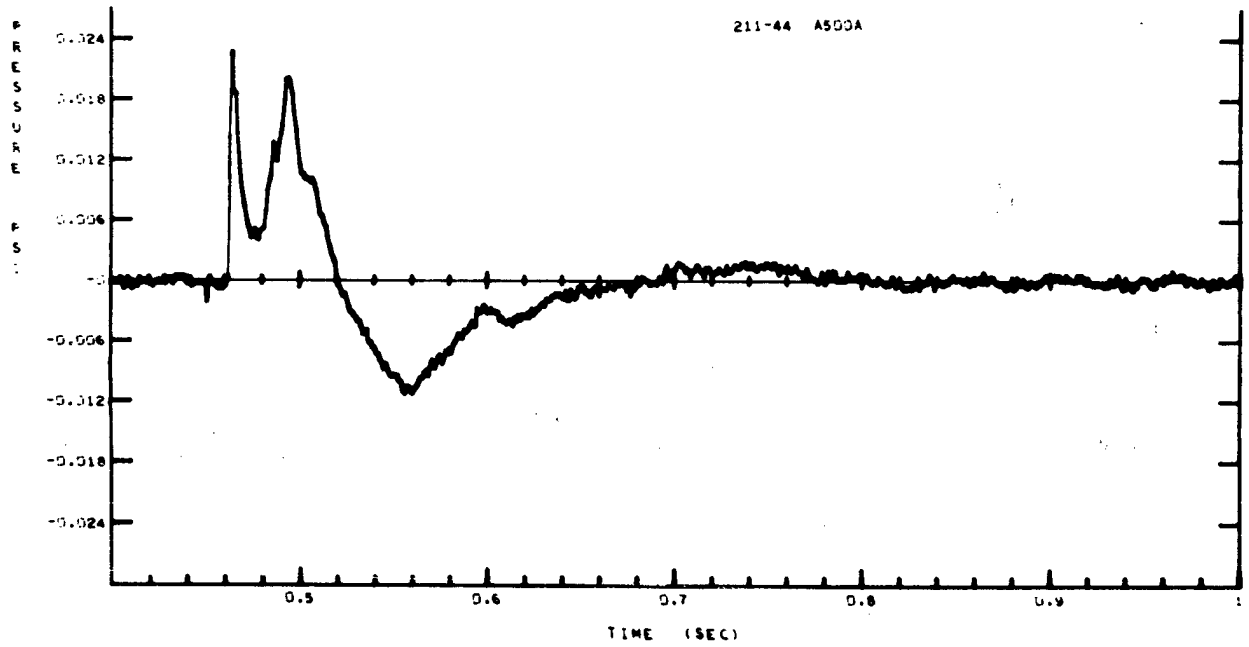

Figure A-49

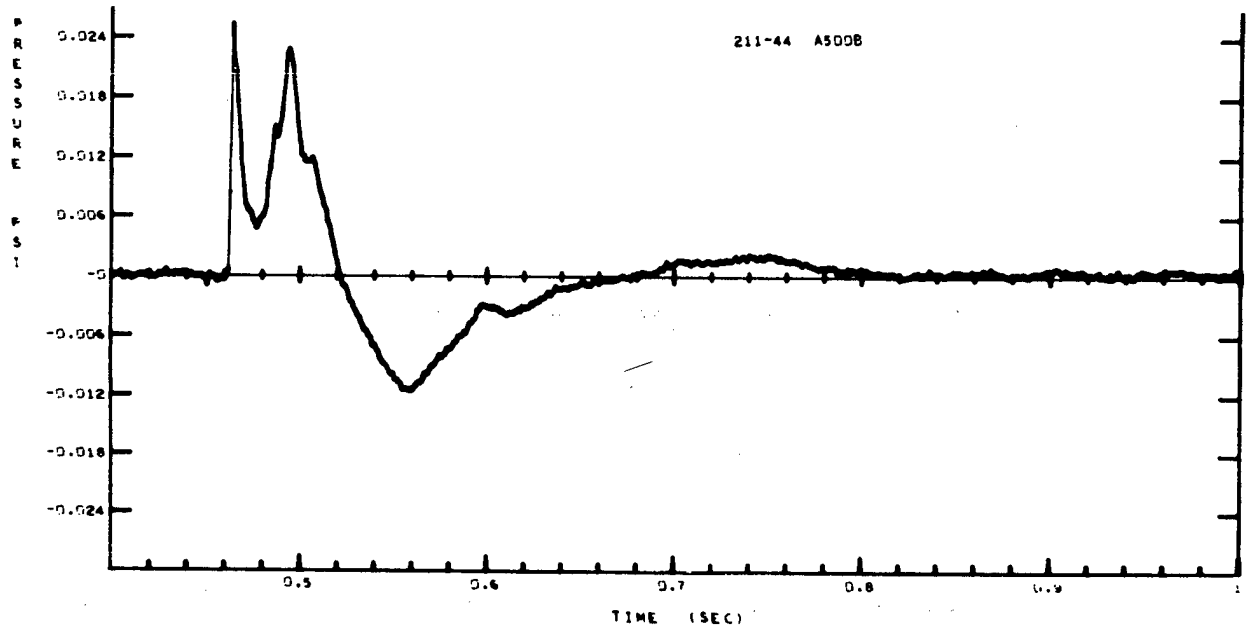

Figure A-50

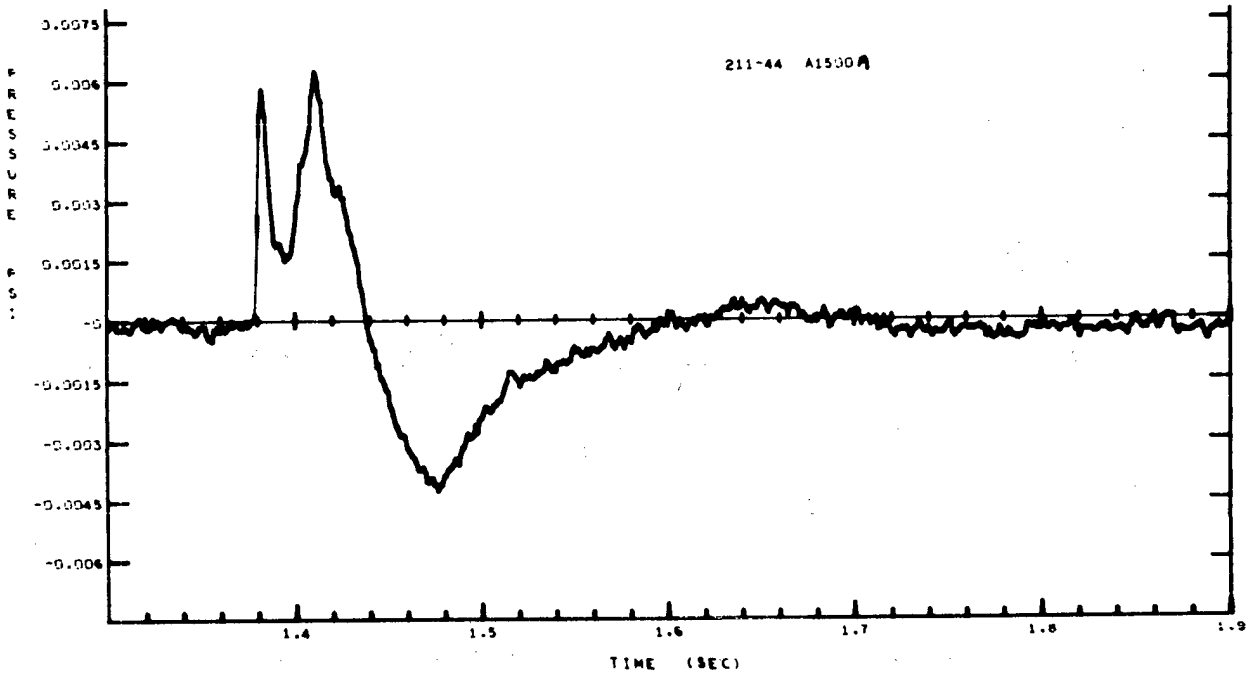

Figure A-51

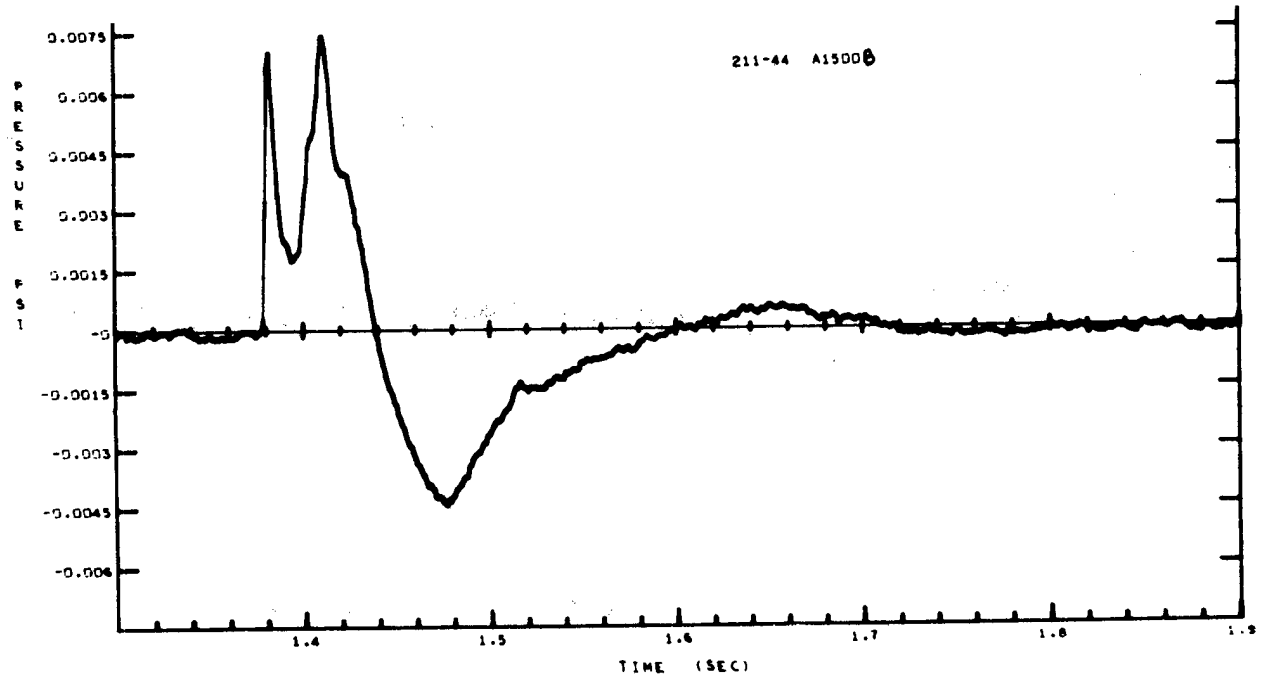

Figure A-52

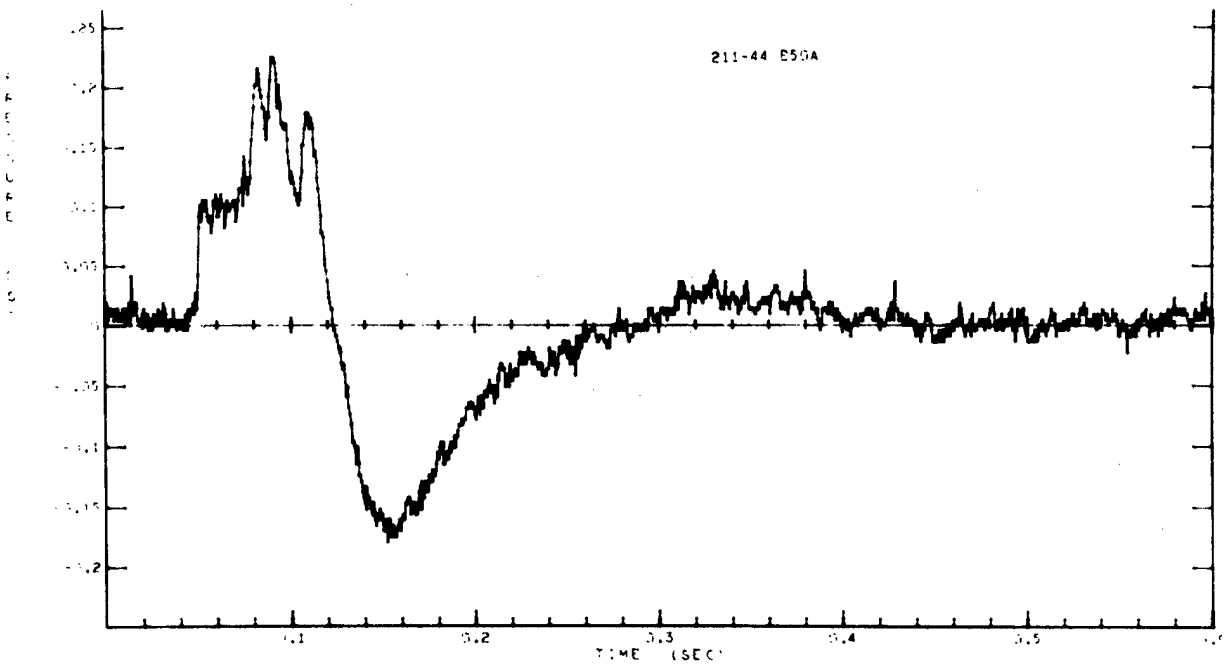

Figure A-53

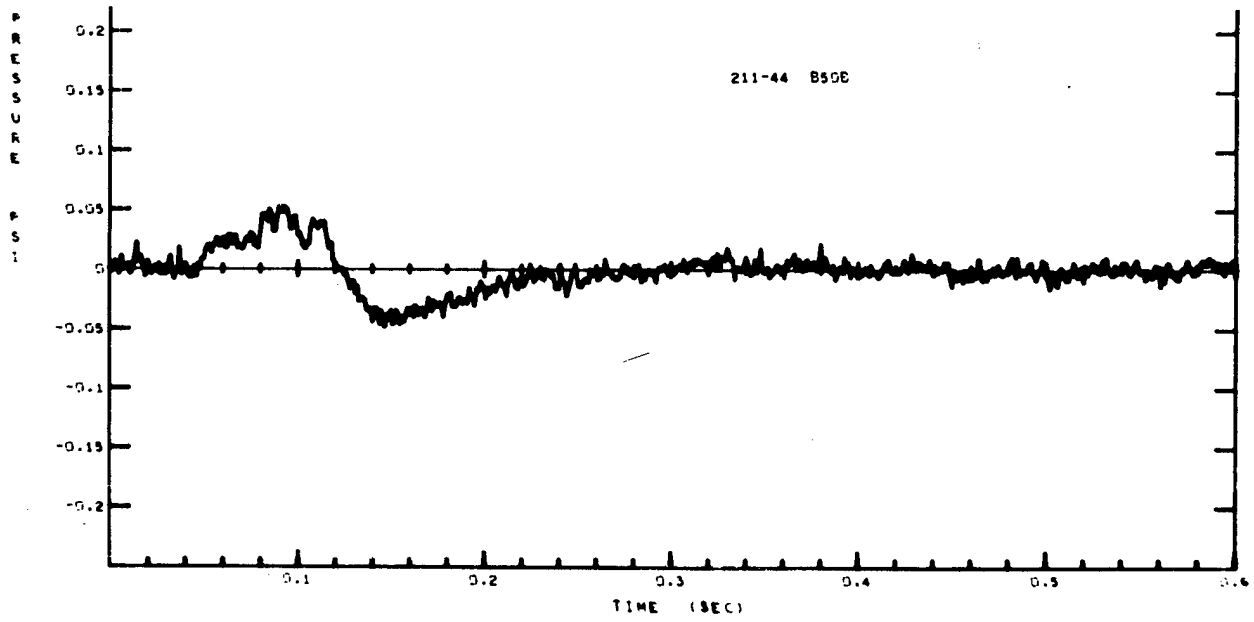

Figure A-54

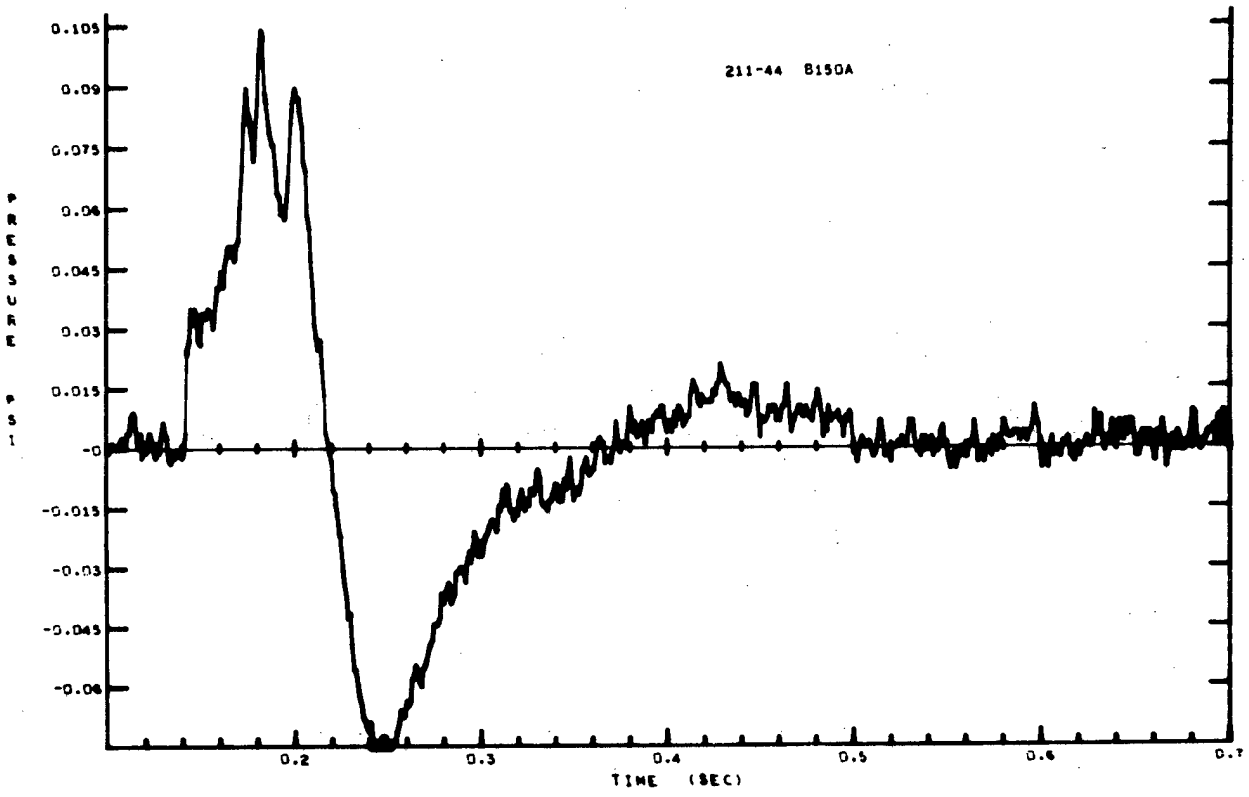

Figure A-55

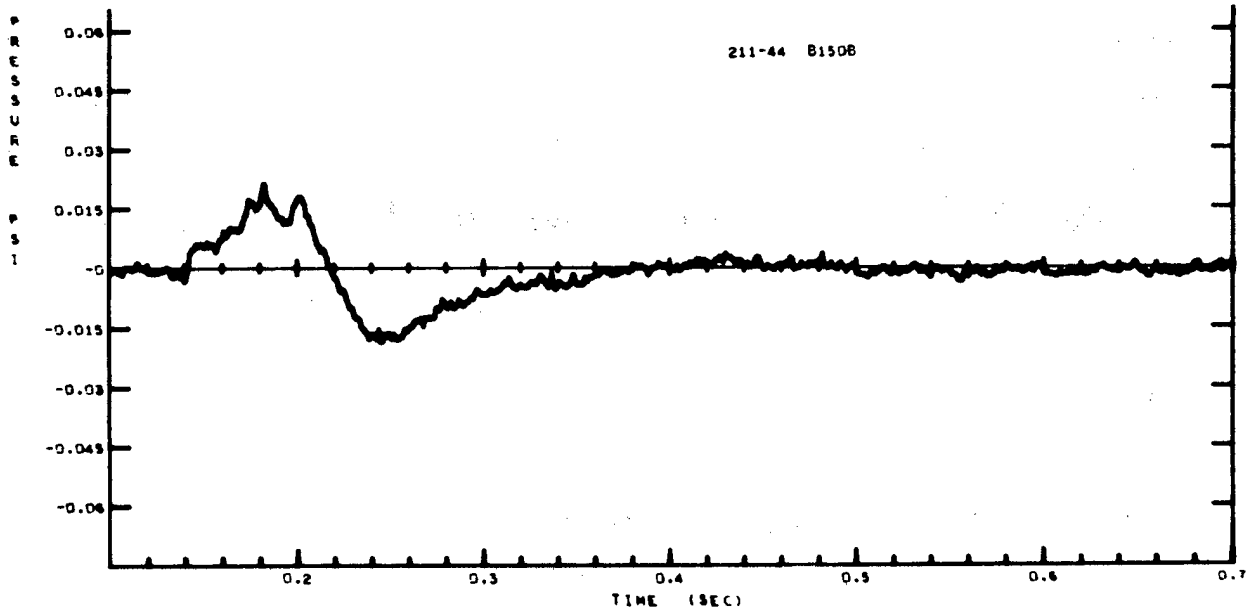

Figure A-56

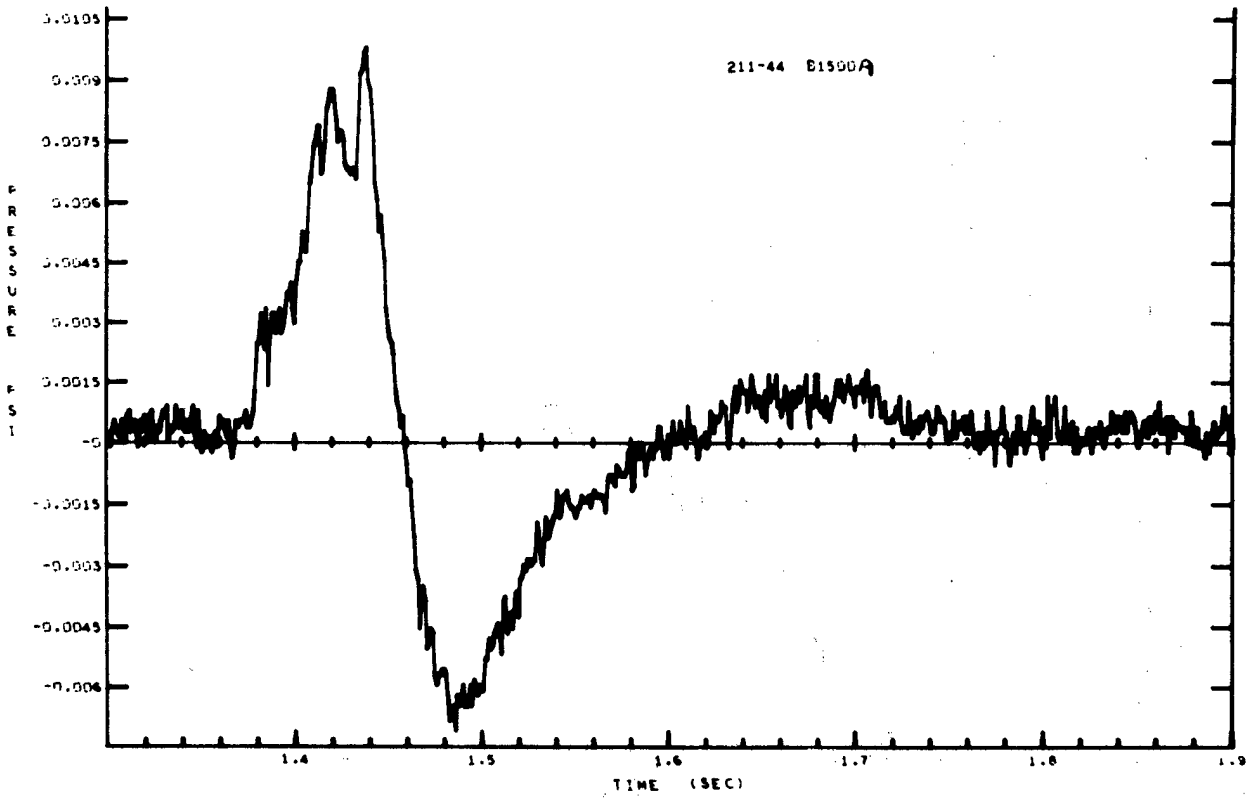

Figure A-57

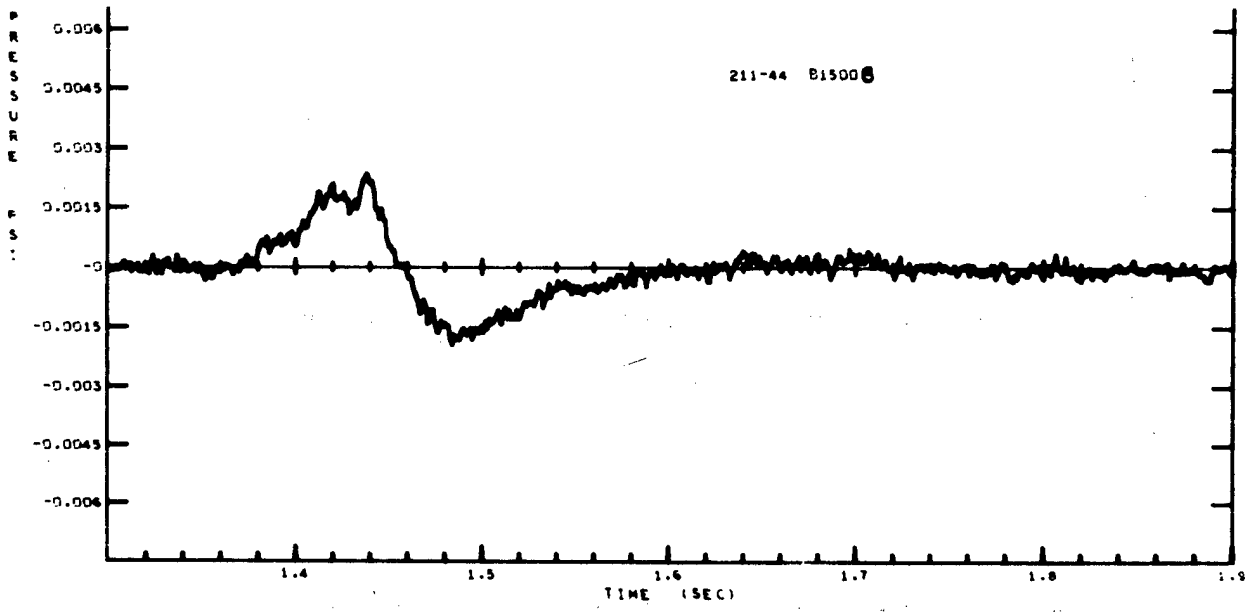

Figure A-58

Shots 211-10, 211-13

Eleven 64-pound charges were buried 6 feet deep, spaced 8 feet apart. There were five blast lines: one perpendicular to center of row (C); one off each end of rows (D,E); and one diagonal between A and C and E and C (B,D), centered on each end charge.

211-10 (Revision)

Station location	Arrival time (sec)	Ground shock induced peak (psi)	Time of peak (sec)	Peak from venting gas (psi)	Time of peak (sec)	Cross-over (sec)	Positive pulse duration (sec)	Maximum negative peak (psi)	Time of peak (sec)	Cross-over (sec)	Negative pulse duration (sec)	First positive impulse (psi-sec)	First negative impulse (psi-sec)
50A	0.048	0.08014	0.052	0.16352	0.080	0.152	0.104	-0.07407	0.182	0.340	0.188	0.00421	0.00603
50B	0.048	0.06335	0.051	0.18330	0.080	0.138	0.090	-0.09709	0.169	0.334	0.196	0.00523	0.00788
50D	0.048	0.08112	0.056	0.18990	0.084	0.133	0.085	-0.12704	0.173	0.340	0.207	0.00637	0.01023
50E	0.048	0.04733	0.058	0.09329	0.080	0.118	0.070	-0.06623	0.173	0.347	0.229	0.00322	0.00473
150A	0.137	0.02426	0.141	0.07653	0.168	0.241	0.104	-0.06226	0.265	0.396	0.155	0.00242	0.00408
150B	0.137	0.02053	0.149	0.06026	0.167	0.228	0.091	-0.04017	0.265	0.402	0.174	0.00235	0.00293
150C	0.136	0.11399	0.139	0.13307	0.169	0.190	0.054	-0.04648	0.225	0.380	0.190	0.00313	0.00326
150D	0.137	0.02394	0.140	0.08047	0.176	0.226	0.089	-0.05671	0.257	0.418	0.192	0.00342	0.00401
150E	0.137	0.01177	0.140	0.04419	0.172	0.240	0.103	-0.04074	0.263	0.420	0.180	0.00210	0.00268
500A	0.448	0.00483	0.450	0.01631	0.480	0.557	0.107	-0.01273	0.581	0.725	0.168	0.00075	0.00082
500B	0.448	0.00646	0.453	0.02283	0.478	0.534	0.086	-0.01836	0.568	0.720	0.186	0.00089	0.00133
500C	0.447	0.04149	0.448	0.05681	0.476	0.502	0.055	-0.02125	0.535	0.678	0.176	0.00129	0.00133
500D	0.449	0.00564	0.458	0.01783	0.485	0.534	0.085	-0.01380	0.569	0.721	0.187	0.00079	0.00103
500E	0.447	0.00353	0.450	0.01502	0.490	0.552	0.105	-0.01446	0.571	0.724	0.172	0.00081	0.00105
1500A	1.338	0.00133	1.343	0.00646	1.369	1.448	0.110	-0.00645	1.474	1.624	0.176	0.00033	0.00045
1500B	1.332			0.00508	1.363	1.422	0.090	-0.00418	1.464	1.609	0.187	0.00024	0.00035
1500C	1.332		1.338	0.01364	1.365	1.394	0.062	-0.00623	1.430	1.598	0.204	0.00035	0.00045
1500E	1.332	0.00125	1.356	0.00273	1.378	1.440	0.108	-0.00290	1.467	1.612	0.172	0.00016	0.00020

211-13

Gage	Arrival time (sec)	Ground shock induced peak (psi)	Time of peak (sec)	Peak from venting gas (psi)	Time of peak (sec)	Cross-over (sec)	Positive phase impulse (psi-sec)	Negative peak (psi)	Time of peak (sec)	Cross-over (sec)	Negative phase impulse (psi-sec)
50A	0.054	0.06536	0.060	0.12578	0.090	0.135	0.00602	-0.08871	0.168	0.338	0.00715
50B	0.054	0.07351	0.059	0.14957	0.084	0.129	0.00644	-0.10129	0.175	0.337	0.00825
50C	0.053	0.29205	0.058	0.46389	0.080	0.110	0.0135	-0.22107	0.151	0.306	0.0173
50D	0.053	0.08734	0.055	0.23134	0.101	0.129	0.00757	-0.11751	0.168	0.307	0.00929
50E	0.053	0.06481	0.057	0.19950	0.109	0.128	0.00643	-0.11693	0.182	0.308	0.00945
150A	0.141	0.02070	0.213	0.06142	0.213	0.228	0.00297	-0.03989	0.286	0.437	0.00323
150B	0.142	0.02897	0.150	0.09633	0.201	0.226	0.00366	-0.05612	0.272	0.418	0.00435
150C	0.143	0.10716	0.147	*	0.147	0.201	0.00435	-0.07471	0.235	0.386	0.00532
150D	0.142	0.03035	0.154	0.11181	0.190	0.226	0.00372	-0.05655	0.272	0.417	0.00416
150E	0.142	0.01649	0.148	0.07888	0.201	0.232	0.00278	-0.04485	0.271	0.437	0.00354
500A	0.464	0.00697	0.471	0.02209	0.532	0.546	0.00102	-0.01578	0.602	0.738	0.00122
500B	0.464	0.00675	0.468	0.03072	0.516	0.547	0.00110	-0.01716	0.584	0.741	0.00125
500C	0.461	0.03443	0.464	*	0.490	0.517	0.00130	-0.02054	0.550	0.722	0.00145
500D	0.464	0.00849	0.472	0.03391	0.510	0.544	0.00111	-0.0184	0.583	0.747	0.00144
500E	0.464	0.00478	0.469	0.02695	0.519	0.561	0.00099	-0.01462	0.601	0.747	0.00111
1500A	1.373	0.00165	1.300	0.00752	1.440	1.467	0.00033	-0.00553	1.526	1.650	0.000431
1500B	1.372	0.00238	1.376	0.01212	1.442	1.456	0.000429	-0.00668	1.498	1.646	0.000520
1500D	1.375	0.00302	1.384	0.01310	1.418	1.458	0.00044	-0.00636	1.490	1.649	0.000523
1500E	1.378	0.00188	1.391	0.00695	1.431	1.470	0.000258	-0.00440	1.526	1.686	0.000333

*Limited

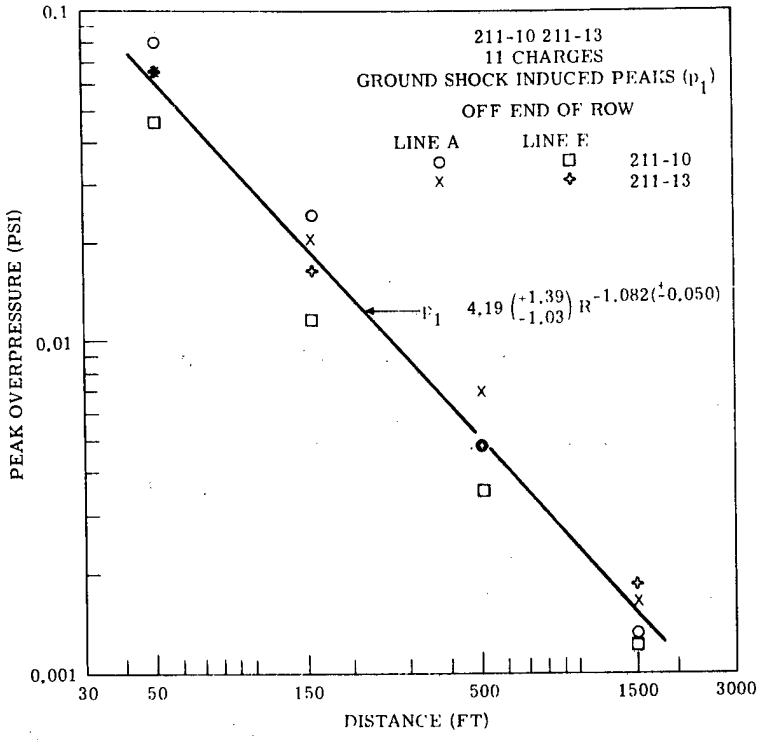

Figure A-59.

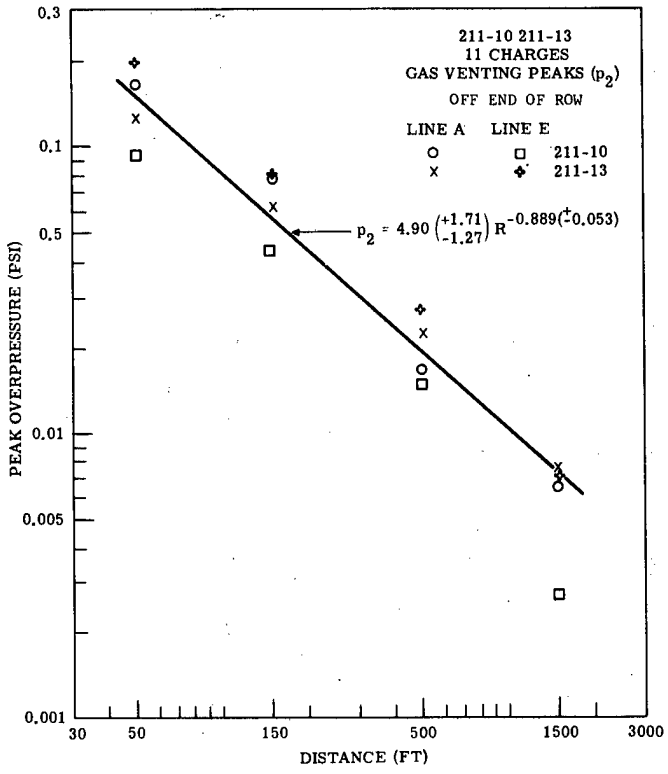

Figure A-60.

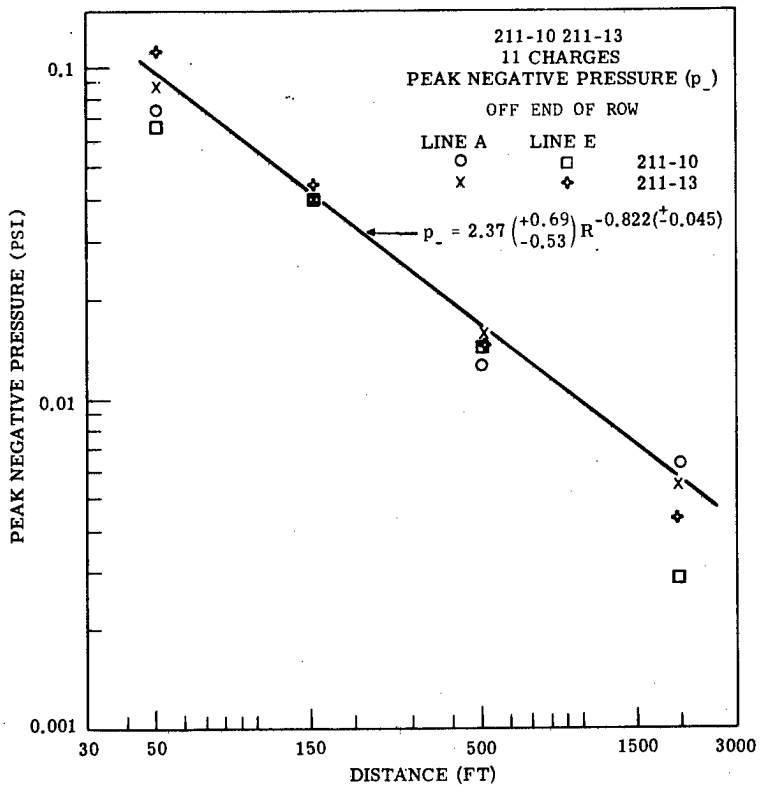

Figure A-61.

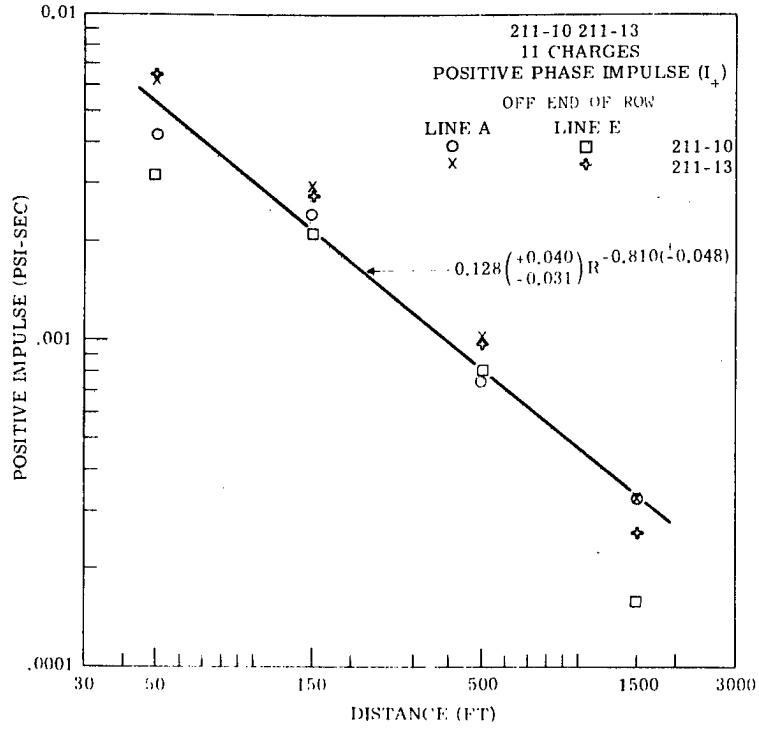

Figure A-62.

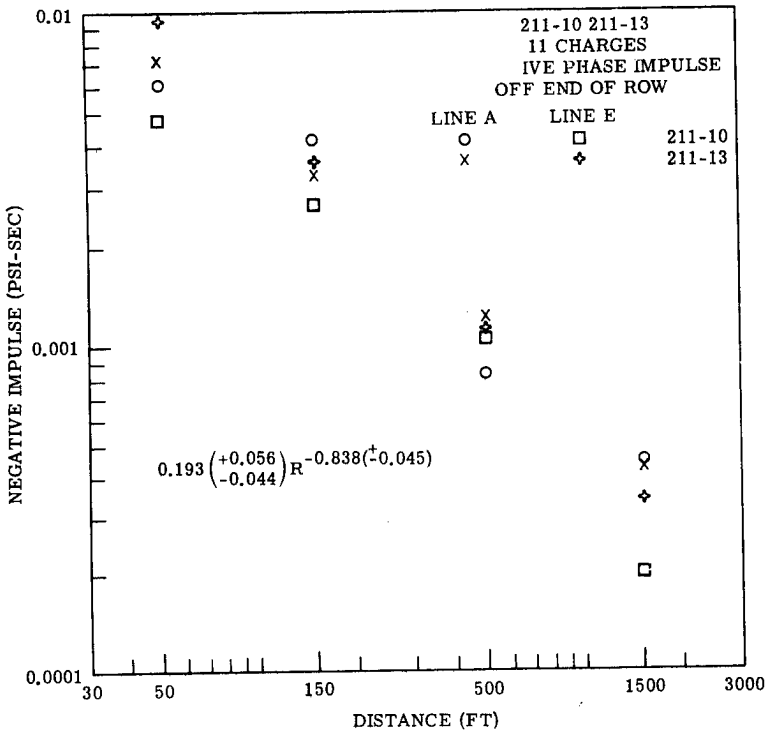
211-10 211-13
11 CHARGES
IVE PHASE IMPULSE
OFF END OF ROW
LINE A
LINE E
211-10
211-13
0.193 (+0.056 / -0.044) R^-0.838(±0.045)
NEGATIVE IMPULSE (PSI-SEC)
0.01
0.001
0.0001
30
50
150
500
1500
3000
DISTANCE (FT)

Figure A-63.

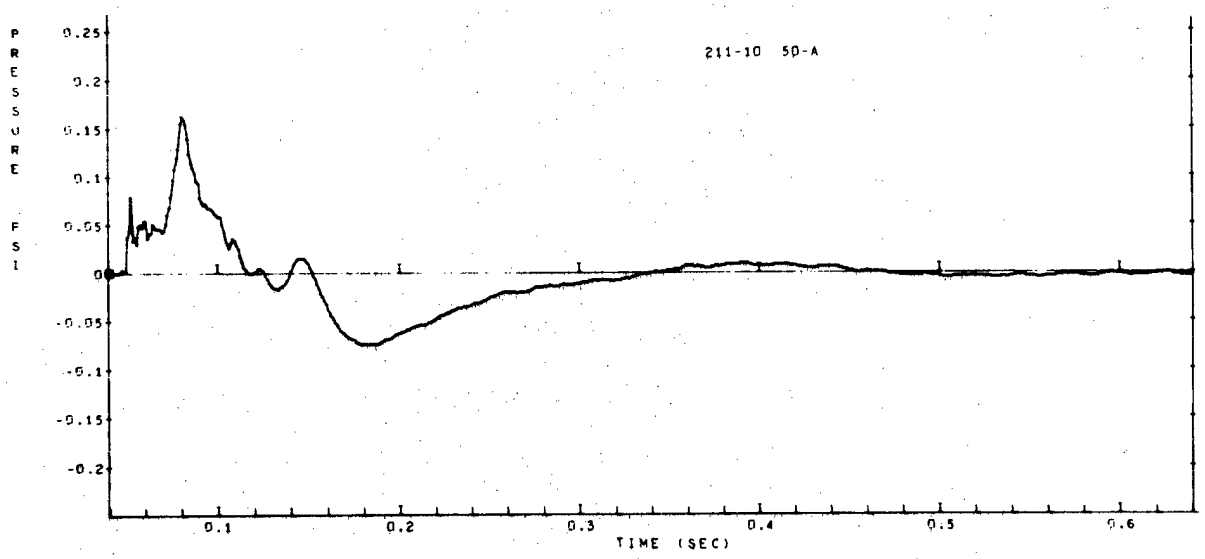

Figure A-64

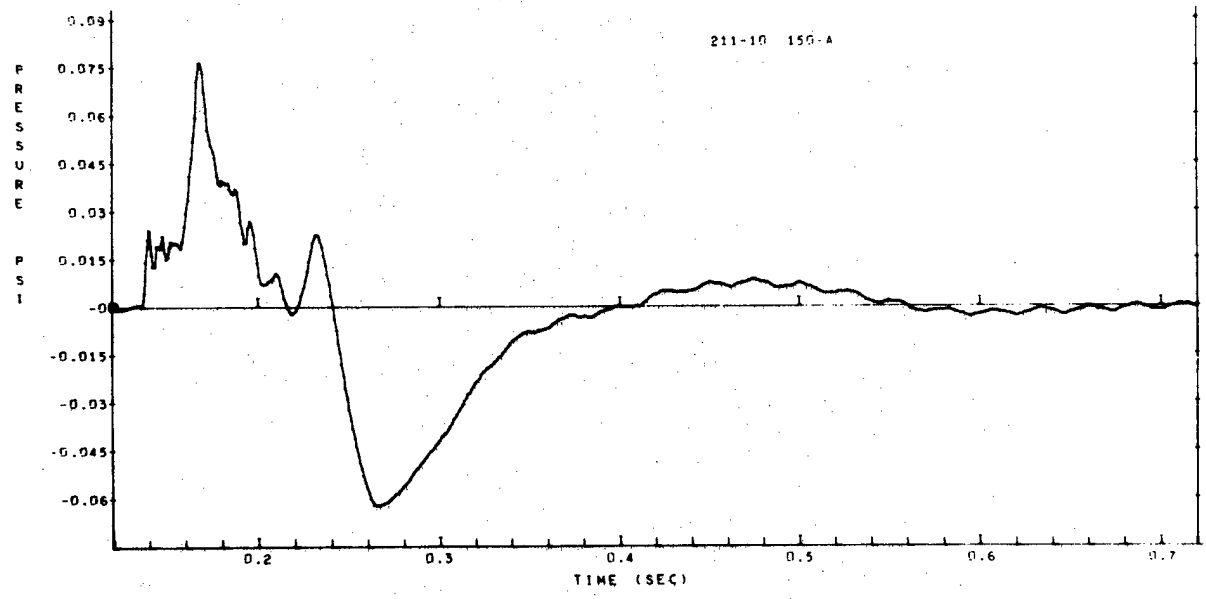

Figure A-65

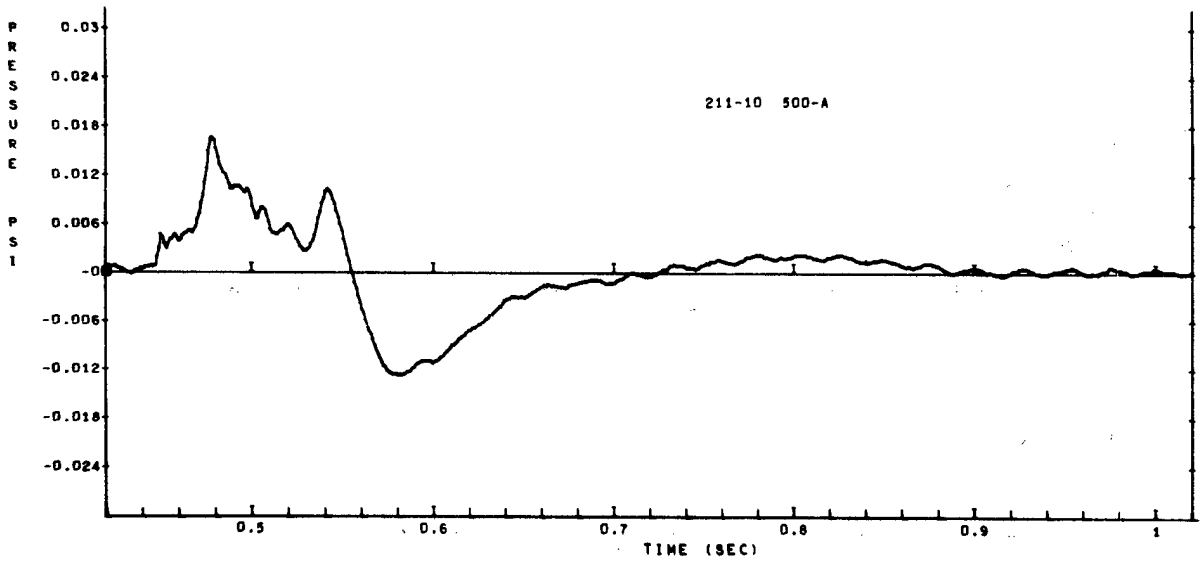

Figure A-66

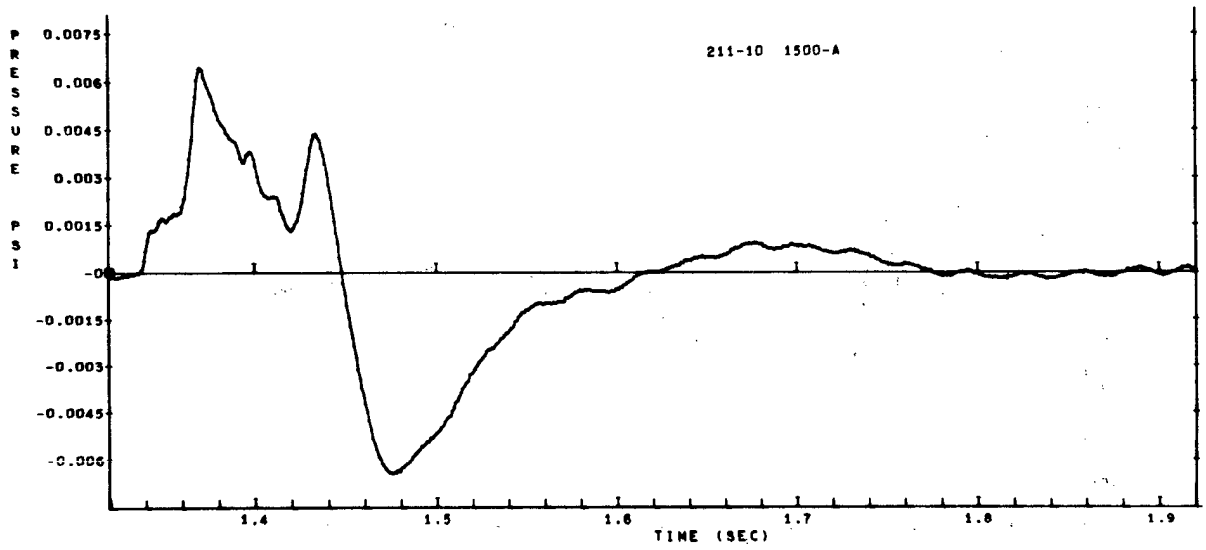

Figure A-67

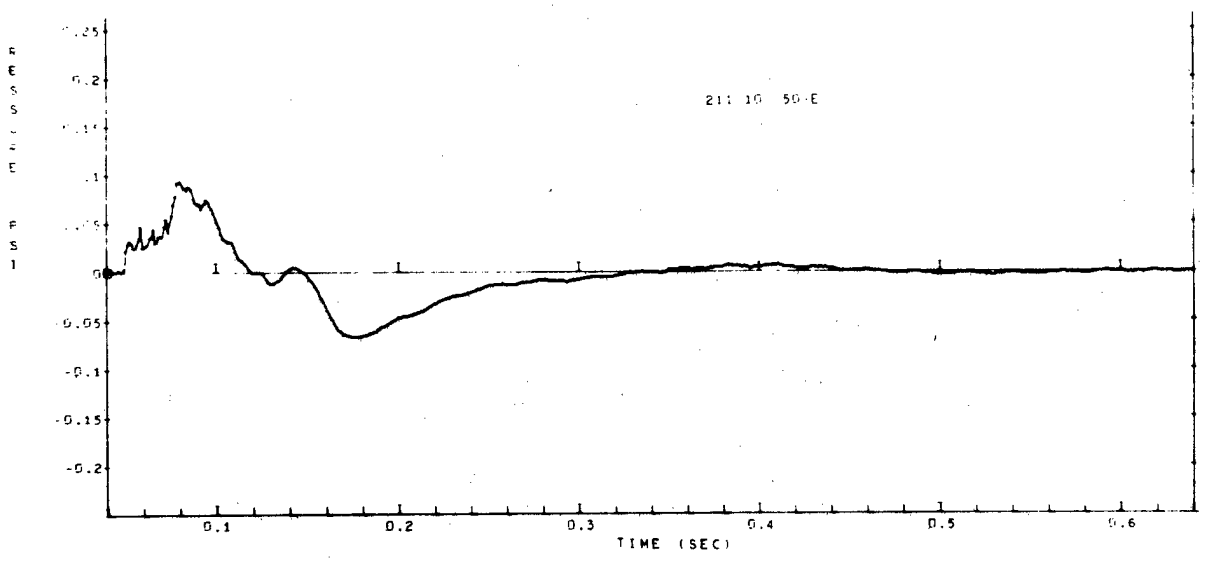

Figure A-68

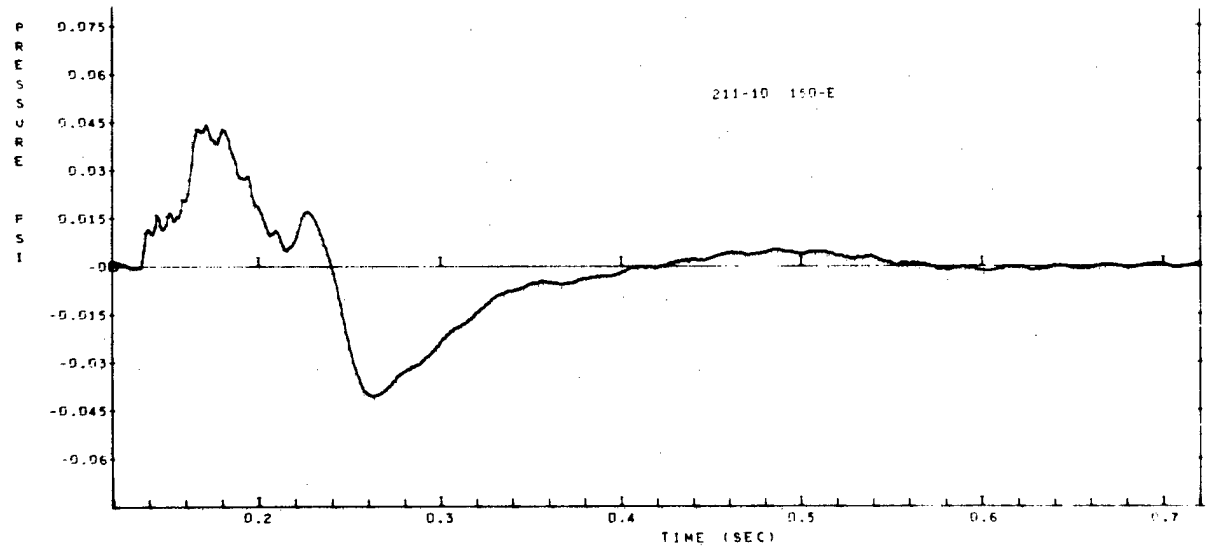

Figure A-69

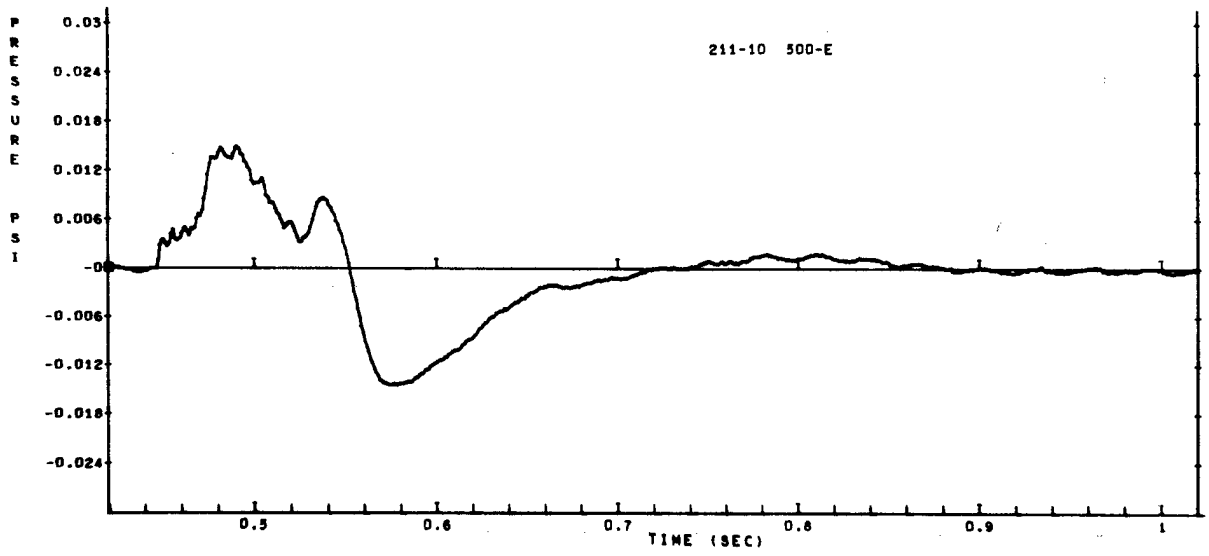

Figure A-70

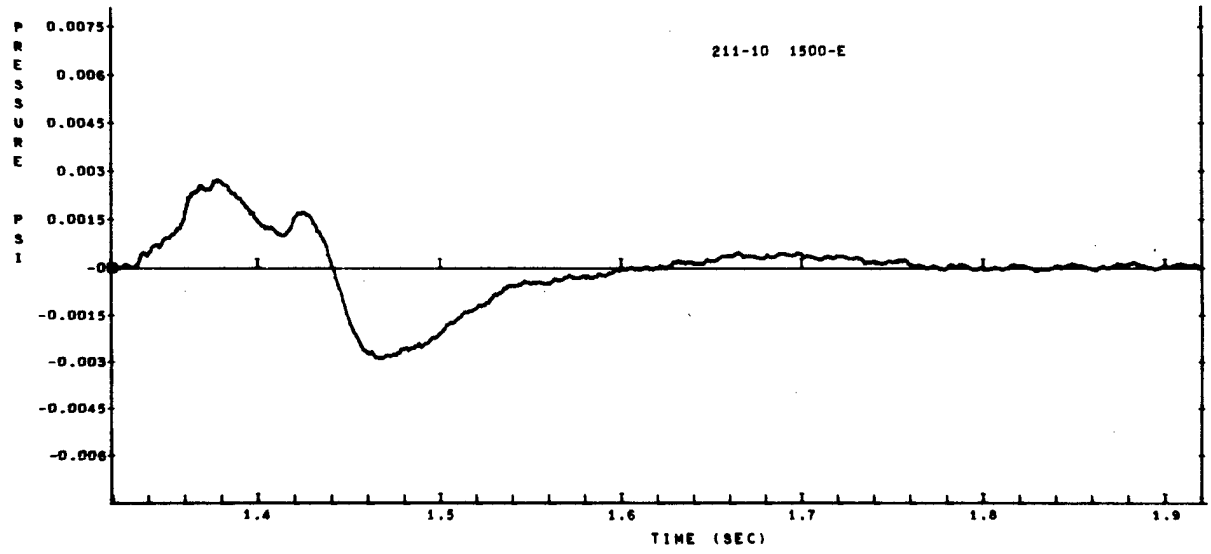

Figure A-71

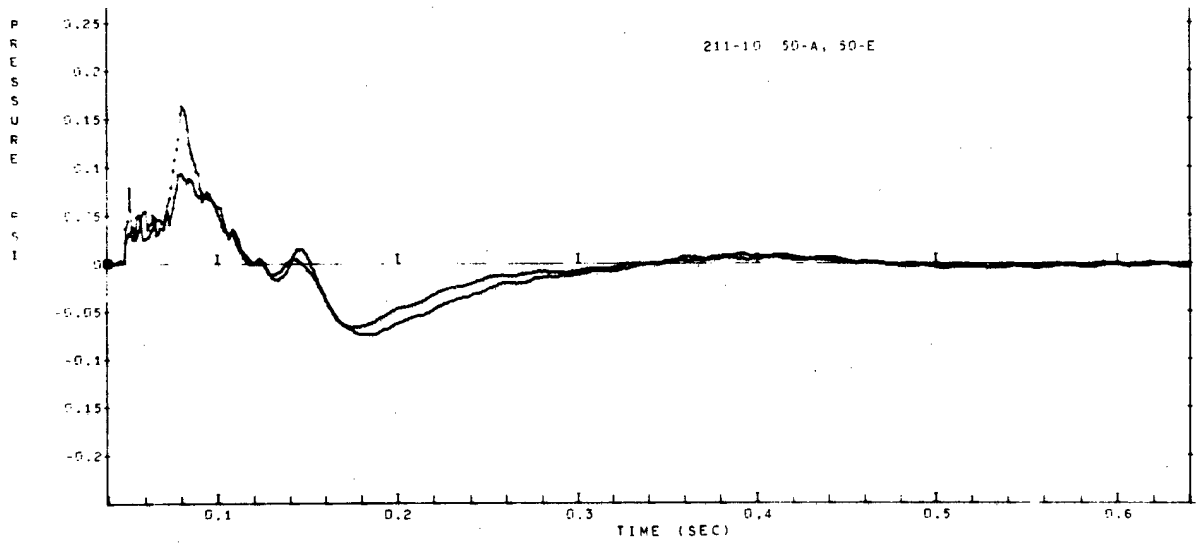

Figure A-72

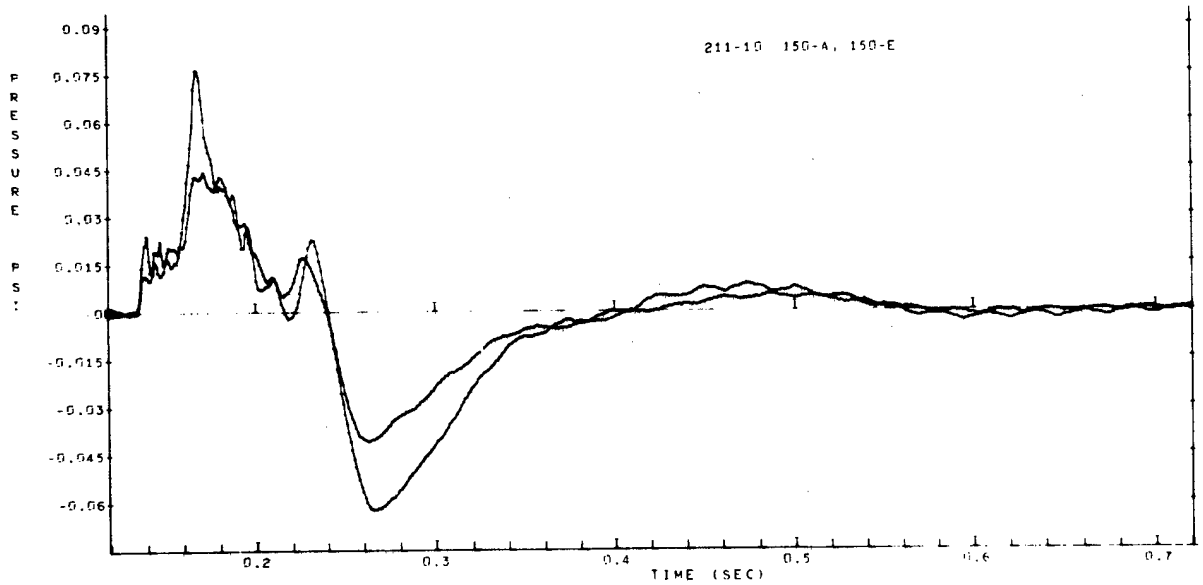

Figure A-73

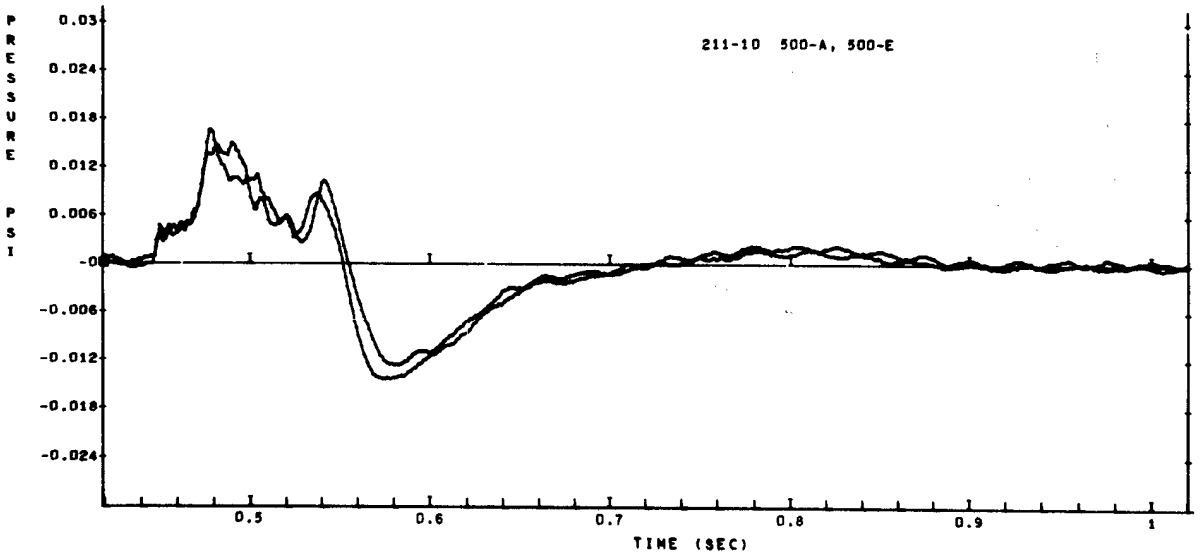

Figure A-74

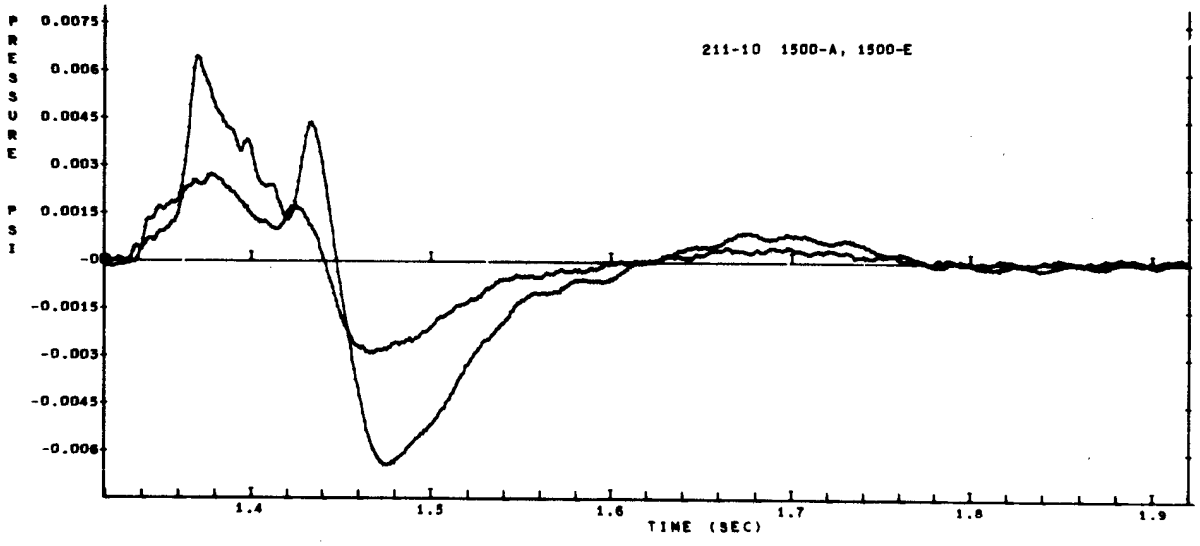

Figure A-75

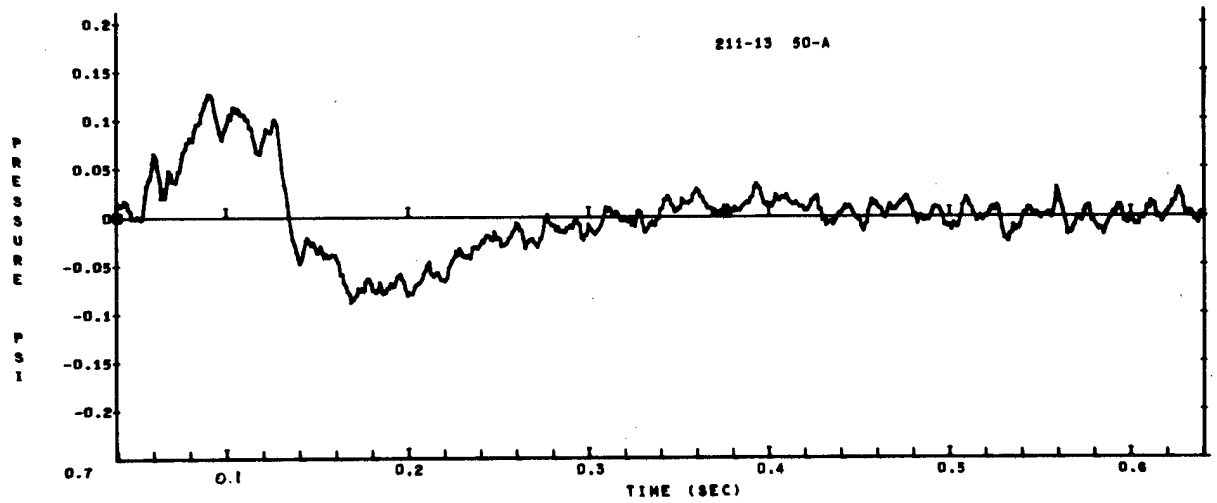

Figure A-76

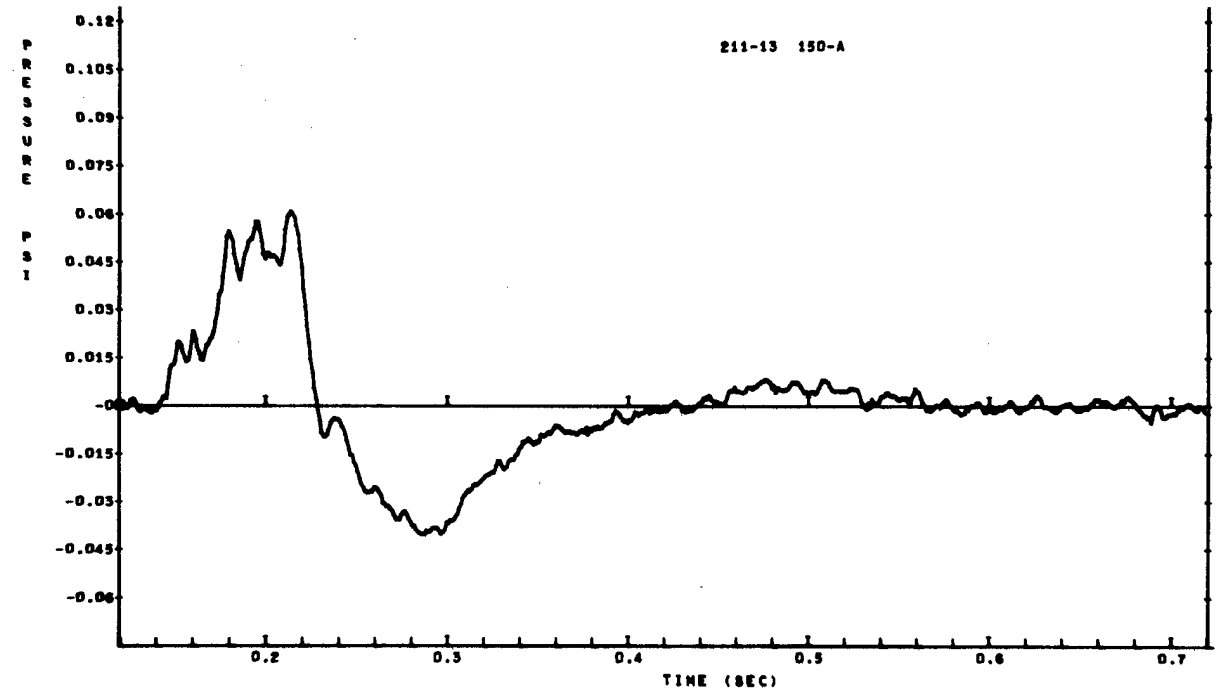

Figure A-77

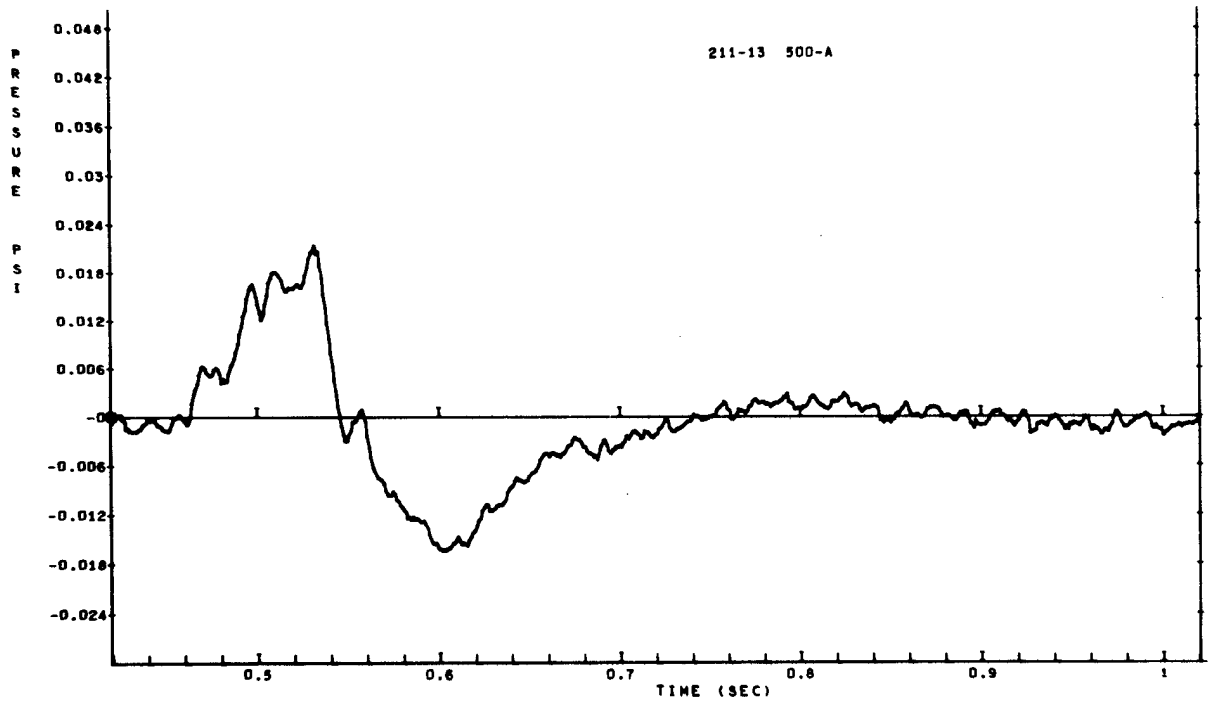

Figure A-78

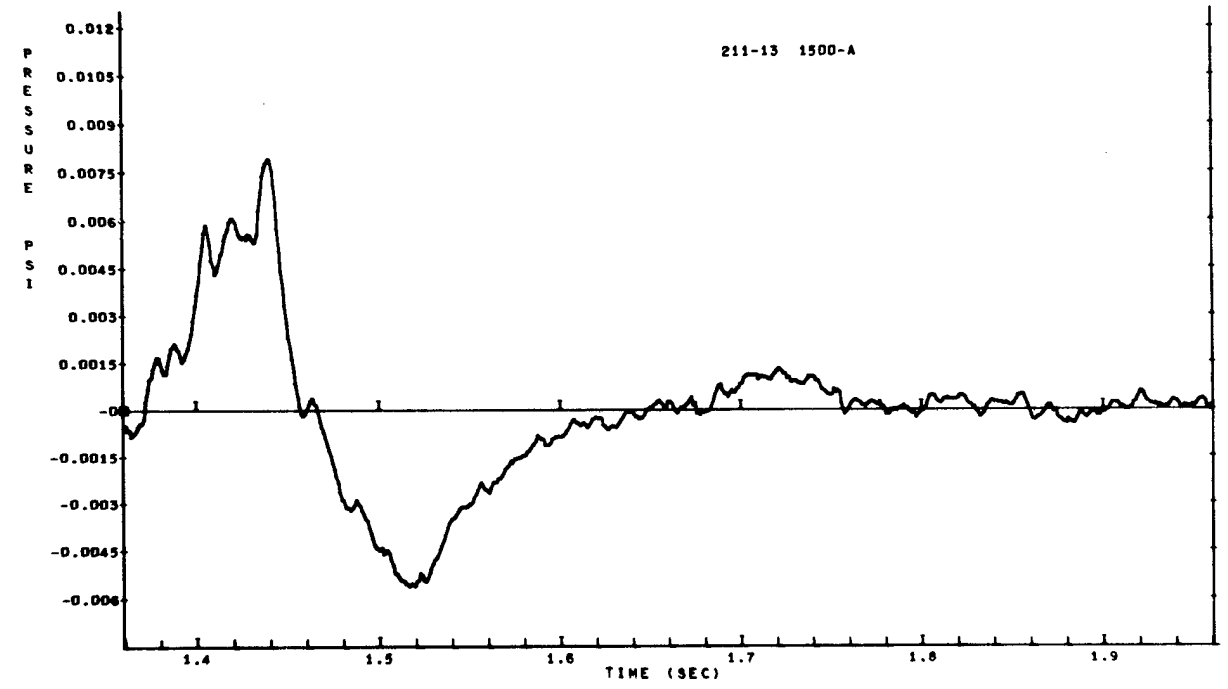

Figure A-79

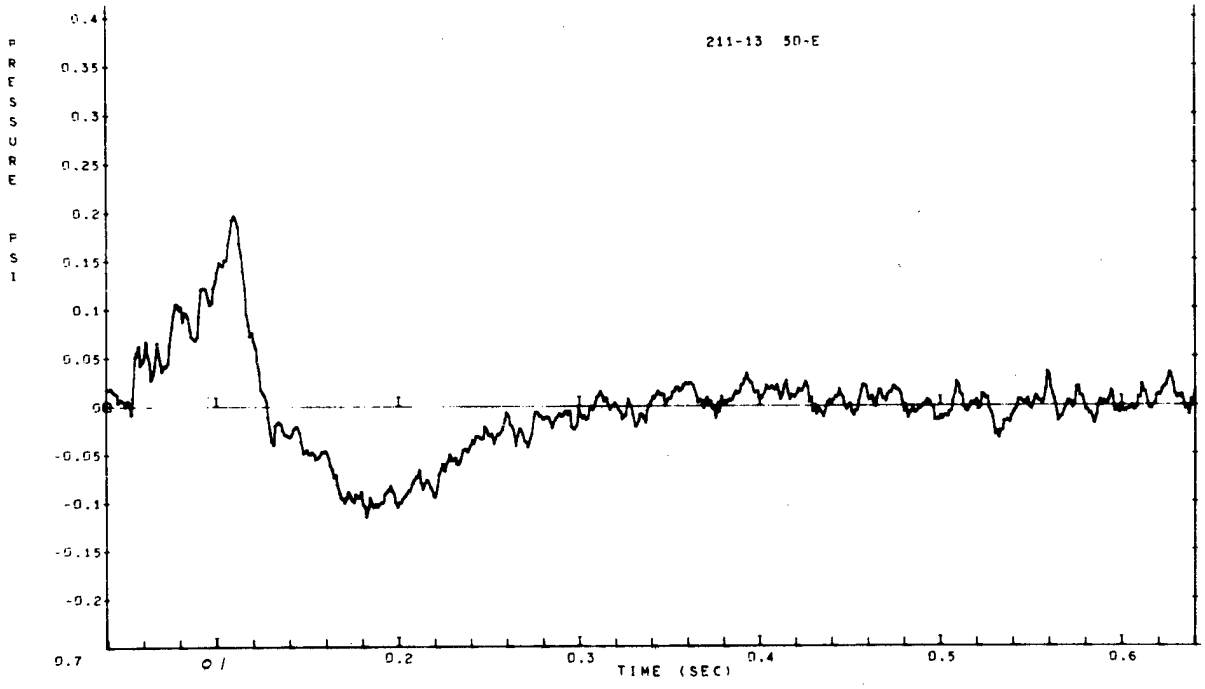

Figure A-80

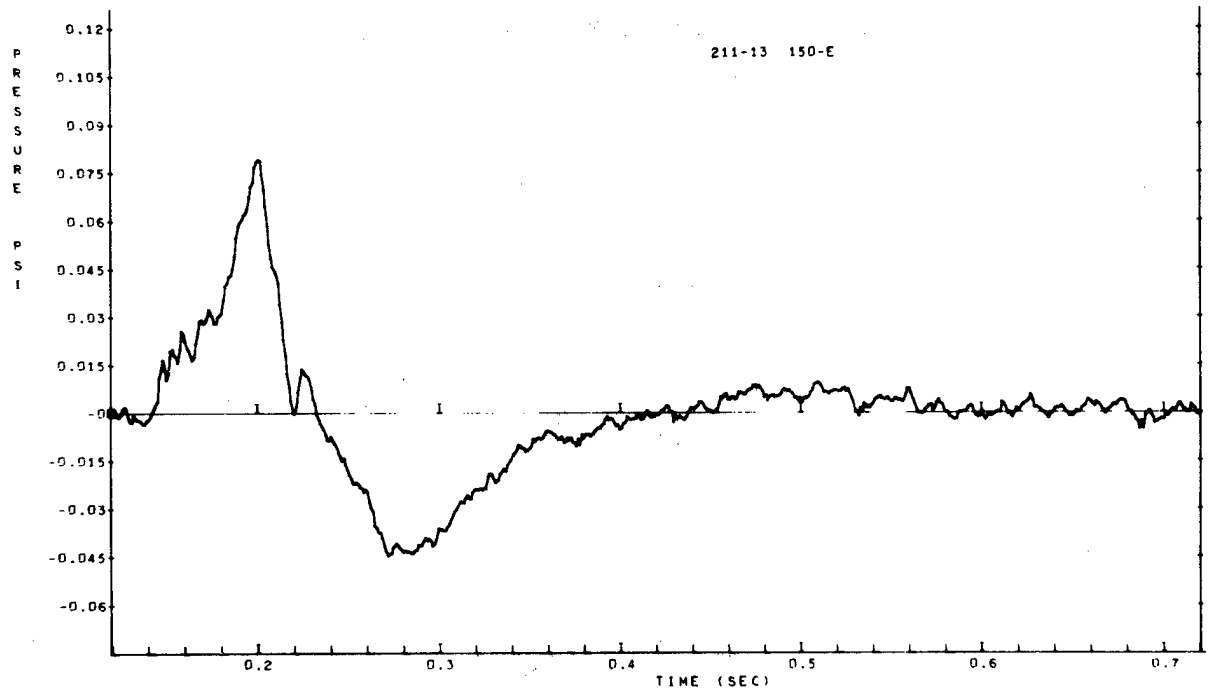

Figure A-81

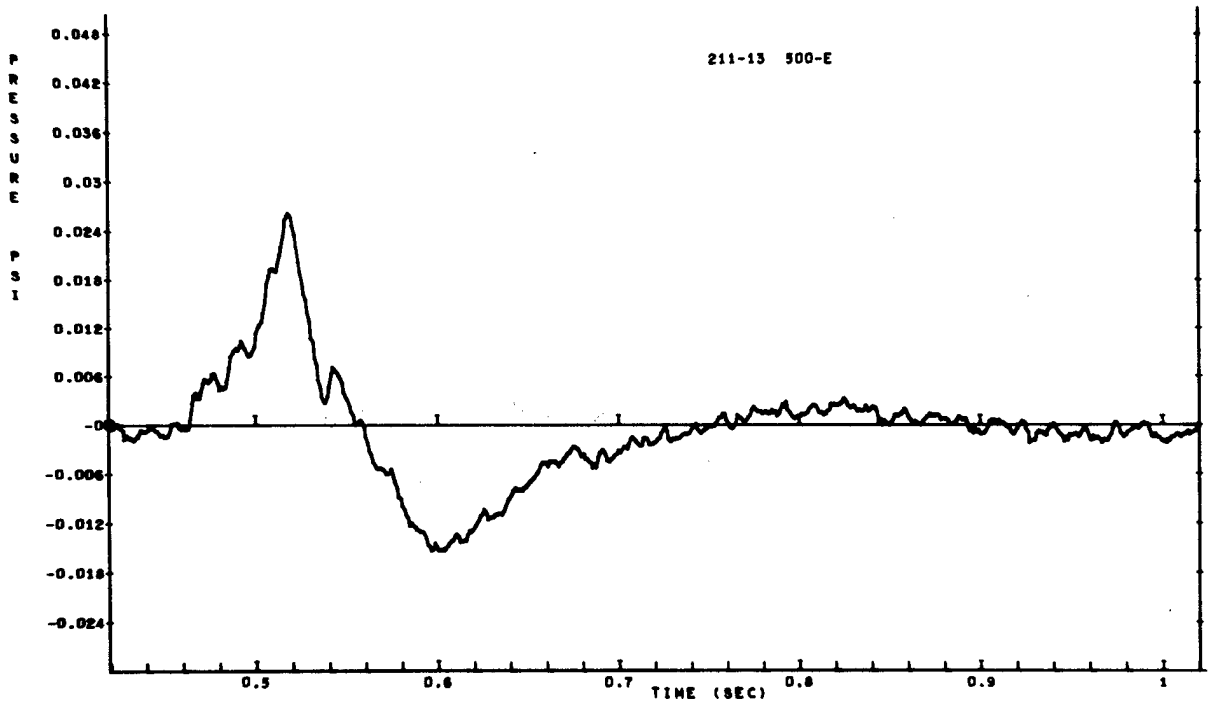

Figure A-82

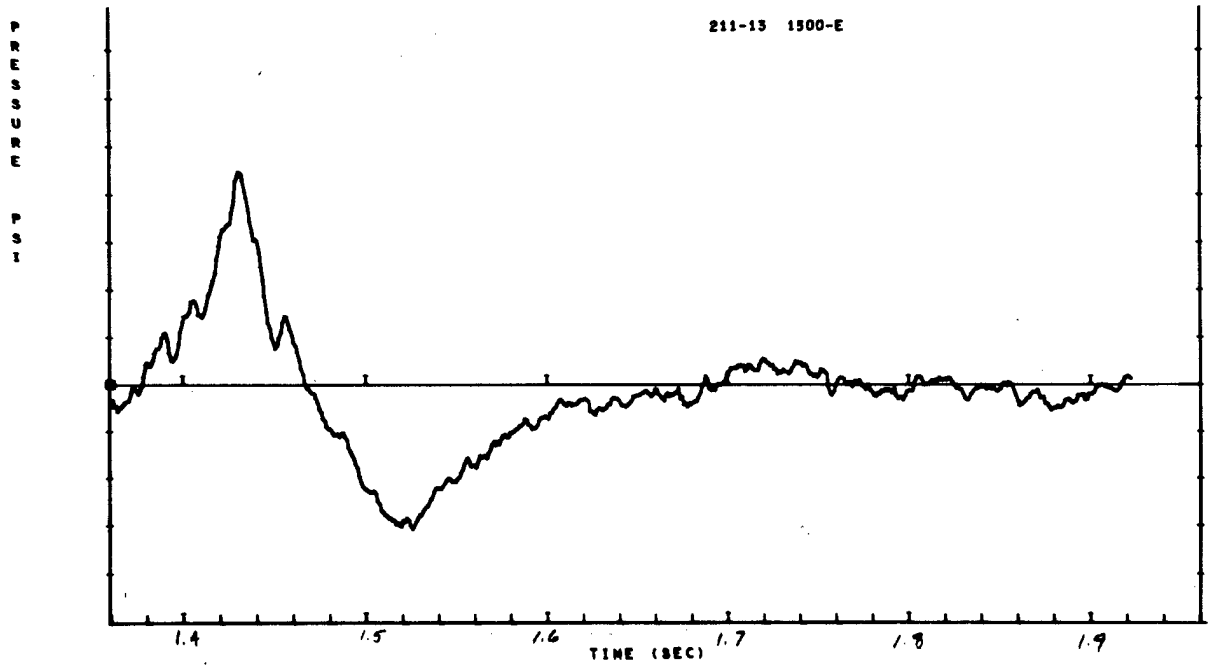

Figure A-83

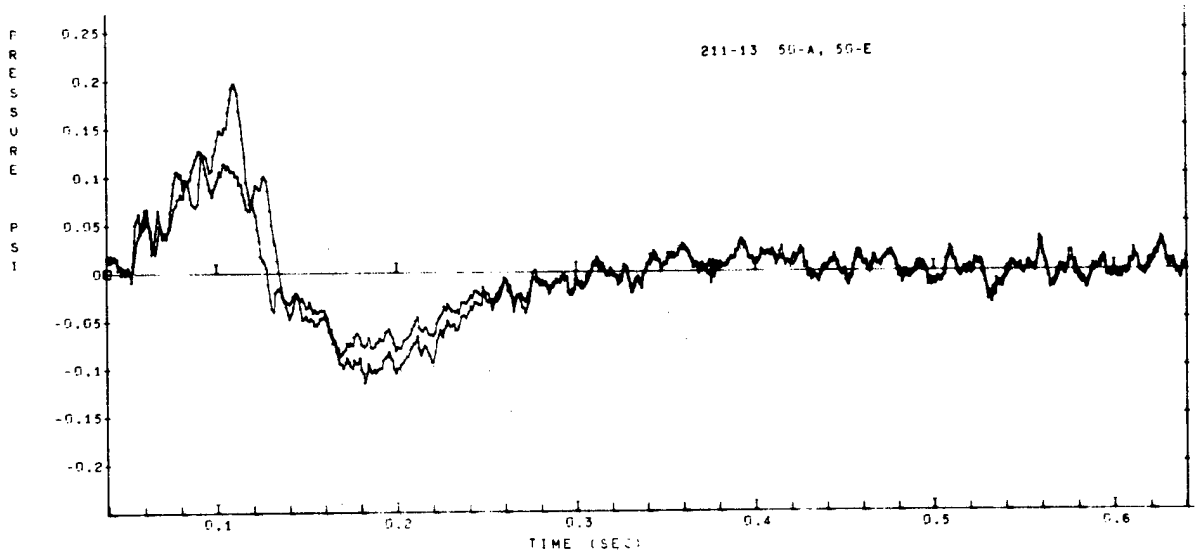

Figure A-84

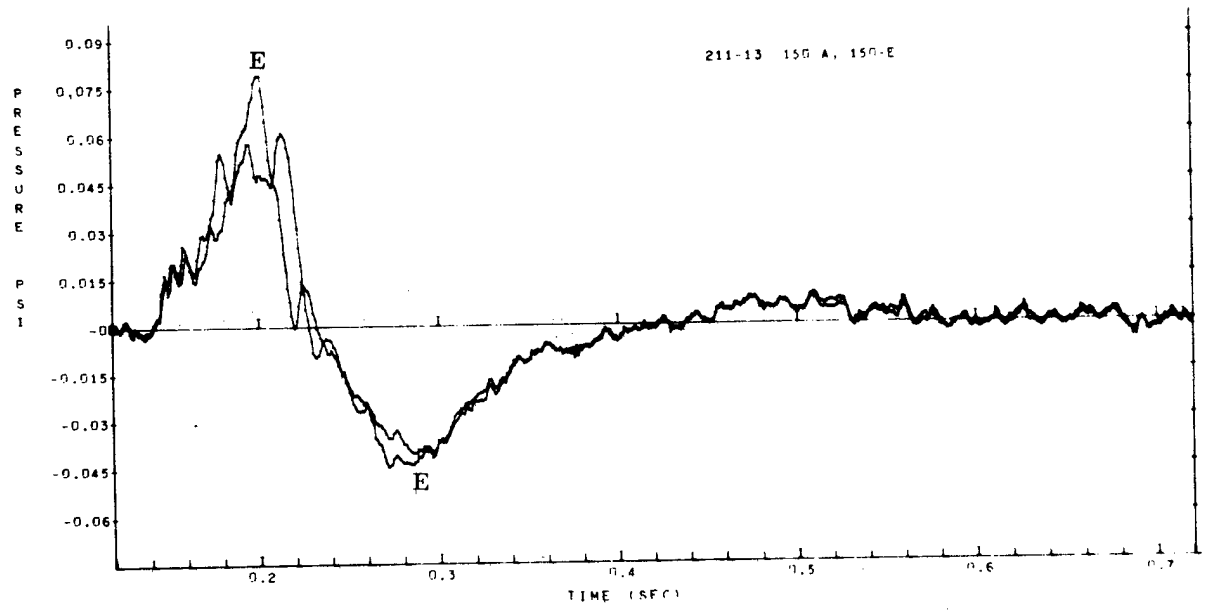

Figure A-85

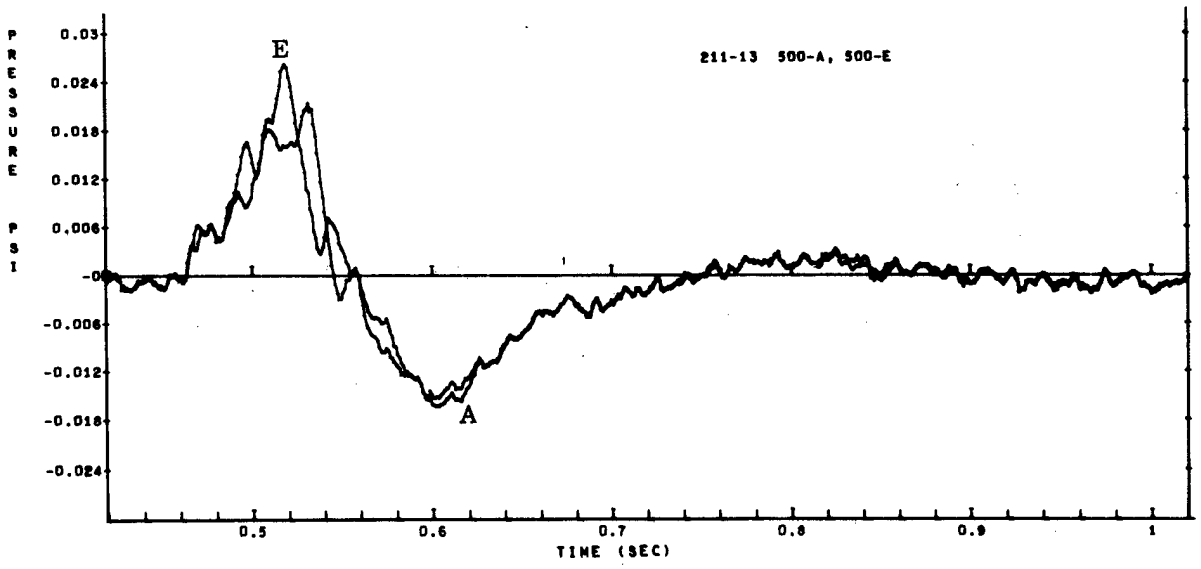

Figure A-86

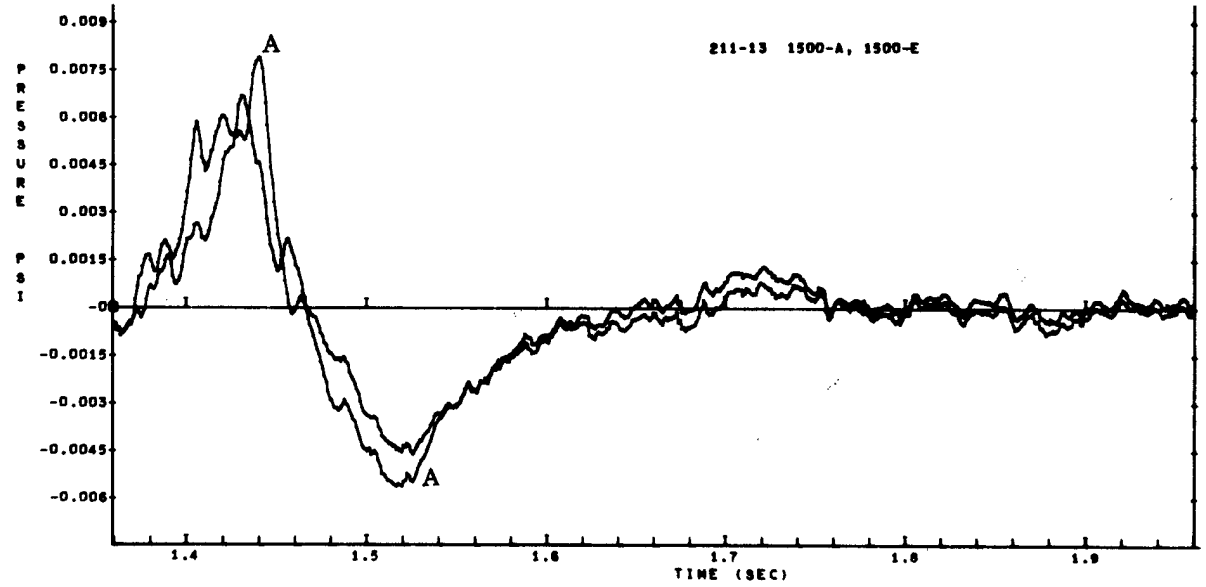

Figure A-87

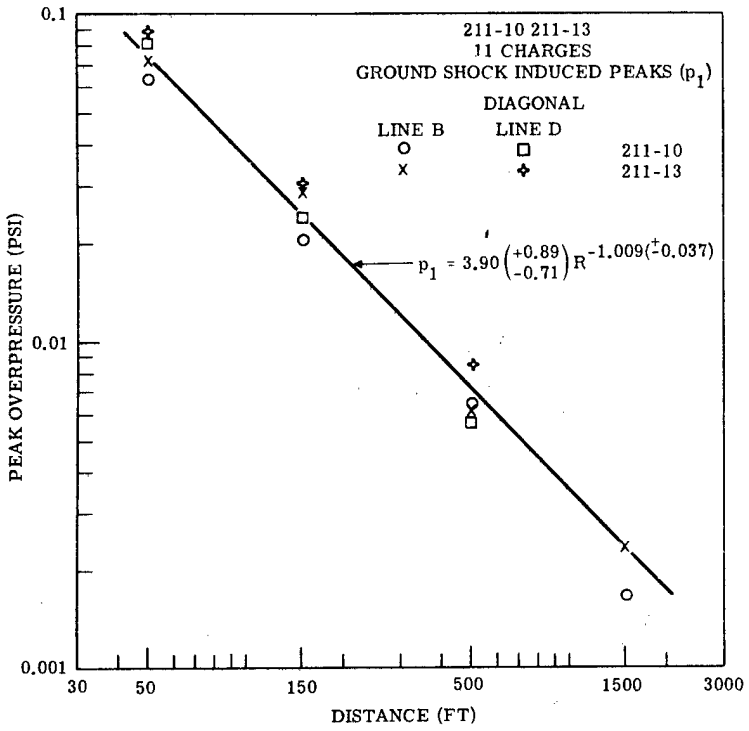

Figure A-88.

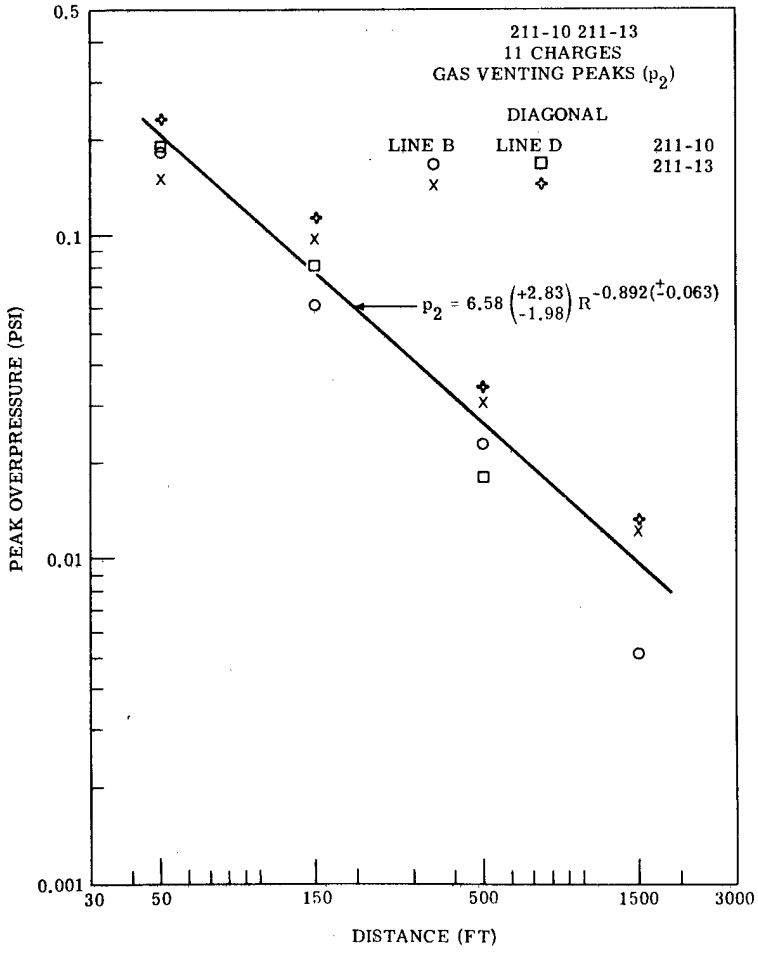

Figure A-89.

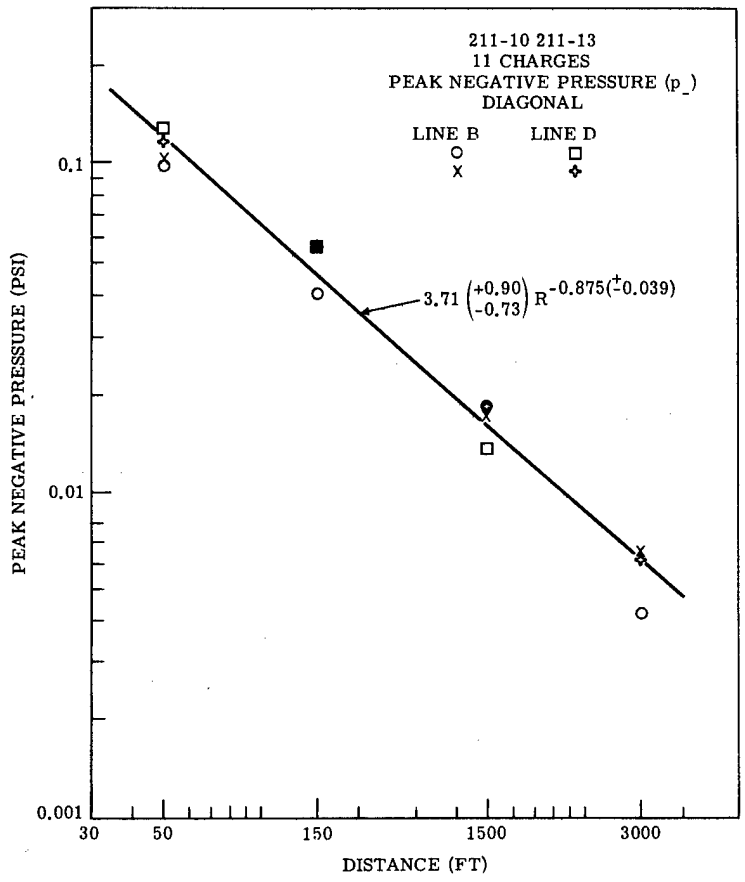
211-10 211-13
11 CHARGES
PEAK NEGATIVE PRESSURE (p_)
DIAGONAL
LINE B
LINE D
3.71 (+0.90 / -0.73) R^-0.875(±0.039)
PEAK NEGATIVE PRESSURE (PSI)
0.1
0.01
0.001
30
50
150
1500
3000
DISTANCE (FT)

Figure A-90.

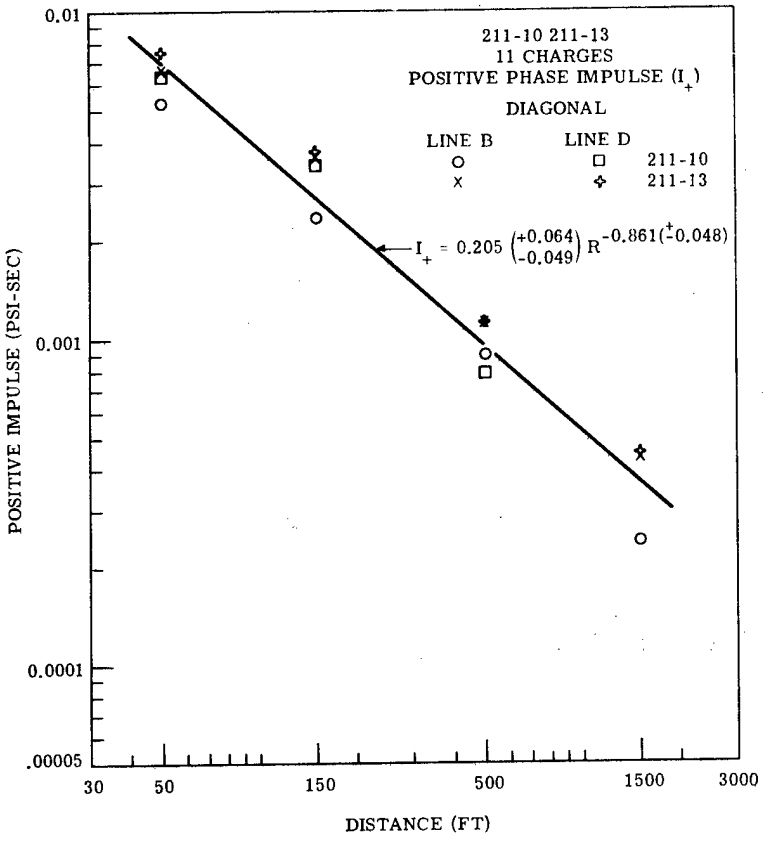

Figure A-91.

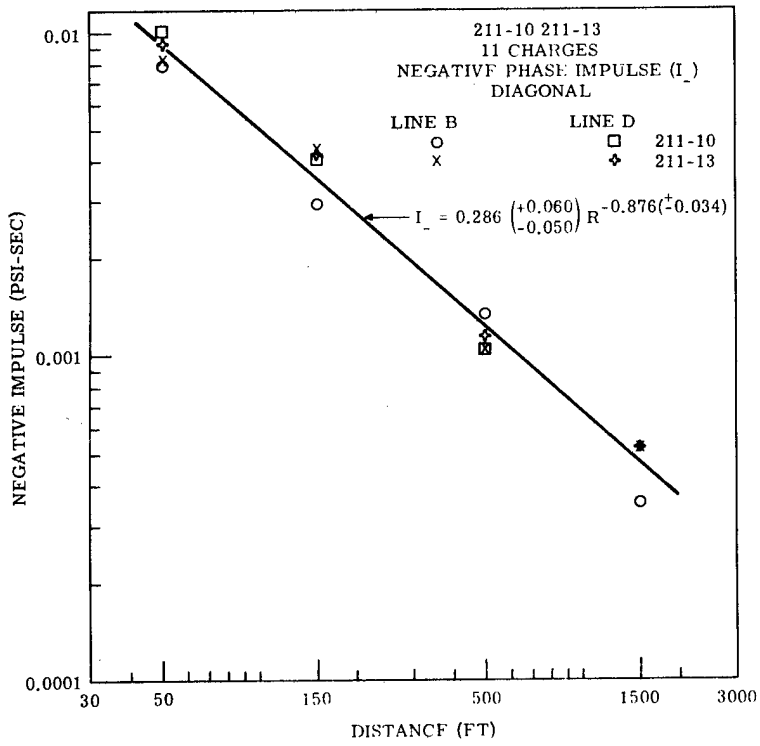

Figure A-92.

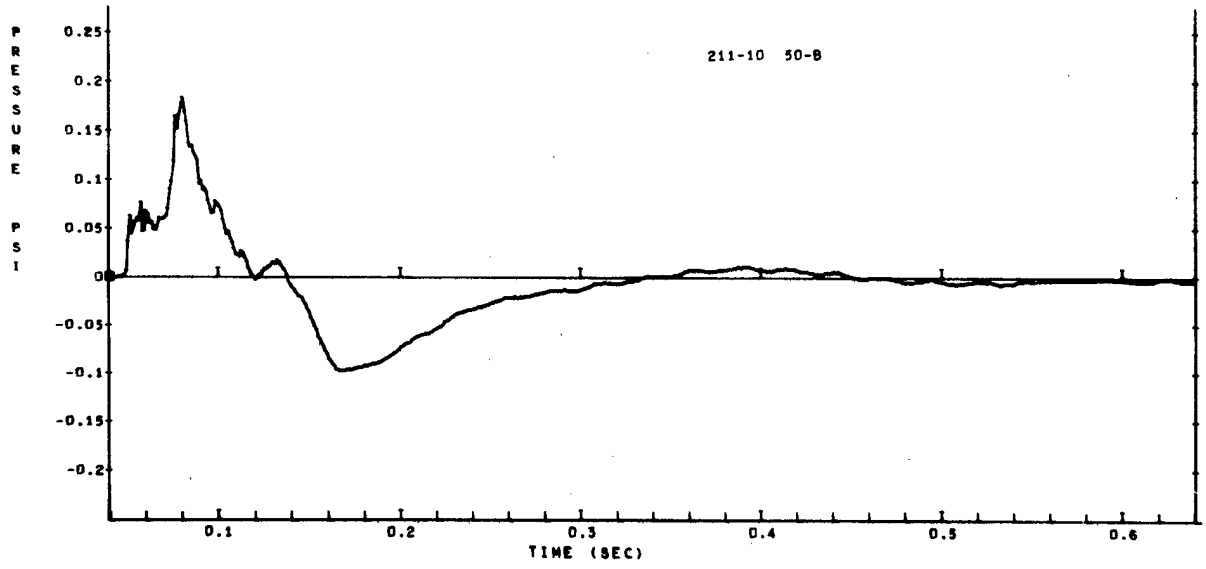

Figure A-93

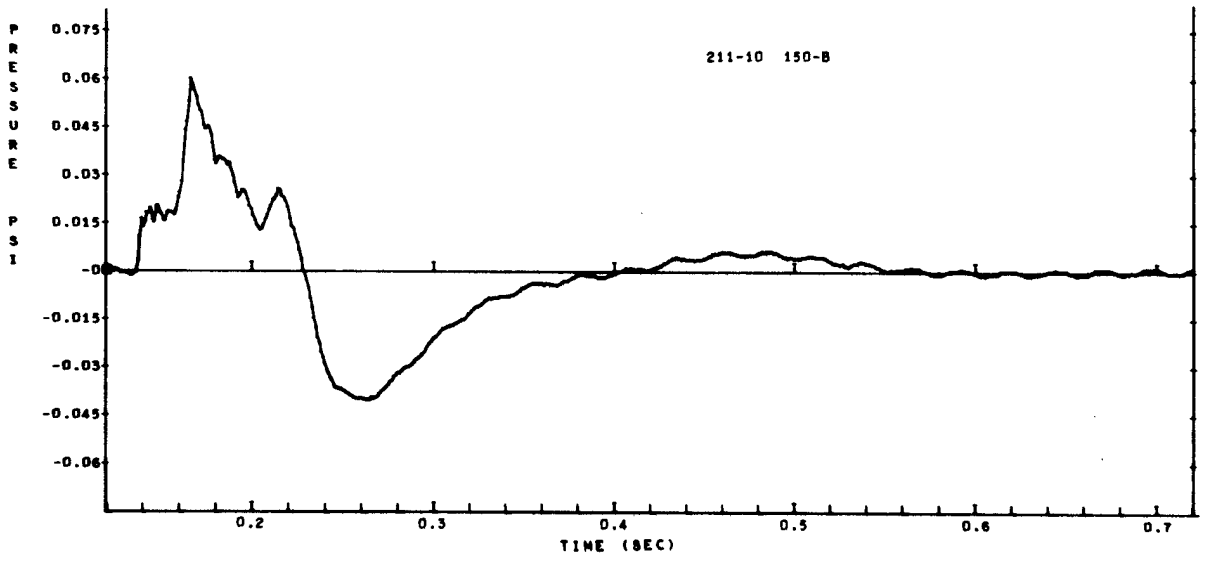

Figure A-94

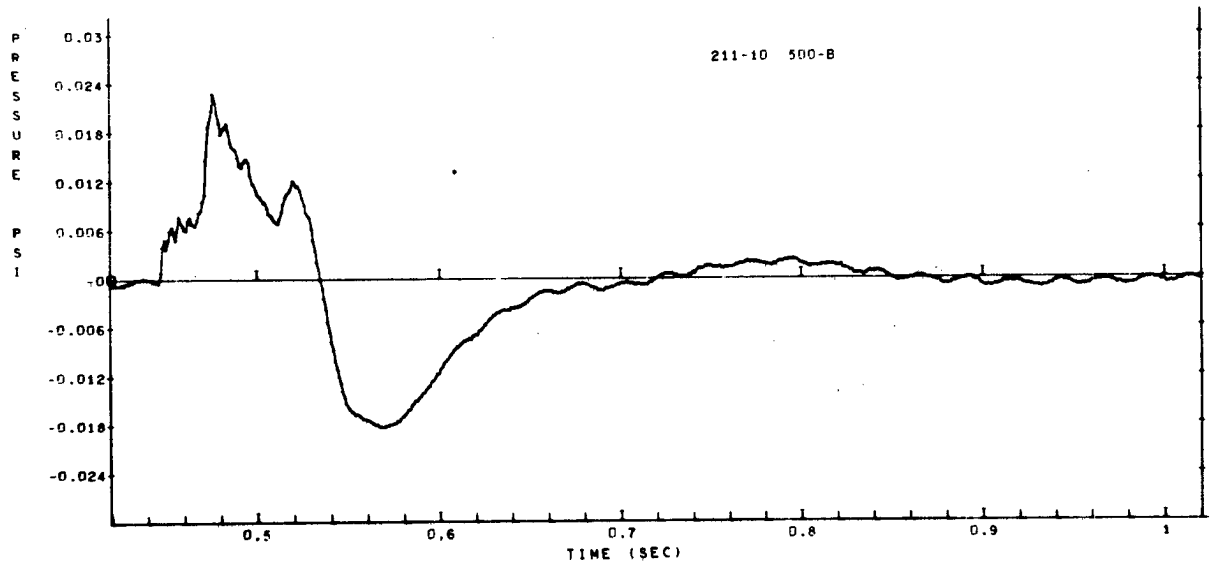

Figure A-95

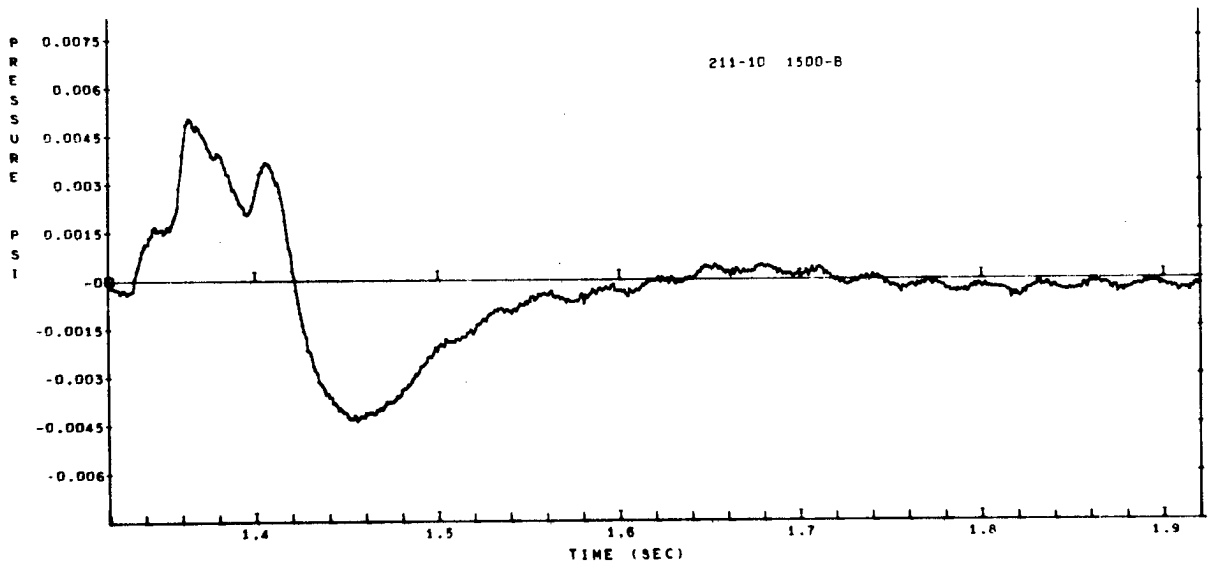

Figure A-96

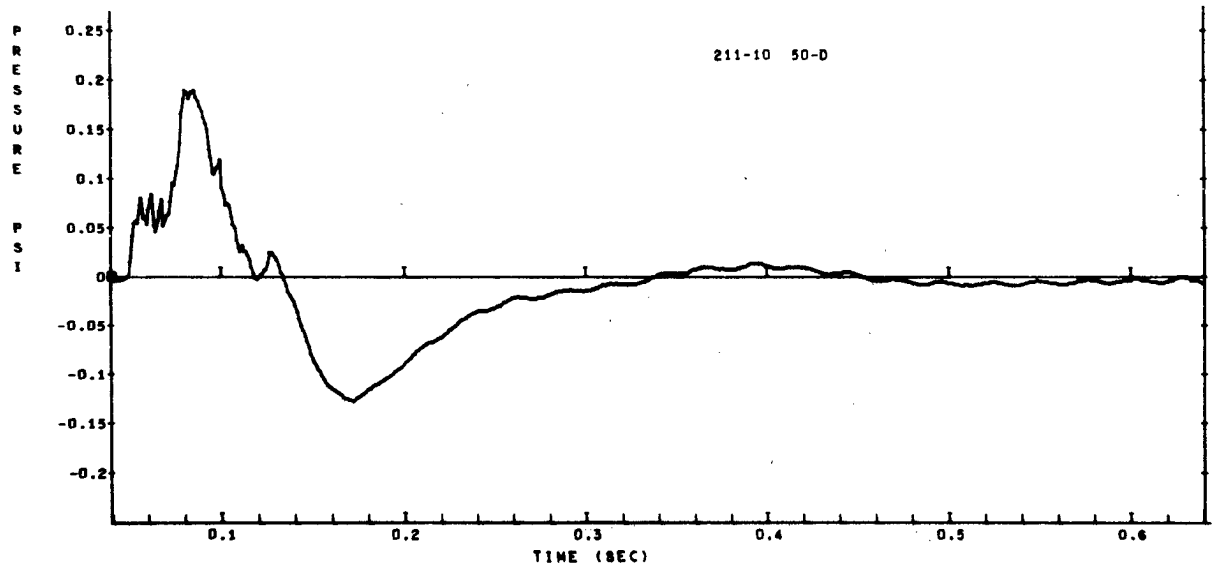

Figure A-97

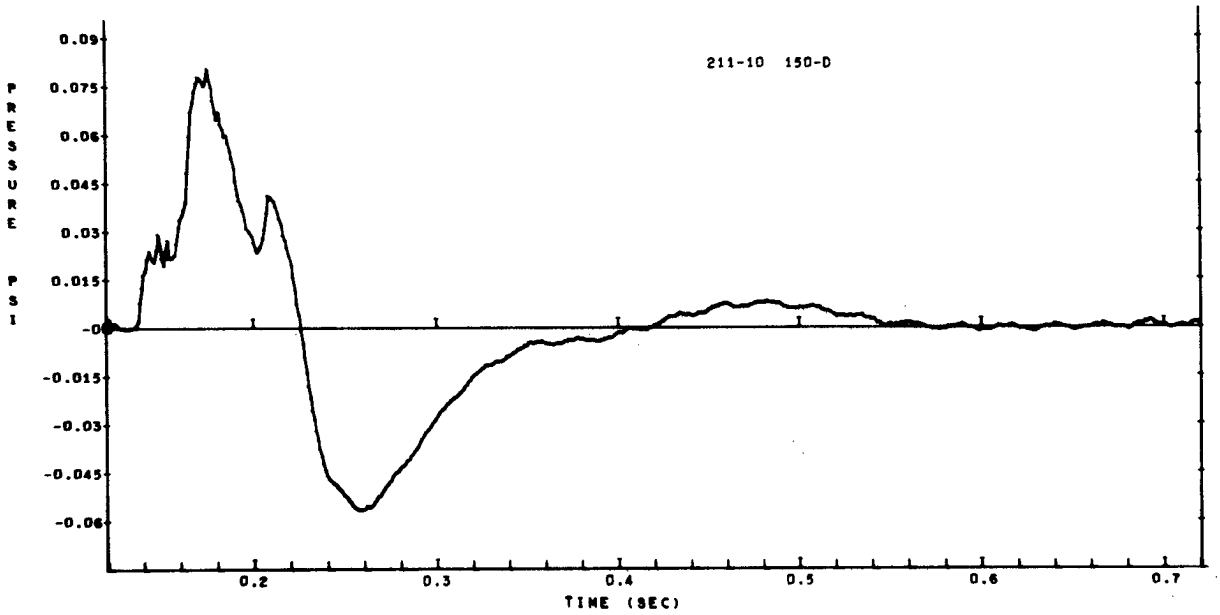

Figure A-98

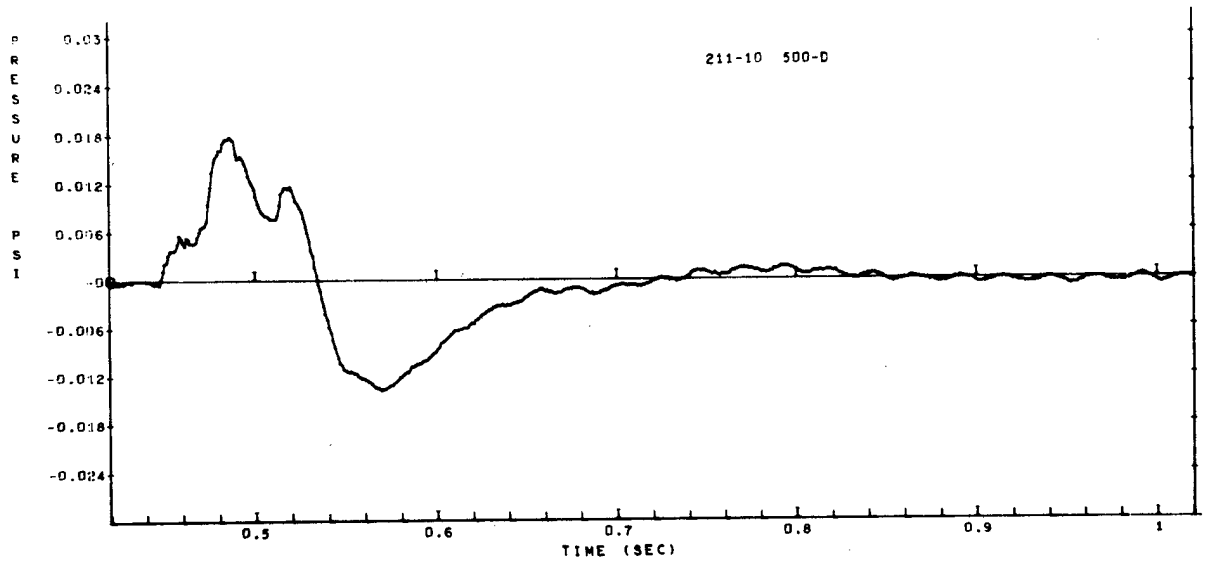

Figure A-99

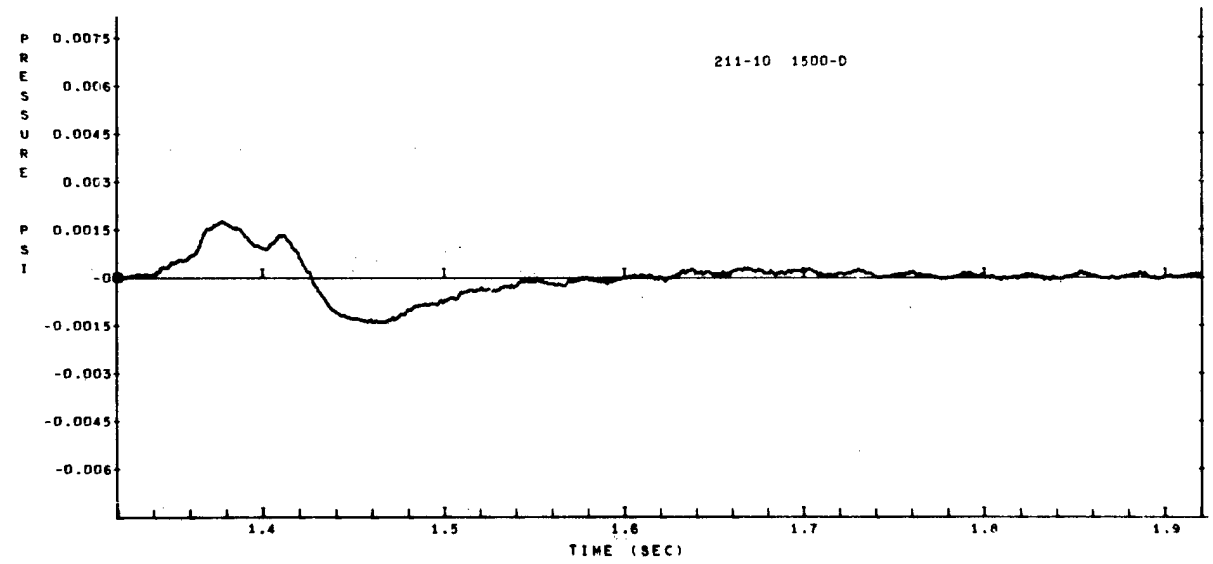

Figure A-100

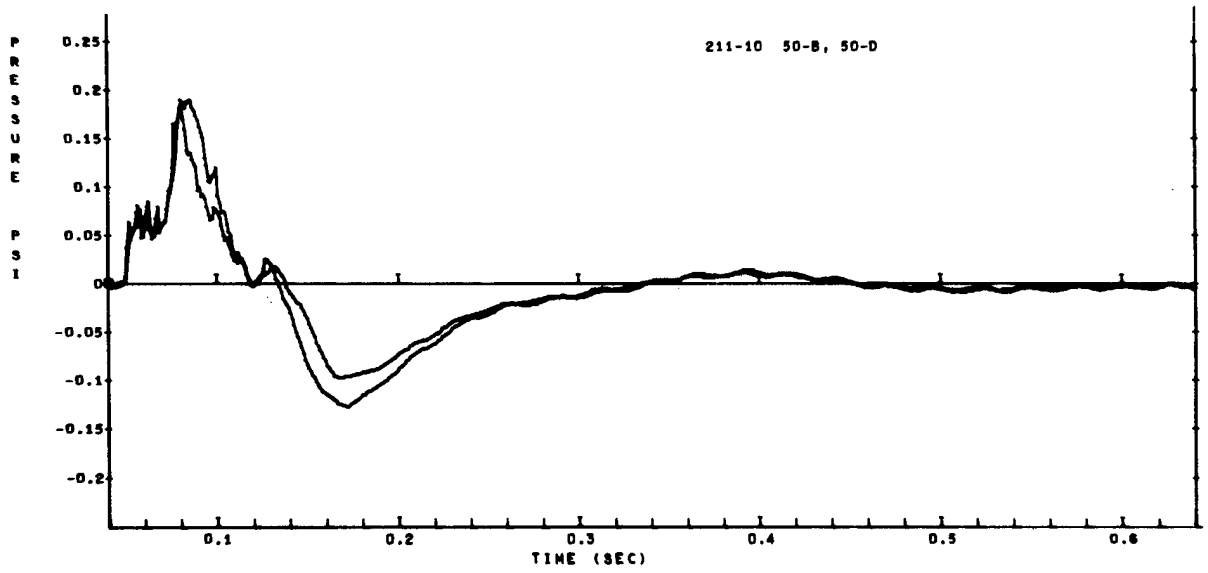

Figure A-101

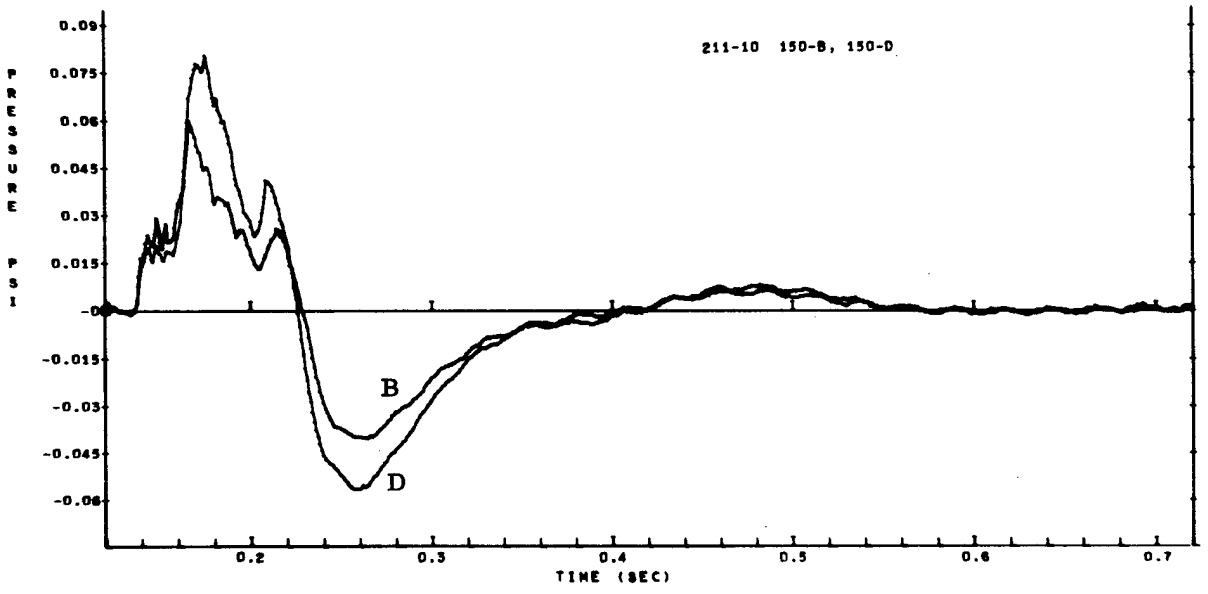

Figure A-102

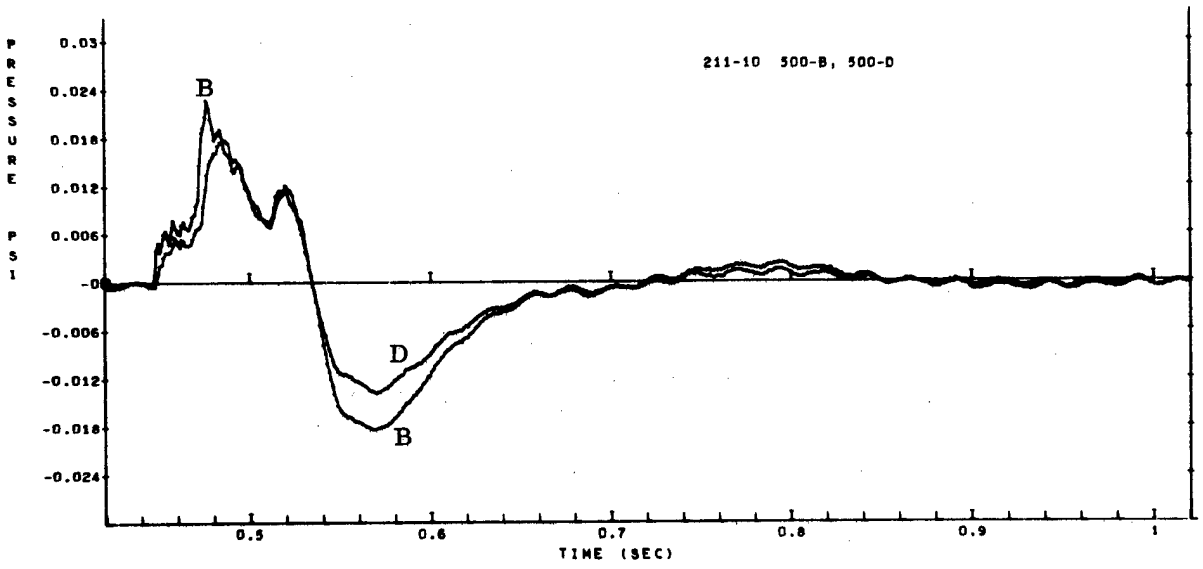

Figure A-103

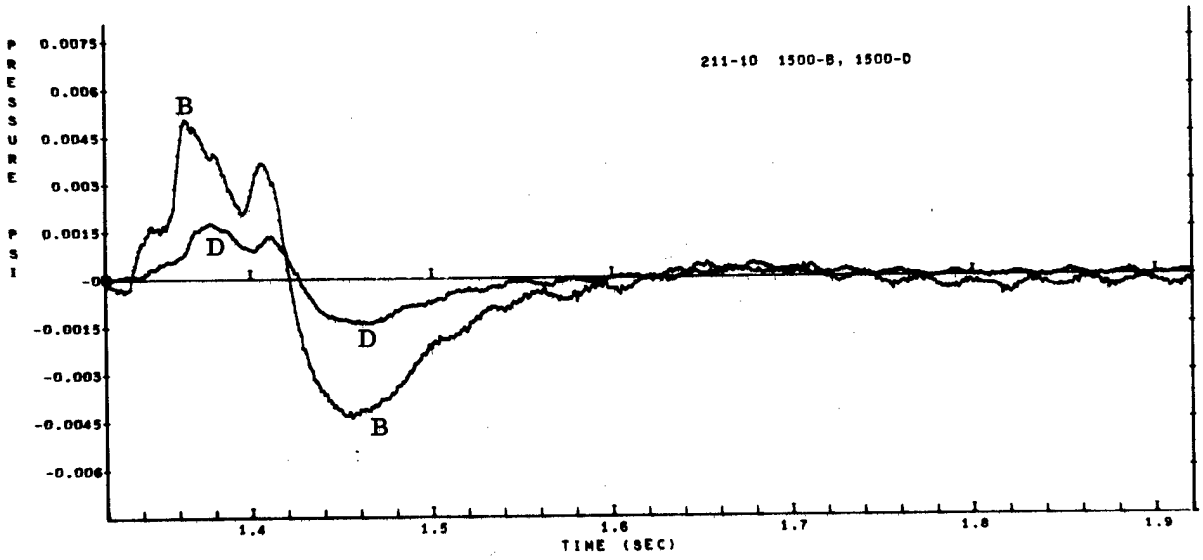

Figure A-104

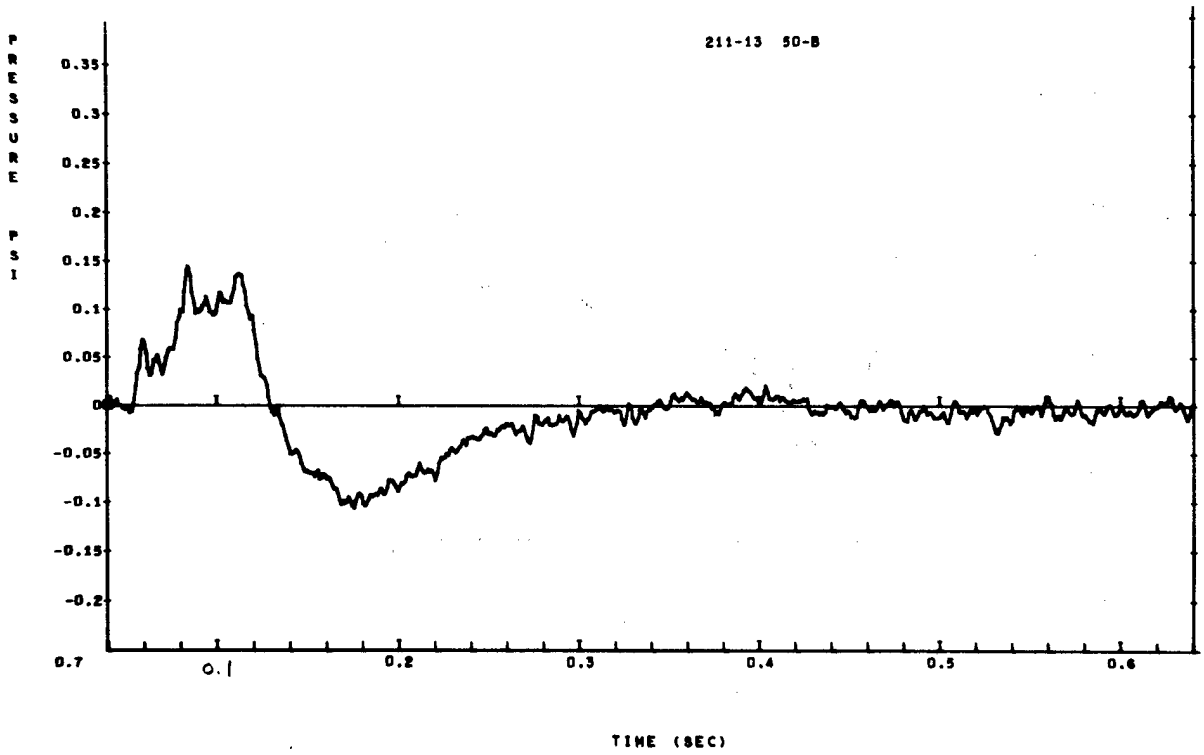

Figure A-105

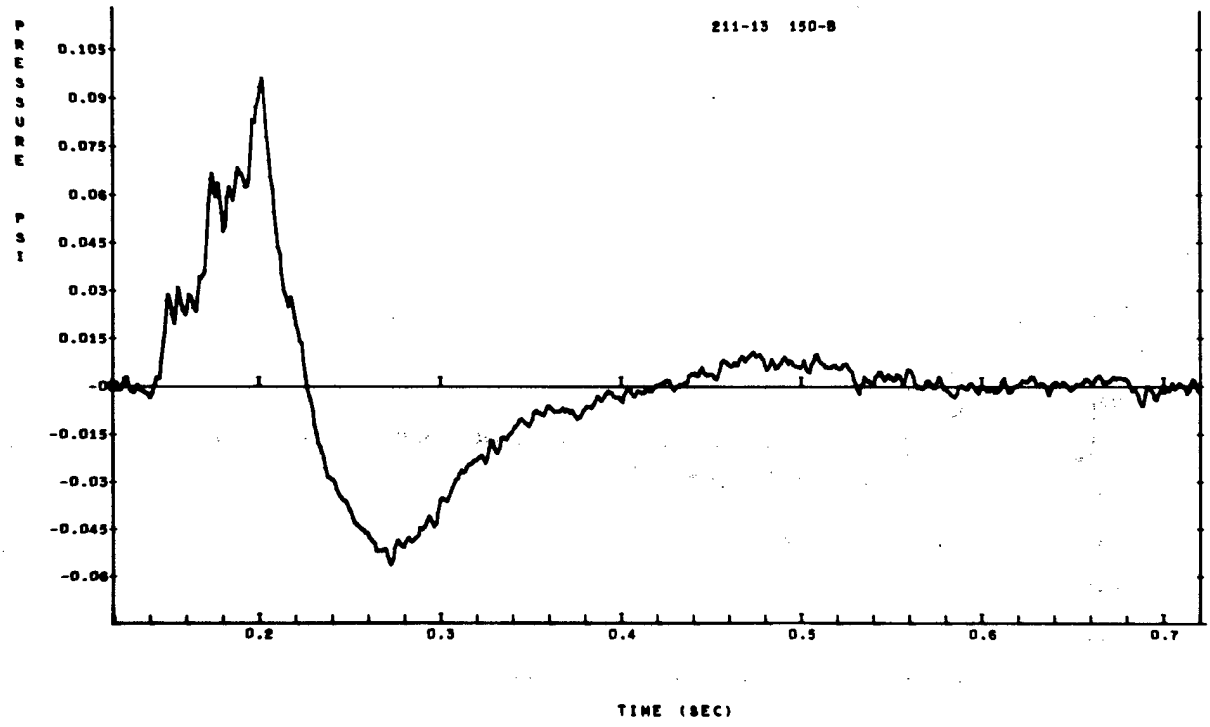

Figure A-106

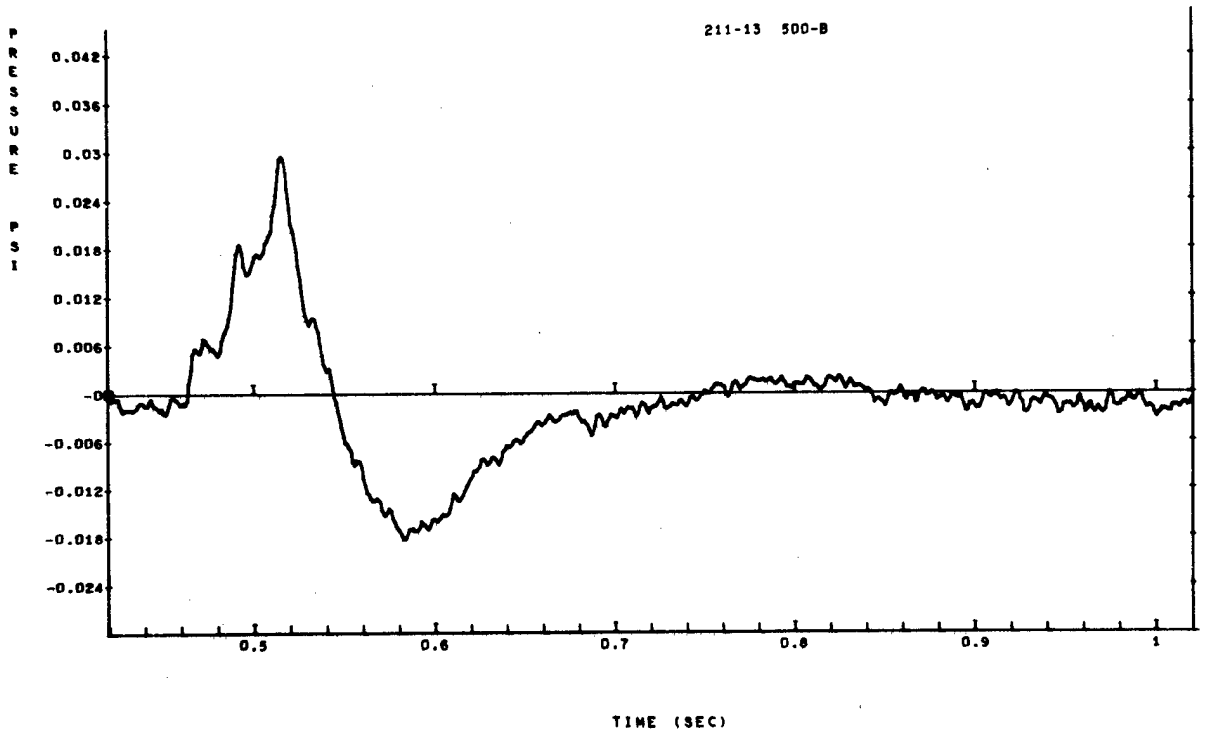

Figure A-107

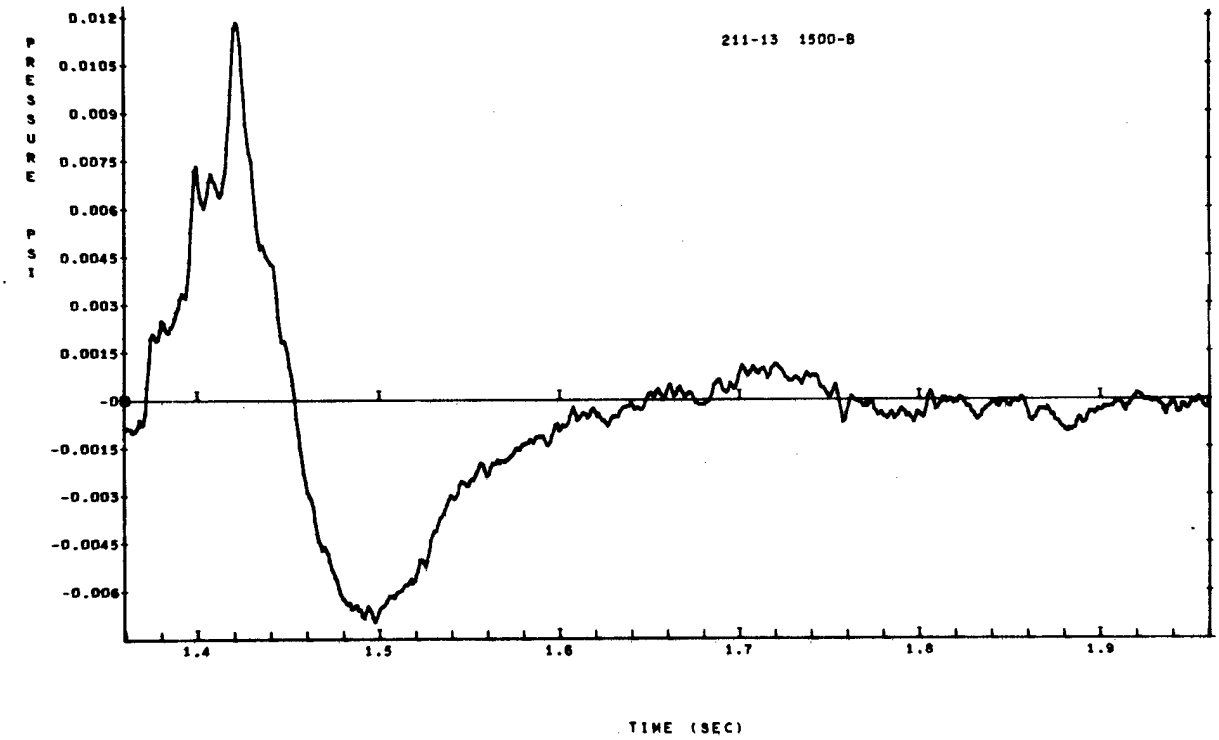

Figure A-108

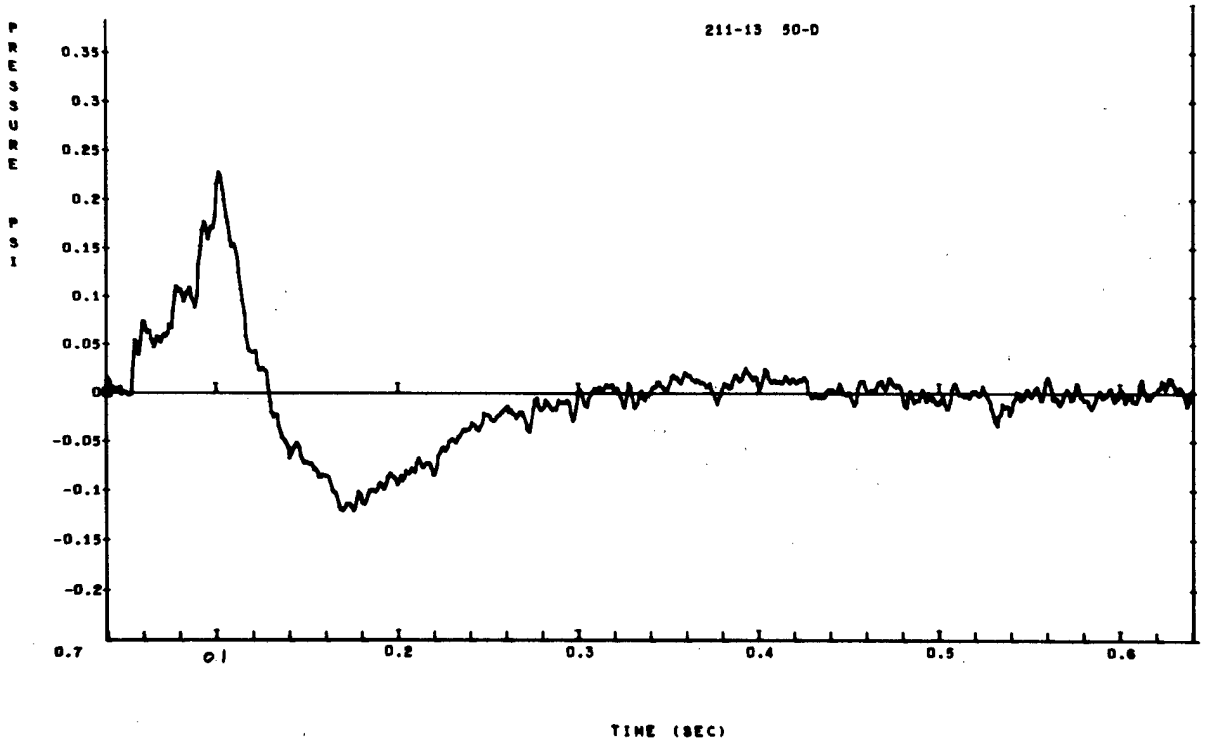

Figure A-109

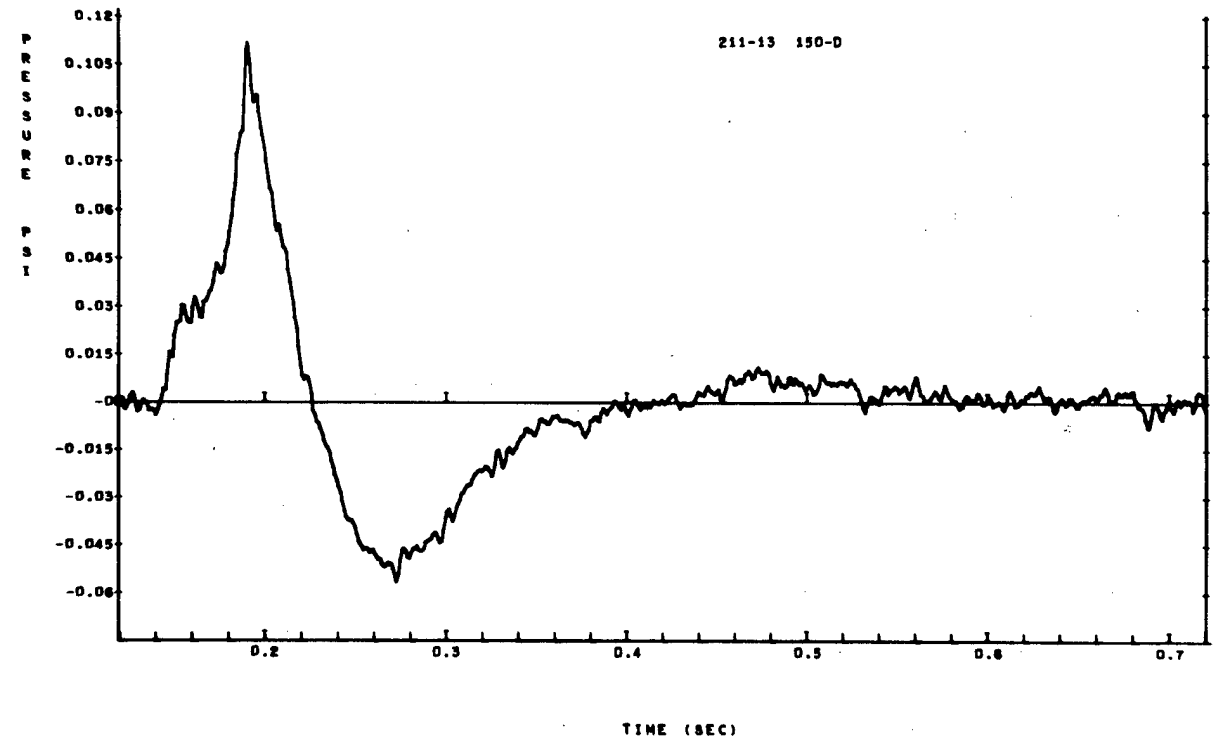

Figure A-110

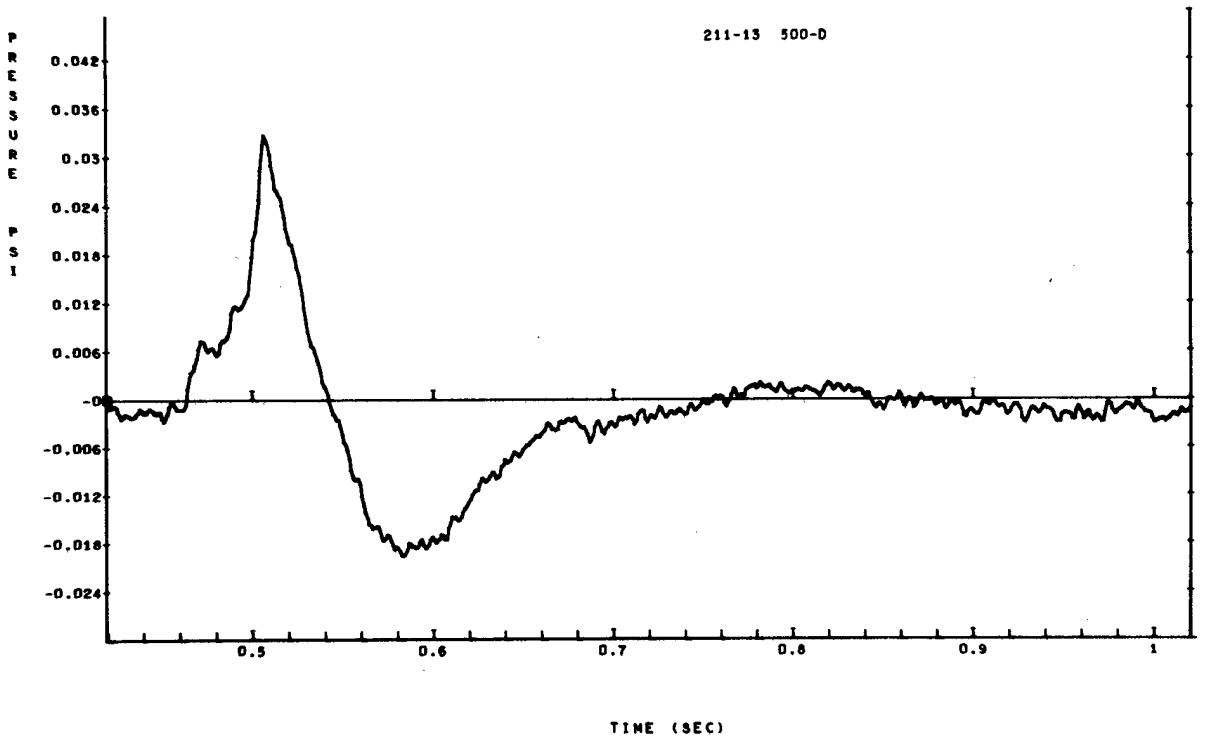

Figure A-111

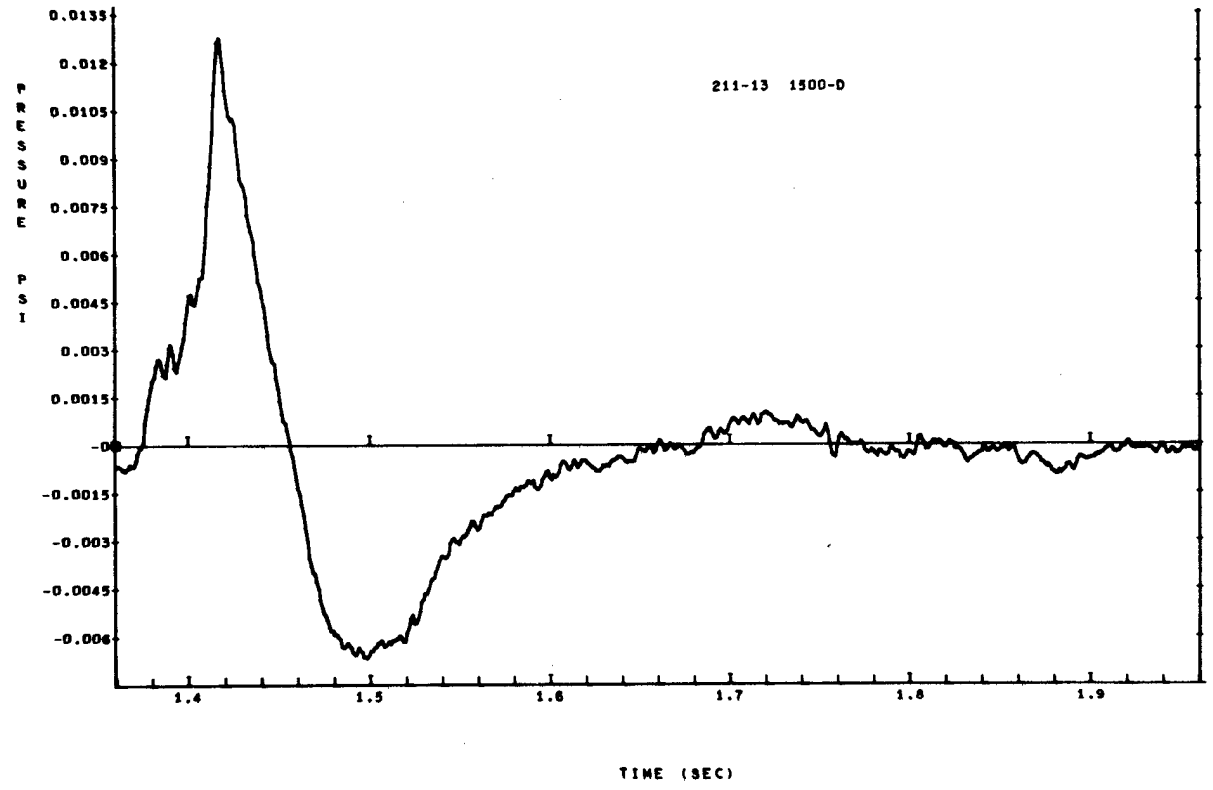

Figure A-112

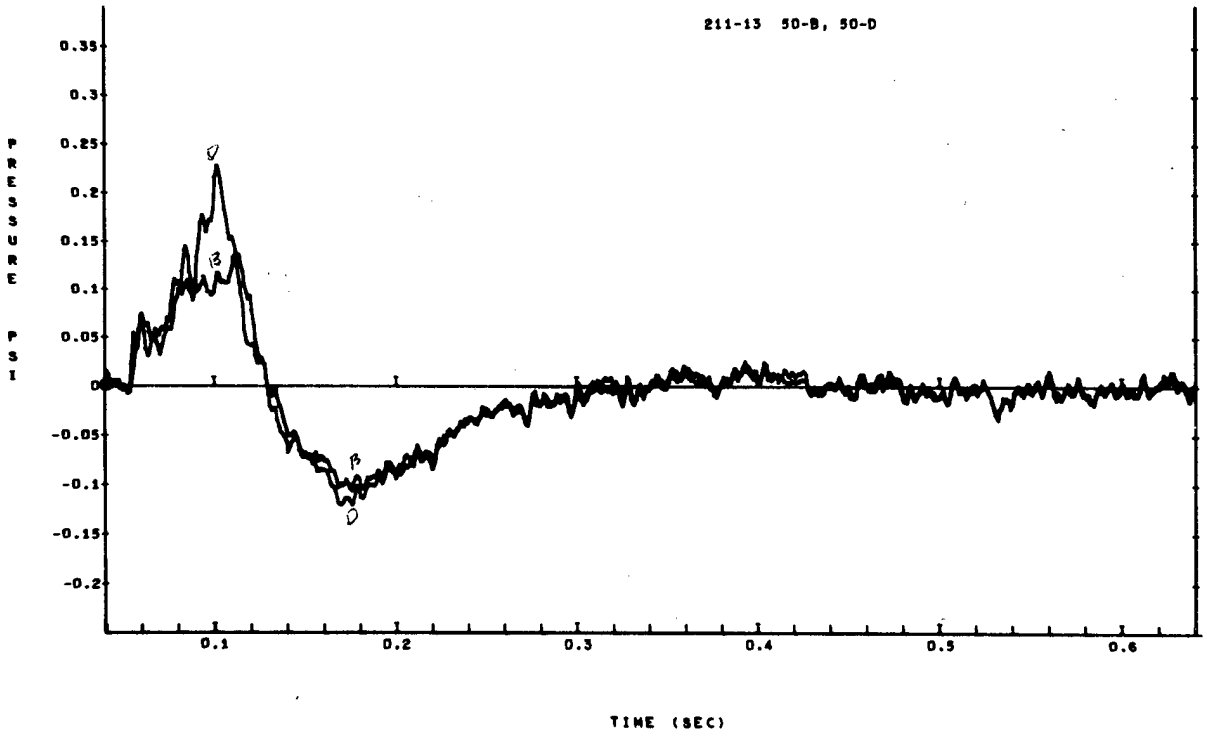

Figure A-113

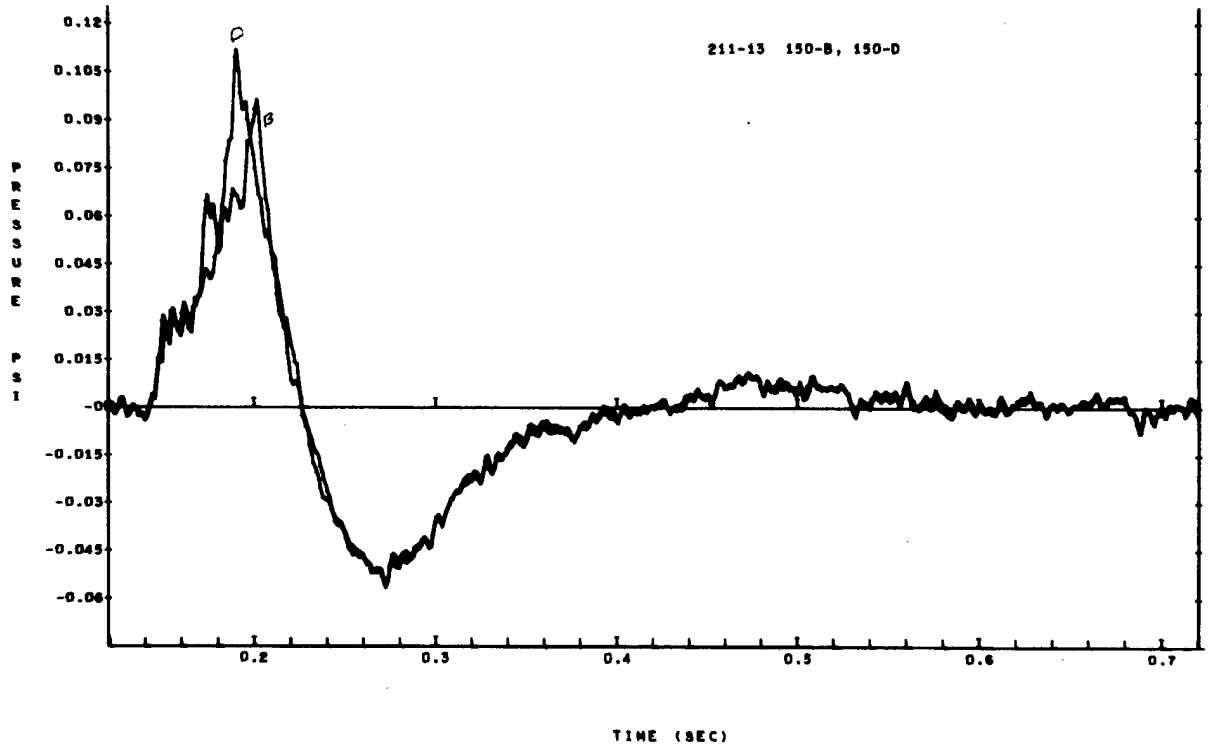

Figure A-114

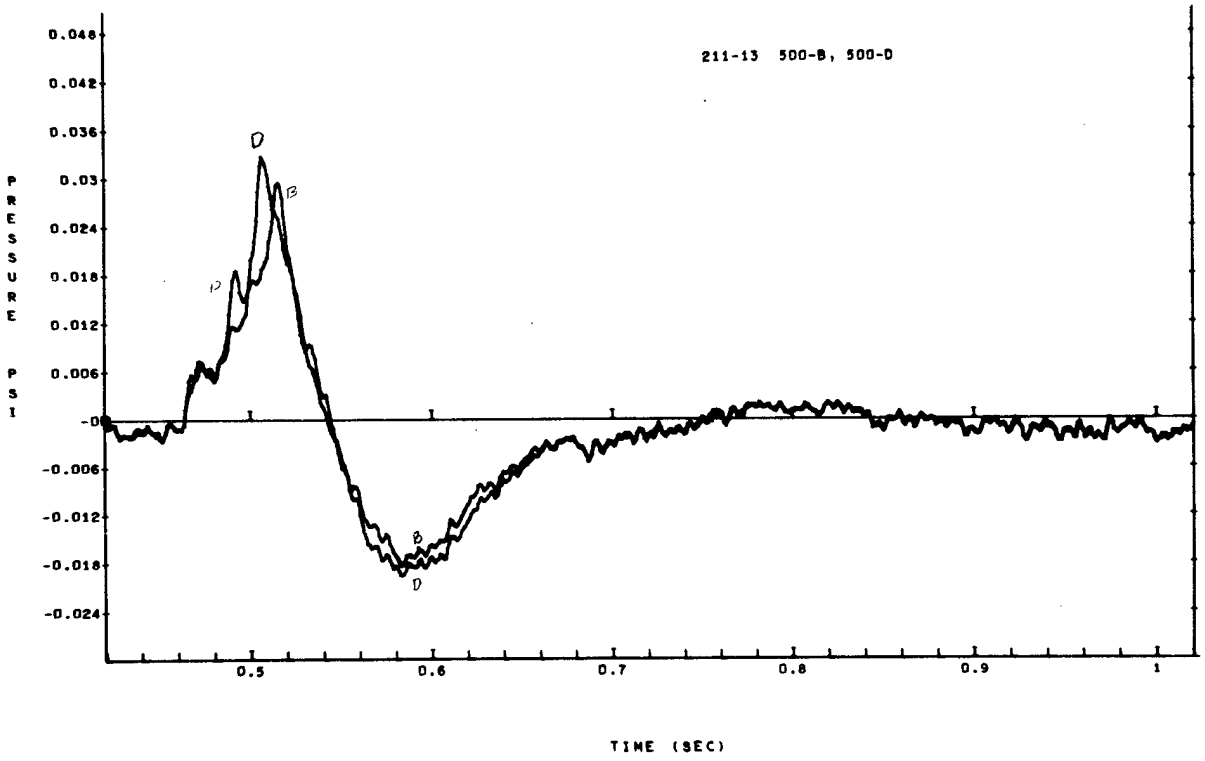

Figure A-115

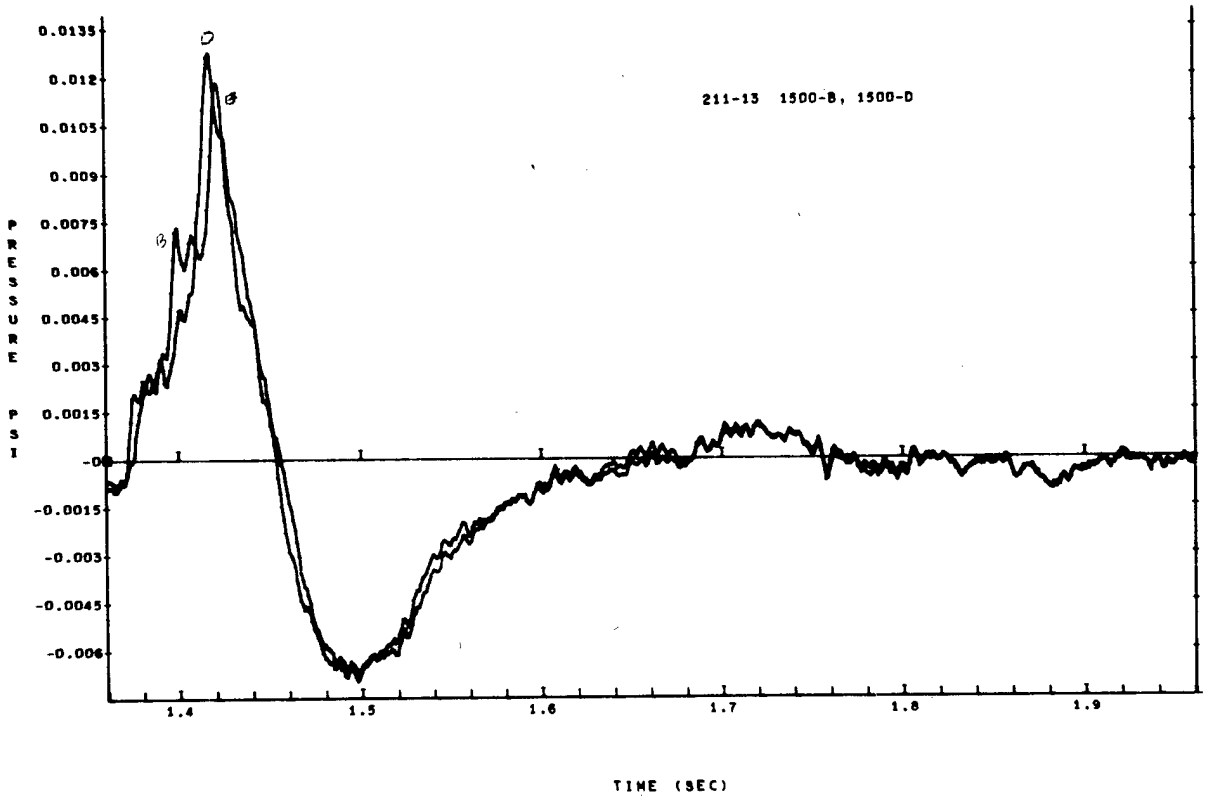

Figure A-116

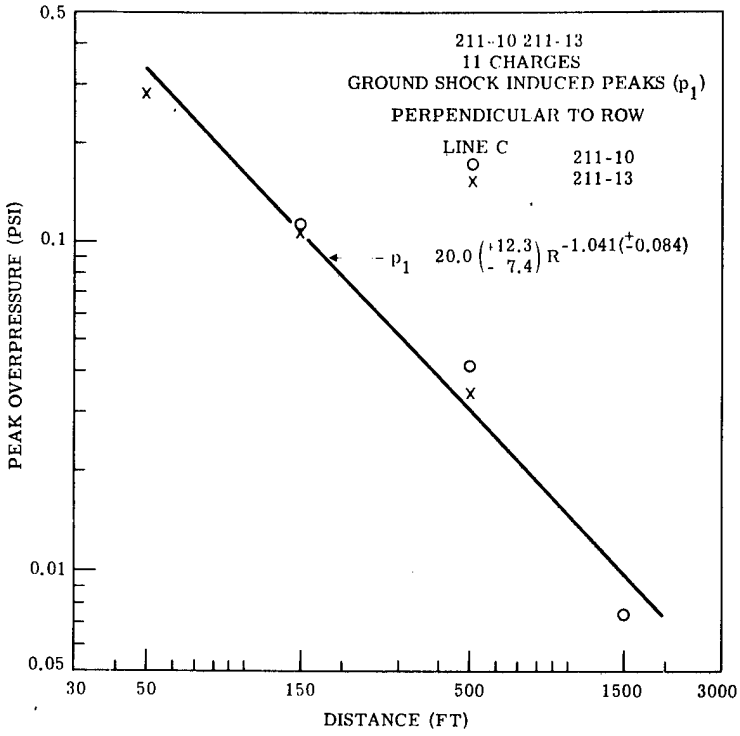

Figure A-117.

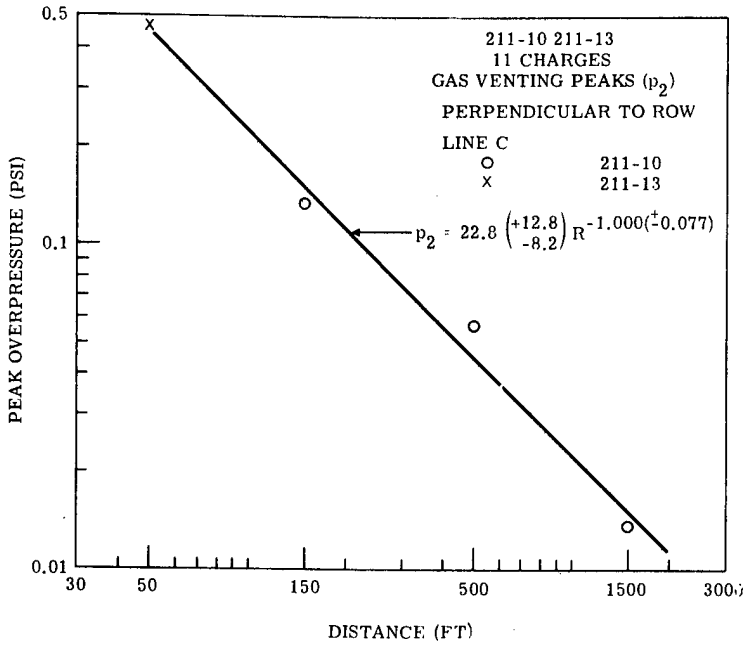

Figure A-118.

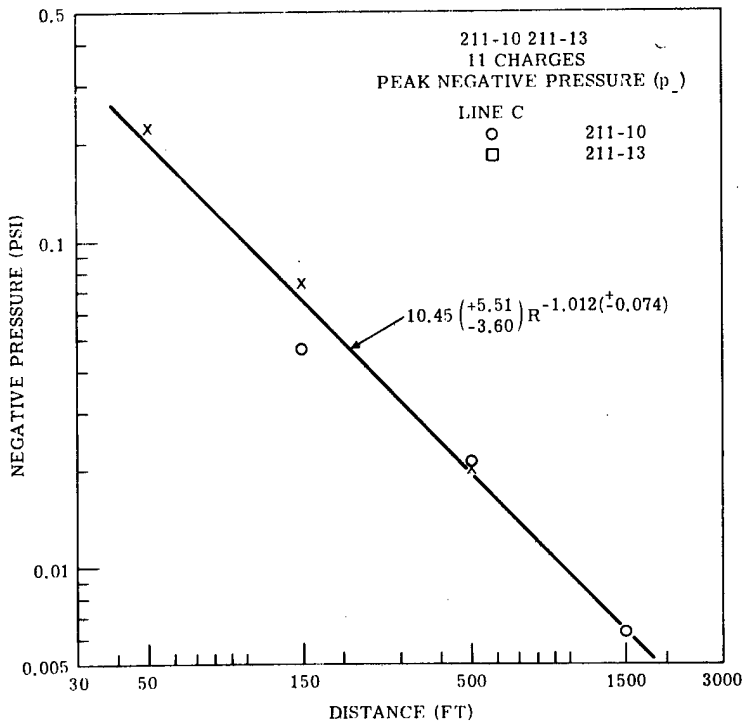

Figure A-119.

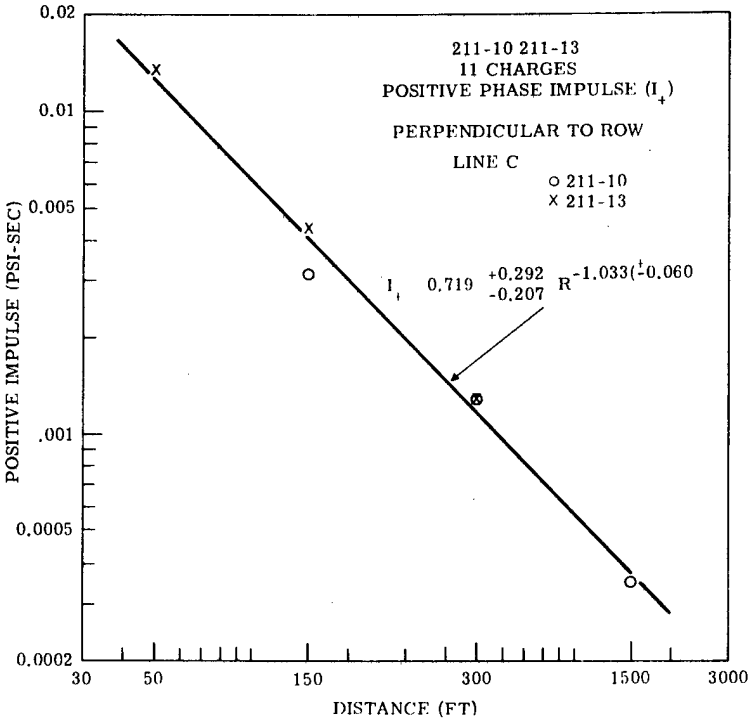

Figure A-120.

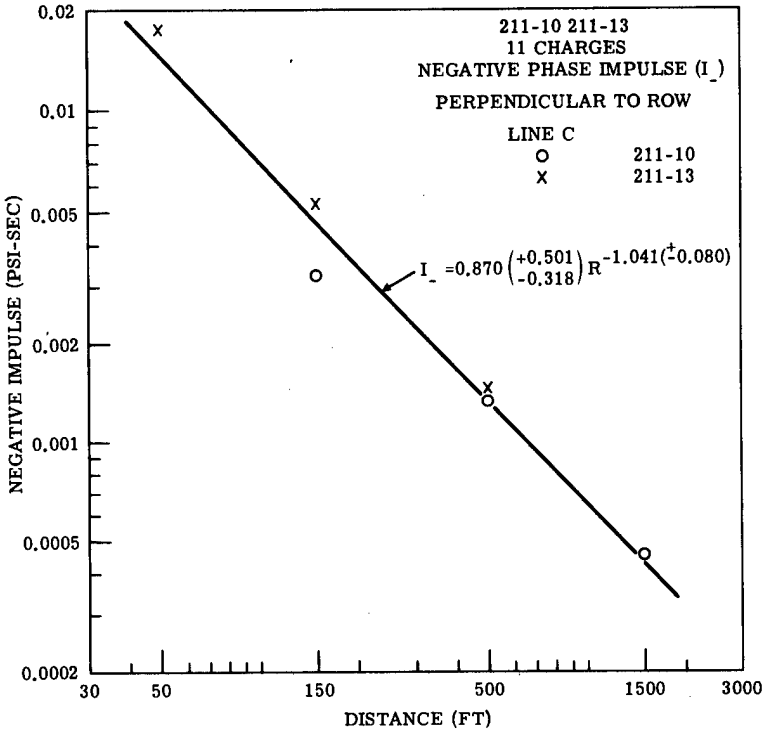
211-10 211-13
11 CHARGES
NEGATIVE PHASE IMPULSE (I_)
PERPENDICULAR TO ROW
LINE C
O 211-10
X 211-13
I_ =0.870 (+0.501 / -0.318) R^-1.041(±0.080)
NEGATIVE IMPULSE (PSI-SEC)
0.02
0.01
0.005
0.002
0.001
0.0005
0.0002
30
50
150
500
1500
3000
DISTANCE (FT)

Figure A-121.

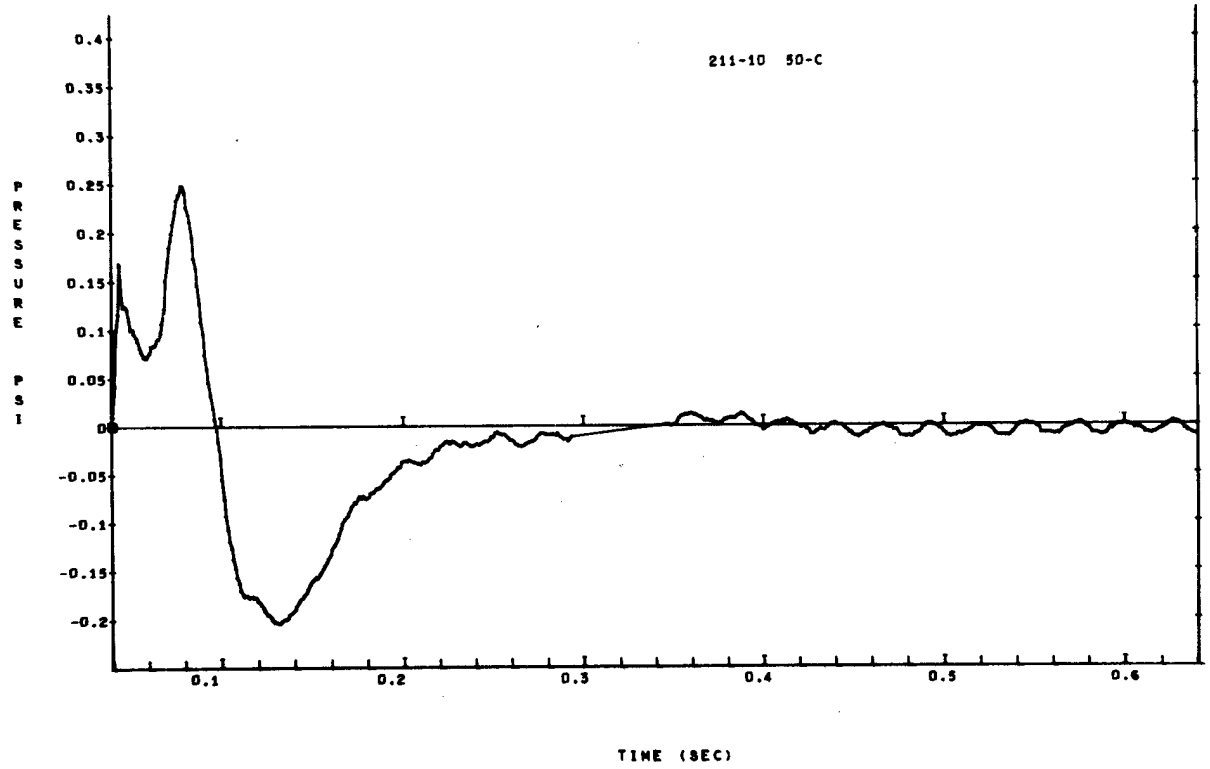

Figure A-122

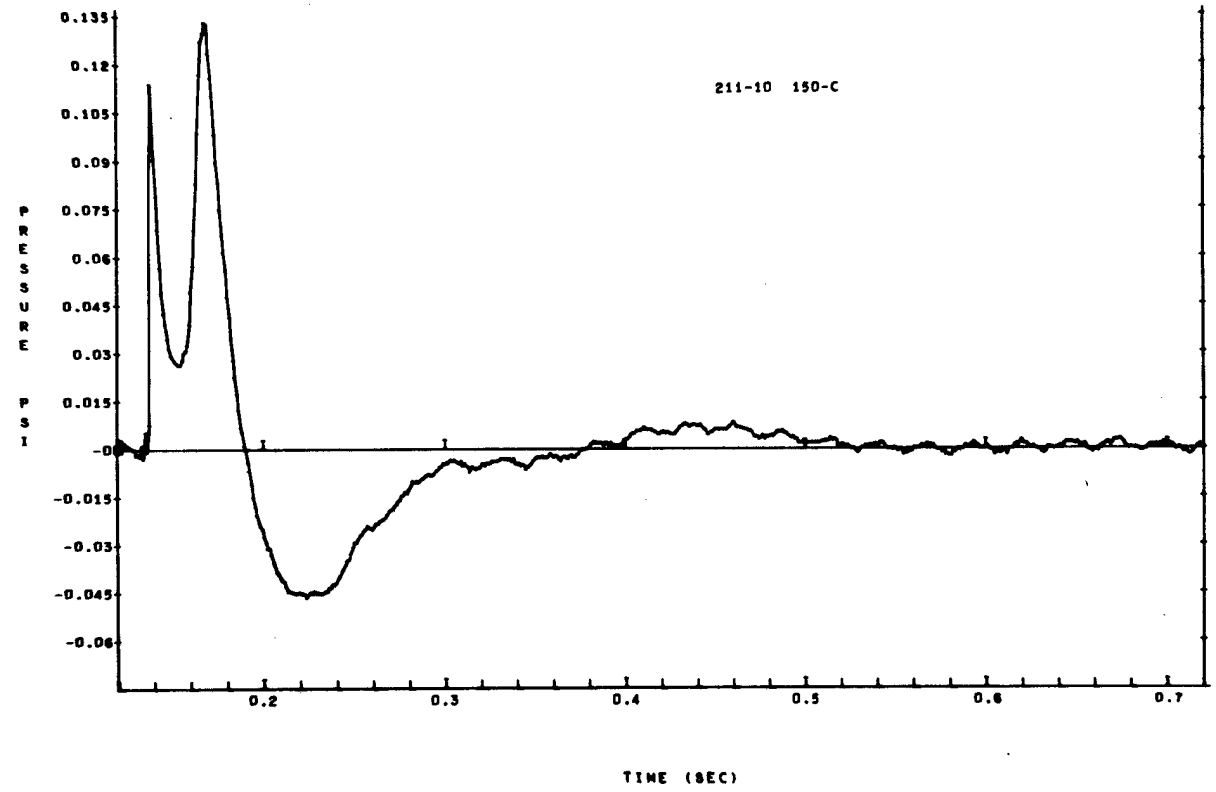

Figure A-123

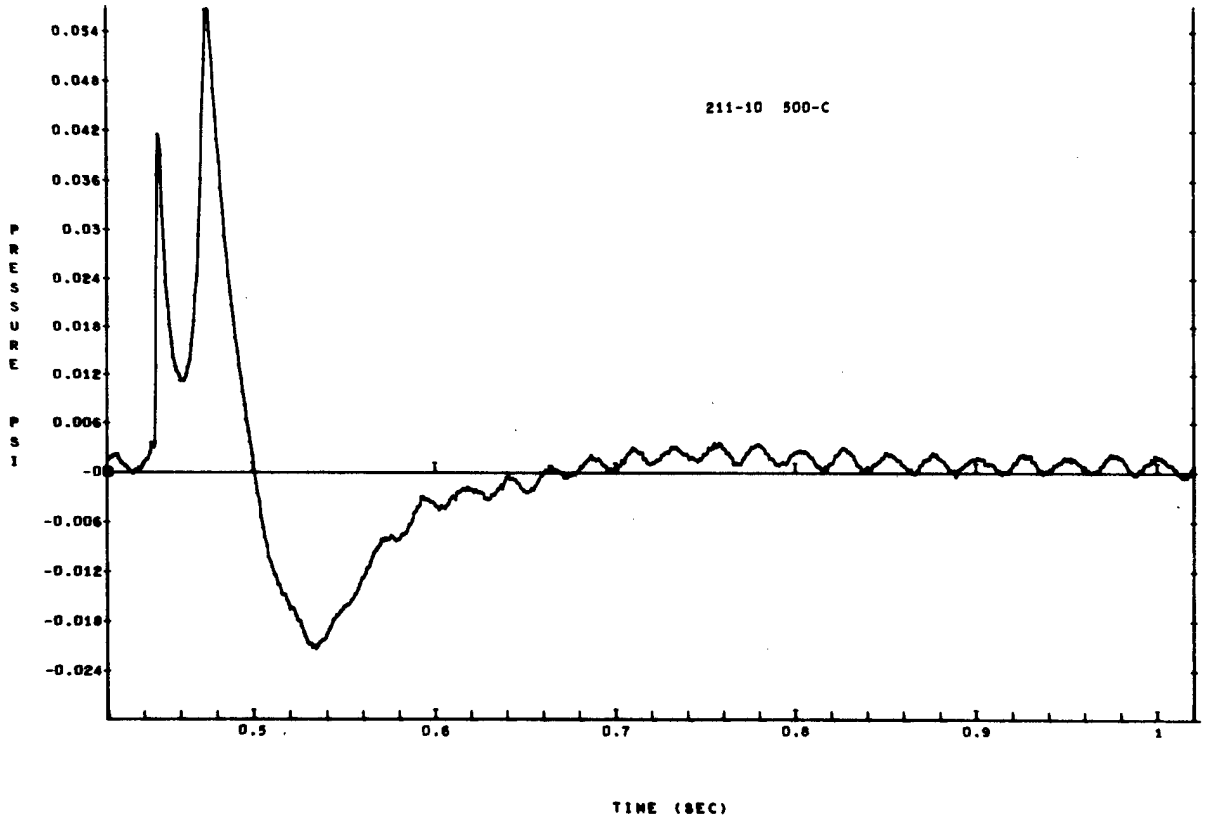

Figure A-124

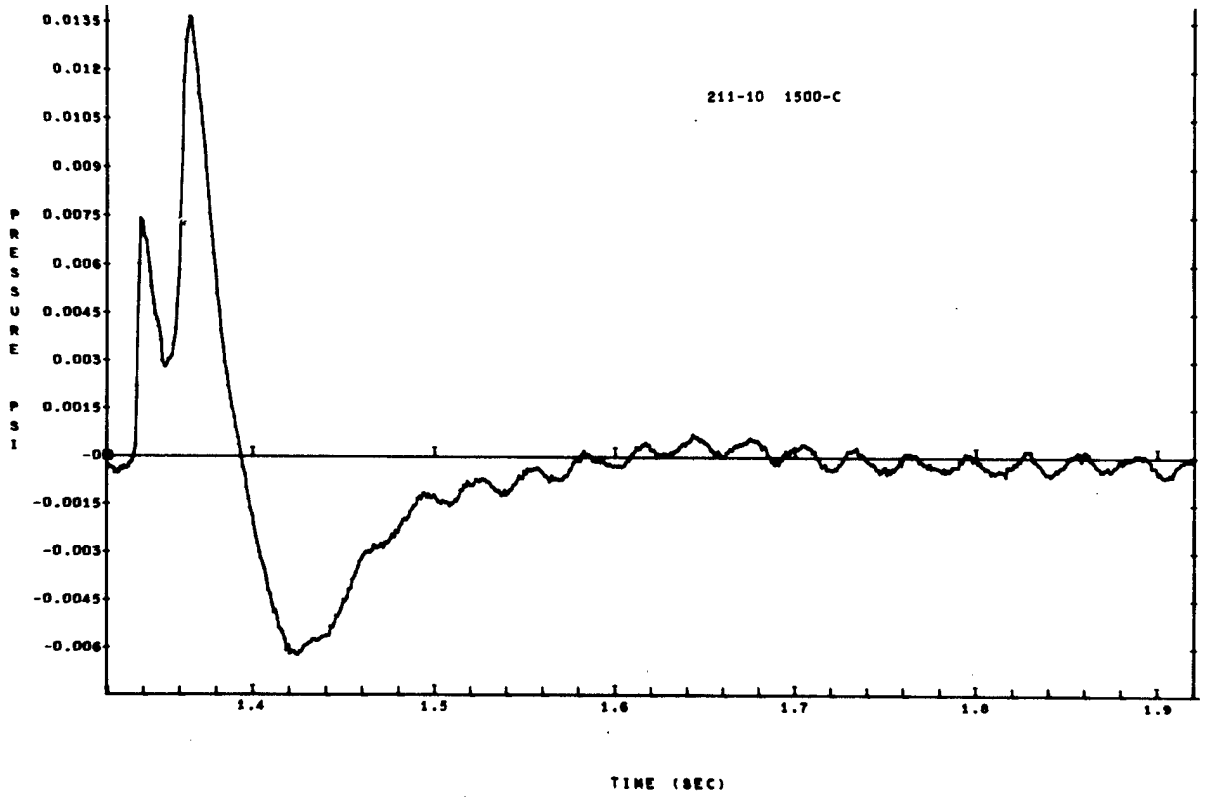

Figure A-125

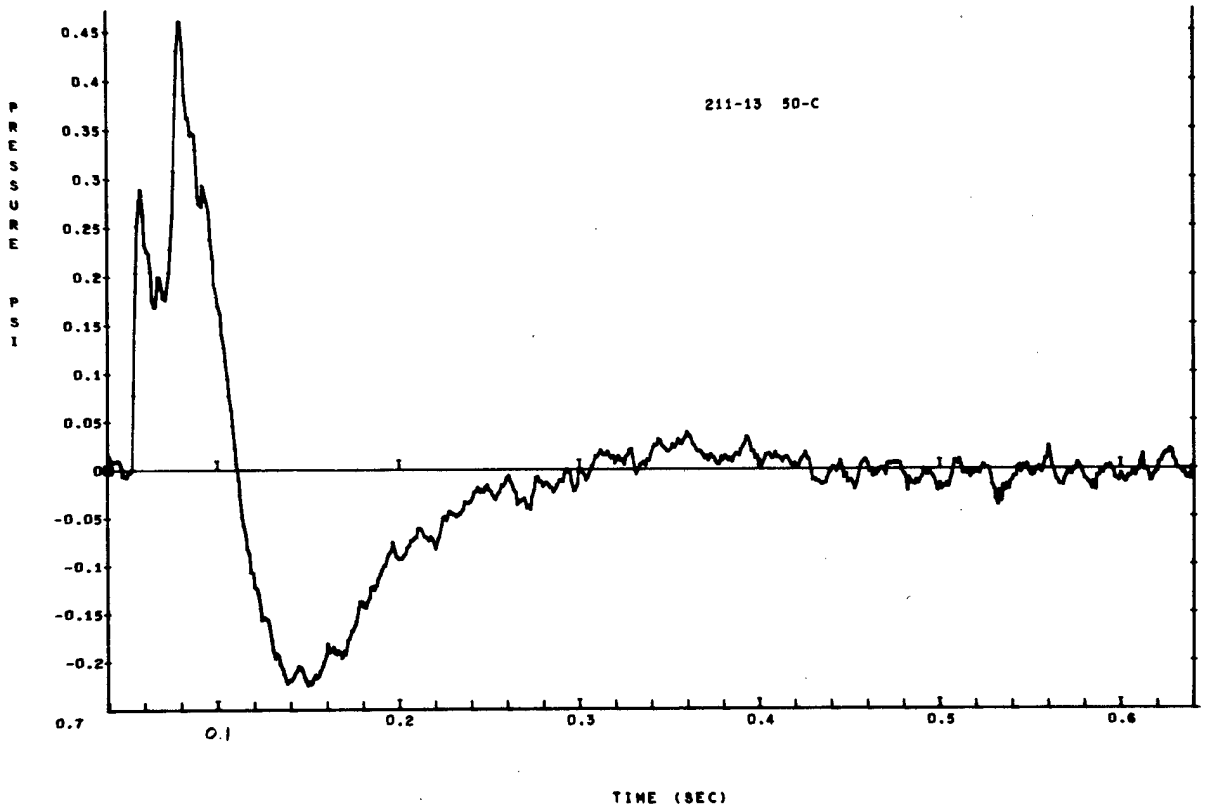

Figure A-126

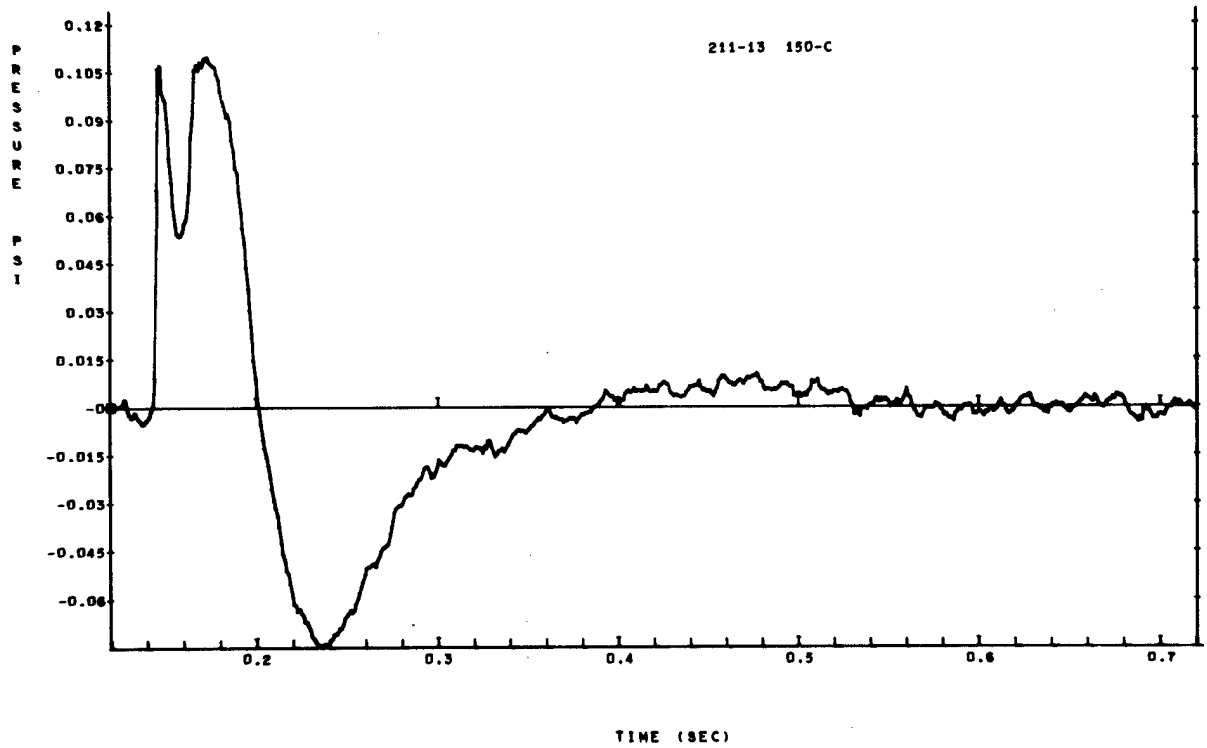

Figure A-127

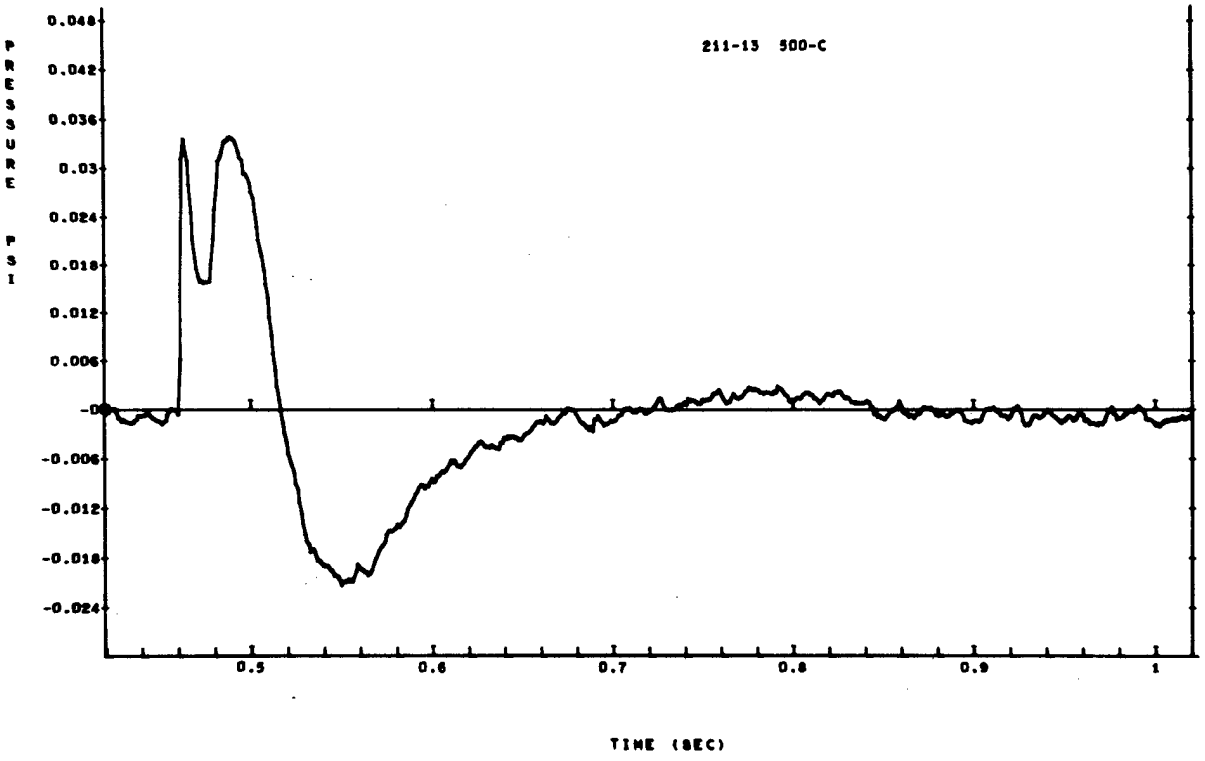

Figure A-128

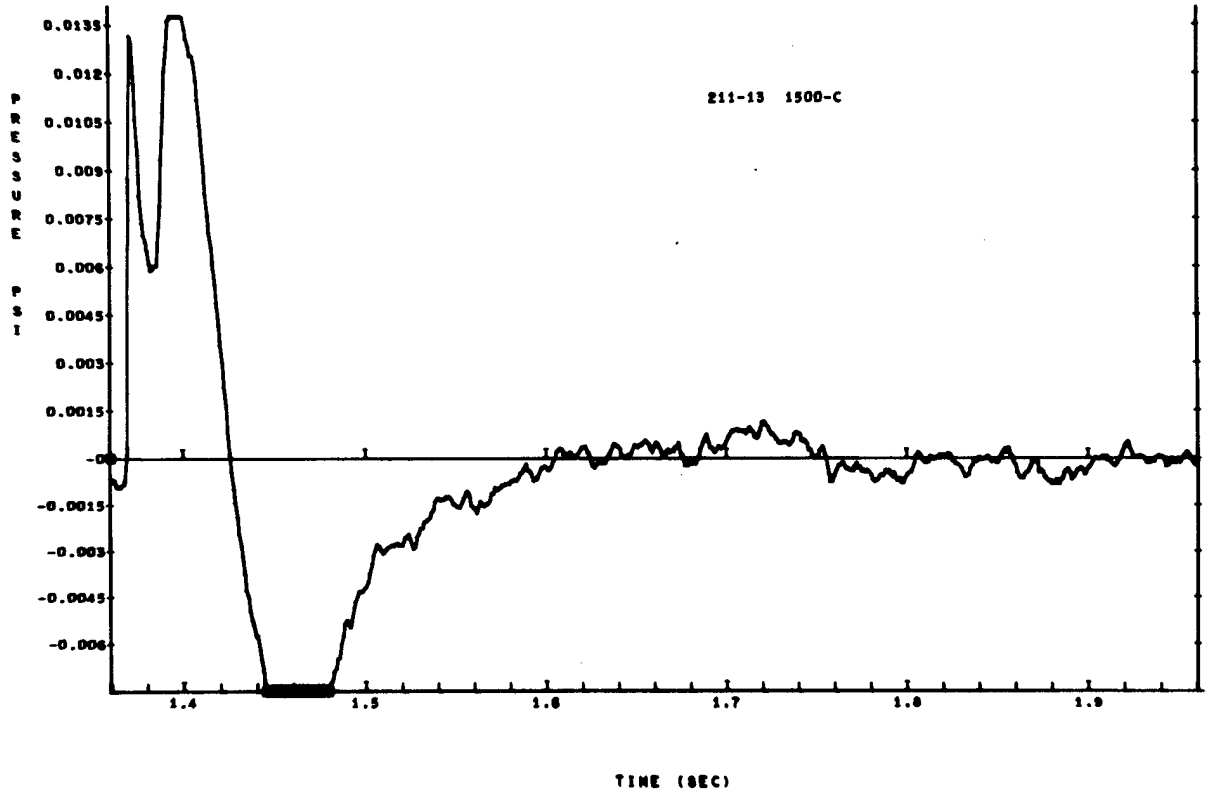

Figure A-129

Shot 211-43

Twenty-five 64-pound charges were buried 6 feet deep, spaced 8 feet apart. There were two blast lines: one off end of row (A), and one perpendicular to row (B). Two gages were placed at each station; gage A is the less sensitive.

Gage	Arrival time (sec)	Ground shock induced peak (psi)	Time of peak (sec)	Peak from venting gas (psi)	Time of peak (sec)	Cross-over (sec)	Positive phase impulse (psi-sec)	Negative peak (psi)	Time of peak (sec)	Cross-over (sec)	Negative phase impulse (psi-sec)
A50A	0.051	0.240	0.060	0.329	0.103	0.133	0.01539	-0.231	0.174	0.346	0.0219
A150A	0.144	0.130	0.147	0.1584	0.184	0.218	0.00729	-0.1229	0.251	0.421	0.0101
A150B	0.144	0.1285	0.147	0.1522	0.184	0.218	0.006918	-0.1155	0.251	0.429	0.00935
A500A	0.454	0.0550	0.458	0.0388	0.484	0.520	0.00186	-0.0326	0.560	0.730	0.00258
A1500A	1.344	0.0297	1.346	0.0166	1.371	1.412	0.000795	-0.0133	1.447	1.591	0.000901
A1500B	1.344	0.0251	1.346	0.0180	1.372	1.415	0.000884	-0.0125	1.449	1.589	0.000816
B50B	0.055	0.0638	0.058	0.1293	0.093	0.130	0.00516	-0.0641	0.281	0.442	0.00936
B150A	0.145	0.0169	0.148	0.051	0.184	0.225	0.00211	-0.03421	0.375	0.543	0.00454
B150B	0.145	0.01486	0.148	0.049	0.184	0.227	0.00206	-0.03275	0.388	0.542	0.00423
B500B	0.457	0.00586	0.460	0.01773	0.497	0.610	0.000856	-0.013653	0.707	0.833	0.00125
B1500A	1.353	0.001895	1.360	0.0057	1.390	1.523	0.000303	-0.005615	1.601	1.714	0.000469
B1500B	1.354	0.00158	1.360	0.005836	1.391	1.523	0.000310	-0.005716	1.601	1.728	0.000578

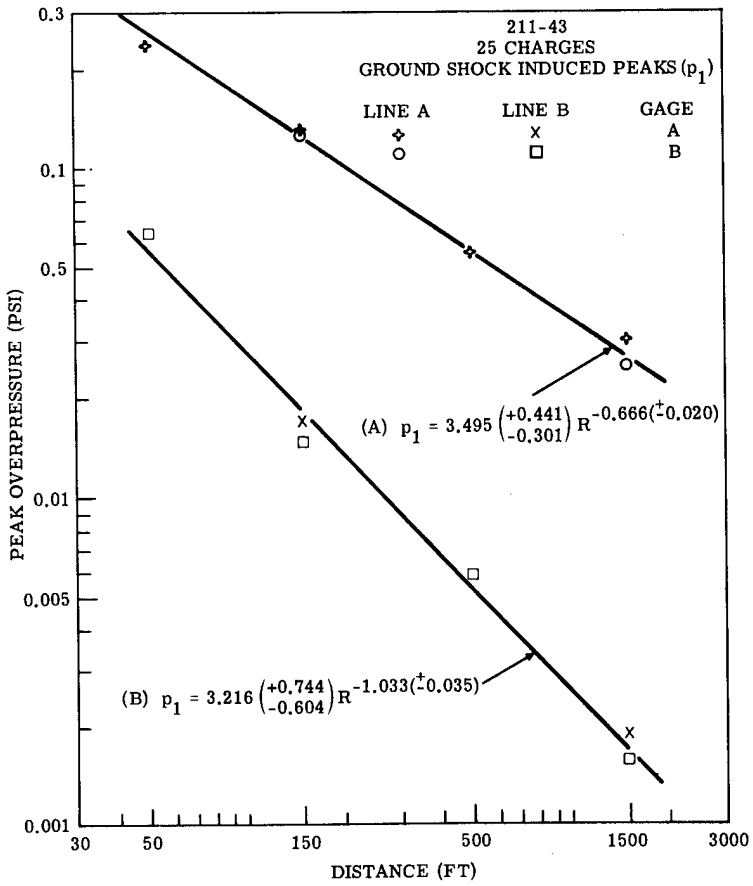

Figure A-130.

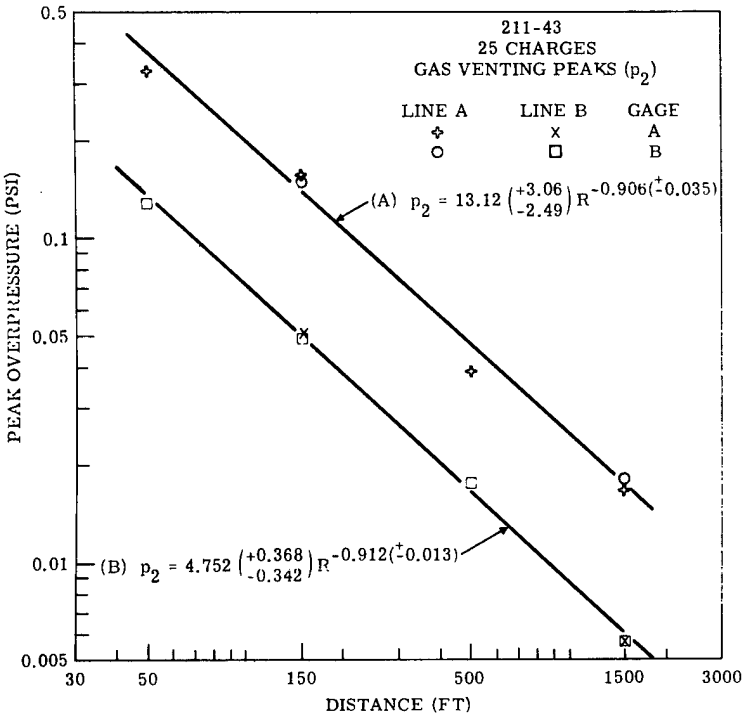

Figure A-131.

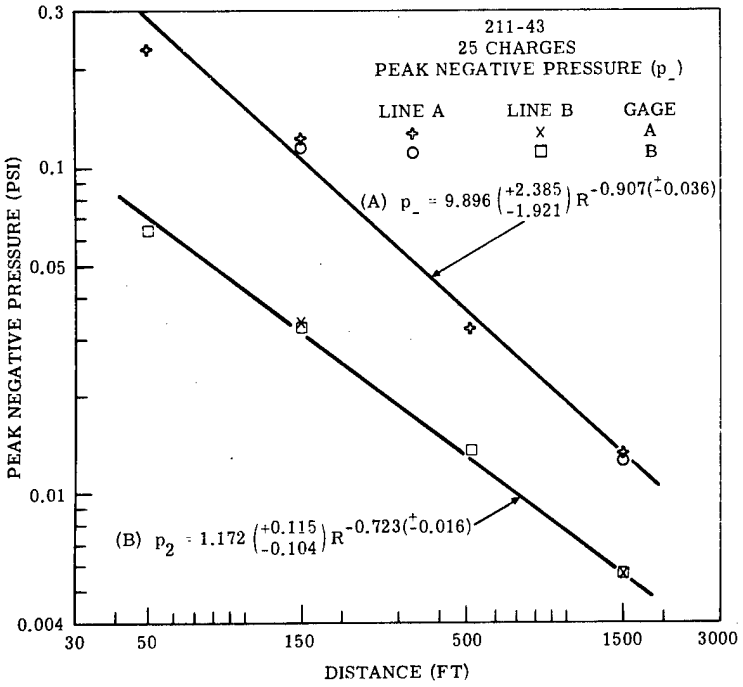

Figure A-132.

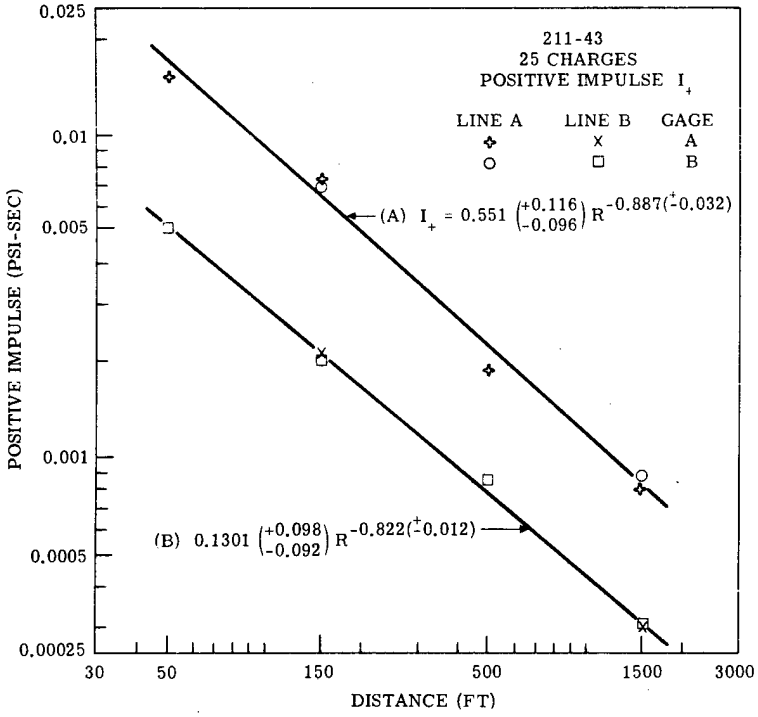

Figure A-133.

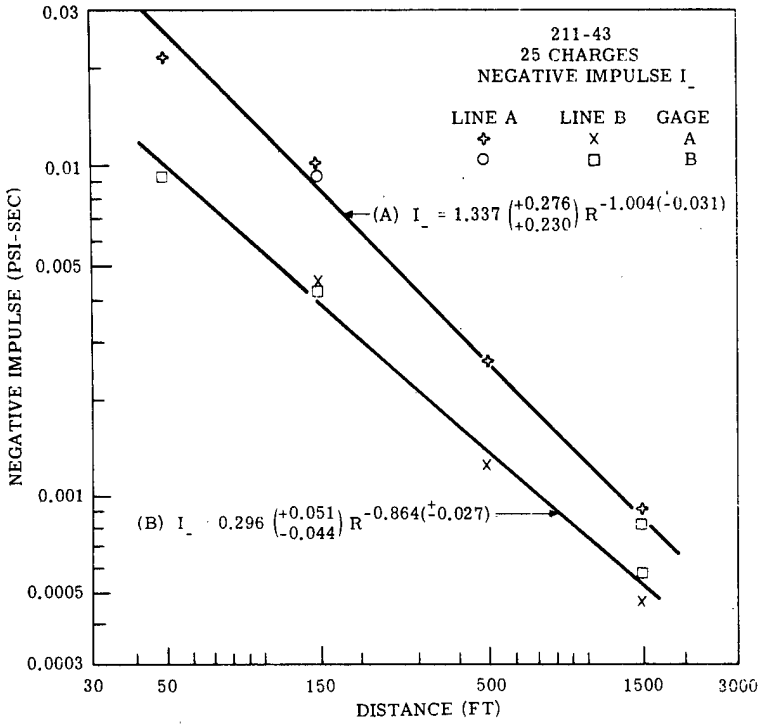
211-43
25 CHARGES
NEGATIVE IMPULSE I_
LINE A LINE B GAGE
A
B
(A) I_ = 1.337 (+0.276 / +0.230) R^-1.004(±0.031)
(B) I_ 0.296 (+0.051 / -0.044) R^-0.864(±0.027)
NEGATIVE IMPULSE (PSI-SEC)
0.03
0.01
0.005
0.001
0.0005
0.0003
30
50
150
500
1500
3000
DISTANCE (FT)

Figure A-134.

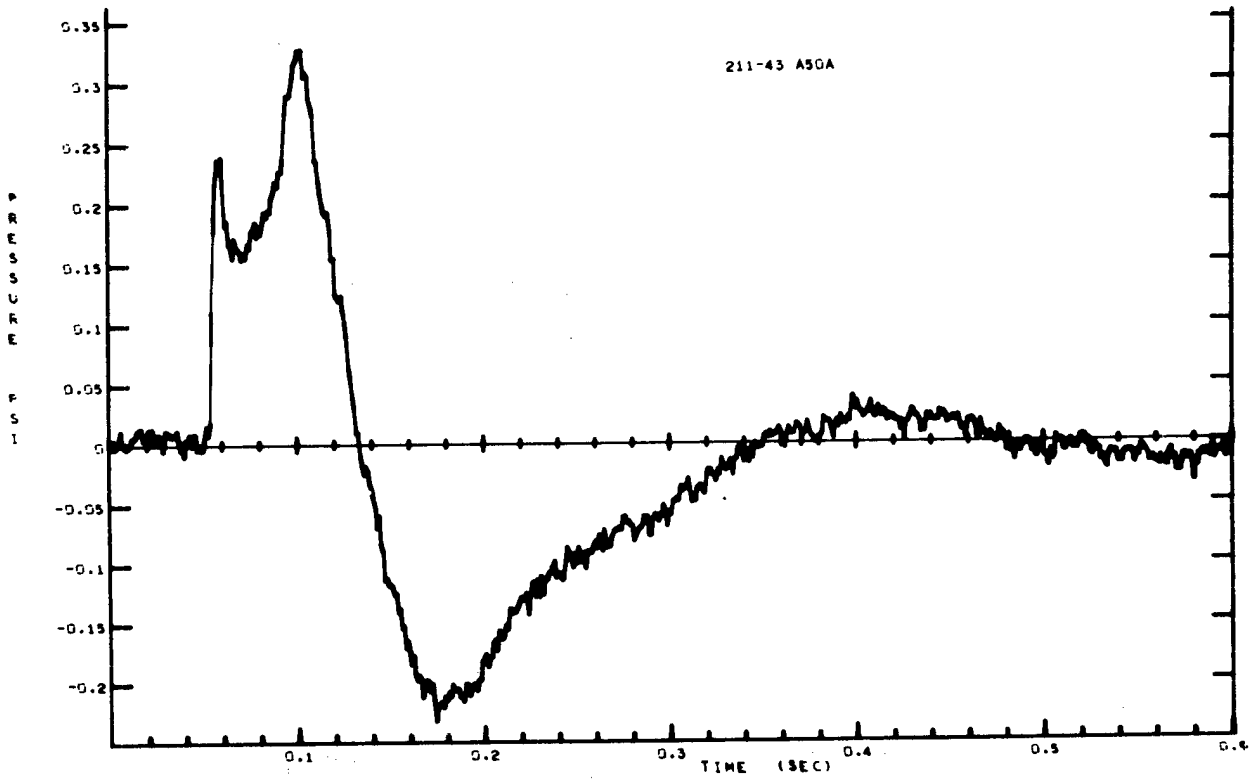

Figure A-135

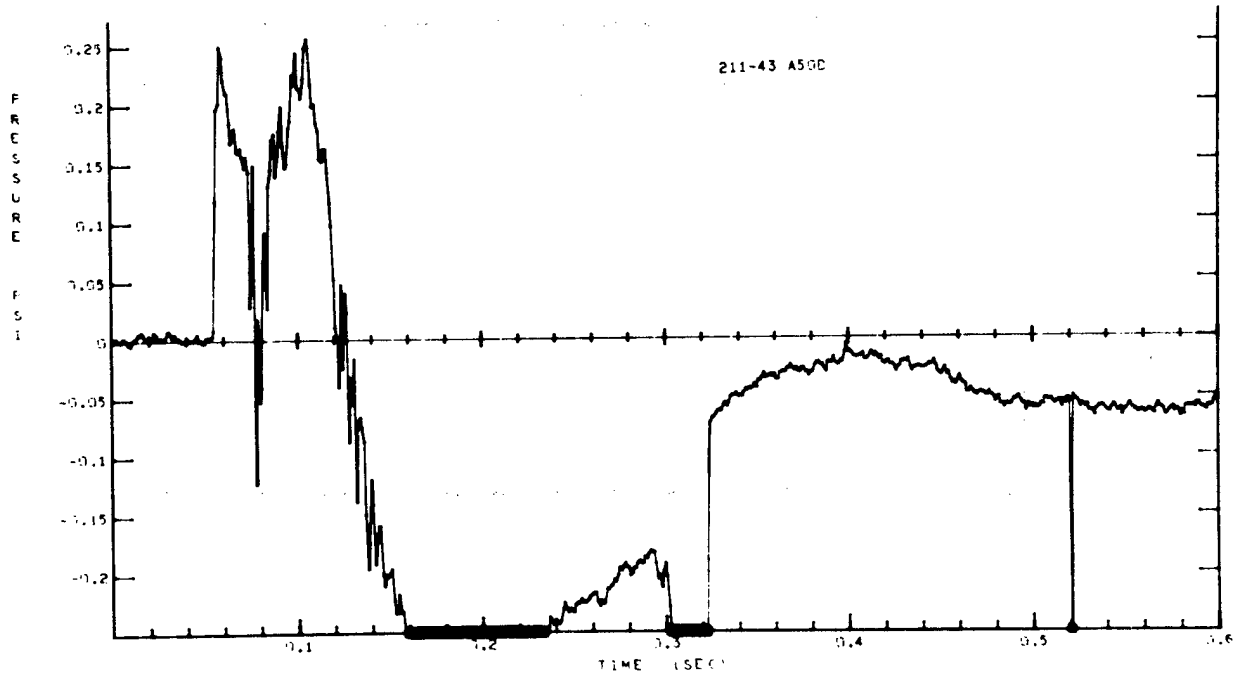

Figure A-136

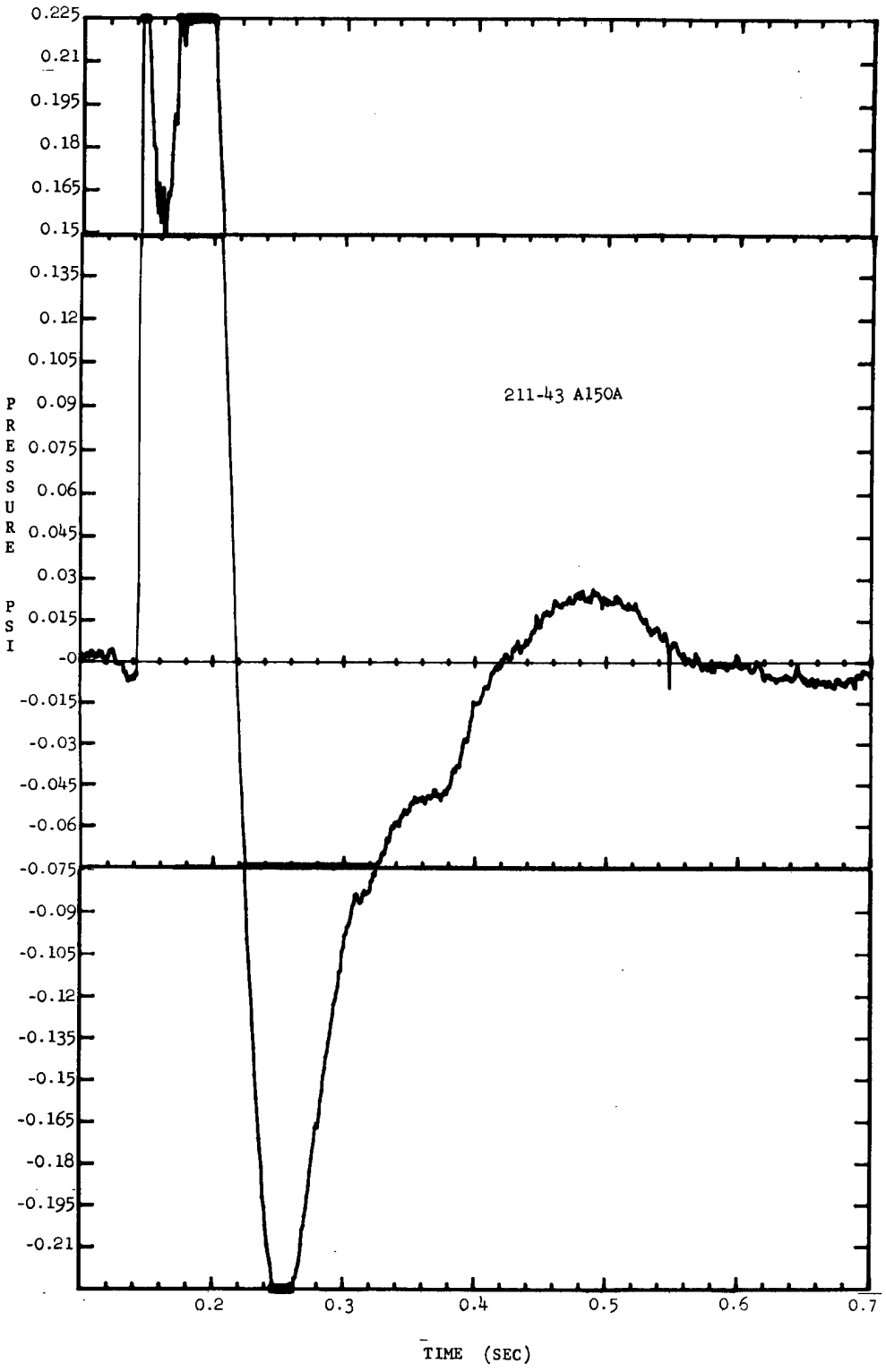
211-43 A150A
PRESSURE PSI
0.225
0.21
0.195
0.18
0.165
0.15
0.135
0.12
0.105
0.09
0.075
0.06
0.045
0.03
0.015
-0
-0.015
-0.03
-0.045
-0.06
-0.075
-0.09
-0.105
-0.12
-0.135
-0.15
-0.165
-0.18
-0.195
-0.21
0.2
0.3
0.4
0.5
0.6
0.7
TIME (SEC)

Figure A-137

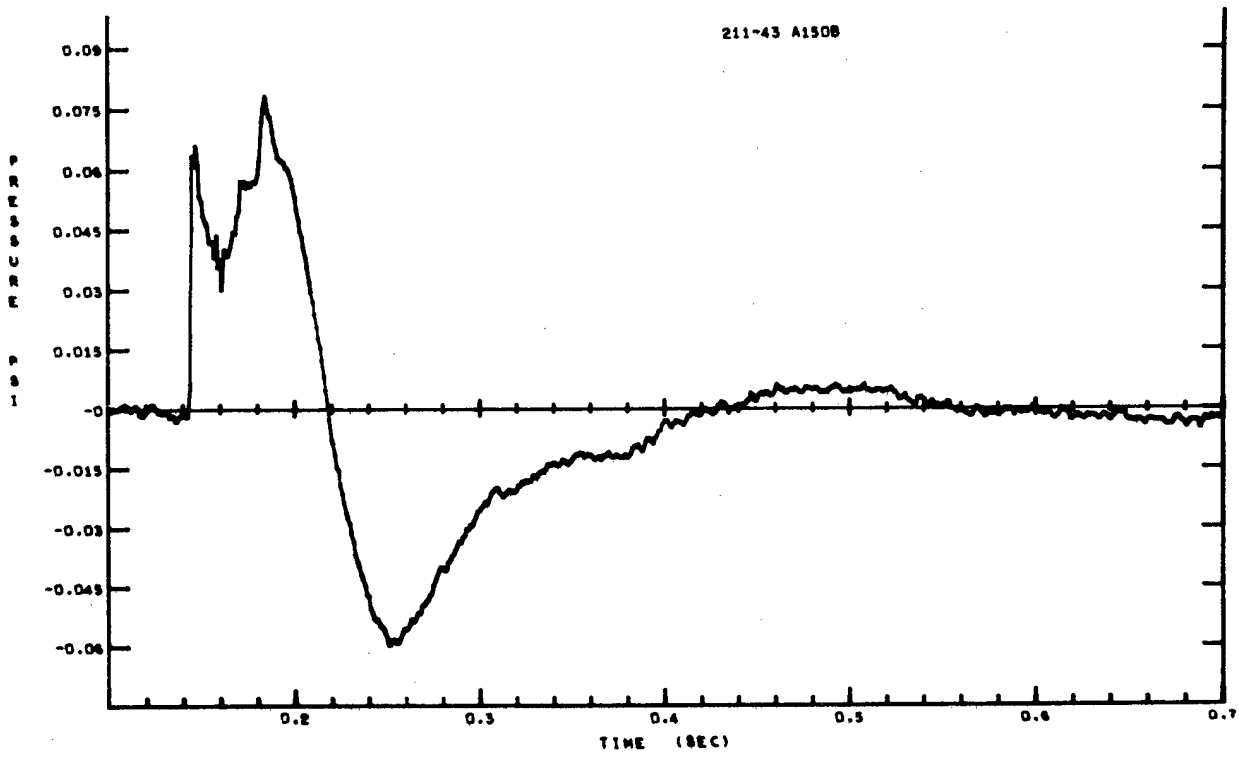

Figure A-138

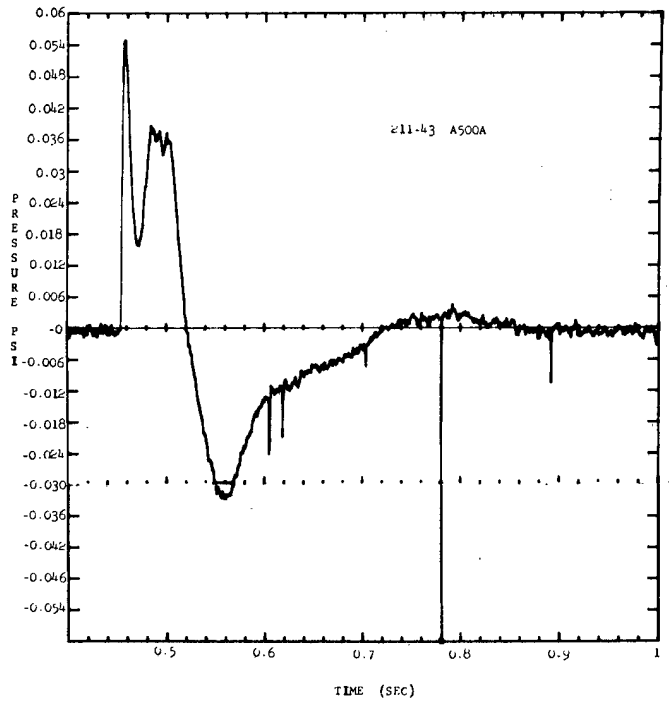

Figure A-139

Figure A-140
(omitted)

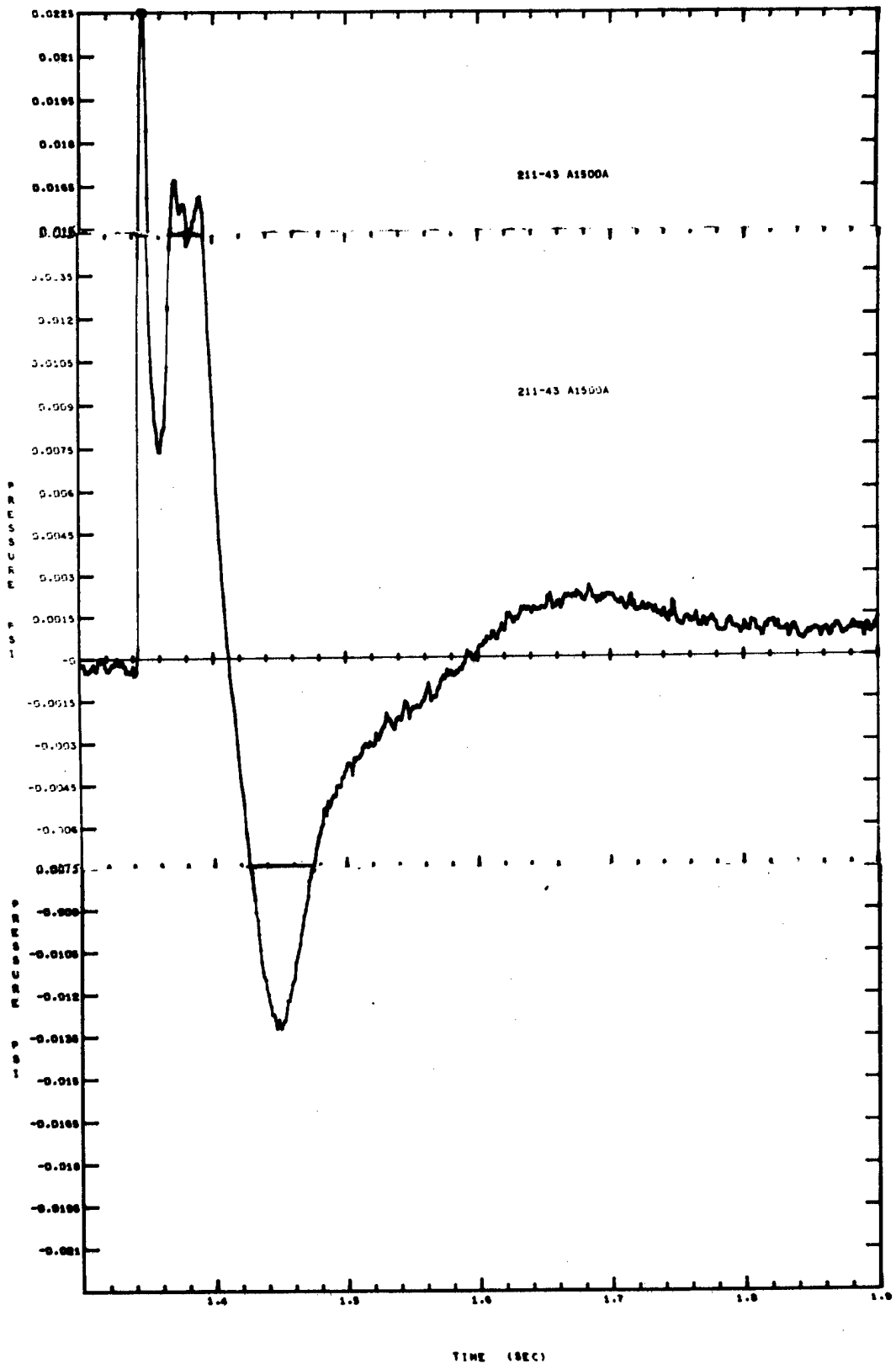
211-43 A1500A
211-43 A1500A
PRESSURE PSI
PRESSURE PSI
TIME (SEC)

Figure A-141.

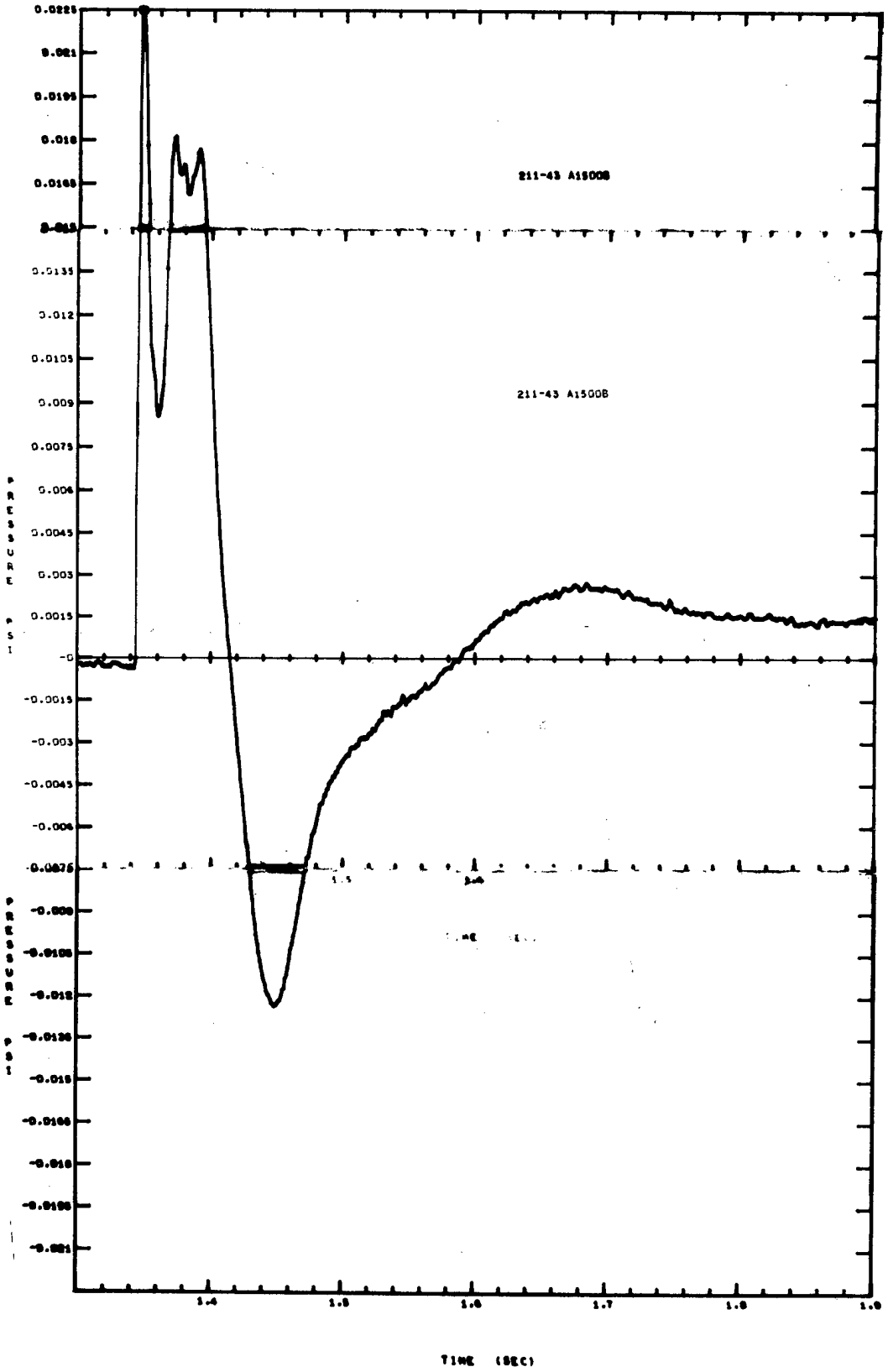

Figure A-142.

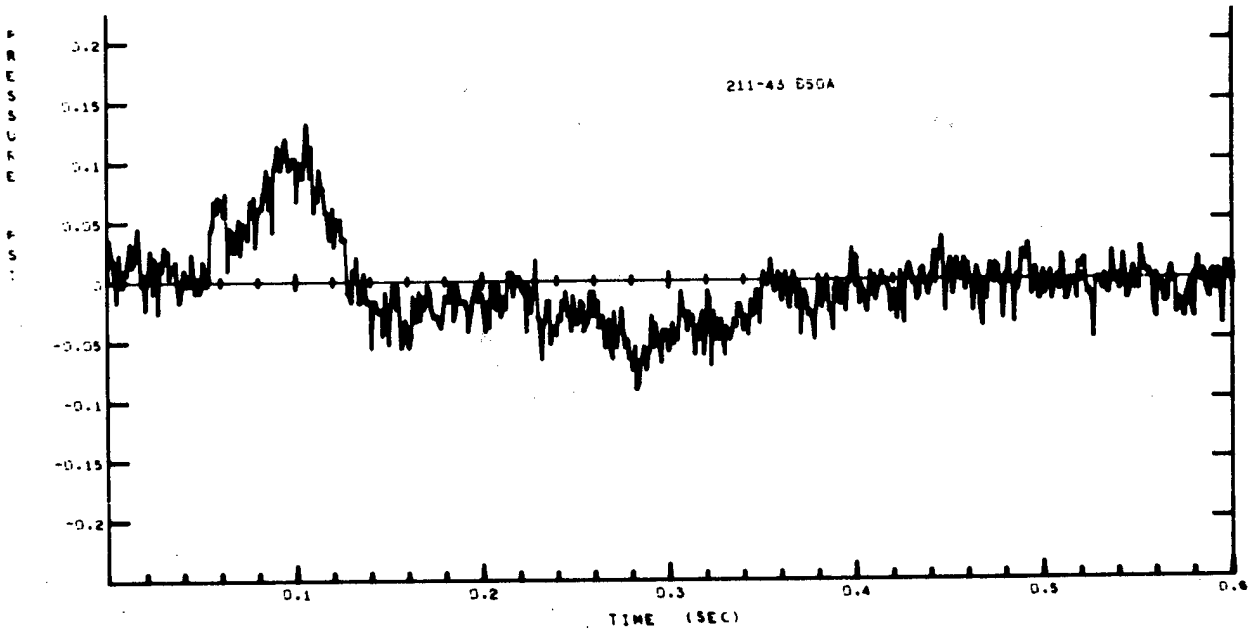

Figure A-143

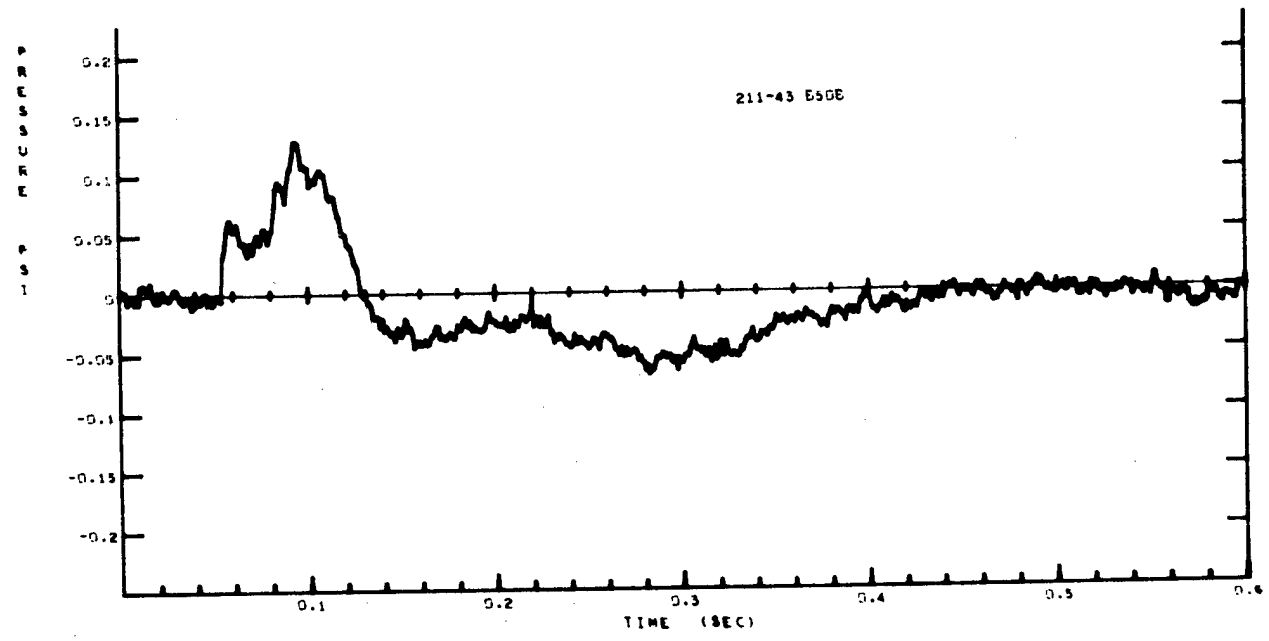

Figure A-144

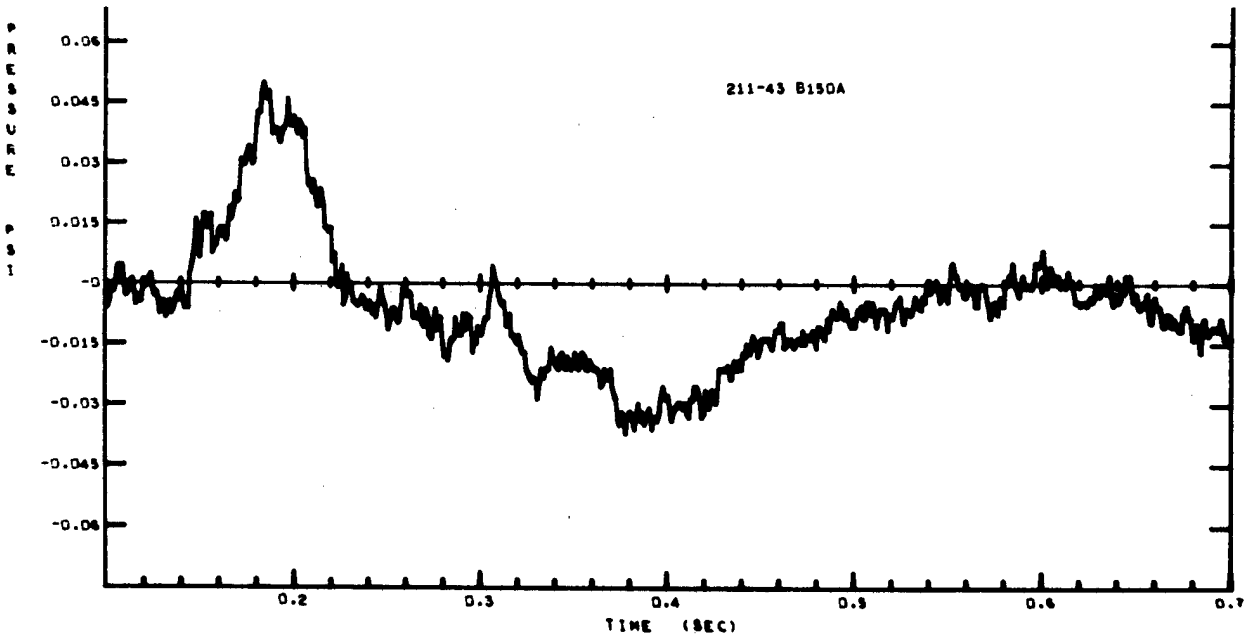

Figure A-145

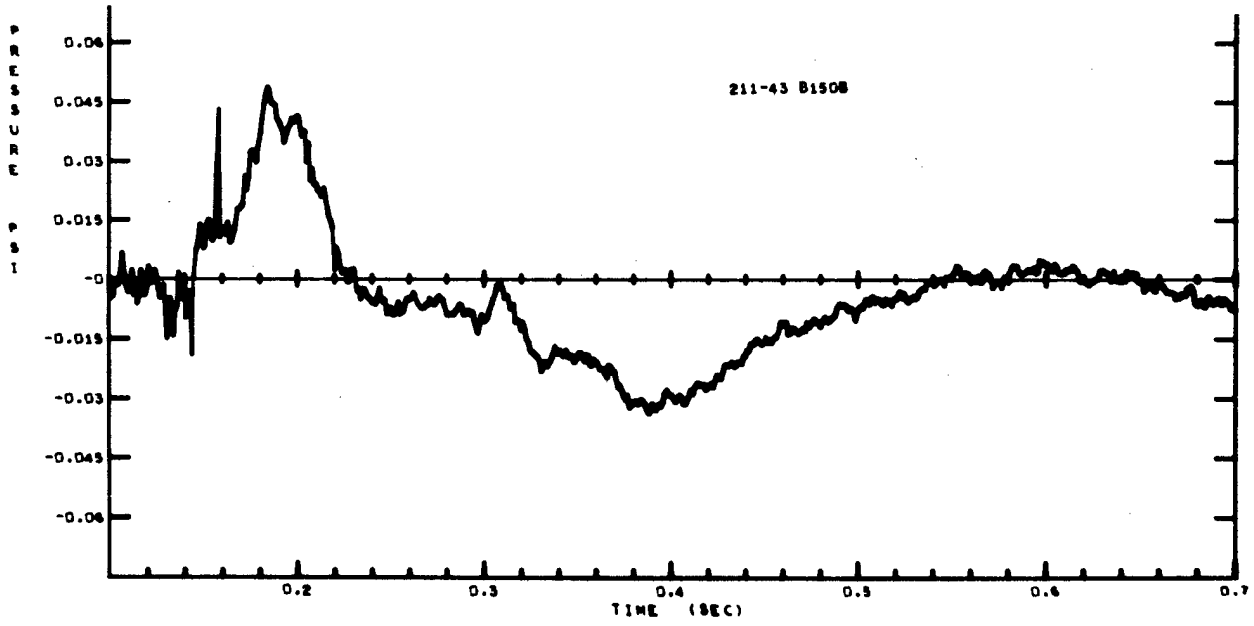

Figure A-146

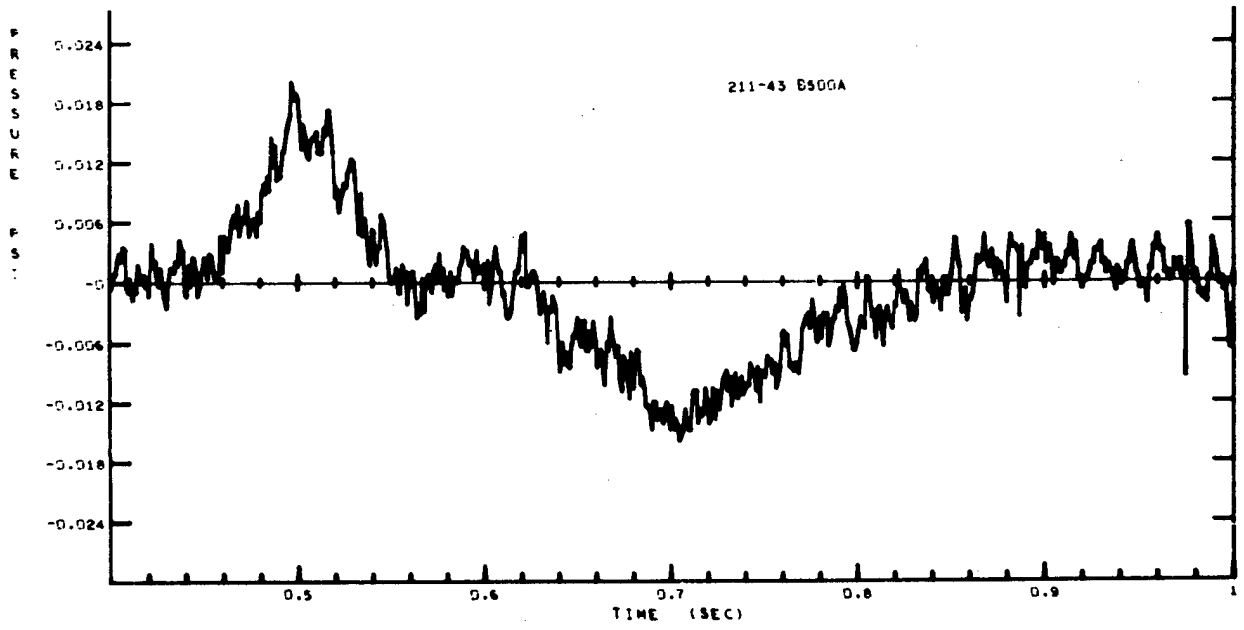

Figure A-147

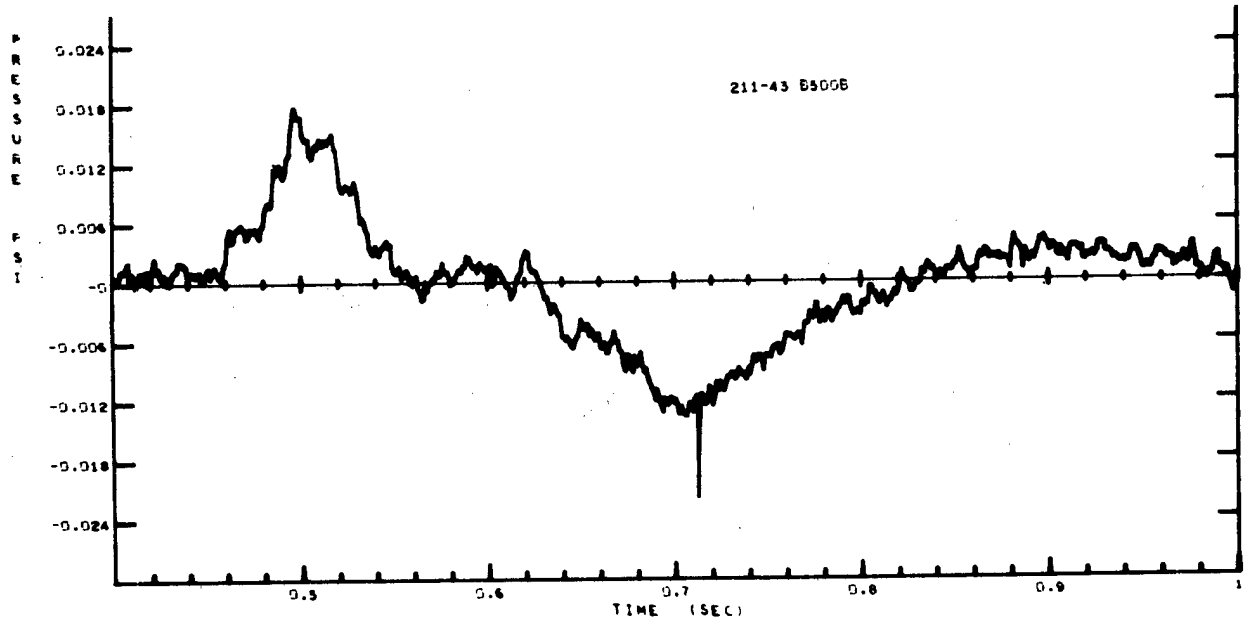

Figure A-148

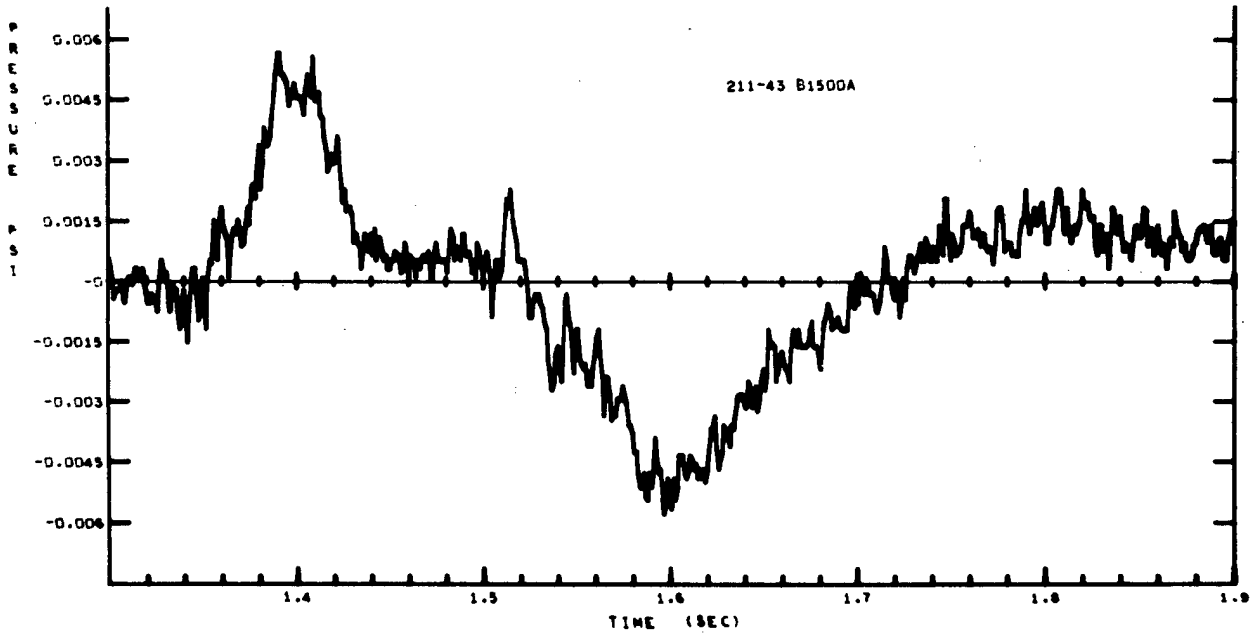

Figure A-149

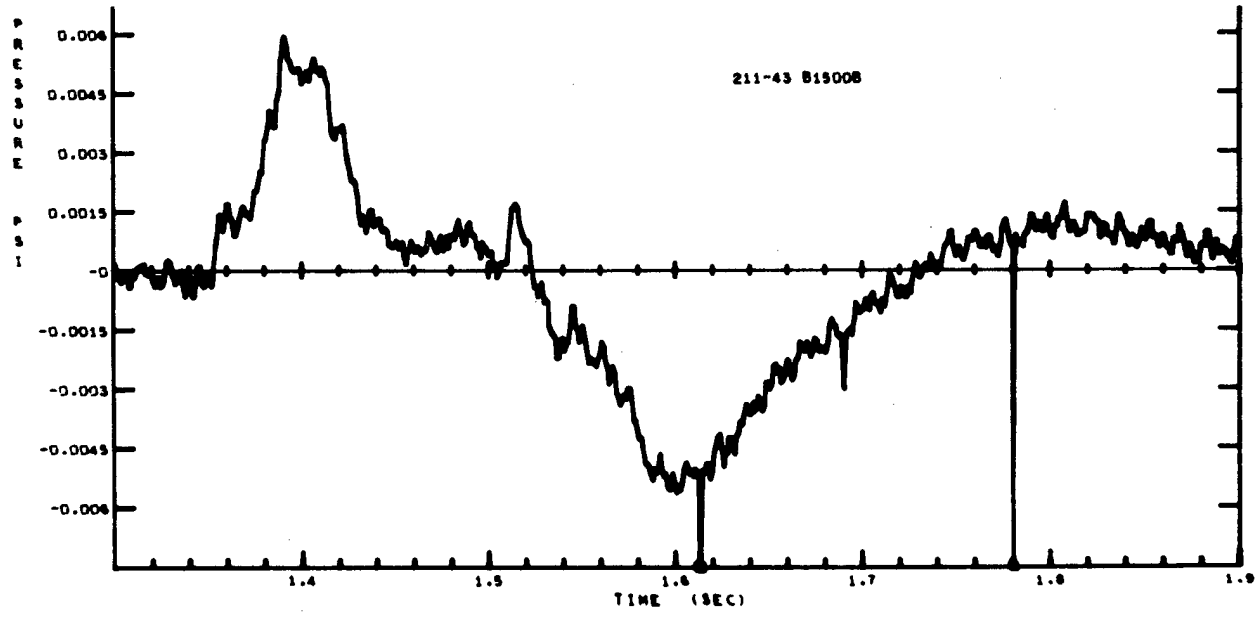

Figure A-150

Shot 211-42

One 64-pound charge was buried 6.9 feet deep. There were two blast lines (A&B), 90° apart. Two gages were placed at each station; gage A is the less sensitive.

Gage	Arrival time (sec)	Ground shock induced peak (psi)	Time of peak (sec)	Peak from venting gas (psi)	Time of peak (sec)	Cross-over (sec)	Positive phase impulse (psi-sec)	Negative peak (psi)	Time of peak (sec)	Cross-over (sec)	Negative phase impulse (psi-sec)
A50A	0.047	0.0366	0.051	0.0226	0.101	0.119	0.00107	-0.0244	0.146	0.257	0.00145
A50B	0.047	0.0368	0.051	0.0233	0.100	0.119	0.00113	-0.0248	0.147	0.254	0.00144
A150B	0.138	0.0112	0.141	0.0095	0.190	0.210	0.000383	-0.0089	0.234	0.328	0.000545
A500A	0.448	0.0032	0.450	0.0027	0.498	0.520	0.000114	-0.0026	0.545	0.643	0.000157
A500B	0.448	0.0028	0.455	0.0022	0.500	0.520	0.000097	-0.0024	0.544	0.641	0.000142
A1500A	1.334	0.0012	1.338	0.0010	1.386	1.408	0.000043	-0.0010	1.436	1.525	0.0000604
A1500B	1.334	0.0010	1.338	0.0008	1.384	1.408	0.000038	-0.0007	1.433	1.525	0.0000433
B50A	0.052	0.0374	0.059	0.0217	0.096	0.123	0.000985	-0.0247	0.155	0.269	0.001285
B50B	0.052	0.0400	0.059	0.0223	0.096	0.123	0.00104	-0.0265	0.153	0.265	0.00142
B150A	0.141	0.0121	0.148	0.0082	0.190	0.215	0.000359	-0.0082	0.244	0.328	0.000462
B150B	0.142	0.0126	0.148	0.0082	0.187	0.215	0.000371	-0.0088	0.245	0.344	0.000525
B1500A	1.344	0.0010	1.349	0.00065	1.391	1.416	0.0000288	-0.000825	1.451	1.549	0.0000469
B1500B	1.345	0.00136	1.349	0.000868	1.388	1.417	0.0000398	-0.000967	1.450	1.540	0.0000572

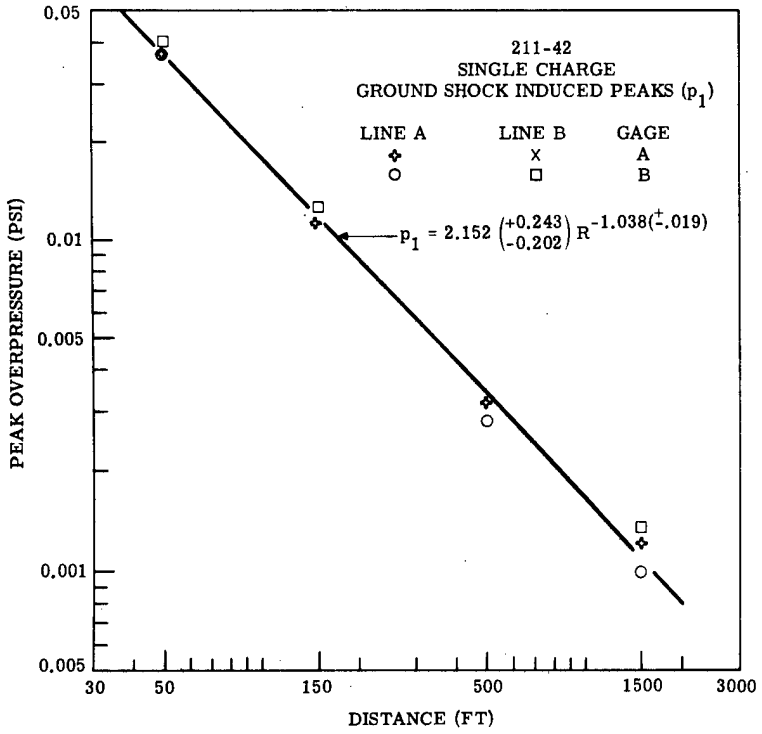

Figure A-151

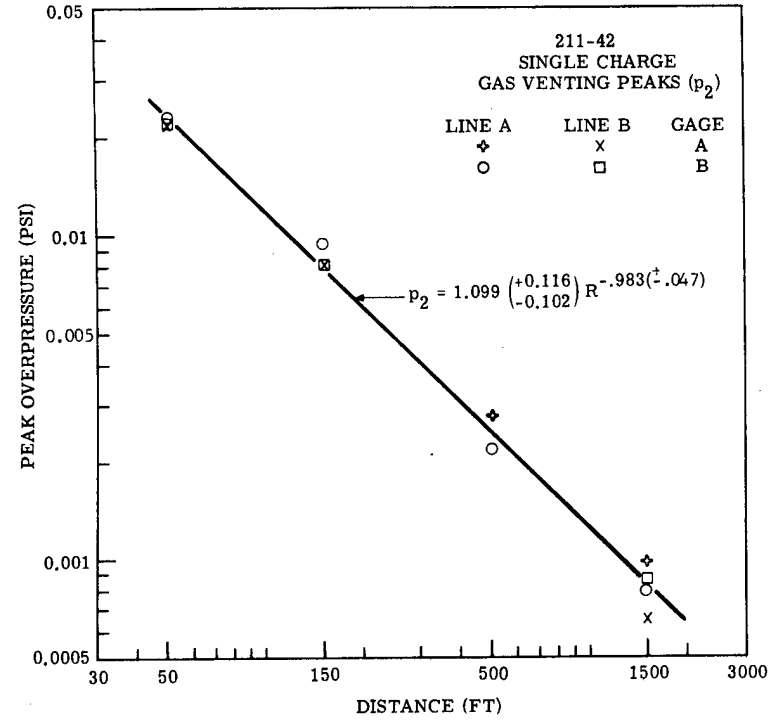

Figure A-152

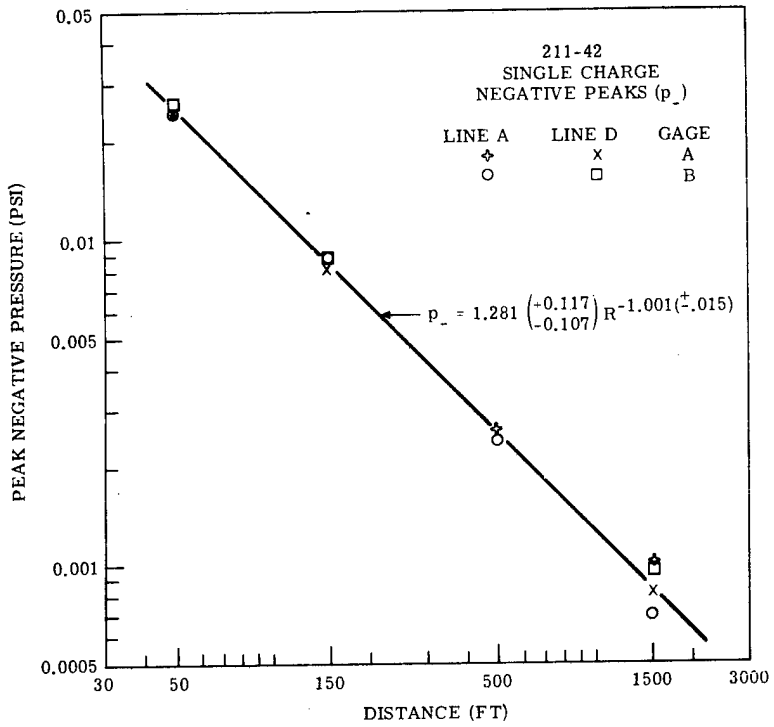

Figure A-153

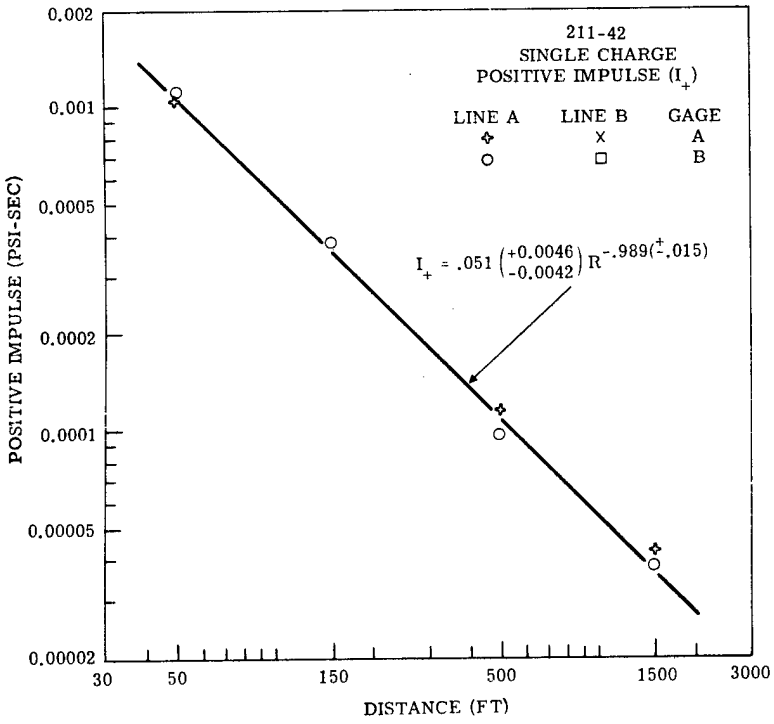

Figure A-154

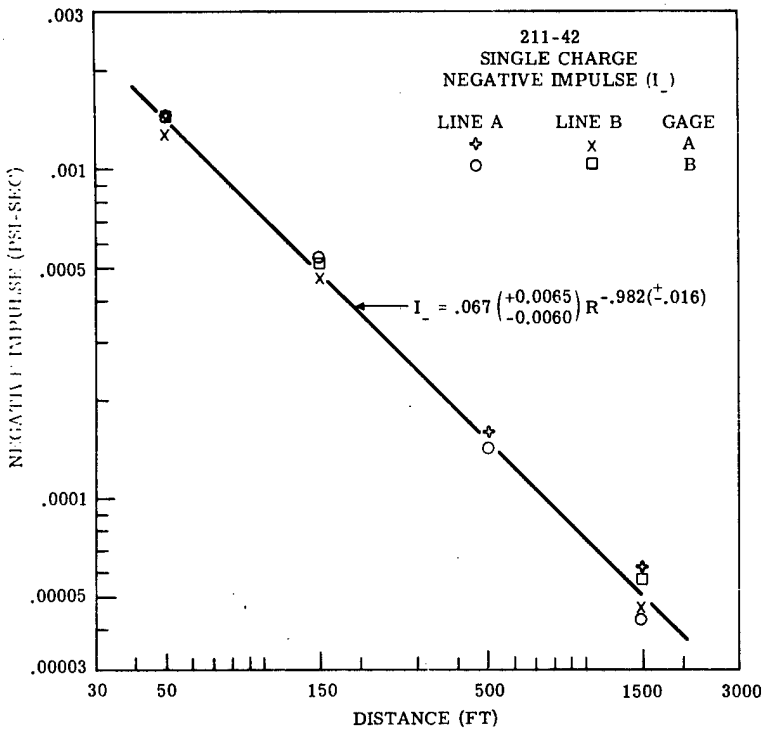
211-42
SINGLE CHARGE
NEGATIVE IMPULSE (I_)
LINE A
LINE B
GAGE
A
B
I_ = .067 (+0.0065 / -0.0060) R^-.982(±.016)
.003
.001
.0005
.0001
.00005
.00003
30
50
150
500
1500
3000
DISTANCE (FT)

Figure A-155

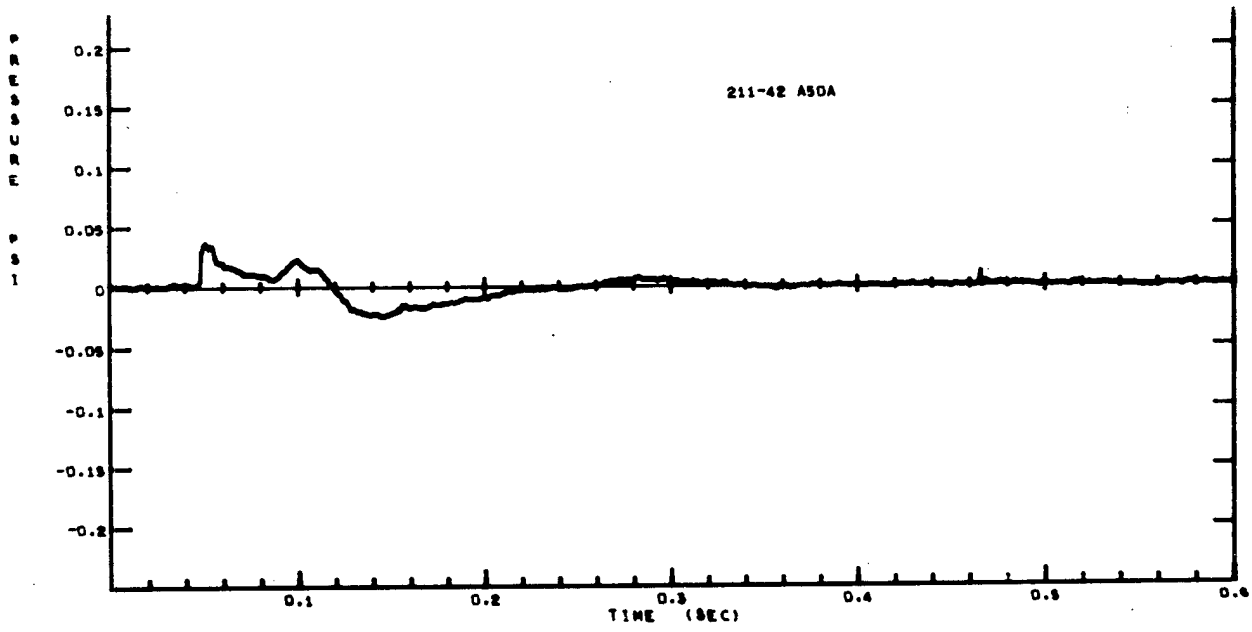

Figure A-156

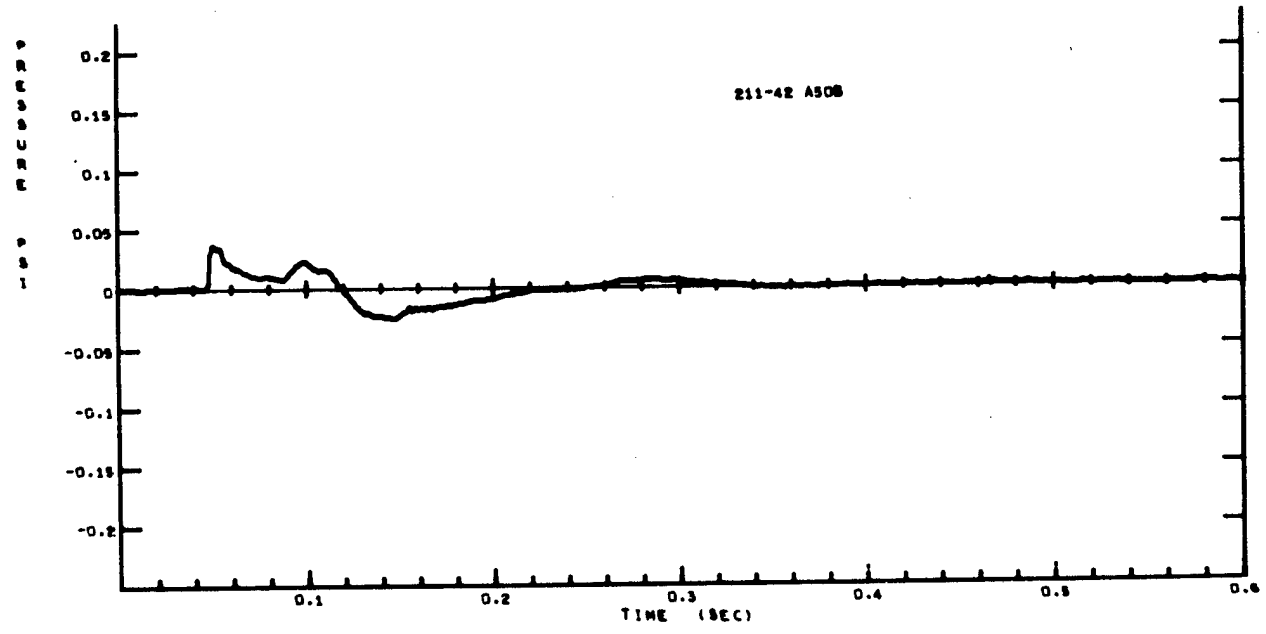

Figure A-157

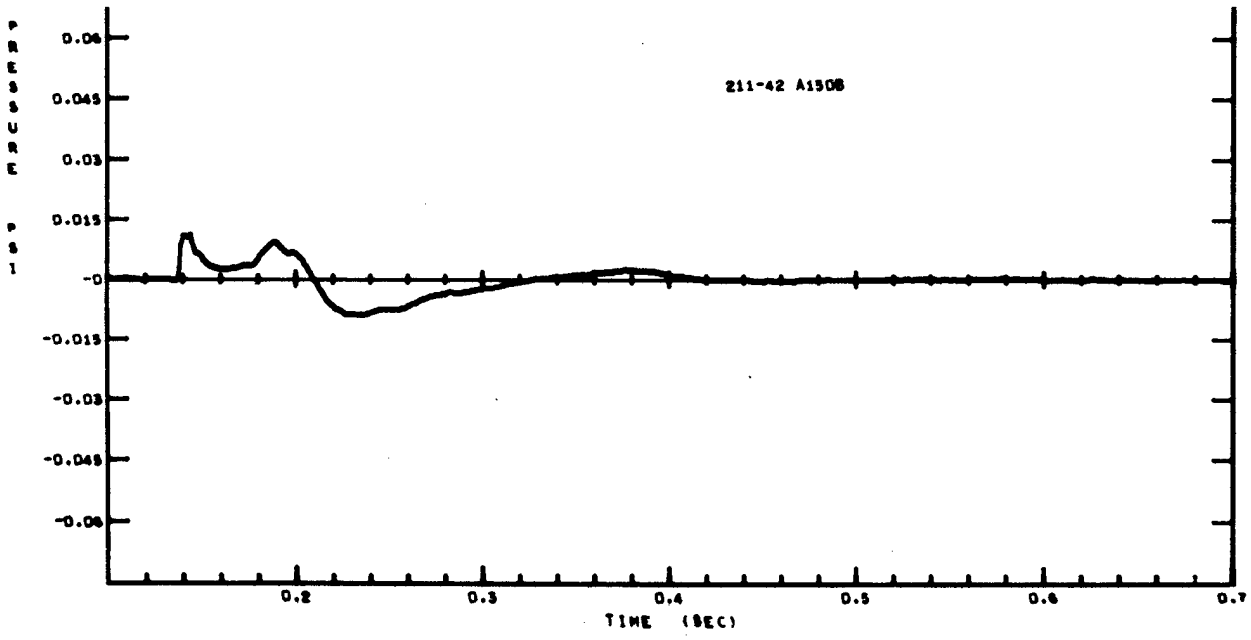

Figure A-158

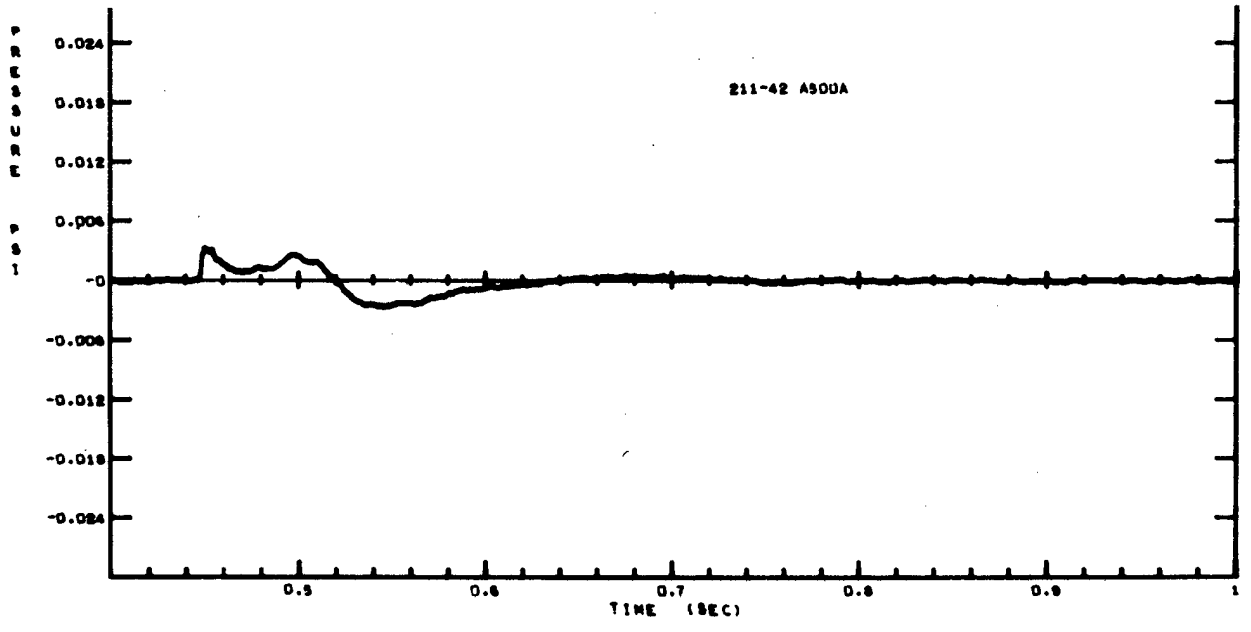

Figure A-159

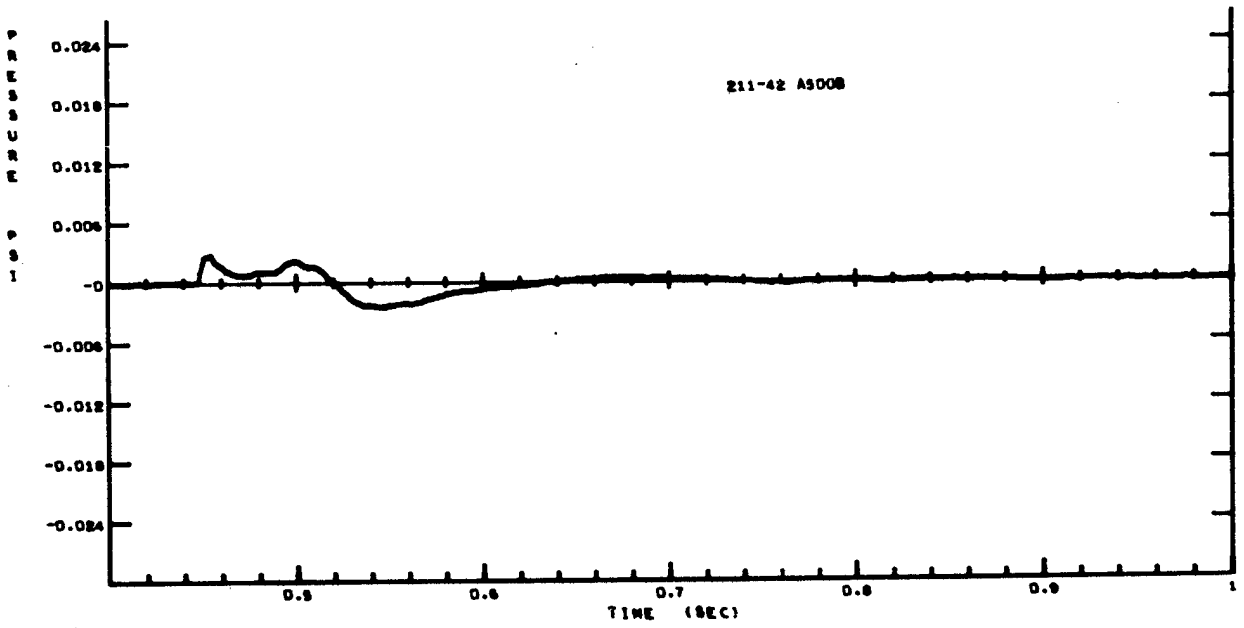

Figure A-160

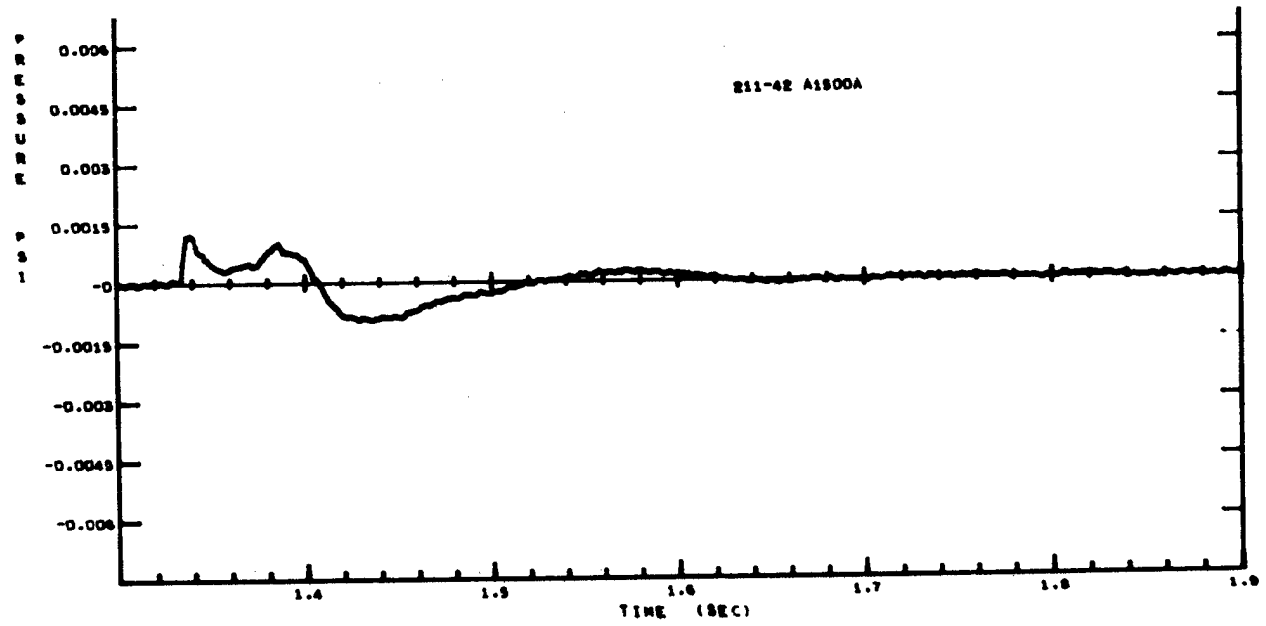

Figure A-161

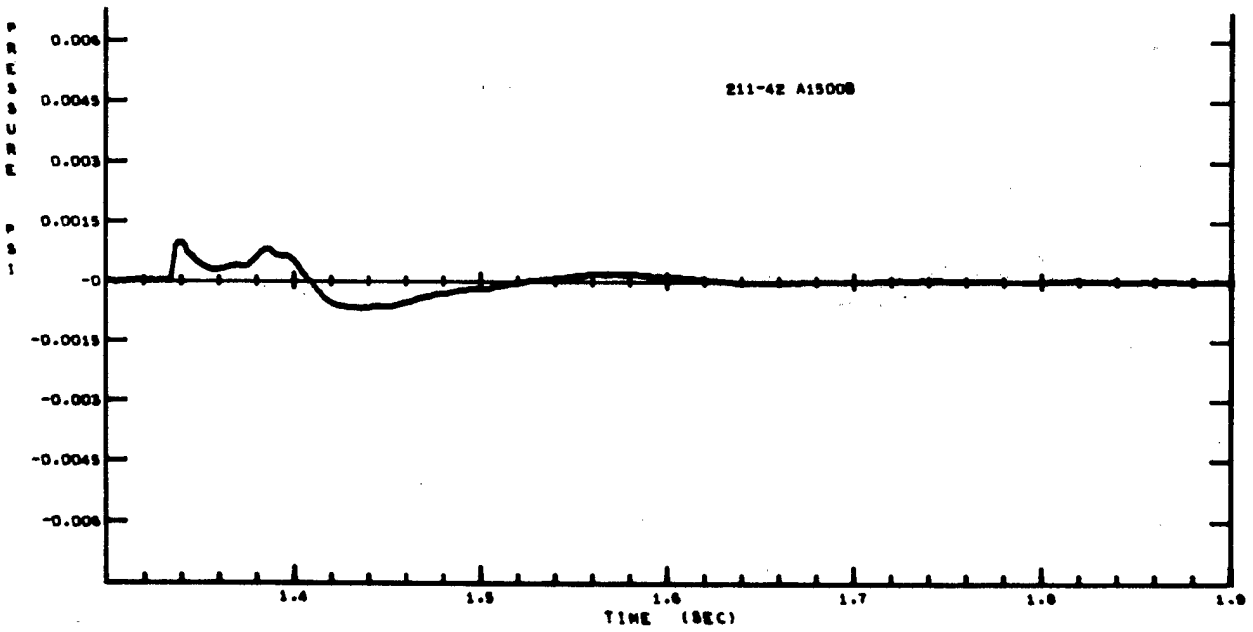

Figure A-162

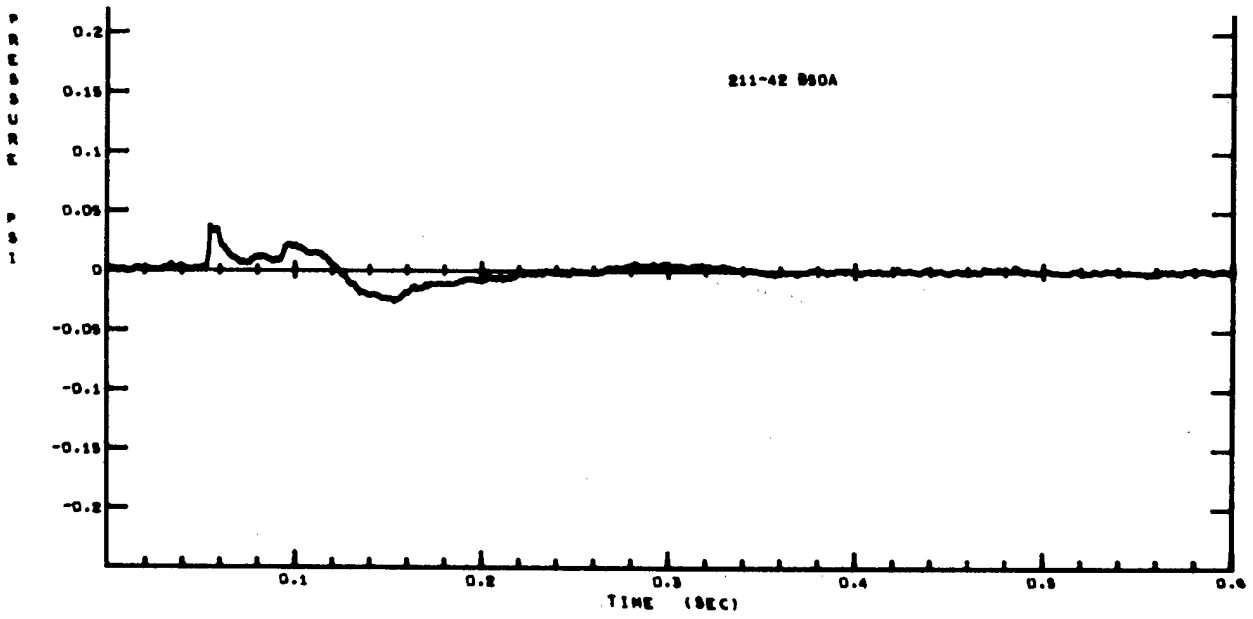

Figure A-163

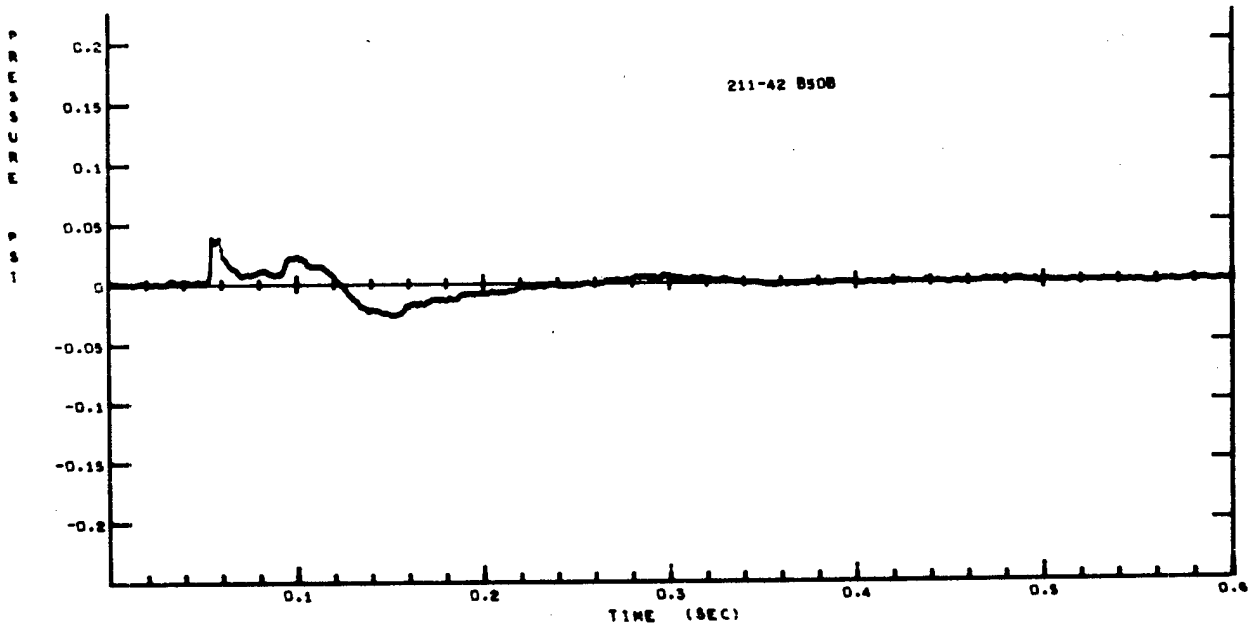

Figure A-164

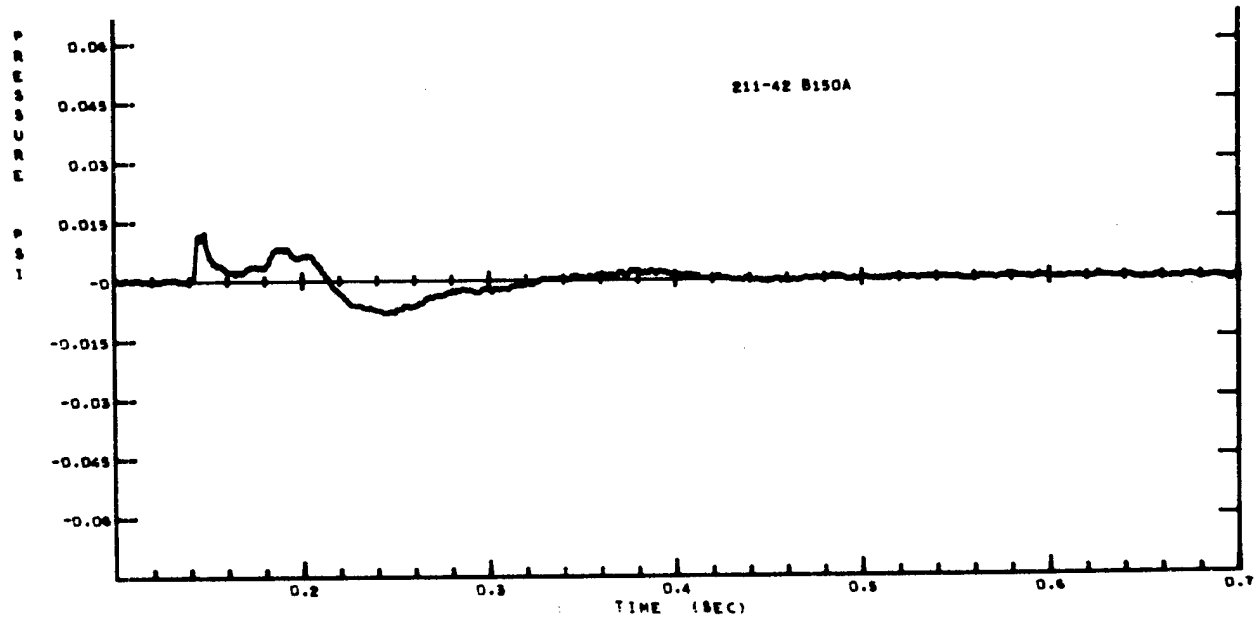

Figure A-165

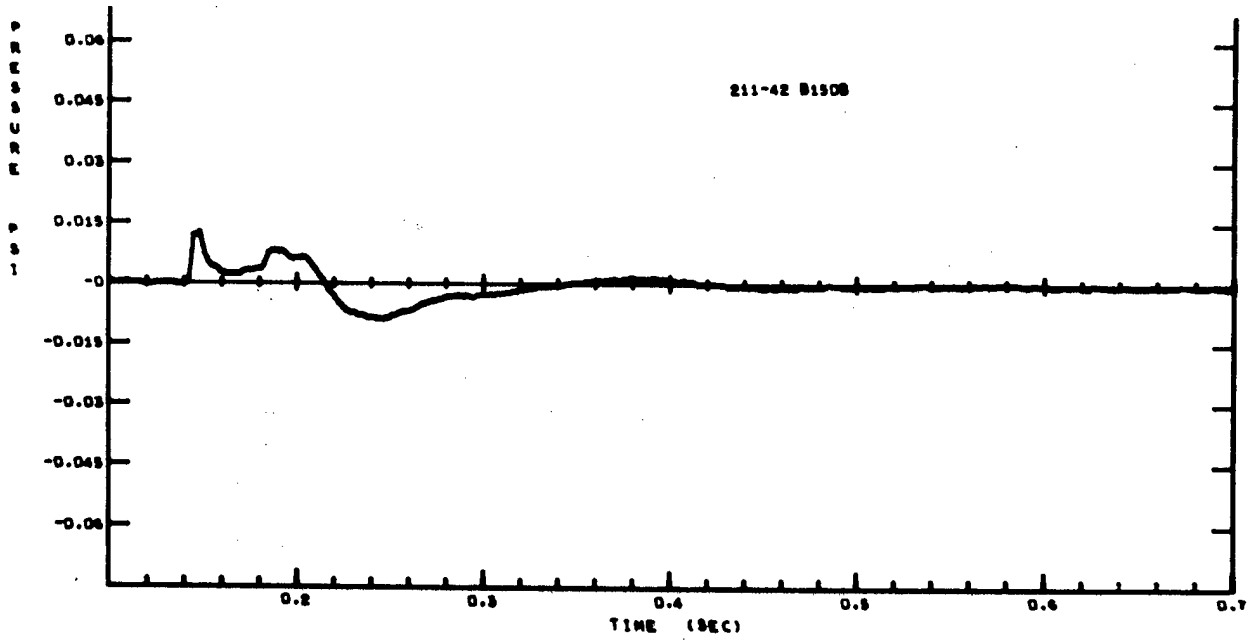

Figure A-166

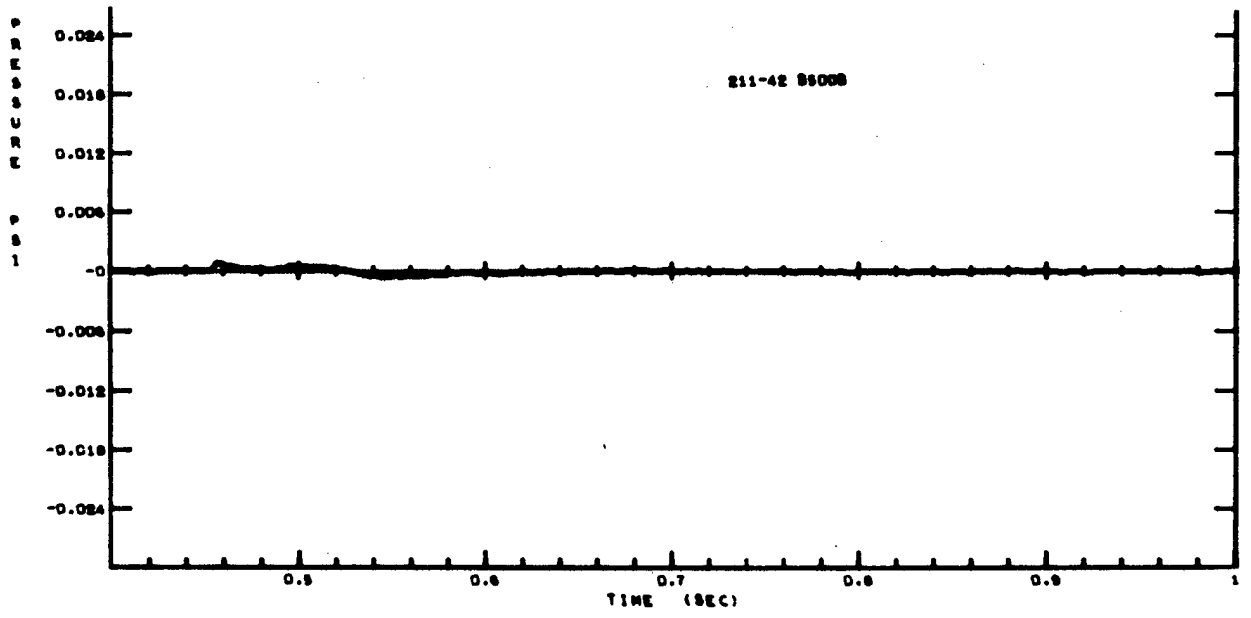

Figure A-167

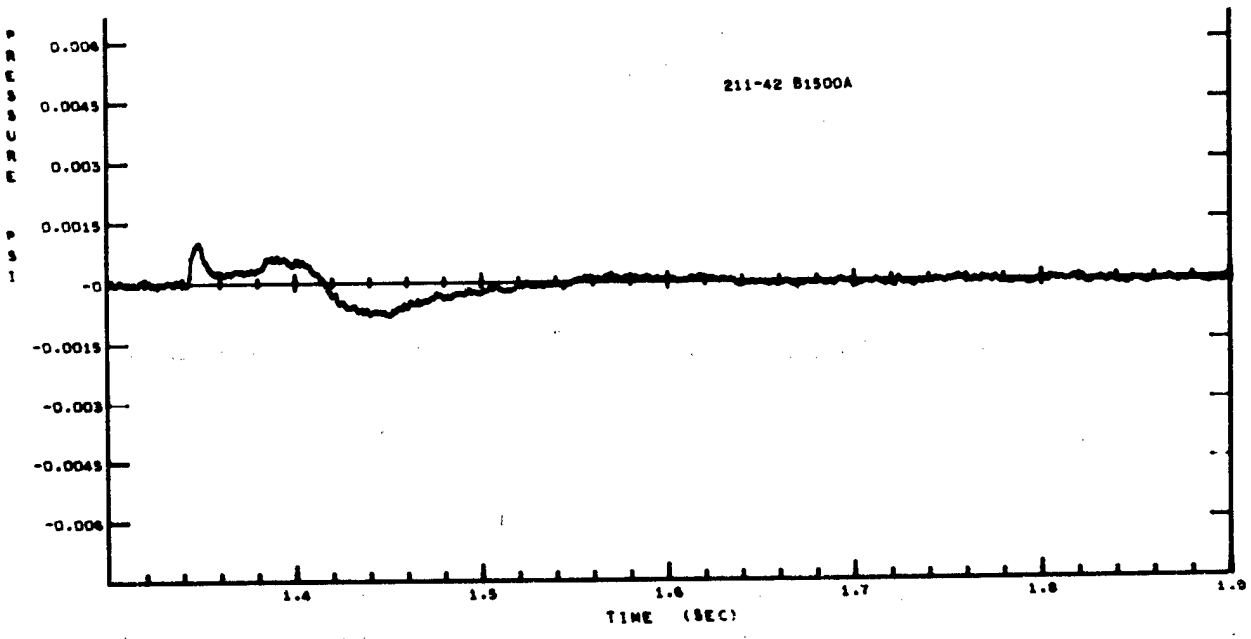

Figure A-168

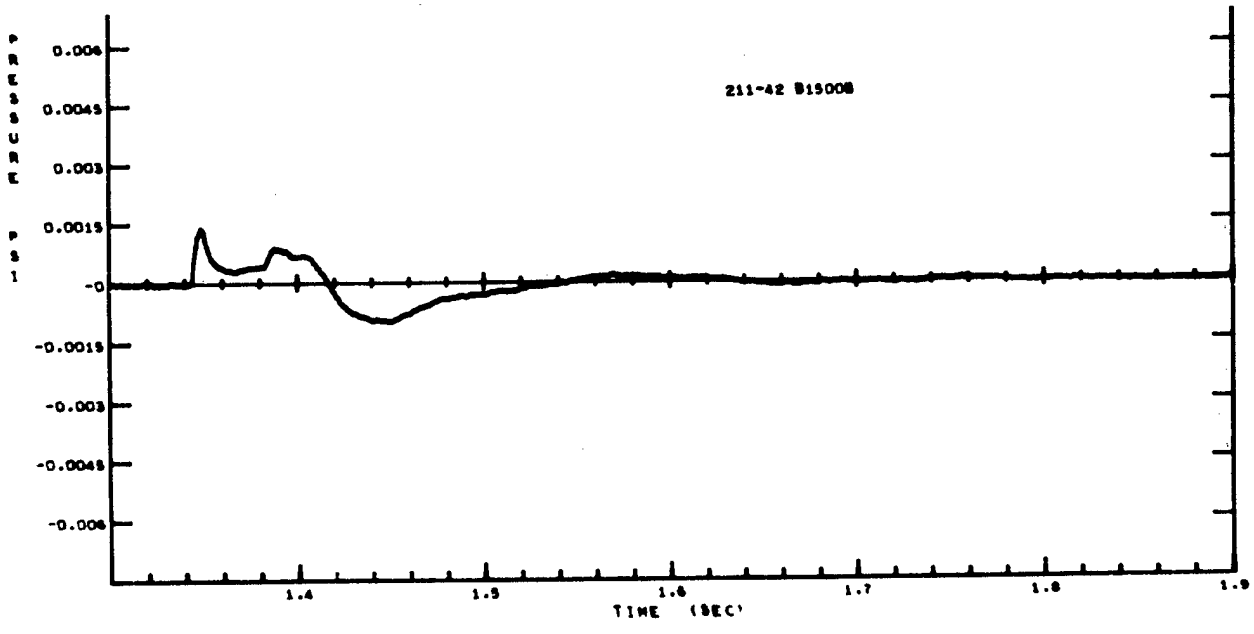

Figure A-169

Shot 211-46

Two 64-pound charges were buried 6.9 feet deep, spread 5.25 feet apart. There were two blast lines (A&B) 90° apart. Two gages were placed at each station; gage A is the less sensitive.

Gage	Arrival time (sec)	Ground shock induced peak (psi)	Time of peak (sec)	Peak from venting gas (psi)	Time of peak (sec)	Cross-over (sec)	Positive phase impulse (psi-sec)	Negative peak (psi)	Time of peak (sec)	Cross-over (sec)	Negative phase impulse (psi-sec)
A50A	0.048	0.09325	0.051	0.03325	0.112	0.122	0.001933	-0.06975	0.158	0.243	0.00386
A50B	0.048	0.08762	0.051	0.03362	0.112	0.122	0.002074	-0.06238	0.160	0.239	0.00342
A150A	0.139	0.02584	0.142	0.01714	0.200	0.213	0.000836	-0.02108	0.242	0.341	0.00144
A150B	0.139	0.02244	0.143	0.01594	0.200	0.213	0.000783	-0.02076	0.242	0.330	0.00126
A500A	0.455	0.0071	0.456	0.0041	0.513	0.524	0.000154	-0.0070	0.558	0.638	0.000375
A500B	0.455	0.0072	0.457	0.0050	0.513	0.528	0.000228	-0.0074	0.559	0.637	0.000396
A1500A	1.356	0.0018	1.362	0.0016	1.415	1.433	0.000082	-0.0019	1.463	1.541	0.000104
A1500B	1.357	0.0016	1.363	0.0014	1.418	1.433	0.000072	-0.0017	1.463	1.541	0.000097
B50A	0.046	0.05375	0.057	0.03775	0.113	0.125	0.00187	-0.05425	0.157	0.241	0.00308
B50B	0.045	0.05247	0.055	0.03747	0.109	0.126	0.00197	-0.05153	0.156	0.240	0.00303
B150A	0.141	0.0166	0.146	0.0139	0.199	0.217	0.000735	-0.0160	0.250	0.332	0.00115
B150B	0.141	0.0176	0.146	0.0147	0.198	0.217	0.000768	-0.0184	0.244	0.330	0.00120
B500A	0.458	0.0053	0.462	0.0040	0.515	0.532	0.000201	-0.0062	0.564	0.642	0.000356
B500B	0.458	0.0048	0.463	0.0039	0.515	0.532	0.000205	-0.0060	0.563	0.642	0.000348
B1500A	1.365	0.001725	1.370	0.001825	1.406	1.442	0.0000792	-0.002075	1.476	1.552	0.000122

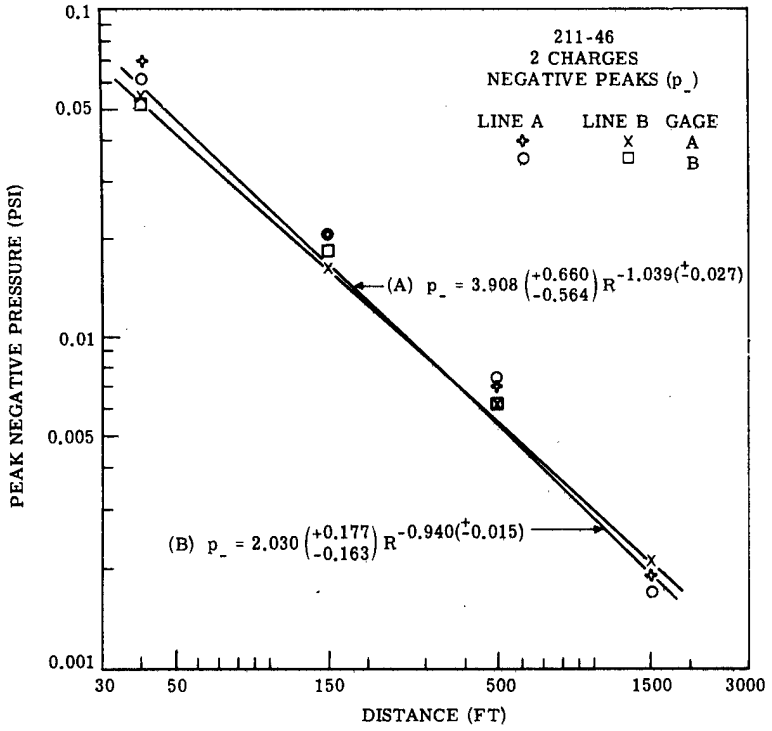

Figure A-172.

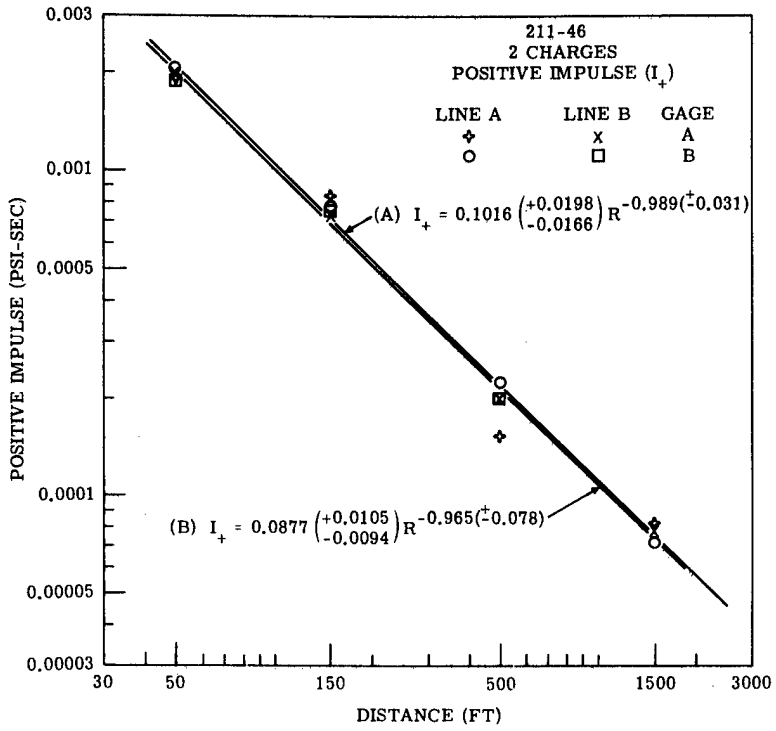

Figure A-173.

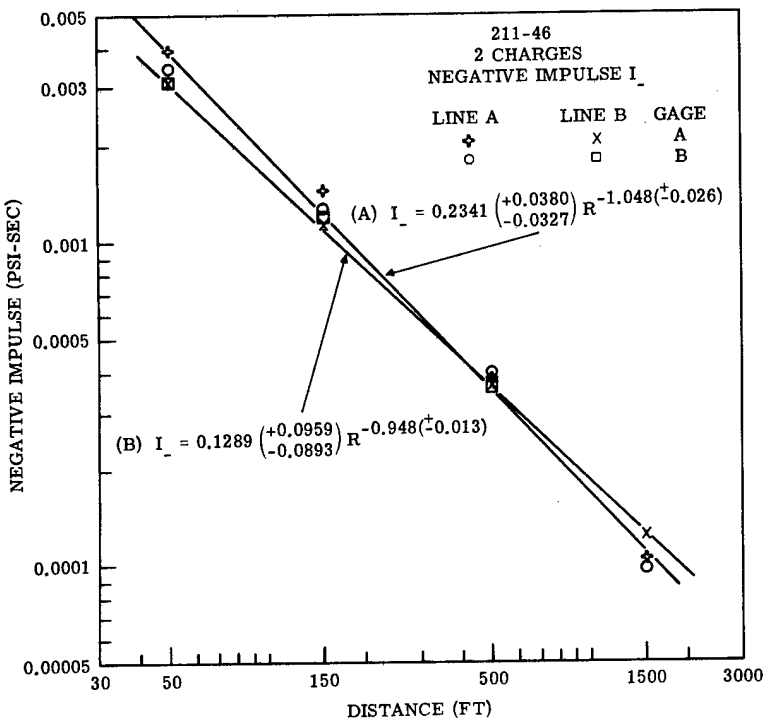
211-46
2 CHARGES
NEGATIVE IMPULSE I_
LINE A
LINE B
GAGE
A
B
(A) I_ = 0.2341 (+0.0380 / -0.0327) R^-1.048(±0.026)
(B) I_ = 0.1289 (+0.0959 / -0.0893) R^-0.948(±0.013)
NEGATIVE IMPULSE (PSI-SEC)
0.005
0.003
0.001
0.0005
0.0001
0.00005
30
50
150
500
1500
3000
DISTANCE (FT)

Figure A-174.

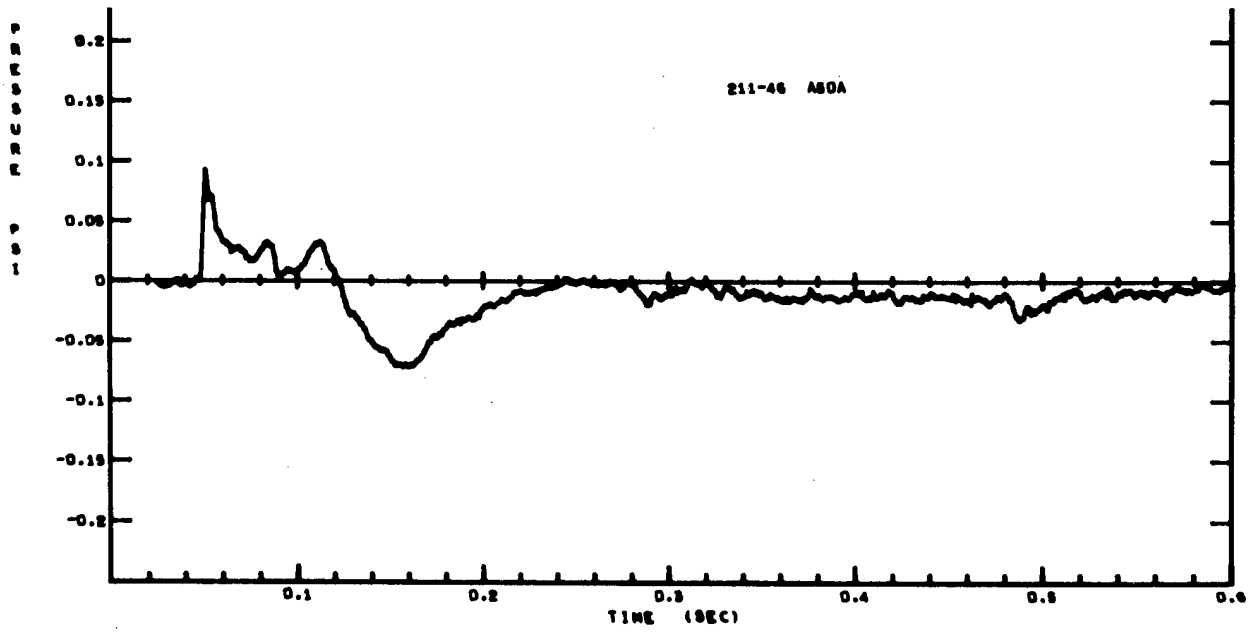

Figure A-175

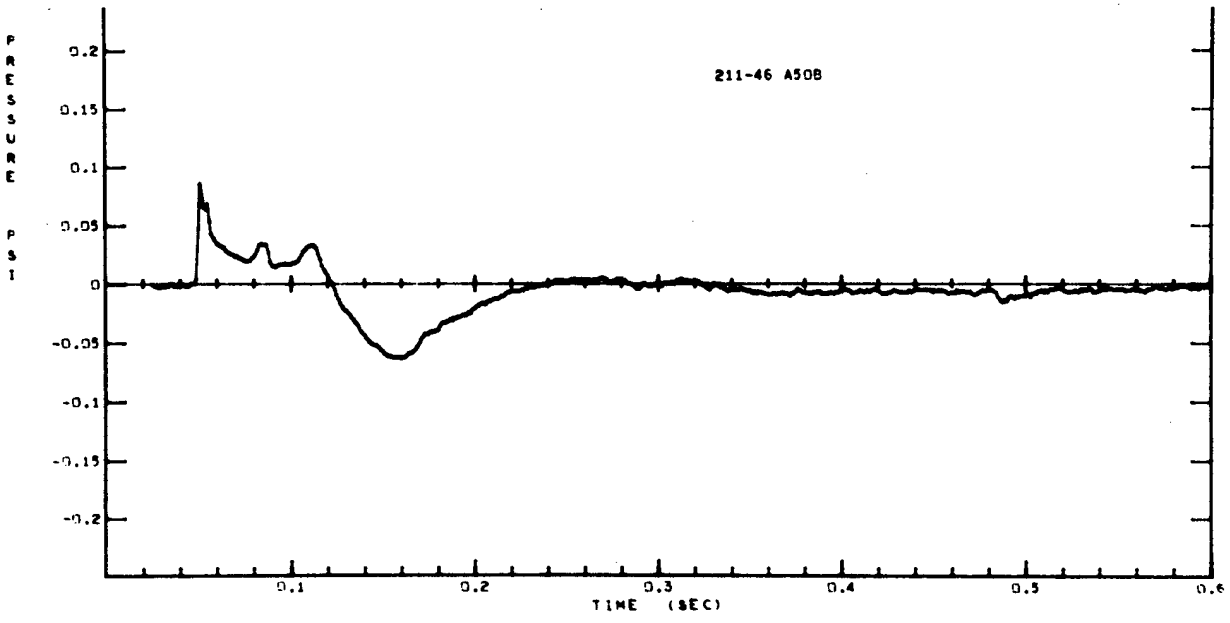

Figure A-176

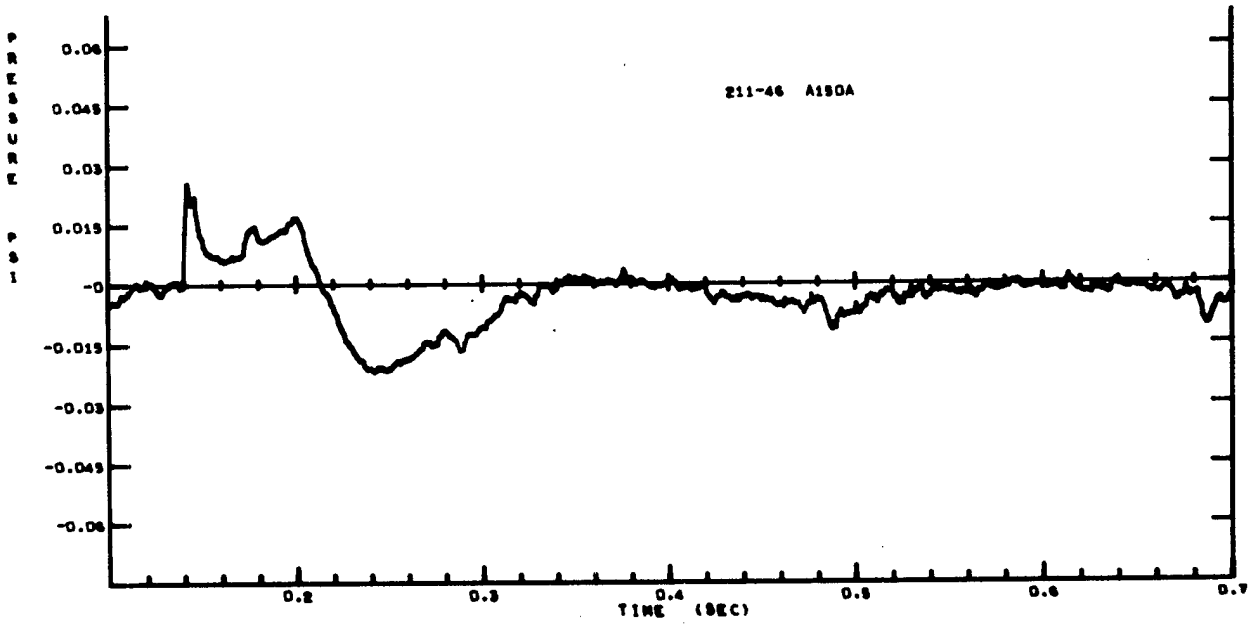

Figure A-177

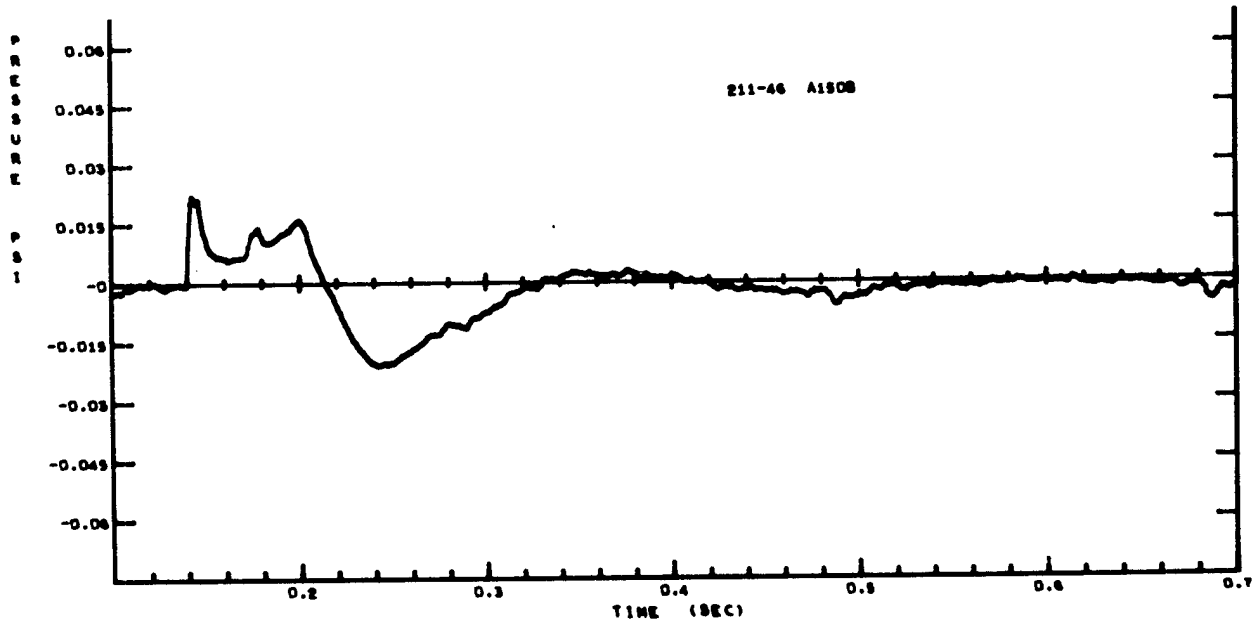

Figure A-178

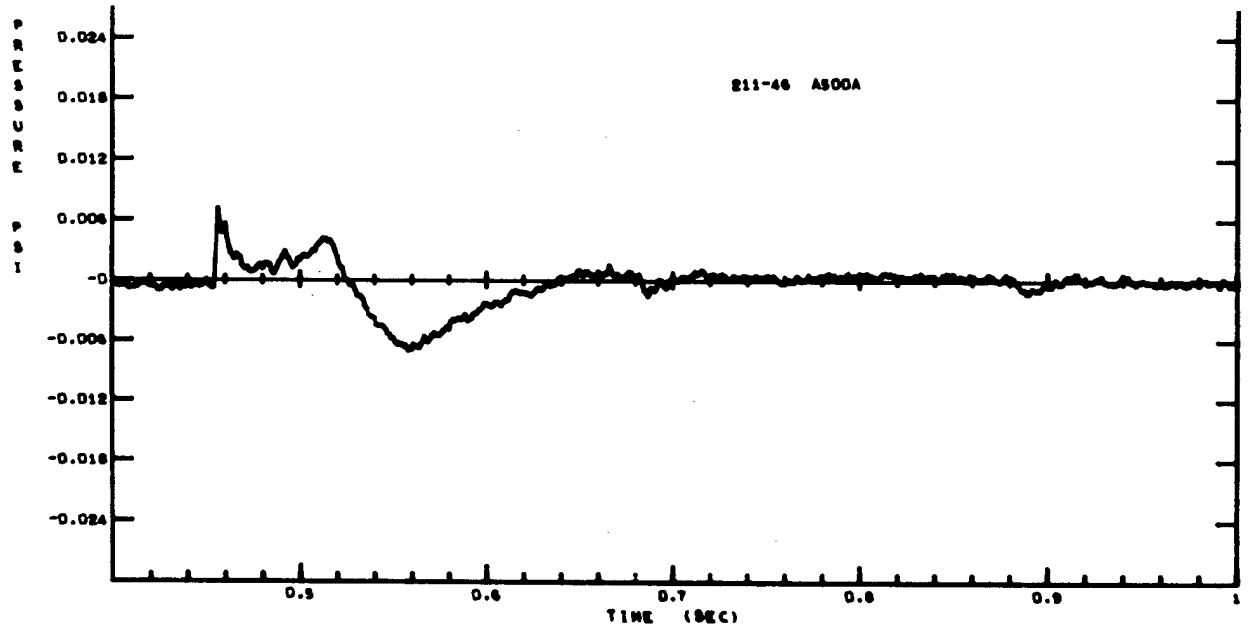

Figure A-179

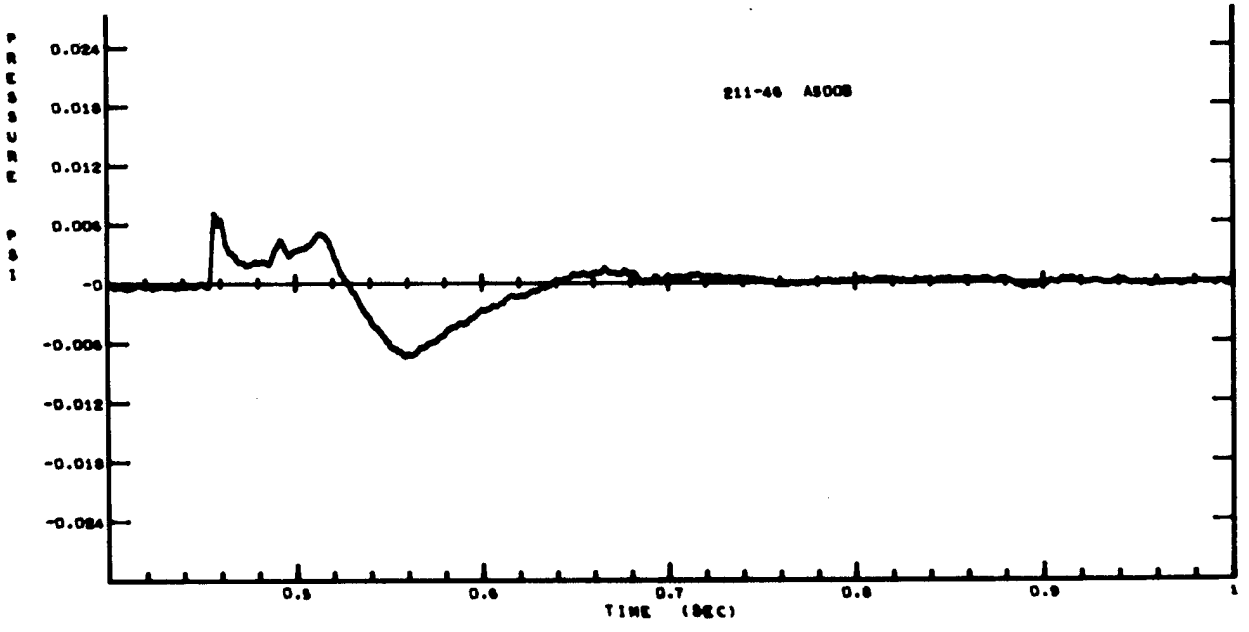

Figure A-180

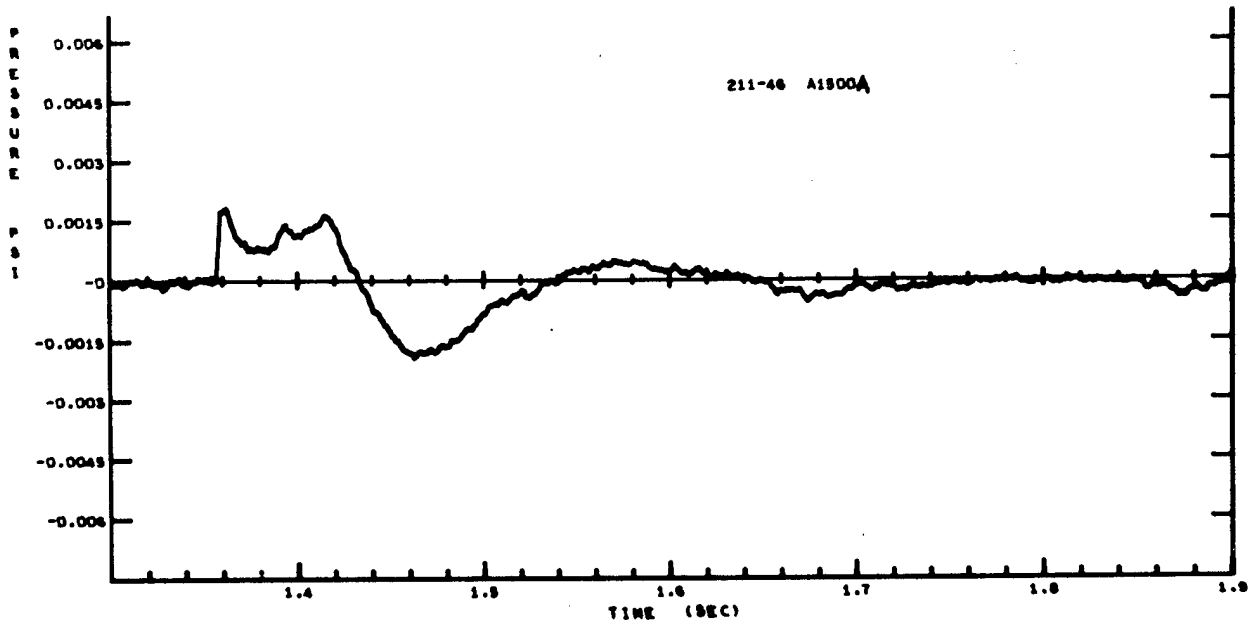

Figure A-181

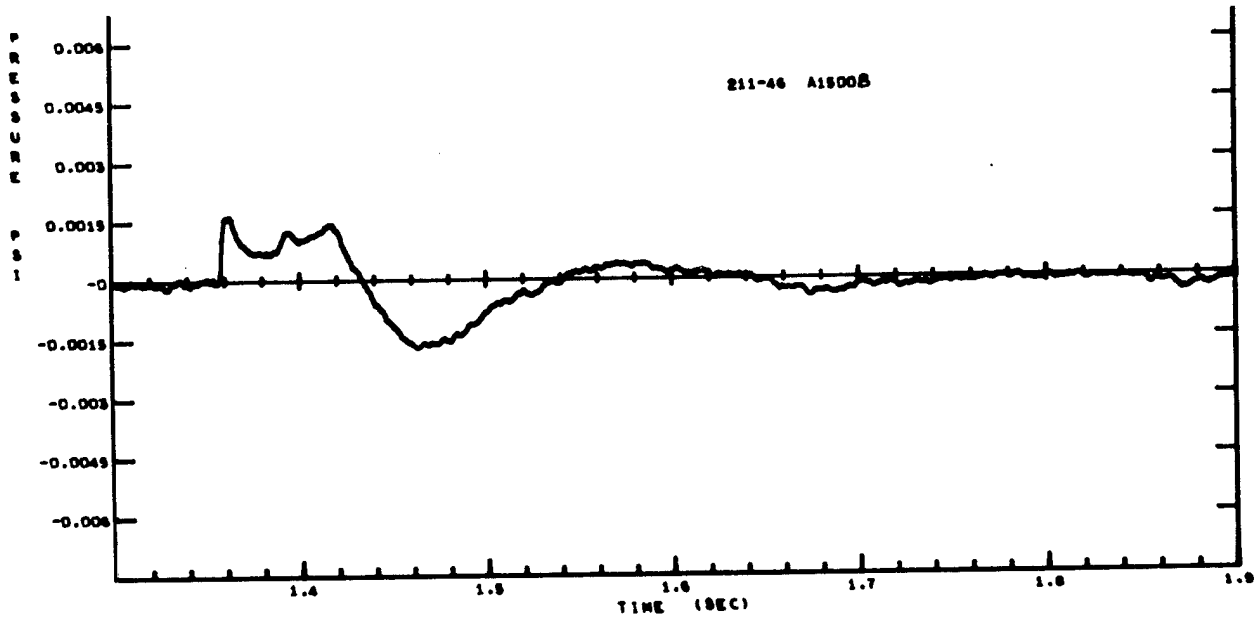

Figure A-182

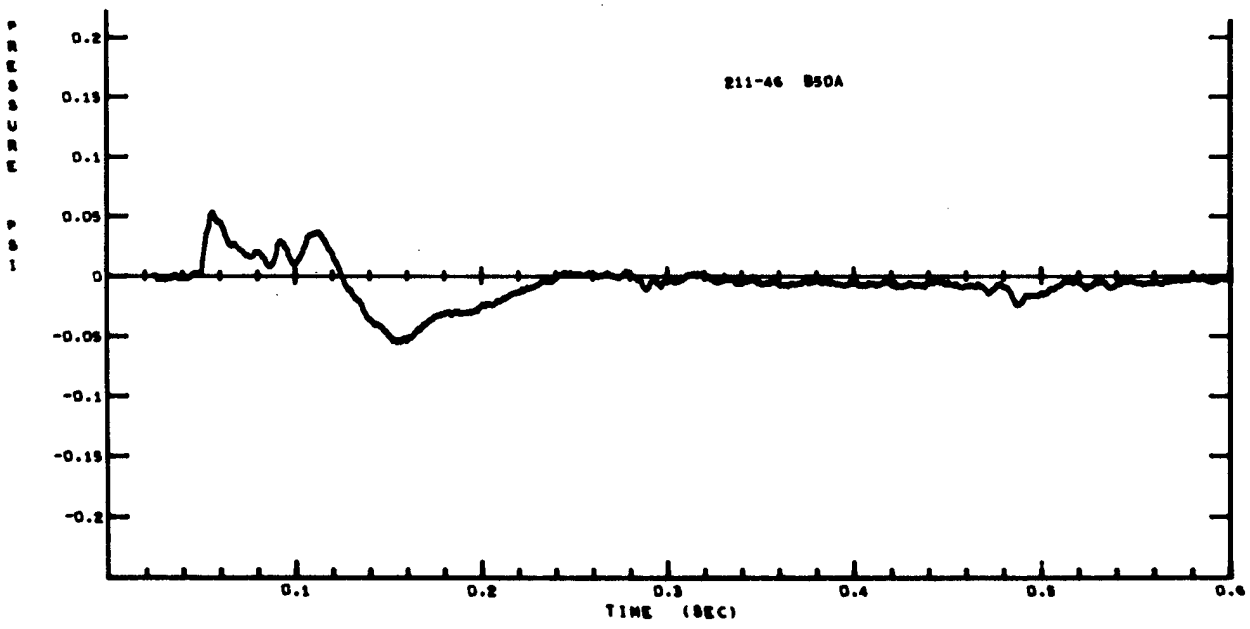

Figure A-183

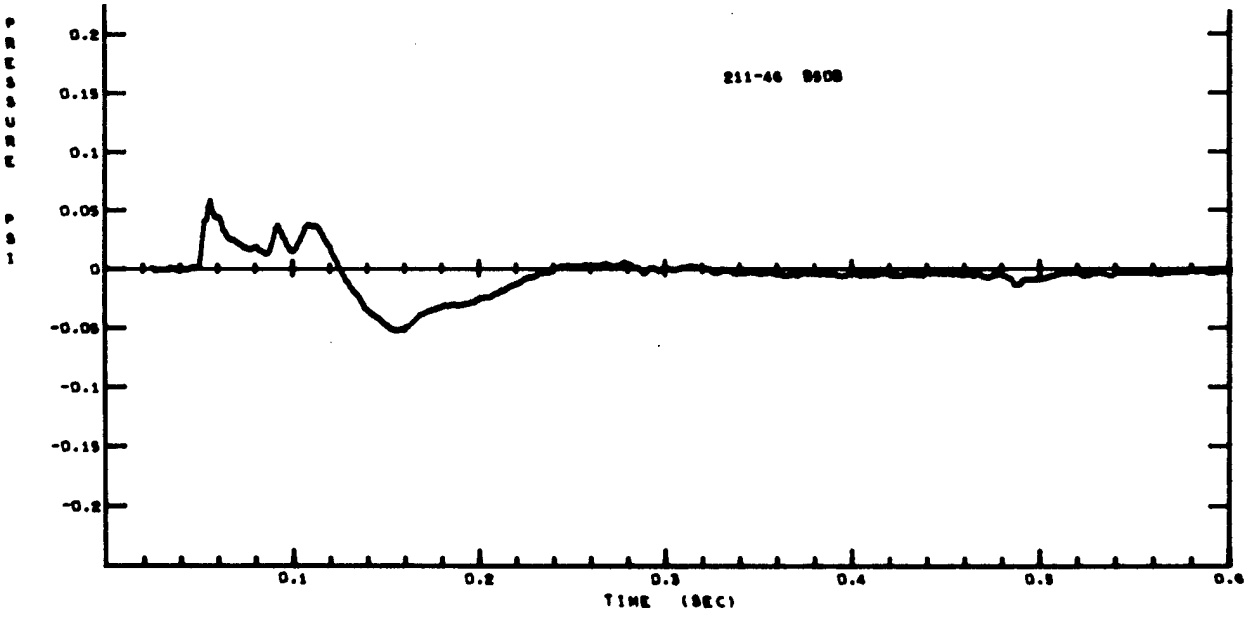

Figure A-184

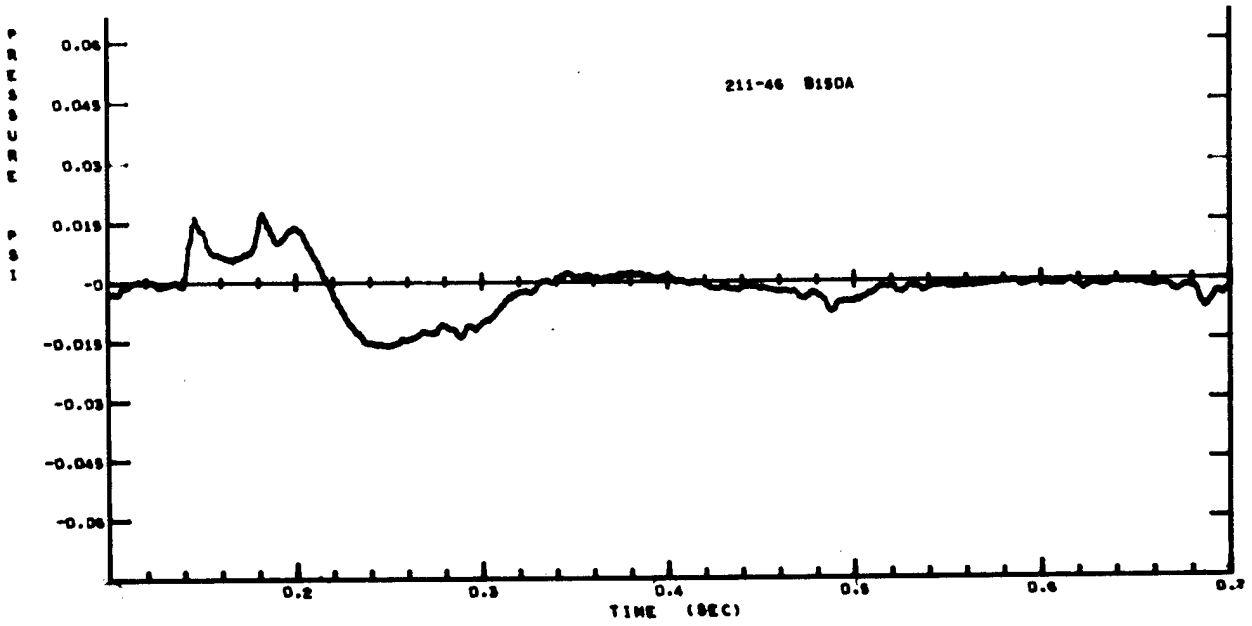

Figure A-185

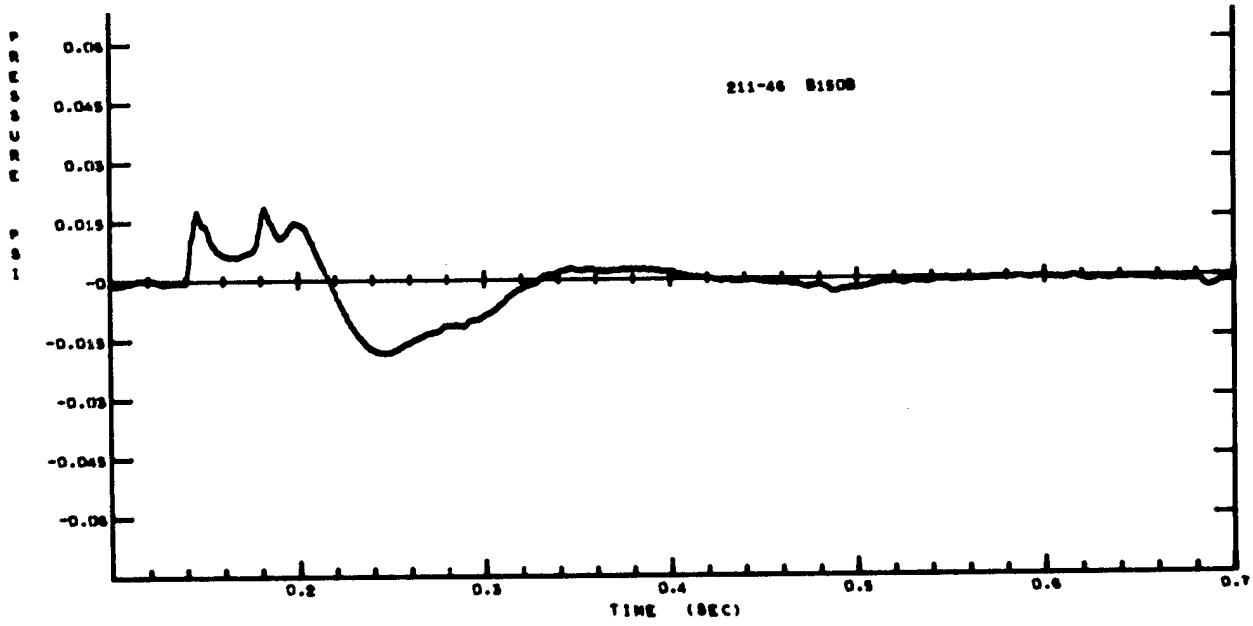

Figure A-186

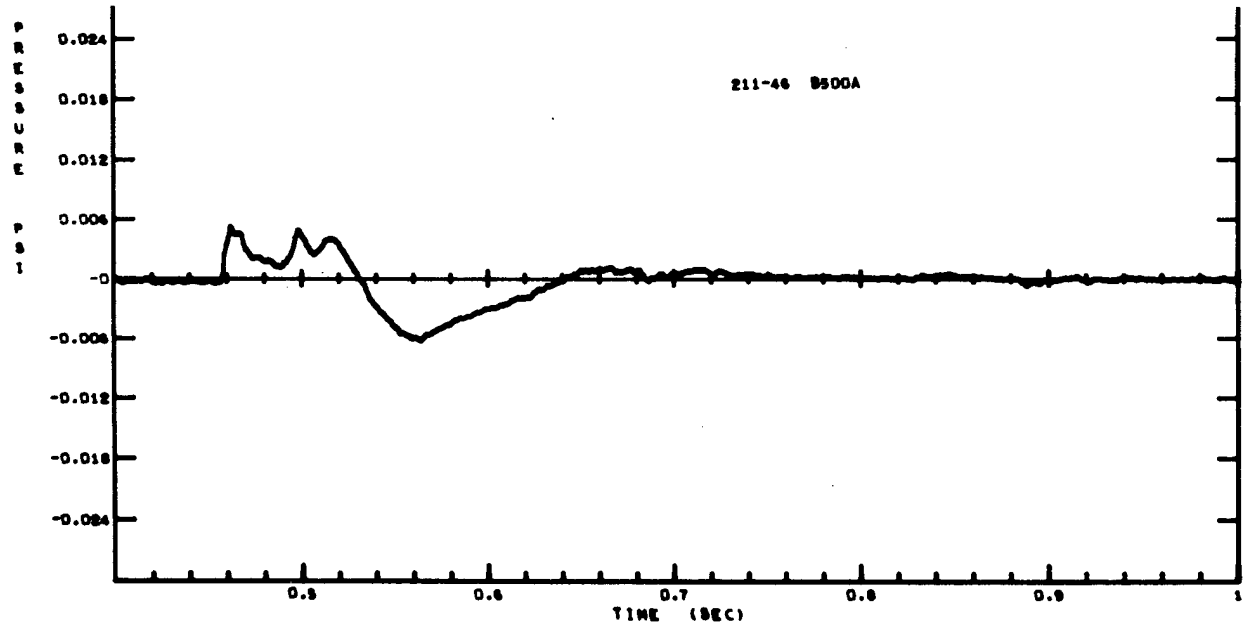

Figure A-187

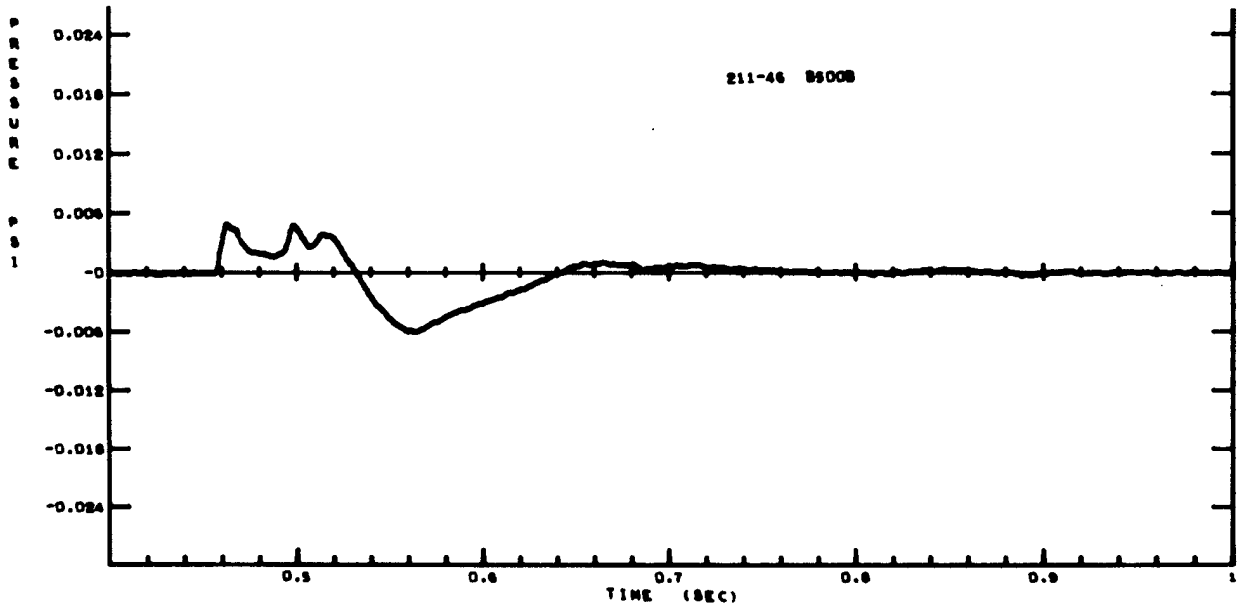

Figure A-188

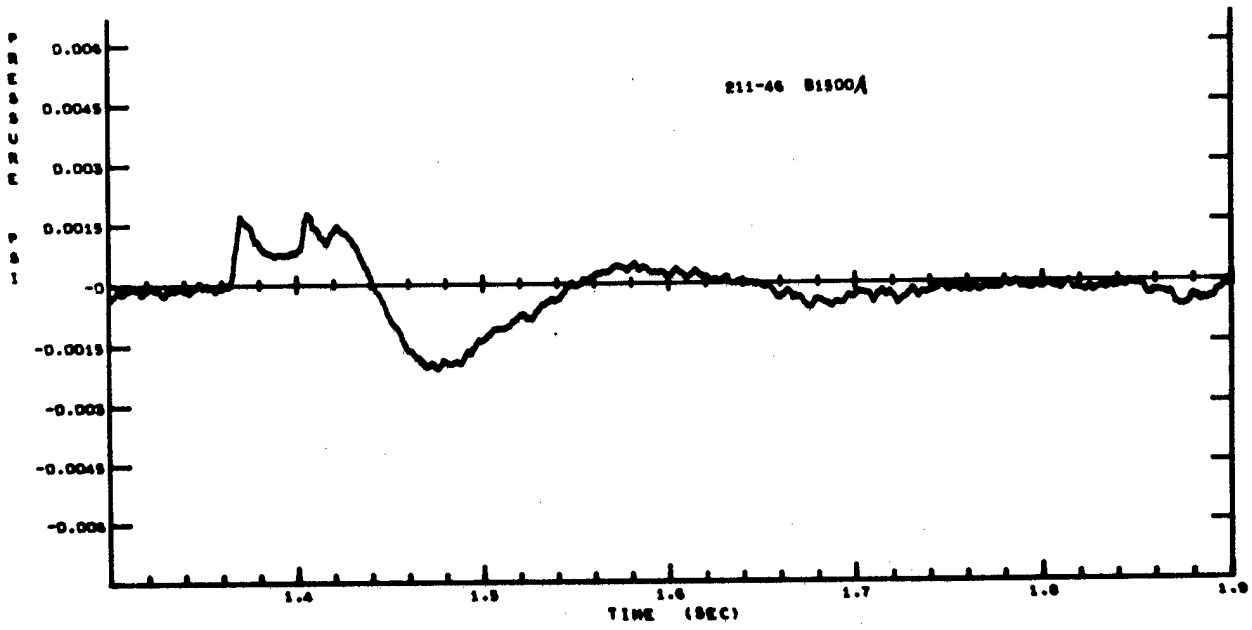
211-46 B1500A
0.006
0.0045
0.003
0.0015
-0
-0.0015
-0.003
-0.0045
-0.006
1.4
1.5
1.6
1.7
1.8
1.9
TIME (SEC)

Figure A-189

Shot 211-16

Five 64-pound charges were buried 6.9 feet deep, spread 5.25 feet apart. There were two blast lines, one off end of row (A) and one perpendicular to center of row (C). One gage was placed at each station.

Station location	Arrival time (sec)	First positive peak (psi)	Time of first positive peak (sec)	Second positive peak (psi)	Time of second positive peak (sec)	Positive cross-over (sec)	Positive pulse duration (sec)	Positive impulse (psi-sec)	First negative peak (psi)	Time of first negative peak (sec)	Negative cross-over (sec)	Negative pulse duration (sec)	Negative impulse (psi-sec)
A19.9	0.027	0.182	0.031	0.156	0.077	0.107	0.080	0.0080	-0.135	0.152	0.280	0.173	0.0124
A40.9	0.045	0.100	0.050	0.090	0.095	0.130	0.085	0.0049	-0.086	0.173	0.297	0.167	0.0071
A99.5	0.099	0.037	0.103	0.045	0.148	0.184	0.085	0.0024	-0.035	0.227	0.342	0.158	0.0031
A269.0	0.248	0.011	0.252	0.017	0.297	0.334	0.086	0.0009	-0.014	0.373	0.480	0.146	0.0011
A567.0		0.0004	0.561						-0.001	0.638			
C19.9	0.022	0.444	0.027	0.201	0.075	0.098	0.076		-0.193	0.152	0.304	0.206	0.0185
C40.9	0.038	0.225	0.046	0.131	0.088	0.117	0.079	0.0066	-0.098	0.168	0.286	0.169	0.0083
C99.5	0.094	0.082	0.100	0.054	0.144	0.176	0.082	0.0026	-0.046	0.213	0.340	0.164	0.0033
C269.0	0.250	0.026	0.254	0.020	0.297	0.331	0.081	0.0009	-0.016	0.368	0.483	0.152	0.0011
C567.0	0.520	0.011	0.525	0.008	0.567	0.601	0.081	0.0004	-0.008	0.637	0.757	0.156	0.0005

Notes: A's denote gages parallel to charges.
C's denote gages perpendicular to center charge.
A567.0 has very gradual break; unable to read arrival, positive, and negative crossover times.
C19.9 has unreasonable drop between first and second positive peak.

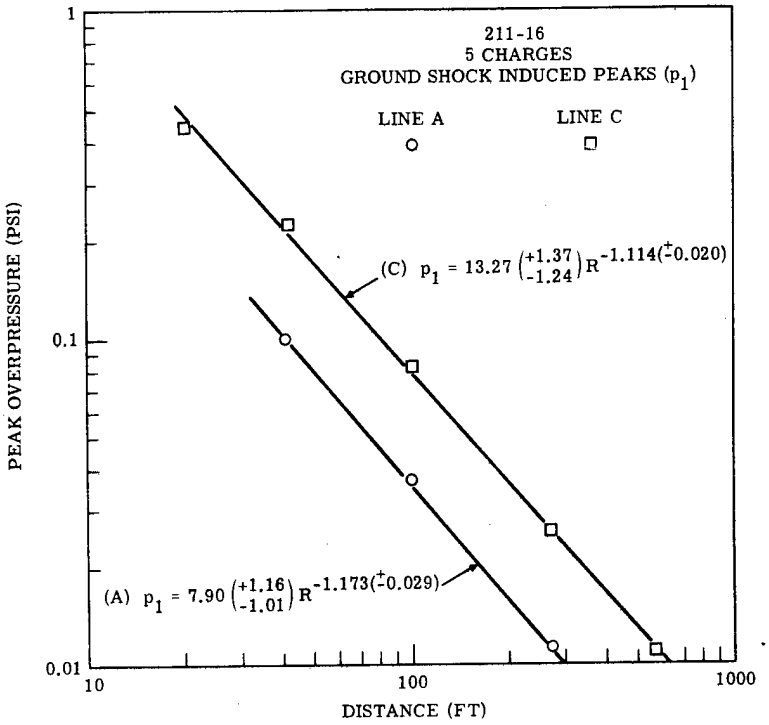

Figure A-190.

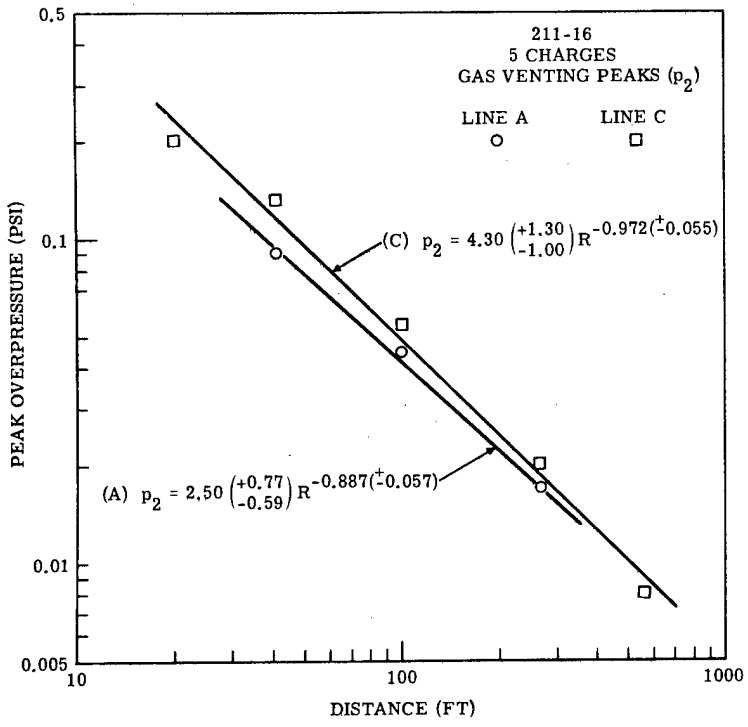

Figure A-191.

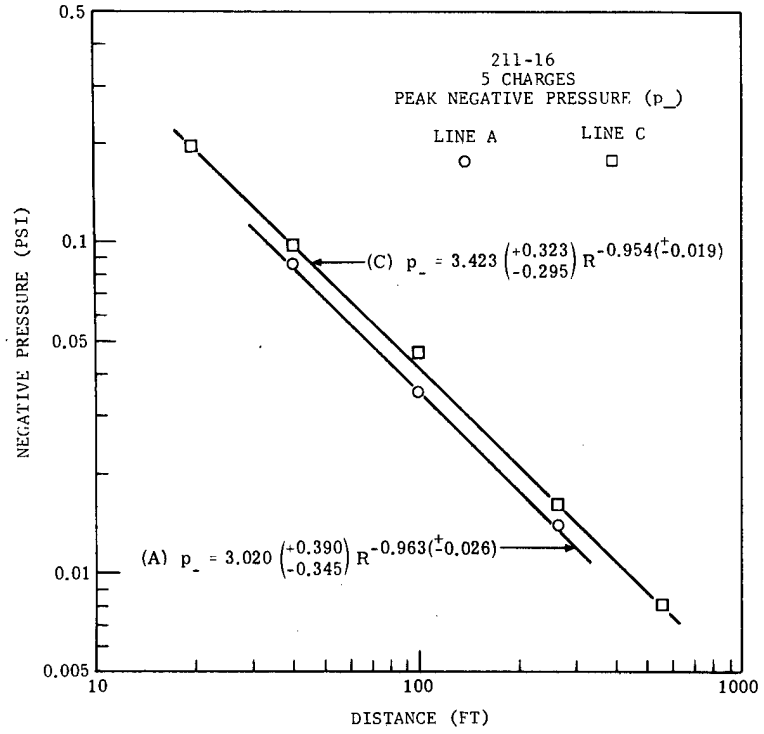

Figure A-192.

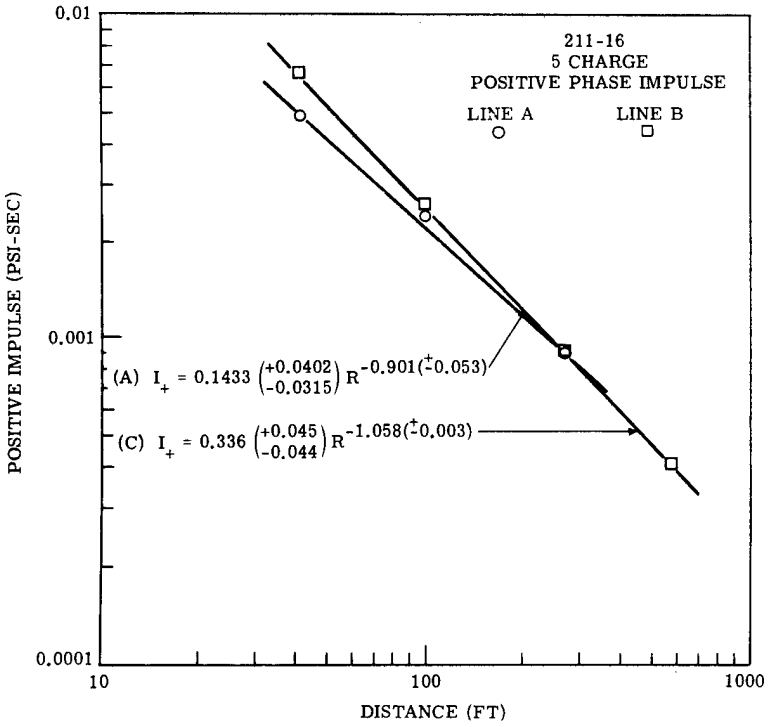

Figure A-193.

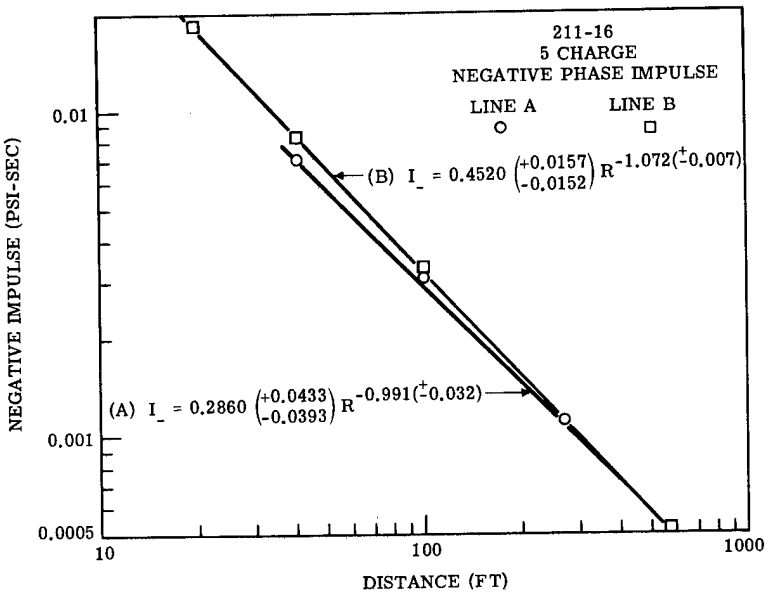
211-16
5 CHARGE
NEGATIVE PHASE IMPULSE
LINE A
LINE B
(B) $I_- = 0.4520 \begin{pmatrix}+0.0157\\-0.0152\end{pmatrix} R^{-1.072(\pm 0.007)}$
(A) $I_- = 0.2860 \begin{pmatrix}+0.0433\\-0.0393\end{pmatrix} R^{-0.991(\pm 0.032)}$
NEGATIVE IMPULSE (PSI-SEC)
0.01
0.001
0.0005
10
100
1000
DISTANCE (FT)

Figure A-194.

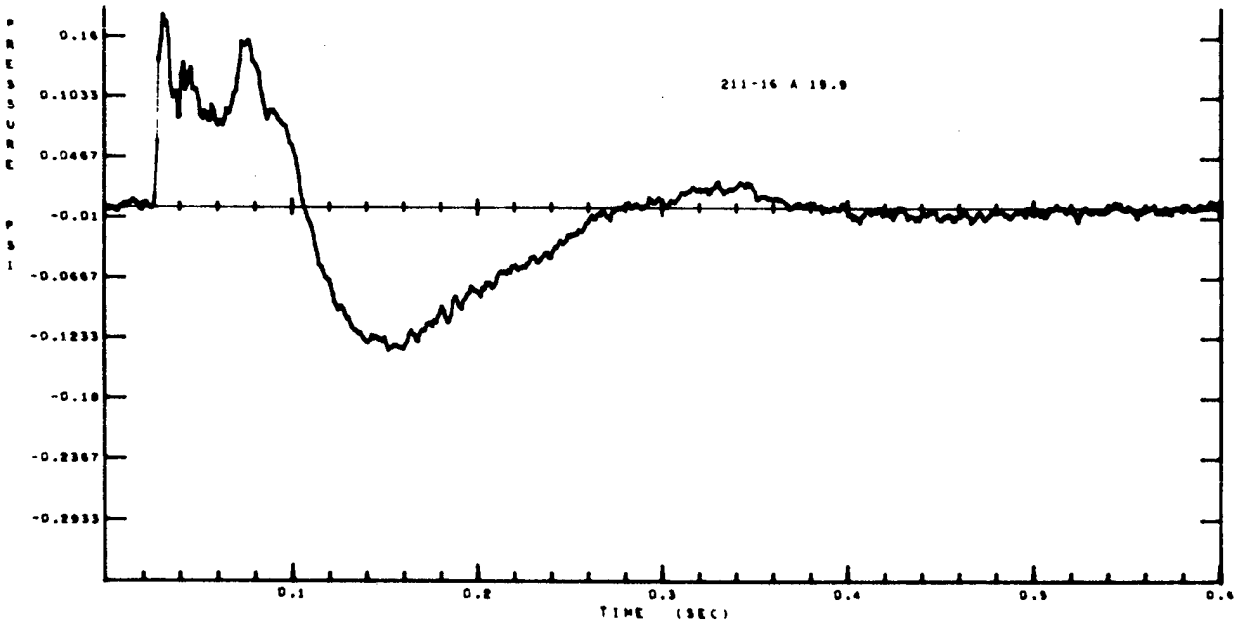

Figure A-195

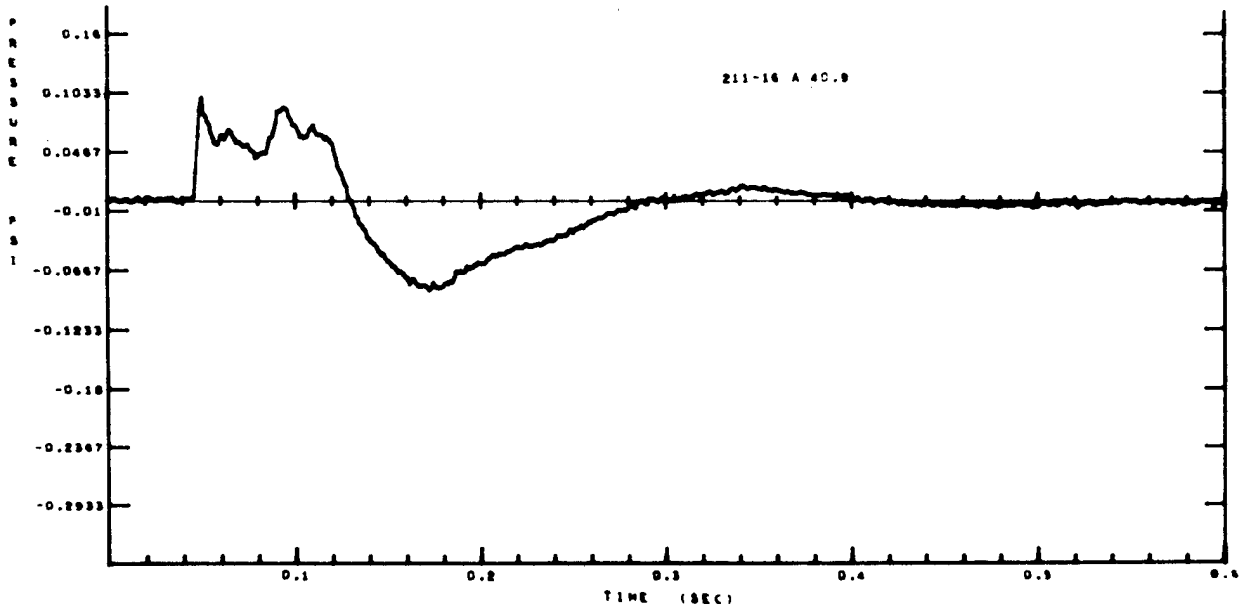

Figure A-196

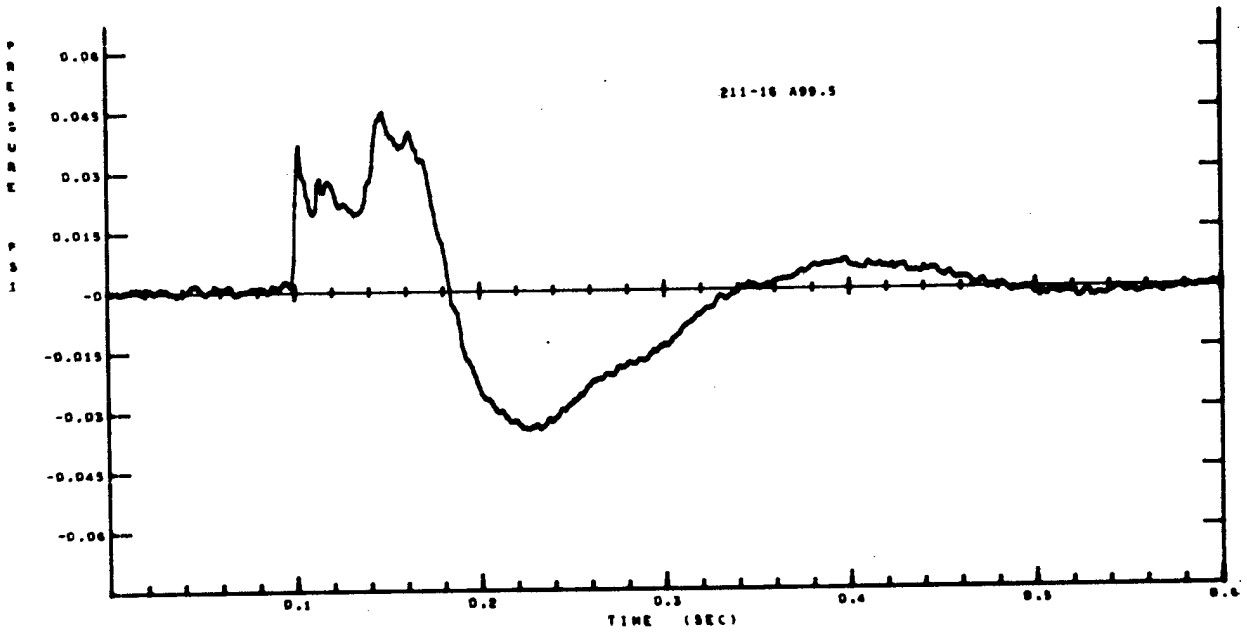

Figure A-197

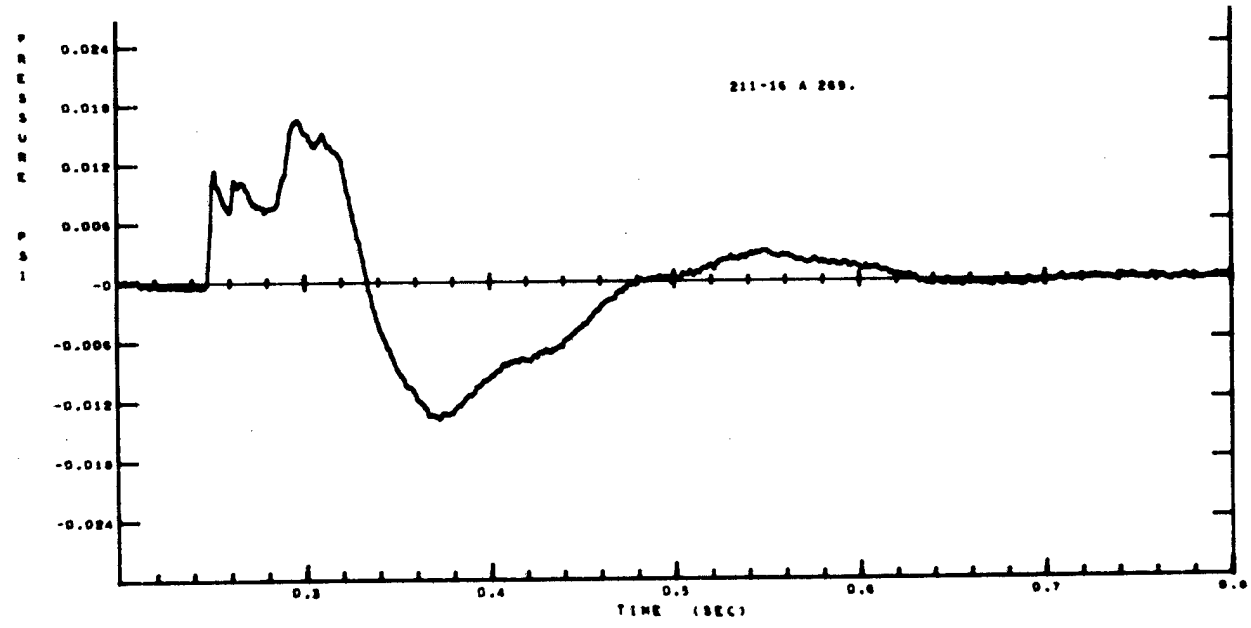

Figure A-198

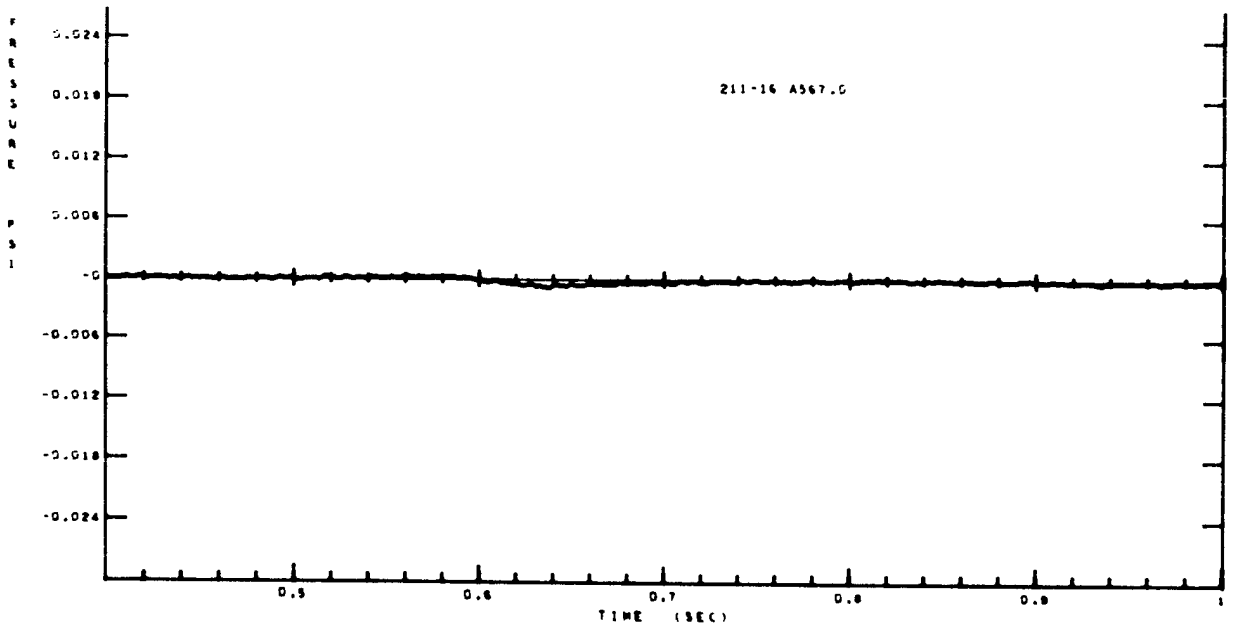

Figure A-199

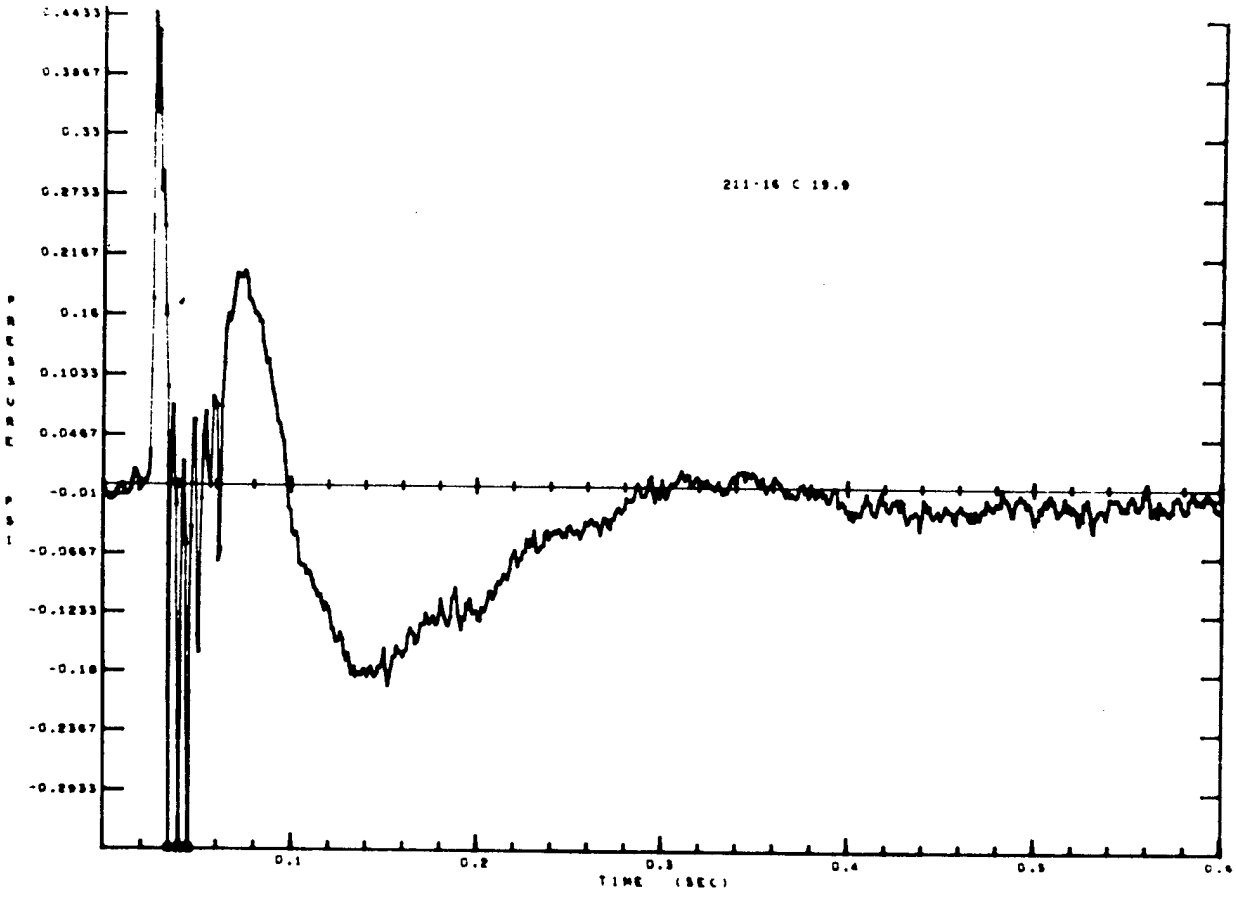

Figure A-200

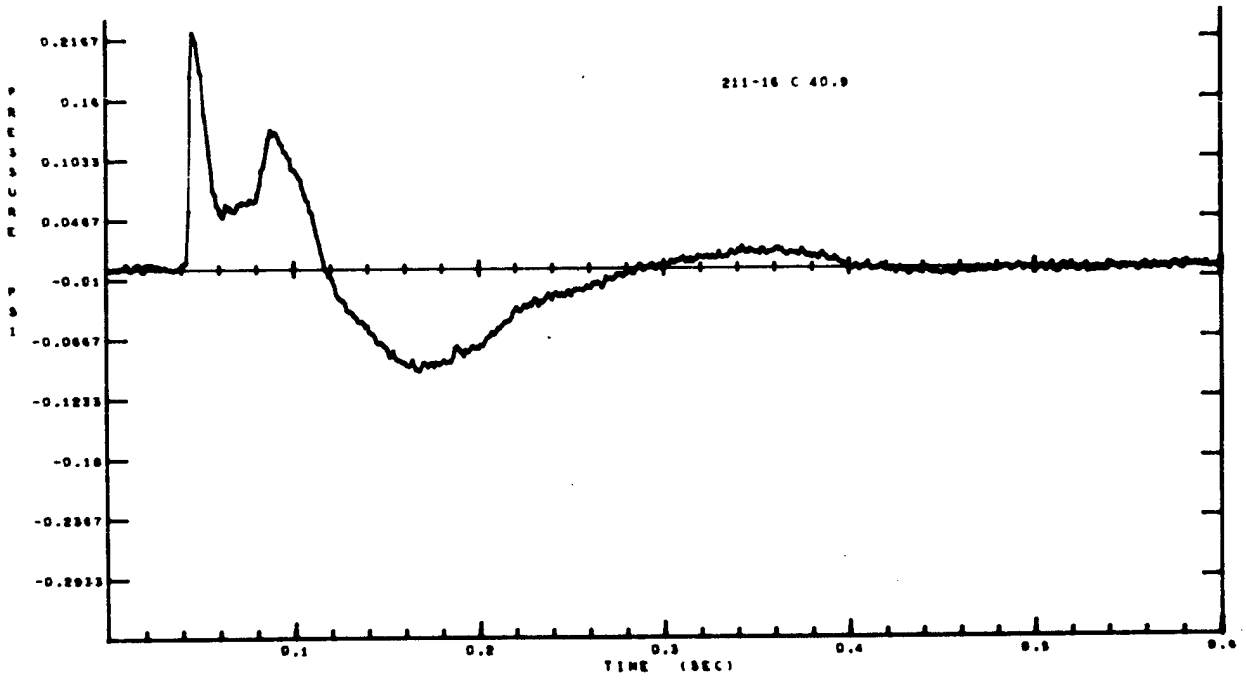

Figure A-201

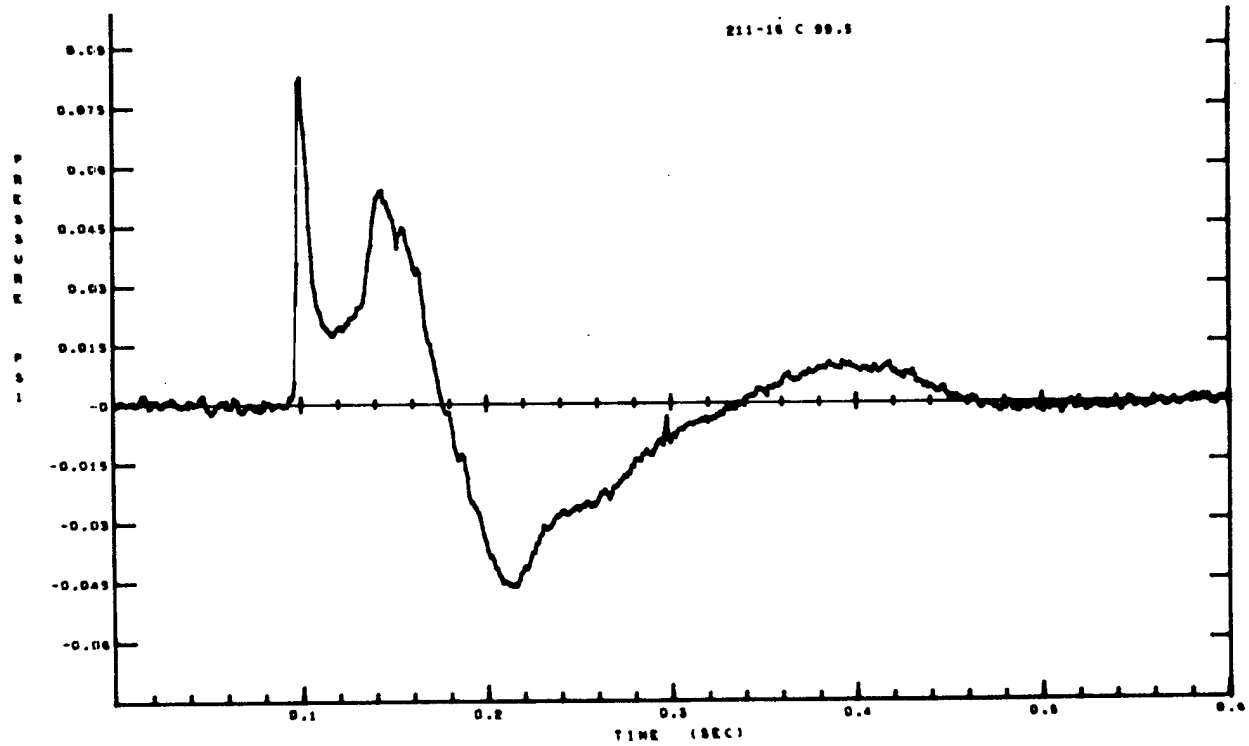

Figure A-202

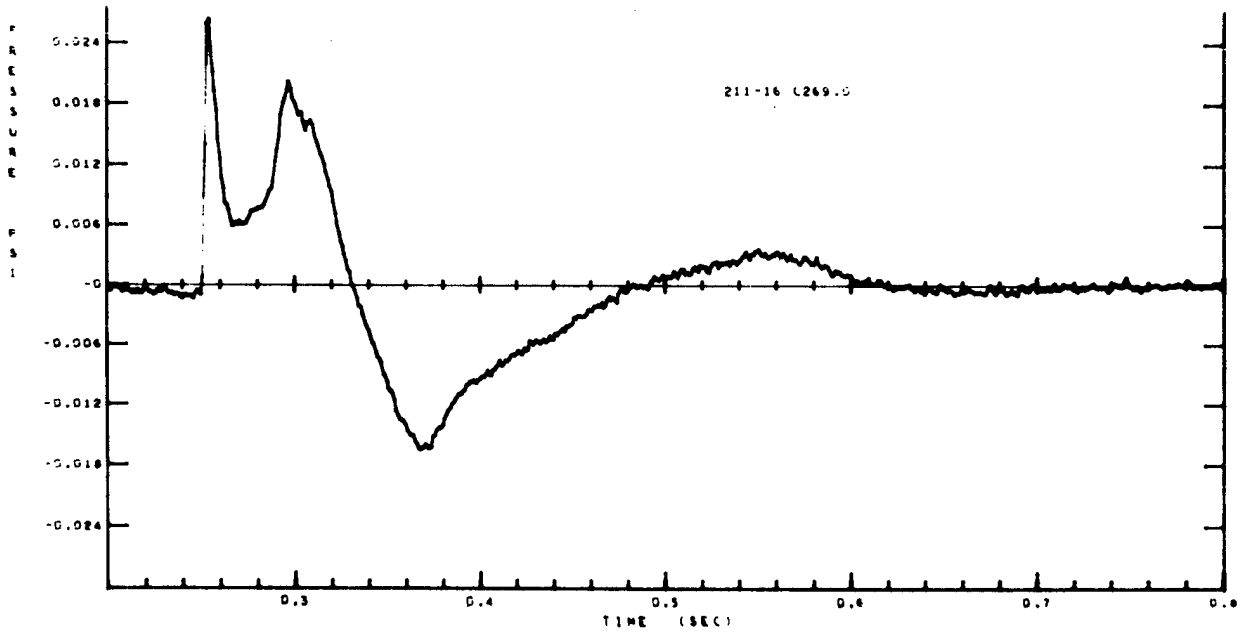

Figure A-203

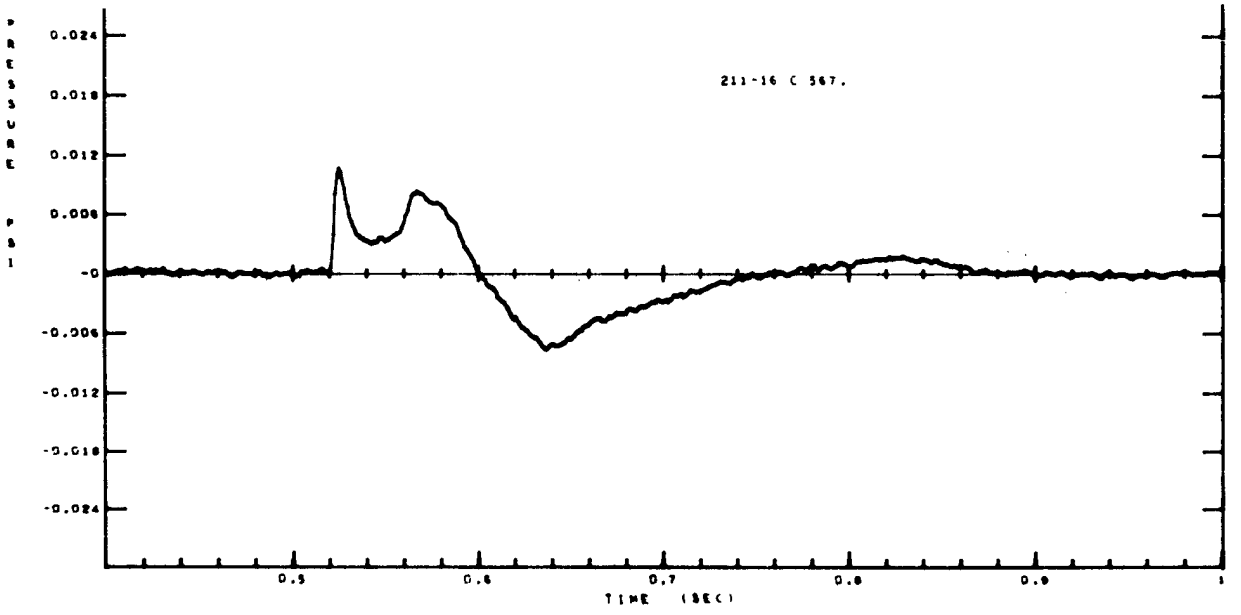

Figure A-204

Shot 211-45

Eleven 64-pound charges were buried 6.9 feet deep, spaced 5.25 feet apart. There were two blast lines (A&B), 90° apart. Two gages were placed at each station; gage A is the less sensitive.

Gage	Arrival time (sec)	Ground shock induced peak (psi)	Time of peak (sec)	Peak from venting gas (psi)	Time of peak (sec)	Cross-over (sec)	Positive phase impulse (psi-sec)	Negative peak (psi)	Time of peak (sec)	Cross-over (sec)	Negative phase impulse (psi-sec)
A50A	0.051	0.33587	0.044	0.17253	0.098	0.129	0.00953	-0.11447	0.179	0.359	0.01417
A50B	0.051	0.29256	0.053	0.17645	0.098	0.129	0.00955	-0.120	0.179	0.351	0.01439
A150A	0.142	0.12292	0.145	0.06818	0.188	0.226	0.00352	-0.05107	0.260	0.432	0.00523
A150B	0.143	Limited	0.145	0.06654	0.187	0.226	0.003185	-0.04792	0.261	0.427	0.00461
A500A	0.462	0.03440	0.464	0.01940	0.506	0.545	0.000983	-0.01517	0.585	0.720	0.00133
A1500A	1.376	0.01508	1.377	0.00759	1.420	1.455	0.000347	-0.00628	1.488	1.648	0.000497
B50A	0.055	0.08942	0.060	0.08282	0.120	0.148	0.00625	-0.08322	0.207	0.422	0.01157
B50B	0.054	0.08682	0.058	0.07853	0.120	0.152	0.00607	-0.08051	0.199	0.366	0.00936
B150A	0.148	0.03363	0.178	0.03658	0.200	0.244	0.00241	-0.03772	0.318	0.455	0.00450
B500B	0.468	0.00765	0.475	0.01356	0.531	0.567	0.000861	-0.01254	0.600	0.755	0.001164
B1500A	1.385	0.00294	1.390	0.00446	1.438	1.484	0.00030	-0.00393	1.523	1.688	0.000421
B1500B	1.385	0.00250	1.390	0.00404	1.438	1.484	0.000275	-0.00358	1.530	1.685	0.000369

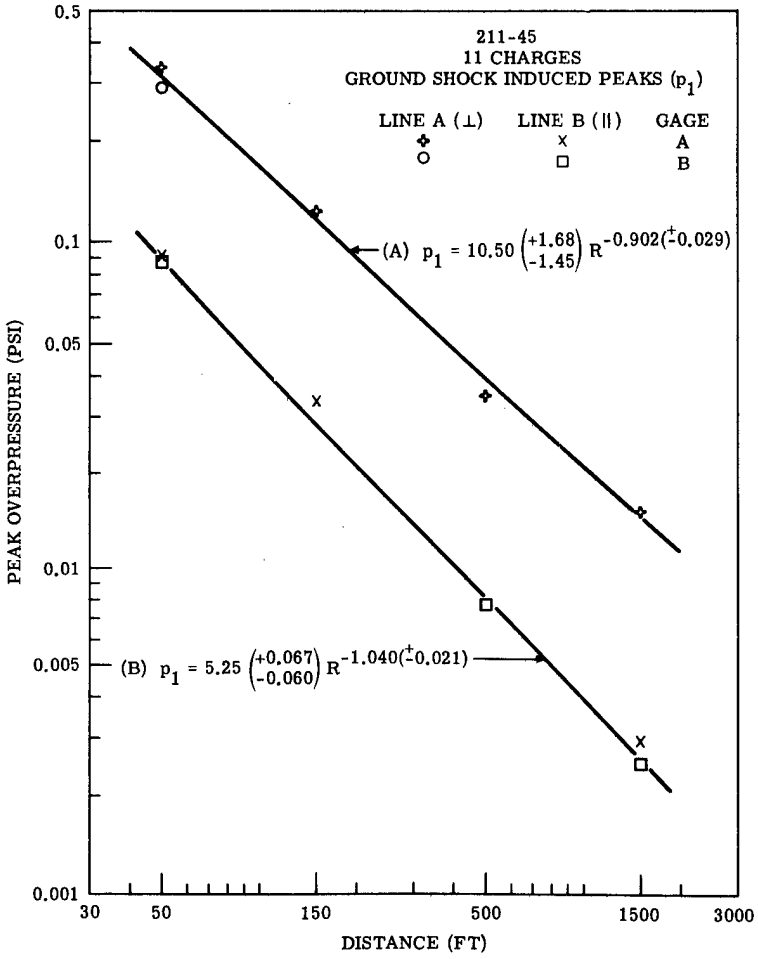
211-45
11 CHARGES
GROUND SHOCK INDUCED PEAKS (p_1)
LINE A (⊥)
LINE B (||)
GAGE
A
B
(A) $p_1 = 10.50 \left(^{+1.68}_{-1.45}\right) R^{-0.902(\pm 0.029)}$
(B) $p_1 = 5.25 \left(^{+0.067}_{-0.060}\right) R^{-1.040(\pm 0.021)}$
PEAK OVERPRESSURE (PSI)
0.5
0.1
0.05
0.01
0.005
0.001
30
50
150
500
1500
3000
DISTANCE (FT)

Figure A-205.

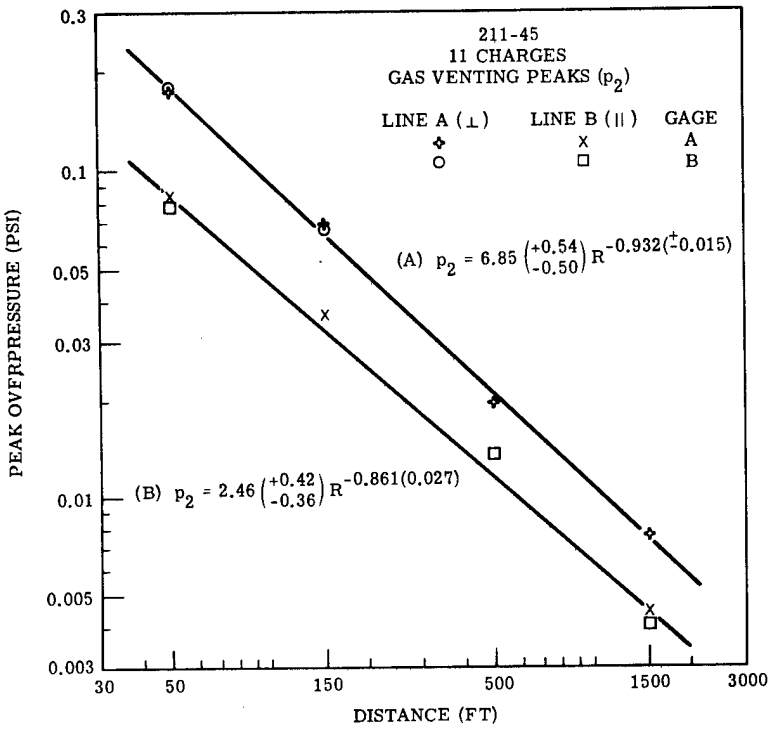

Figure A-206.

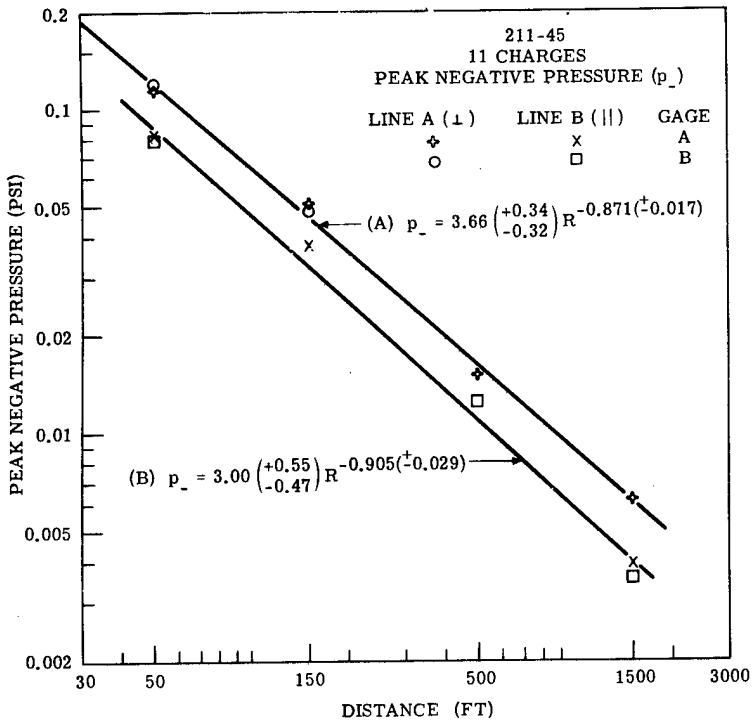

Figure A-207.

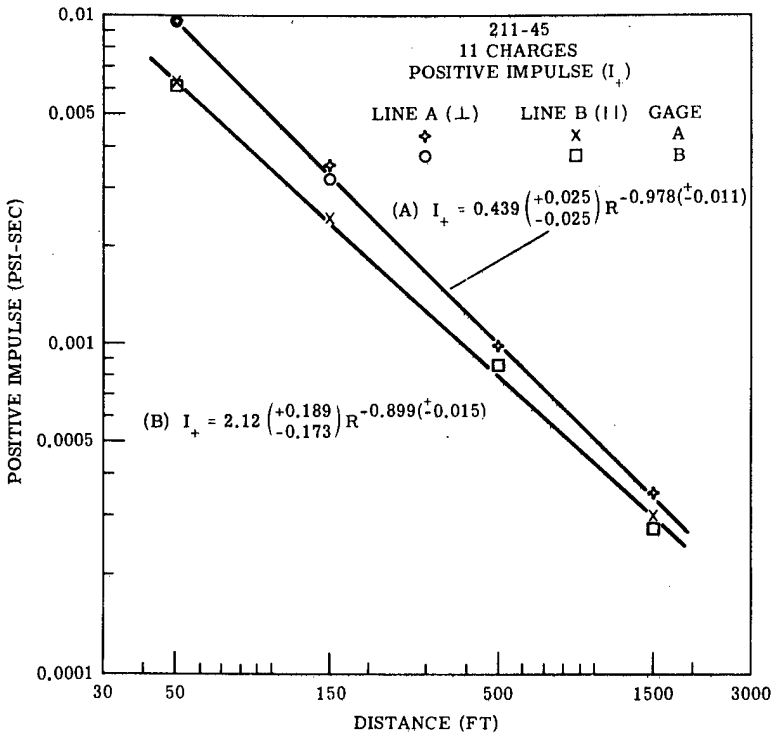

Figure A-208.

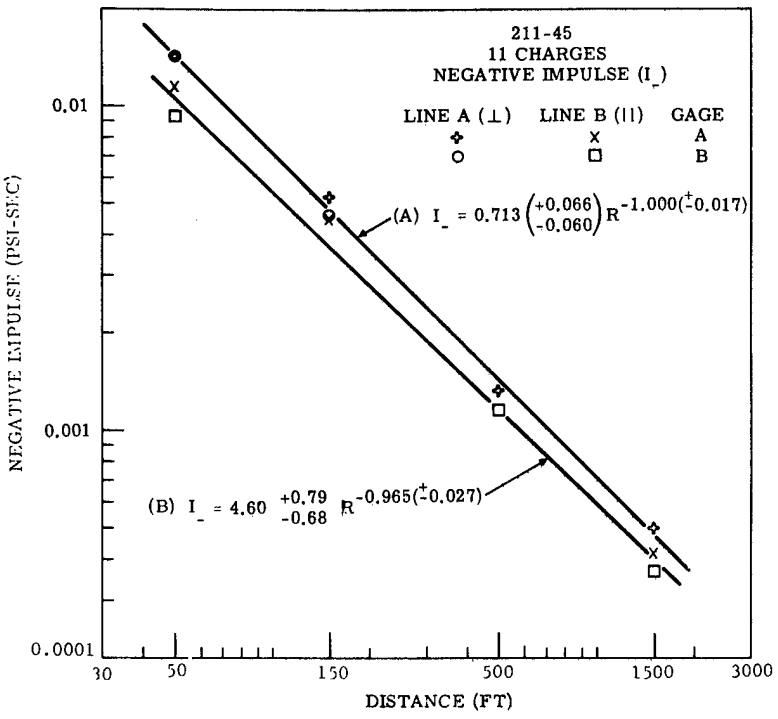

Figure A-209.

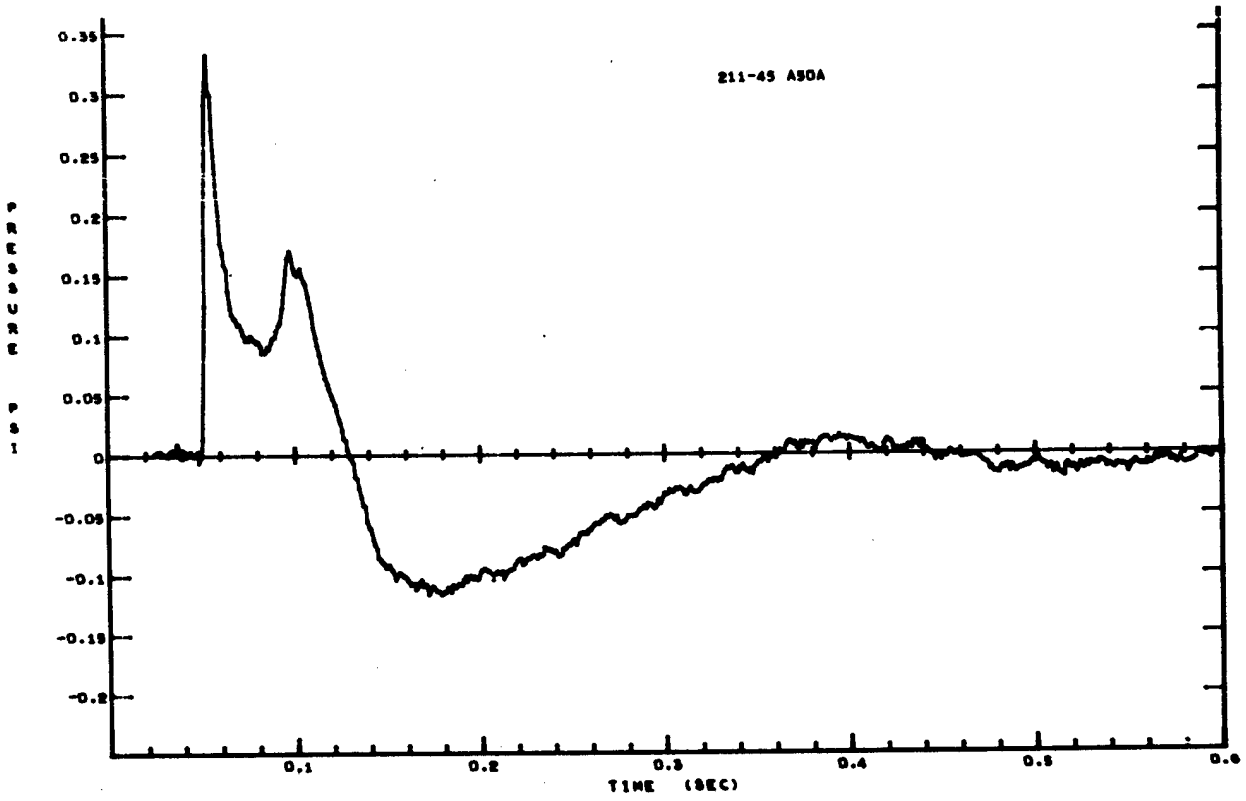

Figure A-210

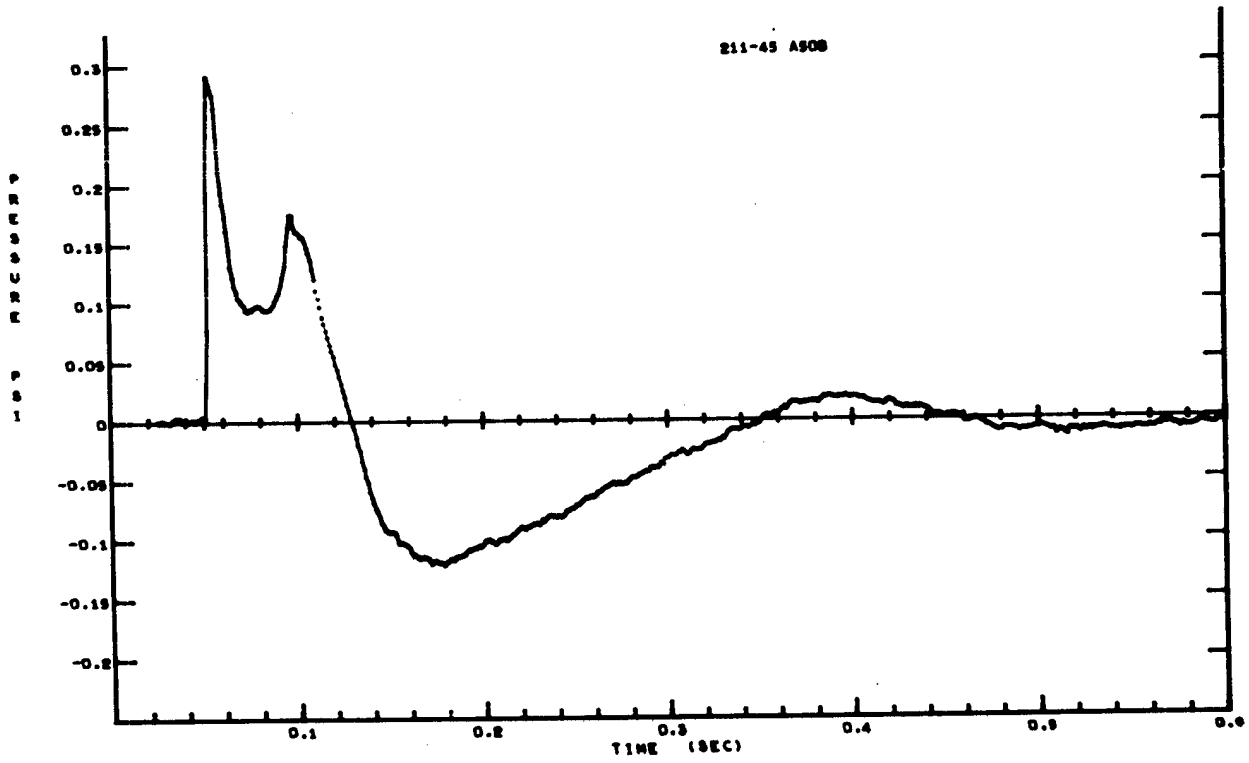

Figure A-211

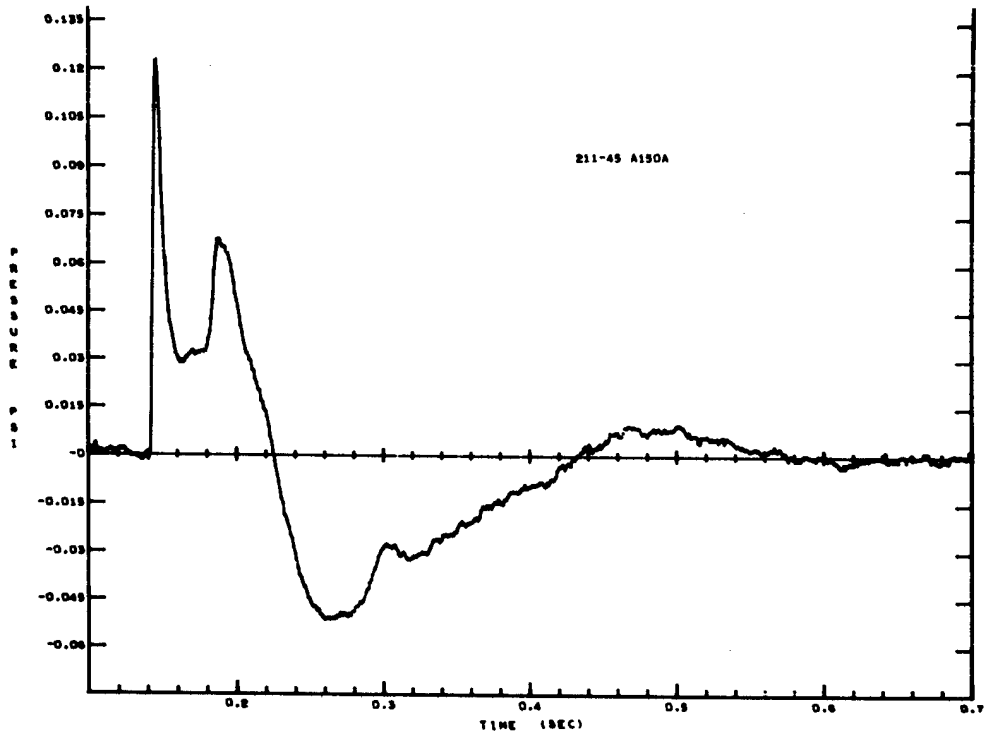

Figure A-212

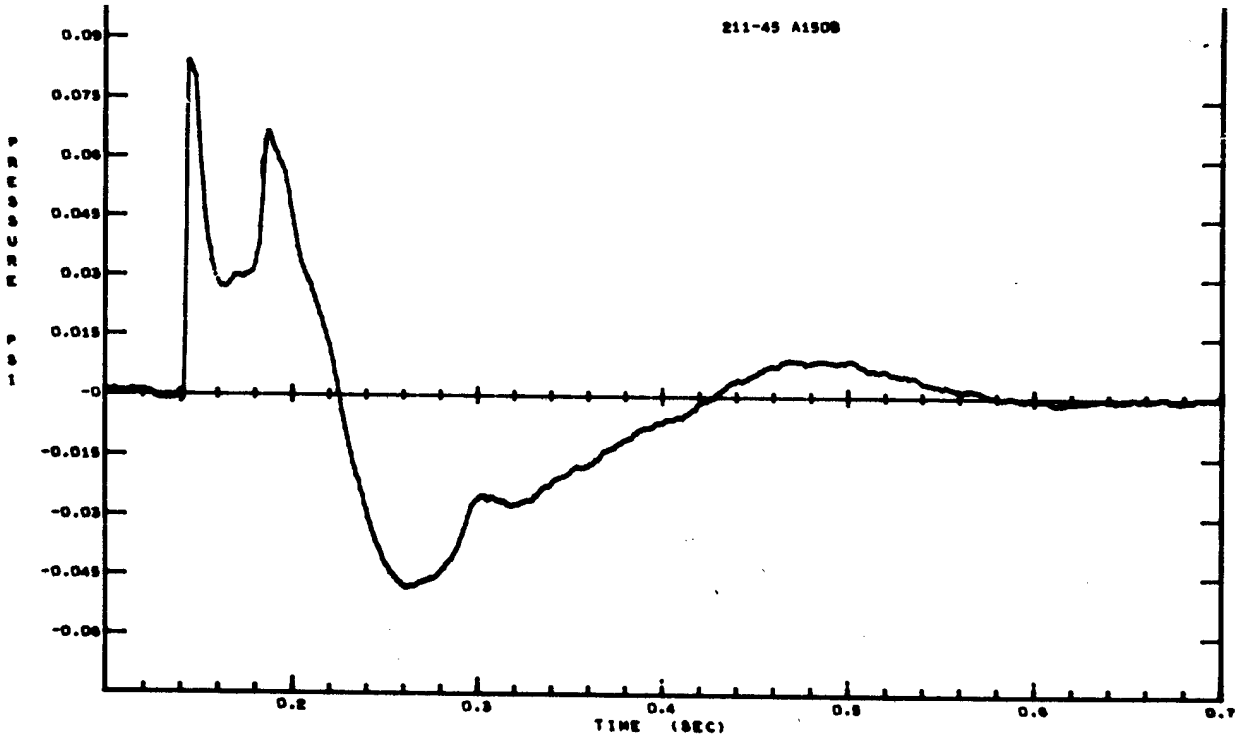

Figure A-213

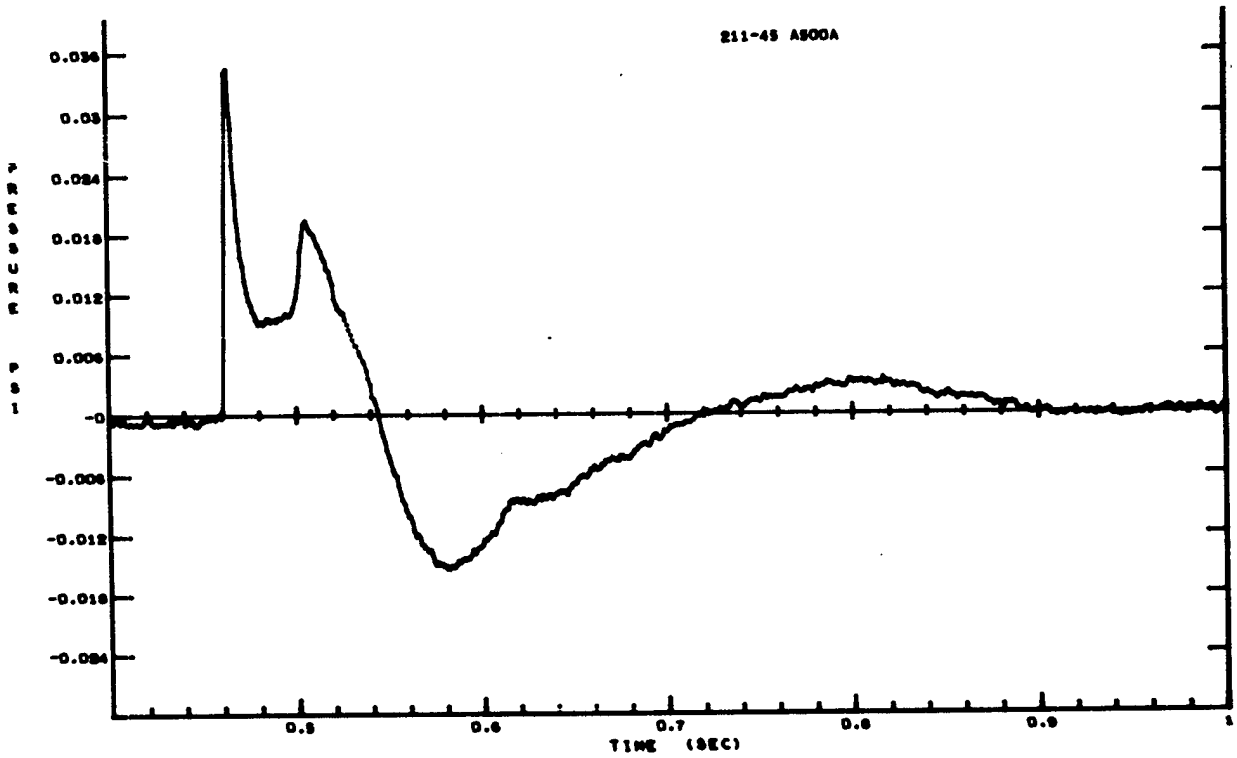

Figure A-214

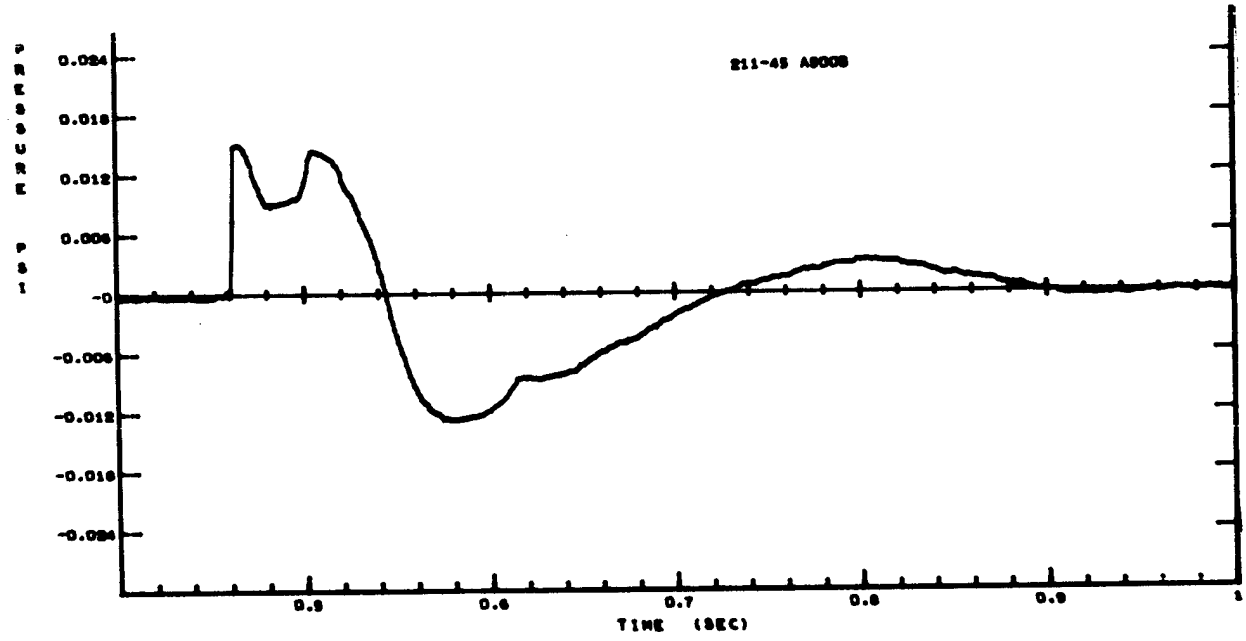

Figure A-215

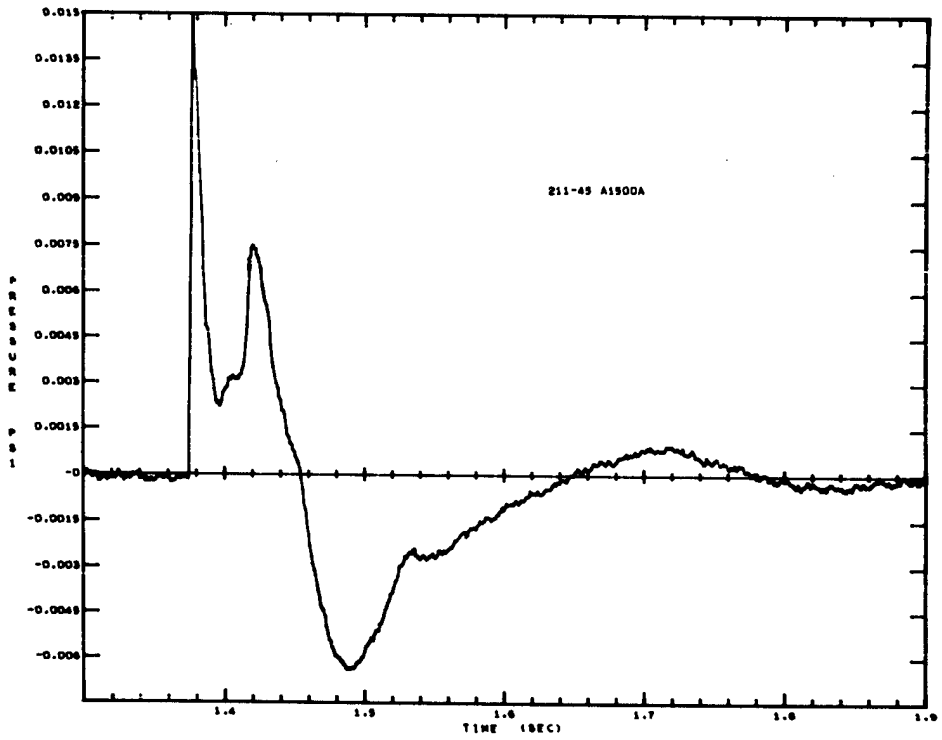

Figure A-216

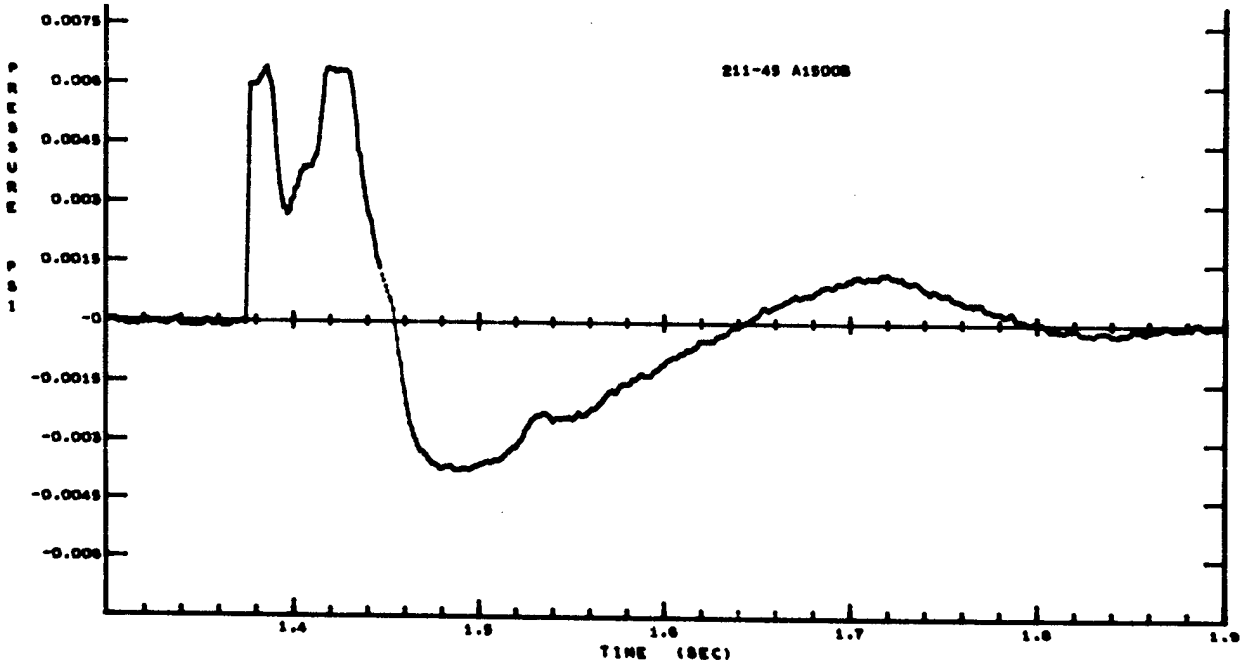

Figure A-217

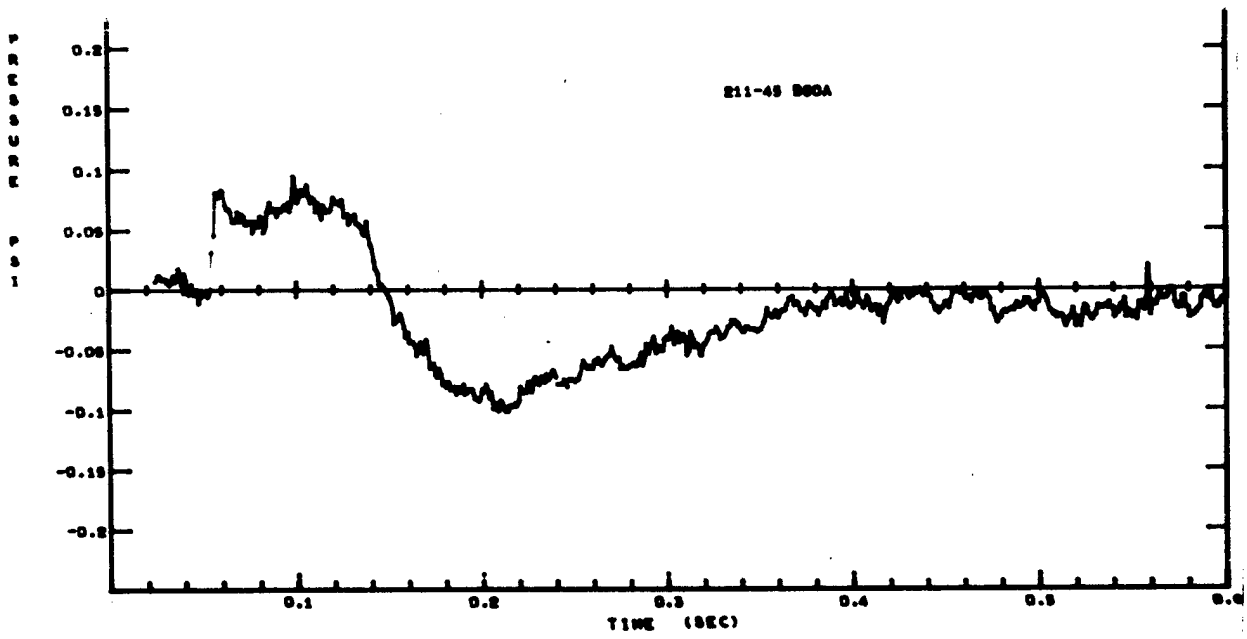

Figure A-218

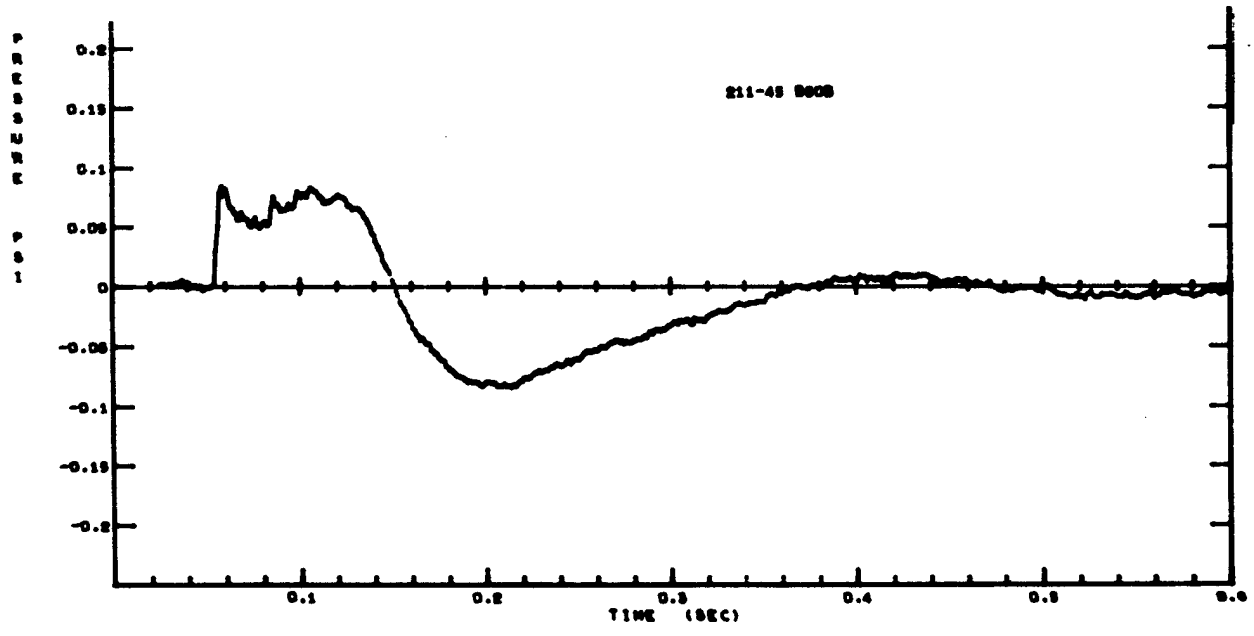

Figure A-219

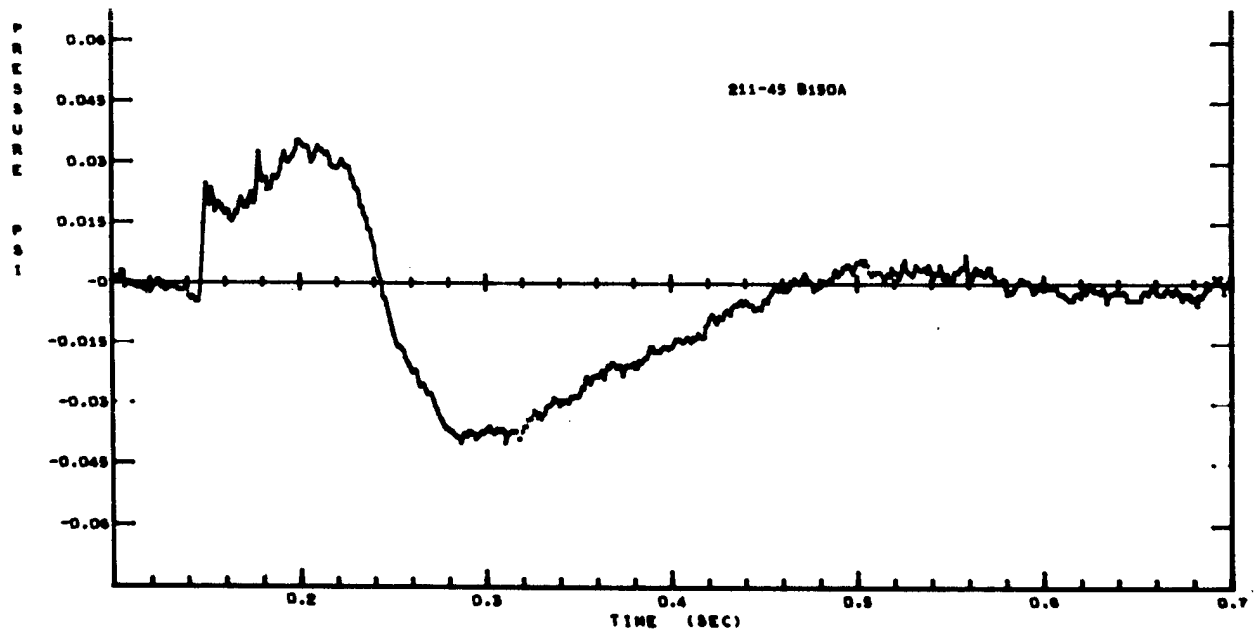

Figure A-220

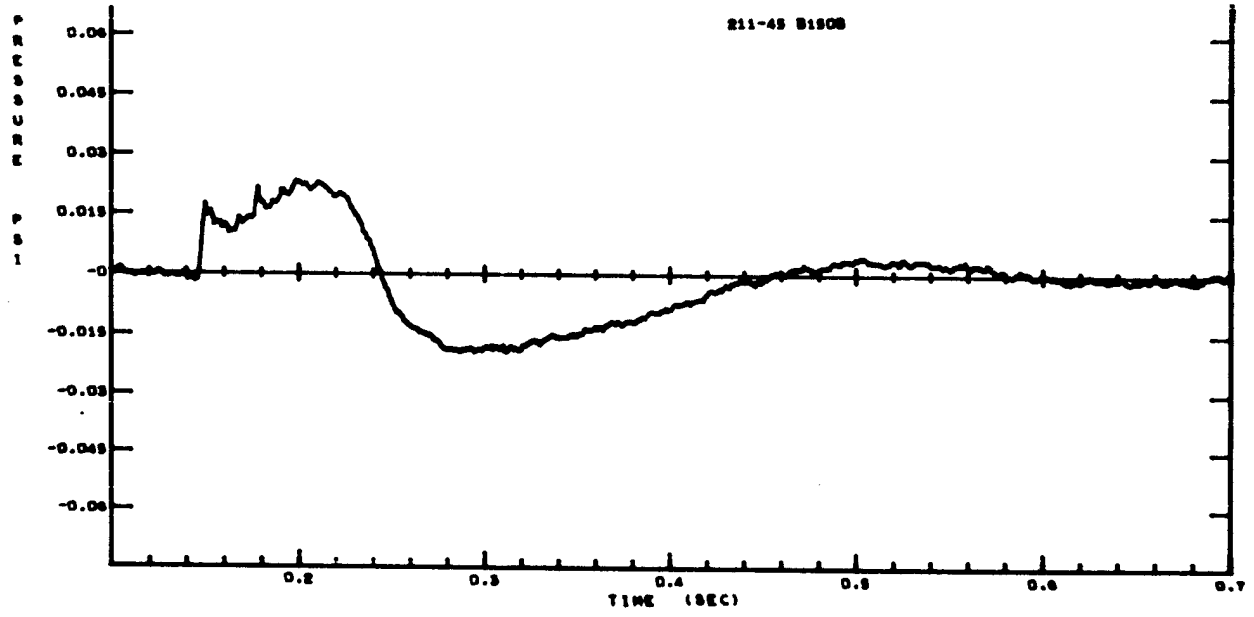

Figure A-221

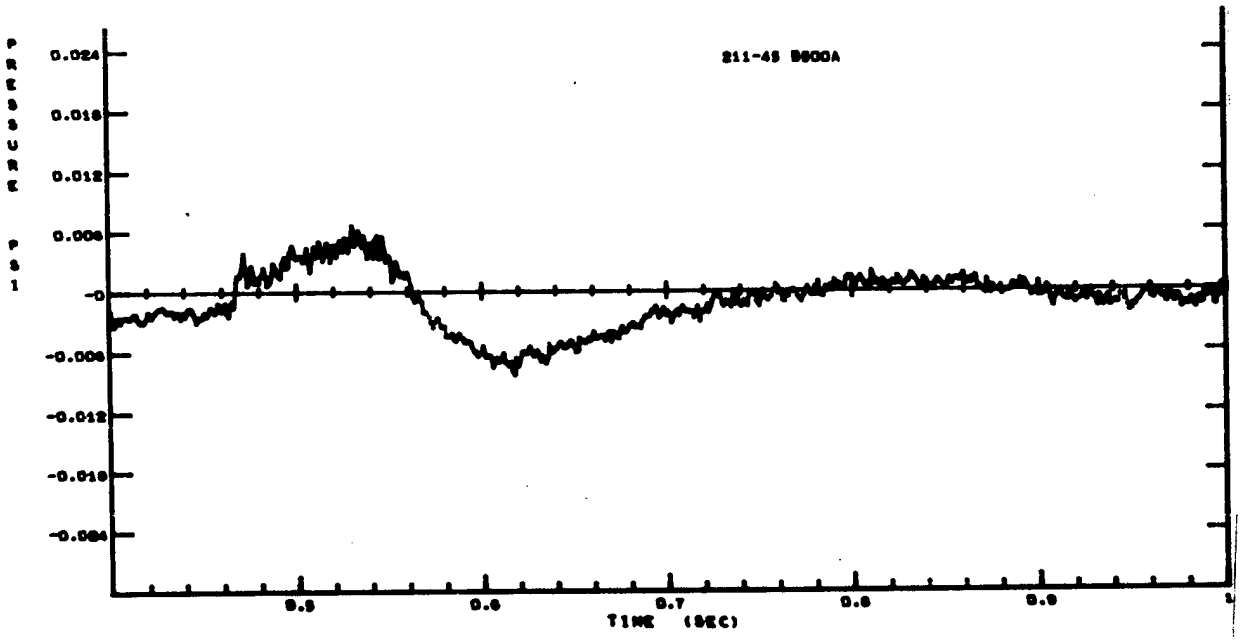

Figure A-222

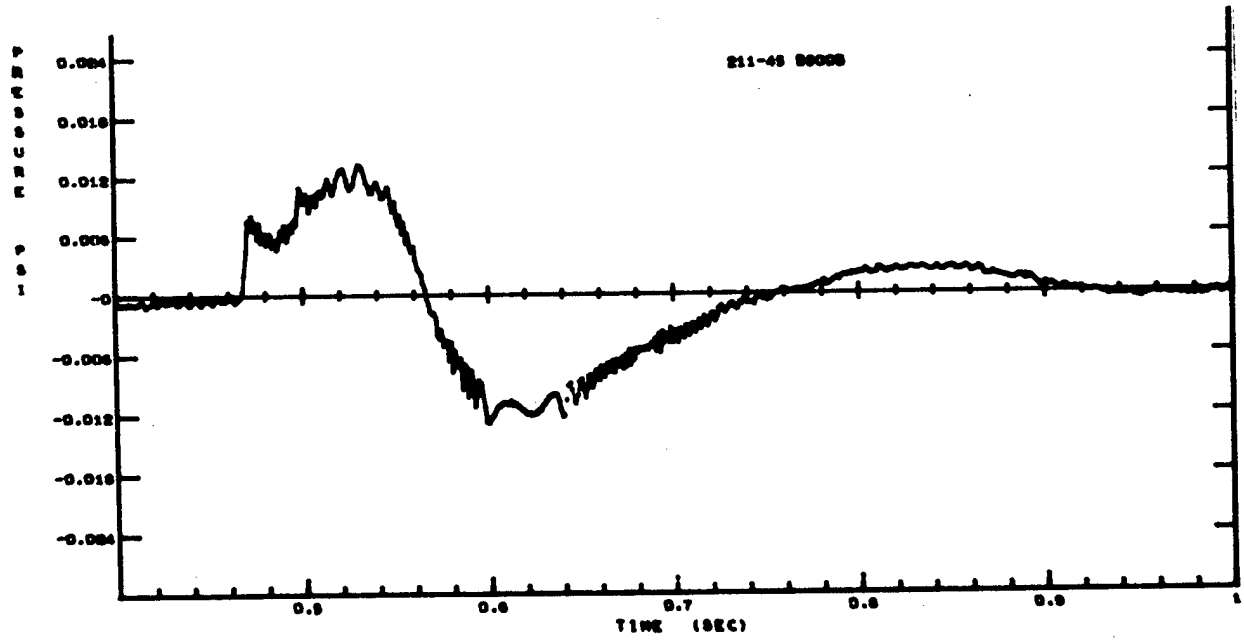

Figure A-223

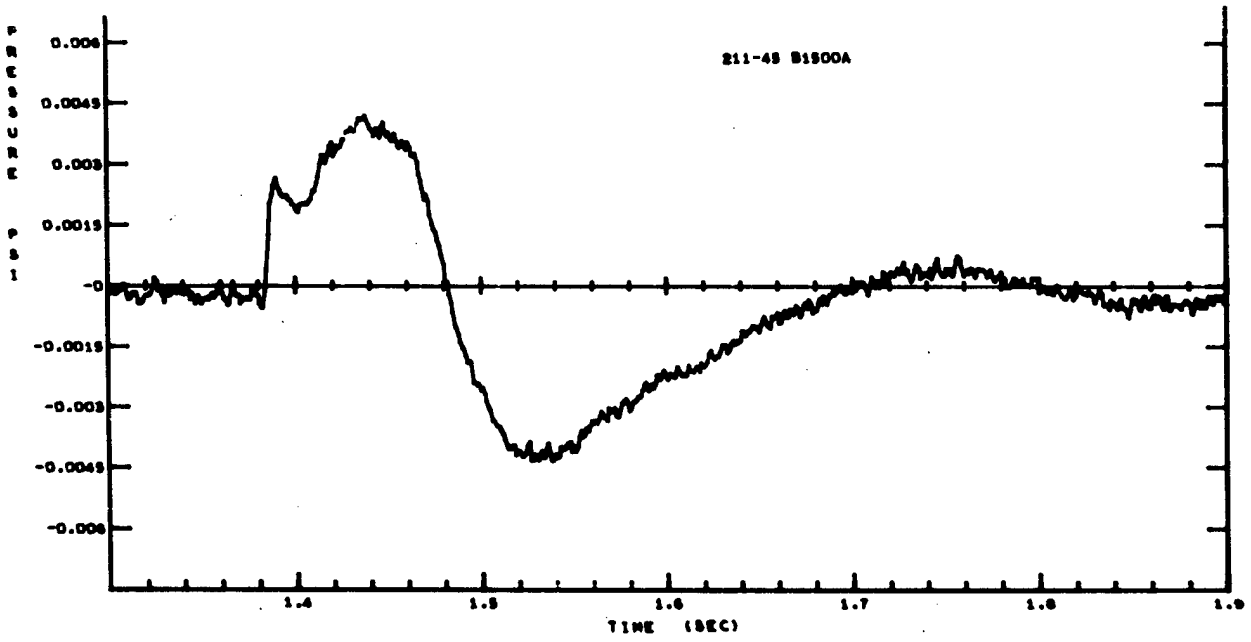

Figure A-224

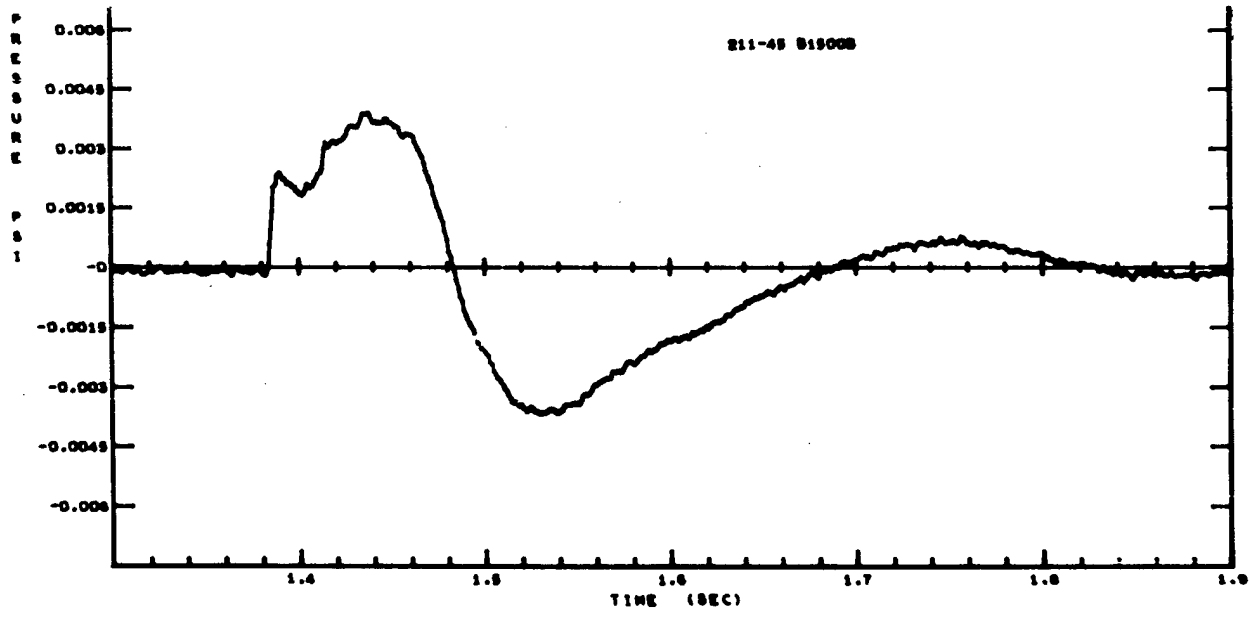

Figure A-225

Shot 211-7

One 700-pound charge was buried 13.3 feet deep. One blast line was used, with 5 gages at each of 4 stations. All gages were of the same sensitivity.

Station and gage location	Arrival time (sec)	Ground shock induced peak (psi)	Time of peak (sec)	Peak from venting gas (psi)	Time of peak (sec)	Cross-over (sec)	Positive pulse duration (sec)	Positive phase impulse (psi-sec)	Negative peak (psi)	Time of peak (sec)	Cross-over (sec)	Negative pulse duration (sec)	Negative phase impulse (psi-sec)
50A-1	0.0355	0.11086	0.061	0.31548	0.113	0.140	0.1045	0.00913	-0.15979	0.170	0.412	0.272	-0.01513
50A-2	0.037	0.09349	0.054	0.28578	0.113	0.139	0.102	0.00783	-0.12465	0.169	0.459	0.320	-0.01228
50A-3	0.037	0.11563	0.063	0.34106	0.114	0.143	0.106	0.00957	-0.16451	0.172	0.463	0.320	-0.01585
50C-4	0.0365	0.11210	0.053	0.35383	0.112	0.139	0.1025	0.00918	-0.12269	0.172	0.463	0.324	-0.01250
50C-5	0.031	0.13137	0.054	0.37380	0.112	0.139	0.108	0.01086	-0.16839	0.168	0.440	0.301	-0.01651
150A-1	0.137	0.03011	0.151	0.13529	0.200	0.231	0.094	0.00392	-0.05572	0.259	0.459	0.228	-0.00474
150A-2	0.137	0.02812	0.150	0.12592	0.200	0.231	0.094	0.00366	-0.05088	0.259	0.460	0.229	-0.00433
150B-3	0.140	0.03158	0.154	0.13419	0.203	0.235	0.095	0.00374	-0.05145	0.259	0.469	0.234	-0.00442
150C-4	0.137	0.02929	0.150	0.12699	0.199	0.231	0.094	0.00348	-0.05074	0.262	0.490	0.241	-0.00434
150C-5	0.137	0.02726	0.150	0.12032	0.199	0.230	0.093	0.00328	-0.04855	0.260	0.488	0.258	-0.00423
500A-1	0.450	0.00920	0.465	0.03754	0.514	0.547	0.097	0.00112	-0.01543	0.574	0.774	0.227	-0.00128
500A-2	0.450	0.00860	0.464	0.03256	0.514	0.547	0.097	0.00104	-0.01443	0.577	0.770	0.223	-0.00118
500C-4	0.450	0.01037	0.464	0.04034	0.514	0.547	0.097	0.00122	-0.01635	0.577	0.773	0.226	-0.00142
500C-5	0.450	0.00796	0.464	0.03006	0.513	0.546	0.096	0.00091	-0.01279	0.572	0.773	0.227	-0.00108
1500A-2	1.344	0.00316	1.364	0.01161	1.420	1.448	0.104	0.00039	-0.00510	1.476	1.677	0.229	-0.00044
1500B-3	1.344	0.00341	1.364	0.01242	1.420	1.448	0.104	0.00044	-0.00552	1.478	1.668	0.220	-0.00046
1500C-4	1.346	0.00317	1.364	0.01139	1.417	1.448	0.102	0.00038	-0.00518	1.477	1.683	0.235	-0.00045

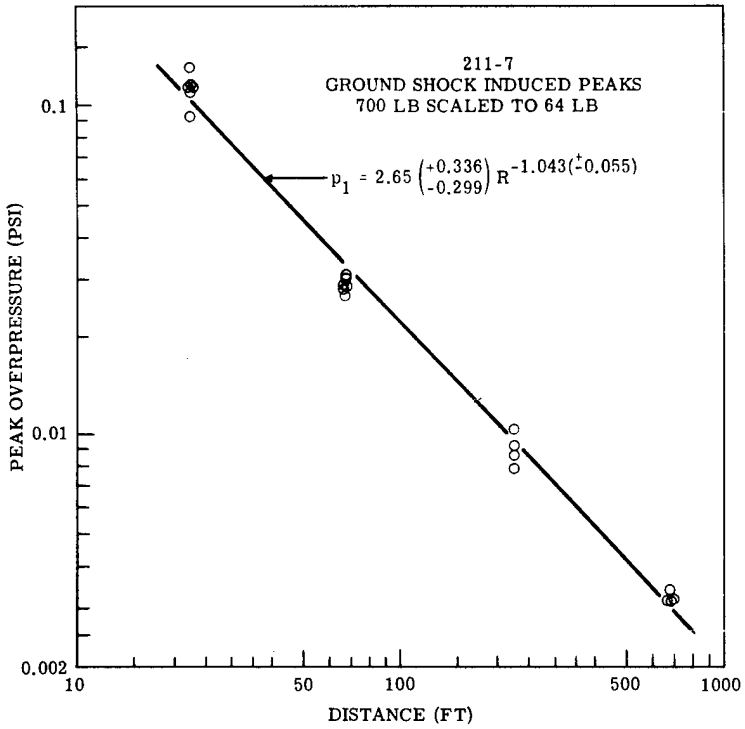

Figure A-226.

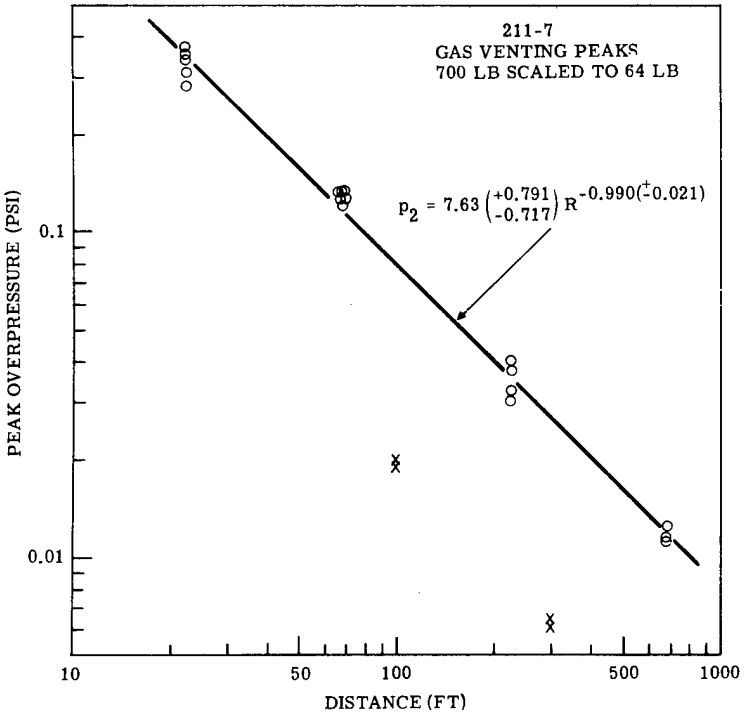

Figure A-227.

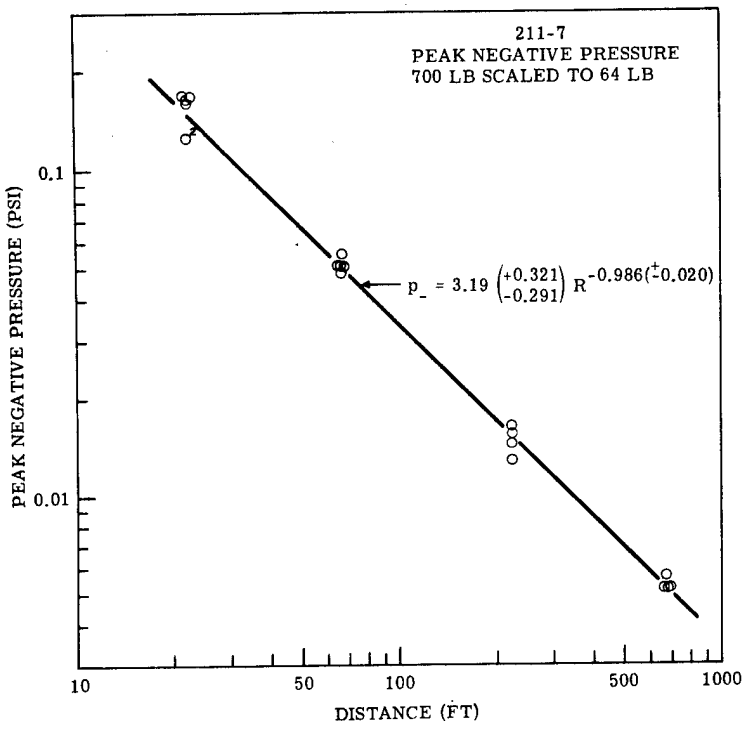

Figure A-228.

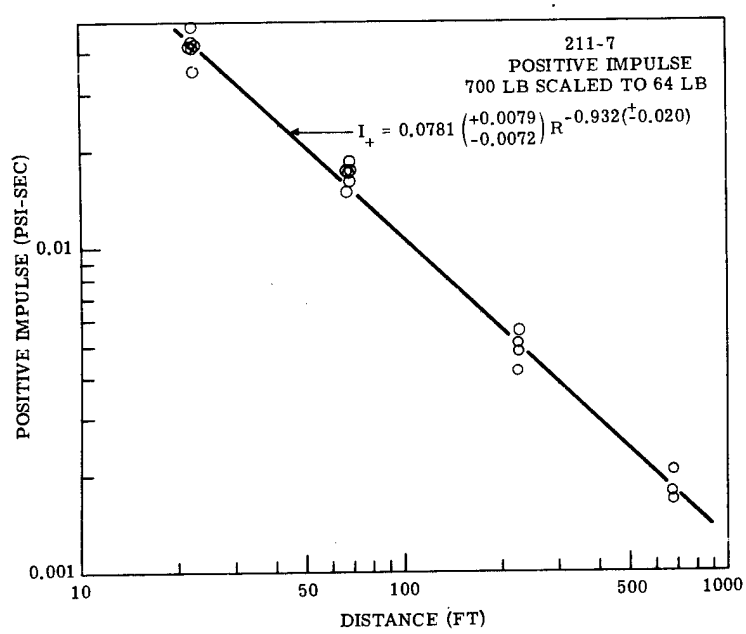

Figure A-229.

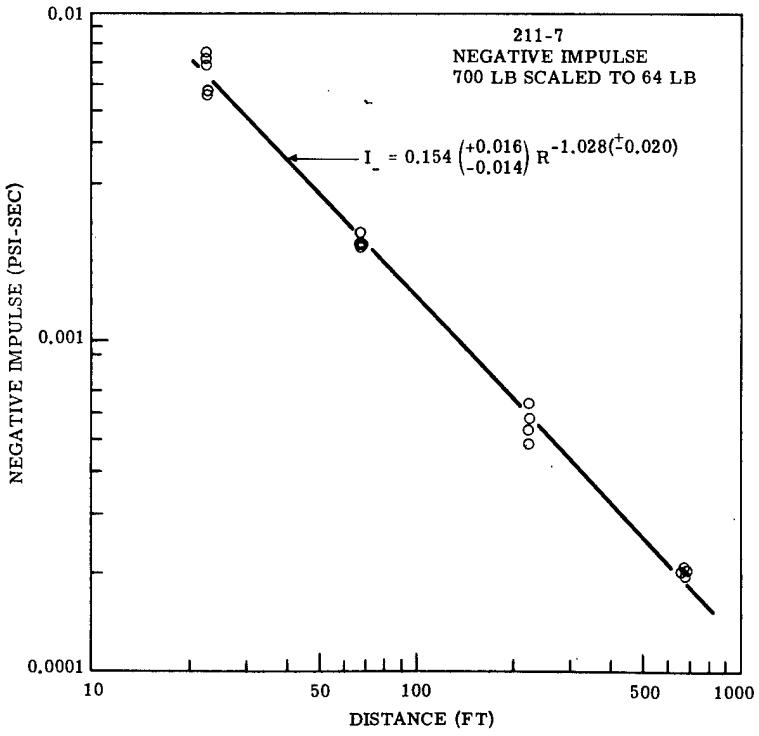

Figure A-230.

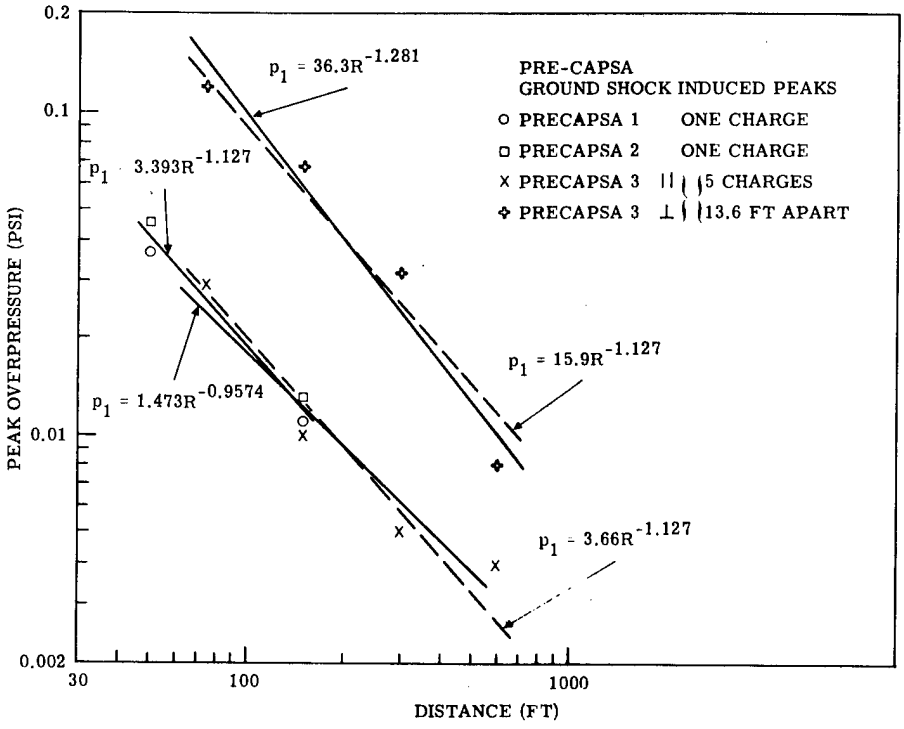

Figure A-231.

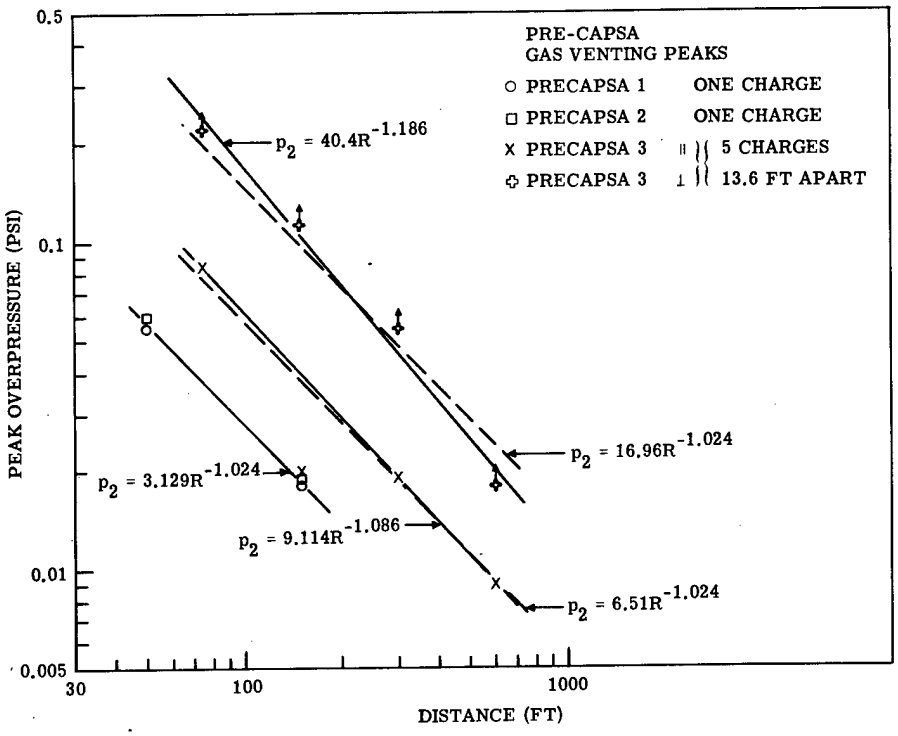

Figure A-232.

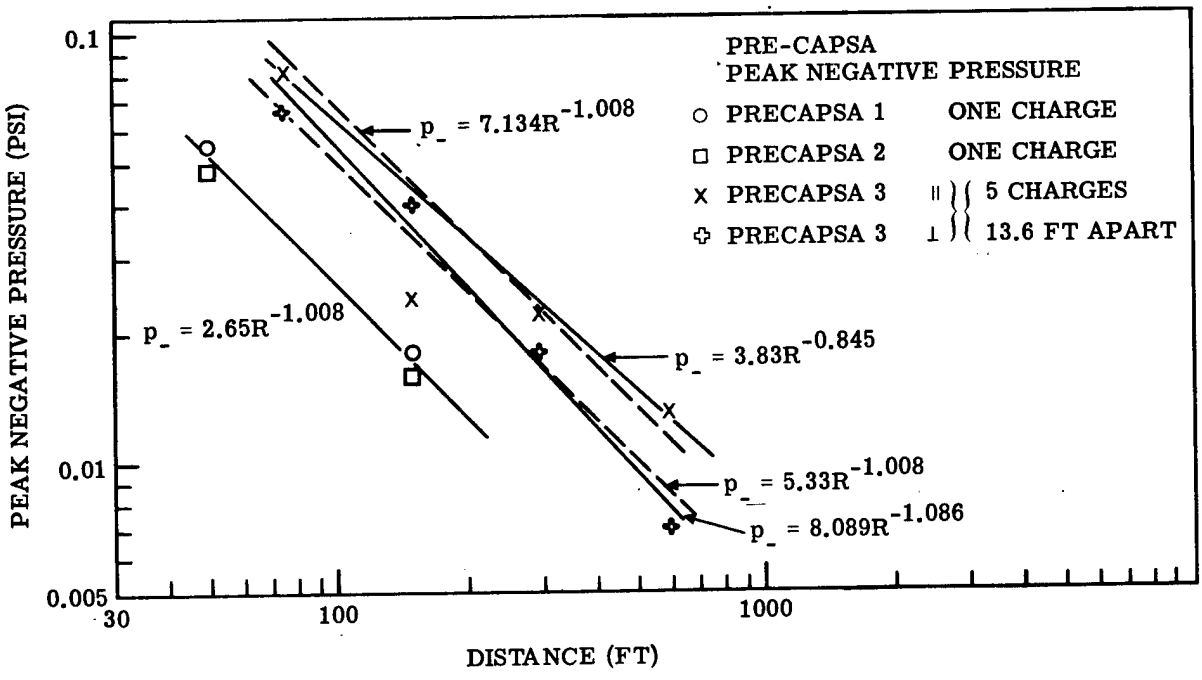

Figure A-233.

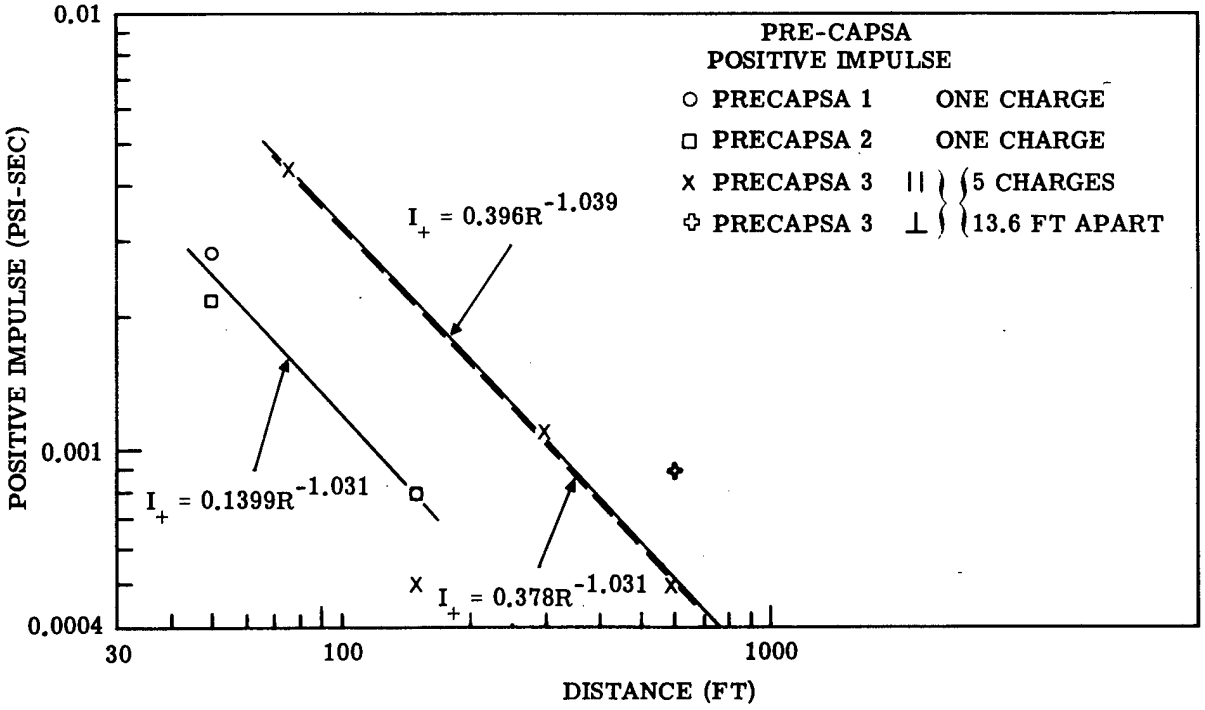

Figure A-234.

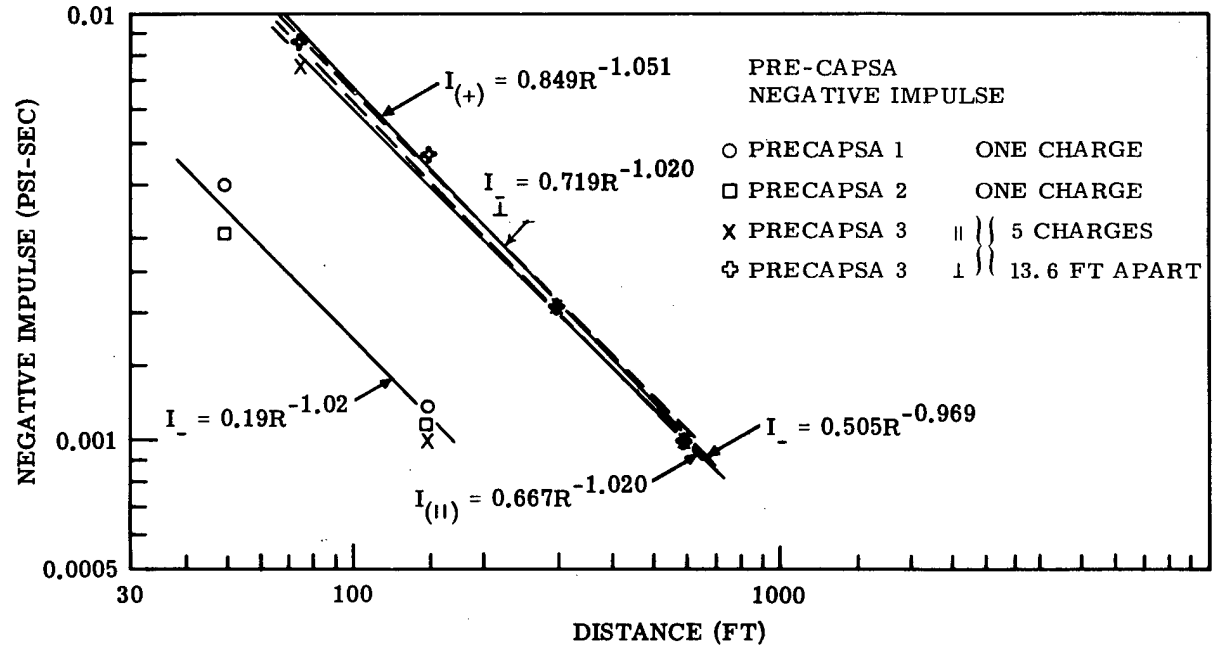

Figure A-235.

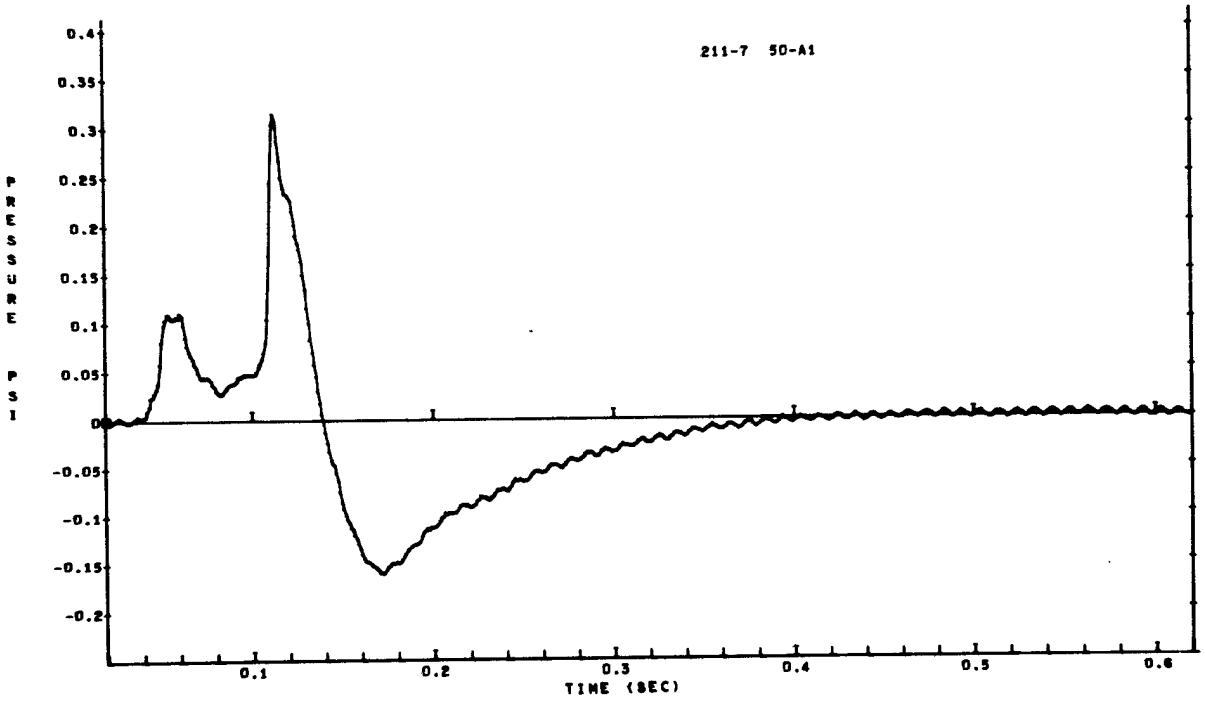

Figure A-236

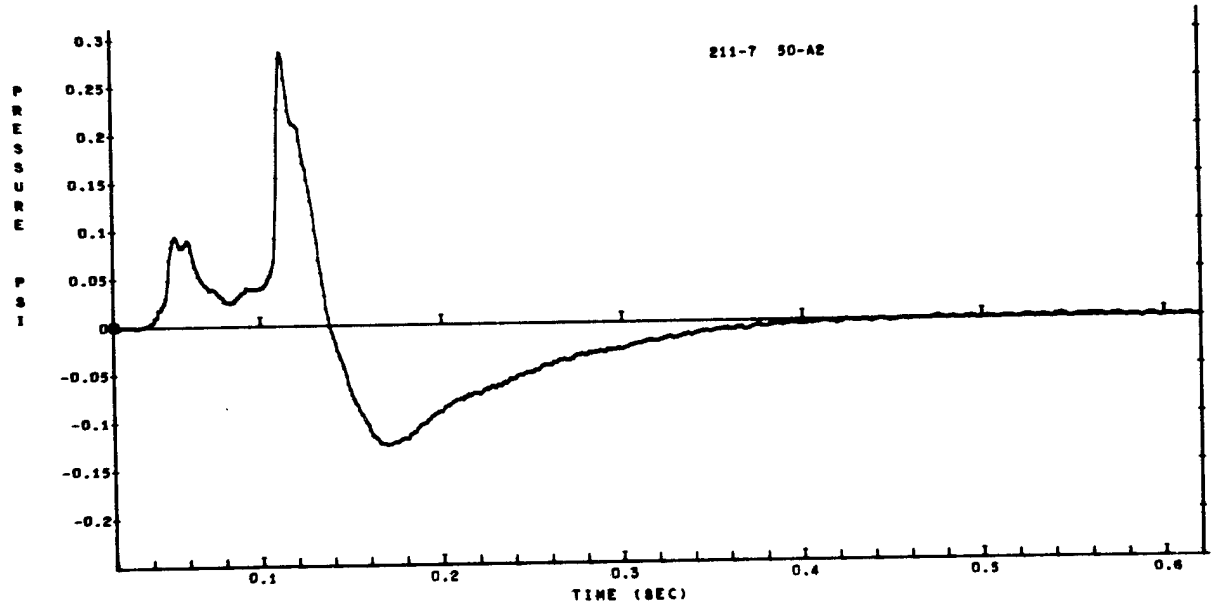

Figure A-237

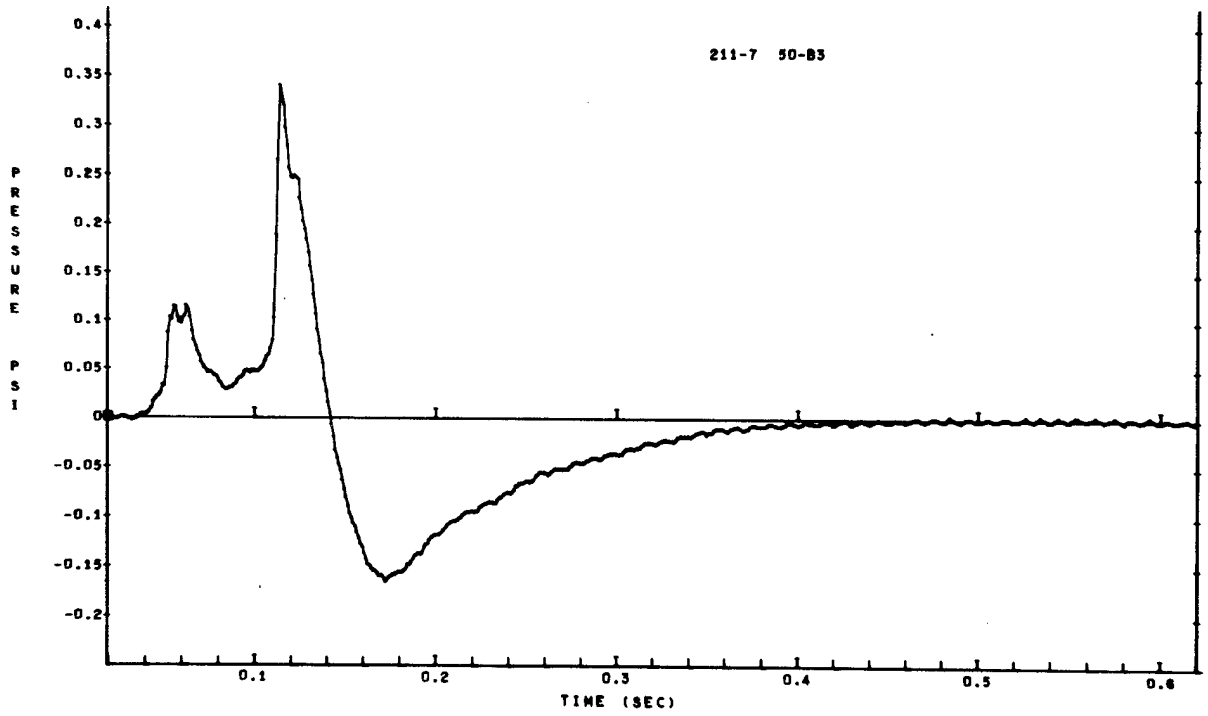

Figure A-238

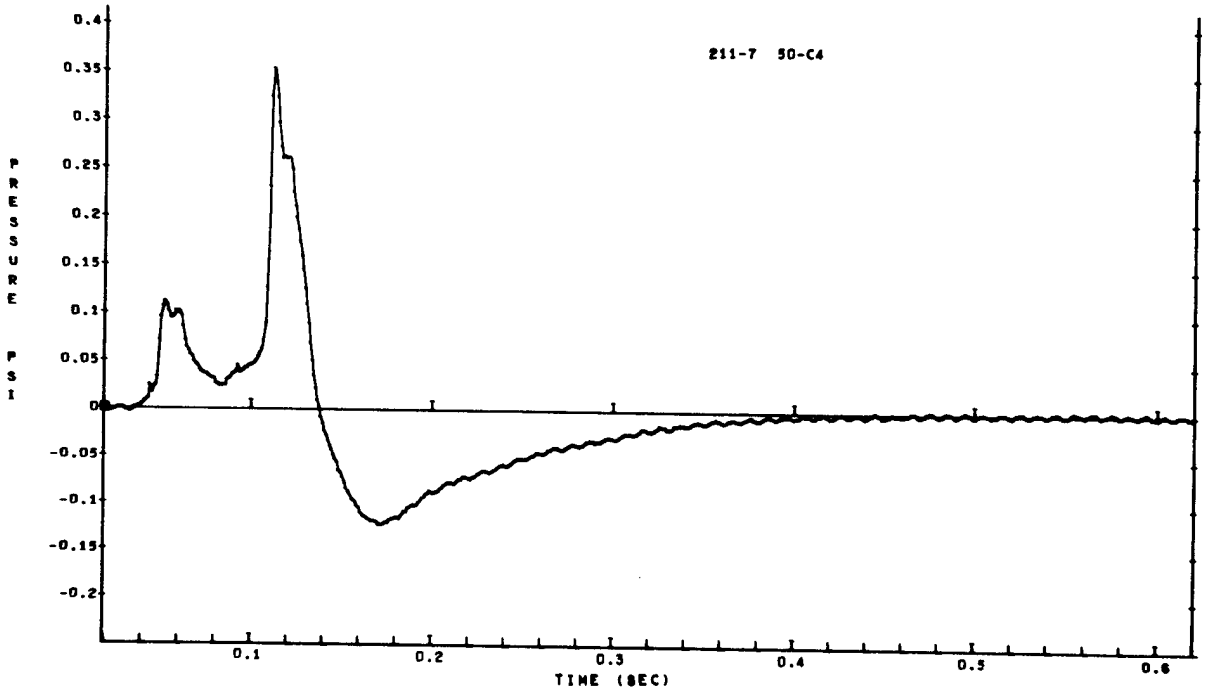

Figure A-239

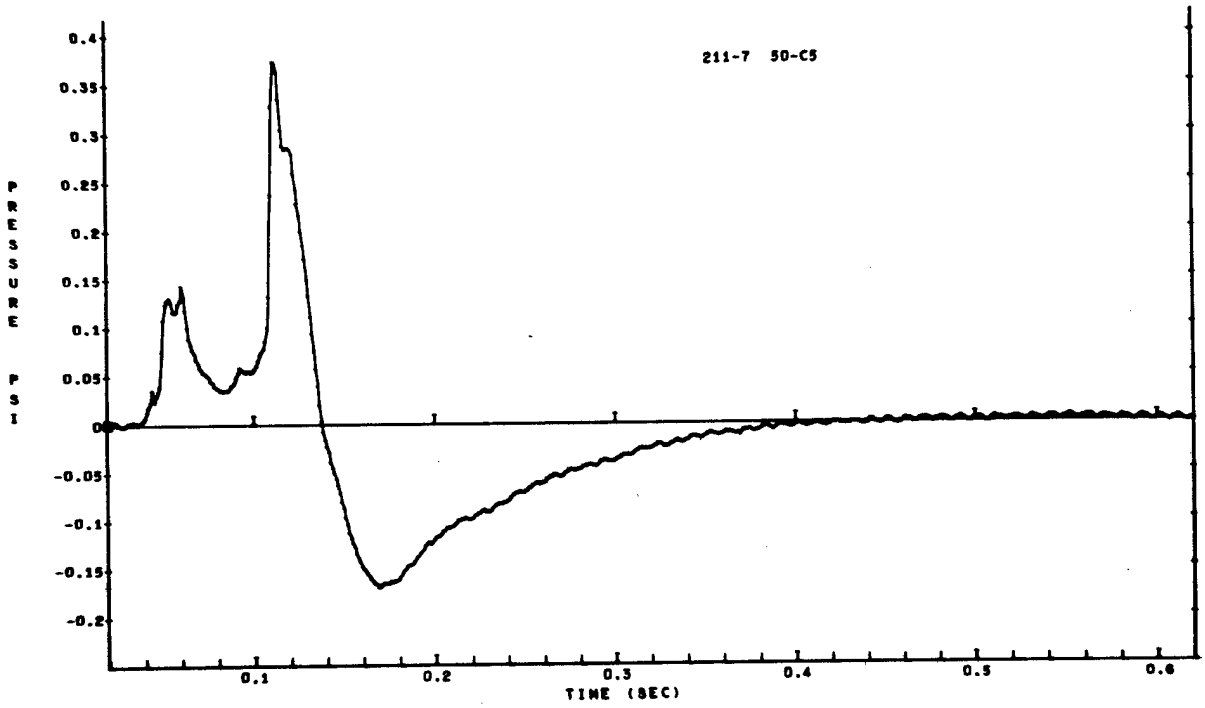

Figure A-240

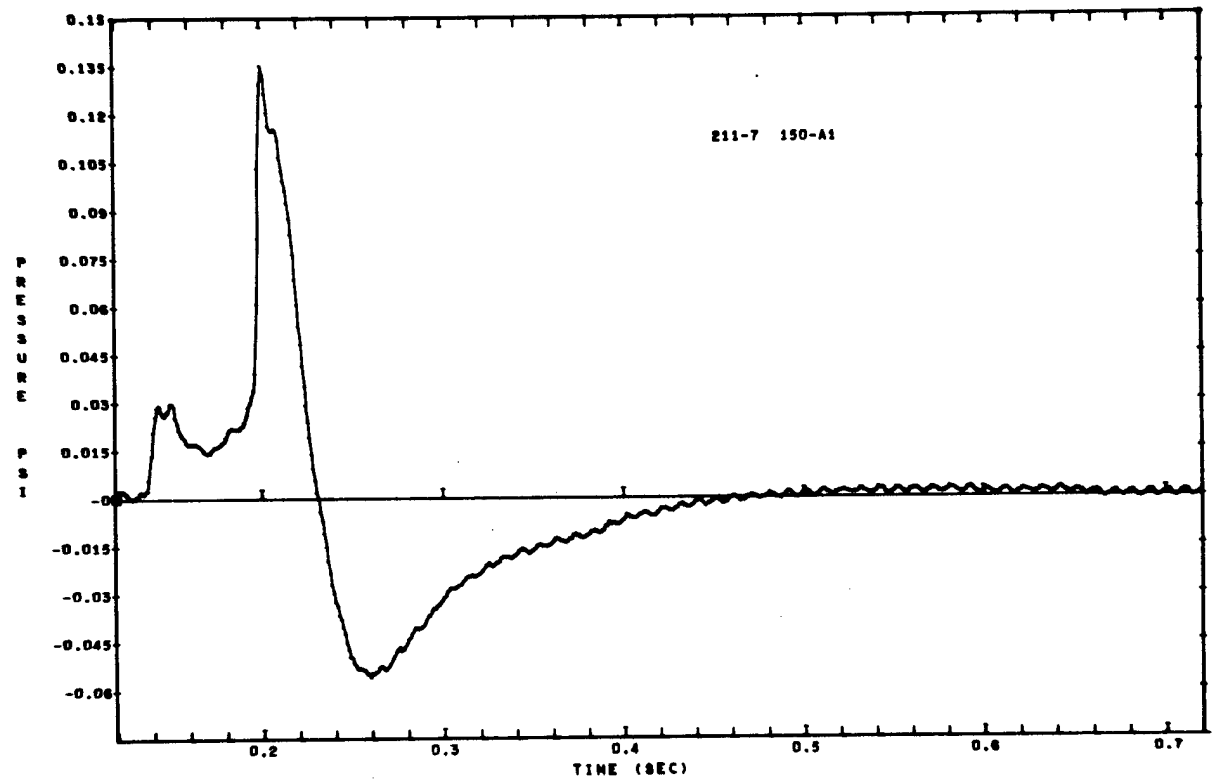

Figure A-241

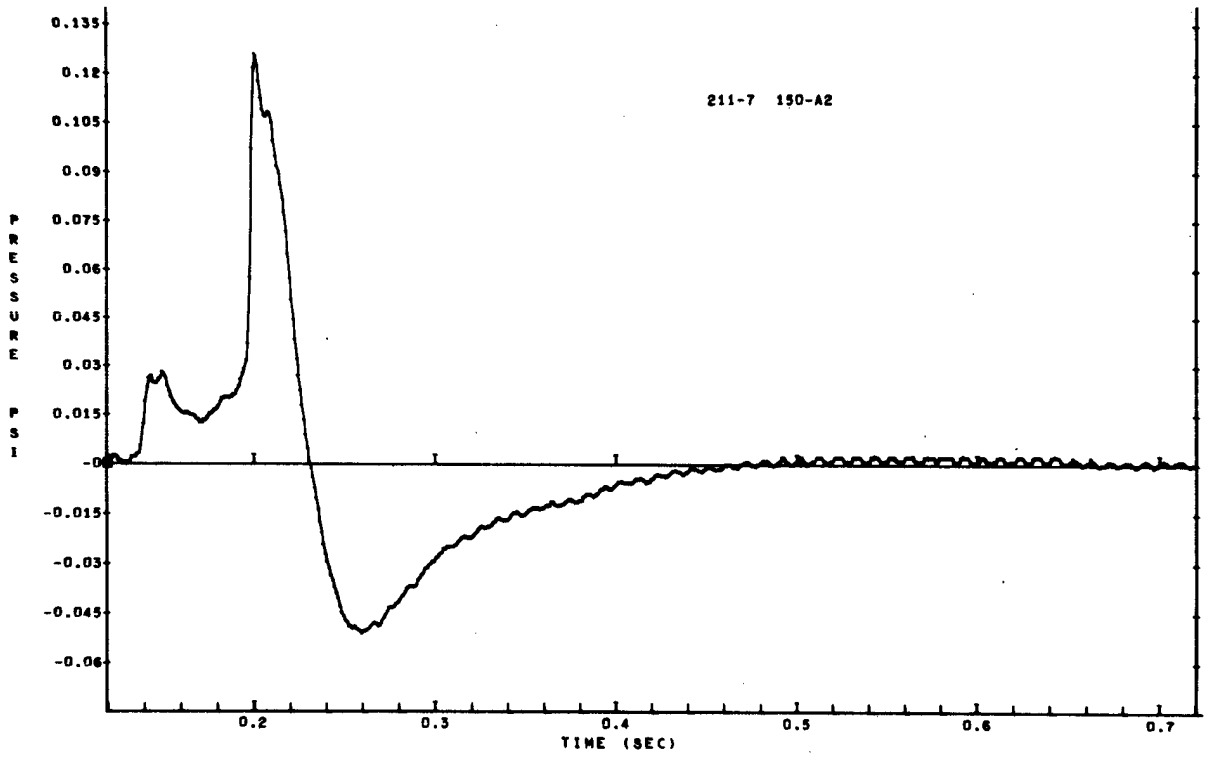

Figure A-242

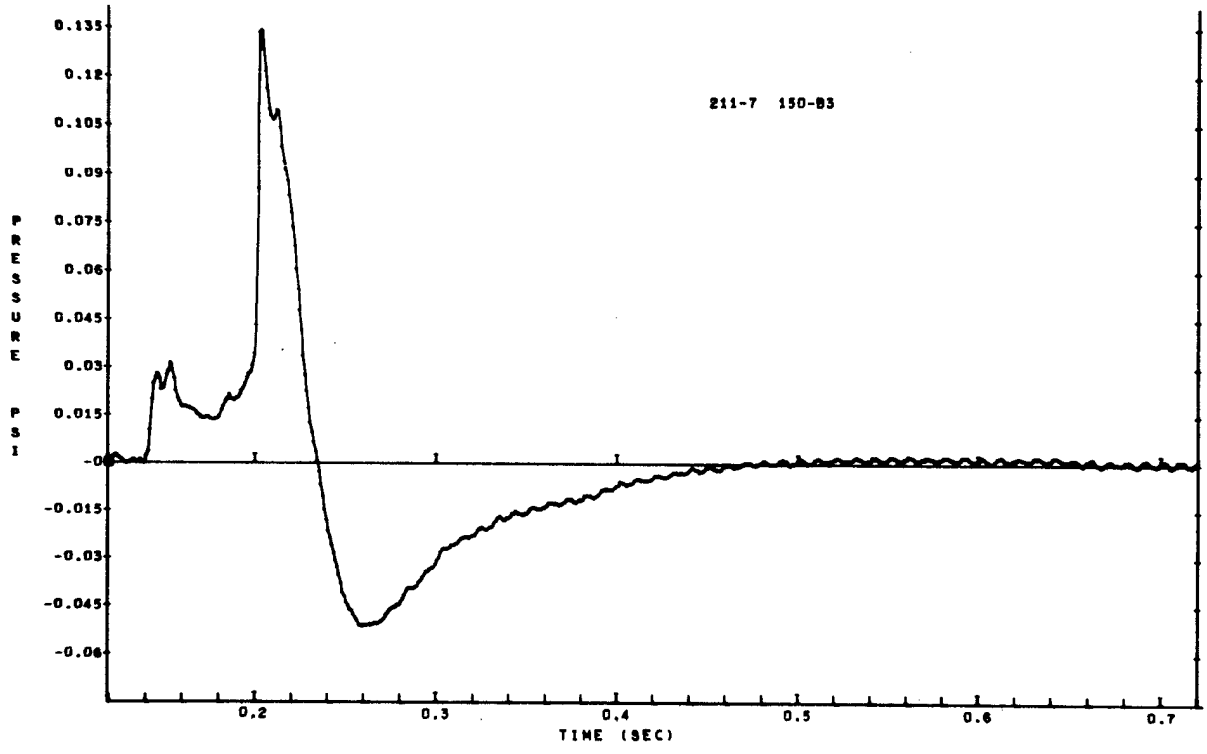

Figure A-243

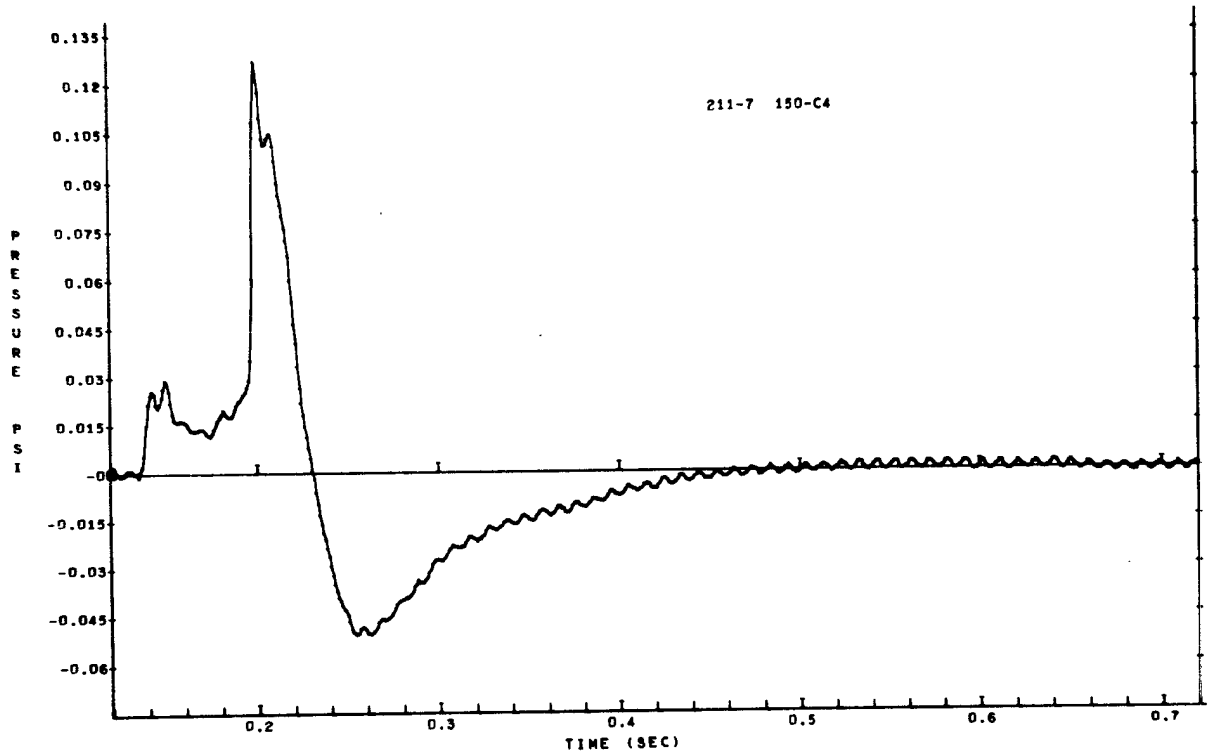

Figure A-244

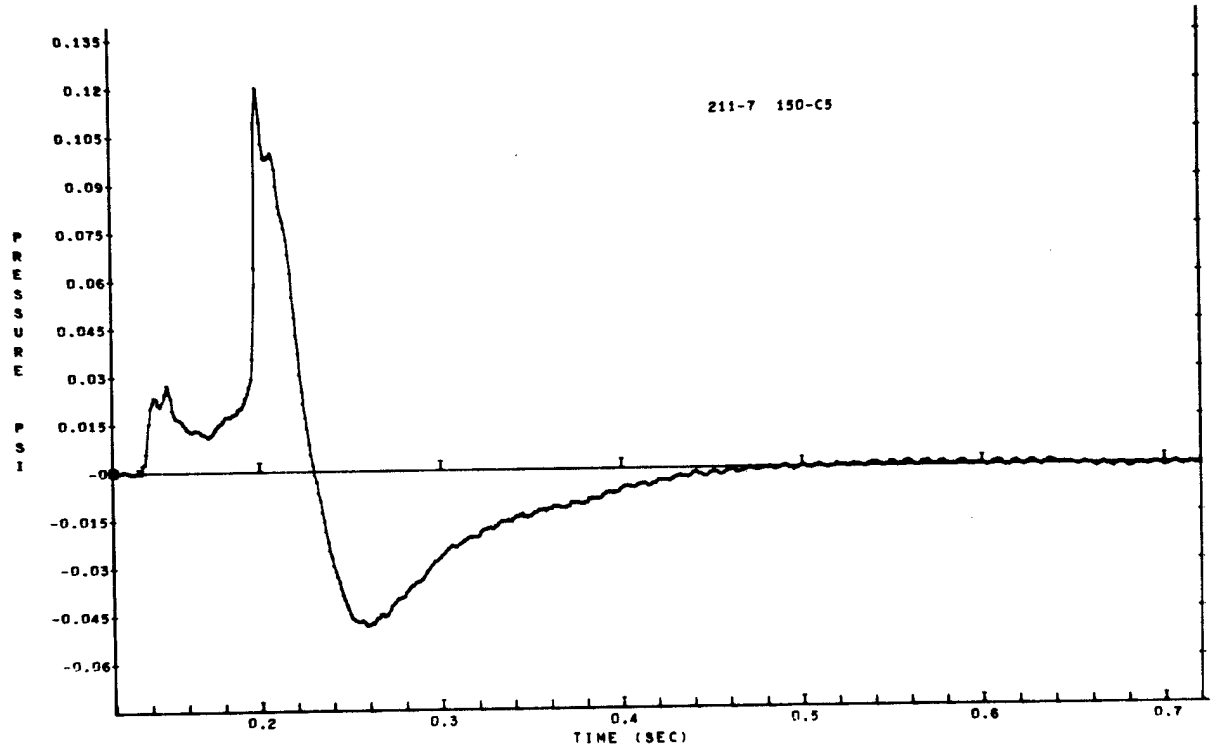

Figure A-245

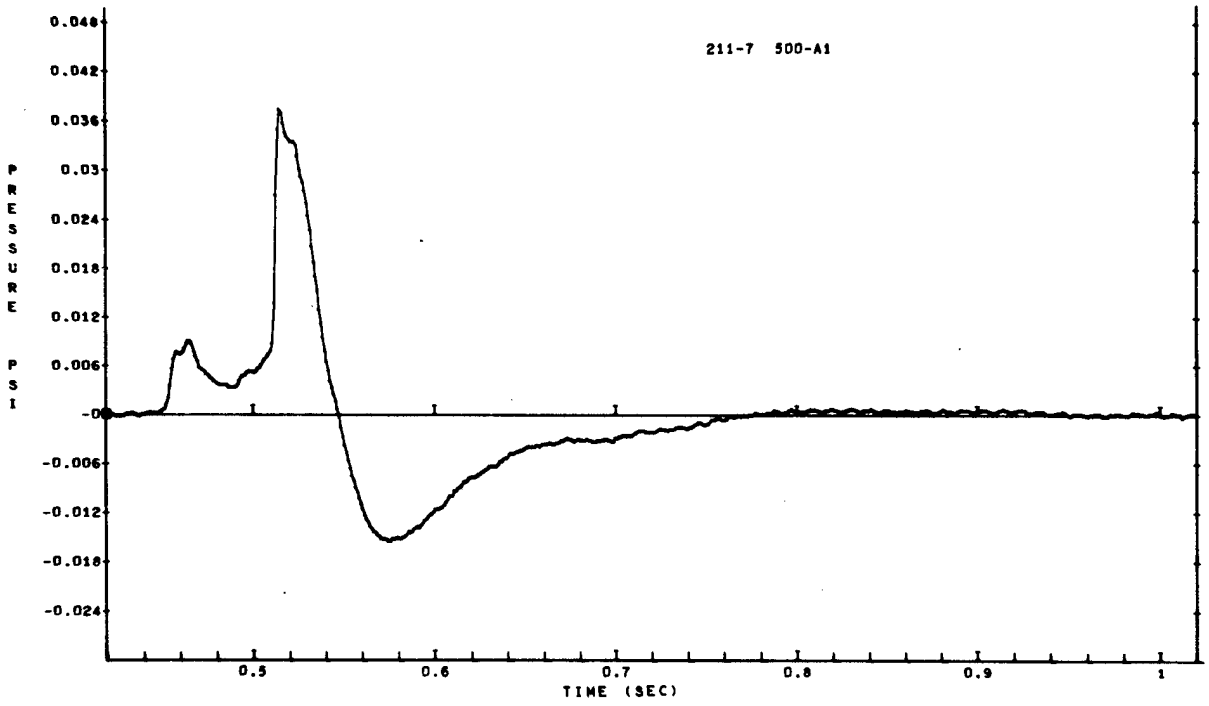

Figure A-246

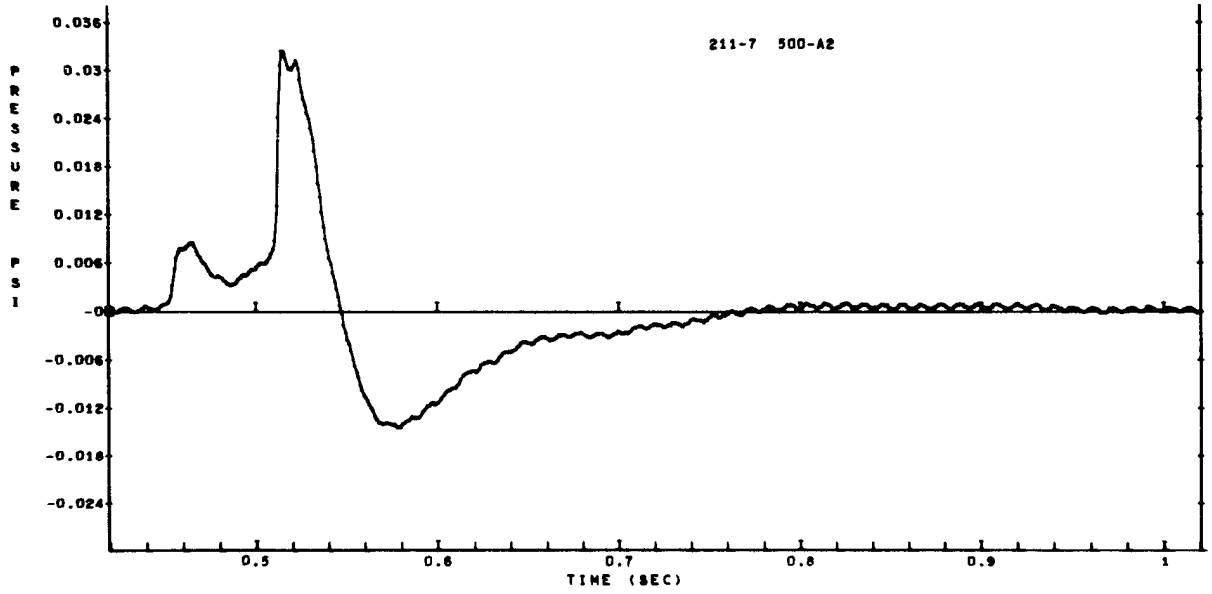

Figure A-247

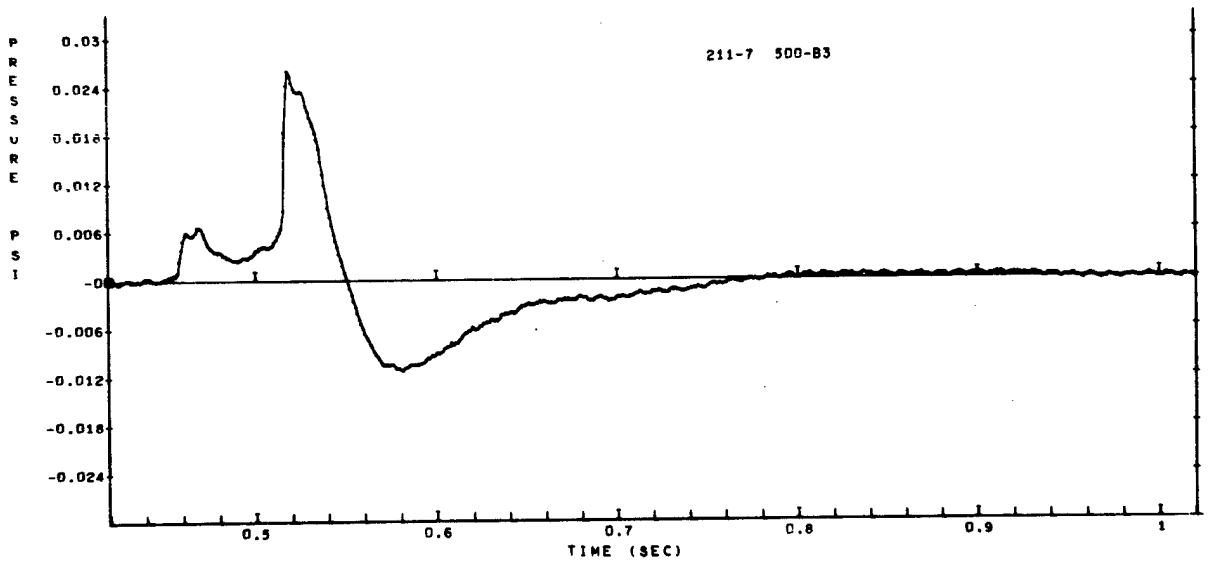

Figure A-248

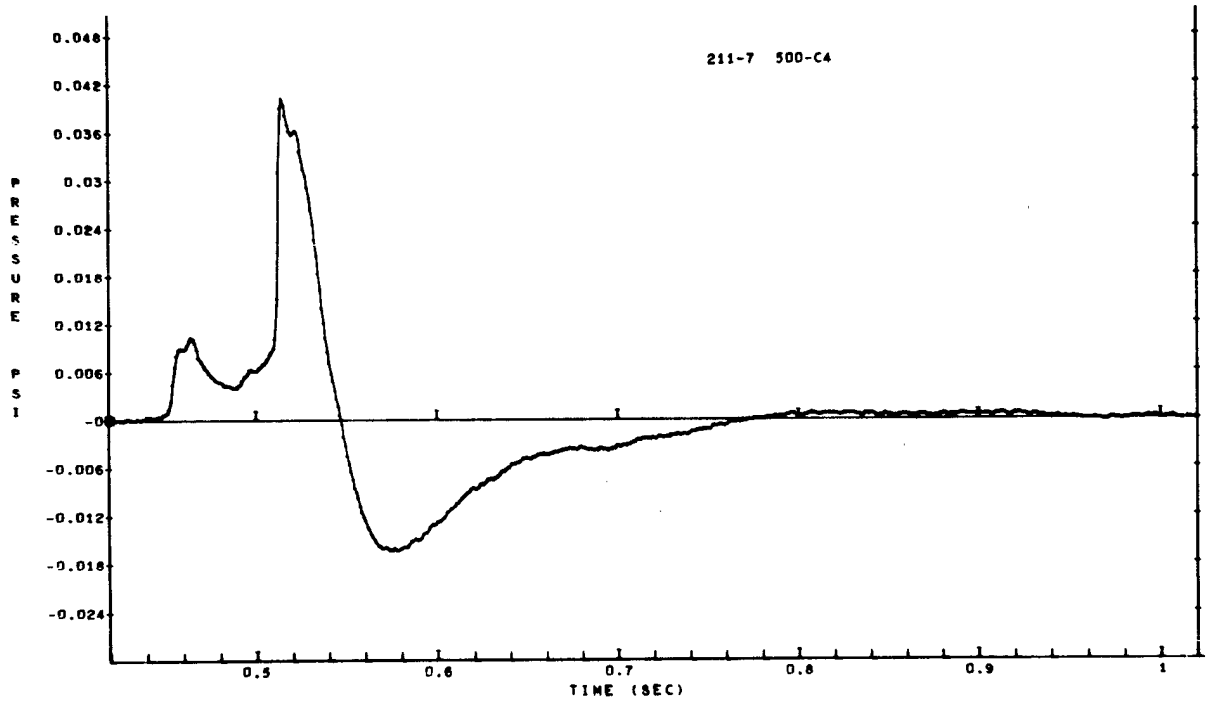

Figure A-249

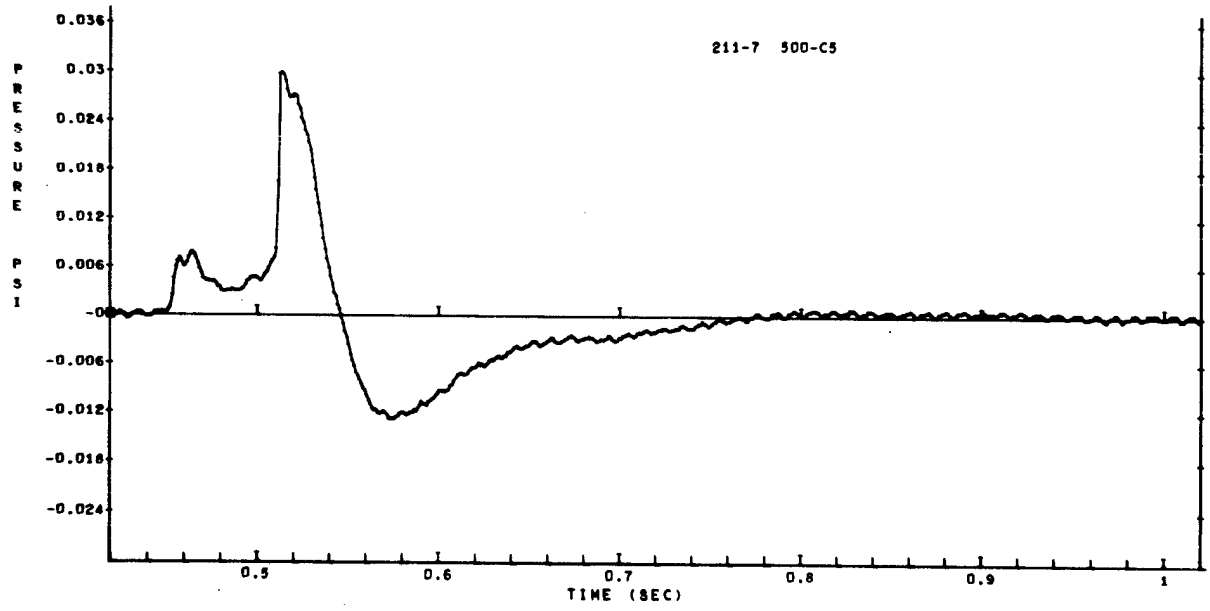

Figure A-250

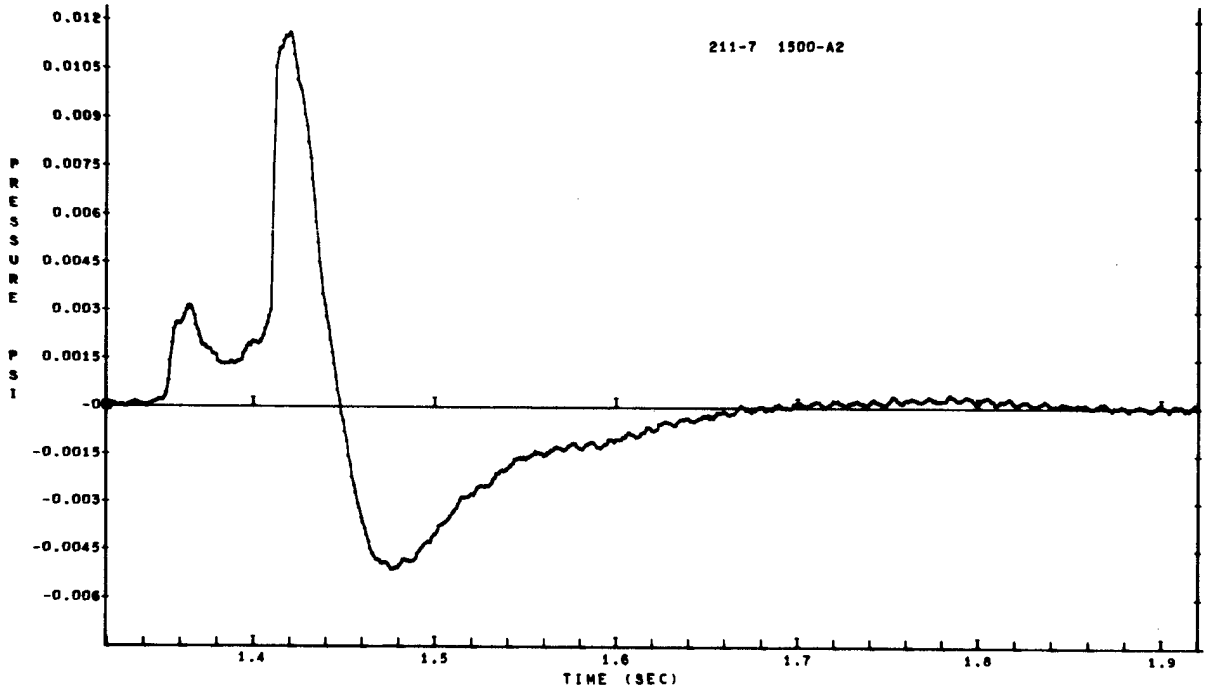

Figure A-251

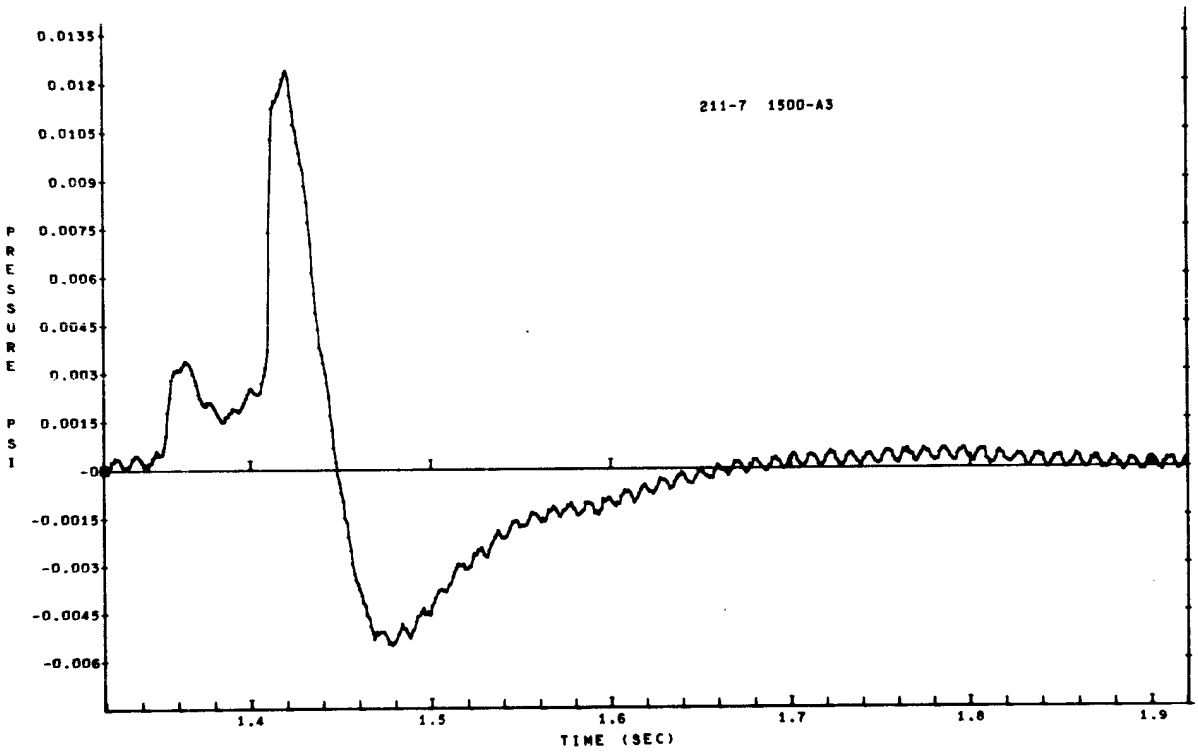

Figure A-252

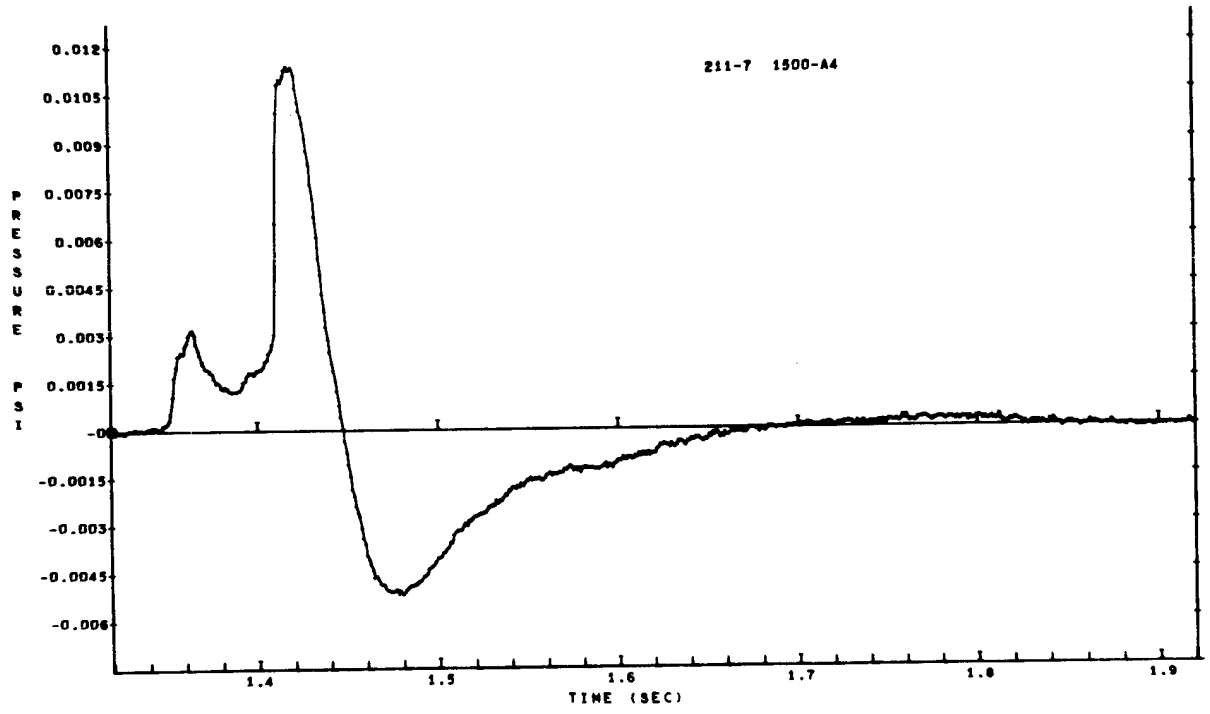

Figure A-253

APPENDIX B

Plots of airblast ratios versus number of charges in the row--values at four distances.

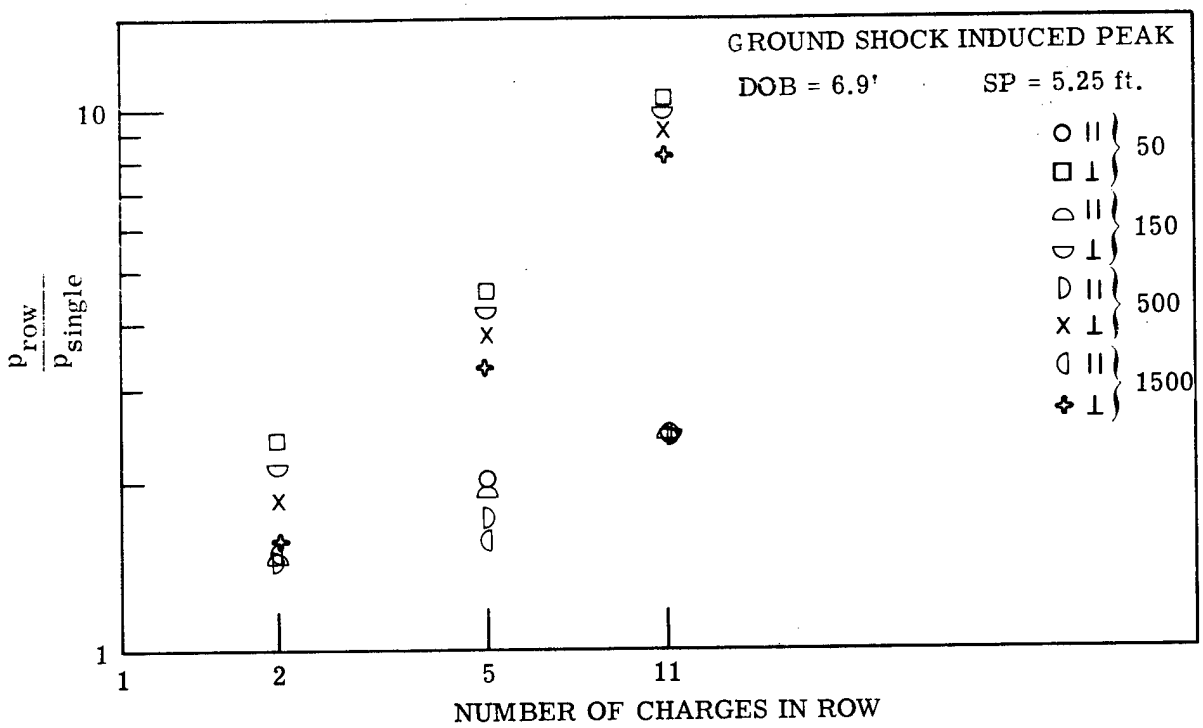

Figure B-1.

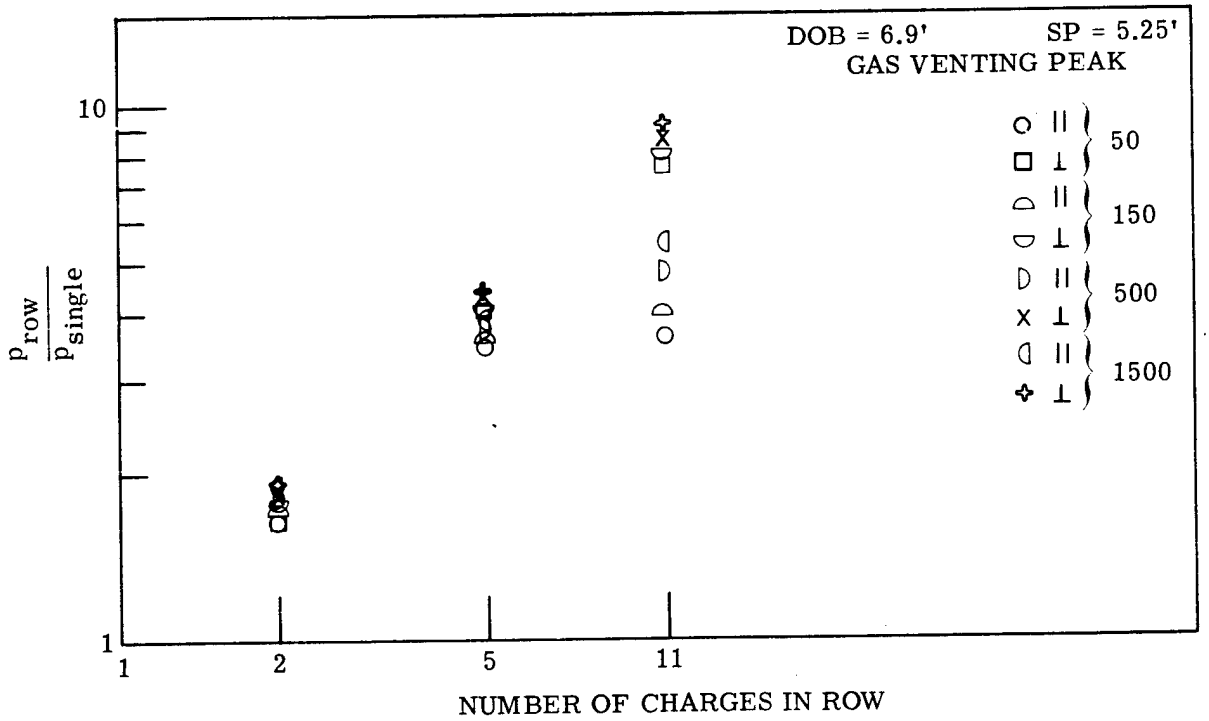

Figure B-2.

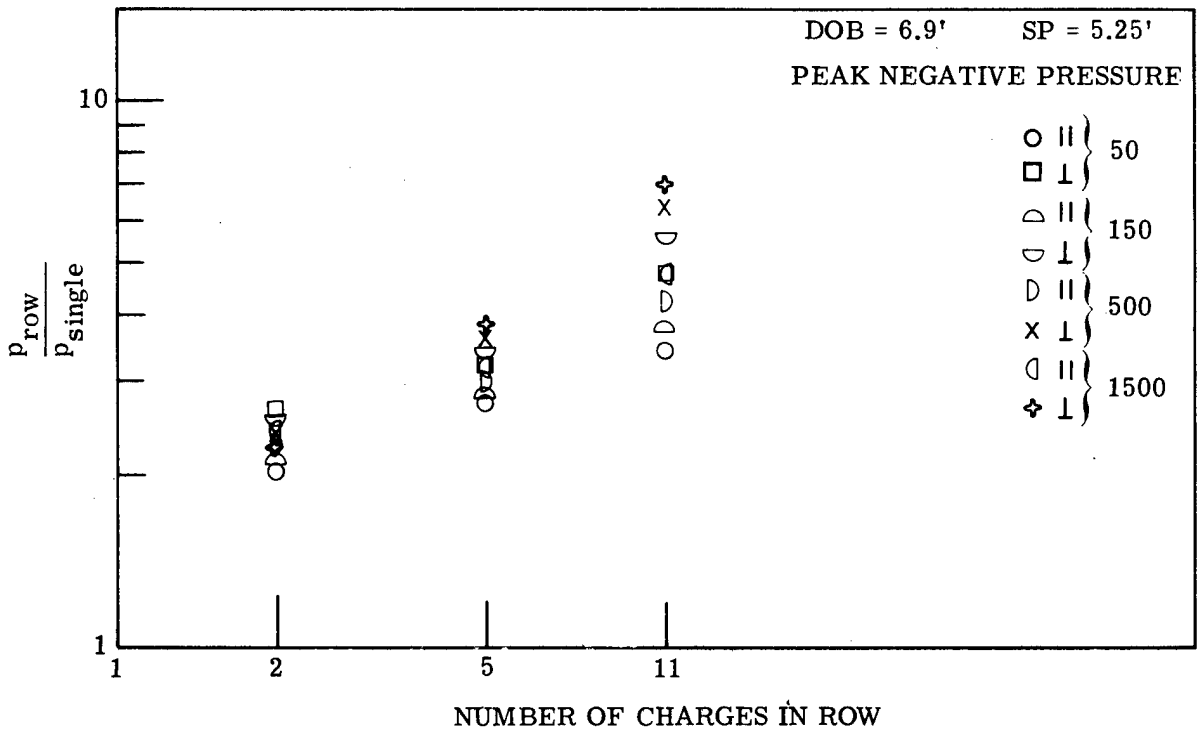

Figure B-3.

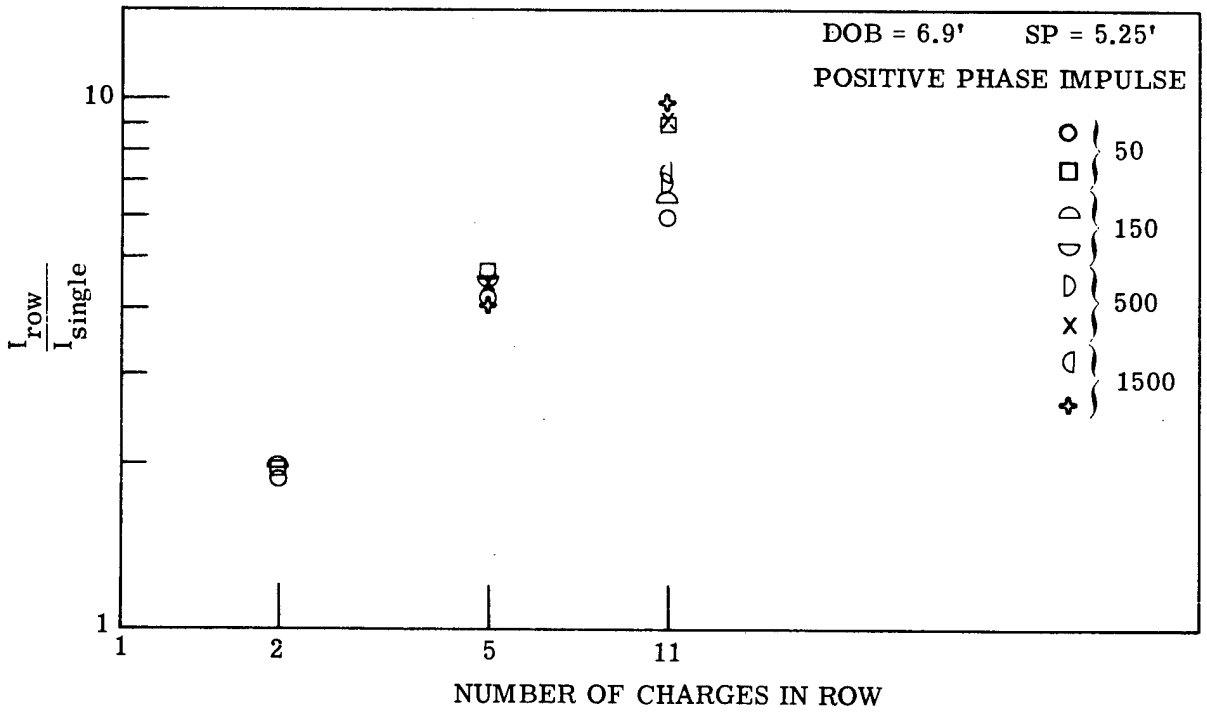

Figure B-4.

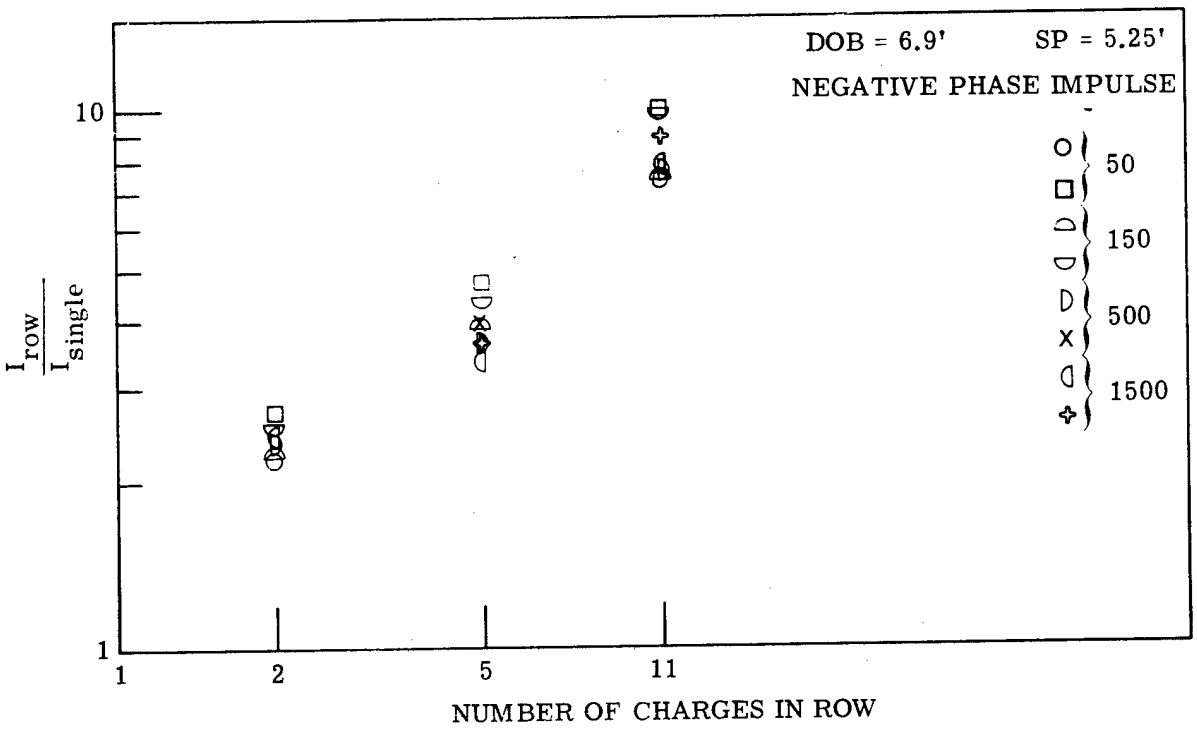

Figure B-5.

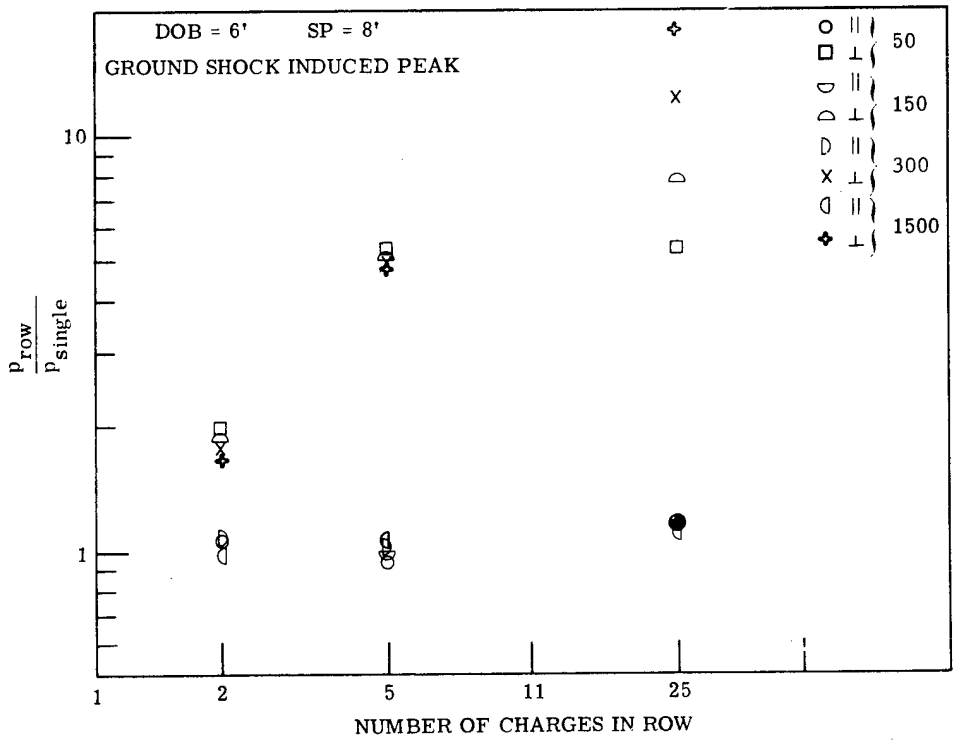

Figure B-6.

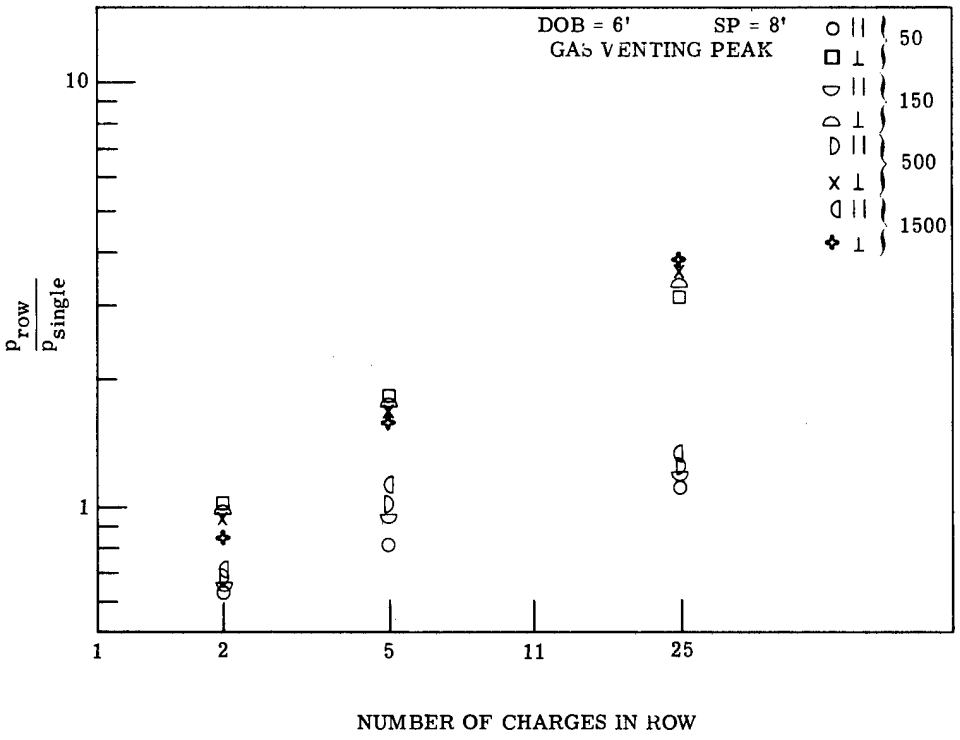

Figure B-7.

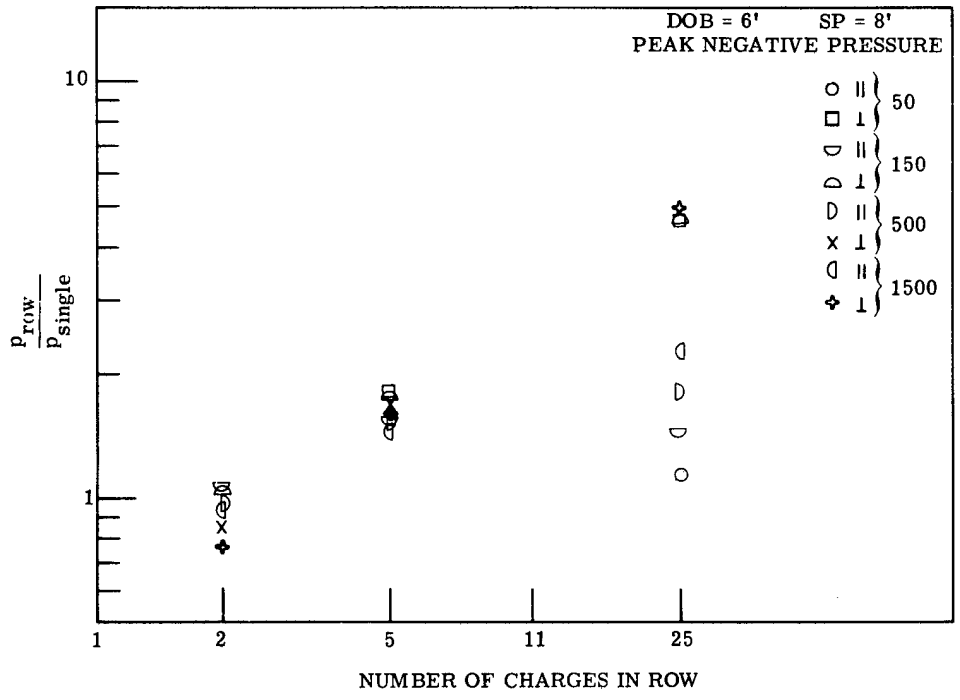

Figure B-8.

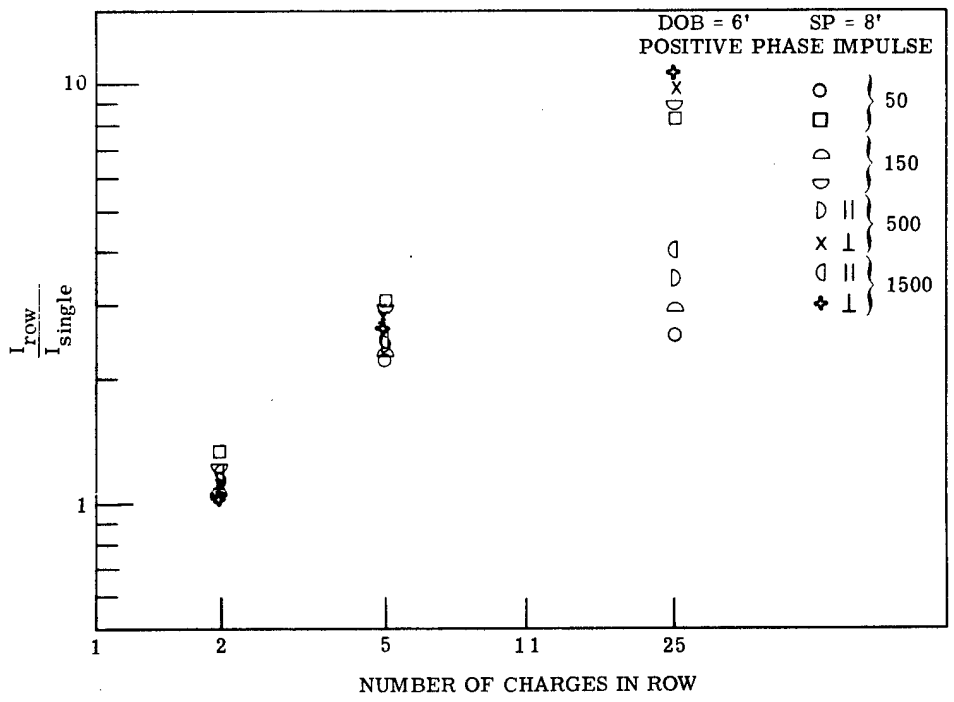

Figure B-9.

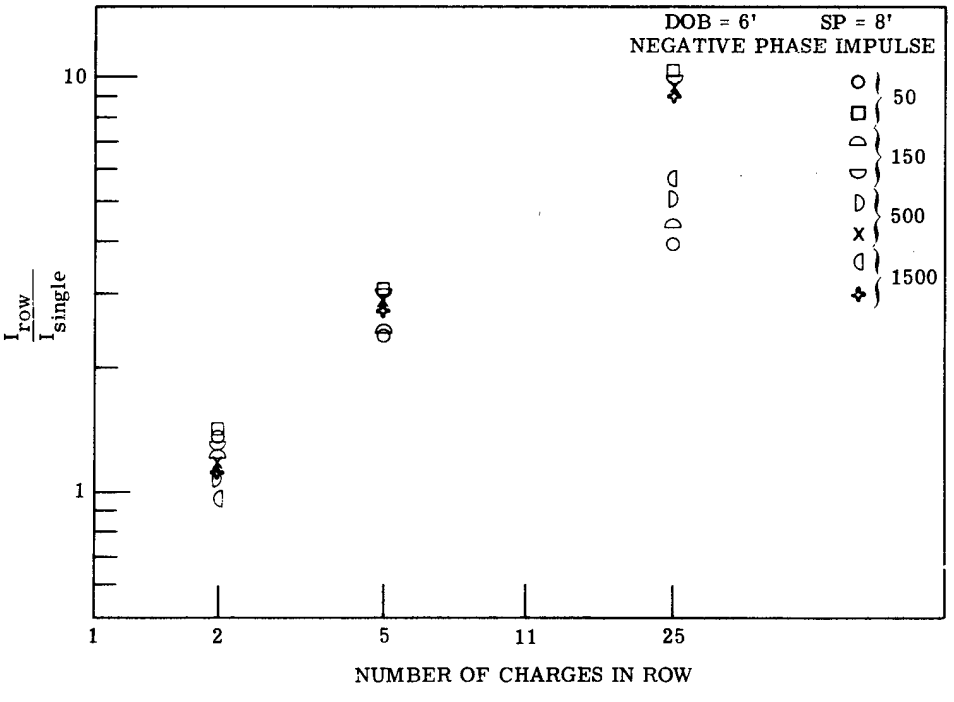

Figure B-10.

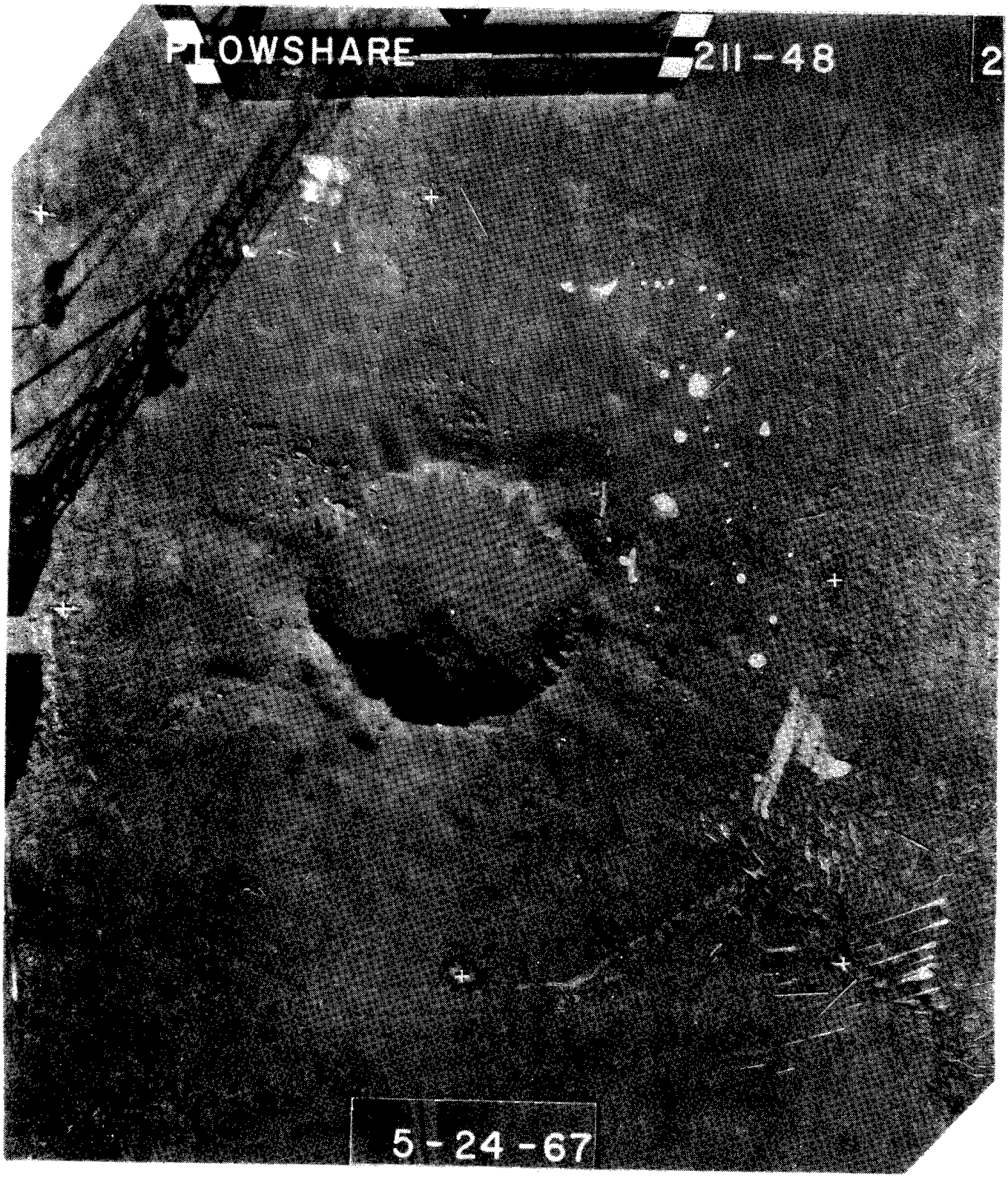
PLOWSHARE
211-48
2
5-24-67

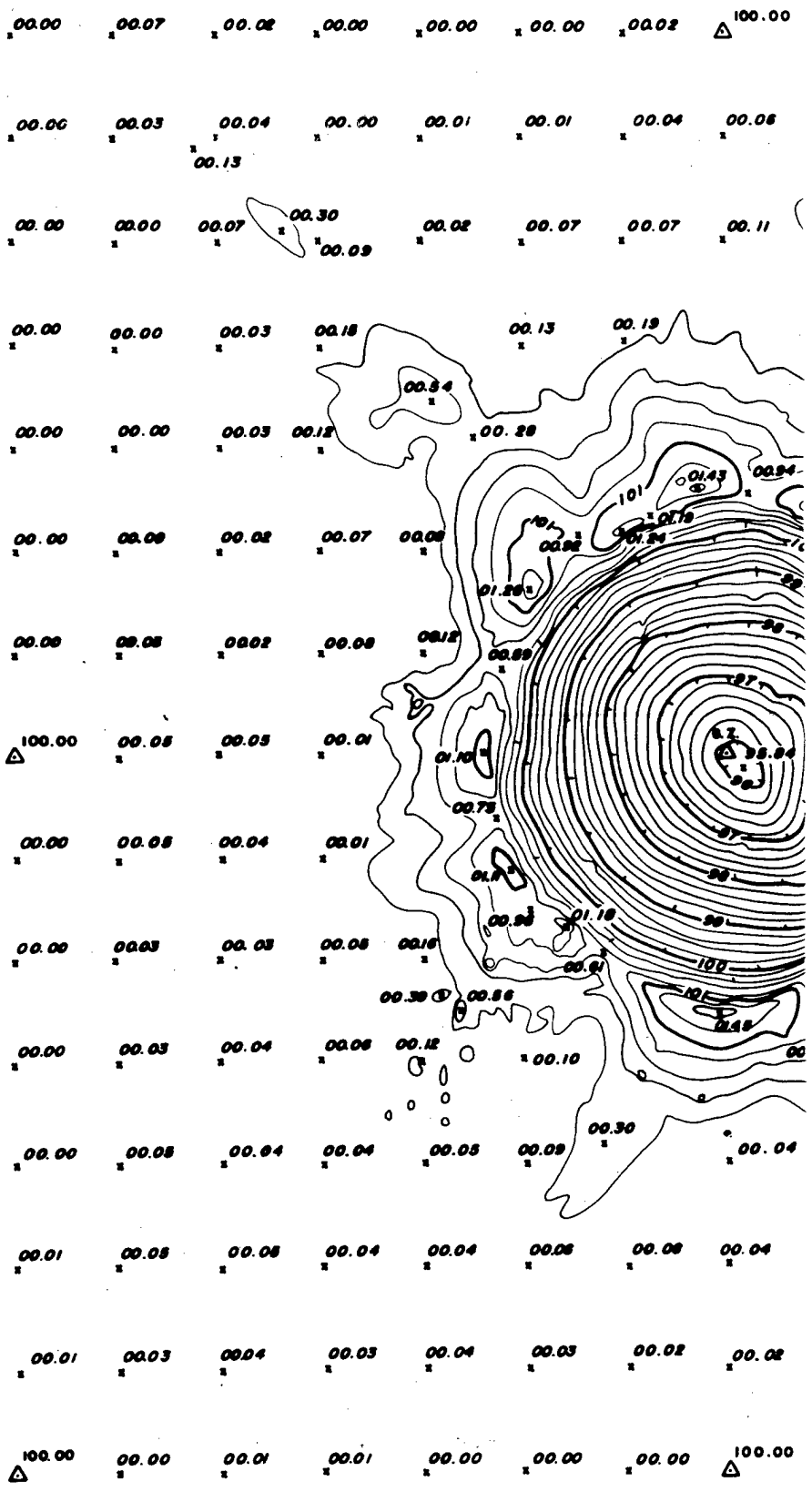
00.00 00.07 00.02 00.00 00.00 00.00 00.02 100.00
00.00 00.03 00.04 00.00 00.01 00.01 00.04 00.06
00.13
00.00 00.00 00.07 00.30 00.09 00.02 00.07 00.07 00.11
00.00 00.00 00.03 00.18 00.13 00.19
00.34
00.00 00.00 00.03 00.18 00.28
01.43 00.94
00.00 00.09 00.02 00.07 00.08 00.82
01.20
00.00 00.08 00.02 00.08 00.12 00.89
100.00 00.08 00.03 00.01 01.10
00.73
00.00 00.08 00.04 00.01
00.00 00.03 00.03 00.06 00.16 00.61
00.39 00.86
00.00 00.03 00.04 00.06 00.12 00.10
00.00 00.08 00.04 00.04 00.05 00.09 00.30 00.04
00.01 00.08 00.06 00.04 00.04 00.06 00.06 00.04
00.01 00.03 00.04 00.03 00.04 00.03 00.02 00.02
100.00 00.00 00.01 00.01 00.00 00.00 00.00 100.00

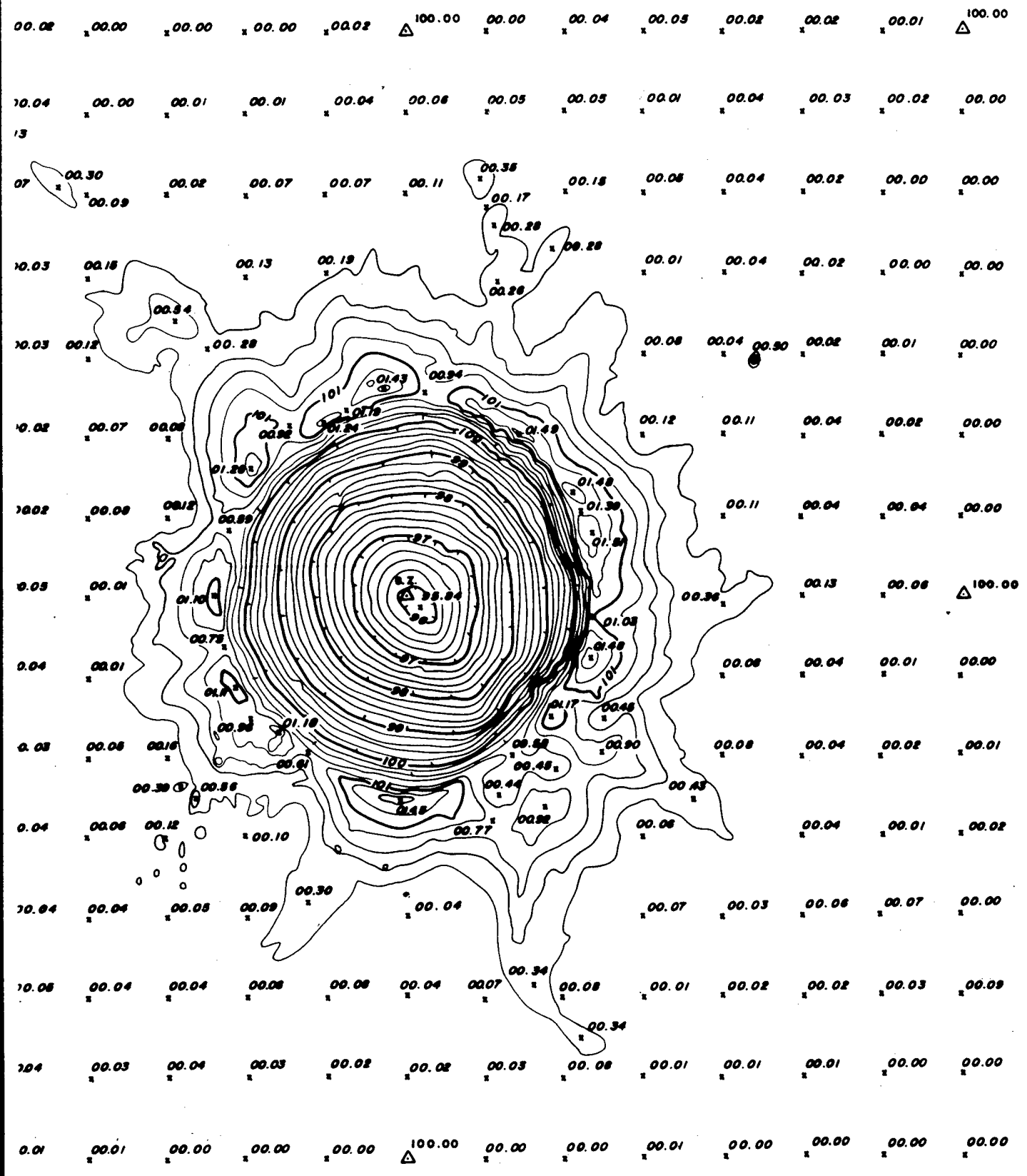
100.00
100.00
100.00
100.00
PROJEC

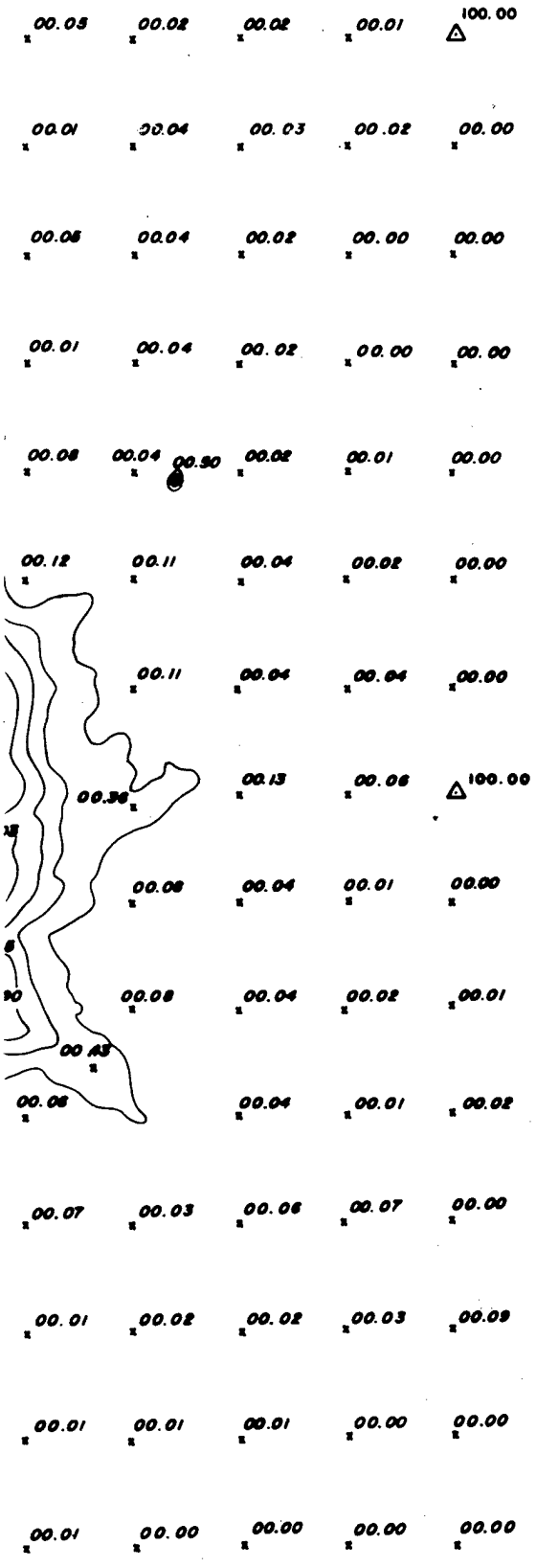

SCALE

0 6 FT. 12 FT.

0.2 FOOT CONTOUR INTERVAL

DATE FLOWN 5-24-67

PROJECT PLOWSHARE TONOPAH 211-48

POST TEST TOPOGRAPHY

Compiled By

AMERICAN AERIAL SURVEYS, INC.

COVINA, CALIF.

(3)

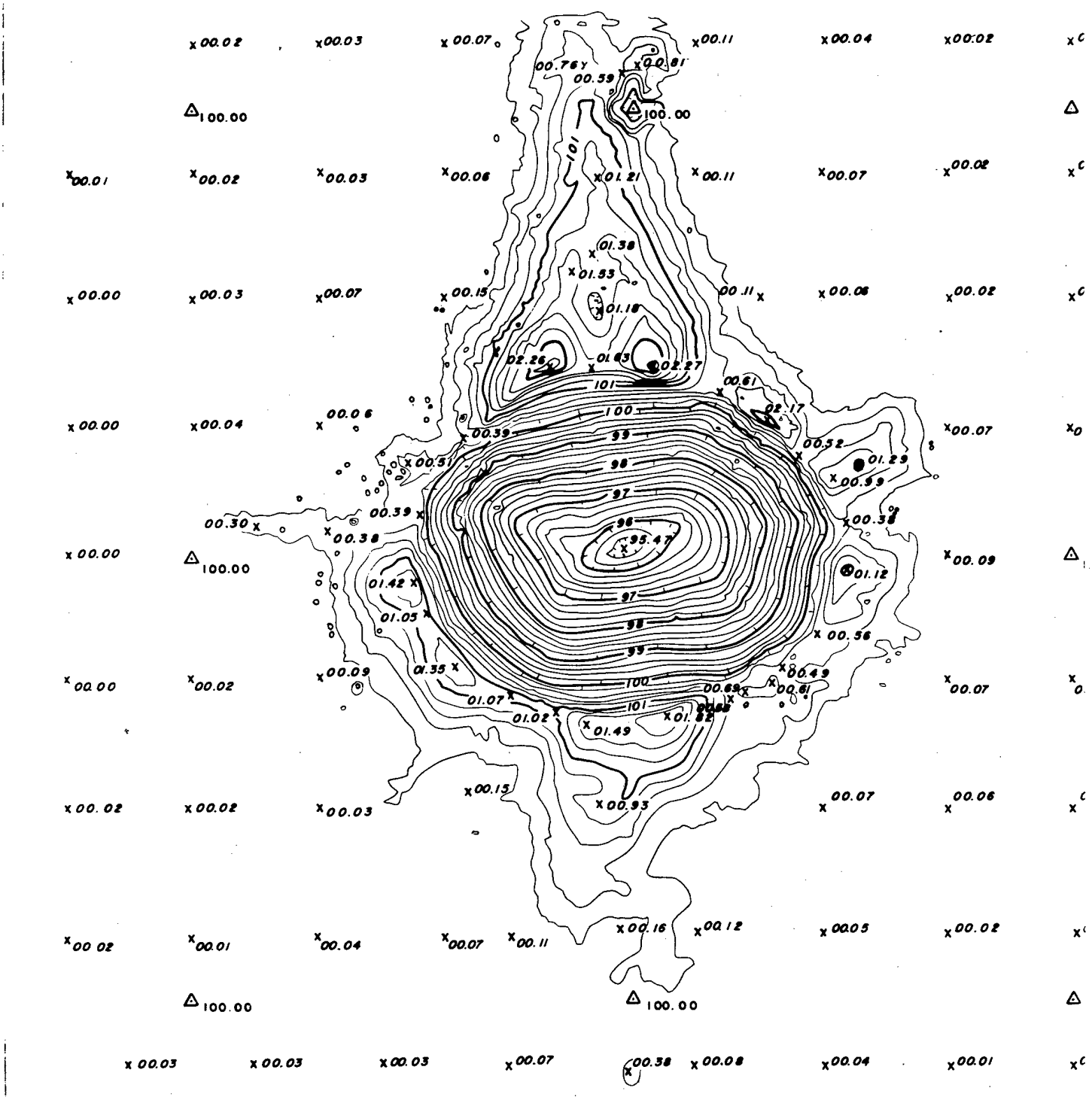
100.00
100.00
100.00
100.00
95.47
101
100
99
98
97
96

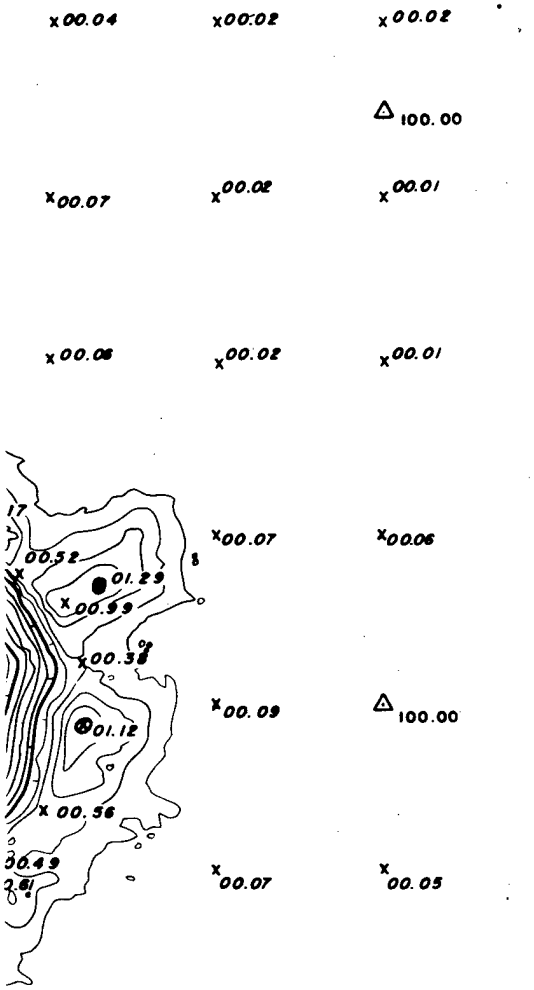

SCALE

0 8FT. 16 FT.

0.2 FOOT CONTOUR INTERVAL

DATE FLOWN 10 - 5 - 66

PROJECT PLOWSHARE TONOPAH 211-41
SHOT NO. 1

POST TEST TOPOGRAPHY

Compiled By

AMERICAN AERIAL SURVEYS, INC.

COVINA, CALIF.

SCALE

0 8FT. 16 FT.

0.2 FOOT CONTOUR INTERVAL

DATE FLOWN 10 - 5 - 66

PROJECT PLOWSHARE TONOPAH 211-41
SHOT NO. 1

POST TEST TOPOGRAPHY

Compiled By

AMERICAN AERIAL SURVEYS, INC.

COVINA, CALIF.

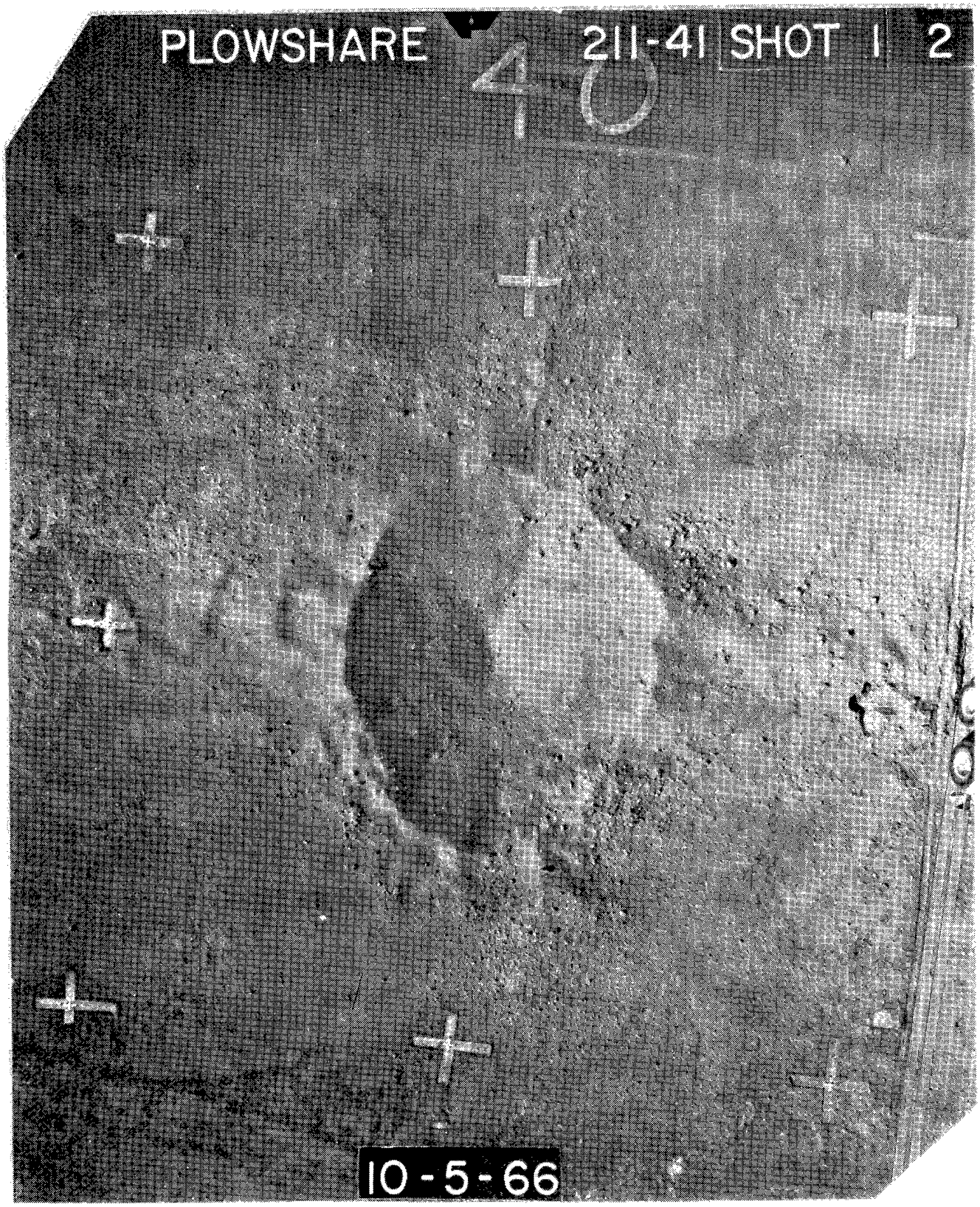
PLOWSHARE 211-41 SHOT 1 2
10-5-66


PLOWSHARE 211-44 2
11-22-66

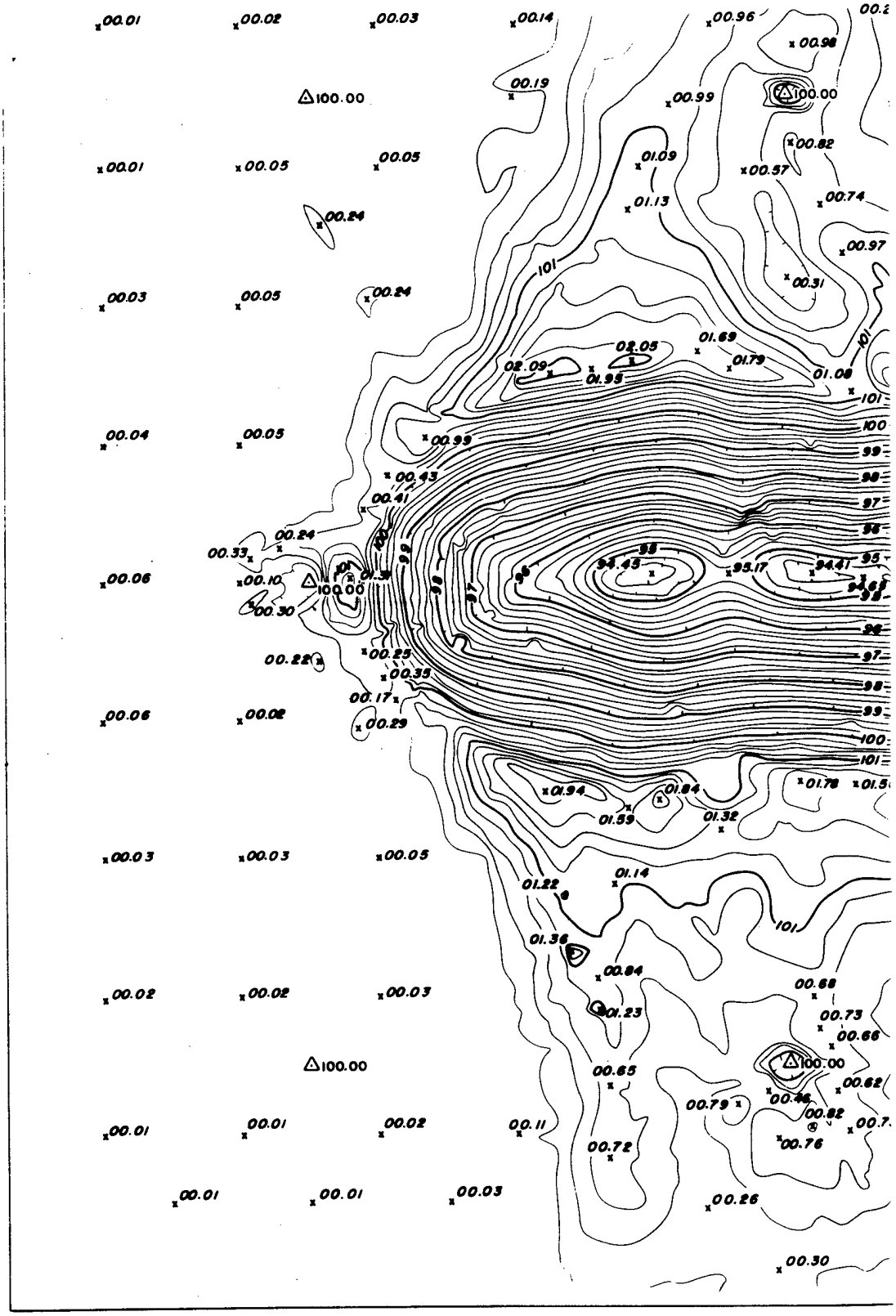
100.00
100.00
100.00
100.00
100.00
00.01
00.02
00.03
00.14
00.96
00.98
00.19
00.99
00.01
00.05
00.05
01.09
00.57
00.82
01.13
00.74
00.24
00.97
00.03
00.05
00.24
00.31
101
02.05
01.69
02.09
01.79
01.95
01.08
00.04
00.05
00.99
00.43
00.41
00.24
00.33
00.06
00.10
00.30
01.39
94.43
95.17
94.41
00.22
00.25
00.35
00.17
00.29
00.06
00.02
01.94
01.84
01.78
01.59
01.32
00.03
00.03
00.05
01.14
01.22
01.36
00.84
00.68
00.73
00.66
01.23
00.65
00.62
00.46
00.79
00.82
00.76
00.02
00.02
00.03
00.01
00.01
00.02
00.11
00.72
00.01
00.01
00.03
00.26
00.30

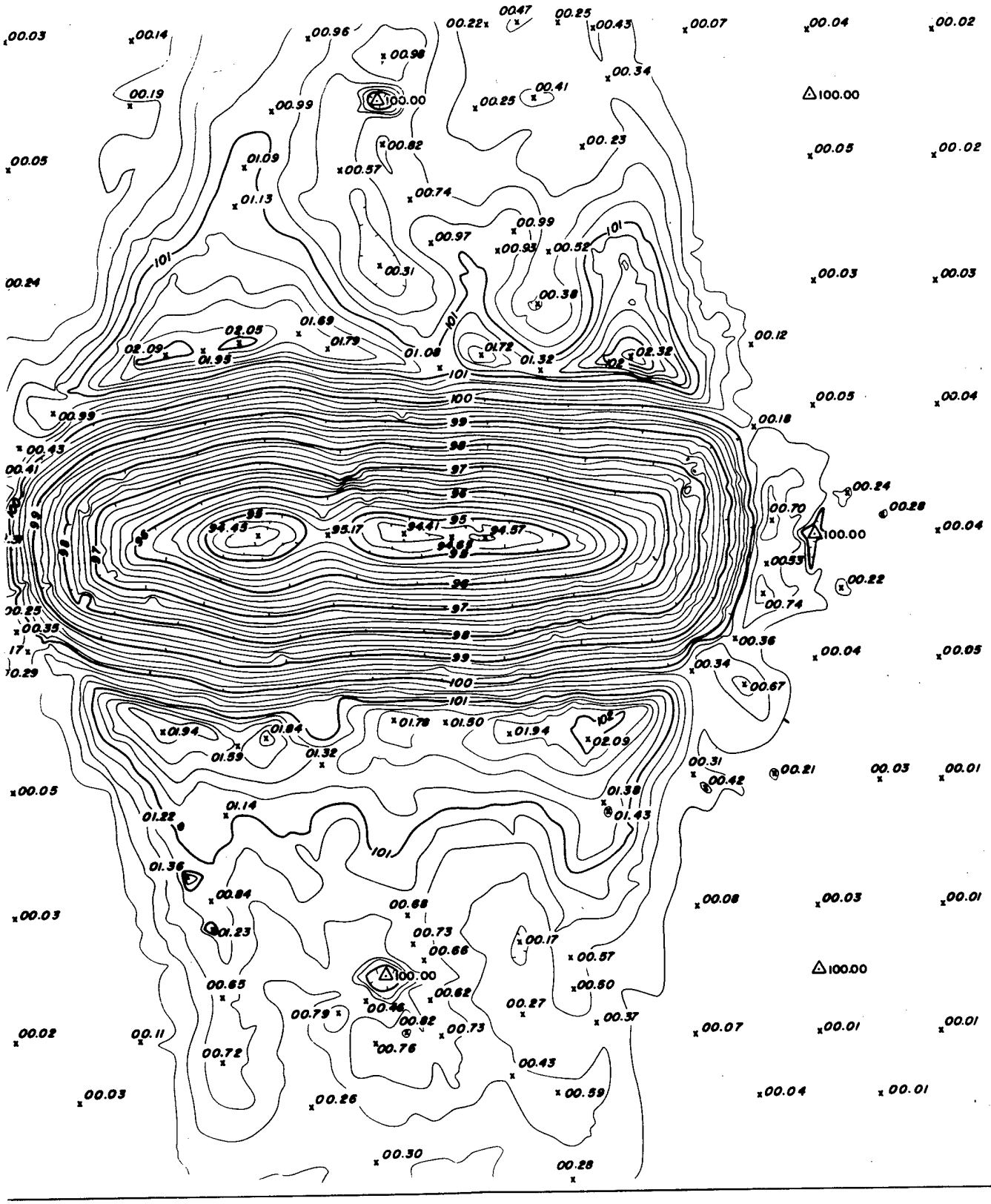
100.00
101
100
99
98
97
96
95
94.43
95.17
94.41
94.57
94.68
PROJECT

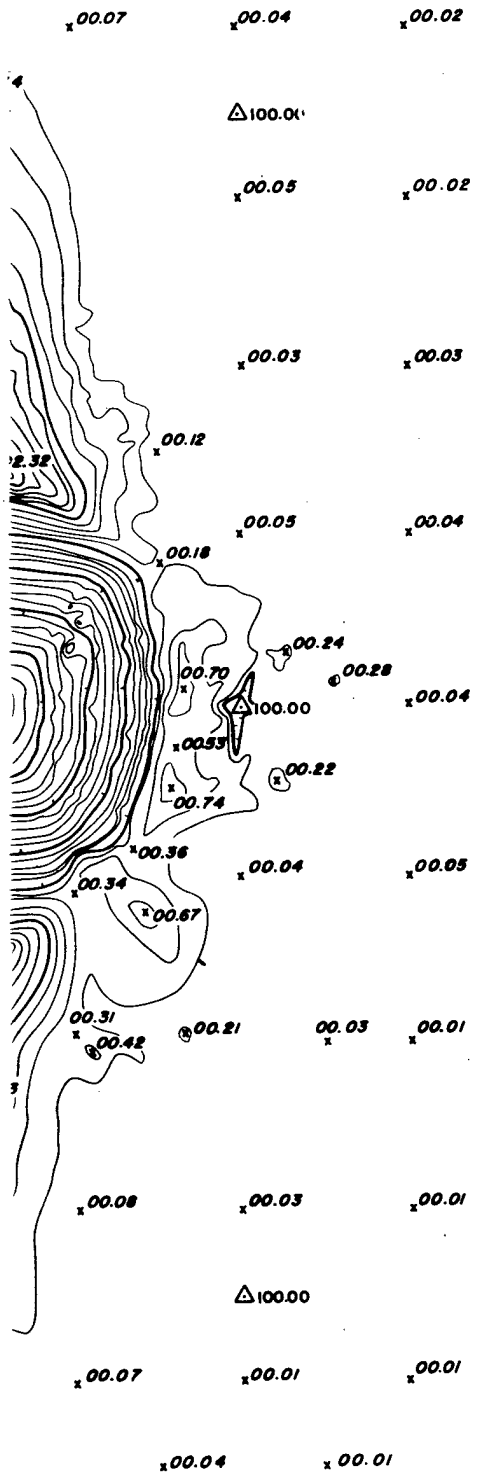

SCALE

0 8 16 FT.

0.2 FOOT CONTOUR INTERVAL

DATE FLOWN – –

PROJECT PLOWSHARE TONOPAH 211-44

POST TEST TOPOGRAPHY

Compiled By

AMERICAN AERIAL SURVEYS, INC.

COVINA, CALIF.

(3)

①

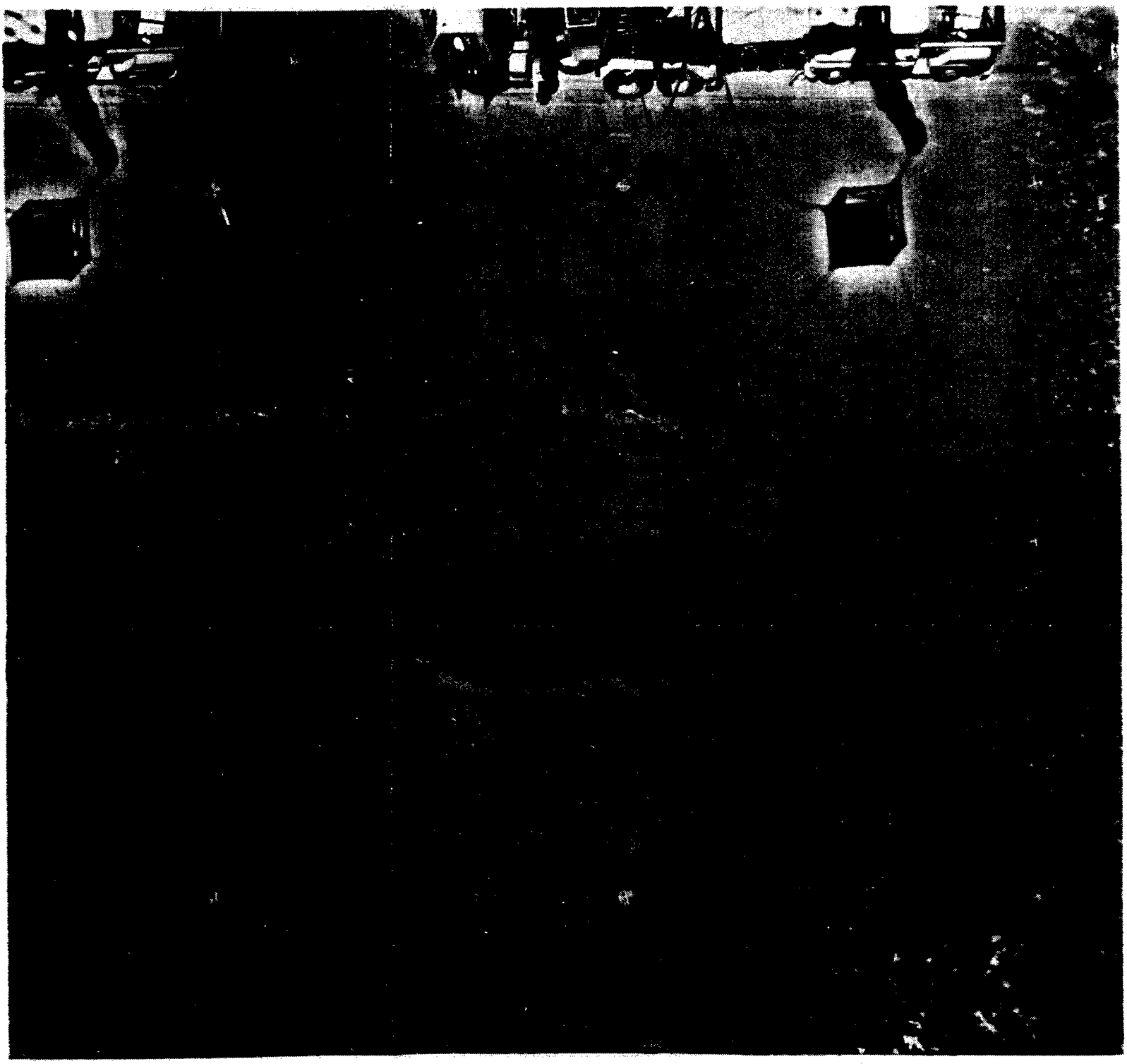

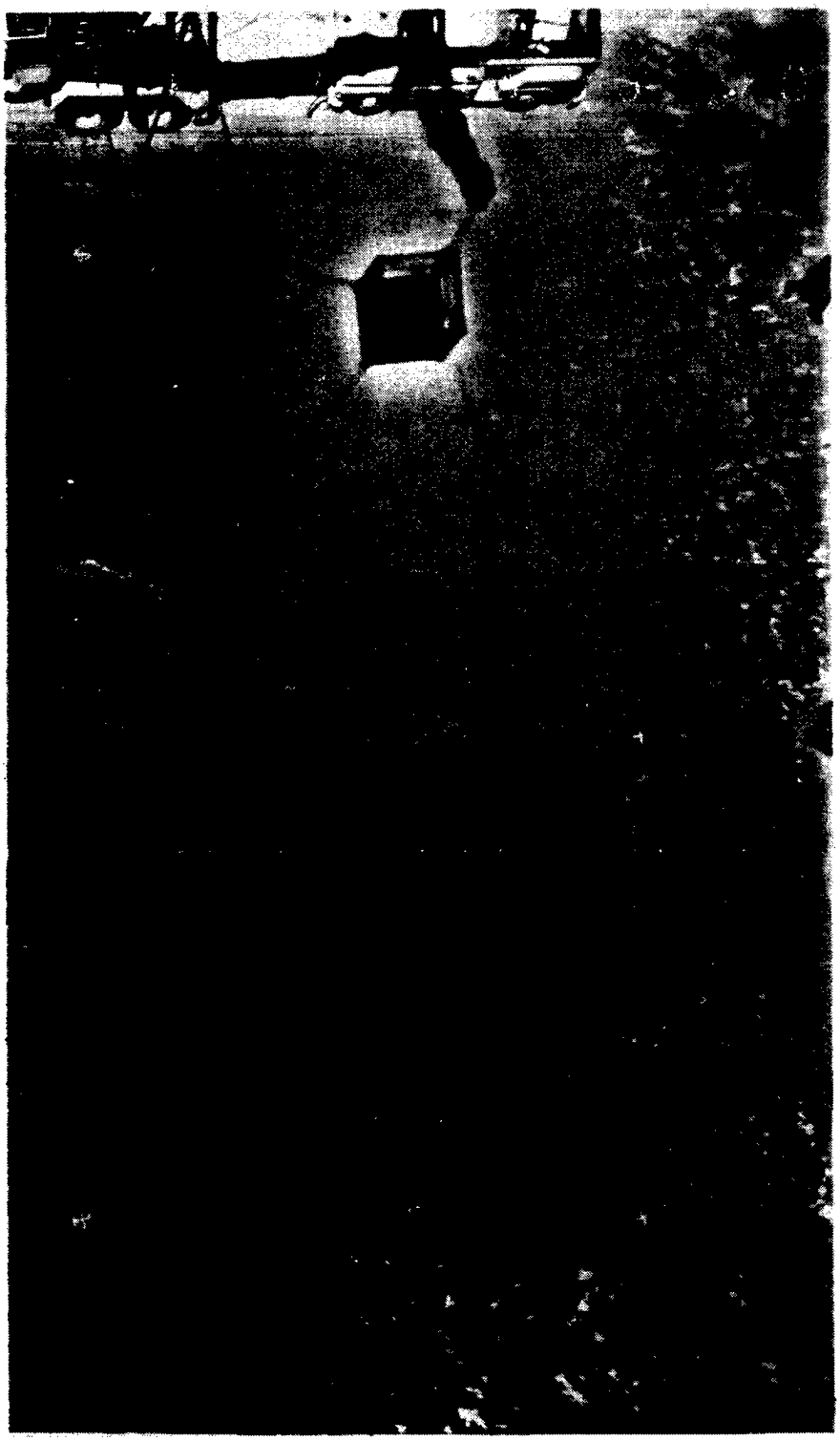

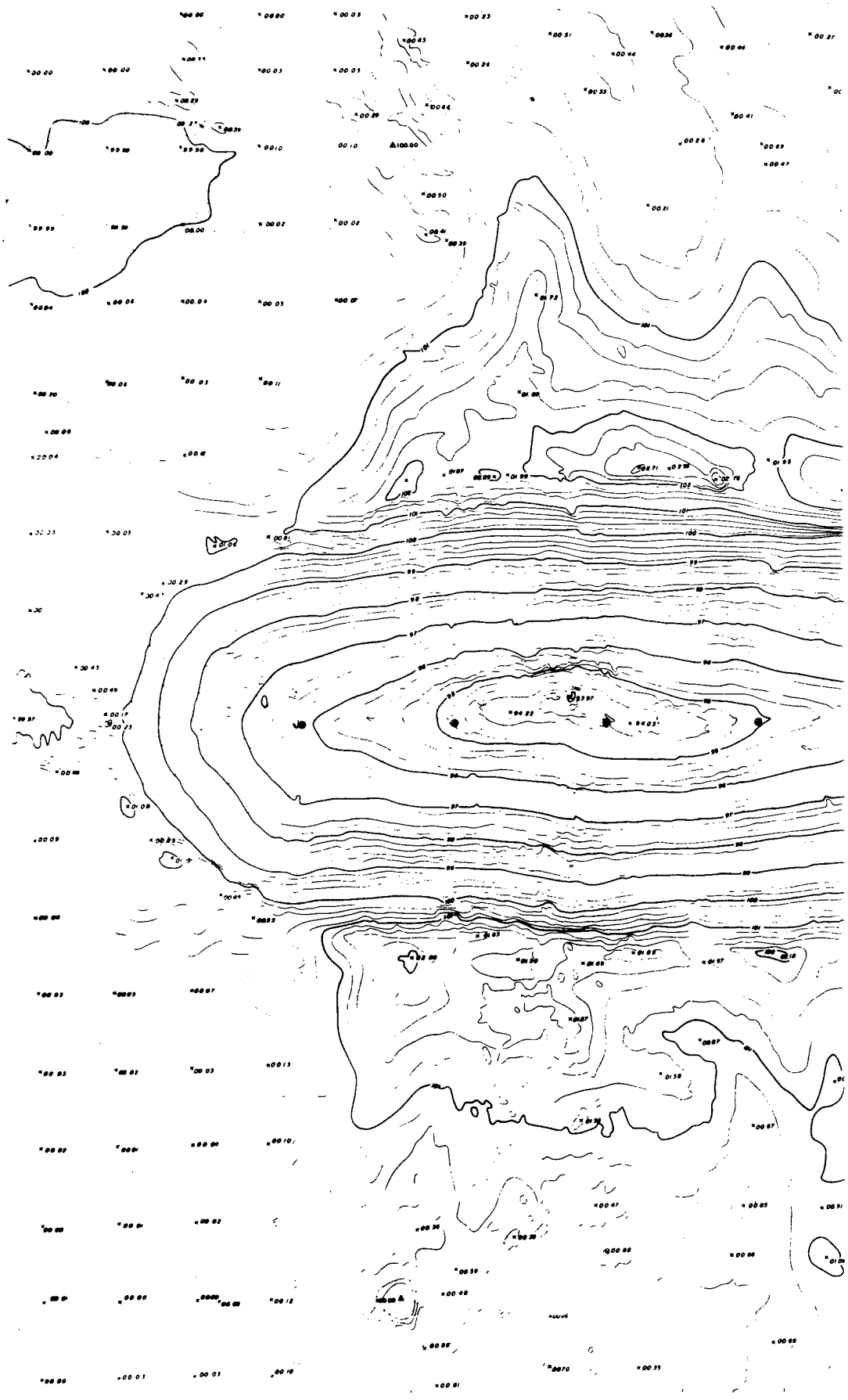

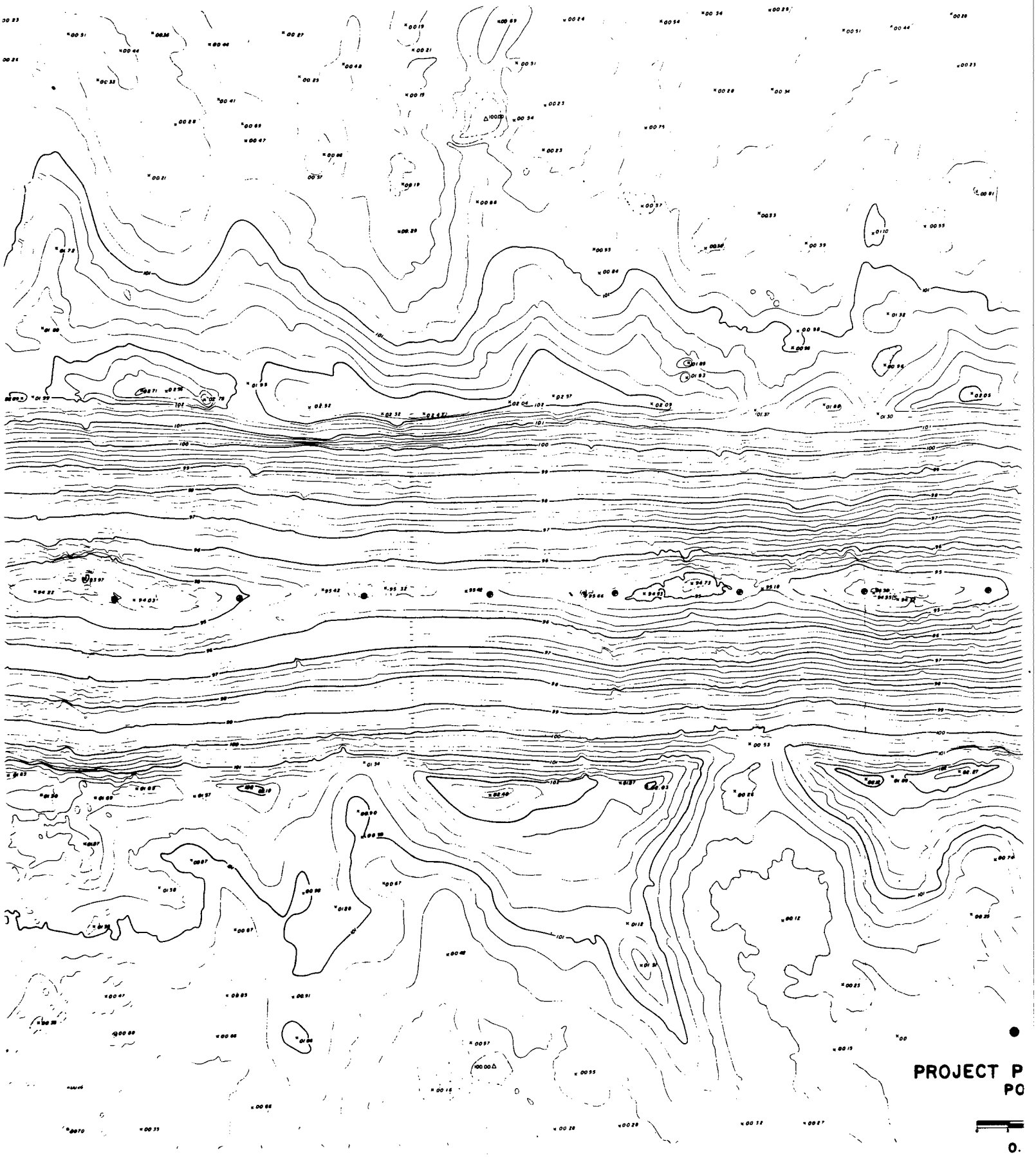
PROJECT P
PO
0.

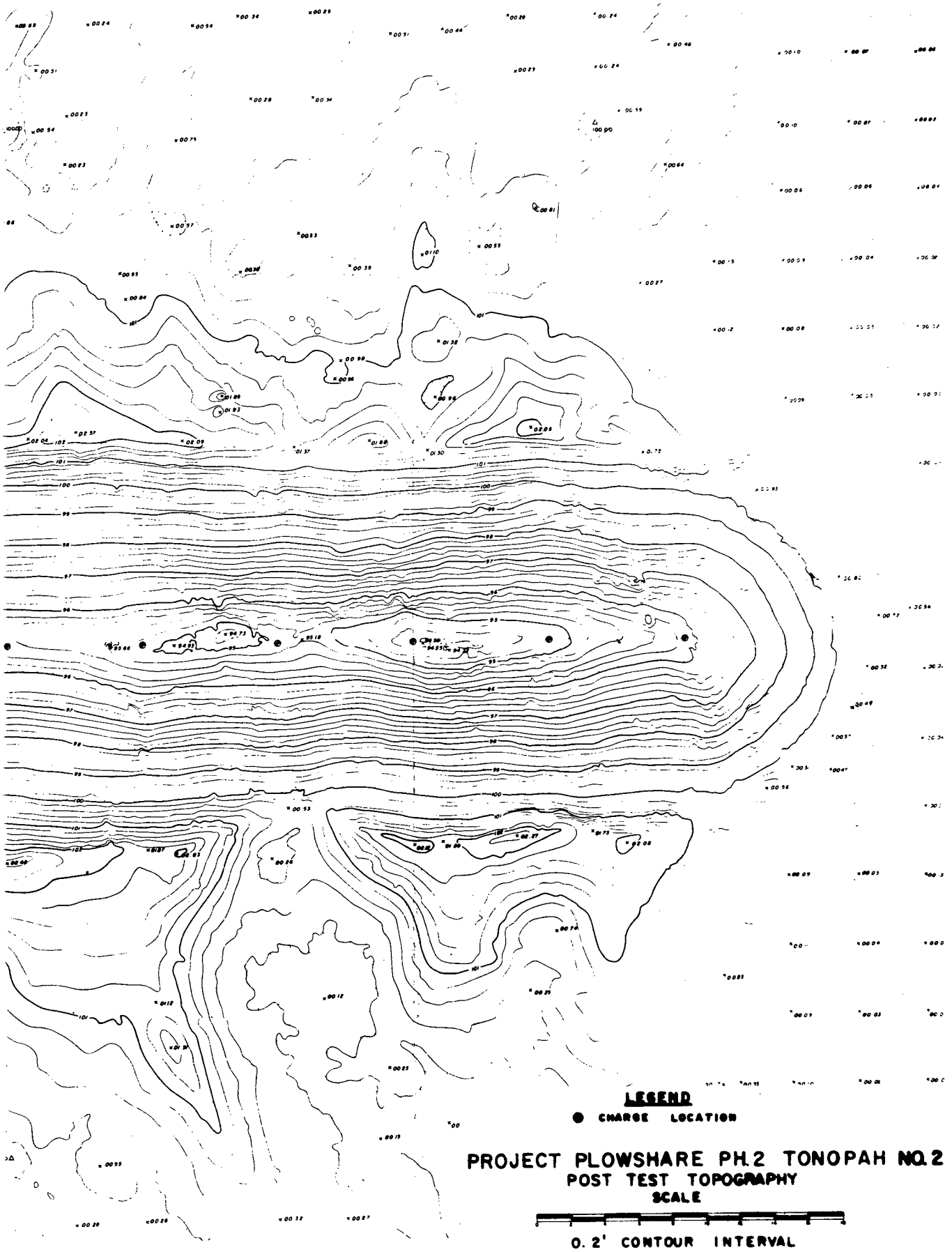

LEGEND

● CHARGE LOCATION

PROJECT PLOWSHARE PH.2 TONOPAH NO.2

POST TEST TOPOGRAPHY

SCALE

0.2' CONTOUR INTERVAL

(3)

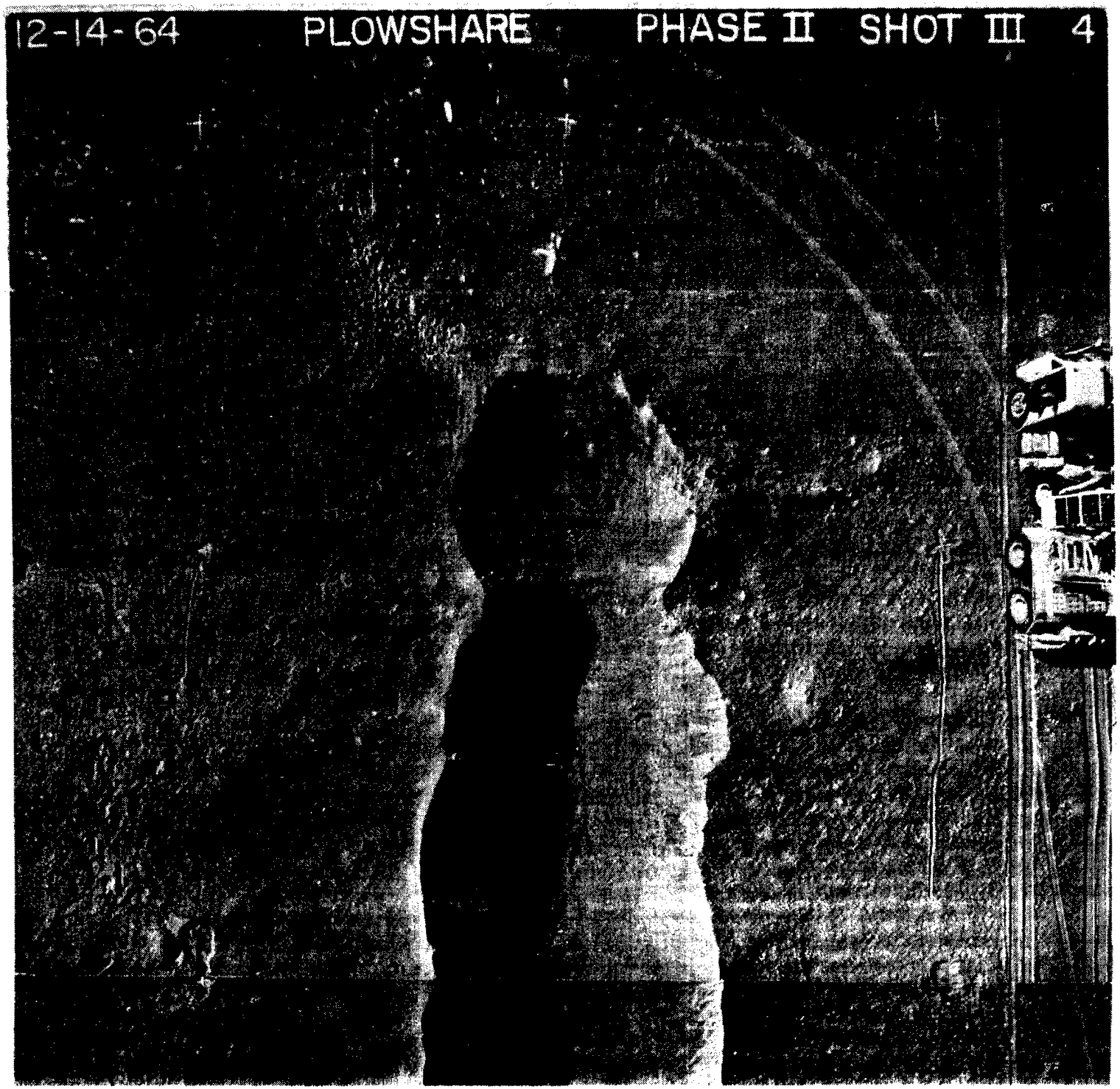
12-14-64 PLOWSHARE PHASE II SHOT III 4

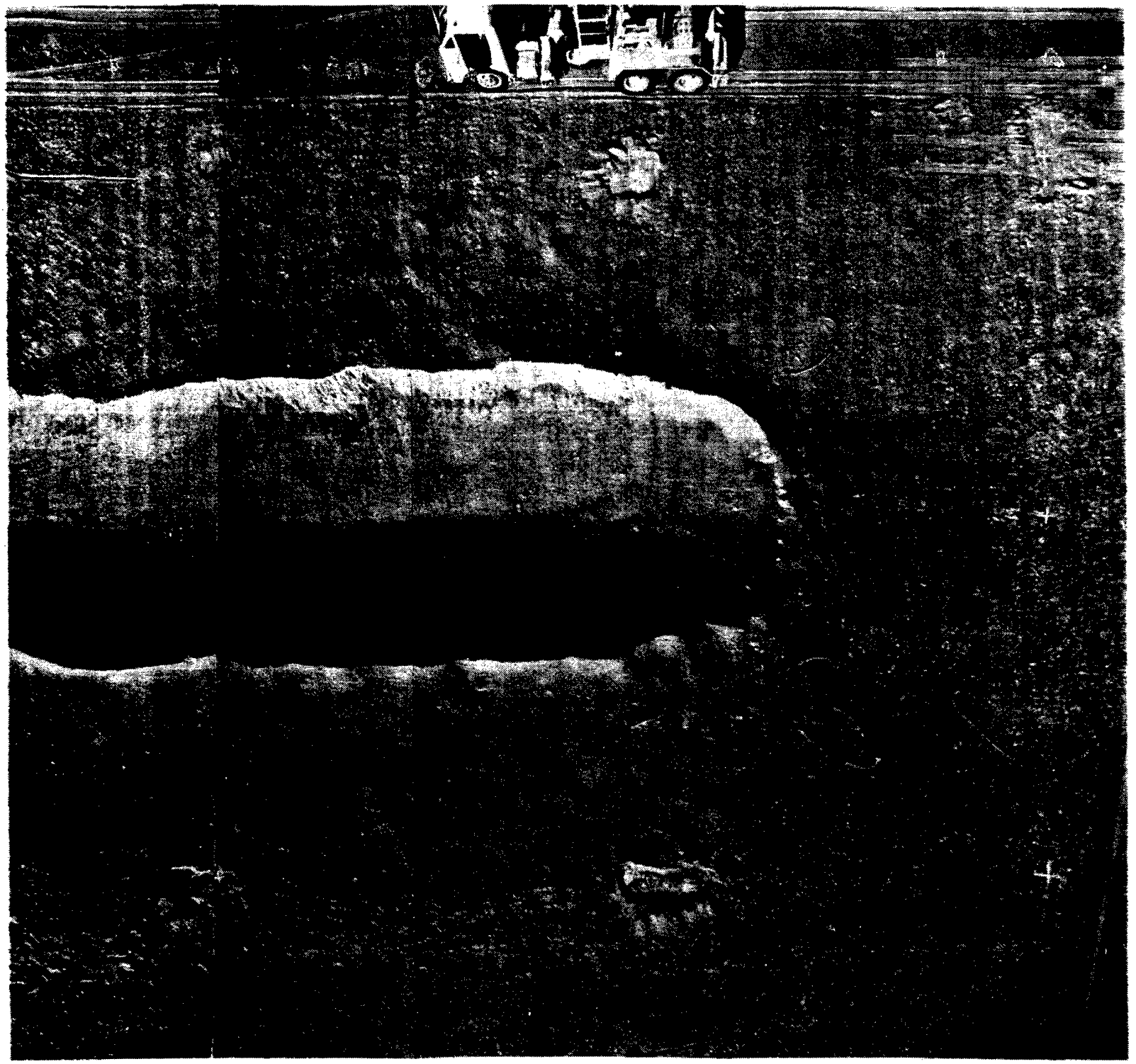

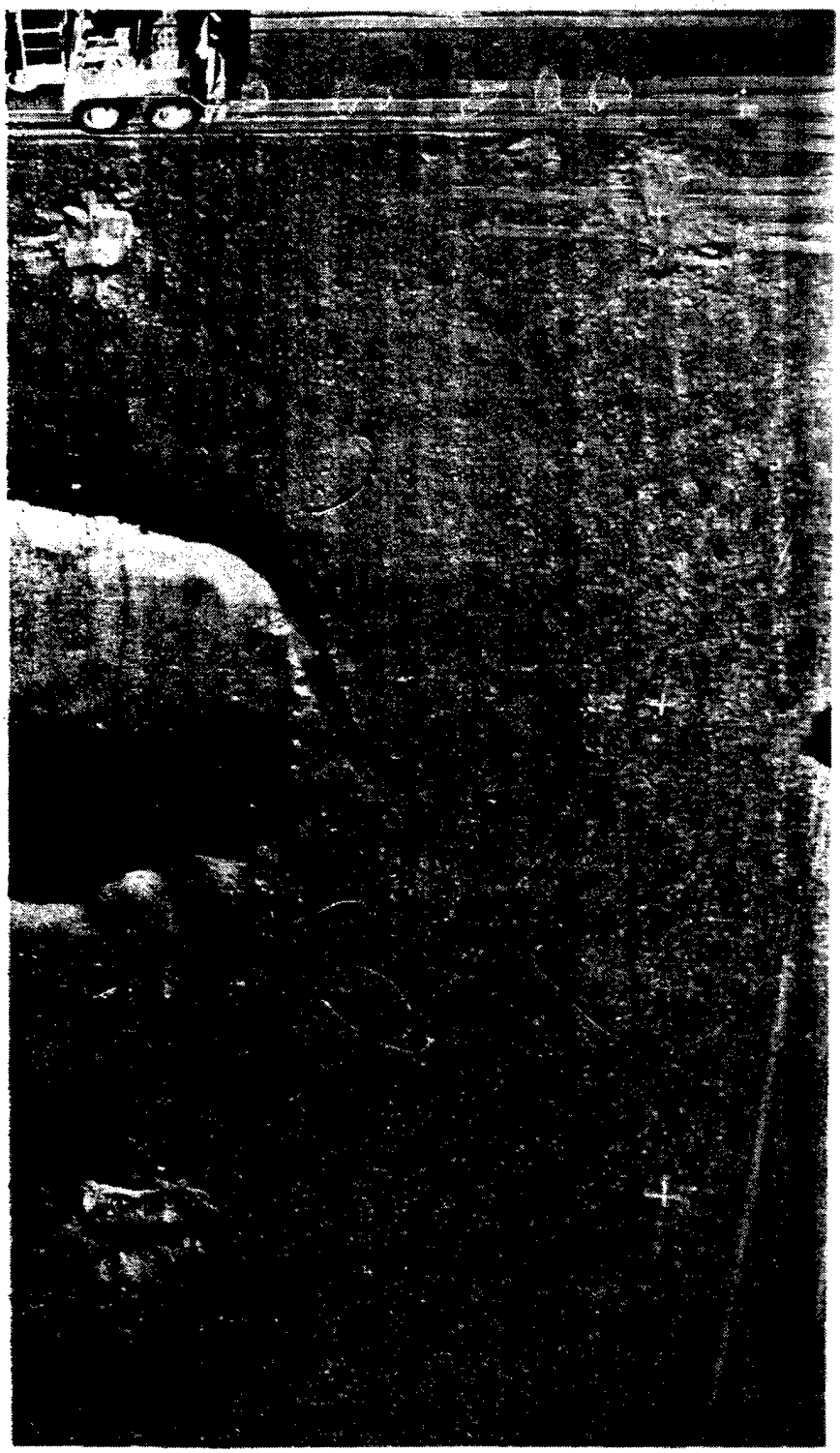

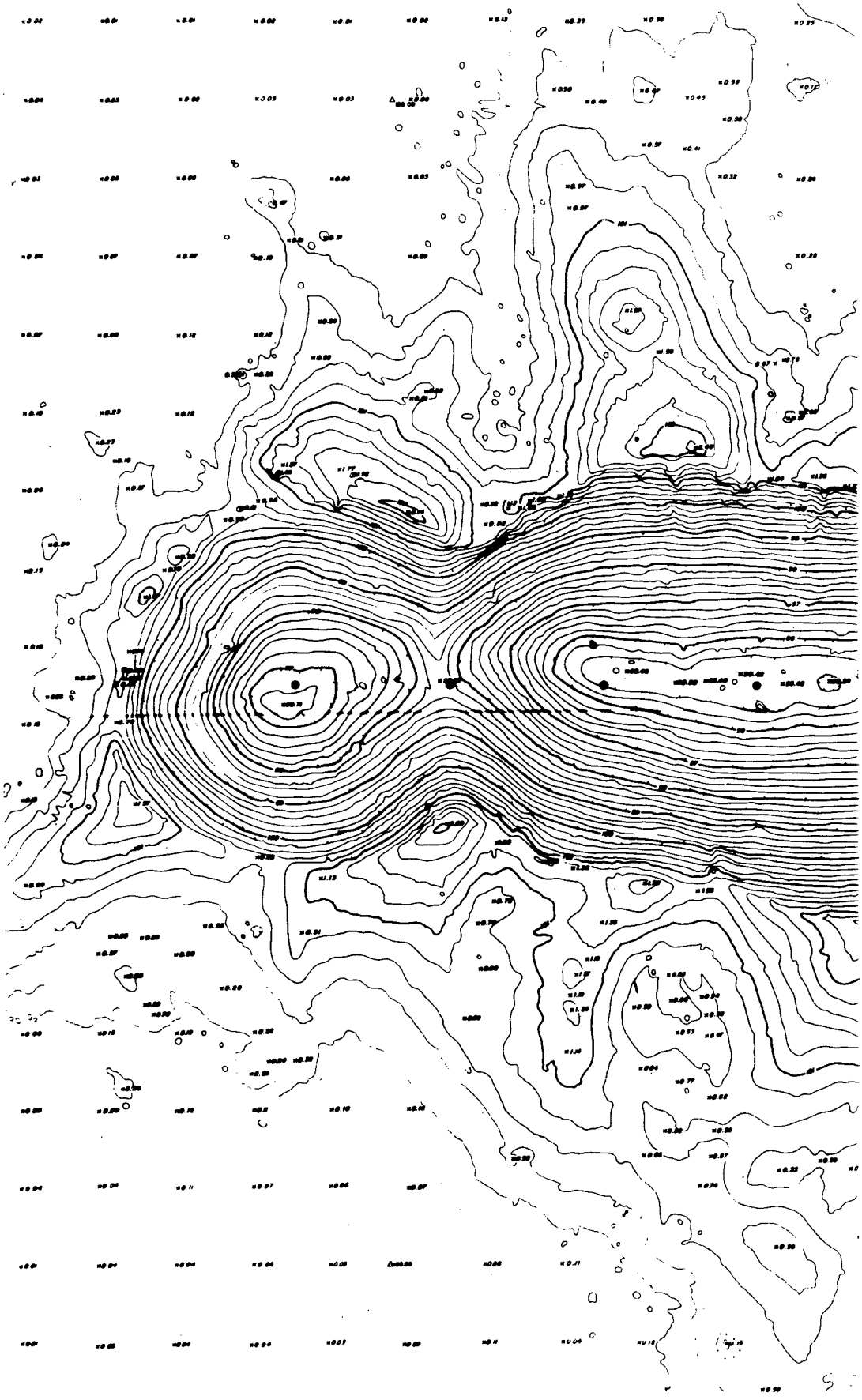

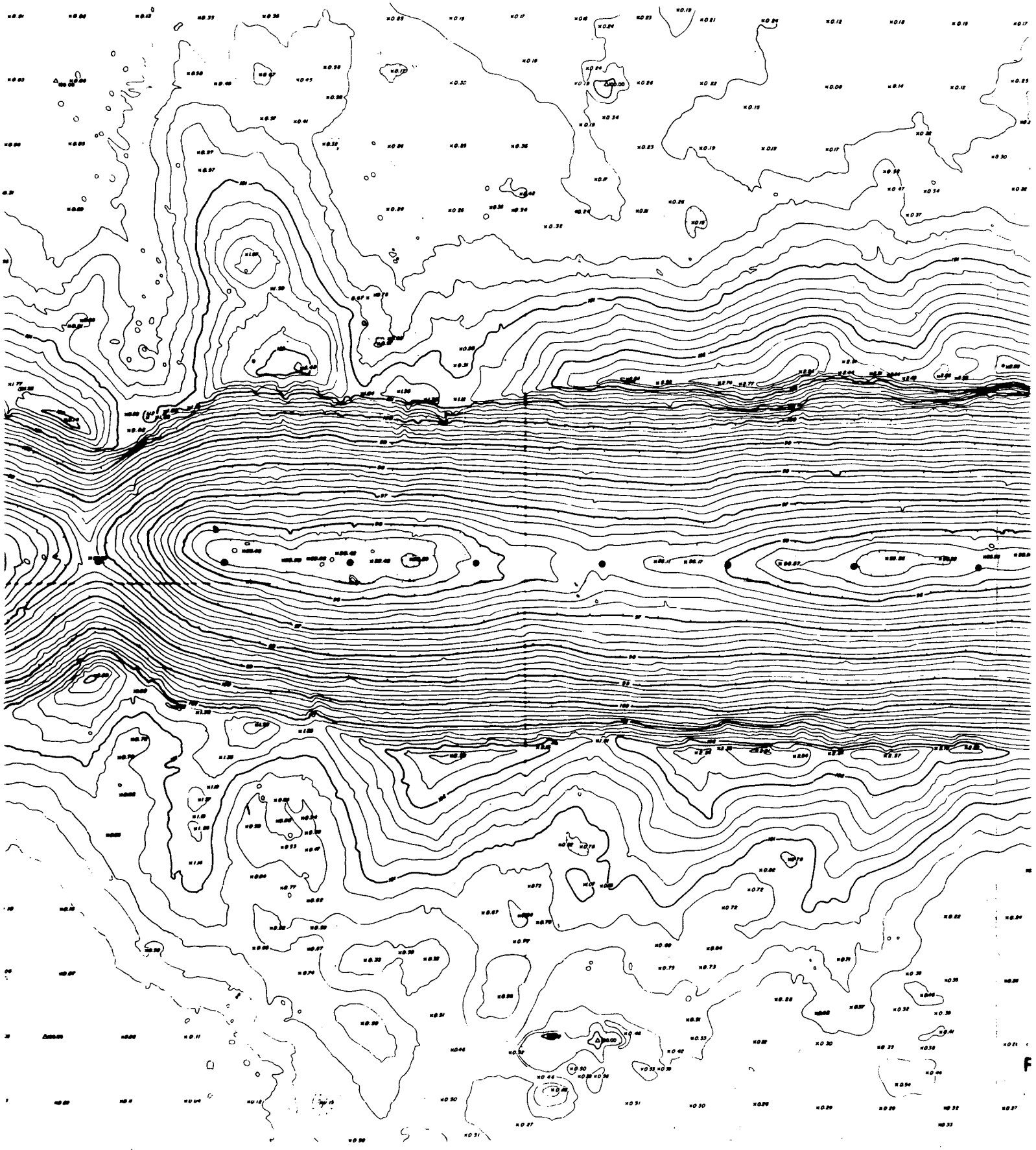

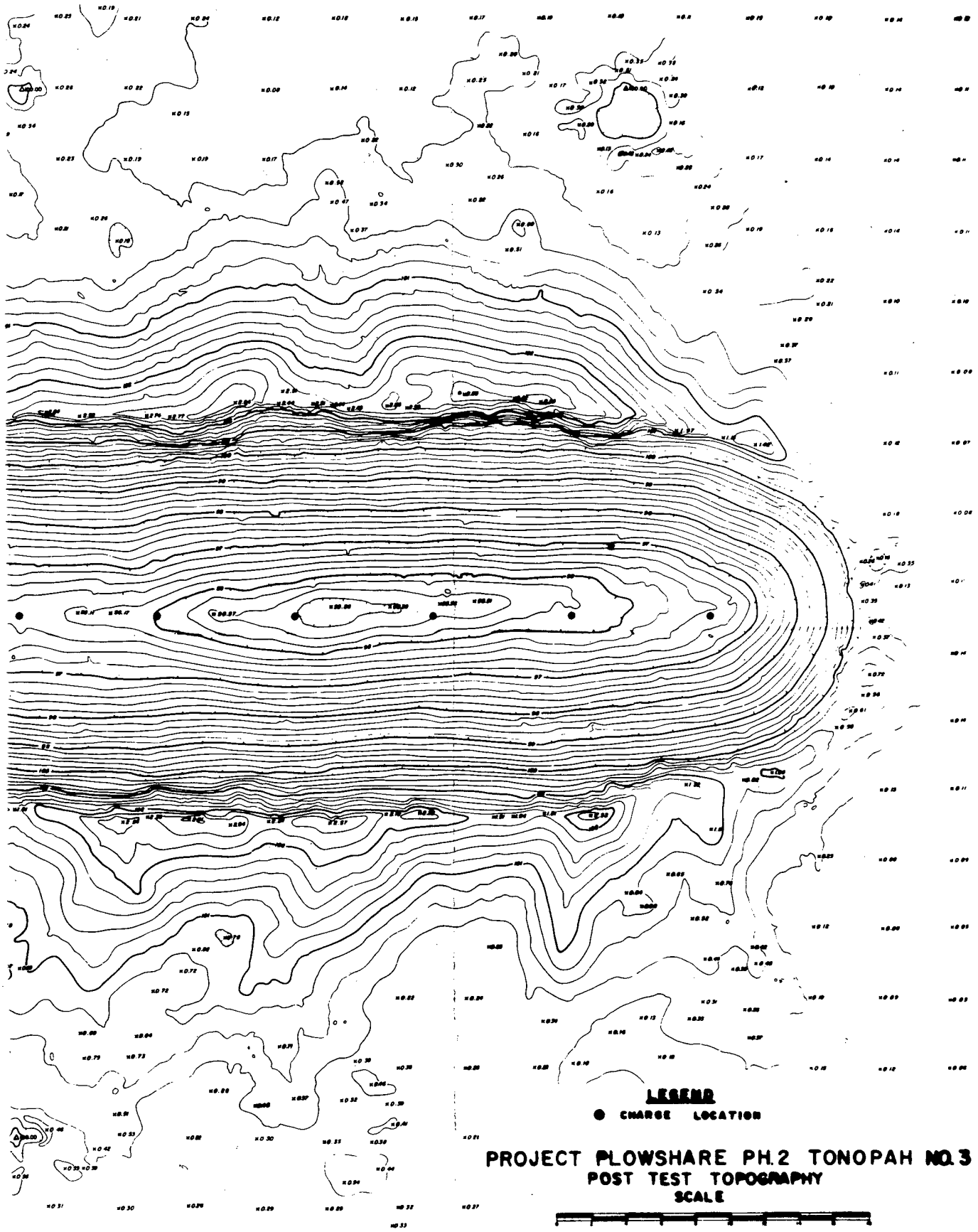

LEGEND

● CHARGE LOCATION

PROJECT PLOWSHARE PH.2 TONOPAH NO.3

POST TEST TOPOGRAPHY

SCALE

0.2' CONTOUR INTERVAL

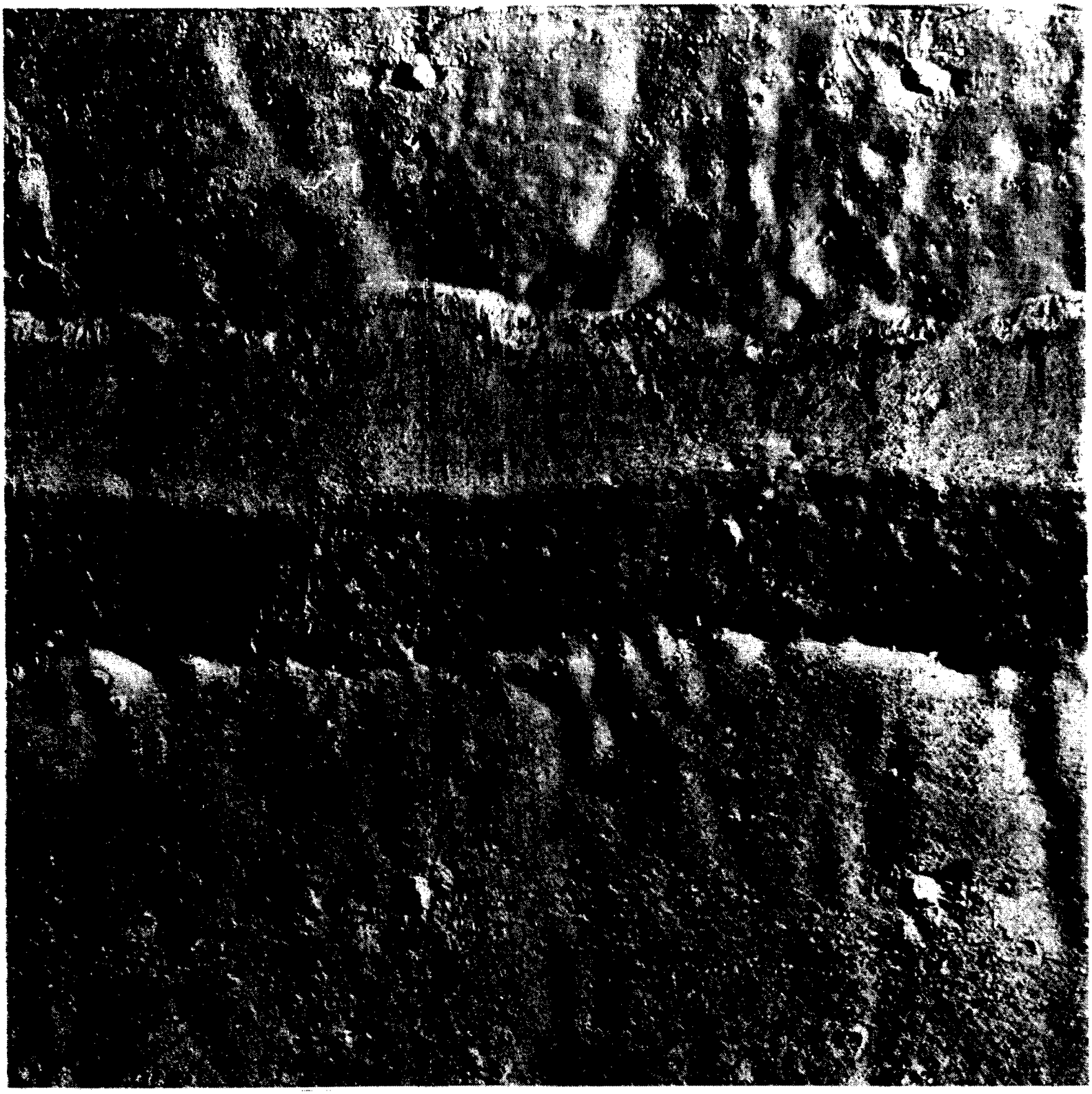

PROJECT PLOWSHARE TONOPAH 21

POST TEST TOPOGRAPHY

Compiled By

AMERICAN AERIAL SURVEYS, INC.

COVINA, CALIF.

(2)

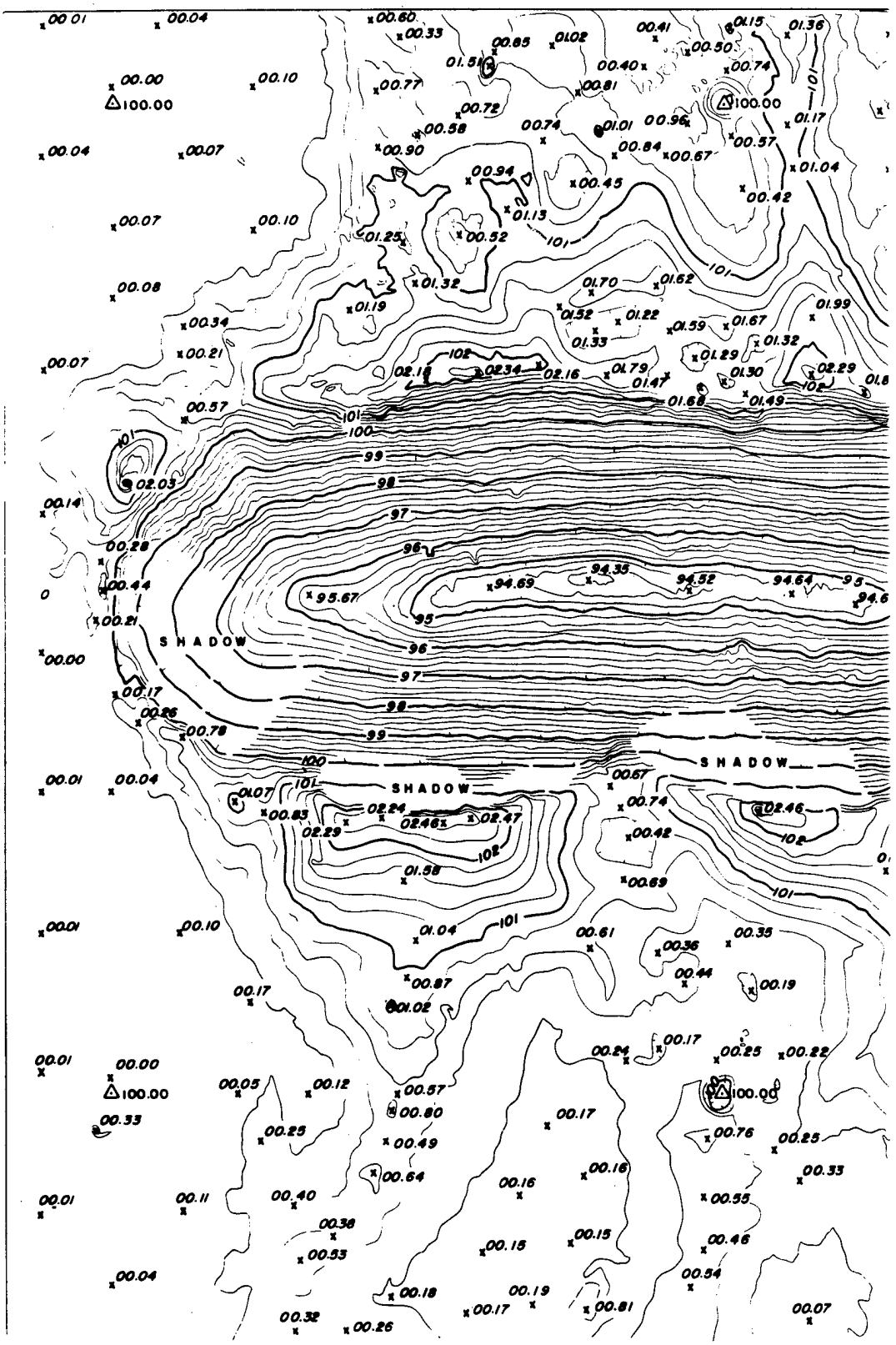
SHADOW
SHADOW
SHADOW
100.00
100.00
100.00
SCALE
0
8
16 FT.
0.2 FOOT CONTOUR INTERVAL
DATE FLOWN - -

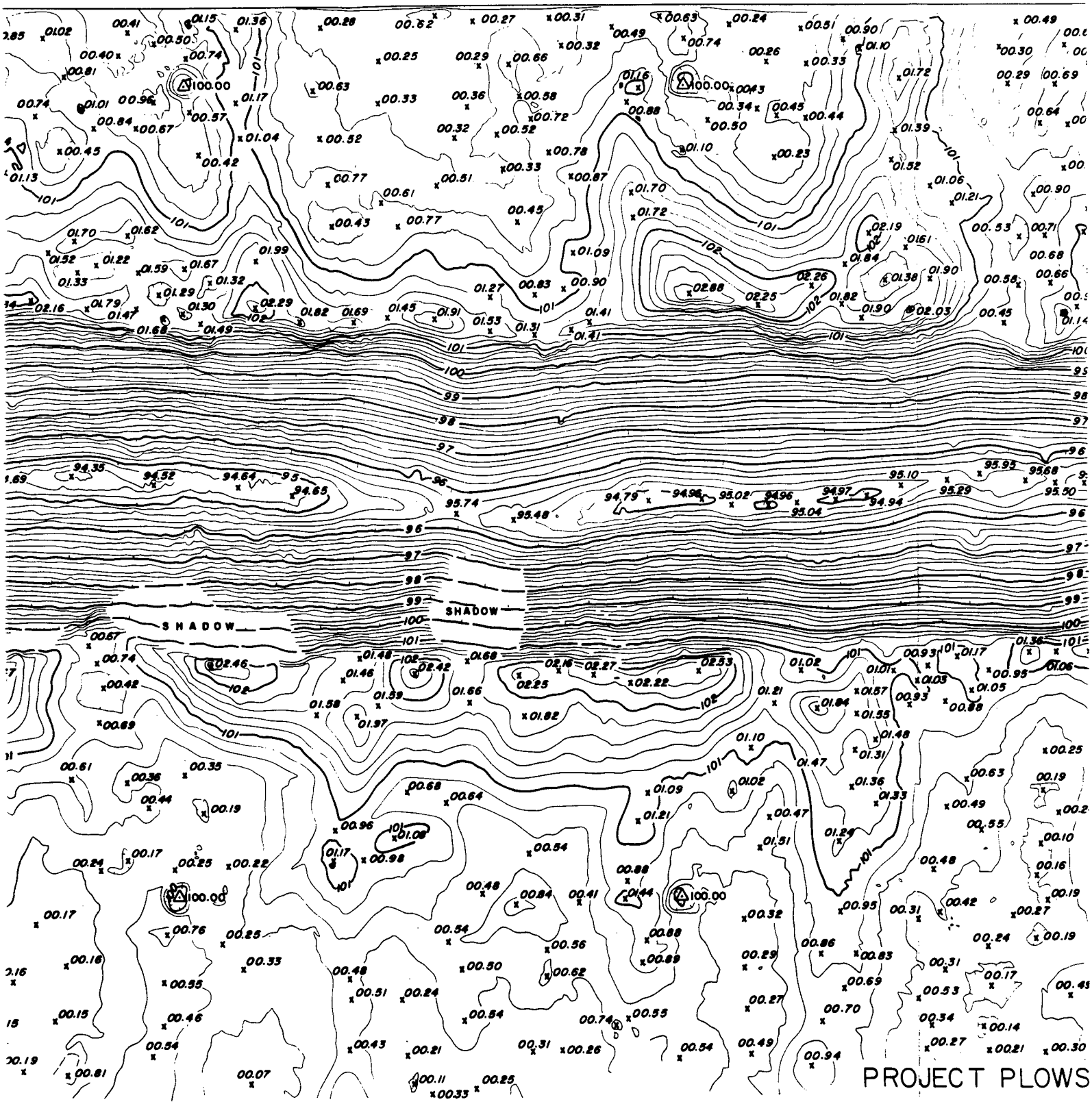
SHADOW
SHADOW
PROJECT PLOWS
POST TE
C
AMERICAN
COV

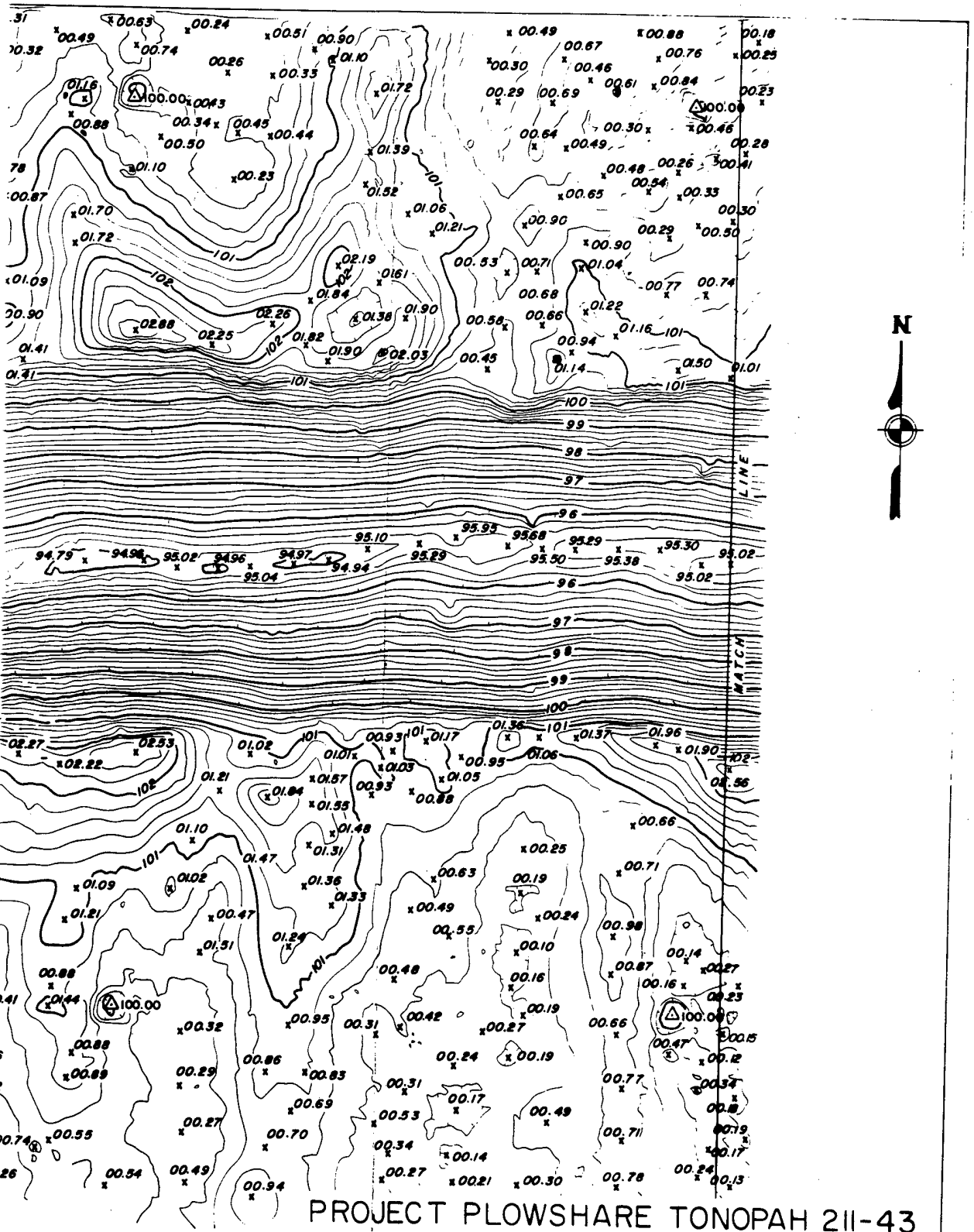

PROJECT PLOWSHARE TONOPAH 211-43

POST TEST TOPOGRAPHY
Compiled By
AMERICAN AERIAL SURVEYS, INC.
COVINA, CALIF.

(3)

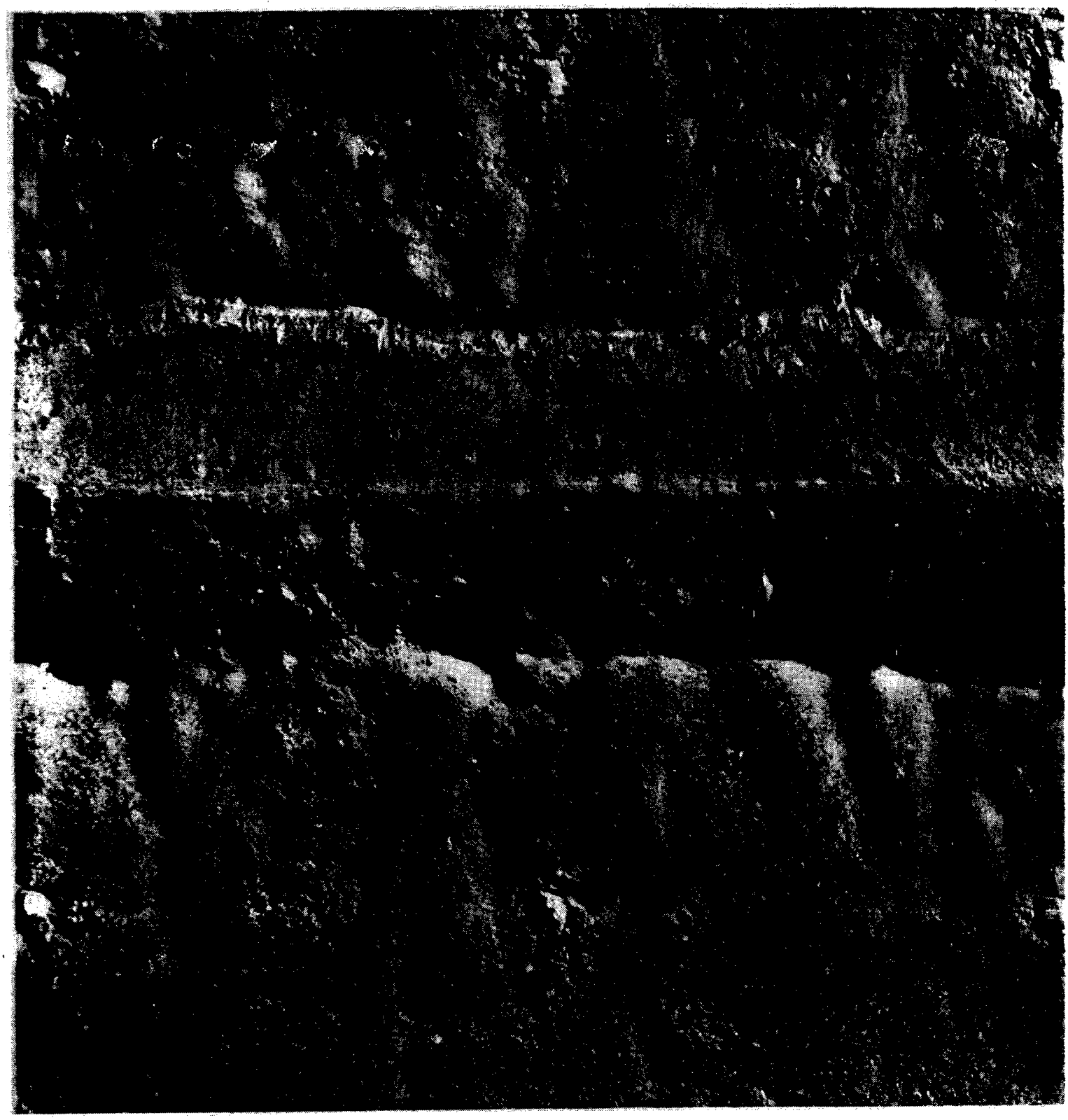

SCALE ±

0 8 16 FT.

0.2 FOOT CONTOUR INTERVAL

(1)

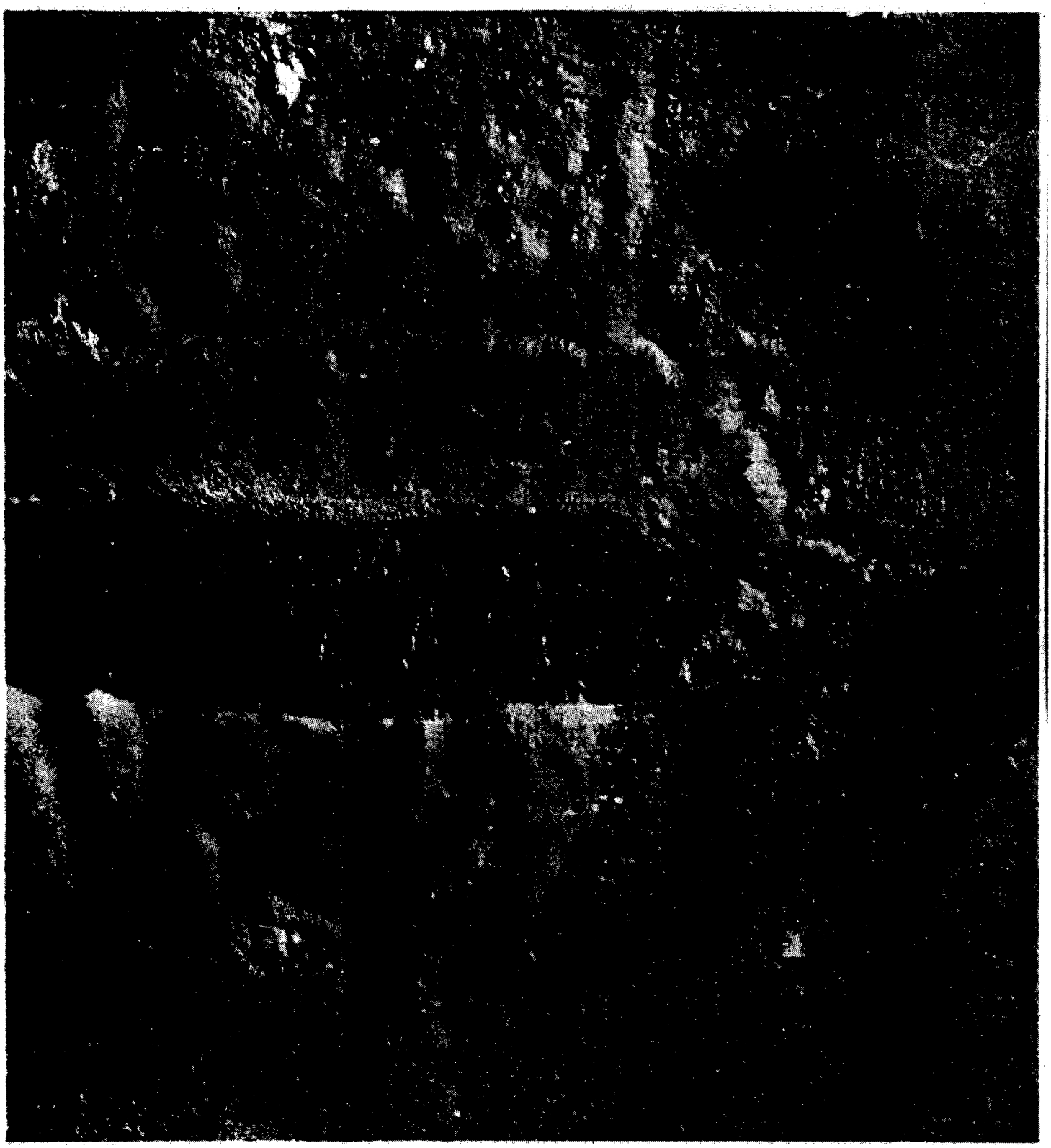

PROJECT PLOWSHARE TONOPAH 211-43

POST TEST TOPOGRAPHY

Compiled By

AMERICAN AERIAL SURVEYS, INC.

COVINA, CALIF.

(2)

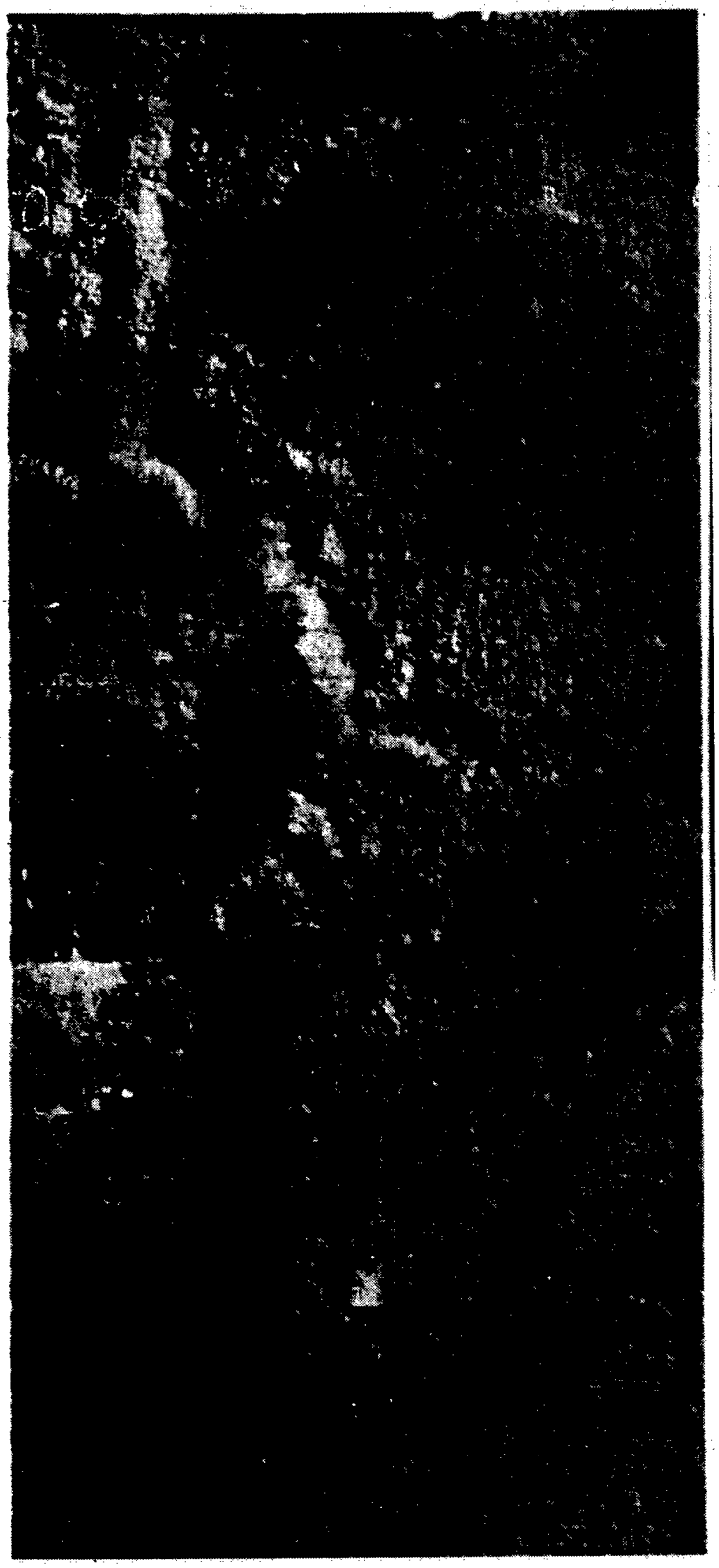

N

PROJECT PLOWSHARE TONOPAH 211-43

POST TEST TOPOGRAPHY

Compiled By

AMERICAN AERIAL SURVEYS, INC.

COVINA, CALIF.

(3)

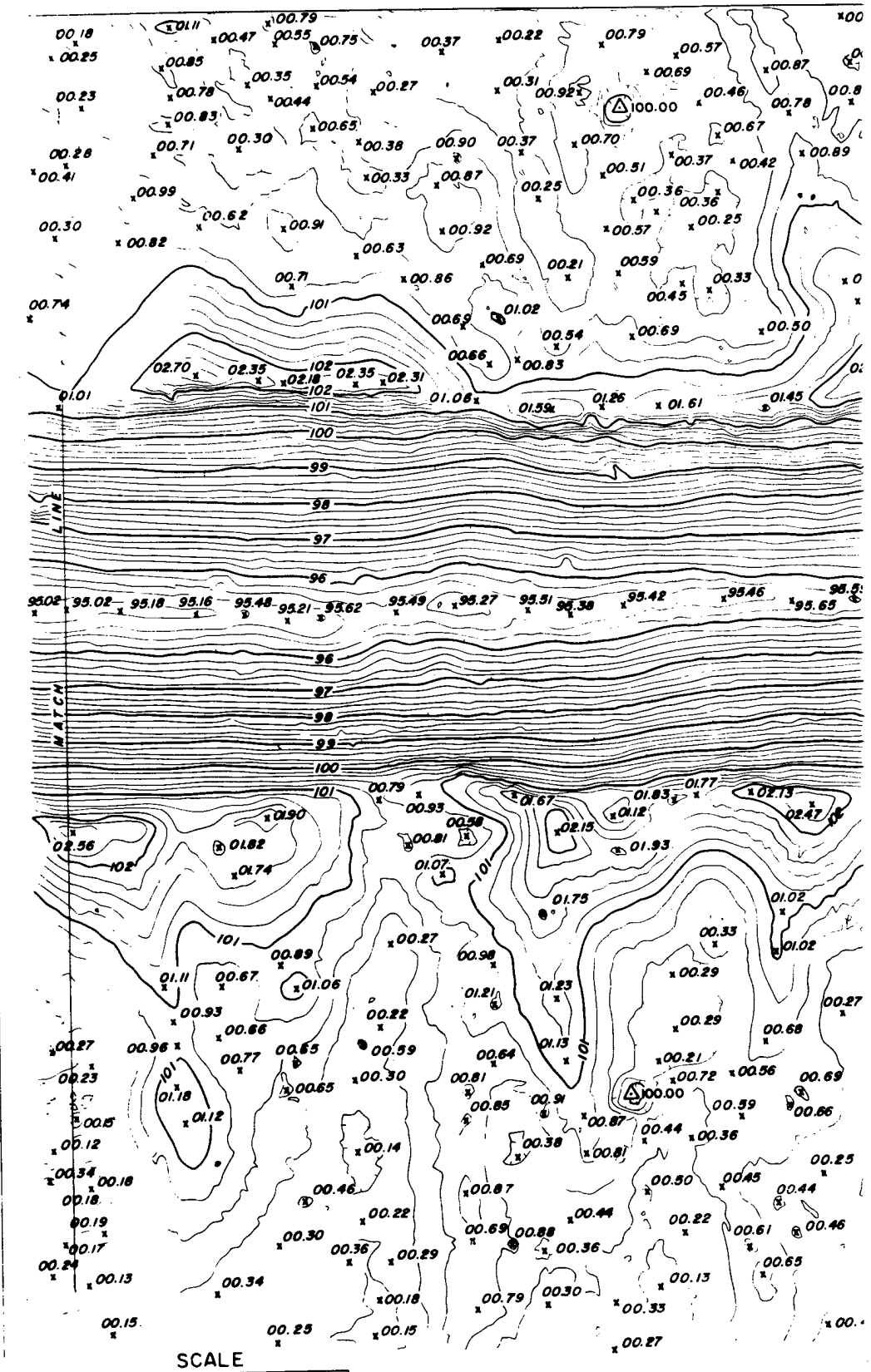
MATCH LINE
MATCH LINE
100.00
100.00
SCALE
0
8
16 FT.
0.2 FOOT CONTOUR INTERVAL
DATE FLOWN - -

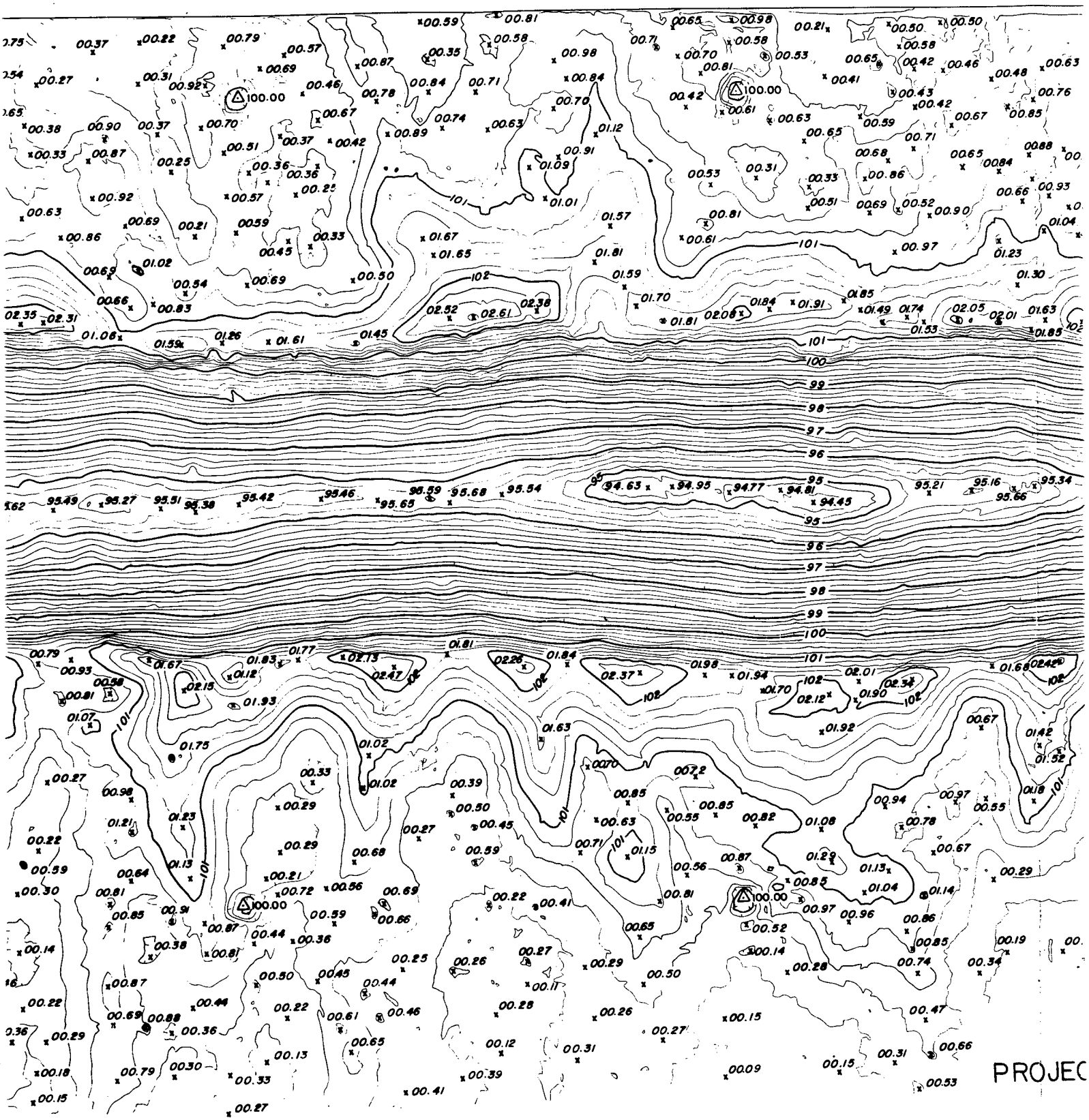

16 FT.

VAL

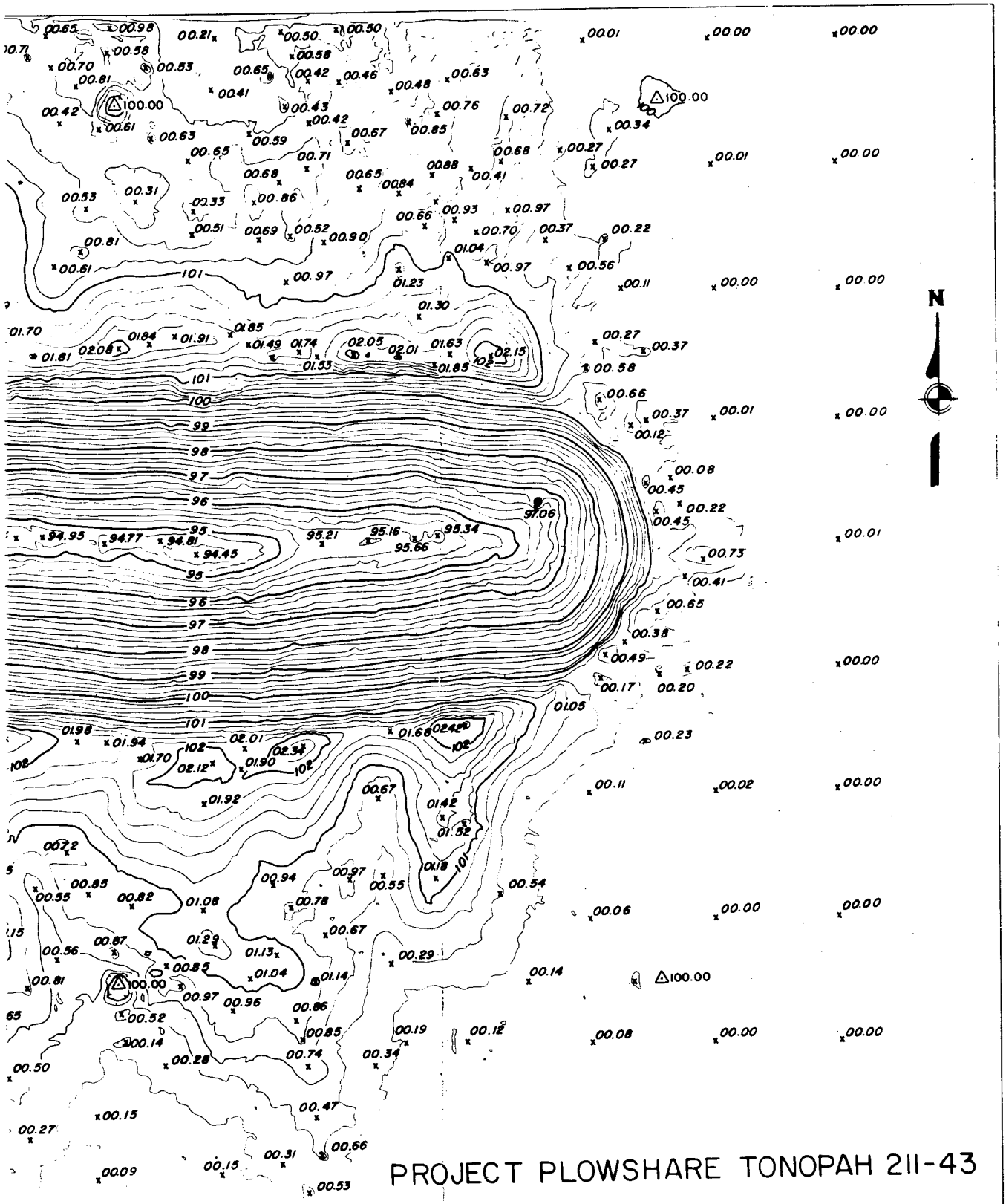
N
PROJECT PLOWSHARE TONOPAH 211-43
POST TEST TOPOGRAPHY
Compiled By
AMERICAN AERIAL SURVEYS, INC.
COVINA, CALIF.

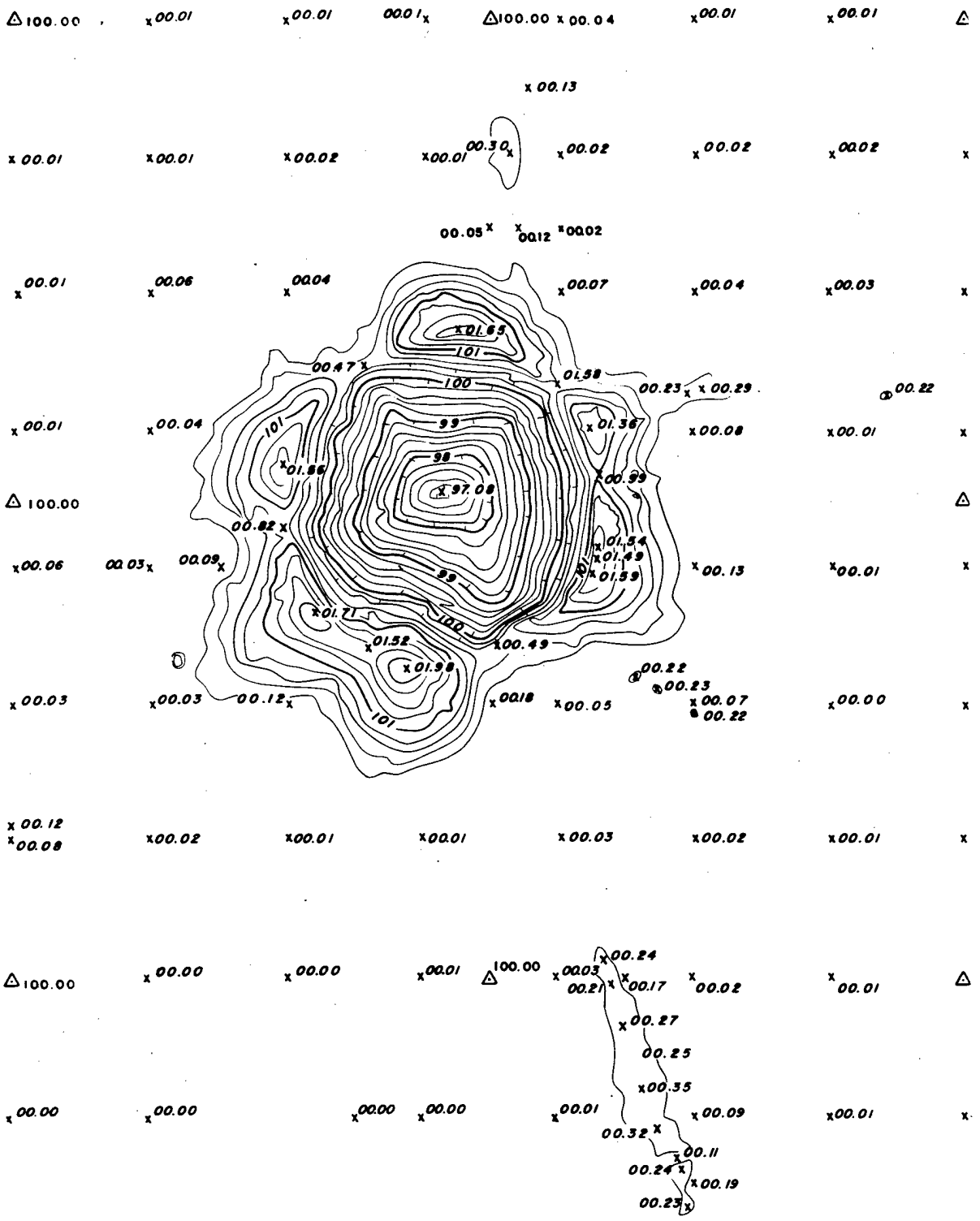
100.00
00.01
00.01
00.01
100.00
00.04
00.01
00.01
00.13
00.01
00.01
00.02
00.01
00.30
00.02
00.02
00.02
00.05
00.12
00.02
00.01
00.06
00.04
00.07
00.04
00.03
01.65
101
00.47
100
01.58
00.23
00.29
00.22
00.01
00.04
101
99
01.36
00.08
00.01
01.86
98
97.08
00.99
100.00
00.82
01.54
01.49
00.06
00.03
00.09
99
01.59
00.13
00.01
01.71
100
01.52
00.49
00.22
00.23
00.03
00.03
00.12
101
00.18
00.05
00.07
00.22
00.00
00.12
00.08
00.02
00.01
00.01
00.03
00.02
00.01
100.00
00.00
00.00
00.01
100.00
00.03
00.24
00.21
00.17
00.02
00.01
00.27
00.25
00.35
00.00
00.00
00.00
00.00
00.01
00.09
00.01
00.32
00.11
00.24
00.19
00.23

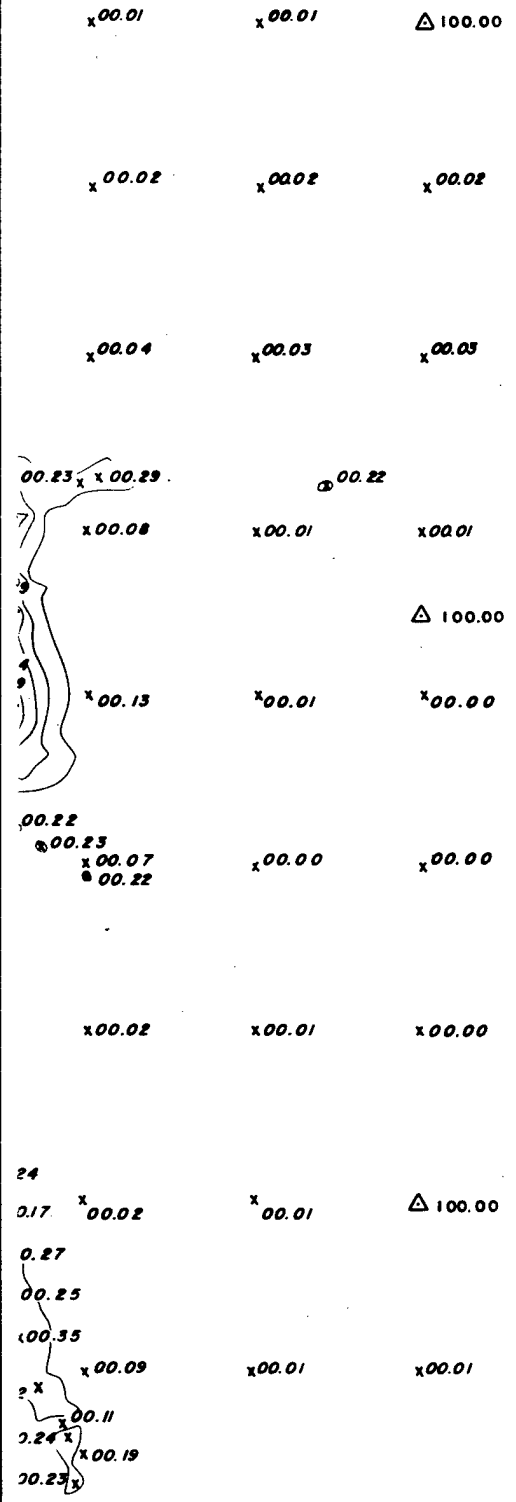

SCALE

0 8FT. 16 FT.

0.2 FOOT CONTOUR INTERVAL

DATE FLOWN 10-25-66

PROJECT PLOWSHARE TONOPAH 211-42

SHOT NO. 1

POST TEST TOPOGRAPHY

Compiled By

AMERICAN AERIAL SURVEYS, INC.

COVINA, CALIF.

SCALE

0 8FT. 16 FT.

0.2 FOOT CONTOUR INTERVAL

DATE FLOWN 10-25-66

ECT PLOWSHARE TONOPAH 211-42

SHOT NO. 1

POST TEST TOPOGRAPHY

Compiled By

AMERICAN AERIAL SURVEYS, INC.

COVINA, CALIF.

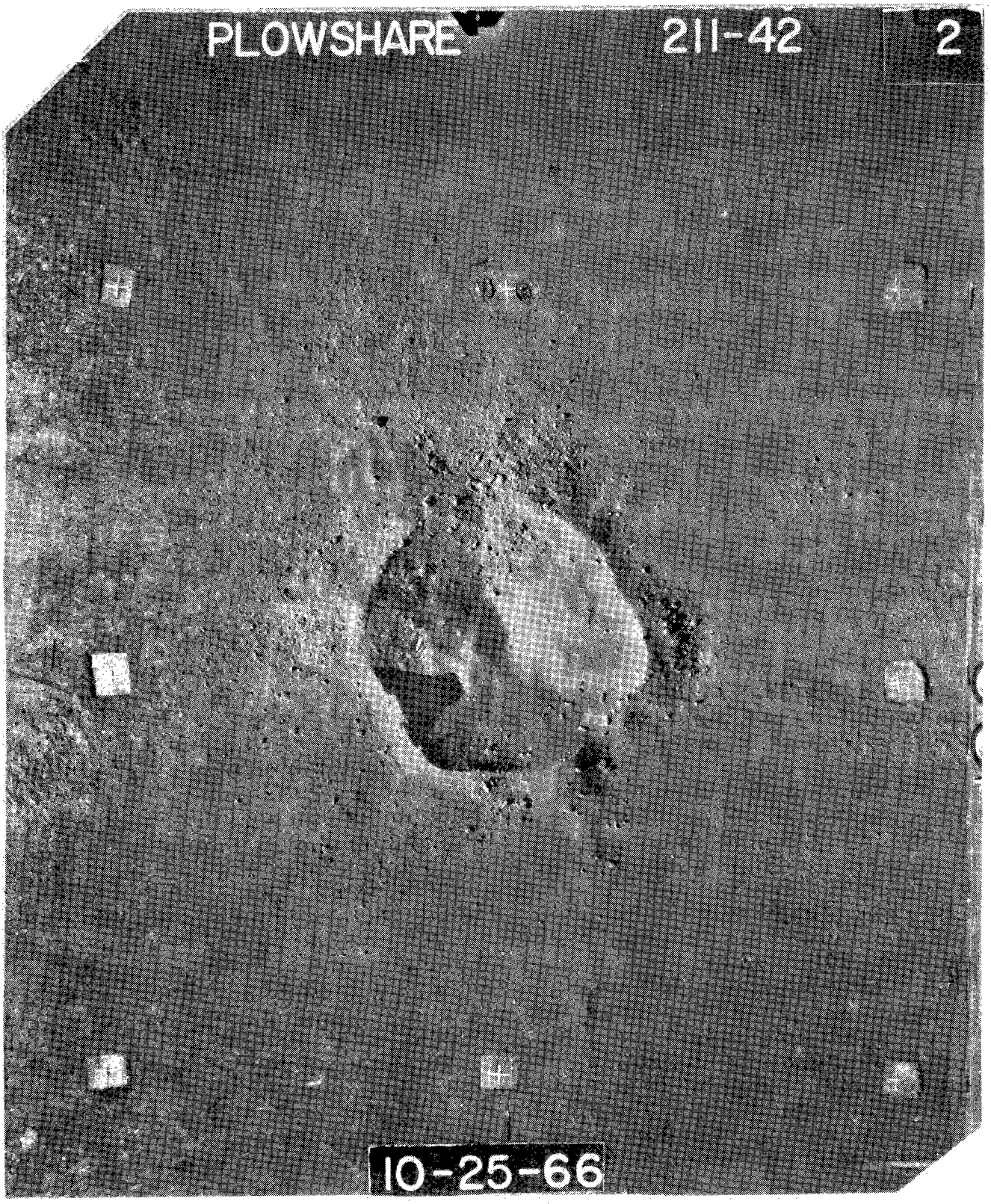
PLOWSHARE
211-42
2
10-25-66

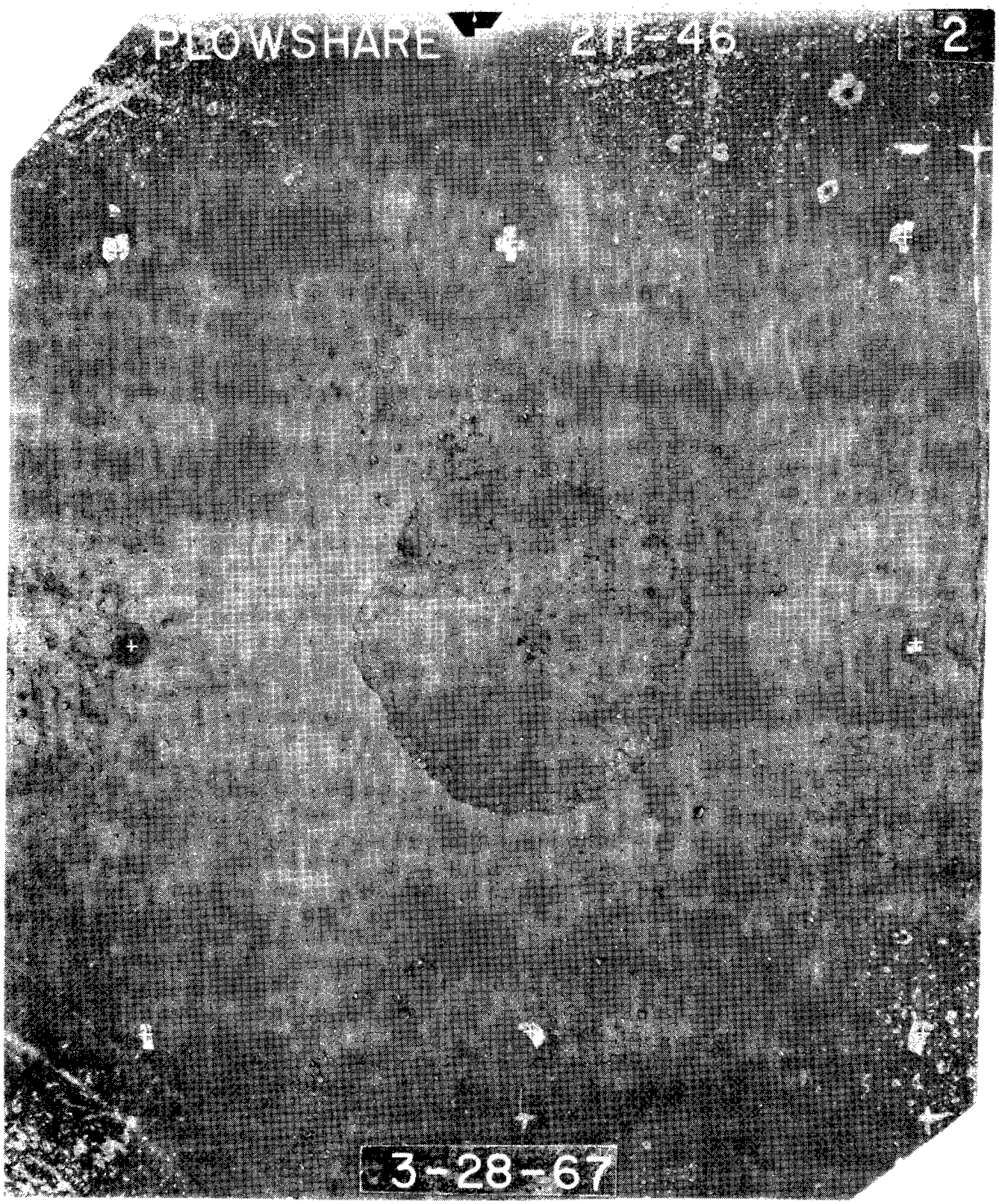
PLOWSHARE
211-46
2
3-28-67

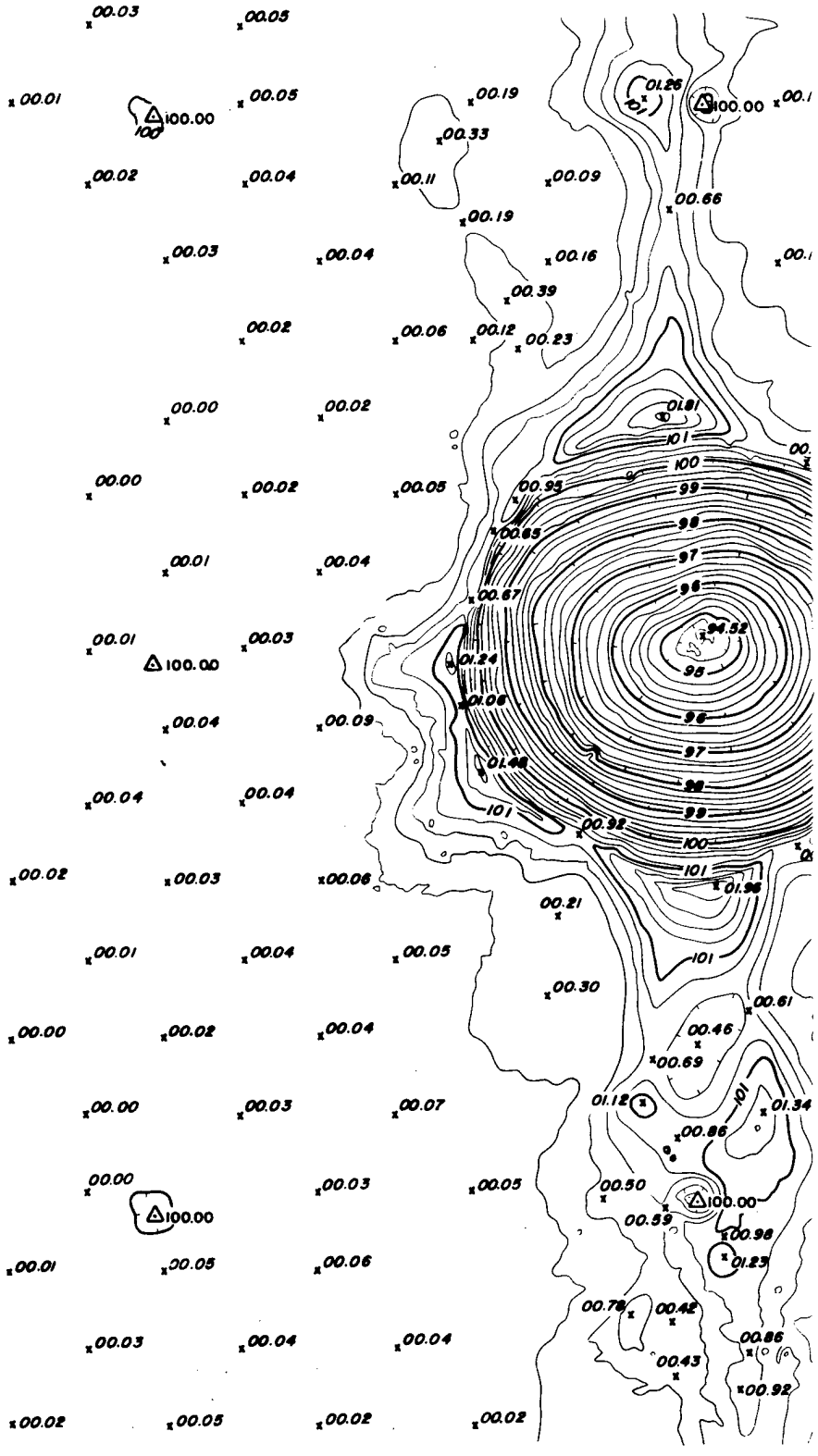
100.00
100.00
100.00
100.00
01.26
00.66
00.33
00.19
00.39
00.23
01.81
00.95
00.65
00.67
94.52
01.24
01.08
01.48
00.92
01.98
00.21
00.30
00.61
00.46
00.69
01.12
01.34
00.86
00.50
00.59
00.98
01.23
00.78
00.42
00.86
00.43
00.92

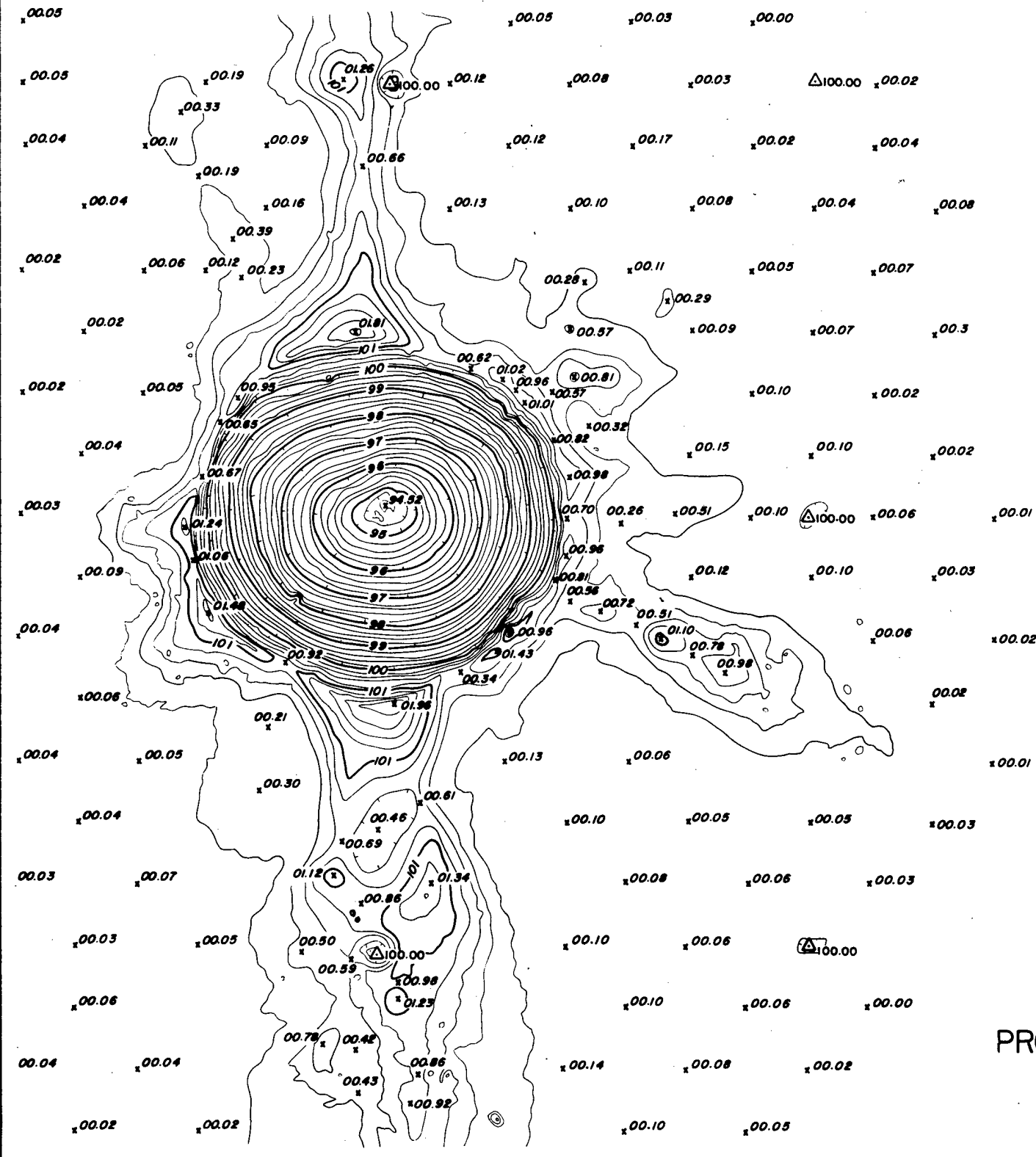
PROJECT PL
POST
AMER
0
0.2
DAT

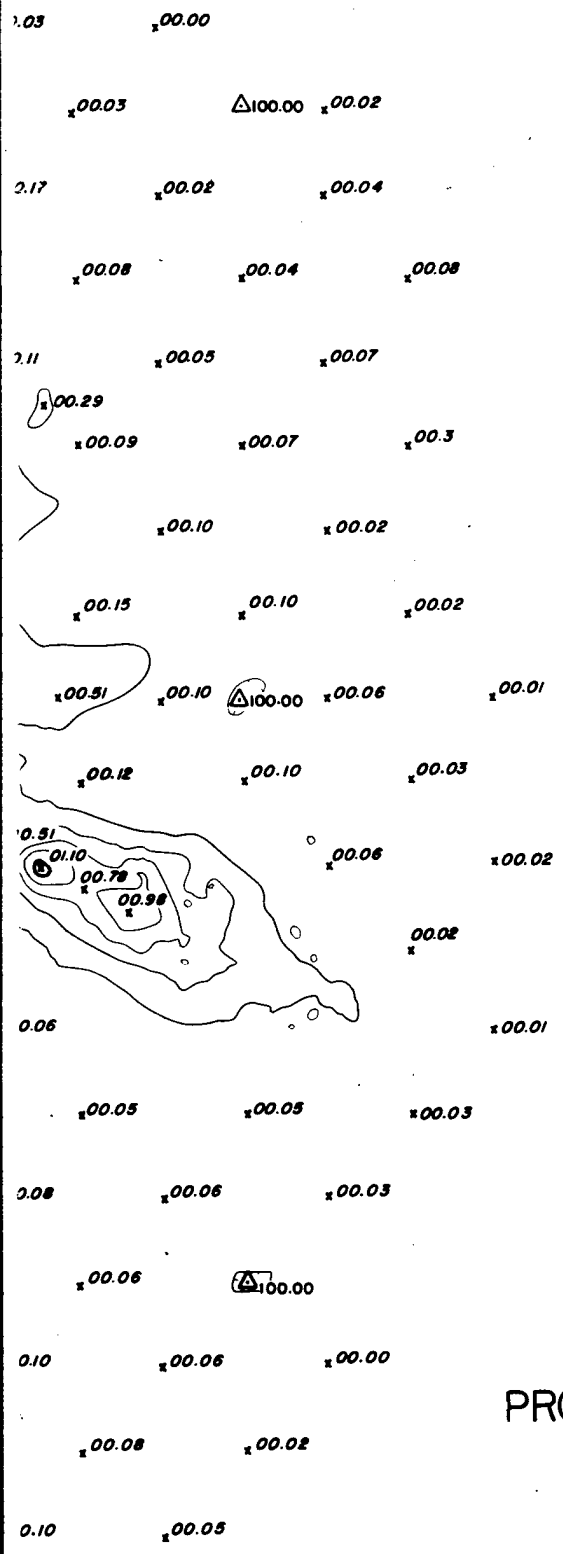

SCALE

0 8 FT. 16 FT.

0.2 FOOT CONTOUR INTERVAL

DATE FLOWN 3-28-67

PROJECT PLOWSHARE TONOPAH 211-46

POST TEST TOPOGRAPHY

Compiled By

AMERICAN AERIAL SURVEYS, INC.

COVINA, CALIF.

(3)

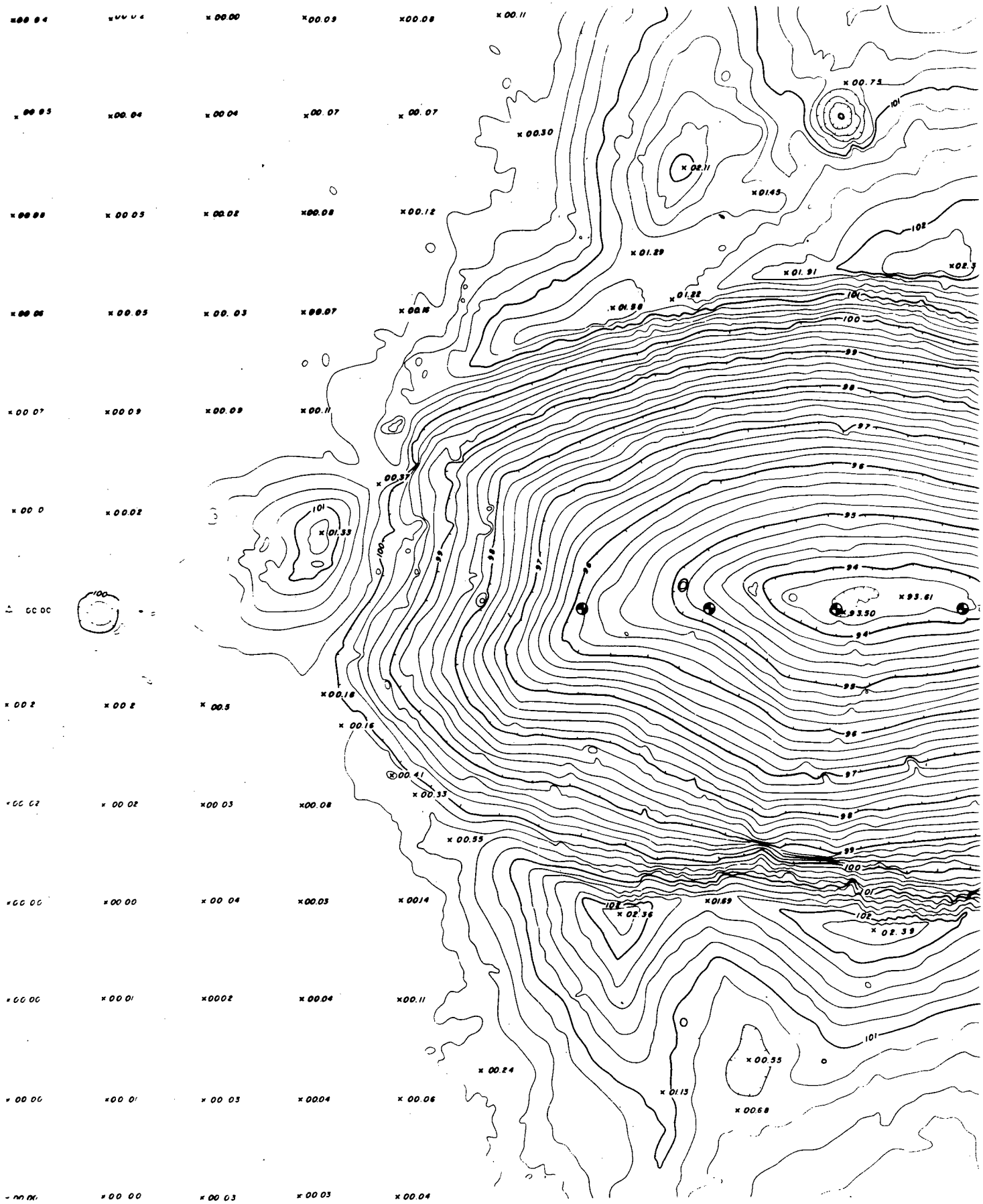
× 00.11
× 00.75
101
× 00.30
× 02.11
× 01.45
102
× 01.29
× 01.91
× 02.3
× 01.22
× 01.58
100
99
98
97
96
93
94
× 93.61
× 93.50
95
× 00.37
101
× 01.33
100
99
98
97
96
× 00.18
× 00.16
× 00.41
× 00.33
96
97
98
× 00.55
99
100
101
× 01.59
102
× 02.36
× 02.39
× 00.24
× 00.55
101
× 01.13
× 00.68

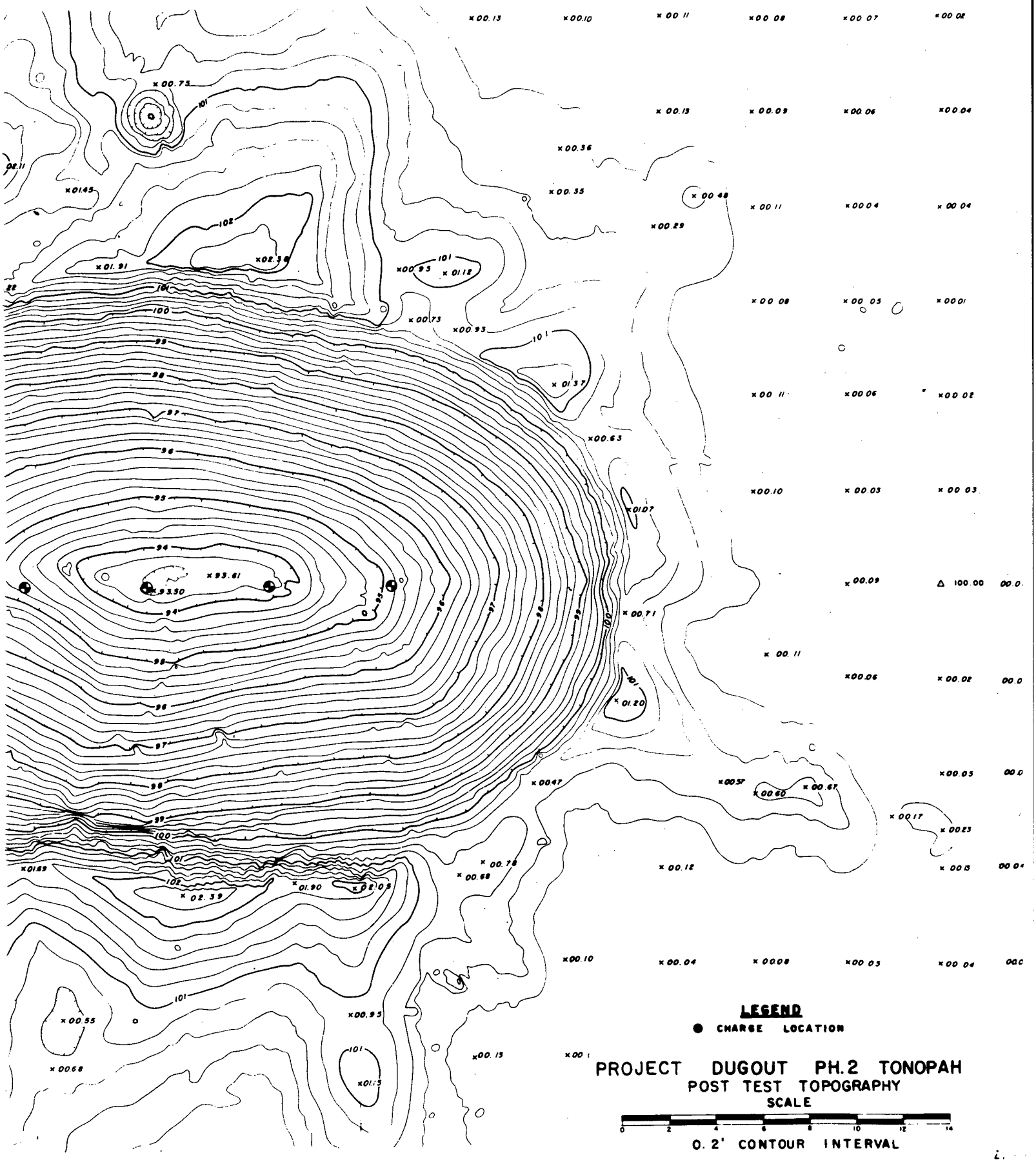
LEGEND
CHARGE LOCATION
PROJECT DUGOUT PH.2 TONOPAH
POST TEST TOPOGRAPHY
SCALE
0 2 4 6 8 10 12 14
0.2' CONTOUR INTERVAL

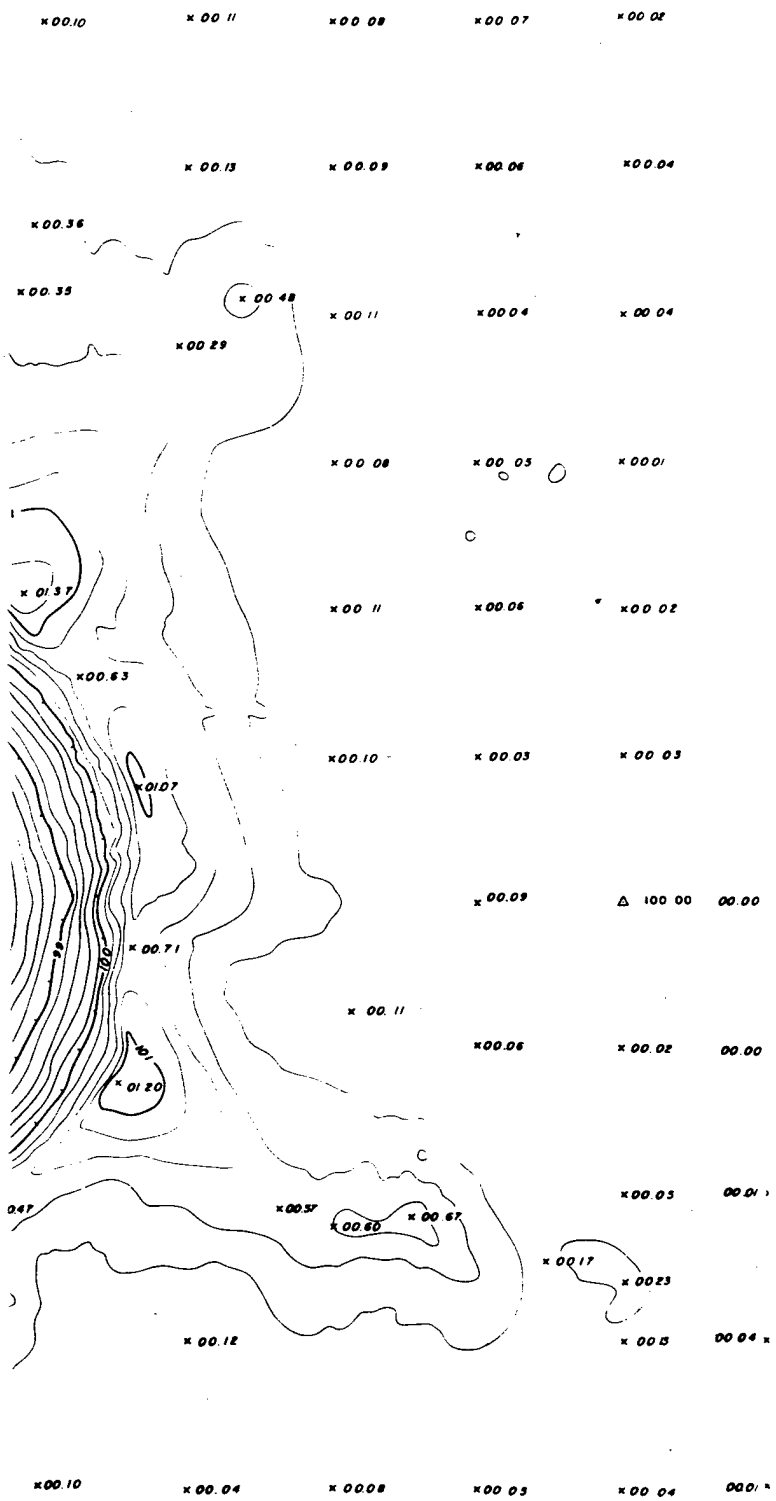

LEGEND

● CHARGE LOCATION

PROJECT DUGOUT PH.2 TONOPAH

POST TEST TOPOGRAPHY

SCALE

0 2 4 6 8 10 12 14

0.2' CONTOUR INTERVAL

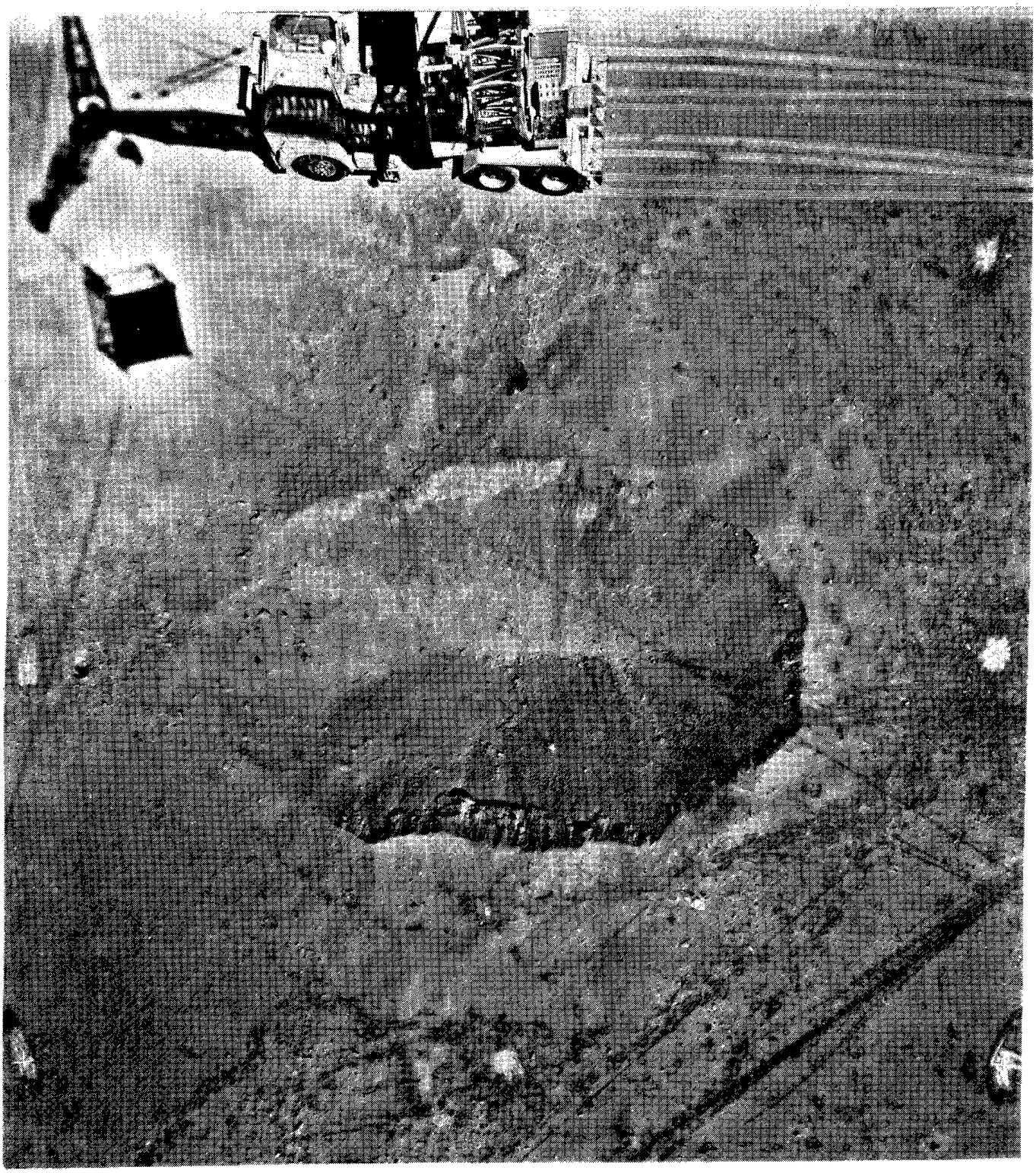

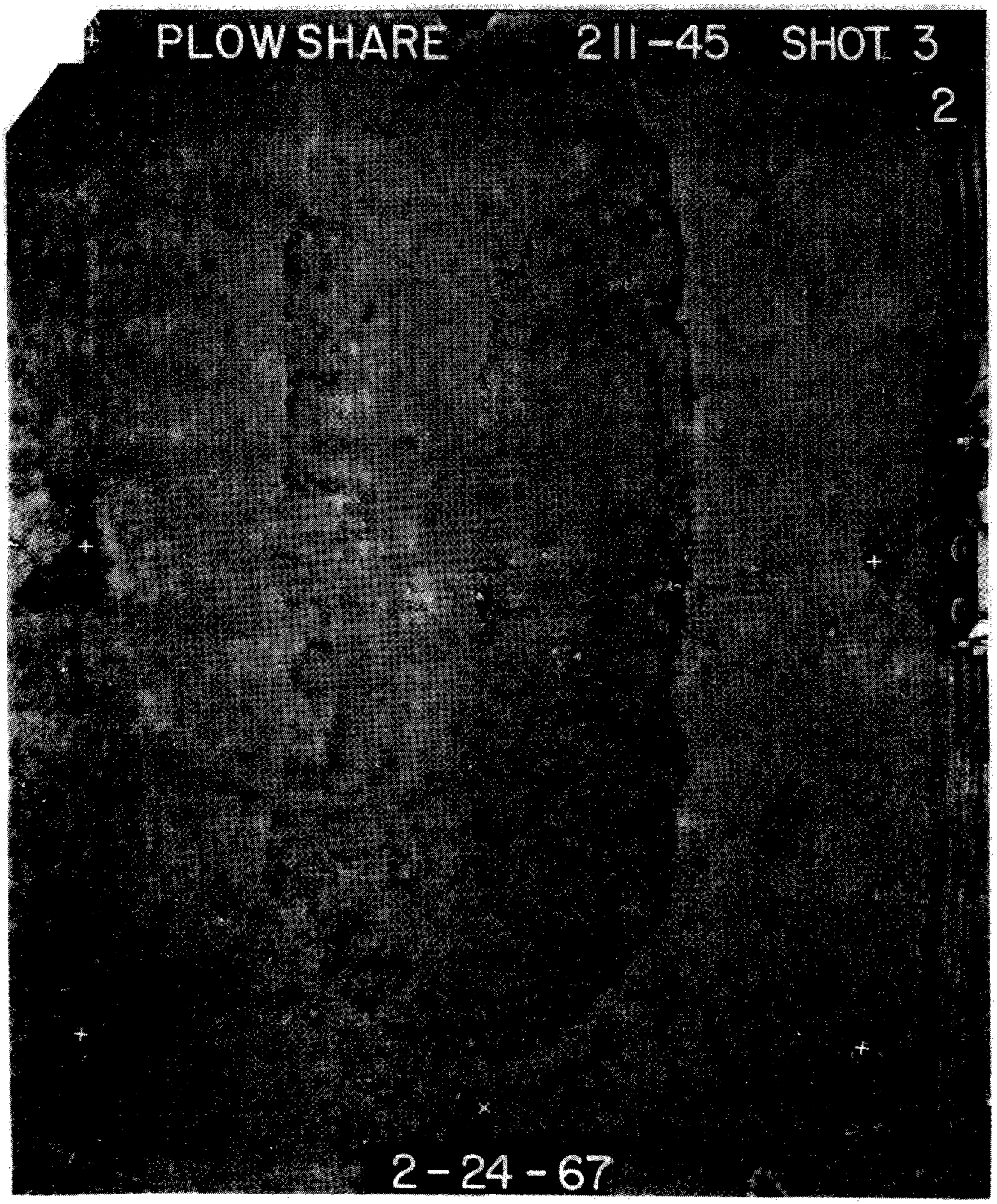
PLOWSHARE 211-45 SHOT 3
2
2-24-67

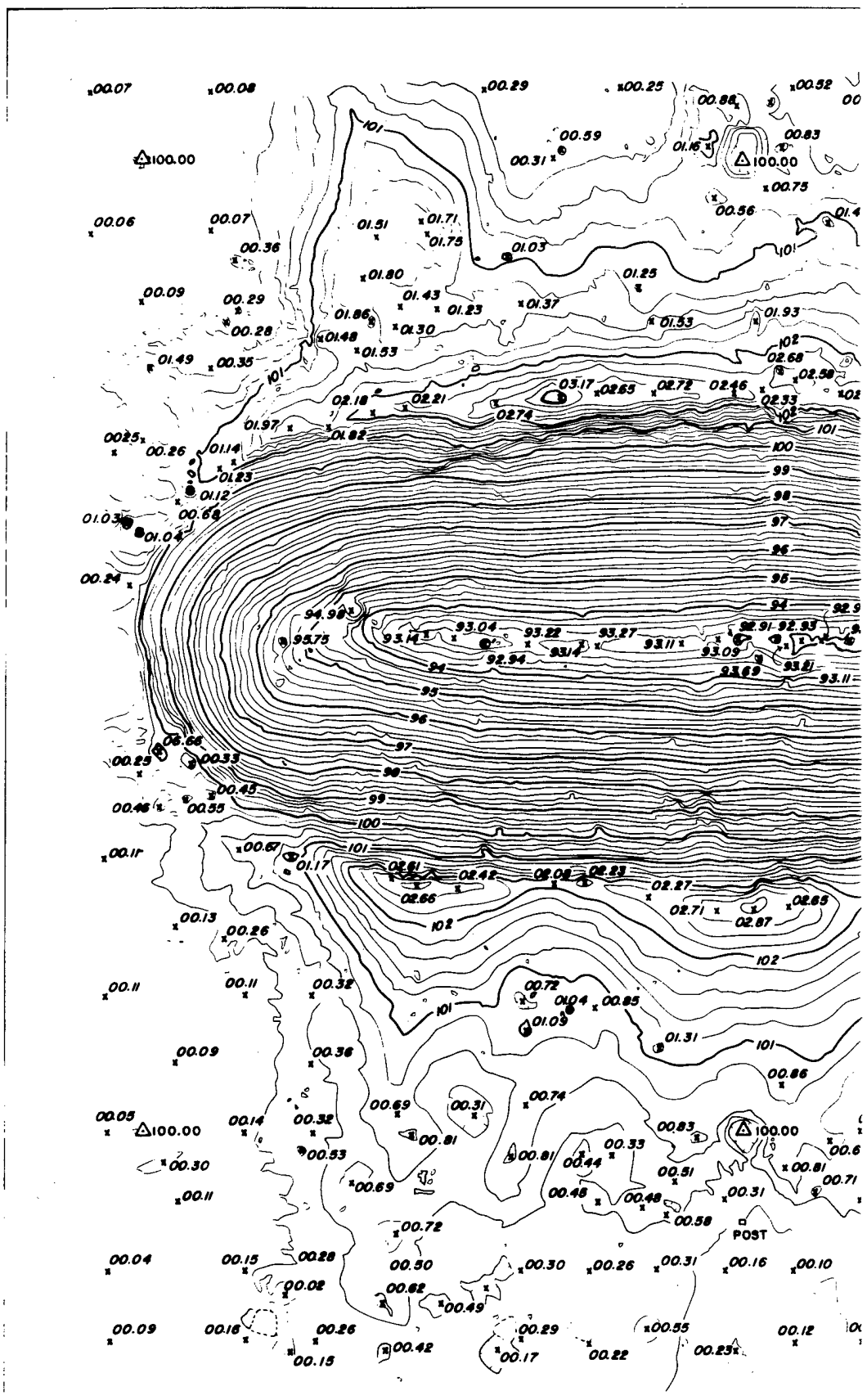
100.00
100.00
100.00
POST

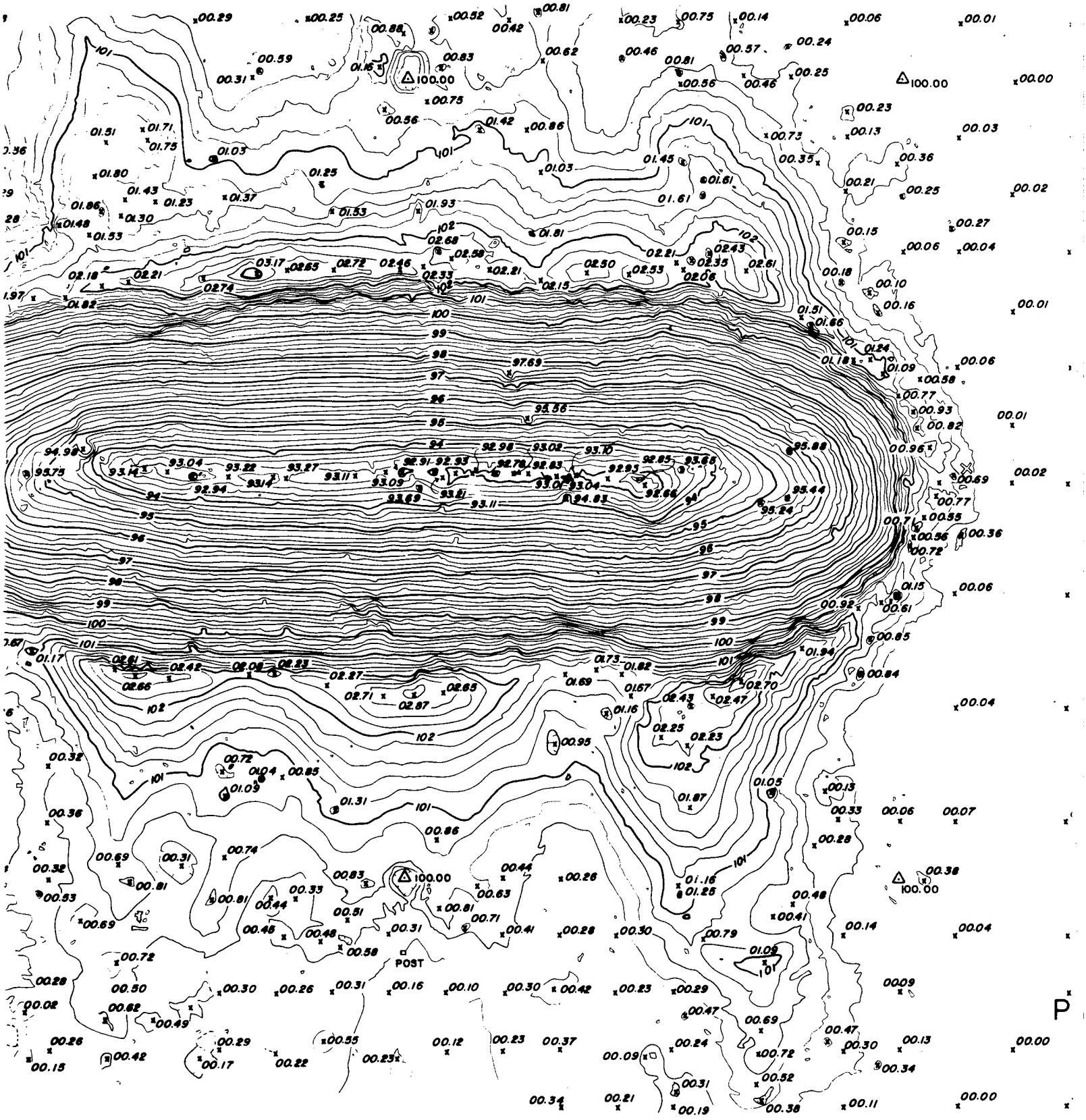
POST

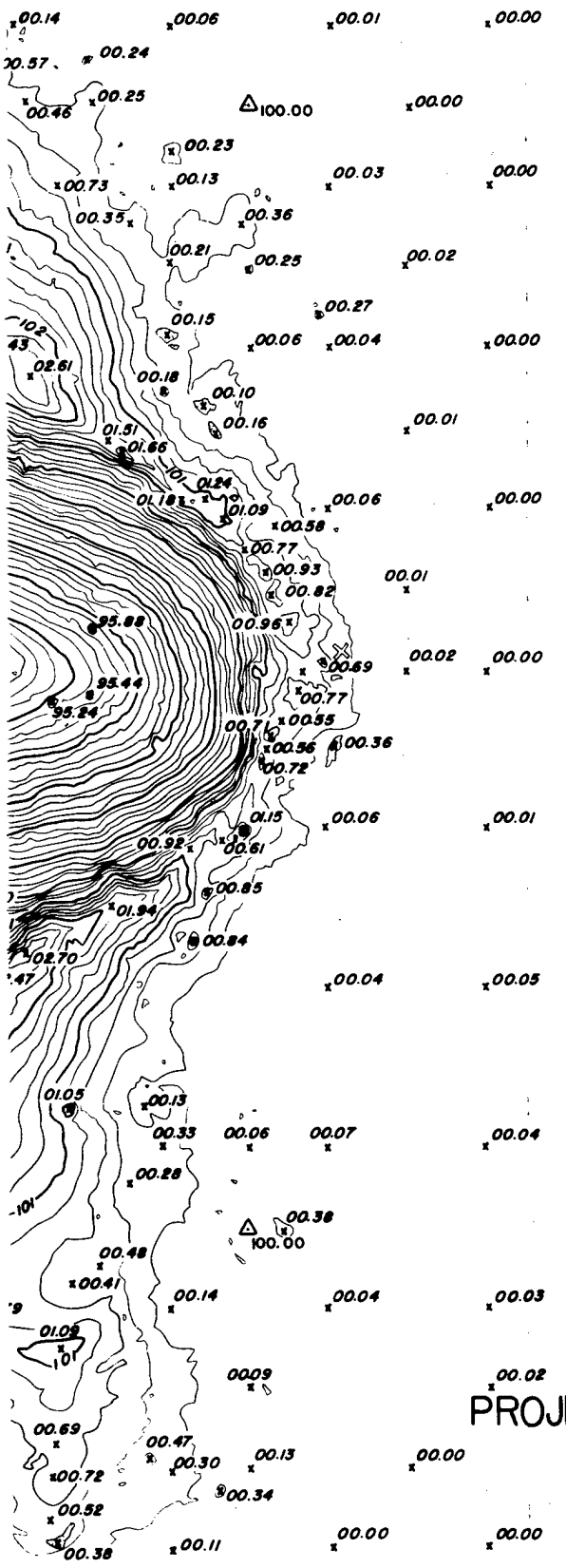

N

SCALE

0 8 FT. 16 FT.

0.2 FOOT CONTOUR INTERVAL

DATE FLOWN 2 - 24 - 67

PROJECT PLOWSHARE TONOPAH 211-45

SHOT 3

POST TEST TOPOGRAPHY

Compiled By

AMERICAN AERIAL SURVEYS, INC.

COVINA, CALIF.

(3)

DISTRIBUTION:
TID-4500, UC-35, (52nd Ed.) (292)

Major Gen. Edward B. Giller, USAF
Asst. General Manager for
Military Application
U.S. Atomic Energy Commission
Washington, D.C. 20545

U.S. Atomic Energy Commission
Dept. Peaceful Nuclear Explosives
Washington, D.C. 20545
Attn: J. S. Kelly, Director (25)
Richard Hamburger (1)
William Oakley (1)

U.S. Atomic Energy Commission
San Francisco Operations Office
2111 Bancroft Way
Berkeley, California 94704 (5)

U.S. Atomic Energy Commission
Albuquerque Operations Office
P. O. Box 5400
Albuquerque, New Mexico 87115 (2)

U.S. Atomic Energy Commission
Nevada Operations Office
P. O. Box 14100
Las Vegas, Nevada 89114
Attn: G. B. Maxey, Consultant (1)
T. F. Thompson,
Consultant (1)

ESSA
Boulder Laboratories
Boulder, Colorado 80302
Attn: John Rinehardt

Colorado School of Mines
Research Foundation, Inc.
P. O. Box 112
Golden, Colorado 80402
Attn: F. L. Smith

The Boeing Co.
Albuquerque Office Suite 1707
First Nat'l Bank Bldg. East
Albuquerque, New Mexico 87108
Attn: R. H. Carlson

Chief
Administrative Services Branch
Defense Atomic Support Agency
Washington, D.C. 20305

U.S. Bureau of Mines
Denver Mining Research Center
Bldg. 20 Denver Federal Center
Denver, Colorado 80225
Attn: Paul L. Russell,
Research Director

Los Alamos Scientific Laboratory
P. O. Box 1663
Los Alamos, New Mexico 87544
Attn: J. C. Mark
W. E. Ogle

Stanford University
School of Engineering
Dept of Civil Engineering
Stanford, California
Attn: Dr. Paul Kruger

Charles W. Martin
201 T and AM Lab
Iowa State University
Ames, Iowa 50010

Robert V. Whitman,
Military Institute of Technology
Cambridge, Massachusetts

N. M. Newmark
University of Illinois
Urbana, Illinois 61801

M. A. Cook
Explosives Research Group
University of Utah
Salt Lake City, Utah 84112

Eugene M. Shoemaker, Chief
Branch of Astrogeology
Geologic Division
U.S. Geologic Survey
P. O. Box 1906
Flagstaff, Arizona

Ralph B. Baldwin
1745 Alexander Rd., SE
East Grand Rapids, Michigan

J. J. Gilvarray
Research Laboratories
Allis-Chalmers Manufacturing Co.
Milwaukee, Wisconsin

DISTRIBUTION (Cont):

U.S. Army Ballistic Research Lab.
Aberdeen Proving Ground
Maryland, 21005
Attn: C. W. Lampson (1)
J. J. Meszaros (1)

William Hardwick
Bureau of Mines
Tucson, Arizona

University of California
Lawrence Radiation Laboratory
P. O. Box 808
Livermore, California 94550
Attn: M. M. May/D. Sewell (1)
G. C. Werth (1)
G. H. Higgins (10)
M. D. Nordyke (1)
B. Hughes, NCG (2)

IIT Research Institute
10 W. 35th St.
Chicago, Illinois 60616
Attn: T. Schiffman

Union Carbide Corp.
Nuclear Division
X-10 Laboratory Records Dept.
P. O. Box X
Oak Ridge, Tennessee 37830
Attn: W. E. Clark

R. M. Stewart
Director Mining Research
The Anaconda Company
1849 W North Temple
Salt Lake City, Utah 84116

Office, Chief of Engineers
Department of the Army
Washington, D.C. 20315
Attn: R. W. Beene (1)
J. H. Tormey (1)
M. D. Kirkpatrick (1)

General Electric Co.
TEMCO - Center for Advanced
Studies
816 State St.
Santa Barbara, California 93101
Attn: George M. Crain

RAND Corporation
1700 Main Street
Santa Monica, California 90406
Attn: D. T. Griggs (1)
H. L. Brode (1)

Stanford Research Institute
P. O. Box 725
Menlo Park, California 94025
Attn: R. B. Vaile (1)
Carl K. Wiehle (1)

Michael R. Dence
Division of Gravity
Department of Energy, Mines and
Resources
Ottawa 3, Ontario, Canada

Chief, Special Projects Branch (2)
Geologic Division
US Geologic Survey
Federal Center
Denver, Colorado 80225

Nuclear Group
El Paso National Gas Company
El Paso, Texas 79999

J. A. Hornbeck, 1
S. A. Moore, 7230
H. J. Bowen, 7233
R. C. Holland, 7233
T. B. Cook, 8000
C. S. Selvage, 8180
G. A. Fowler, 9000
B. F. Murphey, 9100
C. D. Broyles, 9110
L. J. Vortman, 9111
M. L. Merritt, 9111 (5 DPNE)
M. L. Merritt, 9111 (10)
J. W. Reed, 9111
G. E. Hanche, 9120
H. E. Viney, 9130
R. K. Petersen, 9132
R. D. Statler, 9133
B. F. Hefley, 8232 (5)
J. G. Marsh, 3414
B. R. Allen, 3421
L. C. Baldwin, 3412
W. J. Wagoner, 3413 (2)
C. H. Sproul, 3428-2 (15)